frontiers
RESEARCH TOPICS

MECHANISMS OF ION CHANNELS VOLTAGE-DEPENDENCY

Topic Editors
Gildas Loussouarn and Mounir Tarek

frontiers in
PHARMACOLOGY

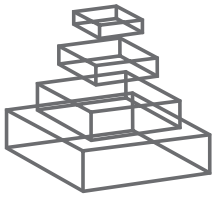

frontiers

Cover image provided by Ibbl sarl, Lausanne CH

ISSN 1664-8714
ISBN 978-2-88919-115-4
DOI 10.3389/978-2-88919-115-4

ABOUT FRONTIERS

Frontiers is more than just an open-access publisher of scholarly articles: it is a pioneering approach to the world of academia, radically improving the way scholarly research is managed. The grand vision of Frontiers is a world where all people have an equal opportunity to seek, share and generate knowledge. Frontiers provides immediate and permanent online open access to all its publications, but this alone is not enough to realize our grand goals.

FRONTIERS JOURNAL SERIES

The Frontiers Journal Series is a multi-tier and interdisciplinary set of open-access, online journals, promising a paradigm shift from the current review, selection and dissemination processes in academic publishing.
All Frontiers journals are driven by researchers for researchers; therefore, they constitute a service to the scholarly community. At the same time, the Frontiers Journal Series operates on a revolutionary invention, the tiered publishing system, initially addressing specific communities of scholars, and gradually climbing up to broader public understanding, thus serving the interests of the lay society, too.

DEDICATION TO QUALITY

Each Frontiers article is a landmark of the highest quality, thanks to genuinely collaborative interactions between authors and review editors, who include some of the world's best academicians. Research must be certified by peers before entering a stream of knowledge that may eventually reach the public - and shape society; therefore, Frontiers only applies the most rigorous and unbiased reviews.
Frontiers revolutionizes research publishing by freely delivering the most outstanding research, evaluated with no bias from both the academic and social point of view.
By applying the most advanced information technologies, Frontiers is catapulting scholarly publishing into a new generation.

WHAT ARE FRONTIERS RESEARCH TOPICS?

Frontiers Research Topics are very popular trademarks of the Frontiers Journals Series: they are collections of at least ten articles, all centered on a particular subject. With their unique mix of varied contributions from Original Research to Review Articles, Frontiers Research Topics unify the most influential researchers, the latest key findings and historical advances in a hot research area!
Find out more on how to host your own Frontiers Research Topic or contribute to one as an author by contacting the Frontiers Editorial Office: researchtopics@frontiersin.org

MECHANISMS OF ION CHANNELS VOLTAGE-DEPENDENCY

Topic Editors:
Gildas Loussouarn, Université de Nantes, France
Mounir Tarek, Centre National de La Recherche Scientifique, France

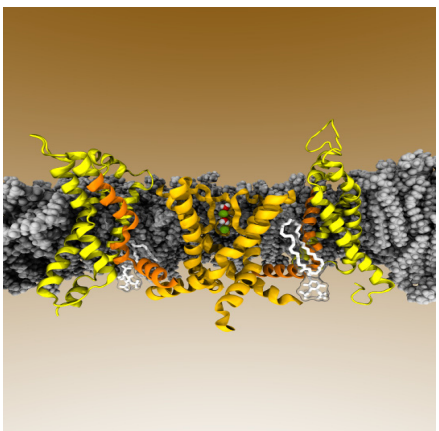

Voltage-gated ion channels are transmembrane proteins in which at least one gate is controlled by the transmembrane potential. They are frequently very selectively permeable to sodium (Nav channels), potassium (Kv channels) or calcium (Cav channels) ions. Depending on the channels, opening of the activation gate is triggered by membrane depolarization (Kv, Nav and Cav channels) or hyperpolarization (HCN channels for instance). In addition, in many voltage-gated channels, a so-called inactivation gate is also present. Compared to the activation gate, the latter is oppositely coupled to the potential: In Kv, Nav and Cav channels, upon membrane depolarization, the inactivation gate closes whereas the activation gate opens.

Depending on the cell types in which they are expressed and their physiological role, various voltage-dependent channels can be characterized by their conductance, ion selectivity, pharmacology and voltage-sensitivity. These properties are mainly dictated by the amino-acids sequence and structure of the pore forming subunit(s), presence of accessory subunit(s), membrane composition, intra- and extracellular ions concentration. Noteworthy, despite a profound variety of these ion channels characteristics, it seems that most of them obey to the same global, four-fold structure now obtained by several X-ray crystallography experiments.

Given the wealth of electrophysiological, biochemical, optical, and structural data regarding ion channels voltage-dependency, we decided to put together in this e-book, up to date reviews describing the molecular details of these complex voltage-gated channels.

Table of Contents

frontiers in
PHARMACOLOGY

EDITORIAL
published: 27 September 2012
doi: 10.3389/fphar.2012.00174

Mechanisms of ion channels voltage-dependency: all about molecular sensors, gates, levers, locks, and grease

Gildas Loussouarn[1,2,3]* and Mounir Tarek[4]

[1] *Institut National de la Santé et de la Recherche Médicale, UMR1087, Nantes, France*
[2] *Centre National de la Recherche Scientifique, UMR 6291, Nantes, France*
[3] *L'institut du Thorax, L'UNAM Université, Université de Nantes, Nantes, France*
[4] *Equipe de Chimie et Biochimie Théoriques, UMR Synthèse et Réactivité de Systèmes Moléculaires Complexes, Centre National de la Recherche Scientifique, Université de Lorraine, Nancy, France*
**Correspondence: gildas.loussouarn@univ-nantes.fr*

Edited by:
Diana Conte Camerino, University of Bari Aldo Moro, Italy

Given the wealth of electrophysiological, biochemical, optical, and structural data regarding ion channels voltage-dependency, we decided to put together in this special issue, up to date reviews describing the molecular details of these complex voltage-gated channels (and in one instance voltage-dependent phosphatases: Villalba-Galea, 2012). The articles focus mostly on the molecular mechanisms underlying channels voltage-dependency, such as the electromechanical coupling governing their activation, but also on molecular mechanisms governing their regulation by lipids. We anticipate that such knowledge will help one to better understand the pathophysiology of channelopathies (Choveau et al., 2012; Delemotte et al., 2012; Jurkat-Rott et al., 2012) and lead to new pharmacological approaches.

Molecular mechanisms underlying voltage-dependent activation and inactivation are complex, especially because channels are behaving in drastically different ways. Many reviews included in the present Research Topic issue describe models that rationalize these different behaviors:

- In some channels, e.g., HCN, KAT, activation is promoted by hyperpolarization while in others, e.g., Kv channels, it is promoted by depolarization, despite a similar global structure and behavior of their voltage sensors. The opposite behavior may come from different kinds of S4-S5/S6 interactions, that can be transient for hyperpolarization activated channel, permanent for depolarization activated channel (Blunck and Batulan, 2012), or bimodal, with the residues implicated in the S4-S5/S6 interaction being different in the open and closed states (Choveau et al., 2012). Along the same lines, the peculiar closed state inactivation observed in Kv4 channels may also come from a transient S4-S5/S6 interaction (Bähring et al., 2012).
- Forced uncoupling between the voltage sensor and the pore leads to opposite effects: this uncoupling favors channel closure of Shaker channels or, conversely, opening of the Kv-KcsA chimeric and KCNQ1 channels. This is most probably due to intrinsic properties of the pore, favoring a closed state in the former case and an open state in the latter (Blunck and Batulan, 2012; Vardanyan and Pongs, 2012).
- The nature of the gating motion of S6 falls into two categories as described in details by Labro and Snyders (2012). This may due to different constraints associated with the origin of the main stimulus, which comes from either the nearby voltage sensor domain or from a distal part of the C-terminus. C-terminal domains of Kv channels are indeed critical for the modulation of channel gating by signal transduction elements (Barros et al., 2012). These two categories may also be related with the intrinsic properties of the pore mentioned above (Vardanyan and Pongs, 2012).
- hERG is a very peculiar channel with slow activation gate and fast inactivation gate. Several molecular mechanisms (differences in voltage sensor dynamics, in the strength of S4-S5/S6 coupling, modulatory role of the N- and C-termini) may be at the origin of that peculiar behavior (Cheng and Claydon, 2012).

Finally, in addition to the pore forming subunits, membrane lipids (Choveau et al., 2012; Moreno et al., 2012; Rodríguez Menchaca et al., 2012), intracellular ions (Goodchild and Fedida, 2012), and β-subunits (Sun et al., 2012) that can associate with multiple stoichiometry (Wrobel et al., 2012) also modulate the channel voltage-dependency.

We hope that this series of reviews will bring researcher in the field (electrophysiologists, biochemists, modelers), a compendium of the knowledge gathered so far on the complex mechanisms of ion channel/enzyme voltage-dependency.

REFERENCES

Bähring, R., Barghaan, J., Westermeier, R., and Wollberg, J. (2012). Voltage sensor inactivation in potassium channels. *Front. Pharmacol.* 3:100. doi: 10.3389/fphar.2012.00100

Barros, F., Domínguez, P., and de la Peña, P. (2012). Cytoplasmic domains and voltage-dependent potassium channel gating. *Front. Pharmacol.* 3:49. doi: 10.3389/fphar.2012.00049

Blunck, R., and Batulan, Z. (2012). Mechanism of electromechanical coupling in voltage-gated potassium channels. *Front. Pharmacol.* 3:166. doi: 10.3389/fphar.2012.00166

Cheng, Y. M., and Claydon, T. W. (2012). Voltage-dependent gating of hERG potassium channels. *Front. Pharmacol.* 3:83. doi: 10.3389/fphar.2012.00083

Choveau, F. S., Abderemane-Ali, F., Coyan, F. C., Es-Salah-Lamoureux, Z., Baró, I., and Loussouarn, G. (2012). Opposite effects of the S4–S5 linker and PIP2 on voltage-gated channel function: KCNQ1/KCNE1 and other channels. *Front. Pharmacol.* 3:125. doi: 10.3389/fphar.2012.00125

Delemotte, L., Klein, M. L., and Tarek, M. (2012). Molecular dynamics simulations of voltage-gated cation channels: insights on voltage-sensor domain function and modulation. *Front. Pharmacol.* 3:97. doi: 10.3389/fphar.2012.00097

Goodchild, S. J., and Fedida, D. (2012). Contributions of intracellular ions to Kv channel voltage sensor dynamics. *Front. Pharmacol.* 3:114. doi: 10.3389/fphar.2012.00114

Jurkat-Rott, K., Groome, J., and Lehmann-Horn, F. (2012). Pathophysiological role of omega pore current in channelopathies. *Front. Pharmacol.* 3:112. doi: 10.3389/fphar.2012.00112

Labro, A. J., and Snyders, D. J. (2012). Being flexible: the voltage-controllable activation gate of Kv channels. *Front. Pharmacol.* 3:168. doi: 10.3389/fphar.2012.00168

Moreno, C., Macias, A., Prieto, A., de la Cruz, A., and Valenzuela, C. (2012). Polyunsaturated fatty acids modify the gating of Kv channels. *Front. Pharmacol.* 3:163. doi: 10.3389/fphar.2012.00163

Rodríguez Menchaca, A. A., Adney, S. K., Zhou, L., and Logothetis, D. E. (2012). Dual regulation of voltage-sensitive ion channels by PIP2. *Front. Pharmacol.* 3:170. doi: 10.3389/fphar.2012.00170

Sun, X., Zaydman, M. A., and Cui, J. (2012). Regulation of voltage-activated K+ channel gating by transmembrane β subunits. *Front. Pharmacol.* 3:63. doi: 10.3389/fphar.2012.00063

Vardanyan, V., and Pongs, O. (2012). Coupling of voltage-sensors to the channel pore: a comparative view. *Front. Pharmacol.* 3:145. doi: 10.3389/fphar.2012.00145

Villalba-Galea, C. A. (2012). Voltage-controlled enzymes: the new Janus Bifrons. *Front. Pharmacol.* 3:161. doi:10.3389/fphar.2012.00161.

Wrobel, E., Tapken, D., and Seebohm, G. (2012). The KCNE tango – how KCNE1 interacts with Kv7.1. *Front. Pharmacol.* 3:142. doi: 10.3389/fphar.2012.00142

Received: 07 September 2012; accepted: 11 September 2012; published online: 27 September 2012.

Citation: Loussouarn G and Tarek M (2012) Mechanisms of ion channels voltage-dependency: all about molecular sensors, gates, levers, locks, and grease. Front. Pharmacol. ***3****:174. doi:10.3389/fphar.2012.00174*

This article was submitted to Frontiers in Pharmacology of Ion Channels and Channelopathies, a specialty of Frontiers in Pharmacology.

frontiers in
PHARMACOLOGY

REVIEW ARTICLE
published: 13 September 2012
doi: 10.3389/fphar.2012.00161

Voltage-controlled enzymes: the new *Janus Bifrons*

Carlos A. Villalba-Galea*

Department of Physiology and Biophysics, Virginia Commonwealth University School of Medicine, Richmond, VA, USA

Edited by:
Gildas Loussouarn, Université de Nantes, France

Reviewed by:
Thomas Knopfel, RIKEN Brain Science Institute, Japan
Thomas Friedrich, Technical University of Berlin, Germany

****Correspondence:***
Carlos A. Villalba-Galea, Department of Physiology and Biophysics, Virginia Commonwealth University School of Medicine, Richmond, VA 23298, USA.
e-mail: cavillalbaga@vcu.edu

The *Ciona intestinalis* voltage-sensitive phosphatase, Ci-VSP, was the first Voltage-controlled Enzyme (VEnz) proven to be under direct command of the membrane potential. The discovery of Ci-VSP conjugated voltage sensitivity and enzymatic activity in a single protein. These two facets of Ci-VSP activity have provided a unique model for studying how membrane potential is sensed by proteins and a novel mechanism for control of enzymatic activity. These facets make Ci-VSP a fascinating and versatile enzyme. Ci-VSP has a voltage sensing domain (VSD) that resembles those found in voltage-gated channels (VGC). The VSD resides in the N-terminus and is formed by four putative transmembrane segments. The fourth segment contains charged residues which are likely involved in voltage sensing. Ci-VSP produces sensing currents in response to changes in potential, within a defined range of voltages. Sensing currents are analogous to "gating" currents in VGC. As known, these latter proteins contain four VSDs which are entangled in a complex interaction with the pore domain – the effector domain in VGC. This complexity makes studying the basis of voltage sensing in VGC a difficult enterprise. In contrast, Ci-VSP is thought to be monomeric and its catalytic domain – the VSP's effector domain – can be cleaved off without disrupting the basic electrical functioning of the VSD. For these reasons, VSPs are considered a great model for studying the activity of a VSD in isolation. Finally, VSPs are also phosphoinositide phosphatases. Phosphoinositides are signaling lipids found in eukaryotes and are involved in many processes, including modulation of VGC activity and regulation of cell proliferation. Understanding VSPs as enzymes has been the center of attention in recent years and several reviews has been dedicated to this area. Thus, this review will be focused instead on the other face of this true *Janus Bifrons* and recapitulate what is known about VSPs as electrically active proteins.

Keywords: voltage-sensitive phosphatases, Ci-VSP, sensing current, 3_{10} helix, VSD relaxation

INTRODUCTION

Voltage sensing phosphatases (VSP) are the first family of enzymes displaying a voltage sensing domain (VSD). The first member of the VSP family was described in 1999, when the human isoform TPTE (Transmembrane Phosphatase with Tensin homology) was reported as a testis-specific protein (Chen et al., 1999; Guipponi et al., 2001; Wu et al., 2001; Tapparel et al., 2003). In spite of the great similarities between the C-terminus of TPTE and members of the protein tyrosine phosphatases (PTP) family (Chen et al., 1999; Guipponi et al., 2000, 2001; Walker et al., 2001; Tapparel et al., 2003), no catalytic activity was – or has been – observed to be mediated by this protein.

Two years later, the findings of a second human VSP (Walker et al., 2001; Wu et al., 2001) and a murine VSP (Guipponi et al., 2001) were reported. In contrast to TPTE, the new human VSP (known as TPTE2 and originally named TPIP: TPTE and PTEN homologous Inositol lipid Phosphatase) displayed phosphoinositide phosphatase activity (Walker et al., 2001; Wu et al., 2001). Another difference between the human VSPs (Hs-VSP, where "Hs-" is for *Homo sapiens*) is that TPTE2 (hereafter Hs-VSP1) is also found expressed in stomach and brain, in addition to testis (Walker et al., 2001). To date, the physiological role of these proteins remains elusive. Likewise, whether or not Hs-VSPs are electrical active remains to be determined – so is the case for the murine VSP (Mm-VSP; known as mTpte). Nevertheless, it is arguably predicted that VSPs are involved in phosphoinositide signaling pathways, which are found in all eukaryotes (Di Paolo and De Camilli, 2006; Balla et al., 2009).

Since the discovery of Hs-VSPs, a number of VSPs have been found – or predicted to exist – in many species (Kumanovics et al., 2002; Sutton et al., 2012). The most conspicuous member of the family is Ci-VSP. This enzyme was isolated from the tunicate *Ciona intestinalis* – hence the acronym "Ci-." In juvenile animals, Ci-VSP has a wide tissue distribution (Ogasawara et al., 2011); whereas it seems to be restricted to testis, neuronal tissues, and sperm in adults (Murata et al., 2005). In contrast to mammals VSPs, Ci-VSP displays robust electrical activity. Indeed, Ci-VSP was the first enzyme proven to be under direct control of the membrane potential (Murata et al., 2005; Murata and Okamura, 2007). Ci-VSP is one of the workhorses for research aimed at understanding the biophysical and biochemical features of the VSP family. In fact, our current understanding of the functioning of VSPs emerges from studies on this enzyme.

The physiological role of VSPs remains unclear. Ci-VSP and other catalytically active VSPs are phosphoinositides phosphatases (Walker et al., 2001; Murata et al., 2005; Murata and Okamura,

2007; Iwasaki et al., 2008; Halaszovich et al., 2009, 2012; Kohout et al., 2010; Ratzan et al., 2011; Kurokawa et al., 2012). As known, phosphoinositides are ubiquitous signaling lipids in eukaryotes (Di Paolo and De Camilli, 2006; Balla et al., 2009). Phosphoinositide signaling is central for a number of processes including development (Leslie and Downes, 2004; Di Paolo and De Camilli, 2006; Leslie et al., 2007, 2008; Balla et al., 2009), ion channels regulation (Suh and Hille, 2008; Logothetis et al., 2010), plasma membrane identity (Hammond et al., 2012), and others. Also, it has been shown that there is a correlation between changes in the membrane potential and regulation of cell proliferation and differentiation (Sundelacruz et al., 2009; Levin and Stevenson, 2012). Thus, VSPs constitute a potential direct link between electrical activity and development.

VSPs are homologs to PTEN, an enzyme critically involved in the control of cell growth and proliferation, as well as in cell differentiation (Leslie and Downes, 2002, 2004; Bai et al., 2004; Menager et al., 2004; Walker et al., 2004; Balla et al., 2005; Leslie et al., 2007, 2008; Endersby and Baker, 2008; Ooms et al., 2009; Arendt et al., 2010; Bunney and Katan, 2010; Davidson et al., 2010; Michailidis et al., 2011). PTEN is known as a *tumor suppressor* – disruption of its function is among the most common causes of cancer in humans (Li et al., 1997; Teng et al., 1997; Maehama and Dixon, 1998, 1999; Leslie and Downes, 2004; Bunney and Katan, 2010). PTEN and the catalytic domain of Ci-VSP display similar mechanisms for activation (Iwasaki et al., 2008; Villalba-Galea et al., 2009a; Kohout et al., 2010; Hobiger et al., 2012), share catalytic targets (Murata et al., 2005; Iwasaki et al., 2008; Halaszovich et al., 2009; Kohout et al., 2010; Lacroix et al., 2011), and have structures that resemble each other (Lee et al., 1999; Matsuda et al., 2011; Liu et al., 2012). Based on these similarities, a series of chimeras, made by attaching the VSD of Ci-VSP to PTEN, were proven to provide control by membrane potential on the activity of PTEN (Lacroix et al., 2011). This study demonstrated for the first time that a cytosolic enzyme can be engineered to become a Voltage-controlled Enzymes (VEnz) and, thus, be directly controlled by membrane potential. More recently, this approach has been used to study the activity of the catalytic domains of the chicken (*Gallus gallus*) VSP (Gg-VSP; Kurokawa et al., 2012) and the Hs-VSP1 (Halaszovich et al., 2012; Kurokawa et al., 2012).

Among enzymes, what is unique about VSPs is that the N-terminus forms a functional VSD controlling catalytic activity – at least in non-mammalian VSPs. In spite of this extraordinary characteristic, it is the C-terminus what has drawn the attention of many researchers in recent years. Presumably, a reason for this is that Ci-VSP displays high structural and functional homology with the tumor suppressor PTEN (Murata et al., 2005; Murata and Okamura, 2007; Iwasaki et al., 2008; Villalba-Galea et al., 2009a; Kohout et al., 2010; Lacroix et al., 2011; Hobiger et al., 2012; Liu et al., 2012). In fact, several review articles on this matter are available in the literature (Worby and Dixon, 2005; Okamura and Dixon, 2011; Villalba-Galea, 2012) and a number of crystal structures have been published recently (Matsuda et al., 2011; Liu et al., 2012). Arguably however, the most striking feature of VSPs is that the VSD controls catalytic activity. Thus, this review will be mainly focused on the electrical properties of VSPs.

SENSING CURRENTS

The VSD of Ci-VSP bears charged residues located within the membrane-embedded region of the protein. As for others VSD proteins, changes in magnitude and/or polarity of the electrical field across the plasma membrane can induce changes in the position of these charges, translating this displacement into conformational changes in the protein itself. This is the underlying process for voltage sensing (Bezanilla, 2005, 2008; Swartz, 2008).

The movement of charged residues down the electrical gradient produces transient currents (**Figure 1A**). These currents are known as "sensing" currents. In voltage-gated channels (VGC), sensing currents are regarded as "gating" currents, since they are involved in the mechanism that opens and closes the "gate" for ion conduction (Bezanilla, 2005, 2008; Tombola et al., 2006). Thus, it is fair to say that "gating" currents were the first instance of sensing currents ever described.

Sensing currents are produced by the movement of VSD intrinsic charges across its membrane-embedded region. In the simplest case, VSD's charges sojourn between two states, one called Resting state and another called Active state (**Figure 1C**, top). The Resting state corresponds to the most probable state found at resting membrane potentials – hence the name. In this condition, the plasma membrane is polarized at negative voltage. On the other hand, the VSD is more likely to be in the Active state as more positive the membrane potential is. The transition rates between Resting and Active states depend exponentially on the voltage across the membrane (Bezanilla, 2000). For a simple two-state model, the transition rate from the Resting to the Active state (α) is greater as the membrane potential is more positive, while the rate for the reverse transition (β) is lesser; for negative potentials, the opposite situation is observed. Thus, the probability of finding the VSD in the Active state (P_{Active}) increases at more positive potentials and is given by the following equation: $P_{\text{Active}} = \alpha/(\alpha + \beta)$.

Usually, the action of changing the membrane potential to more positive values is referred to as "depolarization." This term is inherited from classical electrophysiology in which conductances were evoked by driving the membrane potential toward 0 mV – not polarized membrane. However, in the case of VSPs, maximum activation is typically observed above +60 mV (Murata et al., 2005; Murata and Okamura, 2007; Hossain et al., 2008; Iwasaki et al., 2008; Villalba-Galea et al., 2009a; Ratzan et al., 2011). At these potentials, the membrane is positively polarized and the magnitude of the polarization is larger that the one observed at typical resting potentials. Thus, the term "depolarization" is unsuitable to describe the changes in potential that leads to activation of VSPs. Instead, the term antipolarization (anti-: from the greek αντί that means opposite) is a more accurate descriptor.

THE NATURE OF SENSING CURRENTS

For the voltage-gated channel *Shaker*, it has been proposed that gating currents are composed by the sum of "shot"-like currents events (Sigg et al., 1994; Bezanilla, 2000). There is not reason to believe that VSPs behave differently. Thus, it can be assumed that, as in the case of *Shaker*, the transition of a single VSD from the Resting to the Active state produces an outward "shot"-like current as sensing charges move toward the extracellular space. In

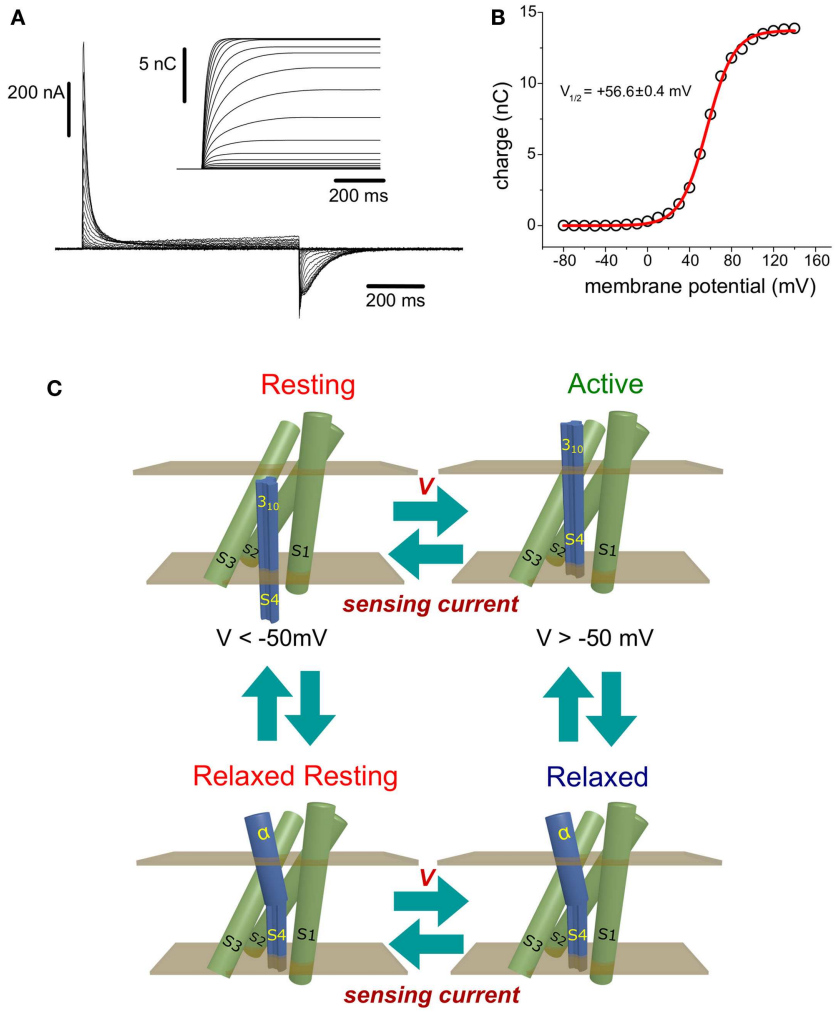

FIGURE 1 | (A) Ci-VSP-C363S sensing currents recorded from *Xenopus* oocytes using the cut-open voltage clamp technique (Taglialatela et al., 1992). The holding potential (HP) was set to −60 mV, and ON-sensing currents were evoked by 800 ms-test pulses ranged −80 to +140 mV. OFF-sensing currents were recorded at −60 mV. Numerical integration of the ON-sensing currents (inset) was performed using a package developed by the author using the programming language Java. **(B)** Maximum (steady state) net charges are calculated by integration were plotted against the voltage applied during the corresponding test pulse. The charge (Q) vs. Potential (V) relationship was fitted to a Boltzmann distribution (see text). For this, particular example, the half-maximum potential fitted was +56.6 ± 0.4 mV. **(C)** Minimum scheme for description of the electrical behavior of the voltage sensing domain of Ci-VSP. At potentials below −50 mV, the VSD resides with high probability in the Resting state. Upon changes in the membrane potential to more positive voltages, sensing currents are observed as consequence of the movement of sensing charges leading the VSD into the active state. If the membrane potential is above +50 mV, a secondary, voltage-independent transition is observed following sensing currents. This process is called relaxation (see text) and promotes the population of the relaxed state. As described in the text, transitions between the resting and active state may occur while the S4 segment is in a 3_{10} helix conformation. However, transit into the relaxed states may be accompanied by a transformation of the upper part of the S4 segment into an α-helix. Finally, repolarization of the plasma membrane causes the return of the VSD to the resting state. This transition is achieved through a hypothetical relaxed resting state.

contrast, the transition from the Active to the Resting state produces an inward "shot"-like current as the sensing charges move in the opposite direction. For a large number of VSDs, the balance between these currents results in a net charge movement across the membrane, thus sensing currents.

When the membrane potential changes from negative to a more positive voltages, sensing currents are observed as outwardly rectifying currents. These currents are referred to as ON-sensing currents, since they are related to the activation of the VSD and phosphatase activity. Likewise, changes from positive to more negative potentials evoke inward sensing current, which are referred to as OFF-sensing currents, since they are related to the deactivation of the VSPs. The net charge movement (Q) at each potential can be determined by numerically integrating sensing currents (**Figure 1A**, inset). The relationship between Q and the membrane potential (V), known as $Q-V$ relationship (**Figure 1B**, open circles), is typically described by one or the sum of two or more Boltzmann distributions $Q = Q_{MAX}/(1 + e^{-zF(V-V_{1/2})/RT})$

(**Figure 1B**, red line). The parameters of these distributions are utilized to characterized voltage dependence of VSD proteins. One of the most commonly used parameters is the half-maximum potential ($V_{1/2}$) that, in the case of a two-state model, defines at which potential the Resting and Active states are equally populated (**Figure 1B**). Other parameters for Boltzmann distributions are: Q_{MAX} which is the maximum charge that can be moved, z which is the apparent sensing charge, and F, R, and T which are the Faraday constant, the universal ideal gas constant, and T in temperature in Kelvin, respectively.

VOLTAGE DEPENDENCE OF VSPs

For Ci-VSP, sensing currents typically become discernible at potentials above −50 mV, when holding the membrane at −60 mV. As describe above, Q increases as antipolarization increases and it reaches its maximum – it saturates – at potentials above +120 mV (**Figure 1B**). The typical $V_{1/2}$ for the Ci-VSP $Q-V$ relationship is around +55 mV (Hossain et al., 2008; Villalba-Galea et al., 2008; **Figure 1B**). Beside Ci-VSP, sensing currents have been only reported from the isoform isolated from *Danio rerio* (zebrafish). This VSP, known as Dr-VSP, shows a $V_{1/2}$ around +96 mV (Hossain et al., 2008).

Three additional VSPs have been shown to be VEnz. These are two isoforms isolated from *Xenopus laevis* (Xl-VSP1 and Xl-VSP2) and one isoform isolated from *Xenopus tropicalis* (Xt-VSP; Ratzan et al., 2011). No sensing currents have been reported from these proteins. However, catalytic activity for Xl-VSP1 and Xl-VSP2 is observed at potential above −20 and 0 mV, respectively, reaching maximum around +60 mV (Ratzan et al., 2011). These observations suggest that Xl-VSPs have steeper voltage dependence than Ci-VSP.

An intriguing feature of VSP is that mutations in the catalytic domain, the effector domain of the VSD, have direct consequences on the electrical activity of the voltage sensor. Particularly, inactivation of Ci-VSP catalytic activity by mutating Cystein 363 to a serine (C363S) causes an apparent change in the dynamics of the VSD Ci-VSP. As reported from experiments using Two-Electrode Voltage Clamp Fluorometry (TE-VCF), the deactivation of the VSD is slower when the catalytic domains has been inactivated by introducing the mutation C363S (Kohout et al., 2010). Likewise, introduction of the equivalent mutation in Dr-VSP (C302S) slightly shifts the $V_{1/2}$ from +97 to +107 mV (Hossain et al., 2008). The basis for these differences in the electrical properties is yet to be determined.

It has also been shown that mutations that affect electrochemical coupling affect sensing currents as well. During the return of the VSD to the resting state, OFF-sensing currents display a slower kinetic than those observed for ON-sensing currents during activation (**Figure 1**). To explain this observation, it has been proposed that the VSD controls the binding of the Phospholipid Binding Motif (PBM) to the membrane, which, in turn, controls catalytic activity (Villalba-Galea et al., 2009a; Kohout et al., 2010; Lacroix et al., 2011; Hobiger et al., 2012). Therefore, the return of sensing charges must overcome PBM binding to the membrane while in transit to the resting state. More recently, it has been shown that the PBM is likely to bind $PI(4,5)P_2$ (Kohout et al., 2010; Villalba-Galea, 2012). Several mutations in the PBM has been identified to disrupts binding, thus, electrochemical coupling (Villalba-Galea et al., 2009a; Kohout et al., 2010; Lacroix et al., 2011; Hobiger et al., 2012). In the presence of some these mutations or when the catalytic domain is deleted, an increase in the speed of OFF-sensing current is observed (Villalba-Galea et al., 2009a; Hobiger et al., 2012). Conversely, when a mutation causes the "trapping" of the catalytic domain on the membrane, the return of the S4 segment to the resting state is much slower. This has been shown in TE-VCF recordings from Ci-VSP bearing a mutation in catalytic domain where Aspartate 331 is replaced to an alanine (D331A; Kohout et al., 2010). Taken together, these observations clearly suggest that as the VSD controls the catalytic domain, this latter one influences the electrical activity of the sensor. Whether the modulation of electrical activity the consequence of electromechanical coupling or whether there is an explicit feedback mechanism for regulation of the VSD remains to be determined.

THE VOLTAGE SENSING DOMAIN

The N-terminus of Ci-VSP displays four putative transmembrane spanning segments forming a VSD (Murata et al., 2005). This domain is homologous to those found in voltage gated channels (Noda et al., 1986). The fourth putative segment of the VSD of Ci-VSP bears five basic residues which are thought to constitute the main sensing charges of the domain (**Figure 2**). In the original description of Ci-VSP, the arginine at position 223 (R223) was alluded as the first sensing charge (Murata et al., 2005). Consistently, it is to be noticed that Arginine 217 (R217) is the only arginine in the S4 segment that is not in the canonical every-third residues array like in many VGC (**Figure 2**; Horn, 2005). However, neutralization of R217 – the outermost extracellular charge – by mutation to a glutamine (R217Q) shifts the voltage dependence of the VSD about 50 mV toward negative potentials (Dimitrov et al., 2007; Kohout et al., 2008). These observations have prompted the idea that R217 may be the first sensing charged residue of the S4 segment (Kohout et al., 2008). Yet, it can be argued that R217 does not participate in voltage sensing and, instead, its charge causes an electrostatic bias in the effective electric field across the VSD. Thus, whether R217 is the first sensing charge or whether it shapes the electrical field across the VSD remains elusive.

The next charged residues are located in positions 223, 226, 229, and 232. These positive charges are also carried by arginines (**Figure 2**). Intriguingly, Ci-VSP is the only example –among the sequences consulted for this review – of a VSP with a S4 segment displaying four arginines in a single every-third-residue array (**Figure 2**). Using the conserved motif NKRRY in the PBM as reference, sequence alignment of Ci-VSP with other VSPs shows that R229 is one the most conserved residues in the S4 segment residues among VSPs (**Figure 2**). This suggests that R229 may constitute a critical residue for electrochemical coupling and for structural stability of the VSD. For Ci-VSP, substitution of residues 229 and 232 for glutamine abrogated voltage-dependent catalytic activity and seems to suppress sensing currents (Murata et al., 2005). These observations indicate that these residues are likely involved in electrochemical coupling in Ci-VSP.

Modeling of the activated VSD of Ci-VSP built based on the crystal structure of the chimeric potassium channel Kv1.2/2.1

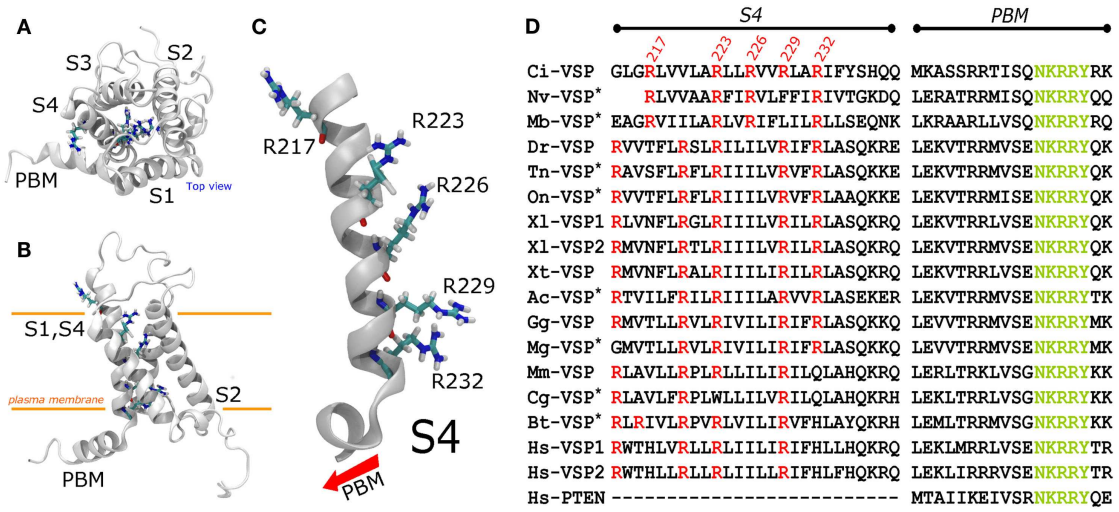

FIGURE 2 | A structural model for the Ci-VSP VSD was generated using the package MODELER and the structure of the chimeric potassium channels Kv1.2–2.1 (2R9R), subjected to minimization and an all-atom simulation for 50 ns using NAMD. For molecular dynamics simulations, the structure was embedded in a DPPC lipid bilayer (not shown). **(A)** Top view displaying four transmembrane segments (S1–S4) in counterclockwise order. **(B)** Side view of the Ci-VSP VSD model. The S4 segment displays five Arginines. Arginines 223, 226, 229, and 232 (R1–R4) are located in the center of the crevice formed by the packing of the helices. In contrast, Arginine 217 remains outside the crevice pointing toward the lipids. **(C)** S4 segment shown in details. All charged residues point to the center of the crevice (right side), except for R217 which faces the opposite direction. **(D)** Alignment of the S4 segment of VSP from several species. The PBM, particularly, the sequence NKRRY, was used as a reference point. The arginine corresponding to Ci-VSP's R223 and R229 are the most conserved arginine among the VSP consulted for this review. Those sequences labeled with an asterisk are predicted proteins. The two letter code before "VSP" represent the species. Mb, *Monosiga brevicollis* (marine choanoflagellate); Ci, *Ciona intestinalis* (sea squirt); Nv, *Nemastotella vectensis* (sea squirt); Dr, *Danio rerio* (zebrafish); Tn, *Tetraodon nigroviridis* (puffer fish); On, *Oreochromis niloticus* (tilapia); Xl, *Xenopus laevis* (african clawed frog); Xt, *Xenopus tropicalis* (frog); Ac, *Anolis carolinensis* (lizard; green anole); Gg, *Gallus gallus* (chicken); Mg, *Meleagris gallopavo* (turkey); Mm, *Mus musculus* (mouse); Cg, *Cricetulus griseus* (chinese hamster); Bt, *Bos taurus* (cow); Hs, *Homo sapiens*. To make the nomenclature uniform, the following changes in notation were made: Hs-VSP1 is TPTE2 or TPIP, Hs-VSP2 is TPTE, and Mm-VSP is mTpte.

(Long et al., 2007) shows that R229 is located in proximity to two negatively charges residues, Aspartate 164 (D164) and Aspartate 186 (D186; **Figure 3**). In *Shaker*, K374 is critical for structural stability and is likely to interact with Glutamate 293 and Aspartate 316 in the S2 and S3 segments, respectively (Papazian et al., 1995; Tiwari-Woodruff et al., 1997; Khalili-Araghi et al., 2010). Likewise, D164 and D186 are conversed in all known VSPs sequence consulted for this review, suggesting that *Shaker's* K374 and Ci-VSP's R229 may play similar roles. Although experimental evidences are to be provided, based on the predicted similarities between these VSD structures, it is likely that R229 is part of a network involving D164 and D186. It is important to emphasize that these interactions might be established at positive potentials, since the model for Ci-VSP shown here was based on the active (maybe relaxed) structure of the Kv1.2–2.1 chimeric channel (Long et al., 2007). Evidently, the accuracy of these predictions is intimately dependent on the initial sequence alignment used for the model construction.

Another residue, Phenylalanines 161 (F161) in Ci-VSP, is also conserved among VSPs (**Figure 3**). This residue seems to be homologous to F290 in *Shaker*, which is known as the "gating charge transfer center" and constitute the core of the so-called "hydrophobic plug" in the VSD of VGC (Tao et al., 2010; Lacroix and Bezanilla, 2011; Pless et al., 2011). However, it is intriguing that mutations of F161 have little effect on the $Q-V$ relationship of Ci-VSP (Lacroix and Bezanilla, 2012) suggesting that the putative "hydrophobic plug" in Ci-VSP may be architecturally different than in VGC.

RELAXATION OF Ci-VSP

An fascinating property of Ci-VSP is that the voltage dependence of sensing currents shifts toward negative voltages when the membrane potential is held antipolarized (Villalba-Galea et al., 2008, 2009a). This phenomenon, known as relaxation, has been proposed to occurs following a voltage-independent transition from the Active state (**Figure 1C**; Villalba-Galea et al., 2008, 2009a). Although the origin of relaxation remains unknown, it has been suggested that one plausible mechanism for it involves local remodeling of the S4 segment. Particularly, a secondary structure transition of the S4 segment from a 3_{10} helix to an α-helix (Villalba-Galea et al., 2008). As known, the carbonyl group of a residue in a 3_{10} helix interacts, via hydrogen bonding, with the amide group of the following third residue. This is different than α-helices in which the equivalent interaction is established with the fourth residue instead. Consequently, as stated by Vieira-Pires and Morais-Cabral (2010), "a 3_{10} helix is more tightly wound, longer, and thinner than an α-helix with the same number of residues."

A transition in the S4 segment from a 3_{10} to an α-helix can be seen as a "local" mechanism. However, relaxation seems to compromise the entire S4 segment as shown from FRET-based optical recording using the Voltage-Sensitive Fluorescence Protein (VSFP)

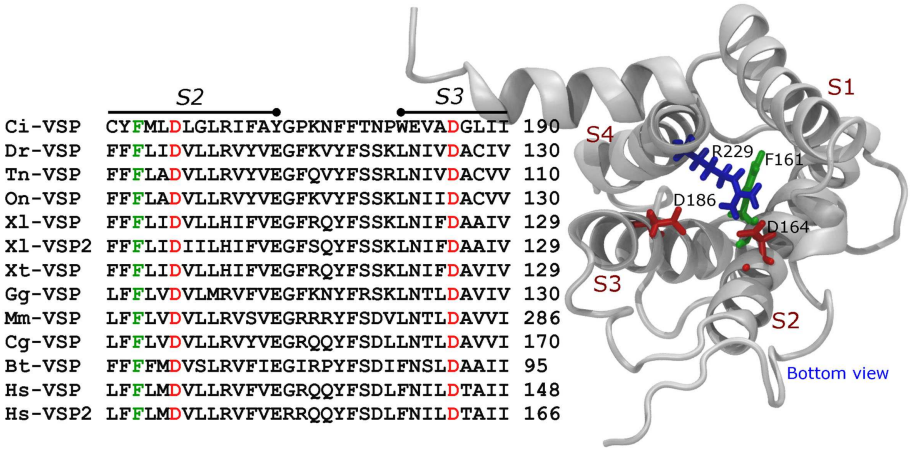

FIGURE 3 | Aligment of the S2 segment, S2–S3 loop, and S3 segment of VSPs. The bottom parts of the S2 and S3 segment contain three of the most conserved residues in VSPs. These are the equivalents to F161, D164, and D186 in Ci-VSP. These residues are also found in VGC (see text).

2.3 (Villalba-Galea et al., 2009b). To know, VSFPs (Sakai et al., 2001; Baker et al., 2007; Dimitrov et al., 2007; Lundby et al., 2008) and similar construct, such as *Nema*, *Zahra*, and *Zahra* 2 (Baker et al., 2012), are artificial proteins built by fusing fluorescence proteins to the C-terminus of a VSD. Detailed analysis by Akemann et al. (2009) has confirmed that optical signals from VSFP 2.3 report conformational changes related to VSD relaxation. Thus, it can be argued that relaxation may arise from rearrangements of the entire VSD to energetically satisfy the new position of the S4 segment after activation. If this is the case, relaxation can be seen as a "global" mechanism.

The structures of several six-transmembrane domain channels display 3_{10} helices in their S4 segments (Long et al., 2007; Clayton et al., 2008; Payandeh et al., 2011). In the structure of the chimeric potassium channel Kv1.2–2.1, a 3_{10} helix is found in the bottom the S4 segment extending from the fourth (R4) to the sixth (R6) arginines (Long et al., 2007). In the case of the NavAb, a member of the NaChBac family isolated from the bacterium *Arcobacter butzleri*, a 3_{10} helix extends along the S4 including the four arginines of this segment (Payandeh et al., 2011). Similarly, the MlotiK1 structure shows its charge-less S4 segment displaying a five-turn 3_{10} helix (Clayton et al., 2008). Because the existence and stability of 3_{10} helices depend on the packing and the interaction with other regions (Vieira-Pires and Morais-Cabral, 2010), these observations grant the possibility that S4 segment could be packed as a 3_{10} helix in the resting state. In support of this idea, several molecular dynamics studies of isolated VSDs suggest that the S4 segment rests as a 3_{10} helix (Bjelkmar et al., 2009; Khalili-Araghi et al., 2010; Schwaiger et al., 2011). In fact, it has been proposed that the S4 segment moves more readily when packed in a 3_{10} helix when compared to an α-helix (Bjelkmar et al., 2009; Schwaiger et al., 2011). In summary, these studies seem to conclude that, indeed, the property of being "tightly wound, longer, and thinner" is likely to be more energetically favorable for voltage sensing. Thus a combination of "local" and "global" events can account for relaxation.

VOLTAGE CLAMP FLUOROMETRY AND RELAXATION

Using the TE-VCF technique, it has been shown that the quenching of tetramethylrhodamine-maleimide (TMRM) attached to a Cysteine replacing *Glycine* 214 (G214) on the top of the S4 segment is sensitive to conformational changes in the VSD (Kohout et al., 2008). Detailed analysis of fluorescence recording using Cut-Open Voltage Clamp Fluorometry (CO-VCF) revealed that TMRM quenching reports two distinct conformational changes during VSD activation (Villalba-Galea et al., 2008). The first (fast) component is correlated with the movement of the sensing charges, constituting about 40% of the change in fluorescence observed (pulsing to +80 mV for 2 s). The second component (slow) is correlated with the settling of relaxation of the VSD as estimated by electrophysiology. This second component develops after sensing currents have faded, suggesting that the conformational changes responsible for this quenching component are not caused by voltage-dependent transitions (Villalba-Galea et al., 2008). Combining both observations, it was concluded that this significant fraction of the fluorescence quenching signal emerge from conformational changes involved in relaxation (Villalba-Galea et al., 2008).

The structure of the chimera Kv1.2–2.1 is regarded as being in the active state. However, since there is no electrical field imposed across the VSD during crystallization, this leads to the possibility that the VSD in structure is in a relaxed-like state and that the top half of the S4 segment displays an α-helix that forms after relaxation (Villalba-Galea et al., 2008). Furthermore, it has been proposed from molecular dynamics studies that the movement of the S4 segment produces little changes in the shape and intensity of the electrical fields across the VSD during deactivation (Delemotte et al., 2011). Extrapolating from this observation, it can be argued that the movement of the sensor during activation occurs before any secondary structure change takes place.

Based on VCF studies in *Shaker*, it has been proposed that the depolarization-induced movement of the S4 segment involves a rotation of the helix along its axis (Tombola et al., 2006; Pathak

et al., 2007). The possibility of a transition from a 3_{10} to an α-helix occurring after sensing (gating) currents inexorably leads us to a simple minded question: Is it possible that the apparent rotation of the S4 is the consequence of the unwinding of the 3_{10} helix? In the case of Ci-VSP, this question has not been answered yet. However, it has been shown that TMRM-labeling at position 208 (a glutamine to cysteine substitution in the S3–S4 loop) yields a fluorescence signals displaying a biphasic behavior. In this case, antipolarization causes an initial dequenching of the fluorophore followed by a slow quenching beyond the resting value (Kohout et al., 2010). This observation suggests that the TMRM attached to position 208 "visits" two different environments causing this differential quenching and – based on what is know for *Shaker* (Pathak et al., 2007) – are consistent with the idea that the top of the S4 segment is rotating. As before however, it can be argued that the unwinding of S4 segment after activation could produce a similar fluorescence signature. These possibilities are not exclusive and can not be ruled out with the reported evidences. So, further confirmation is needed.

It is noteworthy that alternative models for the movement of the S4 segment, such as the "paddle" model (Jiang et al., 2003; Ruta et al., 2003; Long et al., 2007) and the "helical-screw" model (Guy and Seetharamulu, 1986) have not been ruled out. Yet, the model depicted here is more in tune with a third of "the three Major Schools" – as referred to by Borjesson and Elinder (2008) – in which the core of the VSD forms water-filled crevices.

Noteworthy, recent work from the Elinder Lab (Henrion et al., 2012) shows that, in *Shaker*, the S4 segment moves respect to the S3b segment and not with it, suggesting that the paddle model is inadequate. Also, a number of recent theoretical studies support this finding (Pathak et al., 2007; Khalili-Araghi et al., 2010; Delemotte et al., 2011; Schwaiger et al., 2011; Jensen et al., 2012; Yarov-Yarovoy et al., 2012).

Thus far, as reported by fluorescence measurements, the electrically driven movement of the S4 segment seemingly leads to the unwinding (or rotation) of the S4 segment outermost section. This notion might suggest that conformational changes of the VSD during relaxation are confined to the top part of the S4 segment. This implies that relaxation consists of a "local" rearrangement of this segment. However, fluorescence recording from VSFP2.3 expressed in *Xenopus* oocytes argues otherwise (Villalba-Galea et al., 2009b). Reiterating, VSFP2.3 is a member of a genetically encoded optical probes for membrane potential built by attaching fluorescent proteins – or tandem of them – to the C-terminus of a VSD (Sakai et al., 2001; Baker et al., 2007; Dimitrov et al., 2007; Lundby et al., 2008). In the case of VSFP2.3, a tandem of Cyan- and Yellow-Fluorescent Proteins (CFP and YFP, respectively) replaces the catalytic domain of Ci-VSP. Using CO-VCF, fluorescence recordings from this probe have shown that the optical signals are correlated with sensing charge movement and relaxation in a similar fashion than fluorescence signals from TMRM when covalently attached to the other end of the S4 segment (Villalba-Galea et al., 2009b). These observations clearly indicate that relaxation is transmitted along the entire S4 segment, rather to be a "local" event. Thus, it is possible that relaxation involves conformational changes in other regions of the VSD in addition to the S4 segment. If proven, this will make relaxation a "global" phenomenon. Models for the resting state of Kv channels show a rearrangement of the VSD involving all transmembrane segments respect the active state (Pathak et al., 2007; Khalili-Araghi et al., 2010; Yarov-Yarovoy et al., 2012). Therefore, it is very likely that relaxation encompasses conformational changes in the entire VSD. Further investigations of this matter will provided a better understanding of the dynamic of voltage sensor. This facet in the activity of Ci-VSP has constituted – and remains to be – a great tool in doing so.

FINAL REMARKS

Why VSPs operate at positive potentials remains unclear – such is their physiological role. However, membrane potential is not the only parameter determining the activity of VSPs – at least for Ci-VSP. Under physiological conditions, operation of VSPs could be tightly regulated by phosphatidylinositol 4,5-bisphosphate [$PI(4,5)P_2$] beyond activation by PBM binding. Electrochemical coupling is regulated by this lipid (Kohout et al., 2010) and, in turn, Ci-VSP and other VSPs, use this signaling molecule as one of their main catalytic substrates (Murata et al., 2005; Murata and Okamura, 2007; Halaszovich et al., 2009; Kohout et al., 2010; Ratzan et al., 2011). Combining these observations, it can be speculated that VSPs could function as homeostatic regulators for the concentration of $PI(4,5)P_2$, where the combination of electrical activity and $PI(4,5)P_2$, are dynamically tuning phosphatase activity.

REFERENCES

Akemann, W., Lundby, A., Mutoh, H., and Knopfel, T. (2009). Effect of voltage sensitive fluorescent proteins on neuronal excitability. *Biophys. J.* 96, 3959–3976.

Arendt, K. L., Royo, M., Fernandez-Monreal, M., Knafo, S., Petrok, C. N., Martens, J. R., and Esteban, J. A. (2010). PIP3 controls synaptic function by maintaining AMPA receptor clustering at the postsynaptic membrane. *Nat. Neurosci.* 13, 36–44.

Bai, J., Tucker, W. C., and Chapman, E. R. (2004). PIP2 increases the speed of response of synaptotagmin and steers its membrane-penetration activity toward the plasma membrane. *Nat. Struct. Mol. Biol.* 11, 36–44.

Baker, B. J., Jin, L., Han, Z., Cohen, L. B., Popovic, M., Platisa, J., and Pieribone, V. (2012). Genetically-encoded fluorescent voltage sensors using the voltage-sensing domain of Nematostella and Danio phosphatases exhibit fast kinetics. *J. Neurosci. Methods* 208, 190–196.

Baker, B. J., Lee, H., Pieribone, V. A., Cohen, L. B., Isacoff, E. Y., Knopfel, T., and Kosmidis, E. K. (2007). Three fluorescent protein voltage sensors exhibit low plasma membrane expression in mammalian cells. *J. Neurosci. Methods* 161, 32–38.

Balla, A., Tuymetova, G., Tsiomenko, A., Varnai, P., and Balla, T. (2005). A plasma membrane pool of phosphatidylinositol 4-phosphate is generated by phosphatidylinositol 4-kinase type-III alpha: studies with the PH domains of the oxysterol binding protein and FAPP1. *Mol. Biol. Cell* 16, 1282–1295.

Balla, T., Szentpetery, Z., and Kim, Y. J. (2009). Phosphoinositide signaling: new tools and insights. *Physiology (Bethesda)* 24, 231–244.

Bezanilla, F. (2000). The voltage sensor in voltage-dependent ion channels. *Physiol. Rev.* 80, 555–592.

Bezanilla, F. (2005). Voltage-gated ion channels. *IEEE Trans. Nanobioscience* 4, 34–48.

Bezanilla, F. (2008). How membrane proteins sense voltage. *Nat. Rev. Mol. Cell Biol.* 9, 323–332.

Bjelkmar, P., Niemela, P. S., Vattulainen, I., and Lindahl, E. (2009). Conformational changes and slow dynamics through microsecond polarized atomistic molecular simulation of an integral Kv1.2 ion channel. *PLoS Comput. Biol.* 5, e1000289. doi:10.1371/journal.pcbi.1000289

Borjesson, S. I., and Elinder, F. (2008). Structure, function, and modification of the voltage sensor in voltage-gated ion channels. *Cell Biochem. Biophys.* 52, 149–174.

Bunney, T. D., and Katan, M. (2010). Phosphoinositide signalling in cancer: beyond PI3K and PTEN. *Nat. Rev. Cancer* 10, 342–352.

Chen, H., Rossier, C., Morris, M. A., Scott, H. S., Gos, A., Bairoch, A., and Antonarakis, S. E. (1999). A testis-specific gene, TPTE, encodes a putative transmembrane tyrosine phosphatase and maps to the pericentromeric region of human chromosomes 21 and 13, and to chromosomes 15, 22, and Y. *Hum. Genet.* 105, 399–409.

Clayton, G. M., Altieri, S., Heginbotham, L., Unger, V. M., and Morais-Cabral, J. H. (2008). Structure of the transmembrane regions of a bacterial cyclic nucleotide-regulated channel. *Proc. Natl. Acad. Sci. U.S.A.* 105, 1511–1515.

Davidson, L., MacCario, H., Perera, N. M., Yang, X., Spinelli, L., Tibarewal, P., Glancy, B., Gray, A., Weijer, C. J., Downes, C. P., and Leslie, N. R. (2010). Suppression of cellular proliferation and invasion by the concerted lipid and protein phosphatase activities of PTEN. *Oncogene* 29, 687–697.

Delemotte, L., Tarek, M., Klein, M. L., Amaral, C., and Treptow, W. (2011). Intermediate states of the Kv1.2 voltage sensor from atomistic molecular dynamics simulations. *Proc. Natl. Acad. Sci. U.S.A.* 108, 6109–6114.

Di Paolo, G., and De Camilli, P. (2006). Phosphoinositides in cell regulation and membrane dynamics. *Nature* 443, 651–657.

Dimitrov, D., He, Y., Mutoh, H., Baker, B. J., Cohen, L., Akemann, W., and Knopfel, T. (2007). Engineering and characterization of an enhanced fluorescent protein voltage sensor. *PLoS ONE* 2, e440. doi:10.1371/journal.pone.0000440

Endersby, R., and Baker, S. J. (2008). PTEN signaling in brain: neuropathology and tumorigenesis. *Oncogene* 27, 5416–5430.

Guipponi, M., Tapparel, C., Jousson, O., Scamuffa, N., Mas, C., Rossier, C., Hutter, P., Meda, P., Lyle, R., Reymond, A., and Antonarakis, S. E. (2001). The murine orthologue of the Golgi-localized TPTE protein provides clues to the evolutionary history of the human TPTE gene family. *Hum. Genet.* 109, 569–575.

Guipponi, M., Yaspo, M. L., Riesselman, L., Chen, H., De Sario, A., Roizes, G., and Antonarakis, S. E. (2000). Genomic structure of a copy of the human TPTE gene which encompasses 87 kb on the short arm of chromosome 21. *Hum. Genet.* 107, 127–131.

Guy, H. R., and Seetharamulu, P. (1986). Molecular model of the action potential sodium channel. *Proc. Natl. Acad. Sci. U.S.A.* 83, 508–512.

Halaszovich, C. R., Leitner, M. G., Mavrantoni, A., Le, A., Frezza, L., Feuer, A., Schreiber, D. N., Villalba-Galea, C. A., and Oliver, D. (2012). A human phospholipid phosphatase activated by a transmembrane control module. *J. Lipid Res.* doi: 10.1194/jlr.M026021

Halaszovich, C. R., Schreiber, D. N., and Oliver, D. (2009). Ci-VSP is a depolarization-activated phosphatidylinositol-4,5-bisphosphate and phosphatidylinositol-3,4,5-trisphosphate 5'-phosphatase. *J. Biol. Chem.* 284, 2106–2113.

Hammond, G. R., Fischer, M. J., Anderson, K. E., Holdich, J., Koteci, A., Balla, T., and Irvine, R. F. (2012). PI4P and PI(4,5)P2 are essential but independent lipid determinants of membrane identity. *Science* 337, 727–730.

Henrion, U., Renhorn, J., Borjesson, S. I., Nelson, E. M., Schwaiger, C. S., Bjelkmar, P., Wallner, B., Lindahl, E., and Elinder, F. (2012). Tracking a complete voltage-sensor cycle with metal-ion bridges. *Proc. Natl. Acad. Sci. U.S.A.* 109, 8552–8557.

Hobiger, K., Utesch, T., Mroginski, M. A., and Friedrich, T. (2012). Coupling of Ci-VSP modules requires a combination of structure and electrostatics within the linker. *Biophys. J.* 102, 1313–1322.

Horn, R. (2005). Electrifying phosphatases. *Sci. STKE* 2005, pe50.

Hossain, M. I., Iwasaki, H., Okochi, Y., Chahine, M., Higashijima, S., Nagayama, K., and Okamura, Y. (2008). Enzyme domain affects the movement of the voltage sensor in ascidian and zebrafish voltage-sensing phosphatases. *J. Biol. Chem.* 283, 18248–18259.

Iwasaki, H., Murata, Y., Kim, Y., Hossain, M. I., Worby, C. A., Dixon, J. E., McCormack, T., Sasaki, T., and Okamura, Y. (2008). A voltage-sensing phosphatase, Ci-VSP, which shares sequence identity with PTEN, dephosphorylates phosphatidylinositol 4,5-bisphosphate. *Proc. Natl. Acad. Sci. U.S.A.* 105, 7970–7975.

Jensen, M. O., Jogini, V., Borhani, D. W., Leffler, A. E., Dror, R. O., and Shaw, D. E. (2012). Mechanism of voltage gating in potassium channels. *Science* 336, 229–233.

Jiang, Y., Ruta, V., Chen, J., Lee, A., and MacKinnon, R. (2003). The principle of gating charge movement in a voltage-dependent K+ channel. *Nature* 423, 42–48.

Khalili-Araghi, F., Jogini, V., Yarov-Yarovoy, V., Tajkhorshid, E., Roux, B., and Schulten, K. (2010). Calculation of the gating charge for the Kv1.2 voltage-activated potassium channel. *Biophys. J.* 98, 2189–2198.

Kohout, S. C., Bell, S. C., Liu, L., Xu, Q., Minor, D. L. Jr., and Isacoff, E. Y. (2010). Electrochemical coupling in the voltage-dependent phosphatase Ci-VSP. *Nat. Chem. Biol.* 6, 369–375.

Kohout, S. C., Ulbrich, M. H., Bell, S. C., and Isacoff, E. Y. (2008). Subunit organization and functional transitions in Ci-VSP. *Nat. Struct. Mol. Biol.* 15, 106–108.

Kumanovics, A., Levin, G., and Blount, P. (2002). Family ties of gated pores: evolution of the sensor module. *FASEB J.* 16, 1623–1629.

Kurokawa, T., Takasuga, S., Sakata, S., Yamaguchi, S., Horie, S., Homma, K. J., Sasaki, T., and Okamura, Y. (2012). 3' Phosphatase activity toward phosphatidylinositol 3,4-bisphosphate [PI(3,4)P2] by voltage-sensing phosphatase (VSP). *Proc. Natl. Acad. Sci. U.S.A.* 109, 10089–10094.

Lacroix, J., Halaszovich, C. R., Schreiber, D. N., Leitner, M. G., Bezanilla, F., Oliver, D., and Villalba-Galea, C. A. (2011). Controlling the activity of PTEN by membrane potential. *J. Biol. Chem.* 286, 17945–17953.

Lacroix, J. J., and Bezanilla, F. (2011). Control of a final gating charge transition by a hydrophobic residue in the S2 segment of a K+ channel voltage sensor. *Proc. Natl. Acad. Sci. U.S.A.* 108, 6444–6449.

Lacroix, J. J., and Bezanilla, F. (2012). Tuning the voltage-sensor motion with a single residue. *Biophys. J.* 103, L23–L25.

Lee, J. O., Yang, H., Georgescu, M. M., Di Cristofano, A., Maehama, T., Shi, Y., Dixon, J. E., Pandolfi, P., and Pavletich, N. P. (1999). Crystal structure of the PTEN tumor suppressor: implications for its phosphoinositide phosphatase activity and membrane association. *Cell* 99, 323–334.

Leslie, N. R., Batty, I. H., MacCario, H., Davidson, L., and Downes, C. P. (2008). Understanding PTEN regulation: PIP2, polarity and protein stability. *Oncogene* 27, 5464–5476.

Leslie, N. R., and Downes, C. P. (2002). PTEN: the down side of PI 3-kinase signalling. *Cell. Signal.* 14, 285–295.

Leslie, N. R., and Downes, C. P. (2004). PTEN function: how normal cells control it and tumour cells lose it. *Biochem. J.* 382, 1–11.

Leslie, N. R., Yang, X., Downes, C. P., and Weijer, C. J. (2007). PtdIns(3,4,5)P(3)-dependent and -independent roles for PTEN in the control of cell migration. *Curr. Biol.* 17, 115–125.

Levin, M., and Stevenson, C. G. (2012). Regulation of cell behavior and tissue patterning by bioelectrical signals: challenges and opportunities for biomedical engineering. *Annu. Rev. Biomed. Eng.* 14, 295–323.

Li, J., Yen, C., Liaw, D., Podsypanina, K., Bose, S., Wang, S. I., Puc, J., Miliaresis, C., Rodgers, L., McCombie, R., Bigner, S. H., Giovanella, B. C., Ittmann, M., Tycko, B., Hibshoosh, H., Wigler, M. H., and Parsons, R. (1997). PTEN, a putative protein tyrosine phosphatase gene mutated in human brain, breast, and prostate cancer. *Science* 275, 1943–1947.

Liu, L., Kohout, S. C., Xu, Q., Muller, S., Kimberlin, C. R., Isacoff, E. Y., and Minor, D. L. Jr. (2012). A glutamate switch controls voltage-sensitive phosphatase function. *Nat. Struct. Mol. Biol.* 19, 633–641.

Logothetis, D. E., Petrou, V. I., Adney, S. K., and Mahajan, R. (2010). Channelopathies linked to plasma membrane phosphoinositides. *Pflugers Arch.* 460, 321–341.

Long, S. B., Tao, X., Campbell, E. B., and MacKinnon, R. (2007). Atomic structure of a voltage-dependent K+ channel in a lipid membrane-like environment. *Nature* 450, 376–382.

Lundby, A., Mutoh, H., Dimitrov, D., Akemann, W., and Knopfel, T. (2008). Engineering of a genetically encodable fluorescent voltage sensor exploiting fast Ci-VSP voltage-sensing movements. *PLoS ONE* 3, e2514. doi:10.1371/journal.pone.0002514

Maehama, T., and Dixon, J. E. (1998). The tumor suppressor, PTEN/MMAC1, dephosphorylates the lipid second messenger, phosphatidylinositol 3,4,5-trisphosphate. *J. Biol. Chem.* 273, 13375–13378.

Maehama, T., and Dixon, J. E. (1999). PTEN: a tumour suppressor that functions as a phospholipid phosphatase. *Trends Cell Biol.* 9, 125–128.

Matsuda, M., Takeshita, K., Kurokawa, T., Sakata, S., Suzuki, M., Yamashita, E., Okamura, Y., and Nakagawa, A. (2011). Crystal structure of

the cytoplasmic phosphatase and tensin homolog (PTEN)-like region of *Ciona intestinalis* voltage-sensing phosphatase provides insight into substrate specificity and redox regulation of the phosphoinositide phosphatase activity. *J. Biol. Chem.* 286, 23368–23377.

Menager, C., Arimura, N., Fukata, Y., and Kaibuchi, K. (2004). PIP3 is involved in neuronal polarization and axon formation. *J. Neurochem.* 89, 109–118.

Michailidis, I. E., Rusinova, R., Georgakopoulos, A., Chen, Y., Iyengar, R., Robakis, N. K., Logothetis, D. E., and Baki, L. (2011). Phosphatidylinositol-4,5-bisphosphate regulates epidermal growth factor receptor activation. *Pflugers Arch.* 461, 387–397.

Murata, Y., Iwasaki, H., Sasaki, M., Inaba, K., and Okamura, Y. (2005). Phosphoinositide phosphatase activity coupled to an intrinsic voltage sensor. *Nature* 435, 1239–1243.

Murata, Y., and Okamura, Y. (2007). Depolarization activates the phosphoinositide phosphatase Ci-VSP, as detected in *Xenopus* oocytes coexpressing sensors of PIP2. *J. Physiol. (Lond.)* 583, 875–889.

Noda, M., Ikeda, T., Kayano, T., Suzuki, H., Takeshima, H., Kurasaki, M., Takahashi, H., and Numa, S. (1986). Existence of distinct sodium channel messenger RNAs in rat brain. *Nature* 320, 188–192.

Ogasawara, M., Sasaki, M., Nakazawa, N., Nishino, A., and Okamura, Y. (2011). Gene expression profile of Ci-VSP in juveniles and adult blood cells of ascidian. *Gene Expr. Patterns* 11, 233–238.

Okamura, Y., and Dixon, J. E. (2011). Voltage-sensing phosphatase: its molecular relationship with PTEN. *Physiology (Bethesda)* 26, 6–13.

Ooms, L. M., Horan, K. A., Rahman, P., Seaton, G., Gurung, R., Kethesparan, D. S., and Mitchell, C. A. (2009). The role of the inositol polyphosphate 5-phosphatases in cellular function and human disease. *Biochem. J.* 419, 29–49.

Papazian, D. M., Shao, X. M., Seoh, S. A., Mock, A. F., Huang, Y., and Wainstock, D. H. (1995). Electrostatic interactions of S4 voltage sensor in Shaker K+ channel. *Neuron* 14, 1293–1301.

Pathak, M. M., Yarov-Yarovoy, V., Agarwal, G., Roux, B., Barth, P., Kohout, S., Tombola, F., and Isacoff, E. Y. (2007). Closing in on the resting state of the Shaker K(+) channel. *Neuron* 56, 124–140.

Payandeh, J., Scheuer, T., Zheng, N., and Catterall, W. A. (2011). The crystal structure of a voltage-gated sodium channel. *Nature* 475, 353–358.

Pless, S. A., Galpin, J. D., Niciforovic, A. P., and Ahern, C. A. (2011). Contributions of counter-charge in a potassium channel voltage-sensor domain. *Nat. Chem. Biol.* 7, 617–623.

Ratzan, W. J., Evsikov, A. V., Okamura, Y., and Jaffe, L. A. (2011). Voltage sensitive phosphoinositide phosphatases of Xenopus: their tissue distribution and voltage dependence. *J. Cell. Physiol.* 226, 2740–2746.

Ruta, V., Jiang, Y., Lee, A., Chen, J., and MacKinnon, R. (2003). Functional analysis of an archaebacterial voltage-dependent K+ channel. *Nature* 422, 180–185.

Sakai, R., Repunte-Canonigo, V., Raj, C. D., and Knopfel, T. (2001). Design and characterization of a DNA-encoded, voltage-sensitive fluorescent protein. *Eur. J. Neurosci.* 13, 2314–2318.

Schwaiger, C. S., Bjelkmar, P., Hess, B., and Lindahl, E. (2011). 3(1)(0)-Helix conformation facilitates the transition of a voltage sensor S4 segment toward the down state. *Biophys. J.* 100, 1446–1454.

Sigg, D., Stefani, E., and Bezanilla, F. (1994). Gating current noise produced by elementary transitions in Shaker potassium channels. *Science* 264, 578–582.

Suh, B. C., and Hille, B. (2008). PIP2 is a necessary cofactor for ion channel function: how and why? *Annu. Rev. Biophys.* 37, 175–195.

Sundelacruz, S., Levin, M., and Kaplan, D. L. (2009). Role of membrane potential in the regulation of cell proliferation and differentiation. *Stem Cell Rev.* 5, 231–246.

Sutton, K. A., Jungnickel, M. K., Jovine, L., and Florman, H. M. (2012). Evolution of the voltage sensor domain of the voltage-sensitive phosphoinositide phosphatase, VSP/TPTE, suggests a role as a proton channel in Eutherian mammals. *Mol. Biol. Evol.* 29, 2147–2155.

Swartz, K. J. (2008). Sensing voltage across lipid membranes. *Nature* 456, 891–897.

Taglialatela, M., Toro, L., and Stefani, E. (1992). Novel voltage clamp to record small, fast currents from ion channels expressed in *Xenopus* oocytes. *Biophys. J.* 61, 78–82.

Tao, X., Lee, A., Limapichat, W., Dougherty, D. A., and MacKinnon, R. (2010). A gating charge transfer center in voltage sensors. *Science* 328, 67–73.

Tapparel, C., Reymond, A., Girardet, C., Guillou, L., Lyle, R., Lamon, C., Hutter, P., and Antonarakis, S. E. (2003). The TPTE gene family: cellular expression, subcellular localization and alternative splicing. *Gene* 323, 189–199.

Teng, D. H-F., Hu, R., Lin, H., Davis, T., Iliev, D., Frye, C., Swedlund, B., Hansen, K. L., Vinson, V. L., Gumpper, K. L., Ellis, L., El-Naggar, A., Frazier, M., Jasser, S., Langford, L. A., Lee, J., Mills, G. B., Pershouse, M. A., Pollack, R. E., Tornos, C., Troncoso, P., Yung, W. K. A., Fujii, G., Berson, A., Bookstein, R., Bolen, J. B., Tavtigian, S. V., and Steck, P. A. (1997). MMAC1/PTEN mutations in primary tumor specimens and tumor cell lines. *Cancer Res.* 57, 5221–5225.

Tiwari-Woodruff, S. K., Schulteis, C. T., Mock, A. F., and Papazian, D. M. (1997). Electrostatic interactions between transmembrane segments mediate folding of Shaker K+ channel subunits. *Biophys. J.* 72, 1489–1500.

Tombola, F., Pathak, M. M., and Isacoff, E. Y. (2006). How does voltage open an ion channel? *Annu. Rev. Cell Dev. Biol.* 22, 23–52.

Vieira-Pires, R. S., and Morais-Cabral, J. H. (2010). 3(10) Helices in channels and other membrane proteins. *J. Gen. Physiol.* 136, 585–592.

Villalba-Galea, C. A. (2012). New insights in the activity of voltage sensitive phosphatases. *Cell. Signal.* 24, 1541–1547.

Villalba-Galea, C. A., Miceli, F., Taglialatela, M., and Bezanilla, F. (2009a). Coupling between the voltage-sensing and phosphatase domains of Ci-VSP. *J. Gen. Physiol.* 134, 5–14.

Villalba-Galea, C. A., Sandtner, W., Dimitrov, D., Mutoh, H., Knopfel, T., and Bezanilla, F. (2009b). Charge movement of a voltage-sensitive fluorescent protein. *Biophys. J.* 96, L19–L21.

Villalba-Galea, C. A., Sandtner, W., Starace, D. M., and Bezanilla, F. (2008). S4-based voltage sensors have three major conformations. *Proc. Natl. Acad. Sci. U.S.A.* 105, 17600–17607.

Walker, S. M., Downes, C. P., and Leslie, N. R. (2001). TPIP: a novel phosphoinositide 3-phosphatase. *Biochem. J.* 360, 277–283.

Walker, S. M., Leslie, N. R., Perera, N. M., Batty, I. H., and Downes, C. P. (2004). The tumour-suppressor function of PTEN requires an N-terminal lipid-binding motif. *Biochem. J.* 379, 301–307.

Worby, C. A., and Dixon, J. E. (2005). Phosphoinositide phosphatases: emerging roles as voltage sensors? *Mol. Interv.* 5, 274–277.

Wu, Y., Dowbenko, D., Pisabarro, M. T., Dillard-Telm, L., Koeppen, H., and Lasky, L. A. (2001). PTEN 2, a Golgi-associated testis-specific homologue of the PTEN tumor suppressor lipid phosphatase. *J. Biol. Chem.* 276, 21745–21753.

Yarov-Yarovoy, V., DeCaen, P. G., Westenbroek, R. E., Pan, C. Y., Scheuer, T., Baker, D., and Catterall, W. A. (2012). Structural basis for gating charge movement in the voltage sensor of a sodium channel. *Proc. Natl. Acad. Sci. U.S.A.* 109, E93–E102.

Conflict of Interest Statement: The author declares that the research was conducted in the absence of any commercial or financial relationships that could be construed as a potential conflict of interest.

Received: 02 June 2012; accepted: 19 August 2012; published online: 13 September 2012.

Citation: Villalba-Galea CA (2012) Voltage-controlled enzymes: the new Janus Bifrons. Front. Pharmacol. ***3****:161. doi: 10.3389/fphar.2012.00161*

This article was submitted to Frontiers in Pharmacology of Ion Channels and Channelopathies, a specialty of Frontiers in Pharmacology.

frontiers in
PHARMACOLOGY

REVIEW ARTICLE
published: 05 July 2012
doi: 10.3389/fphar.2012.00125

Opposite effects of the S4–S5 linker and PIP_2 on voltage-gated channel function: KCNQ1/KCNE1 and other channels

Frank S. Choveau[1,2,3†], Fayal Abderemane-Ali[1,2,3], Fabien C. Coyan[1,2,3], Zeineb Es-Salah-Lamoureux[1,2,3], Isabelle Baró[1,2,3] and Gildas Loussouarn[1,2,3]*

[1] *UMR 1087, Institut National de la Santé et de la Recherche Médicale, Nantes, France*
[2] *UMR 6291, Centre National de la Recherche Scientifique, Nantes, France*
[3] *L'Institut du Thorax, L'UNAM Université, Université de Nantes, Nantes, France*

Edited by:
Mounir Tarek, Centre National de la Recherche Scientifique, France

Reviewed by:
Nikita Gamper, University of Leeds, UK
David A. Brown, University College London, UK

****Correspondence:***
Gildas Loussouarn, L'Institut du Thorax, UMR 1087/CNRS UMR 6291, IRT-UN, 8 Quai Moncousu, BP 70721, 44007 Nantes Cedex 1, France.
e-mail: gildas.loussouarn@univ-nantes.fr

†Present address:
Frank S. Choveau, UTHSCSA, San Antonio, TX, USA.

Voltage-gated potassium (Kv) channels are tetramers, each subunit presenting six transmembrane segments (S1–S6), with each S1–S4 segments forming a voltage-sensing domain (VSD) and the four S5–S6 forming both the conduction pathway and its gate. S4 segments control the opening of the intracellular activation gate in response to changes in membrane potential. Crystal structures of several voltage-gated ion channels in combination with biophysical and mutagenesis studies highlighted the critical role of the S4–S5 linker ($S4S5_L$) and of the S6 C-terminal part ($S6_T$) in the coupling between the VSD and the activation gate. Several mechanisms have been proposed to describe the coupling at a molecular scale. This review summarizes the mechanisms suggested for various voltage-gated ion channels, including a mechanism that we described for KCNQ1, in which $S4S5_L$ is acting like a ligand binding to $S6_T$ to stabilize the channel in a closed state. As discussed in this review, this mechanism may explain the reverse response to depolarization in HCN-like channels. As opposed to $S4S5_L$, the phosphoinositide, phosphatidylinositol 4,5-bisphosphate (PIP_2), stabilizes KCNQ1 channel in an open state. Many other ion channels (not only voltage-gated) require PIP_2 to function properly, confirming its crucial importance as an ion channel cofactor. This is highlighted in cases in which an altered regulation of ion channels by PIP_2 leads to channelopathies, as observed for KCNQ1. This review summarizes the state of the art on the two regulatory mechanisms that are critical for KCNQ1 and other voltage-gated channels function (PIP_2 and $S4S5_L$), and assesses their potential physiological and pathophysiological roles.

Keywords: voltage-gated potassium channels, S4–S5 linker, phosphatidylinositol 4,5-bisphosphate, patch-clamp, channelopathies

PART 1: ROLE OF THE S4–S5 LINKER IN CHANNEL VOLTAGE DEPENDENCY

Voltage-gated ion channels are all designed according to a common pattern including six transmembrane segments (S1–S6), with S1–S4 forming the voltage-sensing domain (VSD), in which the positively charged S4 is the voltage sensor *per se*, and S5–S6 forming the pore. The N- and C-termini are cytosolic. Whereas voltage-gated K^+ channels are tetrameric assemblies of identical or homologous subunits, eukaryotic Ca^{2+} and Na^+ voltage-gated channels are the result of the fusion of four subunits.

If a general consensus started to emerge on the nature and the (nano-)metrics of the movement of the voltage sensor in voltage-gated channels, it is still not the case for the nature of the coupling between the voltage sensor movement and the gate opening. In this first part, we review most of the results obtained through various experimental approaches on various channels, that can give insights on the nature of the coupling, and we try to classify this coupling into two categories: a strong or a labile coupling between the main actors, namely, the S4–S5 linker (referred here as $S4S5_L$) and the C-terminal part of the S6 transmembrane segment ($S6_T$).

HOW DOES THE VOLTAGE SENSOR REGULATE PORE GATING?

Movement of the voltage sensor

The ability of K_v channels to sense the membrane potential is conferred via the VSD. The S4 segment moves across the plasma membrane in response to changes in membrane potential, allowing the transition of the channel between a closed conformation and an open conformation. Many studies have investigated the nature of the S4 movement, and came up with three different models, with major differences in this movement.

∗ According to the crystal structure of KvAP, S4 coupled to S3 form a helical hairpin, or "paddle," moving 15–20 Å across the lipid bilayer, as confirmed by avidin accessibility to different-length tethered biotin reagents (Jiang et al., 2003; Ruta et al., 2005). However, a number of lines of evidence suggest that the KvAP structure does not correspond to a native conformation, such as the fact that the VSD is in a resting state and in contrast, the pore is in the open state. This non-native state is potentially due to the use of monoclonal antibody fragments in order

to stabilize the structure, but more likely due to the absence of membrane lipids (Lee et al., 2005).
∗ The "transporter" model, described in Shaker, involves a very small movement of S4 (2–3 Å) from a crevice in contact with the intracellular solution to another one in contact with the extracellular solution (Cha et al., 1999; Chanda et al., 2005).
∗ Finally, the helical screw model (Guy and Seetharamulu, 1986) and the similar sliding helix model (Catterall, 1986), originally proposed for sodium channels, have been then adapted to K_v channels (Durell and Guy, 1992). These models suggest that S4 rotates ∼180°, and at the same time, translates ∼13.5 Å along its axis (reviewed in Börjesson and Elinder, 2008). Strikingly, "embryonic" paddle and helical screw models were predicted as early as 1981 (Figures 2 and 9 of Armstrong, 1981).

The variety of these models, and the fact that they predict a magnitude of the S4 movement across the membrane ranging from 2 Å (Cha et al., 1999) to ∼15 Å in Shaker (Larsson et al., 1996), most probably come from the variety of the techniques employed. Some of the techniques (such as FRET) underestimate the distances by capturing rare conformations when the donor and acceptor are nearby. On the contrary, cross-linking or tethered biotin may overestimate distances by capturing and covalently stabilizing rare and extreme conformations in which a cysteine is accessible intracellularly or extracellularly (Tombola et al., 2006).

A structural model of Shaker, based on the crystal structure of Kv1.2, predicts an axial rotation and a translation of S4 (Yarov-Yarovoy et al., 2006) as described in the "helical screw" model. In addition, a subsequent tilting motion of the S4 is also suggested. Very recently, disulfide-locking experiments and structural models of resting and activated state of the VSD in a sodium channel, NaChBac, propose an outward movement (∼6–8 Å) of S4 relative to S1, S2, and S3 and a rotation (∼30°) of the S4 coupled to a tilting motion relative to the $S4S5_L$ (Yarov-Yarovoy et al., 2012). Studies of these different channels support the idea that a common S4 movement may be applied to various channels, including KCNQ channels. The next step will be to solve the crystal structure of KCNQ channels, in an attempt to gain insights on the structural conformation corresponding to gating of these channels. Presently, homology models (Smith et al., 2007) and molecular dynamics are valuable templates to better understand the physiological and pathophysiological mechanisms of voltage dependency (Delemotte et al., 2011).

Coupling between the voltage sensor and the gate: $S4S5_L$ and $S6_T$ play a major role

The $S4S5_L$ interacts with $S6_T$ in many voltage-gated channels. Which part of the channel links the voltage sensor movement to the gate opening? The physical interaction between $S4S5_L$ and $S6_T$ and the role of this interaction in translating the voltage sensor movement to the gate opening have been investigated in many voltage-gated channels by diverse techniques. The results obtained will be detailed below and in other reviews of the present Frontiers Research Topic, but it is important to note that many works stress the major role of this $S4S5_L$–$S6_T$ interaction. Mutagenesis associated to functional studies using chimeras of Shaker and KcsA (Lu et al., 2001, 2002), alanine-scanning of $S4S5_L$ and $S6_T$ in Kv4.2 (Barghaan and Bähring, 2009), cross-linking studies of $S4S5_L$ and $S6_T$ in human ether-a-go-go related gene (hERG; Ferrer et al., 2006), but also in the hyperpolarization-activated channel, spHCN1 (Prole and Yellen, 2006), all converge to the notion that $S4S5_L$ and $S6_T$ play a major role in the coupling between the voltage sensor and the $S6_T$. This is further confirmed by the crystal structures of K_v and Na_v channels, which show that the distance between $S4S5_L$ and $S6_T$ fits with the hypothesis that these regions contact each other (Long et al., 2005; Payandeh et al., 2011).

These studies strongly indicate that the VSD-activation and gate coupling are associated through the $S4S5_L$–$S6_T$ interaction. However, many questions remain to be elucidated. Are other regions of channels involved in this coupling? How exactly does this $S4S5_L$–$S6_T$ interaction make the link between VSD-activation and gate coupling?

The N-terminus and the S1 segment are also involved in the VSD-pore coupling. In addition to $S4S5_L$ and $S6_T$ interaction, other regions influence voltage-dependent channel activity. One of those regions is the N-terminus (Nter). In many signaling proteins, a PAS domain is present where it functions as a signal sensor and its name comes from the transcription factors in which it was first identified: period circadian protein (Per), aryl hydrocarbon receptor nuclear translocator protein (Arnt), and single-minded protein (Sim). The PAS domain is also present in the N-terminus of three K_v channel families, Kv10, Kv11, and Kv12. An interaction between the PAS domain and $S4S5_L$ has been postulated as underlying the slow deactivation process of hERG channels (Wang et al., 1998a; Chen et al., 1999). Long QT syndrome (LQT) is a cardiac disease characterized by prolonged ventricular repolarization, arrhythmias, and sudden death. In some LQT patients, a disruption of the presumed interaction between the PAS domain and $S4S5_L$ would result in an acceleration of the deactivation rate, leading to a decrease in this critical repolarizing current (Chen et al., 1999). Alonso-Ron et al. (2008) showed that channels lacking Nter domain or bearing mutations in $S4S5_L$ exhibited similar slowed deactivation and positive shift in the voltage dependence of activation, supporting the hypothesis of an interaction between these two regions. However, no experiment has unequivocally demonstrated a direct Nter-$S4S5_L$ interaction although a recent study has demonstrated a close proximity between Nter and $S4S5_L$ in hERG (de la Peña et al., 2011). To highlight such interaction, the authors introduced cysteines in the PAS domain and in the $S4S5_L$ and then tested the effects of applying an oxidizing agent, *tert*-butyl hydroperoxide ($TbHO_2$), on channels expressing those cysteines. Formation of disulfide bonds, induced by $TbHO_2$, between cysteines introduced in Nter and $S4S5_L$, dramatically decreases the tail current. This effect is completely reversed by dithiothreitol, a reducing agent. Taken together, these data indicate that Nter can bind to $S4S5_L$, stabilizing the channel in the closed state. A more exhaustive review on the role of cytoplasmic domains (CTD) in voltage-gated potassium channels gating is available in another article of this Frontiers Research topic (Barros et al., 2012).

The coupling between the VSD and the pore may also occur through interactions between transmembrane domains (TMD). Cross-linking studies in Shaker channel showed the proximity between the S4 and S5 segments, and suggested that interactions

may be involved in the coupling between the VSD and the pore (Broomand et al., 2003; Gandhi et al., 2003). Also, statistical analysis of K_v channels sequences and mutagenesis studies suggest that an interface between the S1 domain and the pore helix, both highly conserved in K_v channels, is required for this coupling as well (Lee et al., 2009). Indeed, a tryptophan scanning of residues forming the interaction surface between S1 and the pore helix in Shaker has shown that mutations of those residues affect channels function. Finally, formation of a disulfide bond, forcing the S1-pore helix interaction, leads to an alteration of gating.

In summary, a network of interactions, including Nter, S1, $S4S5_L$, and $S6_T$, seems to be involved in the coupling between VSD and the pore.

INTERACTION BETWEEN $S4S5_L$ AND $S6_T$: TWO MODELS

Model 1: Mechanical lever model (Figure 1A)

Shaker. The Shaker gene from *Drosophila melanogaster* was the first potassium channel to be cloned (Tempel et al., 1987), contributing to the identification of a family of homologous channels in vertebrates (the K_v superfamily) and to the understanding of the role of K_v channels in human diseases. This channel is one of the most extensively studied voltage-activated ion channels and often serves as a model in the study of voltage dependency. In this tetrameric voltage-gated K^+ channel, the four VSDs are covalently connected to the S5 segments of the pore region by the S4–S5 linkers, as mentioned above. Kinetic models predicted that the gating mechanism of this channel involves several relatively independent movements of the four VSDs between resting and activated states, followed by a concerted opening transition where the S6 gate moves from a closed to an open state (Bezanilla et al., 1994; Hoshi et al., 1994; Stefani et al., 1994; Zagotta et al., 1994a,b). This model was further confirmed by using a triplet of mutations in the S4 that make the final concerted step rate limiting in the activation pathway, thus rendering it more detectable (Ledwell and Aldrich, 1999).

In an elegant work using chimeras in which Shaker pore module is replaced by the one of KcsA channel (Lu et al., 2001, 2002), Lu and co-workers showed that $S4S5_L$ and $S6_T$ play a key role in voltage dependency. Incomplete channel closures in Shaker-KcsA chimeras with modified $S4S5_L$ and $S6_T$ suggest that these regions interact in the closed state (Lu et al., 2002). Assuming that the voltage sensors S4 are coupled to the gate in Shaker channels via an obligatory (one S4 in the down state is enough to keep the channel closed) rather than an allosteric mechanism, they proposed a mechanical lever model in which $S4S5_L$ are pushing the S6 gate in a closed conformation at negative voltages. The crystal structure corresponding to the open state of the related vertebrate Kv1.2 (below) is consistent with this mechanism in which all the S4 segments have to be in an "up" state to allow pore opening.

In other functional studies, Shaker mutations in $S4S5_L$ and $S6_T$ were shown to have a dramatic effect on the slow component of the off-gating current. Together with the fact that closing the gate impacts on gating charge return, this has been interpreted as the $S4S5_L$ and $S6_T$ interaction allosterically keeping S4 in the "up" position and stabilizing the open state (Batulan et al., 2010). The same group identified other Shaker mutations in $S4S5_L$ and $S6_T$ that completely uncouple S4 movement from pore opening. They used the mutations to show that the pore domain exerts a mechanical load onto the voltage sensors. Indeed, these mutations lead the voltage sensors to be activated at more negative potentials (they are more free to move), and relieve the mode shift of the voltage sensor, that they interpret as a stabilization of the open state directly impacting the S4 movement (Haddad and Blunck, 2011).

Altogether, these data support both the specificity and the strength of interaction between $S4S5_L$ and $S6_T$, consistent with the mechanical lever mechanism, but in a more complex manner, with potentially state-dependent $S4S5_L$ and $S6_T$ interactions stabilizing the closed (Lu et al., 2002) and the open (Batulan et al., 2010) states. Of note, the critical role of $S4S5_L$ and $S6_T$ interaction in channel open state stabilization has been recently illustrated using high speed molecular dynamics simulation (Jensen et al., 2012). Altogether these data, suggest a mechanism more complex than a pure electromechanical coupling.

Kv1.2. The Kv1.2 channel is a Shaker-like voltage-gated potassium channel expressed in mammalian neurons and involved in the regulation of pre- and post-synaptic membrane excitability. The interaction between the S4–S5 linker and the S6 segment was observed in the crystal structure of Kv1.2 in the open state (Long et al., 2005), confirming the electromechanical coupling between the voltage sensor movement and the pore, as suggested previously by Lu and co-workers in Shaker channels. The S4 were suggested to perform mechanical work on the pore of Kv1.2 through the S4–S5 linkers, which are positioned to constrict or dilate the S6 inner helices of the pore (Long et al., 2005). A prediction of the channel closed state was built based on the hypothesis of a permanent coupling. In this configuration where the S6 helix is presented as a "receptor" of S4–S5 linker, it is easy to understand why its sequence on K_v channels is quite conserved: Pro-X-Pro, where X is any amino-acid (Shaker-like K_v channels), or Gly (other K_v channels) in the corresponding region. This structure allows bending of the S6 helix in order to form the correct interaction with the S4–S5 linker helix. However, the absence of a structure of K_v channels in the closed state prevents from determining the exact molecular nature of the voltage-dependent gate closure. Moreover, the structure of Kv1.2 may not completely correspond to the functional open-activated state, especially for the position of S4 relative to the pore, since this structure is incompatible with the proximity of first S4 arginine R294 and a pore domain residue, A351 (Lewis et al., 2008). Such proximity between R294 and A351 was probed by the generation of a high affinity binding site of Zn^{2+} or Cd^{2+} when the residues were mutated to histidine. As discussed above for cross-linking experiments trying to estimate the S4 position and movement, introduction of the Zn^{2+} or Cd^{2+} high affinity binding site may also capture the channel in a non-native state.

Only the combination of experimental and *in silico* approaches, and the multiplication of channel structures will help understanding the molecular details of the channel voltage dependency. For instance, a recent crystal structure obtained from a prokaryotic voltage-gated sodium channel (structurally similar to eukaryotic voltage-gated K^+ channels) supports the idea of a transient and quite labile coupling between $S4S5_L$ and the $S6_T$ (**Figure 1B**). Indeed, we can observe in this structure that the voltage sensors S4 are in their activated position even though the pore is closed

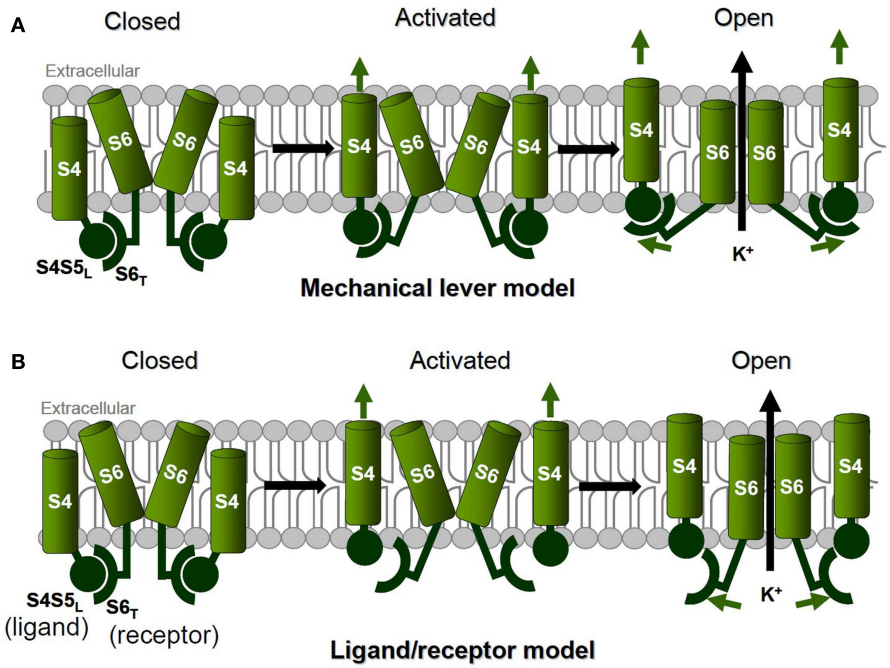

FIGURE 1 | Two models of coupling between voltage sensor movement and pore opening. (A) The mechanical lever model with a strong coupling between voltage sensor movement and pore opening, as suggested for Kv1.2 and Shaker. **(B)** The ligand/receptor model with a loose and state-dependent coupling between voltage sensor movement and pore opening, as suggested for KCNQ1 channels.

(Payandeh et al., 2011), and this corresponds to a decreased interaction of $S4S5_L$ with $S6_T$.

Model 2: Ligand/receptor model (Figure 1B)

KCNQ1. It is now admitted that the VSD-pore coupling is mediated by the interaction between $S4S5_L$ and $S6_T$. Several works on Shaker and Kv1.2 channels (above) suggest that the nature of this interaction is a strong coupling of the pore opening with voltage sensor movement. But in other channels, the interaction between $S4S5_L$ and $S6_T$ may be state-dependent, and leads to stabilization of the channel in the open or closed state. Forcing the interaction between $S4S5_L$ and $S6_T$ seems to stabilize hERG channels in a closed conformation (Ferrer et al., 2006). One interpretation can be that $S4S5_L$ is the equivalent of a ligand, able to bind to $S6_T$ and to stabilize the channel in a closed state. Upon depolarization, S4 drags the $S4S5_L$ ligand away from its receptor, allowing the channel to open (**Figure 1B**). To test this hypothesis on KCNQ1, we designed peptides identical to $S4S5_L$ (the "ligand") and $S6_T$ (the "receptor") based on sequence alignment with Shaker, in which interacting areas in the $S4S5_L$ and the $S6_T$ were suggested (Lu et al., 2001, 2002). KCNQ1 coassembles with the β-subunit KCNE1 to form the channel responsible for the cardiac slowly activating delayed rectifier current, I_{Ks}. In COS-7 cells transfected with the cardiac KCNE1-KCNQ1 channel complex and the $S4S5_L$ or $S6_T$ mimicking peptides, we found that co-expression of $S4S5_L$ peptides ("ligand" or inhibitory peptides) and the channel resulted in a reduction of the voltage-dependent potassium currents. In contrast, $S6_T$ peptides ("receptor" or decoy peptides) up-regulated channels activity, by competing with the endogenous $S6_T$ and decreasing the inhibitory effect of the endogenous $S4S5_L$ binding to the endogenous $S6_T$ (Choveau et al., 2011). This confirms that $S4S5_L$ can be compared to a ligand that locks channels in the closed state by interacting with its receptor, $S6_T$. The specificity of the $S4S5_L/S6_T$ interaction was confirmed by mutating the partners. Previous mutagenesis studies in KCNQ1 channels identified mutations in $S4S5_L$ (V254A) and in $S6_T$ (L353A) that prevent the channels from closing completely at hyperpolarizing potentials (Boulet et al., 2007; Labro et al., 2011), consistent with a decrease in the $S4S5_L$–$S6_T$ interaction. Based on these results, introduction of V254A in $S4S5_L$ peptide or L353A mutations in $S6_T$ peptide should disrupt the channel-peptide interaction and thus abolish their respective effect on the K^+ current. Mutant peptides have indeed no effect on KCNQ1 function (Choveau et al., 2011). To further demonstrate the specificity of the peptides-KCNQ1 interaction, a couple of mutations were tested both on the peptides and on the channel. In the KCNQ1 channel, introduction of L353A mutation located in $S6_T$ leads to an instantaneous current component, that is abolished by the introduction of V254L mutation located in $S4S5_L$ (Labro et al., 2011). The increased side chain volume induced by V254L substitution is probably compensating for the decreased side chain volume induced by the L353A one. We hypothesized (i) that the incomplete L353A channel closure was due to a low binding affinity of the endogenous WT ligand ($S4S5_L$) to its L353A mutated $S6_T$ receptor and (ii) a restored binding affinity of the endogenous V254L mutated ligand ($S4S5_L$) to the mutated $S6_T$ receptor. To confirm this, we showed that the WT $S4S5_L$ peptide has indeed no effect on the L353A KCNQ1 channel, whereas the mutant $S4S5_L$ peptide (V254L) has an effect

on this L353A KCNQ1 channel (Choveau et al., 2011). Altogether, our results are consistent with a ligand/receptor mechanism in which $S4S5_L$ acts as a ligand that binds to its receptor, $S6_T$, stabilizing the pore in a closed conformation. May this ligand/receptor mechanism be applied to other voltage-gated channels?

Human ether-a-go-go related gene. The hERG encodes the voltage-gated potassium channel underlying the cardiac delayed rectifier current, I_{Kr}, participating in the repolarization phase of cardiac action potential (Curran et al., 1995; Sanguinetti et al., 1995; Trudeau et al., 1995). hERG channel structure is similar to that of Shaker-like voltage-gated channels (Warmke and Ganetzky, 1994), possessing six (S1–S6) TMDs that comprise voltage sensor (S1–S4) and ion conduction pore (S5–S6) region. Despite this similarity, hERG channels behave very differently from Shaker-like channels: hERG activation and deactivation gating kinetics are much slower, whereas inactivation and the recovery from inactivation are rapid and intrinsically voltage-dependent (Smith et al., 1996; Sanguinetti and Tristani-Firouzi, 2006). Similarly to KCNQ1, the proximity between the $S4S5_L$ and $S6_T$ in the closed state was suggested by mutagenesis of these regions (Tristani-Firouzi et al., 2002). Most importantly, introducing cysteines in both $S4S5_L$ and $S6_T$ led to a current decrease in an oxidizing environment, and predominantly at a negative holding potential. This potential-dependent channel locking in the closed state is consistent with the formation of a disulfide bond between the cysteines introduced in $S4S5_L$ and $S6_T$ (Ferrer et al., 2006), and suggest that $S4S5_L$ binding to $S6_T$ locks the channel closed. This is in accordance with the ligand-receptor model underlying the voltage dependency of hERG channel activity. In the WT channel, interaction between $S4S5_L$ and $S6_T$ occurs via specific amino-acids since a point mutation (D540K) located in $S4S5_L$ (Sanguinetti and Xu, 1999) fundamentally alters the gating properties of hERG channels and these changes are prevented by additional point mutations (R665A, R665Q, or R665D) located in $S6_T$ (Tristani-Firouzi et al., 2002). The demonstrated specificity of amino-acids interaction further supports the $S4S5_L$ ligand and $S6_T$ receptor model. A companion review (Cheng and Claydon, 2012) in the present Research Topic suggests that the sequence of the $S4S5_L$ may be partly responsible for the slow activation kinetics of hERG channels.

HCN and KAT1. The hyperpolarization-activated, cyclic-nucleotide-gated (HCN) channels represent a family of four members (HCN1-4) that carry I_f ("f" for "funny") or I_h ("h" for "hyperpolarization") currents (DiFrancesco, 1981). Sequence analysis revealed that the primary structure of HCN channels is similar to that of voltage-gated potassium channels, i.e., six TMDs (S1–S6), including the positively charged voltage sensor S4 and the ion-conducting pore between S5 and S6. Ionic currents through HCN channels modulate the intrinsic electrical activity in the heart (DiFrancesco et al., 1979; DiFrancesco, 1993) and in a variety of neurons (Pape, 1996). Intriguingly, these non-specific cation channels are activated upon cell membrane hyperpolarization, contrarily to the classical depolarization-activated ion channels.

How can this difference in the gating behavior be explained? Two competing models have been proposed. The first model proposes that HCN channels are in an inactivated state when the membrane is depolarized and that its hyperpolarization induces channels to recover from inactivation and enter into an open state (Miller and Aldrich, 1996; Gauss et al., 1998). The second suggests that HCN channels gating is opposite to the one of K_v channels. In other words, membrane depolarization induces HCN channels deactivation whereas membrane hyperpolarization results in channel activation. Uncovering hyperpolarization-induced inactivation in KAT1, a six-segment potassium channel cloned from the higher plant *Arabidopsis* and having similar gating characteristics as HCN, has provided an argument that favors the second model for hyperpolarization-dependent activation of HCN channels (Moroni et al., 2000).

Alanine-scanning mutagenesis in HCN2 channel identified three $S4S5_L$ residues playing a major role in the S6 gate stabilization in the closed state (Chen et al., 2001), consistent with the "ligand/receptor" model of voltage dependency described in KCNQ1 and hERG. However, this does not explain in a straightforward way the reversed voltage dependency of the channel compared to other voltage-gated channels. A possible explanation would be that a specific $S4S5_L$–$S6_T$ interaction also favors an open state (in mirror to such interaction favoring a closed state in KCNQ1 or hERG channels). Using a cysteine cross-linking approach, a study showed that forced interaction between the $S4S5_L$ (F359C) and the C-terminus, downstream to S6 (K482C), leads to a constrained and unnatural opening of spHCN1 channel (Prole and Yellen, 2006). Using a homology modeling approach, another study on KAT1 suggested that channel closure occurs via an electrostatic repulsion between $S4S5_L$ (R190 and R197) and $S6_T$ (R307 and R310) while the channel opening occurs when $S4S5_L$ is rotating, allowing an electrostatic interaction between D188 in $S4S5_L$ and R307, R310 in $S6_T$ (Grabe et al., 2007). Again, all these studies are in good agreement with a ligand/receptor model of voltage dependency.

Kv4.2. Kv4.2 channel belongs to the family of voltage-gated potassium channels related to the *Shal* gene of *Drosophila* (Kv4 channels). These channels mediate a subthreshold-activating current (I_{SA}) that controls dendritic excitation and the backpropagation of neuronal action potentials (Hoffman et al., 1997). These Kv4 channels share structural motifs that are conserved in Shaker-like K_v channels, including the positively charged S4 voltage sensor, the TTXGYGD signature sequence in the selectivity filter, and the Pro-X-Pro motif in the S6 segment. One specificity of these channels, as compared to Shaker-like channels, is their significant closed-state inactivation induced by small depolarization (Jerng et al., 2004) and a fast voltage-dependent recovery from inactivation (tens to hundreds of milliseconds). Using functional and modeling approaches, it was demonstrated that this closed-state inactivation is strongly linked to the S4-charge immobilization in Kv4.2 channels, suggesting that the functional availability of Kv4.2 channels is directly regulated by the voltage sensors (Dougherty et al., 2008). Another study based on structural modeling and alanine-scanning, demonstrated that this voltage-dependent regulation involves a dynamic coupling between the $S4S5_L$ and $S6_T$. This

dynamic coupling mediates both transient activation and closed-state inactivation in Kv4.2 channels (Barghaan and Bähring, 2009). While interaction between $S4S5_L$ and $S6_T$ is necessary for channel activation, the Kv4 inactivation process would result from a destabilization of this interaction. This is detailed in another review (Bähring, 2012) of the present Research Topic. A model of labile coupling might thus be applied to Kv4.2 channels the same way as for KCNQ1, hERG, HCN, or KAT1 channels.

Na_v and Ca_v channels. Voltage-gated Na^+ and Ca^{2+} channels (Na_v and Ca_v, respectively), are fused tetrameric subunits with the same structural organization as proper tetrameric K_v channels. Indeed, Na_v and Ca_v subunits contain four homologous but not identical domains, each including six transmembrane segments (S1–S6), a voltage sensor domain with a positively charged S4 segment and a pore region formed by the association of S5 and S6 segments.

Since the voltage-dependent activity of Na^+ and Ca^{2+} channels is mediated by the S4 movements in response to membrane potential variation (Yang and Horn, 1995; Hu et al., 2003) like voltage-gated potassium channels, we hypothesize that the ligand-receptor mechanism we demonstrated for KCNQ1 (Choveau et al., 2011; Labro et al., 2011) may be applied to Na^+ and Ca^{2+} channels. The recent crystal structure of the prokaryotic one-domain voltage-gated sodium channel is consistent with our hypothesis since it can be observed that the channel gate (S6) is closed while the S4 segments are in the "up" position (Payandeh et al., 2011). Moreover, in this pre-open configuration (or pre-locked configuration if we consider the open to close pathway), the interaction surface between $S4S5_L$ and $S6_T$ is reduced as compared to the Kv1.2 channels structure (Payandeh et al., 2011). These observations support the model of a spontaneously opening and closing pore (McCusker et al., 2011; Shaya et al., 2011) with $S4S5_L$ locking the channel in a closed state when the membrane is polarized (**Figure 1B**). It will be interesting to confirm if this model also applies to Na^+ and Ca^{2+} channels, using the approach of exogenous peptides mimicking $S4S5_L$ or $S6_T$, as used in Choveau et al. (2011).

IMPAIRED S4–S5 AND S6 INTERACTION UNDERLIES HUMAN DISEASES

As developed earlier, it is broadly accepted that the interaction between $S4S5_L$ and $S6_T$ is extremely important for voltage-gated ion channels function (activation, deactivation, and inactivation). For that reason, disruption of such interaction may have dramatic physiological effects, and lead to certain forms of disease.

Both cardiac and neurological disorders have been linked to impaired $S4–S5_L$ and $S6_T$ interactions in K_v channels. For instance, many mutations of the KCNQ1 channels lead to the LQT, a cardiac disease characterized by prolonged ventricular repolarization, arrhythmias, and sudden death. Interestingly, looking specifically at the $S4S5_L$, it was shown that LQT1 mutations (type 1 LQT, associated with mutations in KCNQ1) are clustered on the one side of the $S4S5_L$ α-helix structure, that is putatively responsible for interactions with the $S6_T$ region (Boulet et al., 2007; Labro et al., 2011), while several LQT1 mutations are also localized in the interacting $S6_T$ region (http://www.fsm.it/cardmoc/), comforting in the opinion that the interaction of $S4S5_L$ with $S6_T$ is physiologically crucial for a proper heart function. Unfortunately, specific studies that would directly relate the importance of this interaction with disease are still lacking. However, in order to confirm that the ligand/receptor model (**Figure 1B**) fits well with the KCNQ1-E1 complex behavior, we used an atrial fibrillation mutant, S140G, that was shown to deactivate extremely slowly, and thus that presents almost no voltage dependence in the −80 to +80 mV range (Chen et al., 2003; Restier et al., 2008). Interestingly, while "$S6_T$/activator peptides" clearly affect WT KCNQ1-KCNE1 channels, no effect was observed on the S140G-E1 complex. Conversely, "$S4S5_L$/inhibitory peptides" did have a dramatic blocking effect, suggesting that the endogenous $S4S5_L$ of the S140G mutant channel does not reach $S6_T$. Although speculative, these data suggest that in this mutant, the gain-of-function effect might be somehow related to an impaired interaction between $S4S5_L$ and $S6_T$ (Choveau et al., 2011) due to a stabilization of S4 in the "up" state (Restier et al., 2008).

On the other hand, the pathological effect of a Kv1.1 channel mutation is consistent with the mechanical lever model of Kv1 channels (**Figure 1A**): the observation that a mutation located in the $S4S5_L$ prevents Kv1.1 open state stabilization led to the conclusion that disrupted $S4S5_L$ and S6 interactions underlie one type of episodic ataxia disease, in direct support of the mechanical lever model (Batulan et al., 2010).

Recently, it was proven that $S4S5_L$ and S6 regions of the voltage-gated calcium channel Cav2.3 are coupled during the activation process (Wall-Lacelle et al., 2011). Since Ca_v channels are involved in several pathologies, including episodic ataxia, familial hemiplegic migraine, idiopathic generalized epilepsy (Adams and Snutch, 2007), one can easily imagine that an impaired $S4S5_L$–$S6_T$ interaction in these channels might also underlie diseases, knowing that mutations in patients have been found in those critical regions (Adams and Snutch, 2007; Pietrobon, 2007).

PART 2: MODULATION OF VOLTAGE-GATED CHANNELS BY PIP_2

PIP_2 REGULATES SEVERAL VOLTAGE-GATED CHANNELS

KCNQ1 channels

Effect of PIP_2 on I_{Ks} currents. Phosphatidylinositol 4,5-bisphosphate (PIP_2) is a minor acidic membrane lipid found primarily in the inner leaflet of the plasma membrane. PIP_2 was first described as the precursor of the second messengers inositol 1,4,5-trisphosphate (IP_3) and diacylglycerol (DAG) when cleaved by receptor-activated phospholipase C (PLC; Berridge, 1981). It was realized much later that plasma membrane PIP_2 is not simply a precursor, but also a signaling molecule in its own right (reviewed in Logothetis et al., 2010). As also demonstrated for a wide variety of ion channels and transporters (Gamper and Shapiro, 2007; Suh and Hille, 2008; Logothetis et al., 2010), we showed that PIP_2 is a necessary cofactor for KCNQ1 channel activity (Loussouarn et al., 2003). It regulates KCNQ1 channel function by stabilizing its open conformation, leading to increased current amplitude, slower deactivation kinetics, and a negative shift in the steady-state activation curve. Such PIP_2 effect was described by a kinetic model in which only the final concerted step toward opening was affected by PIP_2 levels (**Figure 2**). In this model, when the membrane is depolarized, the movement of the four voltage sensors

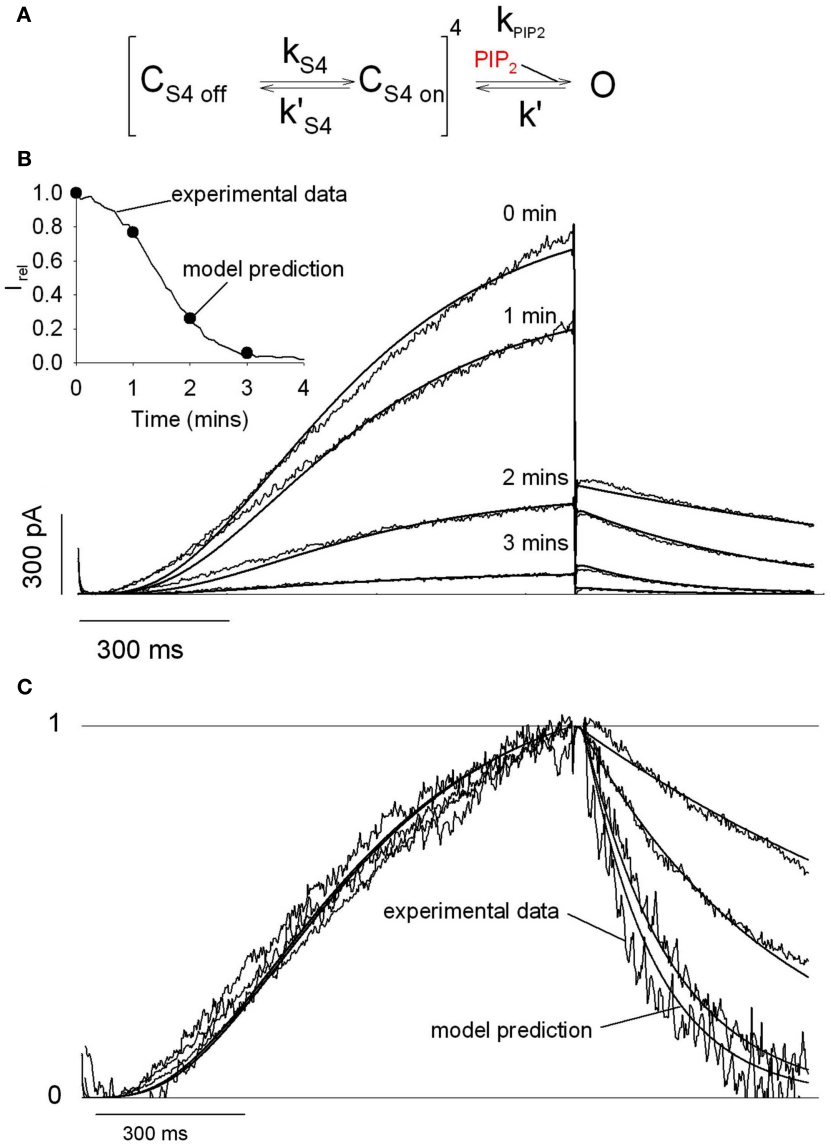

FIGURE 2 | A model based on the stabilization of the open state by PIP2 recapitulates the characteristics of the KCNQ1/KCNE1 currents. (A) During activation, k'_{s4} is negligible whereas $k_{S4} = 3.56$/s, and during deactivation $k'_{s4} = 7.47$/s whereas k_{S4} is negligible. In this model, PIP_2 only affects the transition from a closed state to an open state when the four voltage sensors are in the permissive state ($C_{S4\,on}$). Thus, during simulated rundown, only k_{PIP2} varies ($k' = 87.3$/s). **(B)** Experimental traces were superimposed with the simulated current (solid lines). k_{PIP2} was fixed to 592.74, 176.43, 25.84, and 4.53/s (simulating PIP_2 level decrease) to best fit the decrease in current amplitude during rundown, as shown in the inset. Inset: simulated (circles) and observed current (solid line) amplitudes as a function of time after patch excision. **(C)** Traces in **(B)** were normalized to compare the observed and simulated kinetics of activation and deactivation. From Loussouarn et al. (2003).

in the upward direction is rate limiting, making activation kinetics PIP_2-independent. But, when the membrane is repolarized, the transition of the concerted pore closing becomes rate limiting, making deactivation kinetics PIP_2-dependent. Other KCNQ channels are also PIP_2 sensitive, like the KCNQ2/KCNQ3 complex responsible for the neuronal M-current (cf. below). It is interesting to note that for this channel complex, the biophysical parameters do not seem to vary as PIP_2 levels vary (Shapiro et al., 2000), and more specifically the deactivation kinetics (Zhang et al., 2010). It is possible for those channels, that the concerted pore closing is not rate limiting, making deactivation kinetics PIP_2-independent. In KCNQ4, similar kinetics of "OFF" gating current and ion current deactivation are consistent with this hypothesis (Miceli et al., 2012).

The KCNQ1/KCNE1 kinetic model shares similarities with the one of Kir6.2/SUR1 channel (Enkvetchakul et al., 2000) suggesting similar effects of PIP_2 on six-domain and on two-domain channels. Furthermore, similarly to several inwardly rectifying K^+ (K_{ir}) channels, ROMK, GIRK, and IRK (Huang et al., 1998), direct interaction of PIP_2 with a cluster of basic residues located in the

C-terminus close to S6 was recently shown in KCNQ1 channel (Thomas et al., 2011). This functional homology may give some insights on the nature of PIP_2 regulation of KCNQ1/KCNE1 channels. From the crystal structure of a GIRK channel, Whorton and Mackinnon showed that PIP_2 molecules lie at the interface between the TMD and the CTD (TMD-CTD) and are coordinated by several positively charged residues Lys64, Lys194, Lys199, and Lys200 (Whorton and Mackinnon, 2011). PIP_2 is suggested to couple the G-loop gate (open by GTP binding) and the inner helix gate. But even in the absence of GTP, it allows the outer and interfacial helices to slightly shift downward and outward, and the inner helices to slightly rotate. Even if the motion of the inner helices is not sufficient to open the pore by itself, it shows that PIP_2 binding can lead to the inner helices rearrangements. For KCNQ1, PIP_2 binding to the cluster of basic residues located just after S6 (Thomas et al., 2011) may lead to the stabilization of the inner helices in an open state. In another recent crystallographic study, Hansen et al. (2011) showed that PIP_2 mediates docking of the whole CTD to the TMD and subsequent opening of the inner helix gate of Kir2.2. Thereby, we can speculate that KCNQ1 CTD could interact with the membrane, via interactions with PIP_2. This idea is supported by our previous work showing that substitutions of arginines located at the C-terminus of KCNQ1 channels (R539 and R555, cf. below) decrease the channel-PIP_2 sensitivity. However, crystallographic studies must be done to confirm this hypothesis.

Impact of KCNE1 subunits on PIP_2 sensitivity of I_{Ks}. Although KCNQ1 is a voltage-gated channel on its own, KCNE1 leads to changes in the current properties: it increases the amplitude, shifts the voltage dependence of activation toward more positive potentials, slows activation and deactivation kinetics, and suppresses inactivation (Barhanin et al., 1996; Sanguinetti et al., 1996). More recently, it was shown that KCNE1 alters the function of I_{Ks} by modulating the interaction between PIP_2 and the KCNQ1/KCNE1 complex (Li et al., 2011). It is established that the interaction between proteins and PIP_2 is often based on interaction between basic residues with the negative charges of PIP_2 (Suh and Hille, 2008). In light of this, Li et al. (2011) individually mutated 11 basic residues located in the cytosolic C-terminus of KCNE1 to identify key structural determinants contributing to I_{Ks} regulation by PIP_2. To do this, they studied for each mutant the gradual decrease of KCNQ1/KCNE1 channel activity ("rundown") observed right after excision in the inside-out configuration of the patch-clamp technique, patch excision provoking a decrease in membrane PIP_2 levels. In their study, Li et al. (2011) demonstrated that KCNE1 increases the PIP_2 sensitivity of I_{Ks}. More specifically, they identified 4 basic residues (R67, K69, K70, and H73) in KCNE1 that seem to play a critical role in this PIP_2 sensitivity. They showed that neutralization of these basic residues abolished the delay before rundown that is specifically observed when KCNE1 is co-expressed with KCNQ1, and significantly reduced the time constant of rundown. From a structure obtained by a NMR approach, it appears that these four residues are located on an α-helix, following the TMD (Kang et al., 2008). Kang et al. suggested that the C-terminal end of KCNE1 sits near $S4S5_L$ and $S6_T$, which may explain the changes exerted by KCNE1 on the gating of KCNQ1 (see Part 1: Role of the S4–S5 Linker in Channel Voltage Dependency). Moreover, basic residues in the $S4S5_L$ and in the proximal C-terminus of KCNQ1 have been shown to interact with PIP_2 (Park et al., 2005; Thomas et al., 2011), suggesting that PIP_2 and KCNE1 modulate I_{Ks} through interaction with the same region of KCNQ1. Thus, PIP_2 interacts with amino-acids in the KCNQ1/KCNE1 channel complex, and its capacity to modulate I_{Ks} is regulated by KCNE1, through mechanisms that remain to be clearly identified by crystallographic approach.

Impact of PKA and PKC on PIP_2 sensitivity of I_{Ks}. Neurotransmitter and hormone receptor stimulations activate different signaling pathways that adjust the protein phosphorylation status. Among others, Gq/G11-protein coupled receptors, like muscarinic acetylcholine (ACh) receptors (M1), stimulate the PLC which hydrolyzes PIP_2 (Berridge, 1981) as explained above. The DAG produced by PIP_2 hydrolysis activates protein kinase C (PKC), which has been suggested to regulate I_{Ks} channels. Matavel and Lopes (2009) showed that Gq-coupled receptors regulate I_{Ks} in a biphasic manner: (i) downstream activation of PLC leads to PIP_2 depletion and underlines channel inhibition and (ii) PKC-mediated phosphorylation is responsible for the activation phase.

Protein kinase A (PKA) is another well-characterized kinase that regulates I_{Ks} through receptor-activated signaling pathways (Walsh and Kass, 1988; Marx et al., 2002). Stimulation of the β1-adrenergic receptor leads to activation of adenylyl cyclase (AC) that catalyzes the conversion of ATP to cAMP and activates PKA. This β-adrenergic stimulation activates KCNQ1 via direct phosphorylation by PKA. More recently, Lopes et al. (2007) showed a crosstalk between KCNQ1 phosphorylation by PKA and its regulation by G-proteins of the Gq/G11 family. This study demonstrated that ACh inhibition of KCNQ1/KCNE1 currents in injected *Xenopus laevis* oocytes was lower in activated-PKA conditions and higher in inhibited-PKA conditions as compared to control. Furthermore, invalidation of the KCNQ1 S92 consensus phosphorylation site completely abolished the PKA effect on M1 inhibition of KCNQ1/KCNE1 currents. These results suggest that direct PKA phosphorylation of KCNQ1 is responsible for the PKA modulation of the observed PLC-dependent inhibition. A direct effect of PKA phosphorylation on channel regulation by PIP_2 was suggested by the use of wortmannin, which blocks the PI4-kinase intervening in the PIP_2 synthesis. PKA modulation of wortmannin inhibition was similar to the PKA modulation of M1 inhibition of KCNQ1. All these results suggest that the KCNQ1 sensitivity to PIP_2 is modulated by PKA (**Figure 3**).

More recently, Matavel et al. (2010) gave some new insights on KCNQ1 regulation by PKA and PKC. They tested four point mutations of putative PIP_2 interaction sites of the channel (R174C, R243C, R366Q, and R555C) and observed that mutations located in the proximal and distal C-terminus (R366Q and R555C, respectively), enhance the channel sensitivity to variations of membrane PIP_2 level, suggesting a decrease in the apparent affinity of these mutant channels to PIP_2. This was not the case for two mutations located in the S2–S3 loop (R174C) and in the $S4S5_L$ (R243C). For the latter, this is in contradiction with the enhanced sensitivity to PIP_2 level variation observed by Park et al. (2005) for the R243H

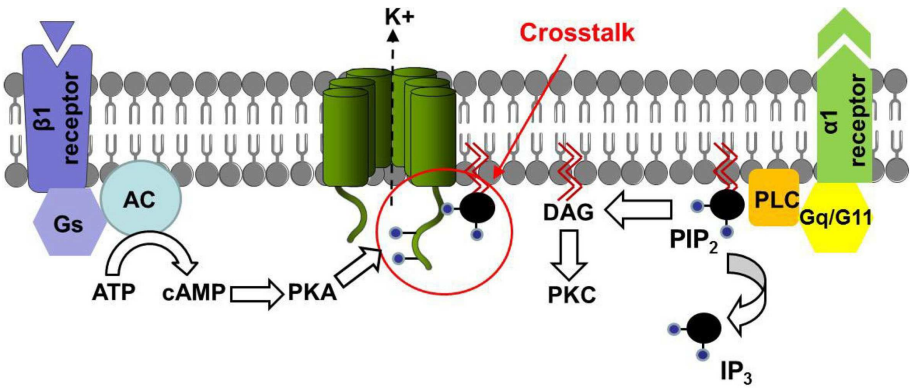

FIGURE 3 | Model of the regulation of channel-PIP2 interactions by PKA. β1-adrenergic receptor regulates channel-PIP_2 interaction through PKA phosphorylation, and simultaneously regulates Gq/G11-protein coupled modulation of the channel. Lopes et al. showed that this model is transposable to KCNQ1 and TREK1 channels. Adapted from Lopes et al. (2007).

mutant. Such discrepancy can be explained by the difference in the nature of the substituted amino-acid (cysteine in one case and histidine in the other) or by differences in experimental conditions (whole-cell configuration on oocytes and giant-patch configuration on COS-7 cells, respectively). Furthermore, Matavel et al. showed that R174C and R243C mutants exhibited an impaired activation by both PKA and PKC, whereas C-terminal KCNQ1 mutants presented an increased activation. Thus, for R366Q and R555C mutant channels, regulation of the channel by PIP_2 was potentiated, suggesting that PKA and PKC activate the channel by strengthening KCNQ1 interactions with PIP_2.

Other KCNQ channels

Five members have been identified in the KCNQ channel family (KCNQ1–5), each with a specific tissue distribution. In the heart, intestine, and inner ear, KCNQ1 subunits, assembling with auxiliary KCNE subunits, are important for repolarization and K^+ transport (Barhanin et al., 1996; Sanguinetti et al., 1996; Neyroud et al., 1997; Wang et al., 1998b). KCNQ2, KCNQ3, and KCNQ5 participate to "M-type" K^+ currents in a variety of neurons (Lerche et al., 2000; Schroeder et al., 2000; Cooper et al., 2001; Roche et al., 2002; Shah et al., 2002) and play a dominant role in regulating neuronal excitability (Jones et al., 1995; Cooper et al., 2001). KCNQ4 primarily localizes to the inner ear (Kubisch et al., 1999). Zhang et al. (2003) studied the PIP_2 dependency of all KCNQ family members. They used various approaches for homomeric KCNQ2 and heteromeric KCNQ2/KCNQ3 channels and showed that PIP_2 application in inside-out macropatches leads to an increase in channel activity, even after an almost complete rundown. Following channel reactivation by PIP_2, they observed that application of polylysine, which was described to act as a PIP_2 scavenger (Lopes et al., 2002; Rohács et al., 2002), results in fast and complete block of the current. Application of PIP_2 antibody to the internal surface of inside-out macropatches also suppresses the current. KCNQ1/KCNE1, KCNQ4, and KCNQ5 channels are also reactivated by PIP_2 after inhibition by polylysine, showing that all KCNQ family members are PIP_2 sensitive.

Similar to KCNQ1 (Loussouarn et al., 2003), PIP_2 may increase the current via a stabilization of the open state of KCNQ2–4 channels (Li et al., 2005). In their study, Li et al. (2011) showed that the maximal single-channel open probability (P_o) of KCNQ2–KCNQ4 and specifically KCNQ2/3 channels is highly governed by diC8-PIP_2 concentration. Furthermore, they observed a strong increase in maximal channel open probability (P_o) of KCNQ2/3 and KCNQ2 in cell-attached patches from cells overexpressing PI5-kinase, which has been shown to increase membrane PIP_2 (Bender et al., 2002; Winks et al., 2005). Conversely, a decrease in free membrane PIP_2 induced by muscarinic stimulation strongly lowers channel P_o. The apparent affinity of the channels for diC8-PIP_2 is strongly different and parallels the differential maximal P_o in cell-attached patches, suggesting that P_o of channels is mainly governed by their sensitivity to membrane PIP_2 (Li et al., 2005). Although not sufficient to nail down the point, these experiments are consistent with PIP_2 stabilizing the open state of all KCNQ channels.

In addition to PIP_2, several kinds of phosphoinositides but also other phospholipids are present in the plasma membrane and are capable of regulating the "M-type" K^+ current (Telezhkin et al., 2012). However, the fact that the current decreases when using tools that specifically decrease PIP_2 (Suh et al., 2006; Lindner et al., 2011) plus consideration of the concentration for half activation for the different phospholipids and their abundance in the membrane suggest a predominant role of PIP_2 for the regulation of KCNQ channels (Telezhkin et al., 2012).

Human ether-a-go-go related gene

The hERG or KCNH2 encodes the pore-forming subunit of the channel that is responsible for the rapid delayed rectifier K^+ current, I_{Kr}, in cardiac cells and several other cell types (cf. Part 1: Role of the S4–S5 Linker in Channel Voltage Dependency). This was the first voltage-gated ion channel described to be sensitive to PIP_2 (Bian et al., 2001). Consistent with this PIP_2 sensitivity, the muscarinic receptor M1, which stimulates enzymatic hydrolysis of PIP_2 by PLC, has been shown to suppress rat ERG currents in a heterologous system (Hirdes et al., 2004). As opposed to KCNQ1/KCNE1 (Loussouarn et al., 2003), Bian et al. (2001) showed that PIP_2 addition on hERG channel led to an accelerated activation with no effect on deactivation. But more recently, we

observed that PIP_2 effects on hERG are very close to those observed on KCNQ1/KCNE1: increased current, slowed deactivation, and no effect on activation kinetics (Rodriguez et al., 2010). This difference could be due to the use of divergent patch-clamp configurations in these studies: whole-cell in Bian et al. versus inside-out in our study. Furthermore, as for KCNQ1/KCNE1 channel complex, a kinetic model showed that PIP_2 effects on hERG can be explained by modifying the late transition rates only, corresponding to pore opening. In addition, we observed that hERG channels present a PIP_2 sensitivity similar to KCNQ1/KCNE1, estimated by (i) polylysine-induced rundown kinetics, (ii) PIP_2 induced run-up kinetics, and (iii) sensitivity to intracellular Mg^{2+}, which is known to screen the PIP_2 negative charges. All these data support the idea that hERG and KCNQ1/KCNE1 channels have a similar affinity to PIP_2. However, the experiments we performed also showed the persistence of a fraction of hERG current at low PIP_2 levels, which may underlie differences in response to physiological decrease in membrane PIP_2 levels.

Other voltage-sensitive channels

In addition to the delayed rectifiers KCNQ1 and hERG, other voltage-gated channels are regulated by PIP_2: the voltage-gated Ca^{2+} channels (Ca_v) channels (Wu et al., 2002), HCN channels (Pian et al., 2006), and also K_v channels (Oliver et al., 2004). At least for Ca_v channels, accessory subunits can regulate the modulation of the current by PIP_2, similar as the β-subunit KCNE1 modulating the PIP_2 sensitivity of KCNQ1 (Suh et al., 2012). Another article of this Frontiers Research topic is focusing on the effect of PIP_2 on these channels (Menchaca et al., under revision).

IMPLICATION OF PIP_2 IN SIGNALING PATHWAYS

Depletion of PIP_2 by activation of the Gq signaling pathway

Many studies have investigated the role of PIP_2 in the regulation of voltage-gated KCNQ channels activity. Recovery of KCNQ2/KCNQ3 current following muscarinic stimulation requires re-synthesis of PIP_2 (Suh and Hille, 2002) and channels activity decreases quickly upon patch excision but is restored upon cytoplasmic addition of PIP_2 (Zhang et al., 2003). In addition, fluorescent PIP_2-sensitive probes showed close correlation between PIP_2 hydrolysis and channel current suppression by muscarinic agonists (Winks et al., 2005). Similar effects of PIP_2 were found for KCNQ1 channels, in recombinant systems (Loussouarn et al., 2003; Zhang et al., 2003; Matavel and Lopes, 2009). Surprisingly, one study shows the opposite effect of PIP_2 on I_{Ks} in guinea-pig cardiomyocytes which would deserve a closer look (Ding et al., 2004).

A decrease in PIP_2 may be the major determinant for a decrease in a KCNQ current upon activation of some Gq/11-coupled receptors, but the mechanism may also be more complex for other Gq/11-coupled receptors. Regarding regulation of the M-current, two distinct pathways following PLC activation and IP_3 and DAG production have been described (**Figure 4**).

The first pathway, for which the decrease in PIP_2 is the major determinant of M-current depression, is induced by the activation of M1 muscarinic ACh and AT1 angiotensin II receptors (Zaika et al., 2006; Suh and Hille, 2007; Matavel and Lopes, 2009; **Figure 4A**).

The second pathway, activated by bradykinin B2 and purinergic P2Y receptors (**Figure 4B**), induces PIP_2 hydrolysis, but also PIP_2 re-synthesis preventing a decrease in PIP_2 abundance. PIP_2 re-synthesis is triggered by the increase of IP_3 concentration leading to calcium release from intracellular stores (Cruzblanca et al., 1998; Bofill-Cardona et al., 2000; Delmas et al., 2002; Zaika et al., 2007). This release is modulated by a IP_3 receptor-binding protein, IRBIT, which leaves and unmasks some IP_3 binding sites at a high enough IP_3 concentration, and increases the IP_3 receptor sensitivity (Zaika et al., 2011). The released Ca^{2+} binds to the calcium sensitive neuronal calcium sensor-1 (NCS-1) that activates PI4-kinase, leading to PIP_2 re-synthesis compensating the hydrolysis of PIP_2 by PLC (Zaika et al., 2007). Ca^{2+} also binds to calmodulin (CaM; Gamper et al., 2005) and Ca^{2+}-CaM binding to the channel might decrease the affinity of channels for PIP_2 (Kwon et al., 2007; Sarria et al., 2011) as their putative binding modules seem to overlap (Hernandez et al., 2008). This decrease in the affinity for PIP_2 may be the cause for current depression in the second pathway (**Figure 4B**).

Binding/unbinding of PIP_2

Localization of PIP_2-binding sites. The location of presumed PIP_2-binding sites and the characteristic of their motifs have been investigated in several channels. For KCNQ channels, evidence support the idea that the PIP_2-binding site(s) is (are) located mainly within the C-terminus. For instance, the H328C mutation in helix A within the C-terminus of KCNQ2 (residue in green in **Figure 5**) renders channels less sensitive to PIP_2 (Zhang et al., 2003). In addition, Shapiro and co-workers localized a cluster of basic residues within the linker connecting helices A and B in the C-terminus of KCNQ2–4 as the primary site of PIP_2 action (Hernandez et al., 2008). Based on the crystal structure of Kir2.1, homology modeling of KCNQ2 has suggested three residues (R459, R461, and R463) to form hydrogen bonds with phosphates of the PIP_2 head group (Hernandez et al., 2008).

Because all KCNQ channels share a common structure and are up-regulated by PIP_2 (Loussouarn et al., 2003; Zhang et al., 2003), PIP_2-binding site may be located at the analogous position in KCNQ1. However, a sequence alignment shows that the putative amino-acids binding to PIP_2 identified by Shapiro and co-workers (blue frame in **Figure 5**) are highly conserved in KCNQ2–5 but not in KCNQ1, suggesting different PIP_2-binding site(s) in this latter. A recent study has identified a cluster of basic residues (K354, K358, R360, and K362) in helix A of KCNQ1 as being involved in PIP_2-binding (Thomas et al., 2011). Three of these residues are conserved in other KCNQ channels (red frame in **Figure 5**), suggesting a potential role of those amino-acids in PIP_2-channel interactions in KCNQ2–4. Other residues, that are located in the S4–S5 linker (R243), downstream of the CaM binding domain (R539) and in helix C of KCNQ1 C-terminus (R555), have also been proposed to interact with PIP_2 (Park et al., 2005). As a result, and especially for KCNQ1, PIP_2 seems to interact with multiple parts of the channel. The crystal structures of Kir2.2 and GIRK 2, corresponding to S4–S5 linker + S5–S6 + C-terminus in KCNQ channels, illustrate such networks of interaction, and may give insights on the nature of PIP_2 regulation of KCNQ channels, as exposed above (Hansen et al., 2011; Whorton and Mackinnon,

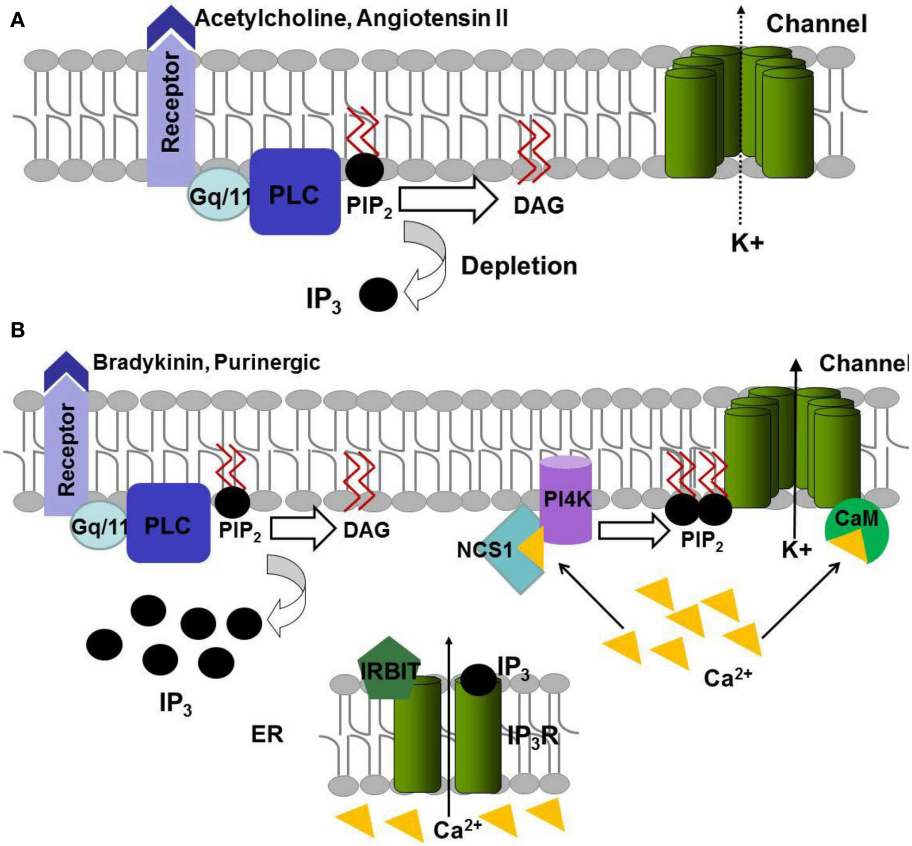

FIGURE 4 | Model of regulation of KCNQ channels function by the Gq signaling pathway. (A) Activation of the PLC by ACh and angiotensin II induces the hydrolysis of PIP_2 to DAG and IP3. **(B)** Activation of bradykinin and purinergic receptors leads to depletion of PIP_2 by PLC but also its re-synthesis. IP_3 allows releasing Ca^{2+} from endoplasmic reticulum via IP_3R receptor. The released Ca^{2+} can bind to NCS-1 that induces the synthesis of PIP_2 via PI4K or bind to CaM and modulate the channel sensitivity to PIP_2.

FIGURE 5 | Alignment of human KCNQ C-terminus and potential PIP2 interacting residues. The residues in KCNQ1, framed in red and indicated in red and italic, are those identified by Thomas et al. (2011) and Park et al. (2005), respectively. The H328 residue identified in KCNQ2 is indicated in green and in italic (Zhang et al., 2003). The region identified in KCNQ2–4 by Shapiro and co-workers is framed in blue (Hernandez et al., 2008).

2011). A more precise mapping and robust structural data remain to be established in KCNQ channels to understand the underlying mechanism.

In hERG also, a PIP_2-binding site seems to be located in the C-terminus. Deletion of a segment (883–894) in the C-terminus of hERG abolished the effects of PIP_2 on channel amplitude and voltage dependence of activation (Bian et al., 2004). However, the exact position remains elusive.

Role of Ca^{2+}-CaM. We described above that activation of Gq/11 signaling pathways leads to PIP_2 depletion and consequently to decreased channel current. However, several works suggest that unbinding of PIP_2 due to decreased affinity for KCNQ channels, rather than PIP_2 depletion, can underlie Gq/11-mediated depression of KCNQ current (Delmas and Brown, 2005). In agreement with this, Ca^{2+}-CaM binding site is very close to the putative binding site for PIP_2: helix A and B for Ca^{2+}-CaM and the A-B helix linker for PIP_2 (Wen and Levitan, 2002; Gamper and Shapiro, 2003; Hernandez et al., 2008). This proximity indicates that occupation of this site by Ca^{2+}-CaM might reduce the binding of PIP_2 to the channel, leading to a down-regulation of channels. Consistent with this, a recent study (Sarria et al., 2011) showed an increase of the open probability by PIP_2 of another six-segment channel, TRPM8, to be reversed by Ca^{2+}-CaM. Conversely, Kwon and co-workers have found that PIP_2 reduced Ca^{2+}-CaM binding to several channels including TRPC1, TRPC5–7, and TRPV1 (Kwon et al., 2007). Interestingly, similar effects are observed in KCNQ1 and Cav1.2, supporting the idea that PIP_2- and Ca^{2+}-CaM binding sites overlap in these channels (Kwon et al., 2007). However, mechanisms by which Ca^{2+}-CaM and PIP_2 antagonize each other effects remain unclear. Does this reduction result from a direct competition or from allosteric conformational changes?

Do phospholipids affect the voltage sensor S4 movement? As previously described in this review, mutagenesis studies have identified clusters of positively charged residues, mainly located in the cytosolic C-terminus of channels that may interact with the negatively charged PIP_2. The S4 segment possesses several positively charged residues, suggesting that PIP_2 might also affect its movement by interacting with some of these residues.

Several studies are consistent with the idea that lipids can interact with the voltage sensor and modulate its motion; although most of these studies focus on interactions in the outer leaflet (PIP_2 is situated in the inner leaflet). Structural studies on KvAP and on a Kv1.2-Kv2.1 chimeric channel show that some residues of S4 are exposed to lipids (Lee et al., 2005; Long et al., 2007). Chimeric Kv2.1 in which the "paddle" motif (S3b and S4) is replaced by one of the paddle motifs of Nav1.4 or of the voltage-dependent phosphatase, Ci-VSP, can be used to evaluate the contribution of the paddle motif to a specific property of the voltage sensor. Hydrolysis of the outer-leaflet lipid sphingomyelin to ceramide-1-phosphate by sphingomyelinase D alters the S4 movement differently in the different chimeric channels, suggesting an interaction between outer-leaf lipids and the paddle motif (Milescu et al., 2009). The sphingomyelin phosphate that persists in ceramide-1-phosphate is critical for their interaction with S4 since sphingomyelinase C, an enzyme which removes this phosphate group, strongly reduced the gating current of Shaker and Kv1.3 (Xu et al., 2008). The importance of the phosphate group of lipids in the S4 movement has also been highlighted in KvAP channels (Schmidt et al., 2006; Zheng et al., 2011). Expression of KvAP in membranes, in which lipids have a positively charged group instead of a phosphate group, renders the channels not functional (Schmidt et al., 2006). This effect would arise from a disruption of the interaction between the arginines of the S4 segment and the phosphate groups of the membrane lipids. Consistent with this, Zheng et al., 2011) showed that the switch of the S4 from the resting to the activated conformation requires more energy in a membrane without phospholipids.

According to those studies, S4 is stabilized in the activated position by interaction with outer-leaflet phospholipids. The structure of the Kv1.2-Kv2.1 chimeric channel suggests that an inner-leaflet phospholipid may also interact with the S4–S5 linker (Long et al., 2007). We suppose that the negatively charged phosphate groups of PIP_2 may bind to positively charged residues at the bottom of S4 or in S4–S5 linker and regulate S4 motions. However, no direct evidence exists for such an interaction.

IMPAIRED CHANNEL-PIP_2 INTERACTION UNDERLIES HUMAN DISEASES

As mentioned above, the importance of PIP_2 regulation of voltage-gated ion channels is now proven and clear. Thus, one might ask how far this crucial factor affects the physiological functions of these channels. Is it limited to a biophysical/regulatory effect, or does it have major impact; for instance, can an impaired interaction with PIP_2 lead to human disease? While this issue was partly answered for non-voltage-gated ion channels (Logothetis et al., 2010), the relationship between PIP_2 and channelopathies implying voltage-gated ion channels is less clear, probably since the study of their regulation is more recent and less developed.

The KCNQ1-KCNE1 potassium channel complex underlies the I_{Ks} repolarizing cardiac current. We showed that this channel function is dependent on PIP_2 regulation, which allows stabilization of the open state (Loussouarn et al., 2003). Importantly, we also demonstrated that residues in intracellular part of KCNQ1 channels ($S4S5_L$ and C-terminus) are important for PIP_2 regulation, and that their substitution, occurring in some LQT1 patients, leads to channel with decreased PIP_2 sensitivity, suggesting a direct connection between channels-PIP_2 interactions and the LQT syndrome (Park et al., 2005).

The KCNE1 beta-subunit is critical for a proper activity of KCNQ1 in the heart, and KCNE1 mutations are also associated with a LQT (type 5 LQT syndrome, LQT5). It was shown that neutralization of positive charges located in KCNE1 C-terminus is associated with LQT5 (Lai et al., 2005; Hedley et al., 2009; Kapplinger et al., 2009). A recent study highlighted the importance of PIP_2 interaction with KCNE1 and suggested that such interaction is critical for a proper function of KCNQ1/KCNE1 in the heart. This study went further by reporting that LQT5 syndrome is directly related to PIP_2-KCNE1 association, since WT channel complex properties were restored by using higher than normal doses of PIP_2, thus also confirming the PIP_2-dependence of LQT5 disease (Li et al., 2011).

Regulation of hERG channels by PIP_2 has been described in Section "Part 2: Human Ether-a-go-go Related Gene." PIP_2

stabilizes hERG open state changing the amplitude and deactivation kinetics (Bian et al., 2001; Rodriguez et al., 2010). In the putative PIP_2-binding sites, phospholipid anionic heads may interact with intracellular positively charged residues separated by, at least, one aromatic residue (Rosenhouse-Dantsker and Logothetis, 2007; Hernandez et al., 2008). One PIP_2 interacting site of hERG is localized to the C-terminal part of S6 (residues 883–864; Bian et al., 2004). Interestingly, three type 2 (hERG-related) LQT mutations that lead to substitution or deletion of arginines (at positions 885, 887, and 892) are localized in this area (Napolitano et al., 2005; Tester et al., 2005; Arnestad et al., 2007). It would thus be informative to investigate the activity of these LQT mutant channels to determine a potential PIP_2 involvement with the LQT2 syndrome.

The importance of PIP_2 regulation for proper voltage-gated ion channels function deserves thus all our attention. Although no direct connection between the phospholipid and channelopathies has been proven, apart from the LQT studies, the data obtained so far open a wide range of possibilities. An impressive list of phosphoinositide-sensitive channels has been presented in a recent review (Logothetis et al., 2010), and many of them are involved in pathologies (Lehmann-Horn and Jurkat-Rott, 1999). Following the example of hERG above, and knowing that several studies brought further details into the PIP_2-binding sites on voltage-gated ion channels (Zhang et al., 2003; Oliver et al., 2004; Hernandez et al., 2008; Flynn and Zagotta, 2011; Thomas et al., 2011), we can certainly imagine that other mutations lead to impaired channels-PIP_2 interaction and thus lead to disease.

ACKNOWLEDGMENTS

Fayal Abderemane-Ali and Fabien C. Coyan are recipients of a grant from the French Ministère de la Recherche. Zeineb Es-Salah-Lamoureux is supported by fellowships from the Lefoulon Delalande foundation and the French Foundation for Medical Research (FRM).

REFERENCES

Adams, P. J., and Snutch, T. P. (2007). Calcium channelopathies: voltage-gated calcium channels. *Subcell. Biochem.* 45, 215–251.

Alonso-Ron, C., de la Peña, P., Miranda, P., Domínguez, P., and Barros, F. (2008). Thermodynamic and kinetic properties of amino-terminal and S4-S5 loop HERG channel mutants under steady-state conditions. *Biophys. J.* 94, 3893–3911.

Armstrong, C. M. (1981). Sodium channels and gating currents. *Physiol. Rev.* 61, 644–683.

Arnestad, M., Crotti, L., Rognum, T. O., Insolia, R., Pedrazzini, M., Ferrandi, C., Vege, A., Wang, D. W., Rhodes, T. E., George, A. L. Jr., Schwartz, P. J. (2007). Prevalence of long-QT syndrome gene variants in sudden infant death syndrome. *Circulation* 115, 361–367.

Bähring, R. (2012). Voltage sensor inactivation in potassium channels. *Front. Pharmacol.* 3:100. doi:10.3389/fphar.2012.00100

Barghaan, J., and Bähring, R. (2009). Dynamic coupling of voltage sensor and gate involved in closed-state inactivation of kv4.2 channels. *J. Gen. Physiol.* 133, 205–224.

Barhanin, J., Lesage, F., Guillemare, E., Fink, M., Lazdunski, M., and Romey, G. (1996). K(V)LQT1 and lsK (minK) proteins associate to form the I(Ks) cardiac potassium current. *Nature* 384, 78–80.

Barros, F., Domínguez, P., and de la Peña, P. (2012). Cytoplasmic domains and voltage-dependent potassium channel gating. *Front. Pharmacol.* 3:49. doi:10.3389/fphar.2012.00049

Batulan, Z., Haddad, G. A., and Blunck, R. (2010). An intersubunit interaction between S4–S5 linker and S6 is responsible for the slow off-gating component in shaker K^+ channels. *J. Biol. Chem.* 285, 14005–14019.

Bender, K., Wellner-Kienitz, M.-C., and Pott, L. (2002). Transfection of a phosphatidyl-4-phosphate 5-kinase gene into rat atrial myocytes removes inhibition of GIRK current by endothelin and alpha-adrenergic agonists. *FEBS Lett.* 529, 356–360.

Berridge, M. J. (1981). Phosphatidylinositol hydrolysis: a multifunctional transducing mechanism. *Mol. Cell. Endocrinol.* 24, 115–140.

Bezanilla, F., Perozo, E., and Stefani, E. (1994). Gating of shaker K^+ channels: II. The components of gating currents and a model of channel activation. *Biophys. J.* 66, 1011–1021.

Bian, J., Cui, J., and McDonald, T. V. (2001). HERG K(+) channel activity is regulated by changes in phosphatidyl inositol 4,5-bisphosphate. *Circ. Res.* 89, 1168–1176.

Bian, J.-S., Kagan, A., and McDonald, T. V. (2004). Molecular analysis of PIP2 regulation of HERG and IKr. *Am. J. Physiol. Heart Circ. Physiol.* 287, H2154–H2163.

Bofill-Cardona, E., Vartian, N., Nanoff, C., Freissmuth, M., and Boehm, S. (2000). Two different signaling mechanisms involved in the excitation of rat sympathetic neurons by uridine nucleotides. *Mol. Pharmacol.* 57, 1165–1172.

Börjesson, S. I., and Elinder, F. (2008). Structure, function, and modification of the voltage sensor in voltage-gated ion channels. *Cell Biochem. Biophys.* 52, 149–174.

Boulet, I. R., Labro, A. J., Raes, A. L., and Snyders, D. J. (2007). Role of the S6 C-terminus in KCNQ1 channel gating. *J. Physiol. (Lond.)* 585, 325–337.

Broomand, A., Männikkö, R., Larsson, H. P., and Elinder, F. (2003). Molecular movement of the voltage sensor in a K channel. *J. Gen. Physiol.* 122, 741–748.

Catterall, W. A. (1986). Voltage-dependent gating of sodium channels: correlating structure and function. *Trends Neurosci.* 9, 7–10.

Cha, A., Snyder, G. E., Selvin, P. R., and Bezanilla, F. (1999). Atomic scale movement of the voltage-sensing region in a potassium channel measured via spectroscopy. *Nature* 402, 809–813.

Chanda, B., Asamoah, O. K., Blunck, R., Roux, B., and Bezanilla, F. (2005). Gating charge displacement in voltage-gated ion channels involves limited transmembrane movement. *Nature* 436, 852–856.

Chen, J., Mitcheson, J. S., Tristani-Firouzi, M., Lin, M., and Sanguinetti, M. C. (2001). The S4–S5 linker couples voltage sensing and activation of pacemaker channels. *Proc. Natl. Acad. Sci. U.S.A.* 98, 11277–11282.

Chen, J., Zou, A., Splawski, I., Keating, M. T., and Sanguinetti, M. C. (1999). Long QT syndrome-associated mutations in the Per-Arnt-Sim (PAS) domain of HERG potassium channels accelerate channel deactivation. *J. Biol. Chem.* 274, 10113–10118.

Chen, Y.-H., Xu, S.-J., Bendahhou, S., Wang, X.-L., Wang, Y., Xu, W.-Y., Jin, H.-W., Sun, H., Su, X.-Y., Zhuang, Q.-N., Yang, Y. Q., Li, Y. B., Liu, Y., Xu, H. J., Li, X. F., Ma, N., Mou, C. P., Chen, Z., Barhanin, J., and Huang, W. (2003). KCNQ1 gain-of-function mutation in familial atrial fibrillation. *Science* 299, 251–254.

Cheng, Y. M., and Claydon, T. W. (2012). Voltage-dependent gating of HERG potassium channels. *Front. Pharmacol.* 3:83. doi:10.3389/fphar.2012.0008

Choveau, F. S., Rodriguez, N., Abderemane-Ali, F., Labro, A. J., Rose, T., Dahimène, S., Boudin, H., Le Hénaff, C., Escande, D., Snyders, D. J., Charpentier, F., Mérot, J., Baró, I., and Loussouarn, G. (2011). KCNQ1 channels voltage dependence through a voltage-dependent binding of the S4–S5 linker to the pore domain. *J. Biol. Chem.* 286, 707–716.

Cooper, E. C., Harrington, E., Jan, Y. N., and Jan, L. Y. (2001). M channel KCNQ2 subunits are localized to key sites for control of neuronal network oscillations and synchronization in mouse brain. *J. Neurosci.* 21, 9529–9540.

Cruzblanca, H., Koh, D. S., and Hille, B. (1998). Bradykinin inhibits M current via phospholipase C and Ca^{2+} release from IP3-sensitive Ca^{2+} stores in rat sympathetic neurons. *Proc. Natl. Acad. Sci. U.S.A.* 95, 7151–7156.

Curran, M. E., Splawski, I., Timothy, K. W., Vincent, G. M., Green, E. D., and Keating, M. T. (1995). A molecular basis for cardiac arrhythmia: HERG mutations cause long QT syndrome. *Cell* 80, 795–803.

de la Peña, P., Alonso-Ron, C., Machín, A., Fernández-Trillo, J., Carretero, L., Domínguez, P., and Barros, F. (2011). Demonstration of physical proximity between the N terminus and the S4–S5 linker of the human ether-a-go-go-related gene (hERG) potassium channel. *J. Biol. Chem.* 286, 19065–19075.

Delemotte, L., Tarek, M., Klein, M. L., Amaral, C., and Treptow, W. (2011). Intermediate states of the Kv1.2 voltage sensor from atomistic molecular dynamics simulations. *Proc. Natl. Acad. Sci. U.S.A.* 108, 6109–6114.

Delmas, P., and Brown, D. A. (2005). Pathways modulating neural KCNQ/M (Kv7) potassium channels. *Nat. Rev. Neurosci.* 6, 850–862.

Delmas, P., Wanaverbecq, N., Abogadie, F. C., Mistry, M., and Brown, D. A. (2002). Signaling microdomains define the specificity of receptor-mediated InsP(3) pathways in neurons. *Neuron* 34, 209–220.

DiFrancesco, D. (1981). A new interpretation of the pace-maker current in calf Purkinje fibres. *J. Physiol. (Lond.)* 314, 359–376.

DiFrancesco, D. (1993). Pacemaker mechanisms in cardiac tissue. *Annu. Rev. Physiol.* 55, 455–472.

DiFrancesco, D., Noma, A., and Trautwein, W. (1979). Kinetics and magnitude of the time-dependent potassium current in the rabbit sinoatrial node: effect of external potassium. *Pflugers Arch.* 381, 271–279.

Ding, W.-G., Toyoda, F., and Matsuura, H. (2004). Regulation of cardiac IKs potassium current by membrane phosphatidylinositol 4,5-bisphosphate. *J. Biol. Chem.* 279, 50726–50734.

Dougherty, K., De Santiago-Castillo, J. A., and Covarrubias, M. (2008). Gating charge immobilization in Kv4.2 channels: the basis of closed-state inactivation. *J. Gen. Physiol.* 131, 257–273.

Durell, S. R., and Guy, H. R. (1992). Atomic scale structure and functional models of voltage-gated potassium channels. *Biophys. J.* 62, 238–247; discussion 247–250.

Enkvetchakul, D., Loussouarn, G., Makhina, E., Shyng, S. L., and Nichols, C. G. (2000). The kinetic and physical basis of K(ATP) channel gating: toward a unified molecular understanding. *Biophys. J.* 78, 2334–2348.

Ferrer, T., Rupp, J., Piper, D. R., and Tristani-Firouzi, M. (2006). The S4–S5 linker directly couples voltage sensor movement to the activation gate in the human ether-a'-go-go-related gene (hERG) K^+ channel. *J. Biol. Chem.* 281, 12858–12864.

Flynn, G. E., and Zagotta, W. N. (2011). Molecular mechanism underlying phosphatidylinositol 4,5-bisphosphate-induced inhibition of SpIH channels. *J. Biol. Chem.* 286, 15535–15542.

Gamper, N., Li, Y., and Shapiro, M. S. (2005). Structural requirements for differential sensitivity of KCNQ K^+ channels to modulation by Ca^{2+}/calmodulin. *Mol. Biol. Cell* 16, 3538–3551.

Gamper, N., and Shapiro, M. S. (2003). Calmodulin mediates Ca^{2+}-dependent modulation of M-type K^+ channels. *J. Gen. Physiol.* 122, 17–31.

Gamper, N., and Shapiro, M. S. (2007). Regulation of ion transport proteins by membrane phosphoinositides. *Nat. Rev. Neurosci.* 8, 921–934.

Gandhi, C. S., Clark, E., Loots, E., Pralle, A., and Isacoff, E. Y. (2003). The orientation and molecular movement of a k(+) channel voltage-sensing domain. *Neuron* 40, 515–525.

Gauss, R., Seifert, R., and Kaupp, U. B. (1998). Molecular identification of a hyperpolarization-activated channel in sea urchin sperm. *Nature* 393, 583–587.

Grabe, M., Lai, H. C., Jain, M., Jan, Y. N., and Jan, L. Y. (2007). Structure prediction for the down state of a potassium channel voltage sensor. *Nature* 445, 550–553.

Guy, H. R., and Seetharamulu, P. (1986). Molecular model of the action potential sodium channel. *Proc. Natl. Acad. Sci. U.S.A.* 83, 508–512.

Haddad, G. A., and Blunck, R. (2011). Mode shift of the voltage sensors in shaker K^+ channels is caused by energetic coupling to the pore domain. *J. Gen. Physiol.* 137, 455–472.

Hansen, S. B., Tao, X., and MacKinnon, R. (2011). Structural basis of PIP2 activation of the classical inward rectifier K^+ channel Kir2.2. *Nature* 477, 495–498.

Hedley, P. L., Jørgensen, P., Schlamowitz, S., Wangari, R., Moolman-Smook, J., Brink, P. A., Kanters, J. K., Corfield, V. A., and Christiansen, M. (2009). The genetic basis of long QT and short QT syndromes: a mutation update. *Hum. Mutat.* 30, 1486–1511.

Hernandez, C. C., Zaika, O., and Shapiro, M. S. (2008). A carboxy-terminal inter-helix linker as the site of phosphatidylinositol 4,5-bisphosphate action on Kv7 (M-type) K^+ channels. *J. Gen. Physiol.* 132, 361–381.

Hirdes, W., Horowitz, L. F., and Hille, B. (2004). Muscarinic modulation of erg potassium current. *J. Physiol. (Lond.)* 559, 67–84.

Hoffman, D. A., Magee, J. C., Colbert, C. M., and Johnston, D. (1997). K^+ channel regulation of signal propagation in dendrites of hippocampal pyramidal neurons. *Nature* 387, 869–875.

Hoshi, T., Zagotta, W. N., and Aldrich, R. W. (1994). Shaker potassium channel gating. I: transitions near the open state. *J. Gen. Physiol.* 103, 249–278.

Hu, L., Shi, J., Ma, Z., Krishnamoorthy, G., Sieling, F., Zhang, G., Horrigan, F. T., and Cui, J. (2003). Participation of the S4 voltage sensor in the Mg^{2+}-dependent activation of large conductance (BK) K^+ channels. *Proc. Natl. Acad. Sci. U.S.A.* 100, 10488–10493.

Huang, C. L., Feng, S., and Hilgemann, D. W. (1998). Direct activation of inward rectifier potassium channels by PIP2 and its stabilization by Gbetagamma. *Nature* 391, 803–806.

Jensen, M. Ø., Jogini, V., Borhani, D. W., Leffler, A. E., Dror, R. O., and Shaw, D. E. (2012). Mechanism of voltage gating in potassium channels. *Science* 336, 229–233.

Jerng, H. H., Pfaffinger, P. J., and Covarrubias, M. (2004). Molecular physiology and modulation of somatodendritic A-type potassium channels. *Mol. Cell. Neurosci.* 27, 343–369.

Jiang, Y., Lee, A., Chen, J., Ruta, V., Cadene, M., Chait, B. T., and MacKinnon, R. (2003). X-ray structure of a voltage-dependent K^+ channel. *Nature* 423, 33–41.

Jones, S., Brown, D. A., Milligan, G., Willer, E., Buckley, N. J., and Caulfield, M. P. (1995). Bradykinin excites rat sympathetic neurons by inhibition of M current through a mechanism involving B2 receptors and G alpha q/11. *Neuron* 14, 399–405.

Kang, C., Tian, C., Sönnichsen, F. D., Smith, J. A., Meiler, J., George, A. L. Jr, Vanoye, C. G., Kim, H. J., and Sanders, C. R. (2008). Structure of KCNE1 and implications for how it modulates the KCNQ1 potassium channel. *Biochemistry* 47, 7999–8006.

Kapplinger, J. D., Tester, D. J., Salisbury, B. A., Carr, J. L., Harris-Kerr, C., Pollevick, G. D., Wilde, A. A. M., and Ackerman, M. J. (2009). Spectrum and prevalence of mutations from the first 2,500 consecutive unrelated patients referred for the FAMILION long QT syndrome genetic test. *Heart Rhythm* 6, 1297–1303.

Kubisch, C., Schroeder, B. C., Friedrich, T., Lütjohann, B., El-Amraoui, A., Marlin, S., Petit, C., and Jentsch, T. J. (1999). KCNQ4, a novel potassium channel expressed in sensory outer hair cells, is mutated in dominant deafness. *Cell* 96, 437–446.

Kwon, Y., Hofmann, T., and Montell, C. (2007). Integration of phosphoinositide- and calmodulin-mediated regulation of TRPC6. *Mol. Cell* 25, 491–503.

Labro, A. J., Boulet, I. R., Choveau, F. S., Mayeur, E., Bruyns, T., Loussouarn, G., Raes, A. L., and Snyders, D. J. (2011). The S4–S5 linker of KCNQ1 channels forms a structural scaffold with the S6 segment controlling gate closure. *J. Biol. Chem.* 286, 717–725.

Lai, L.-P., Su, Y.-N., Hsieh, F.-J., Chiang, F.-T., Juang, J.-M., Liu, Y.-B., Ho, Y.-L., Chen, W.-J., Yeh, S.-J., Wang, C.-C., Ko, Y. L., Wu, T. J., Ueng, K. C., Lei, M. H., Tsao, H. M., Chen, S. A., Lin, T. K., Wu, M. H., Lo, H. M., Huang, S. K., and Lin, J. L. (2005). Denaturing high-performance liquid chromatography screening of the long QT syndrome-related cardiac sodium and potassium channel genes and identification of novel mutations and single nucleotide polymorphisms. *J. Hum. Genet.* 50, 490–496.

Larsson, H. P., Baker, O. S., Dhillon, D. S., and Isacoff, E. Y. (1996). Transmembrane movement of the shaker K^+ channel S4. *Neuron* 16, 387–397.

Ledwell, J. L., and Aldrich, R. W. (1999). Mutations in the S4 region isolate the final voltage-dependent cooperative step in potassium channel activation. *J. Gen. Physiol.* 113, 389–414.

Lee, S.-Y., Banerjee, A., and MacKinnon, R. (2009). Two separate interfaces between the voltage sensor and pore are required for the function of voltage-dependent K(+) channels. *PLoS Biol.* 7, e47. doi:10.1371/journal.pbio.1000047

Lee, S.-Y., Lee, A., Chen, J., and MacKinnon, R. (2005). Structure of the KvAP voltage-dependent K^+ channel and its dependence on the lipid membrane. *Proc. Natl. Acad. Sci. U.S.A.* 102, 15441–15446.

Lehmann-Horn, F., and Jurkat-Rott, K. (1999). Voltage-gated ion channels and hereditary disease. *Physiol. Rev.* 79, 1317–1372.

Lerche, C., Scherer, C. R., Seebohm, G., Derst, C., Wei, A. D., Busch, A. E., and Steinmeyer, K. (2000). Molecular cloning and functional expression of KCNQ5, a potassium channel subunit that may contribute to neuronal M-current diversity. *J. Biol. Chem.* 275, 22395–22400.

Lewis, A., Jogini, V., Blachowicz, L., Lainé, M., and Roux, B. (2008). Atomic constraints between the voltage sensor and the pore domain in a voltage-gated K^+ channel of

known structure. *J. Gen. Physiol.* 131, 549–561.

Li, Y., Gamper, N., Hilgemann, D. W., and Shapiro, M. S. (2005). Regulation of Kv7 (KCNQ) K^+ channel open probability by phosphatidylinositol 4,5-bisphosphate. *J. Neurosci.* 25, 9825–9835.

Li, Y., Zaydman, M. A., Wu, D., Shi, J., Guan, M., Virgin-Downey, B., and Cui, J. (2011). KCNE1 enhances phosphatidylinositol 4,5-bisphosphate (PIP2) sensitivity of IKs to modulate channel activity. *Proc. Natl. Acad. Sci. U.S.A.* 108, 9095–9100.

Lindner, M., Leitner, M. G., Halaszovich, C. R., Hammond, G. R. V., and Oliver, D. (2011). Probing the regulation of TASK potassium channels by PI4,5P with switchable phosphoinositide phosphatases. *J. Physiol. (Lond.)* 589, 3149–3162.

Logothetis, D. E., Petrou, V. I., Adney, S. K., and Mahajan, R. (2010). Channelopathies linked to plasma membrane phosphoinositides. *Pflugers Arch.* 460, 321–341.

Long, S. B., Campbell, E. B., and Mackinnon, R. (2005). Crystal structure of a mammalian voltage-dependent shaker family K^+ channel. *Science* 309, 897–903.

Long, S. B., Tao, X., Campbell, E. B., and MacKinnon, R. (2007). Atomic structure of a voltage-dependent K^+ channel in a lipid membrane-like environment. *Nature* 450, 376–382.

Lopes, C. M. B., Remon, J. I., Matavel, A., Sui, J. L., Keselman, I., Medei, E., Shen, Y., Rosenhouse-Dantsker, A., Rohacs, T., and Logothetis, D. E. (2007). Protein kinase A modulates PLC-dependent regulation and PIP2-sensitivity of K^+ channels. *Channels (Austin)* 1, 124–134.

Lopes, C. M. B., Zhang, H., Rohacs, T., Jin, T., Yang, J., and Logothetis, D. E. (2002). Alterations in conserved Kir channel-PIP2 interactions underlie channelopathies. *Neuron* 34, 933–944.

Loussouarn, G., Park, K.-H., Bellocq, C., Baró, I., Charpentier, F., and Escande, D. (2003). Phosphatidylinositol-4,5-bisphosphate, PIP2, controls KCNQ1/KCNE1 voltage-gated potassium channels: a functional homology between voltage-gated and inward rectifier K^+ channels. *EMBO J.* 22, 5412–5421.

Lu, Z., Klem, A. M., and Ramu, Y. (2001). Ion conduction pore is conserved among potassium channels. *Nature* 413, 809–813.

Lu, Z., Klem, A. M., and Ramu, Y. (2002). Coupling between voltage sensors and activation gate in voltage-gated K^+ channels. *J. Gen. Physiol.* 120, 663–676.

Marx, S. O., Kurokawa, J., Reiken, S., Motoike, H., D'Armiento, J., Marks, A. R., and Kass, R. S. (2002). Requirement of a macromolecular signaling complex for beta adrenergic receptor modulation of the KCNQ1-KCNE1 potassium channel. *Science* 295, 496–499.

Matavel, A., and Lopes, C. M. B. (2009). PKC activation and PIP(2) depletion underlie biphasic regulation of IKs by Gq-coupled receptors. *J. Mol. Cell. Cardiol.* 46, 704–712.

Matavel, A., Medei, E., and Lopes, C. M. B. (2010). PKA and PKC partially rescue long QT type 1 phenotype by restoring channel-PIP2 interactions. *Channels (Austin)* 4, 3–11.

McCusker, E. C., D'Avanzo, N., Nichols, C. G., and Wallace, B. A. (2011). Simplified bacterial "pore" channel provides insight into the assembly, stability, and structure of sodium channels. *J. Biol. Chem.* 286, 16386–16391.

Miceli, F., Vargas, E., Bezanilla, F., and Taglialatela, M. (2012). Gating currents from Kv7 channels carrying neuronal hyperexcitability mutations in the voltage-sensing domain. *Biophys. J.* 102, 1372–1382.

Milescu, M., Bosmans, F., Lee, S., Alabi, A. A., Kim, J. I., and Swartz, K. J. (2009). Interactions between lipids and voltage sensor paddles detected with tarantula toxins. *Nat. Struct. Mol. Biol.* 16, 1080–1085.

Miller, A. G., and Aldrich, R. W. (1996). Conversion of a delayed rectifier K^+ channel to a voltage-gated inward rectifier K^+ channel by three amino acid substitutions. *Neuron* 16, 853–858.

Moroni, A., Gazzarrini, S., Cerana, R., Colombo, R., Sutter, J. U., DiFrancesco, D., Gradmann, D., and Thiel, G. (2000). Mutation in pore domain uncovers cation- and voltage-sensitive recovery from inactivation in KAT1 channel. *Biophys. J.* 78, 1862–1871.

Napolitano, C., Priori, S. G., Schwartz, P. J., Bloise, R., Ronchetti, E., Nastoli, J., Bottelli, G., Cerrone, M., and Leonardi, S. (2005). Genetic testing in the long QT syndrome: development and validation of an efficient approach to genotyping in clinical practice. *JAMA* 294, 2975–2980.

Neyroud, N., Tesson, F., Denjoy, I., Leibovici, M., Donger, C., Barhanin, J., Fauré, S., Gary, F., Coumel, P., Petit, C., Schwartz, K., and Guicheney, P. (1997). A novel mutation in the potassium channel gene KVLQT1 causes the Jervell and Lange-Nielsen cardioauditory syndrome. *Nat. Genet.* 15, 186–189.

Oliver, D., Lien, C.-C., Soom, M., Baukrowitz, T., Jonas, P., and Fakler, B. (2004). Functional conversion between A-type and delayed rectifier K^+ channels by membrane lipids. *Science* 304, 265–270.

Pape, H. C. (1996). Queer current and pacemaker: the hyperpolarization-activated cation current in neurons. *Annu. Rev. Physiol.* 58, 299–327.

Park, K.-H., Piron, J., Dahimene, S., Mérot, J., Baró, I., Escande, D., and Loussouarn, G. (2005). Impaired KCNQ1-KCNE1 and phosphatidylinositol-4,5-bisphosphate interaction underlies the long QT syndrome. *Circ. Res.* 96, 730–739.

Payandeh, J., Scheuer, T., Zheng, N., and Catterall, W. A. (2011). The crystal structure of a voltage-gated sodium channel. *Nature* 475, 353–358.

Pian, P., Bucchi, A., Robinson, R. B., and Siegelbaum, S. A. (2006). Regulation of gating and rundown of HCN hyperpolarization-activated channels by exogenous and endogenous PIP2. *J. Gen. Physiol.* 128, 593–604.

Pietrobon, D. (2007). Familial hemiplegic migraine. *Neurotherapeutics* 4, 274–284.

Prole, D. L., and Yellen, G. (2006). Reversal of HCN channel voltage dependence via bridging of the S4–S5 linker and Post-S6. *J. Gen. Physiol.* 128, 273–282.

Restier, L., Cheng, L., and Sanguinetti, M. C. (2008). Mechanisms by which atrial fibrillation-associated mutations in the S1 domain of KCNQ1 slow deactivation of IKs channels. *J. Physiol. (Lond.)* 586, 4179–4191.

Roche, J. P., Westenbroek, R., Sorom, A. J., Hille, B., Mackie, K., and Shapiro, M. S. (2002). Antibodies and a cysteine-modifying reagent show correspondence of M current in neurons to KCNQ2 and KCNQ3 K^+ channels. *Br. J. Pharmacol.* 137, 1173–1186.

Rodriguez, N., Amarouch, M. Y., Montnach, J., Piron, J., Labro, A. J., Charpentier, F., Mérot, J., Baró, I., and Loussouarn, G. (2010). Phosphatidylinositol-4,5-bisphosphate (PIP(2)) stabilizes the open pore conformation of the Kv11.1 (hERG) channel. *Biophys. J.* 99, 1110–1118.

Rohács, T., Lopes, C., Mirshahi, T., Jin, T., Zhang, H., and Logothetis, D. E. (2002). Assaying phosphatidylinositol bisphosphate regulation of potassium channels. *Meth. Enzymol.* 345, 71–92.

Rosenhouse-Dantsker, A., and Logothetis, D. E. (2007). Molecular characteristics of phosphoinositide binding. *Pflugers Arch.* 455, 45–53.

Ruta, V., Chen, J., and MacKinnon, R. (2005). Calibrated measurement of gating-charge arginine displacement in the KvAP voltage-dependent K^+ channel. *Cell* 123, 463–475.

Sanguinetti, M. C., Curran, M. E., Zou, A., Shen, J., Spector, P. S., Atkinson, D. L., and Keating, M. T. (1996). Coassembly of K(V)LQT1 and minK (IsK) proteins to form cardiac I(Ks) potassium channel. *Nature* 384, 80–83.

Sanguinetti, M. C., Jiang, C., Curran, M. E., and Keating, M. T. (1995). A mechanistic link between an inherited and an acquired cardiac arrhythmia: HERG encodes the IKr potassium channel. *Cell* 81, 299–307.

Sanguinetti, M. C., and Tristani-Firouzi, M. (2006). hERG potassium channels and cardiac arrhythmia. *Nature* 440, 463–469.

Sanguinetti, M. C., and Xu, Q. P. (1999). Mutations of the S4–S5 linker alter activation properties of HERG potassium channels expressed in *Xenopus* oocytes. *J. Physiol. (Lond.)* 514(Pt 3), 667–675.

Sarria, I., Ling, J., Zhu, M. X., and Gu, J. G. (2011). TRPM8 acute desensitization is mediated by calmodulin and requires PIP(2): distinction from tachyphylaxis. *J. Neurophysiol.* 106, 3056–3066.

Schmidt, D., Jiang, Q.-X., and MacKinnon, R. (2006). Phospholipids and the origin of cationic gating charges in voltage sensors. *Nature* 444, 775–779.

Schroeder, B. C., Hechenberger, M., Weinreich, F., Kubisch, C., and Jentsch, T. J. (2000). KCNQ5, a novel potassium channel broadly expressed in brain, mediates M-type currents. *J. Biol. Chem.* 275, 24089–24095.

Shah, M. M., Mistry, M., Marsh, S. J., Brown, D. A., and Delmas, P. (2002). Molecular correlates of the M-current in cultured rat hippocampal neurons. *J. Physiol. (Lond.)* 544, 29–37.

Shapiro, M. S., Roche, J. P., Kaftan, E. J., Cruzblanca, H., Mackie, K., and Hille, B. (2000). Reconstitution of muscarinic modulation of the KCNQ2/KCNQ3 K(+) channels that underlie the neuronal M current. *J. Neurosci.* 20, 1710–1721.

Shaya, D., Kreir, M., Robbins, R. A., Wong, S., Hammon, J., Brüggemann,

A., and Minor, D. L. Jr. (2011). Voltage-gated sodium channel (NaV) protein dissection creates a set of functional pore-only proteins. *Proc. Natl. Acad. Sci. U.S.A.* 108, 12313–12318.

Smith, J. A., Vanoye, C. G., George, A. L. Jr., Meiler, J., and Sanders, C. R. (2007). Structural models for the KCNQ1 voltage-gated potassium channel. *Biochemistry* 46, 14141–14152.

Smith, P. L., Baukrowitz, T., and Yellen, G. (1996). The inward rectification mechanism of the HERG cardiac potassium channel. *Nature* 379, 833–836.

Stefani, E., Toro, L., Perozo, E., and Bezanilla, F. (1994). Gating of shaker K^+ channels: I. Ionic and gating currents. *Biophys. J.* 66, 996–1010.

Suh, B.-C., and Hille, B. (2002). Recovery from muscarinic modulation of M current channels requires phosphatidylinositol 4,5-bisphosphate synthesis. *Neuron* 35, 507–520.

Suh, B.-C., and Hille, B. (2007). Regulation of KCNQ channels by manipulation of phosphoinositides. *J. Physiol. (Lond.)* 582, 911–916.

Suh, B.-C., and Hille, B. (2008). PIP2 is a necessary cofactor for ion channel function: how and why? *Annu. Rev. Biophys.* 37, 175–195.

Suh, B.-C., Inoue, T., Meyer, T., and Hille, B. (2006). Rapid chemically induced changes of PtdIns(4,5)P2 gate KCNQ ion channels. *Science* 314, 1454–1457.

Suh, B.-C., Kim, D.-I., Falkenburger, B. H., and Hille, B. (2012). Membrane-localized β-subunits alter the PIP2 regulation of high-voltage activated Ca^{2+} channels. *Proc. Natl. Acad. Sci. U.S.A.* 109, 3161–3166.

Telezhkin, V., Reilly, J. M., Thomas, A. M., Tinker, A., and Brown, D. A. (2012). Structural requirements of membrane phospholipids for M-type potassium channel activation and binding. *J. Biol. Chem.* 287, 10001–10012.

Tempel, B. L., Papazian, D. M., Schwarz, T. L., Jan, Y. N., and Jan, L. Y. (1987). Sequence of a probable potassium channel component encoded at shaker locus of *Drosophila*. *Science* 237, 770–775.

Tester, D. J., Will, M. L., Haglund, C. M., and Ackerman, M. J. (2005). Compendium of cardiac channel mutations in 541 consecutive unrelated patients referred for long QT syndrome genetic testing. *Heart Rhythm* 2, 507–517.

Thomas, A. M., Harmer, S. C., Khambra, T., and Tinker, A. (2011). Characterization of a binding site for anionic phospholipids on KCNQ1. *J. Biol. Chem.* 286, 2088–2100.

Tombola, F., Pathak, M. M., and Isacoff, E. Y. (2006). How does voltage open an ion channel? *Annu. Rev. Cell Dev. Biol.* 22, 23–52.

Tristani-Firouzi, M., Chen, J., and Sanguinetti, M. C. (2002). Interactions between S4–S5 linker and S6 transmembrane domain modulate gating of HERG K^+ channels. *J. Biol. Chem.* 277, 18994–19000.

Trudeau, M. C., Warmke, J. W., Ganetzky, B., and Robertson, G. A. (1995). HERG, a human inward rectifier in the voltage-gated potassium channel family. *Science* 269, 92–95.

Wall-Lacelle, S., Hossain, M. I., Sauvé, R., Blunck, R., and Parent, L. (2011). Double mutant cycle analysis identified a critical leucine residue in the IIS4S5 linker for the activation of the Ca(V)2.3 calcium channel. *J. Biol. Chem.* 286, 27197–27205.

Walsh, K. B., and Kass, R. S. (1988). Regulation of a heart potassium channel by protein kinase A and C. *Science* 242, 67–69.

Wang, J., Trudeau, M. C., Zappia, A. M., and Robertson, G. A. (1998a). Regulation of deactivation by an amino terminal domain in human ether-à-go-go-related gene potassium channels. *J. Gen. Physiol.* 112, 637–647.

Wang, W., Xia, J., and Kass, R. S. (1998b). MinK-KvLQT1 fusion proteins, evidence for multiple stoichiometries of the assembled IsK channel. *J. Biol. Chem.* 273, 34069–34074.

Warmke, J. W., and Ganetzky, B. (1994). A family of potassium channel genes related to eag in *Drosophila* and mammals. *Proc. Natl. Acad. Sci. U.S.A.* 91, 3438–3442.

Wen, H., and Levitan, I. B. (2002). Calmodulin is an auxiliary subunit of KCNQ2/3 potassium channels. *J. Neurosci.* 22, 7991–8001.

Whorton, M. R., and Mackinnon, R. (2011). Crystal structure of the mammalian GIRK2 K(+) channel and gating regulation by G proteins, PIP(2), and sodium. *Cell* 147, 199–208.

Winks, J. S., Hughes, S., Filippov, A. K., Tatulian, L., Abogadie, F. C., Brown, D. A., and Marsh, S. J. (2005). Relationship between membrane phosphatidylinositol-4,5-bisphosphate and receptor-mediated inhibition of native neuronal M channels. *J. Neurosci.* 25, 3400–3413.

Wu, L., Bauer, C. S., Zhen, X., Xie, C., and Yang, J. (2002). Dual regulation of voltage-gated calcium channels by PtdIns(4,5)P2. *Nature* 419, 947–952.

Xu, Y., Ramu, Y., and Lu, Z. (2008). Removal of phospho-head groups of membrane lipids immobilizes voltage sensors of K^+ channels. *Nature* 451, 826–829.

Yang, N., and Horn, R. (1995). Evidence for voltage-dependent S4 movement in sodium channels. *Neuron* 15, 213–218.

Yarov-Yarovoy, V., Baker, D., and Catterall, W. A. (2006). Voltage sensor conformations in the open and closed states in ROSETTA structural models of K(+) channels. *Proc. Natl. Acad. Sci. U.S.A.* 103, 7292–7297.

Yarov-Yarovoy, V., DeCaen, P. G., Westenbroek, R. E., Pan, C.-Y., Scheuer, T., Baker, D., and Catterall, W. A. (2012). Structural basis for gating charge movement in the voltage sensor of a sodium channel. *Proc. Natl. Acad. Sci. U.S.A.* 109, E93–E102.

Zagotta, W. N., Hoshi, T., and Aldrich, R. W. (1994a). Shaker potassium channel gating. III: Evaluation of kinetic models for activation. *J. Gen. Physiol.* 103, 321–362.

Zagotta, W. N., Hoshi, T., Dittman, J., and Aldrich, R. W. (1994b). Shaker potassium channel gating. II: Transitions in the activation pathway. *J. Gen. Physiol.* 103, 279–319.

Zaika, O., Lara, L. S., Gamper, N., Hilgemann, D. W., Jaffe, D. B., and Shapiro, M. S. (2006). Angiotensin II regulates neuronal excitability via phosphatidylinositol 4,5-bisphosphate-dependent modulation of Kv7 (M-type) K^+ channels. *J. Physiol. (Lond.)* 575, 49–67.

Zaika, O., Tolstykh, G. P., Jaffe, D. B., and Shapiro, M. S. (2007). Inositol triphosphate-mediated Ca^{2+} signals direct purinergic P2Y receptor regulation of neuronal ion channels. *J. Neurosci.* 27, 8914–8926.

Zaika, O., Zhang, J., and Shapiro, M. S. (2011). Combined phosphoinositide and Ca^{2+} signals mediating receptor specificity toward neuronal Ca^{2+} channels. *J. Biol. Chem.* 286, 830–841.

Zhang, H., Craciun, L. C., Mirshahi, T., Rohács, T., Lopes, C. M. B., Jin, T., and Logothetis, D. E. (2003). PIP(2) activates KCNQ channels, and its hydrolysis underlies receptor-mediated inhibition of M currents. *Neuron* 37, 963–975.

Zhang, X., Chen, X., Jia, C., Geng, X., Du, X., and Zhang, H. (2010). Depolarization increases phosphatidylinositol (PI) 4,5-bisphosphate level and KCNQ currents through PI 4-kinase mechanisms. *J. Biol. Chem.* 285, 9402–9409.

Zheng, H., Liu, W., Anderson, L. Y., and Jiang, Q.-X. (2011). Lipid-dependent gating of a voltage-gated potassium channel. *Nat. Commun.* 2, 250.

Conflict of Interest Statement: The authors declare that the research was conducted in the absence of any commercial or financial relationships that could be construed as a potential conflict of interest.

Received: 23 April 2012; accepted: 14 June 2012; published online: 05 July 2012.
Citation: Choveau FS, Abderemane-Ali F, Coyan FC, Es-Salah-Lamoureux Z, Baró I and Loussouarn G (2012) Opposite effects of the S4–S5 linker and PIP_2 on voltage-gated channel function: KCNQ1/KCNE1 and other channels. Front. Pharmacol. ***3****:125. doi: 10.3389/fphar.2012.00125*
This article was submitted to Frontiers in Pharmacology of Ion Channels and Channelopathies, a specialty of Frontiers in Pharmacology.

frontiers in
PHARMACOLOGY

REVIEW ARTICLE
published: 28 May 2012
doi: 10.3389/fphar.2012.00097

Molecular dynamics simulations of voltage-gated cation channels: insights on voltage-sensor domain function and modulation

Lucie Delemotte[1,2], Michael L. Klein[2] and Mounir Tarek[1]*

[1] *Equipe de Chimie et Biochimie Théoriques, UMR Synthèse et Réactivité de Systèmes Moléculaires Complexes, Centre National de la Recherche Scientifique, Université de Lorraine, Nancy, France*
[2] *Institute for Computational Molecular Science, Temple University, Philadelphia, PA, USA*

Edited by:
Gildas Loussouarn, University of Nantes, France

Reviewed by:
Peter Bond, University of Cambridge, UK
Fredrik Elinder, Linköping University, Sweden

****Correspondence:***
Mounir Tarek, UMR Synthèse et Réactivité de Systèmes Moléculaires Complexes, Faculté des Sciences et Techniques, Université de Lorraine, B.P. 70239, 54506 Vandoeuvre les Nancy Cedex, France.
e-mail: mounir.tarek@univ-lorraine.fr

Since their discovery in the 1950s, the structure and function of voltage-gated cation channels (VGCC) has been largely understood thanks to results stemming from electrophysiology, pharmacology, spectroscopy, and structural biology. Over the past decade, computational methods such as molecular dynamics (MD) simulations have also contributed, providing molecular level information that can be tested against experimental results, thereby allowing the validation of the models and protocols. Importantly, MD can shed light on elements of VGCC function that cannot be easily accessed through "classical" experiments. Here, we review the results of recent MD simulations addressing key questions that pertain to the function and modulation of the VGCC's voltage-sensor domain (VSD) highlighting: (1) the movement of the S4-helix basic residues during channel activation, articulating how the electrical driving force acts upon them; (2) the nature of the VSD intermediate states on transitioning between open and closed states of the VGCC; and (3) the molecular level effects on the VSD arising from mutations of specific S4 positively charged residues involved in certain genetic diseases.

Keywords: Kv1.2, gating charges, VSD intermediate states, molecular models, channelopathies, mutations, omega currents

INTRODUCTION

Voltage-gated cation channels (VGCCs) are transmembrane (TM) proteins ubiquitous to excitable cells of superior organisms. Their role is to transport ions across the cell membrane in a manner that depends on its polarization state. Being implicated in a wide variety of biological functions such as the transmission of the nervous impulse, mutations in genes encoding them may give rise to inherited genetic diseases such as long and short QT syndrome of the heart, epilepsies, periodic paralyses, deafness, diabetes, etc. The physiological role of VGCCs has made them objects of interest since their discovery in the 1950s and understanding their function at a molecular level has benefited greatly from results from a large number of experimental techniques, especially structural biology, electrophysiology, and pharmacology, as well as spectroscopies of various kinds.

Among the body of discoveries that have contributed to increase our knowledge of VGCC structure and function, three of them were recognized to have a remarkable impact: the first was the recording of transient currents of very low amplitude (∼200 times lower than ionic currents). These currents, called today "gating currents," initially measured in the 1970s (Armstrong and Bezanilla, 1973; Schneider and Chandler, 1973; Keynes and Rojas, 1974) follow from the reorganization of charged residues of the protein in response to a change in the TM voltage. Their integral, i.e., the gating charge, *Q*, represent the total charge that is transported through the membrane capacitance during gating (opening or closing) of the channel and is a characteristic feature of VGCC function. The second came from the sequencing of VGCCs (Noda et al., 1984; Tempel et al., 1987), which revealed that they were made of either homo- or hetero-tetramers of 6 TM segments (S1–S6). The segment S4 contains a number of positively charged residues (mostly arginines) and was as such recognized to constitute the "voltage-sensor." Following from this, it was hypothesized that it is the movement of S4 across the membrane capacitance in response to changes in the TM potential that gives rise to the gating currents aforementioned. The third discovery was the X-ray crystal structure of a mammalian member of the VGCC family, the Shaker-like (potassium) Kv1.2 channel (Long et al., 2005b). Indeed, while a previous structure had captured an archeal voltage gated K+ channel, the KvAP from *Aeropyrum pernix*, in a non-native conformation 2 years prior (Jiang et al., 2003a), the Kv1.2 structure revealed for the first time the native 3-D arrangement of the channel: a homo tetramer of S5 and S6 segments forms the central pore (homologous to all K^+ channels) and four separate bundles made of segments S1–S4 each form an auxiliary "voltage-sensor" domain (VSD) on the periphery. In this particular Kv1.2 crystallized structure, S4, which contains six positively charged residues, is located in an "up" position, indicating that the VSD was captured in its "activated" conformation. While leaving open the question of the resting/closed state VSD conformation and the channel's deactivation mechanism, this structure enabled one to start envisioning the molecular level operation mechanism of the

VSD. In particular, it allowed computational approaches such as molecular dynamics (MD) simulations to step in and contribute to answering questions concerning the functional mechanism.

In this review, we will provide the reader with our perspective on the results obtained so far using an MD approach. After describing the technique and depicting the protocols designed to specifically address questions that are peculiar to the study of VGCCs (e.g., how to reproduce voltage clamp conditions *in silico*, and how to estimate the gating charge, etc.), we will review the main molecular insights gleaned on VSD operation. In particular, we will show how the protocols devised have enabled construction of models of the resting/closed state as well as being able to access the conformations of kinetic intermediate states. We also show how MD simulation results have been used to tackle questions of biological and pharmacological interest, namely how mutations of the S4 positively charged residues are involved in genetic diseases.

METHODS IN MOLECULAR DYNAMICS SIMULATIONS

As already mentioned, the field of VGCC research has benefited from a large number of experimental techniques ranging from pharmacology to structural biology (Hille, 2001). Computational methods such as MD simulations contributed only later as high-resolution structures have become available. When performed under conditions corresponding to laboratory scenarios, MD simulations can provide a detailed view of the structure and dynamics of a macromolecular system. They can also be used to perform "computer experiments" that cannot be carried out in the laboratory, either because they do not represent a physical behavior, or because the necessary controls cannot be achieved in the lab. Additionally, information from MD simulations like positions and velocities of atoms can also enable to calculate quantities that can be tested against experimental results to ensure the validity of the protocols employed. As an illustration, voltage clamp electrophysiology measurements record currents flowing through the external clamp circuit, giving indirect access to the currents moving across the membrane, whereas in MD simulations, it is possible to follow directly ionic charge displacement at an atomic level (Aksimentiev and Schulten, 2005; Jensen et al., 2010; Kutzner et al., 2011) and use this information to estimate currents from a statistical sampling (repetition) of such events. A comparison of the simulation results with experiments enables one to validate (or invalidate) the theoretical models and ensures that molecular scale dynamics embodied in the MD simulation are reliable.

In this section, we offer a brief description of the general principles of MD simulations, and present the protocols developed specifically to address questions concerning VGCC structure and function.

GENERAL CONSIDERATIONS

MD simulations refer to a family of computational methods aimed at simulating macroscopic behaviors of a microscopic many-body system through the numerical integration of the classical equations of motion. In this review, we report mainly results from atomistic simulations, in which each atom of the system (particle) is represented by a single interaction center with its net charge, mass and specific interaction characteristics. The macroscopic properties of the whole simulation system are expressed as functions of the particle coordinates and momenta, which are computed along a phase space trajectory generated by classical dynamics (Allen and Tildesley, 1987; Leach, 2001; Frenkel and Smit, 2002). The time evolution of the system trajectories are driven by the forces between particles, which in turn derive from a potential energy function U, also called a force field. The force fields in common use in biophysics, which include GROMOS (Schuler et al., 2001), CHARMM (MacKerell et al., 1998) and AMBER (Case et al., 1999), are based on a classical treatment of particle–particle interactions that does not allow chemical bond dissociation: Specifically, the function U is written in terms of interactions between pairs of atoms and is typically divided into "bonded" and "non-bonded" contributions. Typically, the bonded interactions consist of intramolecular harmonic bond stretching (E_{bond}), angle bending (E_{angle}), and dihedral angle deformation (E_{torsion}). Non-bonded interactions include electrostatic (E_{el}) and van der Waals terms (E_{vdw}). The former are calculated from the Coulomb interaction between partial charges assigned to each atom, whereas the latter describe the short-range repulsion and long-range attraction between pairs of atoms.

Recently, other types of force field have emerged, where a single interaction site encompasses several atoms (Bond et al., 2007; Marrink et al., 2007; Devane et al., 2009; Khalfa et al., 2009). These so-called coarse-grained (CG) models have the advantage of reducing by almost an order of magnitude the number of particles, enabling to increase the size of the system and reach a much longer simulation time. For instance, they were used to investigate biologically interesting processes such as the interaction of VGCCs with lipids (Bond and Sansom, 2007; Mokrab and Sansom, 2011) or with toxins (Wee et al., 2008). On the other hand, as the resolution of the system is reduced, details that may be important are lost. For example, a single water bead often represents several (3–4) water molecules, i.e., 9–12 atoms. In most CG force fields, its molecular polarizability is lost and several of its properties cannot be modeled, limiting therefore the number of applications that can be studied with these force fields.

The number of atoms considered in an MD simulation is typically of the order of 10^5–10^6. To minimize surface effects, and thereby simulate more closely the expected behavior of a macroscopic system, it is customary to use 3-D periodic boundary conditions (PBCs). The system as a whole is divided into cells. Each cell is surrounded on all sides by periodic images of itself. Hence, in the case of a VGCC in its membrane environment, what is usually modeled is in fact a multilamellar lipid bilayer stack with a high density of channels. This setup mimics therefore conditions close to the ones in crystallography or neutron- or x-ray reflectivity studies rather than the ones in physiology experiments.

MD simulations generate a set of atomic positions and velocities as a function of time that evolve deterministically from an initial configuration according to the interaction potential U. Information (positions, velocities or momenta, and forces) at a given instant in time, t, is used to predict the positions and momenta at a later time, $t+\delta t$, by numerically integrating the classical equations of motion. The timestep δt should be typically of the order of a few femtoseconds (fs $= 10^{-15}$ s) for all-atom simulations in order to ensure energy conservation. Accordingly, the time range that can be reached nowadays by this technique on

large systems like ions channels or membrane proteins in their host environment is of the order of microseconds (millisecond in very rare occurrences; Shaw et al., 2009).

In general, the MD technique is a scheme for studying the natural time evolution of a classical system of fixed number of particles N in a volume V. In MD simulations using the Newton equations of motion, the total energy E is conserved and along the trajectory, the system samples the micro-canonical ensemble (NVE). Modified algorithms have been devised to perform simulations in conditions that mimic the laboratory conditions. Temperature (T) and pressure (P) control can then be achieved to simulate the isothermal (NVT) or isothermal-isobaric (NPT) ensembles (Martyna et al., 1992).

EVALUATION OF THE LOCAL ELECTROSTATIC AND TM POTENTIAL

The function of VGCCs is to transport ions through the membrane in a manner that depends on the polarization state of the latter. The main force that drives their opening/closing is the action of TM potentials on their charged residues. In general, the TM potential is defined as the difference between the electrostatic potential (EP) in the cytoplasm and in the cell exterior. In MD simulations, as a convention, the bottom bath represents the cell's inside while the top bath represents its outside. Estimating the TM potential then requires evaluating the difference between the EP in the two baths. The EP may be linked (ignoring electronic polarization) to the charge density distribution through Poisson's equation. This EP can be computed at a location r of the system, provided an MD trajectory, by solving (for instance on a 3-D grid):

$$\nabla^2\varphi(r) \;=\; -4\pi\sum_i \rho_i(r) \tag{1}$$

where the sum runs over all atoms i bearing a partial charge ρ_i in the system. The local electric field at a position r may be obtained as the derivative of the EP. Note that access to such a quantity enables one to verify whether or not and how much the electric field is focused within the VSD, which in turn has been crucial for the proper estimation of the gating charge resulting from a conformational change of the channel (see details below).

APPLYING A TM VOLTAGE

A central question in the study of the VSD operation using MD is the correct modeling of the applied TM potential in a way that complies with experiments. When a cell membrane is subjected to an electrical stress, either naturally, or during a patch clamp experiment, the TM potential arises from a local ionic charge imbalance, i.e., from an excess of charges on one side of the membrane with respect to the other. The correct handling of such an effect in MD simulations is challenging because of the use of 3-D PBCs. Thus, an ionic imbalance along the membrane normal cannot be applied directly, due to the communication of the top of the simulation system with the bottom of its image and vice versa. Two major methods have been proposed to circumvent this technical problem.

Electric field method

In experiments, a charge imbalance gives rise to a TM potential and therefore to an electric field along the membrane normal, z. In MD simulations, the first strategy developed to apply a TM potential, which is also the simplest to implement technically, was to apply a constant electric field E perpendicular to the membrane (Suenaga et al., 1998; Zhong et al., 1998; Crozier et al., 2001; Tieleman et al., 2001). In practice, this is done by applying a force $F = q_i.E$ to all the atoms bearing a charge q_i. Reorganization of the molecules and most particularly of the water dipoles then induces a voltage difference across the bilayer. In experiments, the potential difference arising from the application of an electric field to a capacitor (e.g., a lipid membrane) amounts to $\Delta V = E.d$, d being the thickness of the capacitor. In MD simulations, due to the use of PBCs, evaluation of the TM potential by the Poisson equation shows that ΔV is rather a function of L_z, the box size along z (Tieleman, 2004; Tarek, 2005; Gumbart et al., 2012) resulting in $\Delta V = E.L_z$. Due to this property, it is important to stress here that the quantity that is the most appropriate to consider when comparing simulations with electrophysiology experiments is the TM potential rather than the electric field (Delemotte and Tarek, 2012).

Charge imbalance method

In patch clamp experiments, electrodes are inserted on both sides of the membrane and the TM voltage pulse is long enough (milliseconds, i.e., above the membrane charging time) to generate an ionic reorganization within the solution and subsequent charge of the membrane. To mimic such conditions in MD simulations, another class of methods was proposed, where an explicit ionic charge imbalance is considered. Note that to ensure such an imbalance, communication between the system and periodic images of the solution baths on either side of the membrane needs to be avoided. To do so, a system consisting of three salt-water baths separated by two bilayers was proposed (Sachs et al., 2004; Gurtovenko and Vattulainen, 2005; Kandasamy and Larson, 2006).

A variant of this method consists of using a single bilayer between two independent electrolyte baths, each terminated by an air (vacuum)/water interface (Delemotte et al., 2008). The vacuum slab prevents ionic diffusion from one side of the membrane to the other via the PBC (Bostick and Berkowitz, 2003) and maintains constant the charge imbalance imposed between the two baths. For large enough electrolyte baths (>30 Å) the lipid bilayer behaves as if it was in contact with an infinite solution. In both of these setups, it was shown that the bilayer behaves as a capacitor, and that separation of the charges by a low dielectric medium gives rise to a TM potential $\Delta V = Q_{s/C}$, when a charge imbalance per surface area Q_s is imposed, C being the capacitance of the membrane.

Such a method has an important drawback for applications where the TM voltage should remain constant, namely due to the relatively small size of the system, reorganization of the charges within the membrane in response to an applied voltage (ion conduction, reorganization of charged residues of a protein, etc.) leads to a drop in the TM voltage. Whereas this may be a desired effect in some applications (see next paragraph for the computation of gating charges), a method that enables one to maintain ΔV roughly constant was recently proposed (Kutzner et al., 2011).

GATING CHARGE CALCULATIONS

Gating currents arise from the movements of charged groups (ions or charged residues, dipoles. . .) within the lipid dielectric

in response to the application of a TM voltage. In the case of VGCCs submitted to an activating voltage, the displacements of the charges tethered to the VSD give rise to tiny transient "gating" currents. The time integral of the latter, Q, corresponds to the amount of electric charge translocated across the membrane capacitor, and is characteristic of a specific conformational change. In voltage clamp experiments, when current through the main pore is blocked [using for instance a non-conductive mutant such as the W434F Shaker mutant (Perozo et al., 1993)], the current measured through the external circuit can be related directly to the "gating" current within the protein, the integral of which is Q. Q may also be formally related to the excess free energy due to the applied TM voltage. It is then expressed as the product of the channel's charges by the fraction of the electric field that they traverse during the conformational change that the TM voltage induces (Nonner et al., 2004). Accordingly, in MD simulations, two independent routes can be used to estimate, Q.

Direct measurement or Q-route

Both the charge imbalance and the electric field MD setups enable one to monitor the gating charge, Q mimicking what is done in patch clamp experiments. With the charge imbalance method, if ionic conduction through the channel's pore is prevented, the movement of protein charges across the membrane capacitor is reflected directly by a change in the measured TM potential ΔV (Treptow et al., 2009). In practice, the gating charge, Q associated with the conformational change from state λ_1 to λ_2 can be written as:

$$Q = -\frac{1}{2}\left[q_0^{\text{protein}}(\lambda_2) - q_0^{\text{protein}}(\lambda_1)\right] \tag{2}$$

The TM voltage is related to the charge imbalance q_0 between the electrolytes through:

$$\Delta V = \frac{q_0}{AC} \tag{3}$$

in which q_0 arises from the contribution of both ions (q_0^{ion}) and of the protein (q_0^{Protein}), A is the membrane area and C the membrane capacitance. As C is constant for a channel/membrane system in the TM voltage range considered (Stefani et al., 1994; Treptow et al., 2009), this allows one to combine Eqs. 2 and 3 to express q_0^{Protein} as

$$q_0^{\text{protein}} = -q_0^{\text{ion}} + AC\Delta V \tag{4}$$

As q_0^{ion} is maintained fixed, variations in ΔV are then directly linked to the expression of the protein gating charge.

With the electric field method ensuring a constant ΔV value, it was shown that it is possible to monitor the capacitive charge flowing through the external circuit as in voltage clamp setups (Roux, 2008). To do so, one considers ensemble averages of the displacement charge, Q in conformational state λ under a TM voltage ΔV as:

$$\langle Q\rangle_{\lambda,\Delta V} = \left\langle \sum_{i=1}^{N} q_i \frac{z_i^u}{L_z} \right\rangle_{\lambda,\Delta V} \tag{5}$$

where L_z is the size of the simulation box along the normal to the bilayer, q_i the partial charge of atom i, and Z_i^u the unwrapped coordinate of atom i along the z axis.

Energetic formalism or W-route

In general, the total free energy of a system comprises an intrinsic contribution arising from the molecular environment, and another reflecting the coupling of the system to the applied TM potential ΔV. This second contribution may be linked to the gating charge, Q through:

$$Q = \frac{\Delta G(\lambda_2, \Delta V) - \Delta G(\lambda_1, \Delta V)}{\Delta V} \tag{6}$$

where $\Delta G(\lambda)$ is the excess free energy of the channel (in its conformation λ) due to ΔV. $\Delta G(\lambda)$ may be evaluated directly by summing over all charges the finite difference between two free energy perturbation calculations performed at two different TM voltages (Roux, 2008). However, such time-costly calculation may be avoided since $\Delta G(\lambda)$ can also be directly linked to the "electrical" distance (Sigworth, 1994; Lecar et al., 2003; Jogini and Roux, 2007) by:

$$\Delta G(\lambda, \Delta V) = G(\lambda, \Delta V) - G(\lambda, 0) = \Delta V \sum_i q_i \delta_i^{\lambda} \tag{7}$$

where the sum runs over all charges q_i of the channel and the "electrical distance" is given by:

$$\delta_i^{\lambda} = \frac{\partial}{\partial V}\varphi_i^{\lambda}\big|_{V=0} \tag{8}$$

with φ_i^{λ} the local EP at the charge location (Roux, 1997; Islas and Sigworth, 2001; Grabe et al., 2004). Here, in contrast to experiments, the contributions of individual residues of the protein to the total gating charge, and therefore their role in the voltage-sensing mechanism may be directly evaluated.

MOLECULAR INSIGHT INTO THE FUNCTION OF KV CHANNELS

The Kv1.2 X-ray crystal structure provided the MD community with a robust starting conformation to investigate, for the first time, the structural and dynamical properties of a mammalian K^+ selective VGCC (Long et al., 2005b), while previous investigations had relied on approximate homology models (Ranatunga et al., 2001; Capener and Sansom, 2002; Eriksson and Roux, 2002; Guy, 2002; Durell et al., 2004; Treptow et al., 2004). Naturally, the first studies have focused on elucidating the properties of the activated/open state derived from the crystal structure embedded in a model lipid bilayer mimicking the cell membrane. Such simulations have made it possible to describe in detail the environment of the positive charges of S4, with the goal to gain understanding in the voltage-sensing mechanism (Treptow and Tarek, 2006a; Jogini and Roux, 2007). Others studied the permeation mechanism and the origin of selectivity at the level of the pore. Such investigations were recently reviewed in (Jensen et al., 2010) and will not be discussed here.

Later, efforts were devoted to uncover the resting/closed state and ultimately, the mechanism of VSD deactivation linking the two states. To do so, two different strategies were adopted. The first consisted in building *ab initio* models of the closed/resting state of Kv1.2 by introducing constraints derived from experiments. After relaxation of this structure in a membrane/solution environment, the transition pathway was then deduced by comparing the resting state conformation with the initial activated one. The second strategy has been to "follow" the deactivation of the channel submitted to a hyperpolarized (closing) TM potential. Such a brute force approach required reaching time scales well above those accessible to standard simulations and was made possible only with the advent of large high performance computing (HPC) resources. Importantly, we will show that such an approach enabled the discovery of the early steps of the deactivation mechanism.

MOLECULAR DESCRIPTION OF KV1.2 THE ACTIVATED STATE

Details of the crystal structure

Preceding the first TM segment (S1), the N-terminus from each of the four subunits of the Kv1.2 channel come together to form an intracellular tetramerization (T1) domain. It is believed that this auxiliary subunit is very important as it enables contacts between the proteins of different cells. The T1 domain, of dimension $\sim$135 Å $\times$ 95 Å $\times$ 95 Å has an I_4 symmetry, the four-fold symmetry axis running through the center of the main pore, and extends by $\sim$30 Å in the direction perpendicular to the membrane.

As expected, the Kv1.2 pore domain is quite similar to the pore of the bacterial potassium channel KscA (Doyle et al., 1998). The tetrameric assembly of S5 and S6 forms an inverted teepee. As in other K channels, the pore domain is divided into two major regions: at the extracellular side, the selectivity filter (formed by the P-loop linking S5 and S6) controls the passage of ions and favors the transport of K^+ with respect to other ions whereas at the intracellular side, the gate defines the open and closed states of the channel. The inner helix of the pore (S6) contains the amino-acid sequence PVP at which the helix is kinked. This kink is thought to be important for coupling of the VSD to the gate and for the channel gating (del Camino et al., 2000; Beckstein et al., 2003; Domene et al., 2003). Based on the diameter of the pore at the bundle crossing ($\sim$12 Å), the pore was hypothesized to be in an open state.

The S1–S4 bundles form the VSDs and are organized in a manner that agree with previous experimental results (Broomand et al., 2003; Neale, 2003): the VSD of one subunit sits next to the pore domain of the adjacent subunit and the connection between the VSD and the pore of the same subunit is insured by an S4–S5 helical linker (**Figure 1**). The VSD, of which all the segments are oriented roughly perpendicular to the membrane plane, shows rather tight packing. As electron densities are weak in the VSD region, the backbones were easily identified as TM alpha helices but the side chains were not all resolved: most side chains are present in the model on S2, S4, and the S4–S5 linker but S1 and S3 were built as polyalanine helices. The loops connecting the helices were also omitted in the original structure model.

In Kv1.2, S4 bears six positively charged residues (R294, R297, R300, R303, K306, and R309, referred to hereafter as R1, R2, R3, R4, K5, and R6) and four negative charges are lining the interior

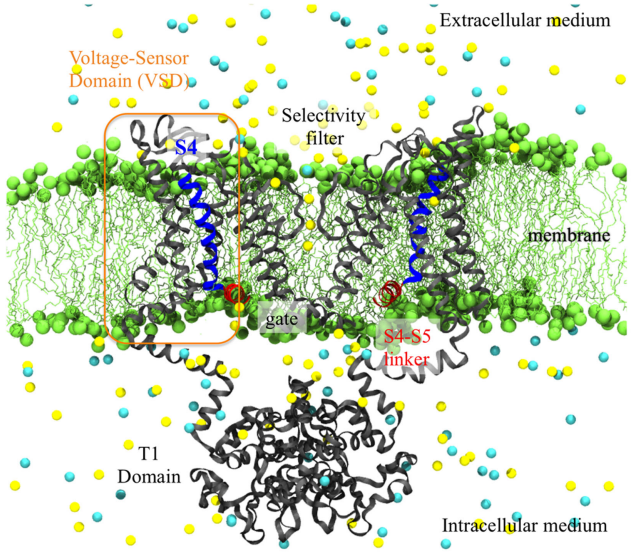

FIGURE 1 | Side view of the activated Kv1.2 (derived from the X-ray crystal structure) embedded in its membrane environment. The entire channel is represented as gray ribbons while the highly charged S4-helix is highlighted in blue and the S4–S5 linker in red. The lipid head groups of the membrane (green) and the ions (K^+ in yellow and Cl^- in cyan) of the solution are represented as spheres. The water molecules are not shown for clarity.

of the VSD (E183 on S1, E226 and E236 and S2 and D259 on S3). In a refined structure (Chen et al., 2010), as well as in a chimera (a Kv1.2 structure in which the S3b/S4 paddle was replaced by its equivalent in Kv2.1; Long et al., 2007), the conformations of side chains and the loops were later uncovered, enabling a better characterization of the VSD and of the salt bridge network stabilizing S4 in a TM orientation. In the refined structure, R3 is engaged in a salt bridge with E183, R4 with E226, K5 with D259 and R6 with E236, while R1 and R2 face the lipid head groups of the top bilayer. This conformation was recognized to correspond to an activated state of the VSD, in agreement with the open pore state.

The coupling between the VSD and the pore is posited to occur through the amphiphatic α-helix bridging between S4 of the VSD and S5 of the pore (S4–S5 linker). This linker is located along the pore, with its hydrophilic face facing the solution and hydrophobic face facing the hydrophobic core of the membrane. It crosses over the top of the S6 inner helix from the same subunit and makes many amino-acid contacts with it. The kink in the S6 helix makes the bottom half of S6 a "receptor" for this linker, which is thought to be involved mechanically in the channel closure mechanism.

MD simulations of the activated Kv1.2 structure

The first studies carried out by the modeling community following publication of the Kv1.2 activated structure were limited to the structural characterization of the channel relaxed in a model membrane/solution environment for a few nanoseconds. MD simulations of Kv1.2 in its membrane environment has indicated that the channel's gate (pore) at the motif is indeed large enough (pore radius >4.5 Å) to let ions through and that the conduction pathway seems to involve passing through the S1–T1 linkers. Along

the S6 segment, MD simulations have enabled the identification of V478 of the PVP motif as the residue constituting the main gate (Treptow and Tarek, 2006b).

At the level of the VSD domain, much effort was dedicated to the elucidation of the environment of the S4 basic residues. Indeed, the location of the S4-helix in a TM environment originally had been challenged because it required setting charges in a hydrophobic, energetically unfavorable environment. Several groups reconstructed the missing side chain residues of the original structure and observed the following properties: in the activated state, the two outermost positive charges of S4, R1, and R2, are turned toward the lipid head groups and seem to interact with them through an electrostatic interaction (Sands and Sansom, 2007). The remaining four charges, R3, R4, K5, and R6 are engaged in salt bridges with negative residues of the remainder of the VSD. Because water crevices protrude into the VSD from the intra- and the extracellular media, all the S4 basic residues lie in a solution environment, rationalizing the stability of S4 in a TM orientation (Freites et al., 2006; Treptow and Tarek, 2006a; Jogini and Roux, 2007; Nishizawa and Nishizawa, 2008; Krepkiy et al., 2009). Such a property also accounts for the focused electric field necessary to transport 12–14e during activation while the vertical translation of S4 remains of intermediate magnitude. Using continuum electrostatic computations, Jogini and Roux (2007) determined that the TM potential sensed by the S4 basic residues varies mostly over the outer part of the membrane ("focused electric field") while others find that the electric field is most focused in the inner region of the membrane (Treptow and Tarek, 2006a); a discrepancy that remains to be explained. Looking further at the interaction of a single VSD with the membrane using a CG model, Bond and Sansom (2007) found that the insertion of the protein leads to considerable local membrane deformation, mainly due to the interaction of S4 with the surrounding lipids. Such a property is proposed to participate to the focusing of the electric field. These results were later confirmed by neutron diffraction, solid-state nuclear magnetic resonance (NMR) spectroscopy and all-atom MD simulations (Krepkiy et al., 2009).

AB INITIO MOLECULAR MODELS OF THE KV1.2 CLOSED STATE

After the activated Kv1.2 structure was resolved, protocols were designed to develop a model of the resting state and to gain a complete view of the process associated with the response of the channel to depolarization. The first resting state model to be proposed was built on the basis of the ROSETTA Membrane *ab initio* structural modeling program (Yarov-Yarovoy et al., 2006). A candidate was selected using as constraints the experimentally probed distances between E226 (S2) and R1 and the exposure of two of the four potential gating charge-carrying arginines in S4 to the intracellular water-accessible environment, supposed to account for the 12–14e gating charge. In the gating mechanism derived from the comparison between this closed state model and the activated structure, S4 moves outwards by ∼3 Å and rotates clockwise ∼180° about its axis while the extracellular part of S4 changes its tilt angle from ∼10° to ∼45° relative to the membrane normal vector. The same modeling method was used by a different group, only introducing new experimental constraints derived from fluorescence scan data (Pathak et al., 2007). While the coarse features were similar, the models differ in that the activation now involves a vertical translation of S4 by 6–8 Å. Independently, Grabe et al. (2007) constructed a down state model of the channel using homology modeling with six pairs of interacting residues as structural constraints and verified this model by engineering suppressor mutations on the basis of spatial considerations. Tombola et al. (2006a) proposed yet another model of the resting conformation of the VSD of Kv1.2 that they tested using leak current measurements concomitant with S4 mutations (see next paragraph).

Recently, Clayton et al. (2008) solved the structure of MlotiK in its closed state. In this non-voltage-gated potassium-selective channel, uncharged residues replace the first four basic residues of S4, and two of the acidic countercharges are absent. The packing of the VSD domain as well as the interaction between the VSD and the pore seem to be quite different than the ones in VGCCs. Yet, this structure provides us with a good idea of what a closed Kv channel looks like, mostly in the pore region. Hence, models of the resting states of other channels (Hv1, NaChBac, and the plant KAT channel) have been derived from homology modeling methods, using among others, the MlotiK structure as templates (Shafrir et al., 2008; Schow et al., 2010; DeCaen et al., 2011; Wood et al., 2012). All these models bear similarities, as they place S4 inwards. The deactivation mechanisms derived involve a sliding helix motion for S4 while the bundle made of S1–S3 remains static. The details of the process, however, depend on the particular channel, with the S4 vertical translation ranging from 3 to 15 Å and its tilt from a few degrees to a much larger angle.

Han and Zhang (2008) were the first to relax the closed state model by Pathak et al. (2007) in a membrane environment using MD simulations. They observed differences in a variety of properties between the open and closed state channel (stability, environment of the S4 basic residues, salt bridge arrangements, and further interactions between the VSD and the pore), concluding that only the sliding helix model could enable going from one to the other state. Khalili-Araghi et al. (2010) then pushed the MD simulations further and measured the total gating charge associated with the activation of the channel. They revealed that in the down state, S4 had to be placed in a slightly lower position than originally proposed by Pathak et al. to reach a total $Q = 12$–14e transported across the membrane capacitor. As the applied electric field varies rapidly over a narrow region of 10–15 Å in the outer leaflet of the membrane, they confirmed that the gating charge could reach 12–14e without full translocation of S4 across the membrane.

IN SILICO VSD DEACTIVATION BY THE APPLICATION OF A TM POTENTIAL

Interestingly, even without applying a TM voltage, an early study using a coarse grained (CG) representation of the Kv1.2 (Treptow et al., 2008) revealed the first computationally induced conformational change of Kv1.2. Such a representation, in which few atoms are regrouped into one interaction center, allowed the simulation to reach time scales where large conformational changes could be sampled. The gating mechanism revealed suggested a downward movement of S4 combined with a lateral displacement of the S4–S5 linker acts on the gate to induce closure of the channel. Because of the low resolution of the method, results obtained with

CG force fields are only qualitative but they nevertheless gave first indications on the route followed by Kv1.2 to deactivate.

Fully atomistic MD simulations applying membrane hyperpolarization have been conducted recently mainly by three groups in order to observe directly the deactivation of the channel by "brute force." Two groups followed the protocol employed by Treptow et al. (2004) in a pioneering study of a homology model of Shaker. By submitting the system to an electric field, this simulation triggered a conformational response, including displacement of the S4-charges in response to a change in the TM voltage. Applying a strong electric field (0.1 V/nm) to an isolated Kv1.2 VSD (for 30 ns), Nishizawa and Nishizawa (2008) sampled a 6.7 Å displacement of S4 in a screw-like axial rotation, in which the S4 basic residues formed serial interactions with E183 (E0) and E226 (E1). The authors identified two intermediate states, which they found to be in good agreement with kinetic models such as the ZHA (Zagotta et al., 1994a) one. Their subsequent work brought more information on the coupling mechanism between VSD operation and gate closure/opening: this mechanism involves the S4–S5 linker, which brings S6 in its open/closed position through salt bridges between a positive charge at the end of S4 and a negative charge at the end of S6 (Nishizawa and Nishizawa, 2009).

The group of Lindahl carried out a long MD simulation (1 μs) of an entire Kv1.2 channel (Bjelkmar et al., 2009) submitted to a hyperpolarized potential. The response they described involved a large rotation of S4 (120°), changes in hydrogen bonding patterns and an extension of the 3_{10} helical stretch but almost no translation of S4. They implied that the final downwards translation that is necessary to complete the deactivation process is partly entropic explaining the slow nature of the process. The same authors continued by investigating the energetic cost of dragging S4 basic residues downwards when S4 is in a 3_{10} helical conformation compared to a α-helical one (Schwaiger et al., 2011). For the first transition toward the resting state, i.e., when R4 passes through the hydrophobic seal at the center of the VSD, the free energy is lower by about a factor of two with the 3_{10} helix conformation and leads to less distortion of the rest of the VSD; a finding that supports the hypothesis that S4 adopts a 3_{10} helix conformation during activation/deactivation (see next paragraph for more discussion).

Others have adopted the charge imbalance setup (see Methods in Molecular Dynamics Simulations; Denning et al., 2009; Treptow et al., 2009; Delemotte et al., 2011). Delemotte et al. (2011) have used an extensive 2.2 μs MD simulation of the membrane-bound Kv1.2 channel subject to a hyperpolarized potential to reveal the VSD response and reorganization during the initial steps of the channel deactivation. The conformational changes taking place within the VSD involved a zipper-like motion of the S4 basic residues in sequential ion pairing with nearby counter charges and lipid head groups from both the upper and lower membrane leaflets (**Figure 2**). This essential feature is in agreement with early mutagenesis experiments (Papazian et al., 1995; Tiwari-Woodruff et al., 2000; Zhang et al., 2005) and with the recent hypotheses from the groups of Cui and Catterall. The former probed the salt bridge interactions in the different states of Kv7.1 by charge reversal mutagenesis (Wu et al., 2010). The latter probed these interactions in NaChBac, a bacterial Nav channel, whose VSD is very similar to that of Kv, by disulfide locking (DeCaen et al., 2009) and showed indeed that, during activation, the S4 segment moves from an inward position to an outward position by forming sequentially state-dependent salt bridges (c.f. also Catterall, 2010).

Overall, the Delemotte et al. (2011) study has uncovered five states of the channel. In addition to the α (open) state and the two intermediate states (β, γ) arising from the unbiased MD trajectory, one more (δ) was identified resorting to biased MD simulations using so-called steered MD simulations (thus using additional forces to pull certain atoms in the desired direction) in which the imposed "reaction" pathway was consistent with the zipper-like motion (**Figure 2**). To further validate their resting state model of the VSD, the authors evaluated the gating charge associated with the transition from α to ε. The latter, computed using the direct measurement, is most appropriate to compare with electrophysiology measurements of the gating charge. It is associated with the whole channel deactivation. For the entire system, it amounts to $12.8 \pm 0.3e$ which is in good agreement with values obtained for Shaker-like channels (12–14e) in the 1990s (Schoppa et al., 1992; Aggarwal and MacKinnon, 1996; Seoh et al., 1996). Also, the position of S4 basic residues in the ε-state was checked by probing the effect of mutations of the arginines, R1 and R2 (see next paragraph). Importantly, the final down state (ε) arising from the

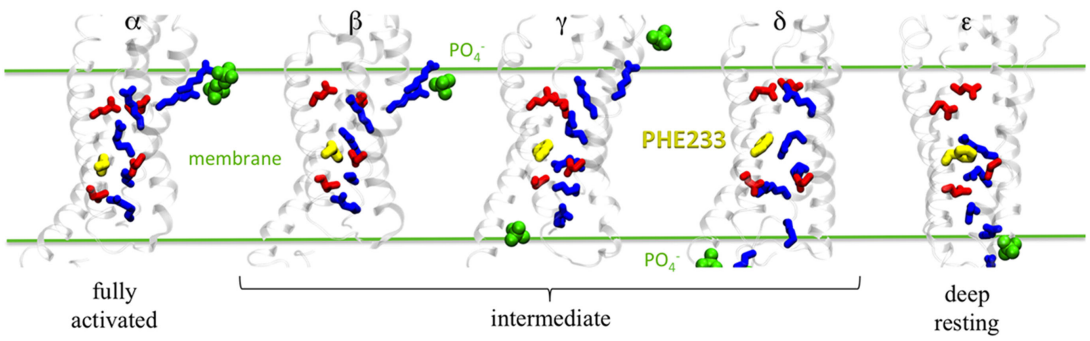

FIGURE 2 | Salt bridge network in each Kv1.2 conformation (α to ε). Basic residues are in blue and acidic residues in red. F233 is represented as yellow spheres and lipid PO_4^- groups within 6 Å of the basic residues are shown in green. Adapted from Delemotte et al. (2011).

biased MD bears similarities with the ones generated by *de novo* (*ab initio*) modeling (Tombola et al., 2005a; Pathak et al., 2007) or by further using restrained all-atom MD simulation of the channel embedded in a membrane environment to bias the conformation toward the hypothetical resting state (Khalili-Araghi et al., 2010; Vargas et al., 2011). Note however there is a difference between the resting state models proposed by the two groups concerning the position and orientation of R1, which is slightly different. The Delemotte et al. model places R1 in a lower position, i.e., close to D2 (D259), in agreement with recent (Tao et al., 2010) and subsequent work (Lin et al., 2011) placing R1 in the so-called catalytic center (c.f. below). The probable discrepancy from these two models comes from the fact that there are multiple closed, non-conductive states, as proposed in various kinetic models. The relative population of these states depends on the length and the magnitude of the hyperpolarizing pulse. The Khalili-Araghi model then likely represents the closed state that is most populated at a slightly less negative voltage, which may be referred to as a "penultimate closed state" as proposed by (Lin et al., 2011), while the Delemotte et al. (2011) model is reached only at more negative TM voltages, and in that sense is possibly a candidate for the "deep resting state."

The overall VSD activation mechanism proposed by Delemotte et al. (2011) is consistent with experiments and kinetic models devised to fit the curves of the gating current, which assume that activation of each of the VSDs proceeded in multiple sequential steps. Interestingly, the gating charge measured for each transition (∼0.45–1.2e per subunit) is of the same order of magnitude as the elementary charge movements estimated from measurements of gating current fluctuations (Sigworth, 1994) and as the "loose" charges, an early component of the gating current in Shaker channels (∼1e per VSD unit; Sigg et al., 2003), indicating that the intermediate states uncovered are of functional significance. Naturally, early models, e.g., the Zagotta–Hoshi–Aldrich model (Zagotta et al., 1994a) have considered a small number of states (a minimum of three was required for proper fitting). Later, other groups, extending the study to a broader voltage range, have proposed the same types of models, but introducing additional states (Baker et al., 1998; Schoppa and Sigworth, 1998; Zheng and Sigworth, 1998; Kanevsky and Aldrich, 1999; Loboda and Armstrong, 2001; Sigg et al., 2003). One of the most recent proposals suggested that the VSD can adopt five conformational states (Tao et al., 2010). This last investigation by Mackinnon and co-workers demonstrated indeed that the VSD transitions involve sequential passage of the S4 basic residues through a catalytic center involving the conserved F233 residue. This feature is captured in the five states (α to ε), in each of which a different basic residue occupies the gating charge transfer center. Furthermore, the unbiased MD simulation have clearly indicated the response of the four VSDs of the channel and particularly the intermediate transitions are not occurring simultaneously for all VSDs, in agreement with electrophysiology experiments that all indicate that only the final opening transition is concerted (Zagotta et al., 1994b).

Concerning the overall displacement of S4 which was subject to much debate in the literature, the overall conformational change from the active to the resting states of the VSD is shown in the Delemotte et al. (2011) study to necessitate a large displacement of the S4 backbone amounting to 10–15 Å, which is in closer agreement with estimates from avidin binding experiments (Ruta et al., 2005) than previous models (Catterall, 2010). Up to 2005, two main contradictory models were competing to describe VSD activation (Börjesson and Elinder, 2008): (1) the helical screw model, in which S4 moves independently from the rest of the VSD in a screw-like motion, involving a large translation of the latter by ∼10–20 Å while rotating about its own axis by 180°, advocated mostly by cysteine accessibility studies and disulfide scanning experiments and (2) the transporter model involving instead a large reorganization of the electric field in the vicinity of S4 with only a small overall displacement of S4, which had been put forward mostly to rationalize fluorescence measurements. Since then however, several attempts have been undertaken at reconciling these various views (Tombola et al., 2006b; Jogini and Roux, 2007; Pathak et al., 2007). It was claimed that all the experiments involving mutagenesis introduce an alteration of the structure, of the function and probably of the dynamics of the channel (Durell et al., 2004), and that all the fluorescence studies have a tendency to underestimate measured distances (Selvin, 2002). Also, avidin binding may lock the channel in extreme positions, which are scarcely visited otherwise, leading to overestimation of measured distances (Jiang et al., 2003b). Taking this into account, the molecular conformations of the transition states identified by the computational study of Delemotte et al. (2011) appear to be not only consistent with the sliding helix model, but also complying with most experiments, and thus likely provide a picture of the complete operation of the VSD.

In order to satisfy the charge pairing of the basic and acidic residues, some studies have suggested that the movement of S4 and particularly the passage of S4 through the catalytic center require the transitory switch of a stretch of S4 into a 3_{10} helix (DeCaen et al., 2009). Recent simulations have found results pointing toward this direction: Khalili-Araghi et al. (2010) found a spontaneous conversion of the 10 residue stretch of S4 located in the catalytic center into a 3_{10} helix in their Rosetta model of the resting state. The group of Lindahl (Bjelkmar et al., 2009) found an extension of 3_{10} helix stretch when submitting the open Kv1.2/2.1 paddle chimera channel to a hyperpolarized electric field. They further showed that the free energy of dragging S4 downward is much lower for the 3_{10} helix conformation (Schwaiger et al., 2011). Interestingly, Delemotte et al. (2011) simulations have shown that for one subunit, the short stretch around the residue transferring through the gating charge transfer center takes the form of a 3_{10} helix, for each of the four transitions. In contrast, all the other subunits underwent the four transitions without such secondary structure change. From this data, it is not clear therefore which mechanism would be most favorable from an energetic point of view and further investigations are needed before drawing firm conclusions. In addition, it is important to stress here that secondary structure stability and conformational changes are likely to be dependent on the force field used and interpretation of related data should be with caution (Yoda et al., 2004; Matthes and de Groot, 2009).

Perhaps the most interesting feature revealed by MD simulations and the analysis of the electrical activity of the channel is the finding that the cumulative gating charge transported by the S4 basic residues can be described by a unique sigmoidal function,

which defines the electromechanical coupling mechanism that the VSD charges undergo (Delemotte et al., 2011). As inferred by early MD studies, because water crevices protrude into the VSD from the intra- and the extracellular media, all the S4 basic residues lie in a solution environment. Such a shape ensures the presence of a focused electric field, which is required to transport 12–14e during activation without having to translate S4 vertically in an excessive manner (Freites et al., 2006; Treptow and Tarek, 2006a; Jogini and Roux, 2007; Nishizawa and Nishizawa, 2008; Krepkiy et al., 2009). However, while Jogini and Roux determined using continuum electrostatic computations that the TM potential sensed by the S4 basic residues varies mostly over the outer half of the membrane, Delemotte et al. (2011) found that such a variation is maximal at the level of the gating charge transfer center, just under the middle of the VSD. As mentioned earlier, the origin of this discrepancy is not yet understood. The former model agrees better with the fluorescence measurements from the Bezanilla lab (Asamoah et al., 2003), while the latter agrees better with the hypothesis of a charge transfer center within the hydrophobic plug (Tao et al., 2010). Note that in addition, and as importantly, Delemotte et al. (2011) show that the shape and intensity of the focused electric field is hardly modified during deactivation, thus invalidating the transporter model.

Though the ensemble of these results is specific to the VSD of the Kv1.2 channel, the coarse features can likely be generalized to other VGCCs. Also, when combined with electrophysiology measurements, they may allow a better characterization of the molecular mechanisms implicated in the modulation of these channels. Among others, for instance, one finds those implicating the interaction of VGCCs with their lipidic environment. Indeed, recent studies have shown that the presence or absence of the phosphate groups has a dramatic influence on VGCCs function: the activation of K^+ channels may indeed be suppressed when they are embedded in bilayers formed by cationic lipids (Schmidt et al., 2006). Removal of the lipid head groups by enzymes also results in an immobilization of the VSD motion, thereby inhibiting function (Ramu et al., 2006; Xu et al., 2008; Zheng et al., 2011). As inferred from electrophysiology experiments, MD simulations confirmed that lipids, and in particular their negatively charged phosphate head group moieties provide counter charges for the S4 basic residues, during the gating process. While earlier molecular models of the VSD (Bjelkmar et al., 2009; Treptow et al., 2009; Khalili-Araghi et al., 2010) have shown that lipids from the upper and lower bilayer leaflets stabilize, respectively the activated and resting states of the VSD, Delemotte et al. (2011) provided evidence that lipids are also crucial in stabilizing conformations of the intermediate states (**Figure 2**).

CHANNELOPATHIES ARISING FROM VSD MUTATIONS

Due to their ubiquity, genetic mutations in VGCCs give rise to a variety of inherited diseases, called channelopathies. Neuromuscular disorders were the first to be described but we now know that they can affect tissues of any excitable cell such as the heart. Moreover, one gene encoding a particular ion channel can suffer from various mutations, causing either the same disease, or a different one. For example, Kv7.1, encoded by the KCNQ1 gene and found in heart cells, has a total of 49 mutations that lead to 5 different phenotypes: long QT syndrome types 1 and 2, short QT syndrome, Jervell and Lange-Nielsen syndrome 1 or atrial fibrillation (listed in the Online Mendelian Inheritance in Man (OMIM) database). Usually these mutations can be spread throughout the ion channel sequence, in the VSD, the pore, or in the N- and C-termini domains, leading to molecular scale effects that should in principle be drastically different.

Here, we focus particularly on the mutations within the VSD, especially those affecting the S4 basic residues. Mutations of the charged residues of S4 in K^+, Na^+, or Ca^{2+} VGCCs have been shown to impair cellular function and have been linked to a number of inherited channelopathies leading to epilepsy, long QT syndrome, and paralyses (Lehmann-Horn and Jurkat-Rott, 1999). Most of these mutations modify the physical properties of VGCCs, e.g., sensitivity to voltage changes, which in turn alters conduction through the central (alpha) pore (Bao et al., 1999; Jurkat-Rott et al., 2000; Soldovieri et al., 2007). Recently, however, specific mutations have been identified that lead to the appearance of another current component aside from the alpha conduction. In Shaker for instance, such so-called "omega" or gating-pore current was attributed to a non-specific leakage of cations through a conduction pathway within the VSD, indicating that R1 in the S4 segment sterically hinders ion passage through the gating-pore (Tombola et al., 2005b). Substitution of the latter in the VSD by histidine, R1H, allows a H^+ current to flow at hyperpolarized potentials (Starace and Bezanilla, 2004), while a R4H mutant allows a proton flux at depolarized potentials (Starace and Bezanilla, 2001). Moreover, mutations of R1 into smaller, uncharged residues give rise to an influx of a non-selective cation current, called "omega current," through an unidentified pathway through the VSD (Tombola et al., 2006a). Interestingly, it seems that such mutants may have also evolved into "useful" channels: A member of the Kv3 family was identified in a flatworm, N.at-Kv3.2, which has an inward rectifier phenotype, and in which two S4 basic residues are replaced by neutral amino-acids. It was shown that this channel mediates ion permeation through the modified gating (omega) pore, yielding qualitatively different ion permeability when compared to all other members of this gene family (Klassen et al., 2008).

In Na^+ VGCCs, omega currents were correlated with mutations that cause normo- and hypo-kalemic periodic paralysis (Sokolov et al., 2005, 2007, 2008; Struyk and Cannon, 2007). Interestingly, in such a channel, it was shown that the mutation of residues R2 or R3 in one of the four S4 helices allows an influx of cations through the omega pore in a state-dependent manner: the omega current is observed only when the channel is in its hyperpolarized conformation. Under depolarization, the omega pore closes and the canonical ion-selective pore opens.

In the following, we show how the study of mutations via MD simulations performed both for the open and closed conformations of Kv1.2, which serves as a prototype for the entire Kv family, can unveil the elementary molecular processes involved in the omega currents detected by electrophysiology.

MD SIMULATIONS OF THE EFFECTS OF VSD S4 MUTATIONS

In Kv1.2, no "natural" mutations of S4 basic residues were shown to give rise to channelopathies. To take advantage of the molecular

conformations at hand, Delemotte et al. (2010) designed artificial mutants (double and single mutants) that enabled them to use Kv1.2 as a prototype to study the effect of S4 basic mutations. Two key conformations of the channel were considered: the first corresponds to the X-ray crystal structure of the open channel, the aforementioned α state (Long et al., 2005a), while the other corresponds to the closed state, in which the VSD has the resting conformation (conformation ε). Interestingly, in both conformations, the topology of the VSD has shared characteristics: whereas the salt bridge network between the basic residues of S4 and acidic residues of the S1–S3 bundle is state-dependent, the solvent-accessible volume has the shape of an hourglass. The constriction, i.e., the region of lowest diameter, where diffusion of water is shown to be hampered, is located around the salt bridge that involves D259 (and R1 in the closed and K5 in the open state). Such a shape was described also in independent work (Bezanilla, 2005; Sokolov et al., 2005; Treptow and Tarek, 2006a; Krepkiy et al., 2009).

Accordingly, to investigate leak currents through the VSD, Delemotte et al. (2010) chose to mutate one or two residues around the constriction. Mutants away from the constriction were used as controls. As expected, several MD simulations showed that the mutation of the residues (to their uncharged homolog) not involved in the water constriction does not change the overall topology of the VSD. The salt bridge in which the residue is involved is indeed broken, but the interaction being away from the constriction, the VSD retains its hourglass like shape. In contrast, mutation of residues involved in the constriction, i.e., that of K5 in the open structure and that of R1 in the closed one opens up in each case a hydrophilic path (omega pore), drastically changing the topology of the VSD (**Figure 3**).

Submitting each of these mutants to TM potentials using explicit ion dynamics showed that the hydrophilic pathway within the VSD of the closed state is permeable to K^+cations. In agreement with experiments on the other hand, in the open state K5 mutant, only a partial conduction event was witnessed. Due to the neutralization of basic residues, the resulting omega pore contains an excess of negative charge (one or more glutamates). Accordingly, the K^+ diffusion followed a jump diffusion model in which the acidic residues serve as binding sites, and in agreement with experiments (Gamal El-Din et al., 2010), despite the presence of chloride ions in the electrolyte baths, the omega pores were selective to cations. Repetition of permeation events and transposition to physiological conditions (TM voltage ∼100 mV and ionic concentration ∼100 mM) enabled evaluation of the leak conductance $\sim 10^6$ ions/s, which is over one order of magnitude below the alpha currents ($\sim 10^7$ ions/s).

Recently, Khalili-Araghi et al. (2012) studied the same type of mutations in their model of the resting state of Kv1.2, where R1 is in interaction with E1 of S2. Simulation of four mutants (R1S, R1N, E1D-R1N, and E1D-R1S) under a depolarized TM voltage indicates a similar process: K^+ ions are transported stochastically, more favorably than Cl^- ions, due to the presence of a negatively charged constriction in the mutated VSD. The need to resort to double mutants to achieve more conduction than in the WT VSD, however, is in disagreement with experimental data (Tombola et al., 2005b; Gamal El-Din et al., 2010) and may indicate

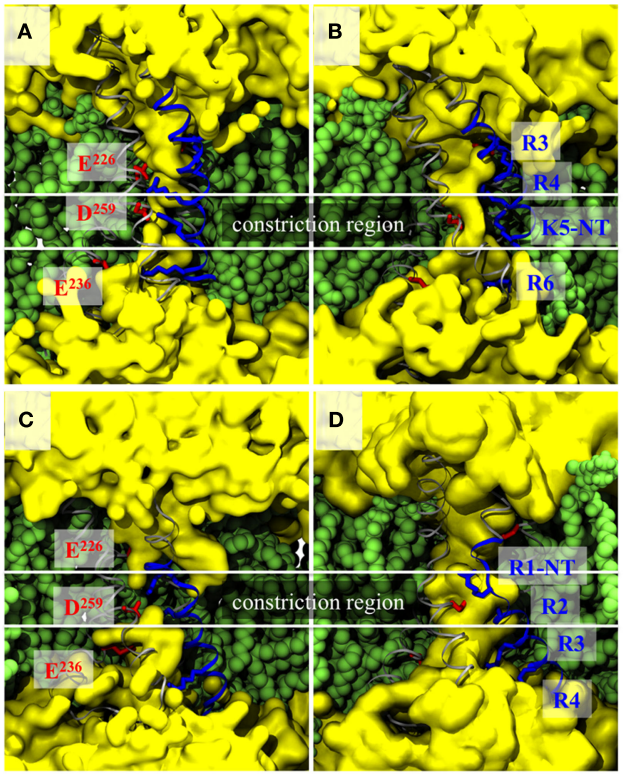

FIGURE 3 | VSD topologies of the activated (A,B) and resting (C,D) states of the Kv1.2 VSDs before mutation, i.e., in the wild-type channel (A,C) and after mutation of a single residue, i.e., K5 in the activated (B) and R1 in the resting (D) state. Representations and colors are the same as in **Figure 2**. The water is represented as a continuous surface (yellow) and highlights the presence of a constriction in the WT VSDs and not in the mutants.

(as also discussed in In silico VSD Deactivation by the Application of a TM Potential) that the Khalili-Araghi et al. resting state model is a "penultimate" closed state rather than a fully resting closed state (Lin et al., 2011).

RELATIONSHIP TO DISEASES

The results from MD simulations may be summarized as follows: at rest, VGCCs are in a closed non-conducting conformation and S4 is in the so-called "down" state. Within the VSD, the salt bridges that maintain the constriction between the intra- and extracellular water crevices involve the top S4 residues and only their mutation leads to omega currents (**Figure 4**, top). Under depolarized TM potentials, S4 positive residues are dragged upwards (S4 moves to the "up" state) and the VGCCs adopt the open conformation. Within the VSD, the bottom S4 basic residues become critical in maintaining the constriction (Tombola et al., 2005b; Nishizawa and Nishizawa, 2008). Accordingly, mutations of the latter destabilize the VSDs and lead to omega currents (**Figure 4**, bottom). Hence, mutations of the S4 basic residues give rise to state-dependent omega currents. Overall, these results are consistent with experiments showing that (1) mutations (synthetic or genetic) of the S4 top basic

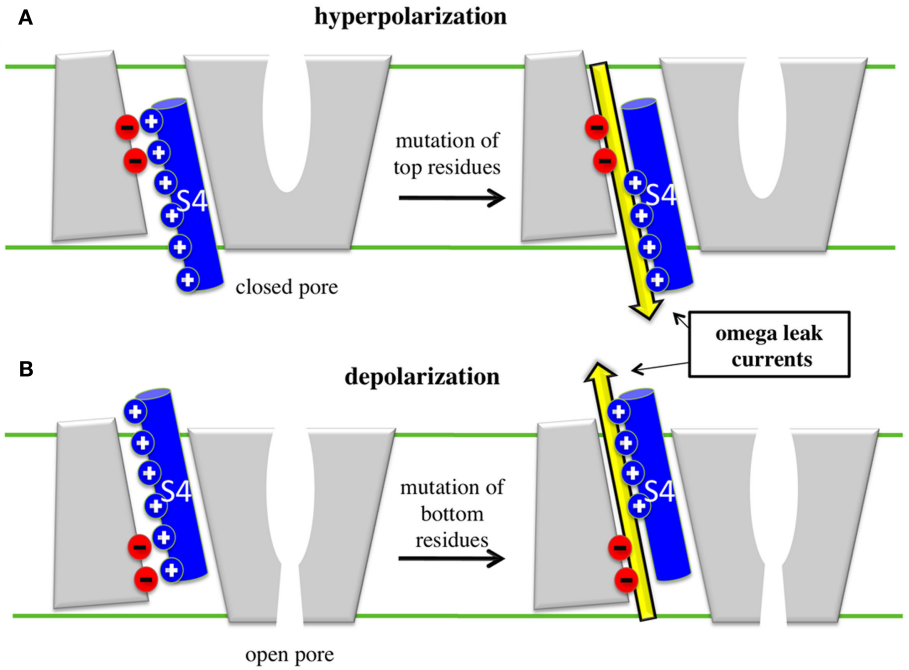

FIGURE 4 | Cartoon representation of the appearance of omega leaks. **(A)** Under hyperpolarized potentials, when the VSD is in its resting position, mutation of top residues give rise to omega currents, which then represent an inward cation leak (yellow arrow). **(B)** Under depolarized potentials, when the VSD is activated, mutation of bottom residues gives rise to outward omega currents.

residues of the Na^+ VGCCs Nav1.2a (Sokolov et al., 2005) and Nav1.4 (Sokolov et al., 2007) and of Shaker channels (Tombola et al., 2005b) lead to inward omega currents under hyperpolarized potentials and (2) mutations of the S4 bottom basic residues of Nav1.2a (Sokolov et al., 2005) and Nav1.4 (Sokolov et al., 2008) lead to outward omega currents under depolarized potentials.

In VGCCs, the positive residues of S4 are the main sensors of the TM voltage and are directly implicated in the conformational changes of the VSD, which control switching (gating) of the channels from open to closed conformations (Schoppa et al., 1992; Seoh et al., 1996). A mutation of any S4 basic residue alters the sensitivity of the channels and modifies their gating kinetics as shown for several VGCCs. In Kv1.2. Delemotte et al. (2010) have identified the mutations that are critical for the stability of α and ε VSD conformations, and determined in which conformational state these mutations give rise to omega currents. Under hyperpolarized TM potentials, omega currents affect directly the channel's function since they constitute a leak through a closed channel supposedly impermeable to ions. Quite interestingly, most mutations associated with genetic diseases, e.g., epilepsy, hypo- or hyper-kalemic periodic paralysis, or long QT syndrome fall in this category. Under depolarized TM potentials, VGCCs are open and omega currents are a mere modulation of the main alpha current (the omega pore conductance is ∼2 orders of magnitude lower than the alpha pore conductance (Sokolov et al., 2005, 2007, 2008). Such small conductance must however have a more dramatic consequence on VGCCs that undergo N-type inactivation – i.e., become non-conductive under extended depolarized potentials – as shown for Nav1.4, for which omega leak currents were implicated in NormoPP symptoms (Sokolov et al., 2008).

To generalize these results to other members of the large VGCC family (Nav, Cav, and Kv), however, more structural data is required. Indeed, whereas the general characteristics of omega conduction should be similar in other more or less homologous channels, a more precise knowledge of the salt bridge network within each conformation of the VSD, and therefore of the location of the constriction, is necessary to enable identification of the mutations that would give rise to omega currents. Finally, although the appearance of an omega current is the easiest effect of S4 mutations to characterize using MD simulations, one should recall that it is most likely not the only effect of such mutations. Indeed, mutating such charges probably results in the alteration of the response of the VSD to TM voltage change, as manifested by shifts in G/V and Q/V curves and modified kinetics of ON and OFF currents (Miceli et al., 2008). To explain the molecular origin of such experimental observations, it would be most insightful to compare the free energy surface of activation/deactivation of the WT and of the mutants, which requires sophisticated MD simulations protocols (Hénin and Chipot, 2004; Maragliano et al., 2006; Laio and Gervasio, 2008).

CONCLUSION

Since the release of the first crystal structure of a mammalian voltage gated K^+ channel, Kv1.2 in 2005, theoretical and computational methods have been used to gain insights into the molecular level function of these ubiquitous proteins. The focus of this review has been directed at the specific contribution from MD

simulations to advance our understanding of the function and modulation of the VSD.

Starting from the open/activated state crystal structure, we have presented different protocols that have been devised to uncover the resting/closed state structure and, in some occurrences, the conformation of kinetic intermediate states. We have shown how these models may be tested and validated against experimental data such as the gating charge value, molecular contacts, etc. and how such molecular level insights may help reconcile diverging views derived from different sets of experimental data. We have then shown how the availability of these computational-based models has enable done to tackle questions with direct biological or pharmacological implication, i.e., to look into the molecular details of the appearance of leak currents, which follow from genetic mutations involved in inherited diseases.

Since it seems unlikely that a crystal structure of the closed state will be resolved in the near future, results from computational methods, in combination with the ones from all other experimental techniques, are crucial to gain a molecular level picture of the entire activation/deactivation cycle. As ever, larger computer resources become available, the accessible time scale will exceed the millisecond domain. Thus the day where a complete brute force MD calculation will uncover the entire deactivation/activation pathway is not so far away; an event that will finally bridge the gaps between the results from the different studies described in this review.

Finally, as a crystal structure of the first bacterial voltage-gated Na^+ channel was released last year (Payandeh et al., 2011), modelers have already started to take a serious interest in unraveling the structure/function behavior of Na^+ selective channels (Carnevale et al., 2011; Corry and Thomas, 2011). Such an achievement opens up a whole new world that should enable, together with the results on voltage-gated K^+ channels, to explain the basis of cellular excitability at a molecular level.

ACKNOWLEDGMENTS

We thank Werner Treptow for his collaboration and input on the ion channels studies we carried out. This work was performed using HPC resources from GENCI-CINES (grant No. c2010075137, c2011075137, c2011076742).

NOTE ADDED IN PROOF

A recent paper by Jensen et al. (2012) reports on an impressive over 200 μs MD simulation of Kv1.2 channel switching between deactivated and activated states, that quite interestingly confirms essentially all the findings of Delemotte et al. (2010, 2011).

REFERENCES

Aggarwal, S. K., and MacKinnon, R. (1996). Contribution of the S4 segment to gating charge in the Shaker K+ channel. *Neuron* 16, 1169–1177.

Aksimentiev, A., and Schulten, K. (2005). Imaging a-hemolysin with molecular dynamics: ionic conductance, osmotic permeability, and the electrostatic potential map. *Biophys. J.* 88, 3745–3761.

Allen, M. P., and Tildesley, D. J. (1987). *Computer Simulation of Liquids.* Oxford: Clarendon Press.

Armstrong, C. M., and Bezanilla, F. (1973). Currents related to movement of the gating particles of the sodium channels. *Nature* 242, 459–461.

Asamoah, O. K., Wuskell, J. P., Loew, L. M., and Bezanilla, F. (2003). A fluorometric approach to local electric field measurements in a voltage-gated ion channel. *Neuron* 37, 85–97.

Baker, O., Larsson, H., Mannuzzu, L., and Isacoff, E. (1998). Three transmembrane conformations and sequence-dependent displacement of the S4 domain in Shaker K channel gating. *Neuron* 20, 1283–1294.

Bao, H., Hakeem, A., Henteleff, M., Starkus, J. G., and Rayner, M. D. (1999). Voltage-insensitive gating after charge-neutralizing mutations in the S4 segment of Shaker channels. *J. Gen. Physiol.* 113, 139–151.

Beckstein, O., Biggin, P. C., Bond, P., Bright, J. N., Domene, C., Grottesi, A., Holyoake, J., and Sansom, M. S. P. (2003). Ion channel gating: insights via molecular dynamics. *FEBS Lett.* 555, 85–90.

Bezanilla, F. (2005). The voltage-sensor structure in a voltage-gated ion channel. *Trends Biochem. Sci.* 30, 166–168.

Bjelkmar, P., Niemelä, P. S., Vattulainen, I., and Lindahl, E. (2009). Conformational changes and slow dynamics through microsecond polarized atomistic molecular simulation of an integral Kv1.2 ion channel. *PLoS Comput. Biol.* 5, e1000289. doi:10.1371/journal.pcbi.1000289

Bond, P. J., Holyoake, J., Ivetac, A., Khalid, S., and Sansom, M. S. (2007). Coarse-grained molecular dynamics simulations of membrane proteins and peptides. *J. Struct. Biol.* 157, 593–605.

Bond, P. J., and Sansom, M. S. P. (2007). Bilayer deformation by the Kv channel voltage sensor domain revealed by self-assembly simulations. *Proc. Natl. Acad. Sci. U.S.A.* 104, 2631–2636.

Börjesson, S. I., and Elinder, F. (2008). Structure, function, and modification of the voltage sensor in voltage-gated ion channels. *Cell Biochem. Biophys.* 52, 149–174.

Bostick, D., and Berkowitz, M. L. (2003). The implementation of slab geometry for membrane-channel molecular dynamics simulations. *Biophys. J.* 85, 97–107.

Broomand, A., Männikkö, R., Larsson, P., and Elinder, F. (2003). Molecular movement of the voltage sensor in a K channel. *J. Gen. Physiol.* 122, 741–748.

Capener, C. E., and Sansom, M. S. P. (2002). Molecular dynamics simulations of a K+ channel model: sensitivity to changes in ions, waters, and membrane environment. *J. Phys. Chem.* 106, 4543–4551.

Carnevale, V., Treptow, W., and Klein, M. L. (2011). Sodium ion binding sites and hydration in the lumen of a bacterial ion channel from molecular dynamics simulations. *J. Phys. Chem. Lett.* 2, 2504–2508.

Case, D. A., Pearlman, D. A., Caldwell, J. W., Cheatham, T. E. III, Ross, W. S., Simmerling, C. L., Darden, T. A., Merz, K. M., Stanton, R. V., and Cheng, A. L. (1999). *AMBER6.* San Francisco: University of California.

Catterall, W. A. (2010). Ion channel voltage sensors: structure, function, and pathophysiology. *Neuron* 67, 915–928.

Chen, X., Wang, Q., Ni, F., and Ma, J. (2010). Structure of the full-length Shaker potassium channel Kv1. 2 by normal-mode-based X-ray crystallographic refinement. *Proc. Natl. Acad. Sci. U.S.A.* 107, 11352.

Clayton, G., Altieri, S., Heginbotham, L., Unger, V., and Morais-Cabral, J. (2008). Structure of the transmembrane regions of a bacterial cyclic nucleotide-regulated channel. *Proc. Natl. Acad. Sci. U.S.A.* 105, 1511–1515.

Corry, B., and Thomas, M. (2011). Mechanism of ion permeation and selectivity in a voltage gated sodium channel. *J. Am. Chem. Soc.* 134, 1840–1846.

Crozier, P. S., Henderson, D., Rowley, R. L., and Busath, D. D. (2001). Model channel ion currents in NaCl extended simple point charge water solution with applied-field molecualr dynamics. *Biophys. J.* 81, 3077–3089.

DeCaen, P. G., Yarov-Yarovoy, V., Scheuer, T., and Catterall, W. A. (2011). Gating charge interactions with the S1 segment during activation of a Na+ channel voltage sensor. *Proc. Natl. Acad. Sci. U.S.A.* 108, 18825–18830.

DeCaen, P. G., Yarov-Yarovoy, V., Sharp, E. M., Scheuer, T., and Catterall, W. A. (2009). Sequential formation of ion pairs during activation of a sodium channel voltage sensor. *Proc. Natl. Acad. Sci. U.S.A.* 106, 22498.

del Camino, D., Holmgren, M., Liu, Y., and Yellen, G. (2000). Blocker protection in the pore of a voltage-gated K+ channel and its structural implications. *Nature* 403, 321–325.

Delemotte, L., Dehez, F., Treptow, W., and Tarek, M. (2008). Modeling membranes under a transmembrane potential. *J. Phys. Chem. B* 112, 5547–5550.

Delemotte, L., and Tarek, M. (2012). Molecular dynamics simulations of lipid membranes

electroporation. *J. Memb. Biol.* doi:10.1007/s00232-012-9434-6

Delemotte, L., Tarek, M., Klein, M. L., Amaral, C., and Treptow, W. (2011). Intermediate states of the Kv1.2 voltage sensor from atomistic molecular dynamics simulations. *Proc. Natl. Acad. Sci. U.S.A.* 108, 6109–6114.

Delemotte, L., Treptow, W., Klein, M. L., and Tarek, M. (2010). Effect of sensor domain mutations on the properties of voltage-gated ion channels: molecular dynamics studies of the potassium channel Kv1.2. *Biophys. J.* 99, L72–L74.

Denning, E. J., Crozier, P. S., Sachs, J. N., and Woolf, T. B. (2009). From the gating charge response to pore domain movement: initial motions of Kv1.2 dynamics under physiological voltage changes. *Mol. Membr. Biol.* 26, 397–421.

Devane, R., Shinoda, W., Moore, P. B., and Klein, M. L. (2009). A transferable coarse grain nonbonded interaction model for amino acids. *J. Chem. Theory. Comput.* 5, 2115–2124.

Domene, C., Haider, S., and Sansom, M. S. P. (2003). Ion channel structures: a review of recent progress. *Curr. Opin. Drug Discov. Devel.* 6, 611–619.

Doyle, D. A., Cabral, J. M., Pfuetzner, R. A., Kuo, A., Gulbis, J. M., Cohen, S. L., Chait, B. T., and MacKinnon, R. (1998). The structure of the potassium channel: molecular basis of K+ conduction and selectivity. *Science* 280, 69–77.

Durell, S. R., Shrivastava, I. H., and Guy, H. R. (2004). Models of the structure and voltage-gating mechanism of the Shaker K+ channel. *Biophys. J.* 87, 2116–2130.

Eriksson, M. A. L., and Roux, B. (2002). Modeling the structure of Agitoxin in complex with the Shaker K+ channel: a computational approach based on experimental distance restraints extracted from thermodynamic mutant cycles. *Biophys. J.* 83, 2595–2609.

Freites, J. A., Tobias, D. J., and White, S. H. (2006). A voltage-sensor water pore. *Biophys. J.* 91, L90–L92.

Frenkel, D., and Smit, B. (2002). *Molecular Simulations – From Algorithms to Applications*, 2nd Edn. Salt Lake City: Academic Press.

Gamal El-Din, T. M., Heldstab, H., Lehmann, C., and Greeff, N. G. (2010). Double gaps along Shaker S4 demonstrate omega currents at three different closed states. *Channels (Austin)* 4, 93–100.

Grabe, M., Lai, H. C., Jain, M., Jan, Y. N., and Jan, L. Y. (2007). Structure prediction for the down state of a potassium channel voltage sensor. *Nature* 445, 550–553.

Grabe, M., Lecar, H., Jan, Y. N., and Jan, L. Y. (2004). A quantitative assessment of models for voltage-dependent gating ion channels. *Proc. Natl. Acad. Sci. U.S.A.* 101, 17640–17645.

Gumbart, J., Khalili-Araghi, F., Sotomayor, M., and Roux, B. (2012). Constant electric field simulations of the membrane potential illustrated with simple systems. *Biochim. Biophys. Acta* 1818, 294–302.

Gurtovenko, A. A., and Vattulainen, I. (2005). Pore formation coupled to ion transport through lipid membranes as induced by transmembrane ionic charge imbalance: atomistic molecular dynamics study. *J. Am. Chem. Soc.* 127, 17570–17571.

Guy, H. R. (2002). Computational simulations of peptide binding to proteins: how scorpions sting K+ channels. *Biophys. J.* 83, 2325–2326.

Han, M., and Zhang, J. Z. H. (2008). Molecular dynamic simulation of the Kv1.2 voltage-gated potassium channel in open and closed state conformations. *J. Phys. Chem. B* 112, 6966–16974.

Hénin, J., and Chipot, C. (2004). Overcoming free energy barriers using unconstrained molecular dynamics simulations. *J. Chem. Phys.* 121, 2904–2914.

Hille, B. (2001). *Ion Channels of Excitable Membranes*, 3rd Edn. Sunderland: Sinauer Associates.

Islas, L. D., and Sigworth, F. J. (2001). Electrostatic and the gating pore of Shaker potassium channels. *J. Gen. Physiol.* 117, 69–89.

Jensen, M. Ø., Borhani, D. W., Lindorff-Larsen, K., Maragakis, P., Jogini, V., Eastwood, M. P., Dror, R. O., and Shaw, D. E. (2010). Principles of conduction and hydrophobic gating in K+ channels. *Proc. Natl. Acad. Sci. U.S.A.* 107, 5833–5838.

Jensen, M. Ø., Jogini, V., Borhani, D. W., Leffler, A. E., Dror, R. O., and Shaw, D. E. (2012). Mechanism of voltage gating in potassium channels. *Science* 336, 229–233.

Jiang, Y., Lee, A., Chen, J., Ruta, V., Cadene, M., Chait, B. T., and MacKinnon, R. (2003a). X-ray structure of a voltage-dependent K+ channel. *Nature* 423, 33–41.

Jiang, Y., Ruta, V., Chen, J., Lee, A., and MacKinnon, R. (2003b). The principle of gating charge movement in a voltage-dependent K+ channel. *Nature* 423, 42–48.

Jogini, V., and Roux, B. (2007). Dynamics of the Kv1. 2 voltage-gated K+ channel in a membrane environment. *Biophys. J.* 93, 3070–3082.

Jurkat-Rott, K., Mitrovic, N., Hang, C., Kouzmekine, A., Iaizzo, P., Herzog, J., Lerche, H., Nicole, S., Vale-Santos, J., Chauveau, D., Fontaine, B., and Lehmann-Horn, F. (2000). Voltage-sensor sodium channel mutations cause hypokalemic periodic paralysis type 2 by enhanced inactivation and reduced current. *Proc. Natl. Acad. Sci. U.S.A.* 97, 9549–9554.

Kandasamy, S. K., and Larson, R. G. (2006). Cation and anion transport through hydrophilic pores in lipid bilayers. *J. Chem. Phys.* 125, 074901.

Kanevsky, M., and Aldrich, R. W. (1999). Determinants of voltage-dependent gating and open-state stability in the S5 segment of Shaker potassium channels. *J. Gen. Physiol.* 114, 215–242.

Keynes, R. D., and Rojas, E. (1974). Kinetics and steady-state properties of the charged system controlling sodium conductance in the squid giant axon. *J. Gen. Physiol.* 239, 393–434.

Khalfa, A., Treptow, W., Maigret, B., and Tarek, M. (2009). Self assembly of peptides near or within membranes using coarse grained MD simulations. *Chem. Phys.* 358, 161–170.

Khalili-Araghi, F., Jogini, V., Yarov-Yarovoy, V., Tajkhorshid, E., Roux, B., and Schulten, K. (2010). Calculation of the gating charge for the Kv1.2 voltage-activated potassium channel. *Biophys. J.* 98, 2189–2198.

Khalili-Araghi, F., Tajkhorshid, E., Roux, B., and Schulten, K. (2012). Molecular dynamics investigation of the ω-current in the Kv1.2 voltage sensor domains. *Biophys. J.* 102, 258–267.

Klassen, T. L., Spencer, A. N., and Gallin, W. J. (2008). A naturally occurring omega current in a Kv3 family potasium channel from a platyhelminth. *BMC Neurosci.* 9, 52–64. doi:10.1186/1471-2202-9-52

Krepkiy, D., Mihailescu, M., Freites, J. A., Schow, E. V., Worcester, D. L., Gawrisch, K., Tobias, D. J., White, S. H., and Swartz, K. J. (2009). Structure and hydration of membranes embedded with voltage-sensing domains. *Nature* 462, 473–479.

Kutzner, C., Grubmüller, H., de Groot, B. L., and Zachariae, U. (2011). Computational electrophysiology: the molecular dynamics of ion channel permeation and selectivity in atomistic detail. *Biophys. J.* 101, 809–817.

Laio, A., and Gervasio, F. L. (2008). Metadynamics: a method to simulate rare events and reconstruct the free energy in biophysics, chemistry and material science. *Rep. Prog. Phys.* 71, 126601.

Leach, A. R. (2001). *Molecular Modeling – Principles and Applications*, 2nd Edn. Upper Saddle River: Pearson Education Limited.

Lecar, H., Larsson, H. P., and Grabe, M. (2003). Electrostatic model of S4 motion in voltage-gated ion channels. *Biophys. J.* 85, 2854–2864.

Lehmann-Horn, F., and Jurkat-Rott, K. (1999). Voltage-gated ion channels and hereditary disease. *Physiol. Rev.* 79, 1517.

Lin, M. A., Hsieh, J.-Y., Mock, A. F., and Papazian, D. M. (2011). R1 in the Shaker S4 occupies the gating charge transfer center in the resting state. *J. Gen. Physiol.* 138, 155–163.

Loboda, A., and Armstrong, C. M. (2001). Resolving the gating charge movement associated with late transitions in K channel activation. *Biophys. J.* 81, 905–916.

Long, B. S., Campbell, E. B., and Mackinnon, R. (2005a). Voltage sensor of Kv1.2: Structural basis of electromechanical coupling. *Science* 309, 903–908.

Long, B. S., Campbell, E. B., and MacKinnon, R. (2005b). Crystal structure of a mammalian voltage-dependent Shaker family K+ channel. *Science* 309, 897–903.

Long, S. B., Tao, X., Campbell, E. B., and MacKinnon, R. (2007). Atomic structure of a voltage-dependent K+ channel in a lipid membrane-like environment. *Nature* 450, 376–382.

MacKerell, J. A. D., Bashford, D., Bellott, M., Dunbrack, R. L., Evanseck, J. D., Field, M. J., Fischer, S., Gao, J., Guo, H., Ha, S., Joseph-McCarthy, D., Kuchnir, L., Kuczera, K., Lau, F. T. K., Mattos, C., Michnick, S., Ngo, T., Nguyen, D. T., Prodhom, B., Reiher, W. E., Roux, B., Schlenkrich, M., Smith, J. C., Stote, R., Straub, J., Watanabe, M., Wiorkiewicz-Kuczera, J., Yin, D., and Karplus, M. (1998). All-atom empirical potential for molecular modeling and dynamics studies of proteins. *J. Phys. Chem. B* 102, 3586–3616.

Maragliano, L., Fischer, A., Vanden-Eijnden, E., and Ciccotti, G. (2006). String method in collective variables:

minimum free energy paths and isocommittor surfaces. *J. Chem. Phys.* 125, 024106–24115.

Marrink, S. J., Risselda, H. J., Yelfinov, S., Tieleman, D. P., and de Vries, A. H. (2007). The MARTINI force field: coarse grained model for biomolecular simulations. *J. Phys. Chem. B* 111, 7812–7824.

Martyna, G. J., Tuckerman, M. E., and Klein, M. L. (1992). Nosé-hoover chains: the canonical ensemble via continuous dynamics. *J. Chem. Phys.* 97, 2635–2643.

Matthes, D., and de Groot, B. L. (2009). Secondary structure propensities in peptide folding simulations: a systematic comparison of molecular mechanics interaction schemes. *Biophys. J.* 97, 599–608.

Miceli, F., Soldovieri, M. V., Hernandez, C. C., Shapiro, M. S., Annunziato, L., and Taglialatela, M. (2008). Gating consequences of charge neutralization of arginine residues in the S4 segment of Kv7.2, an epilepsy-linked K+ channel subunit. *Biophys. J.* 95, 2254–2264.

Mokrab, Y., and Sansom, M. S. P. (2011). Interaction of diverse voltage sensor homologs with lipid bilayers revealed by self-assembly simulations. *Biophys. J.* 100, 875–884.

Neale, E. J. (2003). Evidence for intersubunit interactions between S4 and S5 transmembrane segments of the Shaker potassium channel. *J. Biol. Chem.* 278, 29079–29085.

Nishizawa, M., and Nishizawa, K. (2008). Molecular dynamics simulation of Kv channel voltage sensor helix in a lipid membrane with applied electric field. *Biophys. J.* 95, 1729–1744.

Nishizawa, M., and Nishizawa, K. (2009). Coupling of S4 helix translocation and S6 gating analyzed by molecular-dynamics simulations of mutated Kv channels. *Biophys. J.* 97, 90–100.

Noda, M., Shimizu, S., Tanabe, T., Takai, T., Kayano, T., Ikeda, T., Takahashi, H., Nakayama, H., Kanaoka, Y., and Minamino, N. (1984). Primary structure of electrophorus electricus sodium channel deduced from cDNA sequence. *Nature* 312, 121–127.

Nonner, W., Peyser, A., Gillespie, D., and Eisenberg, B. (2004). Relating microscopic charge movement to macroscopic currents: the Ramo-Schockley theorem applied to ion channels. *Biophys. J.* 87, 3716–3722.

Papazian, D. M., Shao, X. M., Seoh, S., Mock, A. F., Huang, Y., and Wainstock, D. H. (1995). Electrostatis interactions of S4 voltage sensor in Shaker K+ channel. *Neuron* 14, 1293–1301.

Pathak, M. M., Yarov-Yarovoy, V., Agarwal, G., Roux, B., Barth, P., Kohout, S., Tombola, F., and Isaccoff, E. Y. (2007). Closing in on the resting state of the Shaker K+ channel. *Neuron* 56, 124–140.

Payandeh, J., Scheuer, T., Zheng, N., and Catterall, W. A. (2011). The crystal structure of a voltage-gated sodium channel. *Nature* 475, 353–358.

Perozo, E., MacKinnon, R., Bezanilla, F., and Stefani, E. (1993). Gating currents from a nonconducting mutant reveal open-closed conformations in Shaker K+ channels. *Neuron* 11, 353–358.

Ramu, Y., Xu, Y., and Lu, Z. (2006). Enzymatic activation of voltage-gated potassium channels. *Nature* 442, 696–699.

Ranatunga, K. M., Law, R. J., Smith, G. R., and Sansom, M. S. (2001). Eletrostatics studies and molecular dynamics simulations of a homology model of the Shaker K+ channel pore. *Eur. Biophys. J.* 30, 295–303.

Roux, B. (2008). The membrane potential and its representation by a constant electric field in computer simulations. *Biophys. J.* 95, 4205–4216.

Roux, B. T. (1997). Influence of the membrane potential on the free energy of an intrinsic protein. *Biophys. J.* 73, 2980–2989.

Ruta, V., Chen, J., and Mackinnon, R. (2005). Calibrated measurement of gating-charge arginine displacement in the KvAP voltage-dependent K+ channel. *Cell* 123, 463–475.

Sachs, J. N., Crozier, P. S., and Woolf, T. B. (2004). Atomistic simulations of biologically realistic transmembrane potential gradients. *J. Chem. Phys.* 121, 10847–10851.

Sands, Z. A., and Sansom, M. S. P. (2007). How does a voltage sensor interact with a lipid bilayer? Simulations of a potassium channel domain. *Structure* 15, 235–244.

Schmidt, D., Jiang, Q., and MacKinnon, R. (2006). Phospholipids and the origin of cationic gating charges in voltage sensors. *Nature* 444, 775–779.

Schneider, M. F., and Chandler, W. K. (1973). Voltage dependent charge movement in skeletal muscle: a possible step in excitation-contraction coupling. *Nature* 242, 244–246.

Schoppa, N. E., McCormack, K., Tanouye, M. A., and sigworth, F. J. (1992). The size of gating charge in wild-type and mutant Shaker potassium channels. *Science* 255, 1712–1715.

Schoppa, N. E., and Sigworth, F. J. (1998). Activation of Shaker potassium channels. III. An activation gating model for wild-type and V2 mutant channel. *J. Gen. Physiol.* 111, 313–342.

Schow, E. V., Freites, J. A., Gogna, K., White, S. H., and Tobias, D. J. (2010). Down-state model of the voltage-sensing domain of a potassium channel. *Biophys. J.* 98, 2857–2866.

Schuler, L. D., Daura, X., and van Gunsteren, W. F. (2001). An improved GROMOS96 force field for aliphatic hydrocarbons in the condensed phase. *J. Comput. Chem.* 22, 1205–1218.

Schwaiger, C. S., Bjelkmar, P., Hess, B., and Lindahl, E. (2011). 310-helix conformation facilitates the transition of a voltage sensor S4 segment toward the down state. *Biophys. J.* 100, 1446–1454.

Selvin, P. R. (2002). Principles and biophysical applications of lanthanide-based probes. *Annu. Rev. Biophys. Biomol. Struct.* 31, 275–302.

Seoh, S. A., Sigg, D., Papazian, D. M., and Bezanilla, F. (1996). Voltage-sensing residues in the S2 and S4 segments of the Shaker K+ channel. *Neuron* 16, 1159–1167.

Shafrir, Y., Durell, S. R., and Guy, H. R. (2008). Models of voltage-dependent conformational changes in NaChBac channels. *Biophys. J.* 95, 3663–3676.

Shaw, D., Dror, R., Salmon, J., Grossman, J., Mackenzie, K., Bank, J., Young, C., Deneroff, M., Batson, B., Bowers, K., Chow, E., Eastwood, M. P., Ierardi, D. J., Klepeis, J. L., Kuskin, J. S., Larson, R. H., Larsen, K. L., Maragakis, P., Moraes, M. A., Piana, S., Shan, Y., and Towles, B. (2009). "Millisecond-scale molecular dynamics simulations on Anton," in *SC '09: Proceedings of the Conference on High Performance Computing Networking, Storage and Analysis* (Portland, OR: ACM), 1–11.

Sigg, D., Bezanilla, F., and Stefani, E. (2003). Fast gating in the Shaker K+ channel and the energy landscape of activation. *Proc. Natl. Acad. Sci. U.S.A.* 100, 7611–7615.

Sigworth, F. J. (1994). Voltage gating of ion channels. *Q. Rev. Biophys.* 27, 1–40.

Sokolov, S., Scheuer, T., and Catterall, W. A. (2005). Ion permeation through a voltage-sensitive gating pore in brain sodium channels having voltage sensor mutations. *Neuron* 47, 183–189.

Sokolov, S., Scheuer, T., and Catterall, W. A. (2007). Gating pore current in an inherited ion channelopathy. *Nature* 446, 76–78.

Sokolov, S., Scheuer, T., and Catterall, W. A. (2008). Depolarization-activated gating pore current conducted by mutant sodium channels in potassium-sensitive normokalemic periodic paralysis. *Proc. Natl. Acad. Sci. U.S.A.* 105, 19980–19985.

Soldovieri, M. V., Miceli, F., Bellini, G., Coppola, G., Pascotto, A., and Tagliatela, M. (2007). Correlating the clinical and genetic features of benign familial neonatal seizures (BFNS) with the functional consequences of underlying mutations. *Channels (Austin)* 1, 228–233.

Starace, D. M., and Bezanilla, F. (2001). Histidine scanning mutagenesis of basic residues of the S4 segment of the Shaker potassium channel. *J. Gen. Physiol.* 117, 469–490.

Starace, D. M., and Bezanilla, F. (2004). A proton pore in a potassium channel voltage sensor reveals a focused electric field. *Nature* 427, 548–553.

Stefani, E., Toro, L., Perozo, E., and Bezanilla, F. (1994). Gating of Shaker K+ channels: I. Ionic and gating currents. *Biophys. J.* 66, 996–1010.

Struyk, A. F., and Cannon, S. C. (2007). A Na+ channel mutation linked to hypokalemic periodic paralysis exposes a proton selective gating Pore. *J. Gen. Physiol.* 130, 11–20.

Suenaga, A., Komeiji, Y., Uebayasi, M., Meguro, T., Saito, M., and Yamato, I. (1998). Computational observation of an ion permeation through a channel protein. *Biosci. Rep.* 18, 39–48.

Tao, X., Lee, A., Limapichat, W., Dougherty, D. A., and MacKinnon, R. (2010). A gating charge transfer center in voltage sensors. *Science* 328, 67–73.

Tarek, M. (2005). Membrane electroporation: a molecular dynamics simulation. *Biophys. J.* 88, 4045–4053.

Tempel, B. L., Papazian, D. M., Schwarz, T. L., Jan, Y. N., and Jan, L. Y. (1987). Sequence of a probable potassium channel component encoded at Shaker locus of *Drosophila*. *Science* 237, 770–775.

Tieleman, D. P. (2004). The molecular basis of electroporation. *BMC Biochem.* 5, 10. doi:10.1186/1471-2091-5-10

Tieleman, D. P., Biggin, P. C., Smith, G. R., and Sansom, M. S. P. (2001). Simulation approaches to ion channel structure-function relationships. *Q. Rev. Biophys.* 34, 473–561.

Tiwari-Woodruff, S. K., Lin, M. A., Schulteis, C. T., and Papazian, D. M. (2000). Voltage-dependent structural interactions in the Shaker K+ channel. *J. Gen. Physiol.* 115, 123–138.

Tombola, F., Pathak, M. M., Gorostiza, P., and Isacoff, E. Y. (2006a). The twisted ion-permeation pathway of a resting voltage-sensing domain. *Nature* 445, 546–549.

Tombola, F., Pathak, M. M., and Isacoff, E. Y. (2006b). How does voltage open an ion channel? *Annu. Rev. Cell Dev. Biol.* 22, 23–52.

Tombola, F., Pathak, M. M., and Isacoff, E. Y. (2005a). How far will you go to sense voltage? *Neuron* 48, 719–725.

Tombola, F., Pathak, M. M., and Isacoff, E. Y. (2005b). Voltage-sensing arginines in a potassium channel permeate and occlude cation-selective pores. *Neuron* 45, 379–388.

Treptow, W., Maigret, B., Chipot, C., and Tarek, M. (2004). Coupled motions between pore and voltage-sensor domains: a model for Shaker B, a voltage-gated potassium channel. *Biophys. J.* 87, 2365–2379.

Treptow, W., Marrink, S. J., and Tarek, M. (2008). Gating motions in voltage-gated potassium channels revealed by coarse-grained molecular dynamics simulations. *J. Phys. Chem. B* 112, 3277–3282.

Treptow, W., and Tarek, M. (2006a). Environment of the gating charges in the Kv1.2 Shaker potassium channel. *Biophys. J.* 90, L64–L66.

Treptow, W., and Tarek, M. (2006b). K+ conduction in the selectivity filter of potassium channels is monitored by the charge distribution along their sequence. *Biophys. J.* 91, L81–L83.

Treptow, W., Tarek, M., and Klein, M. L. (2009). Initial response of the potassium channel voltage sensor to a transmembrane potential. *J. Am. Chem. Soc.* 131, 2107–2110.

Vargas, E., Bezanilla, F., and Roux, B. (2011). In search of a consensus model of the resting state of a voltage-sensing domain. *Neuron* 72, 713–720.

Wee, C. L., Gavaghan, D., and Sansom, M. S. P. (2008). Lipid bilayer deformation and the free energy of interaction of a Kv channel gating-modifier toxin. *Biophys. J.* 95, 3816–3826.

Wood, M. L., Schow, E. V., Freites, J. A., White, S. H., Tombola, F., and Tobias, D. J. (2012). Water wires in atomistic models of the Hv1 proton channel. *Biochim. Biophys. Acta* 1818, 286–293.

Wu, D., Delaloye, K., Zaydman, M. A., Nekouzadeh, A., Rudy, Y., and Cui, J. (2010). State-dependent electrostatic interactions of S4 arginines with E1 in S2 during Kv7.1 activation. *J. Gen. Physiol.* 135, 595–606.

Xu, Y., Ramu, Y., and Lu, Z. (2008). Removal of phospho-head groups of membrane lipids immobilizes voltage sensors of K+ channels. *Nature* 451, 826–829.

Yarov-Yarovoy, V., Baker, D., and Catterall, W. A. (2006). Voltage sensor conformations in the open and closed states in Rosetta structural models of K+ channels. *Proc. Natl. Acad. Sci. U.S.A.* 103, 7292–7297.

Yoda, T., Sugita, Y., and Okamoto, Y. (2004). Secondary-structure preferences of force fields for proteins evaluated by generalized-ensemble simulations. *Chem. Phys.* 307, 269–283.

Zagotta, W. N., Hoshi, T., and Aldrich, R. W. (1994a). Shaker potassium channel gating. III: Evaluation of kinetic models for activation. *J. Gen. Physiol.* 103, 321.

Zagotta, W. N., Hoshi, T., Dittman, J., and Aldrich, R. W. (1994b). Shaker potassium channel gating. II: Transitions in the activation pathway. *J. Gen. Physiol.* 103, 279–319.

Zhang, M., Liu, J., Jiang, M., Wu, D.-M., Sonawane, K., Guy, H. R., and Tseng, G.-N. (2005). Interactions between charged residues in the transmembrane segments of the voltage-sensing domain in the hERG channel. *J. Membr. Biol.* 207, 169–181.

Zheng, H., Liu, W., Anderson, L. Y., and Jiang, Q.-X. (2011). Lipid-dependent gating of a voltage-gated potassium channel. *Nat. Commun.* 2, 250.

Zheng, J., and Sigworth, F. J. (1998). Intermediate conductances during deactivation of heteromultimeric Shaker potassium channels. *J. Gen. Physiol.* 112, 457–474.

Zhong, Q., Jiang, Q., Moore, P. B., Newns, D. M., and Klein, M. L. (1998). Molecular dynamics simulation of a synthetic ion channel. *Biophys. J.* 74, 3–10.

Conflict of Interest Statement: The authors declare that the research was conducted in the absence of any commercial or financial relationships that could be construed as a potential conflict of interest.

Received: 21 March 2012; accepted: 01 May 2012; published online: 28 May 2012.

*Citation: Delemotte L, Klein ML and Tarek M (2012) Molecular dynamics simulations of voltage-gated cation channels: insights on voltage-sensor domain function and modulation. Front. Pharmacol. **3**:97. doi: 10.3389/fphar.2012.00097*

This article was submitted to Frontiers in Pharmacology of Ion Channels and Channelopathies, a specialty of Frontiers in Pharmacology.

frontiers in
PHARMACOLOGY

REVIEW ARTICLE
published: 11 June 2012
doi: 10.3389/fphar.2012.00112

Pathophysiological role of omega pore current in channelopathies

Karin Jurkat-Rott[1]*, James Groome[2] and Frank Lehmann-Horn[1]

[1] *Department of Neurophysiology, Ulm University, Ulm, Germany*
[2] *Department of Biological Sciences, Idaho State University, Pocatello, ID, USA*

Edited by:
Gildas Loussouarn, University of Nantes, France

Reviewed by:
Stephen Cannon, University of Texas Southwestern Medical Center, USA
Domenico Tricarico, University of Bari, Italy

****Correspondence:***
Karin Jurkat-Rott, Department of Neurophysiology, Ulm University, Albert-Einstein-Allee 11, 89069 Ulm, Germany.
e-mail: karin.jurkat-rott@uni-ulm.de

In voltage-gated cation channels, a recurrent pattern for mutations is the neutralization of positively charged residues in the voltage-sensing S4 transmembrane segments. These mutations cause dominant ion channelopathies affecting many tissues such as brain, heart, and skeletal muscle. Recent studies suggest that the pathogenesis of associated phenotypes is not limited to alterations in the gating of the ion-conducting alpha pore. Instead, aberrant so-called omega currents, facilitated by the movement of mutated S4 segments, also appear to contribute to symptoms. Surprisingly, these omega currents conduct cations with varying ion selectivity and are activated in either a hyperpolarized or depolarized voltage range. This review gives an overview of voltage sensor channelopathies in general and focuses on pathogenesis of skeletal muscle S4 disorders for which current knowledge is most advanced.

Keywords: epilepsy and neuromyotonia, long QT syndrome, familial hemiplegic migraine, myotonia and paramyotonia, hyperkalemic and hypokalemic periodic paralysis, sodium overload, cytotoxic edema, degeneration

INTRODUCTION

The basic motif of the alpha subunit of voltage-gated cation channels is a tetrameric association of four domains I–IV, each consisting of six transmembrane helical segments S1–S6, connected by intracellular and extracellular loops. At the resting potential, open probability is low. Activation results from a depolarization-induced conformational change leading to the opening of the alpha pore. When the pore is pharmacologically blocked, charge movements in the electrical membrane field are measurable as so-called gating currents. These gating currents are a result of the outward movement of highly conserved voltage-sensitive S4 segments which display an arginine or lysine residue at every third amino acid position, almost vertically aligned (denoted as R1, R2, R3, etc.). At resting potential, the outermost S4 charge separates the extracellular fluid from the cytoplasm. With membrane depolarization, each S4 moves outwardly shifting deeper situated arginines to the critical position of extra-intracellular separation. During their outward movement, the S4 segments move in a spiral path through canaliculi of the channel protein made up of segments S1–S3 (**Figures 1** and **2**). Likewise, during recovery from channel inactivation, the S4 segments are thought to move back to their original position. Because of the narrow constriction separating extracellular from intracellular compartments, mutations of the S4 charges may cause either a hyperpolarization-activated or a depolarization-activated non-specific cation leak called the omega current (**Figure 2**).

An omega current was first described in the voltage-gated potassium channel of drosophila *Shaker*. In this channel the mutation R1H in S4 generates an inward-directed hyperpolarization-induced proton current that becomes increasingly prominent as the proton reversal potential E_H is shifted to more positive values (Starace and Bezanilla, 2004). R1 substitutions to residues other than histidine result in a hyperpolarization-induced inward current carried by alkali metal cations rather than protons (Tombola et al., 2005) indicating that this mutation creates a short-circuit connection of intracellular and extracellular compartments in the canaliculus. This current varies with the identity of the substituted residue: R1S > R1C > R1V ~ R1A, has the selectivity $Cs^+ > K^+ > Li^+$, and is not affected by alpha pore blockers. *Shaker* mutants R2H and R3H conduct protons at potentials corresponding to the voltage-dependent movement of S4 charges, as the current is maximal at potentials close to midpoint of the Q_{ON}-voltage relation (Starace et al., 1997; Starace and Bezanilla, 2001). Further depolarization blocks the omega pore, consistent with the model that outward S4 movement shifts the short-circuiting mutant residues out of the canaliculus.

Studies on *Shaker* potassium channel and domain II of rat brain sodium channel $Na_v1.2$ suggest that substitution of a single S4 arginine may be insufficient to produce a non-proton omega current, but that two adjacent mutations (i.e., R2/R3 or II-R1/R2) are required (Sokolov et al., 2005; Gamal El-Din et al., 2010). In this respect, the presence of alanine at the position equivalent to R0 in *Shaker* may therefore enhance the omega current of R1S. The motif of adjacent arginine replacements recurs in some of the potassium channel disorders and may be explained by the degree of accessibility of arginines to the extracellular or intracellular compartments. However, this does not hold true for all channels suggesting that position and orientation of the S4 segment and its environment play an important role as well. Based on current knowledge of S4 position, in this review R0 designates charge positions of S4 outside of the canaliculus and R1 the first charge inside of it.

For human diseases, the channelopathies result from mutations in voltage-gated ion channels. In several of these disorders,

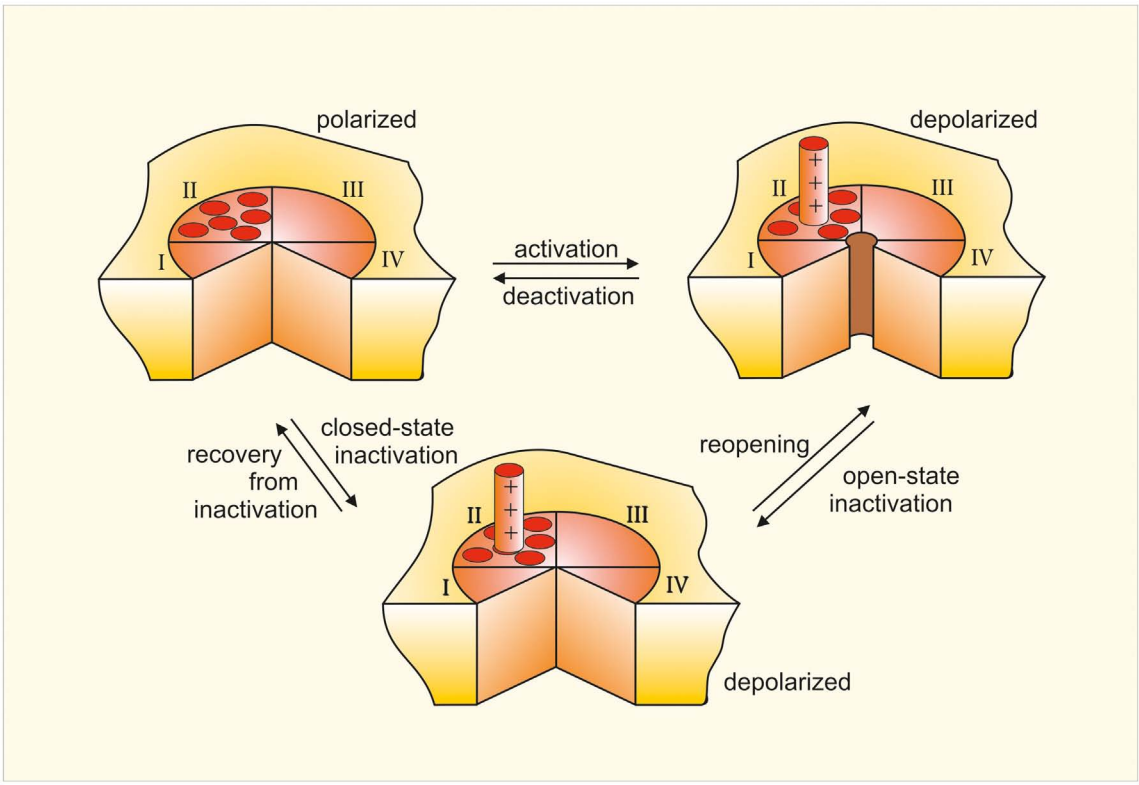

FIGURE 1 | Scheme of a voltage-gated ion channel. Bird's eye view of the channel consisting of four similar repeats (I to IV). The channel has been cut open between repeats I and IV to show the opening and closing of the central pore. The model also shows one of the four voltage sensors S4, which moves outward when the membrane becomes depolarized and remains in this position until repolarization.

mutations of specific charges of S4 segments are known, such as in epilepsy, hemiplegic migraine, long QT (LQT) syndrome, paramyotonia congenita, and periodic paralyzes (**Table 1**). The underlying mutations generally modify voltage sensitivity of gating and maximal amplitude of alpha current. Additionally, some of these mutations have been reported to produce an omega current. Most of these are inward currents that result in enhanced membrane depolarization, contributing to the symptoms of the channelopathy. Depending on the position of the S4 mutation and the voltage threshold of activation of the channel, the omega current can appear in very different voltage ranges.

This review briefly outlines the clinical features and pathogenesis of the S4 channelopathies with a focus on mutation-dependent changes of alpha and omega currents as well as their contributions to the phenotype. It also introduces the concept of membrane bistability in general and in computer simulations incorporating omega current. Also discussed are the consequences of intracellular sodium overload and tissue degeneration to explain the non-episodic features of the channelopathies and the ideas behind best practice treatment. For further reading, there are reviews with more emphasis on S4 structure and function (Catterall, 2010), S4 mutations in channels of skeletal muscle (Cannon, 2010; Jurkat-Rott et al., 2010), or drug action in periodic paralyzes and related channelopathies (Matthews and Hanna, 2010; Tricarico and Camerino, 2011).

EPILEPSY AND NEUROMYOTONIA

Epilepsy is characterized by recurring episodes of synchronized electrical discharges of neurons caused by their facilitated depolarization within the central nervous system. The symptoms of a seizure depend on age of the patient, the underlying cause, and the brain region involved.

Generalized epilepsy with febrile seizures plus (GEFS+) is a childhood-onset syndrome featuring febrile seizures (FS) and afebrile epileptic convulsions within the same pedigree. The penetrance is ∼60%. In two-thirds of affected individuals either FS persist after the sixth year of life or afebrile generalized tonic-clonic seizures additionally occur (FS+). GEFS+ type II is caused among others by missense mutations in the alpha subunit of the neuronal sodium channel $Na_v1.1$, encoded by *SCN1A*. Mutations frequently destabilize the fast-inactivated state, resulting in a persistent inward sodium current that depolarizes the membrane potential to a value closer to the $Na_v1.1$ threshold (facilitated spike generation). Additionally, a few mutations result in loss-of-function by trafficking defects (Catterall et al., 2010; Escayg and Goldin, 2010). S4 mutations II-R1C, IV-R4H, and IV-R7C (**Figure 3**) result in additional loss-of-function effects such as decreased current amplitude and stabilization of the inactivated state (Alekov et al., 2000; Spampanato et al., 2001; Lossin et al., 2003; Barela et al., 2006; Vanoye et al., 2006). Apparently, loss-of-function in inhibitory neurons produces overexcitability (Martin et al., 2010)

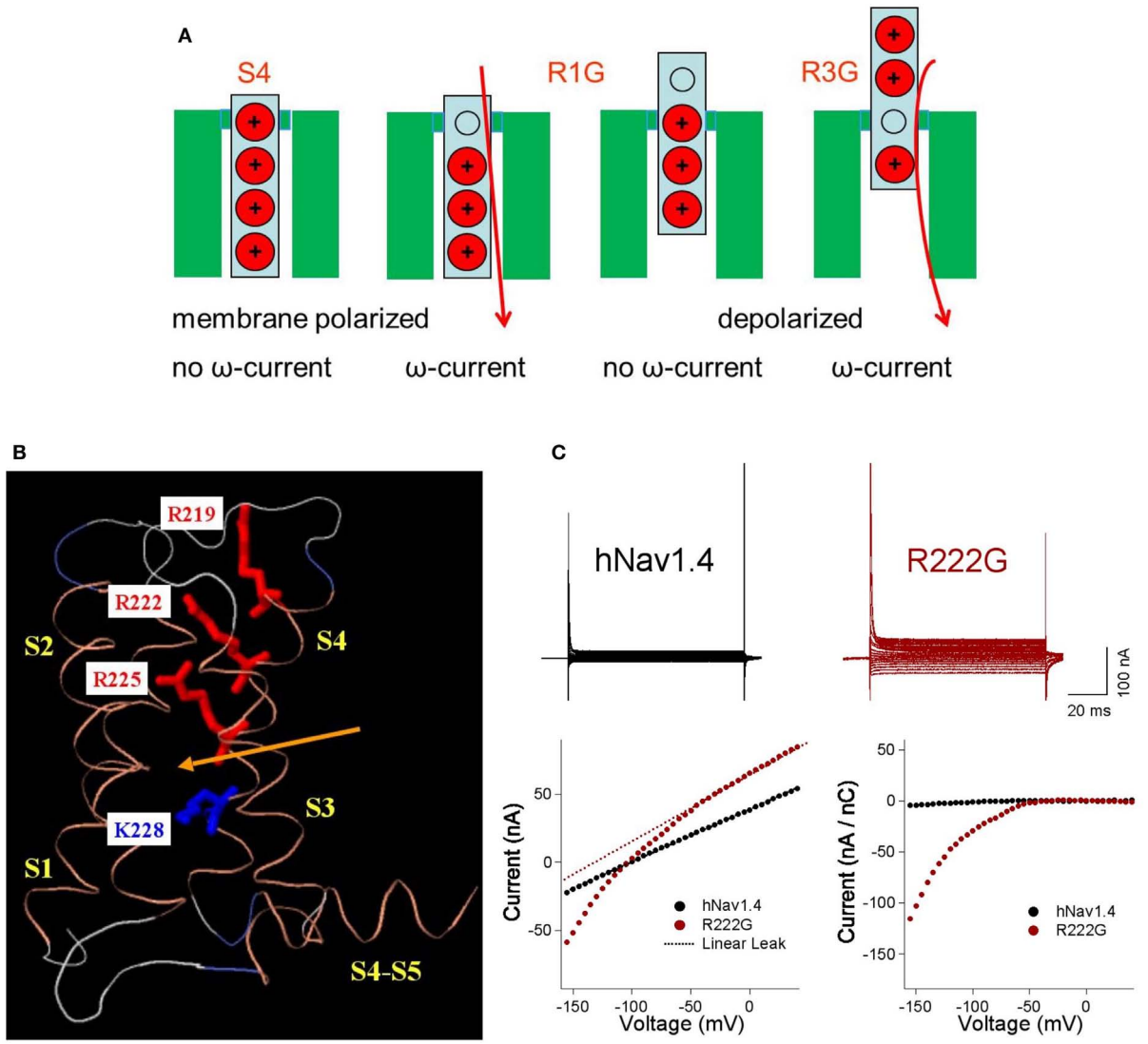

FIGURE 2 | Omega pores and currents dependent on the R position. **(A)** Replacement of the outermost arginine (red) by a neutral amino acid (gray) such as glycine (R1G) opens a conductive pathway through the polarized membrane, resulting in an omega current (red). At depolarized potentials at which the S4 segment moves outward, the conductive pathway is closed by a deeper arginine and the omega current ceases. In contrast the replacement of a deeper arginine (R3G) only opens the omega pore if the membrane is depolarized. **(B)** Homology model of domain I in hNa$_v$1.4 based on crystal structure of NaVAb (activated-closed; crystal structure at 0 mV), using Modeller. Positions of arginine and lysine residues of DIS4 are shown, relative to the putative gating pore constriction (arrow). Modified from Groome and Winston (2012). **(C)** Comparison of current-voltage (*I/V*) traces for wild type hNa$_v$1.4 and R222G, with plots of raw *I/V*, linear leak, and normalized current (linear leak subtracted from IV and normalized to gating current at +40 mV). The mutation R222G causes HypoPP type 2. External solution contained 120 mM K^+ and 1 μM TTX. Modified from Holzherr et al. (2010).

similar to gain-of-function effects in excitatory neurons (Kahlig et al., 2006, 2010).

Severe myoclonic epilepsy of infancy (SMEI), or Dravet syndrome, is characterized by clonic or tonic-clonic seizures that occur in the first year of life, are often prolonged, and are typically associated with fever. During the course of the disease, patients develop additional afebrile generalized and partial seizures. Cognitive deterioration appears in early childhood. In contrast to GEFS+, the syndrome is resistant to pharmacotherapy, although stiripentol seems to have a positive effect by enhancing GABAergic neurotransmission. Cranial magnetic resonance (MR) imaging in patients reveals focal and generalized atrophy. Because some patients with SMEI have a family history of febrile or afebrile seizures, and in some families GEFS+ and SMEI overlap, SMEI may therefore be regarded as the most severe phenotype of the GEFS+ spectrum (Mullen and Scheffer, 2009). SMEI is caused by mutations in *SCN1A* encoding Na$_v$1.1. Most SMEI mutations cause loss-of-function due to nonsense mutations demonstrating that haploinsufficiency of *SCN1A* is pathogenic (Oakley et al., 2011). The loss-of-function of Na$_v$1.1 channels results in reduced action potential (AP) firing in hippocampal inhibitory neurons, thus generating overexcitability. IV-R4C causes gain-of-function

Table 1 | Voltage sensor mutations in K^+, Na^+, and Ca^{2+} channelopathies.

Channel	Gene	Disease	Mutation	Location		Reference genetics	Reference function
$K_V7.1$	*KCNQ1*	LQT-1	R231C	S4	R1	Lupoglazoff et al. (2004), Fodstad et al. (2004)	Bartos et al. (2011)
			R243H/C		R5	Mohammad-Panah et al. (1999), Franqueza et al. (1999)	Mohammad-Panah et al. (1999), Franqueza et al. (1999), Chouabe et al. (2000)
$K_V7.2$	*KCNQ2*	BFNS-PNH	R207W/Q	S4	R3	Dedek et al. (2001), Wuttke et al. (2007)	Dedek et al. (2001), Wuttke et al. (2007), Miceli et al. (2012)
$K_V11.1$	*KCNH2*	LQTS-2	K525N-R528P	S4	R0–R1	Millat et al. (2006)	–
			R534C		R3	Itoh et al. (1998)	Nakajima et al. (1999)
$Na_V1.1$	*SCN1A*	GEFS+	R859C	IIS4	R1	Barela et al. (2006)	Barela et al. (2006)
			R1648H	IVS4	R4	Escayg et al. (2000)	Alekov et al. (2000), Spampanato et al. (2001), Kahlig et al. (2006), Vanoye et al. (2006), Martin et al. (2010), Kahlig et al. (2010)
		SMEI	R1648C		R4	Rhodes et al. (2004)	Rhodes et al. (2004), Kahlig et al. (2010)
		GEFS+	R1657C		R7	Lossin et al. (2003)	Lossin et al. (2003), Vanoye et al. (2006)
$Na_V1.4$	SCN4A	HypoPP-2	R222W	IS4	R2	Matthews et al. (2009)	–
		Myotonia	R225W		R3	Lee et al. (2009)	–
		HypoPP-2	R669H	IIS4	R1	Bulman et al. (1999)	Bulman et al. (1999), Struyk et al. (2000), Kuzmenkin et al. (2002), Sokolov et al. (2007), Struyk and Cannon (2007), Wu et al. (2011)
			R672H/G/S/C		R2	Jurkat-Rott et al. (2000), Davies et al. (2001), Kim et al. (2007)	Jurkat-Rott et al. (2000), Bendahhou et al. (2001), Kuzmenkin et al. (2002), Sokolov et al. (2007), Struyk et al. (2008), Sokolov et al. (2010)
		HypoPP-2/NormoPP	R675G/Q/W		R3	Vicart et al. (2004)	Wu et al. (2008), Sokolov et al. (2008)
		HypoPP-2	R1129Q	IIIS4	R1	Hong et al. (2010)	–
			R1132Q		R2	Carle et al. (2006)	Carle et al. (2006), Francis et al. (2011)
			R1135H		R3	Matthews et al. (2009)	–

		Paramyotonia	R1448H/C/S/L/P	IVS4	R0	Ptacek et al. (1992), Lerche et al. (1996), Matthews et al. (2008)	Lerche et al. (1996), Fan et al. (1996), Featherstone et al. (1998), Groome et al. (1999), Mitrovic et al. (1999), Francis et al. (2011)
$Na_v1.5$	*SCN5A*	LQT-3	R225Q/W	IS4	R3	Bezzina et al. (2003), Millat et al. (2006)	Bezzina et al. (2003)
			R814Q	IIS4	R3	Frigo et al. (2007)	–
			R1623L/Q	IVS4	R0	Makita et al. (1998), Yamagishi et al. (1998), Splawski et al. (2000)	Makita et al. (1998)
			R1626P		R1	Ruan et al. (2007)	Ruan et al. (2007), Banderali et al. (2010)
			R1644C/H		R7	Splawski et al. (2000)	Dumaine et al. (1996)
$Ca_v1.1$	*CACNA1S*	HypoPP-1	R528H/G	IIS4	R1	Jurkat-Rott et al. (1994), Matthews et al. (2009)	Lapie et al. (1996), Jurkat-Rott et al. (1998), Morrill et al. (1998), Morrill and Cannon (1999), Kuzmenkin et al. (2007), Jurkat-Rott et al. (2009)
			R897S	IIIS4	R1	Chabrier et al. (2008)	–
			R900S		R2	Matthews et al. (2009)	–
			R1239H/G	IVS4	R2	Ptacek et al. (1994), Lehmann-Horn et al. (1995)	Lehmann-Horn et al. (1995), Morrill and Cannon (1999), Kuzmenkin et al. (2007), Jurkat-Rott et al. (2009)
$Ca_v2.1$	*CACNA1A*	FHM	R192Q	IS4	R0	Ophoff et al. (1996)	Kraus et al. (1998), Hans et al. (1999), van den Maagdenberg et al. (2004)
			R195Q		R1	Ducros et al. (2001)	–
			R583Q	IIS4	R1	Battistini et al. (1999)	Kraus et al. (2000)
			R1346Q	IIIS4	R1	Alonso et al. (2004)	–
			R1661H	IVS4	R1	Friend et al. (1999)	–
			R1664Q		R2	Tonelli et al. (2006)	–
			R1667W		R3	Ducros et al. (2001)	–

Bold print: proof of omega currents or omega-analogous leaks in native tissue.

by destabilizing fast inactivation and producing persistent currents (Rhodes et al., 2004) that may be inhibited by the sodium channel blocker ranolazine (Kahlig et al., 2010; **Figure 3**).

Benign familial neonatal seizures (BFNS) are dominantly inherited with a penetrance of 85%. The seizures manifest within the first weeks of life and typically disappear spontaneously after weeks to months. Seizures may have a partial onset or may appear as generalized. Accordingly, ictal EEGs show focal and generalized discharges. Interictal EEGs are mostly normal. The risk of seizures recurring in adulthood is ∼15%, but psychomotor development is usually normal. Causative mutations have been identified in $K_v7.2$ and $K_v7.3$ potassium channels encoded by *KCNQ2* and *KCNQ3* respectively that interact with each other and constitute the so-called *M*-current, an important regulator of membrane potential near the AP threshold. Co-expression of heteromeric wild type and mutant $K_v7.2/K_v7.3$ channels usually reveals a potassium current reduction of ∼20–30% in the setting of haploinsufficiency. This causes BFNS by depolarizing the membrane and facilitating AP firing (Maljevic et al., 2008). In contrast, S4 mutations of the pattern R3W/Q (**Figure 3**) produce a dominant negative effect on co-expressed wild type brought about by a drastic depolarizing shift of the activation curve and slowing of the activation time course (Dedek et al., 2001; Wuttke et al., 2007; Miceli et al., 2012). This suppression of inhibitory neurons explains the hyperexcitability that affects central as well as peripheral neurons. The latter locus of hyperexcitability leads to additional neuromyotonia also termed peripheral nerve hyperexcitability (PNH). This disorder is characterized by short spells of spontaneous skeletal muscle overactivity resulting in twitching, undulation, or rippling of the muscles and painful cramps, so that the phenotype for these S4 mutation carriers is BFNS-PNH. Omega currents have been implicated in BFNS for the analogous $K_v7.4$ channel. There, corresponding R3W/Q mutations generate non-specific depolarization-induced cation outward currents of ∼1% of the pore current amplitude, at the +40 mV voltage step (Miceli et al., 2012). In K_v7 channels, single mutations of R1 and R3 fulfill the concept of adjacent arginine replacements because there is a glutamine at position R2.

LONG QT SYNDROME

Long QT syndrome is named for an elongated QT interval in the electrocardiogram. It is caused by lengthening of the repolarization phase of the cardiac ventricular AP. Because duration of the cardiac AP is dispersed in different regions of the ventricle depending on regional channel expression, any disproportionate

motif	*Shaker*	Kv7.1	Kv7.2	Kv11.1	Nav1.1				Nav1.4				Nav1.5				Cav1.1				Cav2.1				omega current
					I	II	III	IV	I	II	III	IV	I	II	III	IV	I	II	III	IV	I	II	III	IV	
	359	228	198	525	213	856	1313	1636	216	666	1126	1448	216	805	1300	1623	162	525	894	1233	192	580	1343	1658	
R0	A	R	R	K	S	S	K	R	S	S	K	R	S	S	K	R	K	S	K	A	R	S	K	S	
X	I	G	S	T	A	V	S	V	A	V	S	V	A	V	S	V	A	V	I	F	T	V	S	F	
X	L	I	L	A	L	L	L	I	L	L	L	I	L	L	L	I	L	L	L	F	L	L	L	L	at hyperpolar.
R1	R	R	R	R	R	R	R	R	R	R	R	R	R	R	R	R	R	R	R	R	R	R	R	R	
X	V	F	F	L	T	S	T	L	T	S	T	L	T	S	T	L	A	C	V	L	A	A	V	L	
X	I	L	L	L	F	F	L	A	F	F	L	A	F	F	L	A	F	I	L	F	V	L	L	F	
R2	R	Q	Q	R	R	R	R	R	R	R	R	R	R	R	R	R	R	R	R	R	R	R	R	R	
X	L	I	I	L	V	L	A	I	V	L	A	I	V	L	A	I	V	L	V	V	V	L	V	A	
X	V	L	L	V	L	L	L	G	L	L	L	G	L	L	L	G	L	L	L	M	L	L	L	A	at depolarization
R3	R	R	R	R	R	R	R	R	R	R	R	R	R	R	R	R	R	R	R	R	R	R	R	R	
X	V	M	M	V	A	V	P	I	A	V	P	V	A	V	P	I	P	I	P	L	P	I	P	L	
X	F	L	I	A	L	F	L	L	L	F	L	L	L	F	L	L	L	F	L	I	L	F	L	I	
R4	R	H	R	R	K	K	R	R	K	K	R	R	K	K	R	R	R	K	R	K	K	K	K	K	
X	I	V	M	K	T	L	A	L	T	L	A	L	T	L	A	L	L	I	A	L	L	V	T	L	
X	F	D	D	L	I	A	L	I	I	A	L	I	I	A	L	I	V	T	I	L	V	T	I	L	
R5	K	R	R	D	S	K	S	K	T	K	S	R	S	K	S	R	S	K	N	S	S	K	K	R	
X	L	Q	R	R	V	S	R	G	V	S	R	G	V	S	R	G	G	Y	R	R	G	Y	R	Q	
X	S	G	G	Y	I	W	F	A	I	W	F	A	I	W	F	A	V	W	A	A	I	W	L	G	
R6	R	G	G	S	P	P	E	K	P	P	E	K	S	P	E	K	P	T	K	E	P	A	P	Y	

FIGURE 3 | S4 sequences of channels with an R0 to R6 mutation. Positively charged residues in R0 to R6 positions are delineated with a shaded background (gray). The constriction of the omega pore lies between R2 and R3. Therefore an inward movement of S4 due to hyperpolarization opens the omega pore if R1 or R2 is replaced by a neutral amino acid. An outward movement of S4 due to depolarization opens the omega pore if R3 or R4 is replaced by a neutral amino acid. These gray-background arginines are boxed. The *Shaker* K^+ channel serves as reference. Neutral replacements of its arginines R2 and R3 have been described as proton transporters.

prolongation of the AP increases the probability for re-entry of the depolarization wave, early after-depolarizations and thus, arrhythmia. Associated ECG findings may be ventricular bigemini and *torsade de pointes* in which the QRS complex twists around the isoelectric axis in the electrocardiogram. By this, syncope and sudden death may result in young and otherwise healthy individuals. LQT syndrome (LQTS) is caused among others by loss-of-function of potassium channels K_v7.1 encoded by *KCNQ1* or K_v11.1 encoded by *KCNH2* and by gain-of-function of the Na_v1.5 sodium channel encoded by *SCN5A*.

K_v7.1 currents deactivate very slowly allowing adaptive shortening of the AP during tachycardia by incomplete deactivation. Therefore, loss-of-function in K_v7.1 leads to arrhythmia especially at elevated heart rate due to physical or emotional stress. R1C decreases current amplitude which explains the LQT in the electrocardiogram, but also produces a hyperpolarizing shift of the voltage dependence of activation and tail currents, thereby explaining the additional atrial fibrillation in these patients (Bartos et al., 2011). R5H/C produce a slowed rate of activation, a positive voltage shift of activation and/or dominant suppression of co-expressed wild type (Franqueza et al., 1999; Mohammad-Panah et al., 1999; Chouabe et al., 2000). R1, R3, and R5 mutants all fulfill the concept of adjacent arginine replacements because there is a glutamine at R2 and a histidine at R4 (**Figure 3**).

K_v11.1 activates and deactivates relatively slowly in comparison to a rapid inactivation. LQT mutations suppress repolarization of the myocardial AP and lengthen the QT interval by either loss-of-function or haploinsufficiency. A dominant negative effect may be achieved by current reduction of the tetrameric channel complex. For the LQT double mutation of R0/R1, there is no functional data but there two adjacent arginines are changed (**Figure 3**). The point mutation R3C reduces current amplitude and accelerates deactivation thereby slowing repolarization of the cardiac AP in its final phase (Nakajima et al., 1999).

Na_v1.5 initiates the cardiac AP. LQT mutants frequently conduct a persistent inward current during membrane depolarization and single channel recordings show fluctuation between normal and non-inactivating gating modes. I-R3Q/W shift the steady-state inactivation curve to the right (Bezzina et al., 2003). IV-R0L/Q delay inactivation (Makita et al., 1998), IV-R1P impairs inactivation or shifts the steady-state inactivation curve to the left (Ruan et al., 2007) and decreases inactivation upon stretch modulation (Banderali et al., 2010). Mutations IV-R7C/H show dispersed re-openings (Dumaine et al., 1996; **Figure 3**). It has yet to be established that omega currents play a role in the pathogenesis of K_v or Na_v LQTS channelopathies, but the finding of mutations in these cardiac disorders in R1–R3 residues of S4 raises that possibility (**Table 1**; Sokolov et al., 2007).

HEMIPLEGIC MIGRAINE

Familial hemiplegic migraine (FHM) presents with characteristic unilateral migraine headaches accompanied by nausea, phono-, and photophobia. Episodes are typically precipitated by an aura with symptoms of both hyper- and hypo-excitability such as aphasia, dysarthria, vertigo, homonymous hemianopsia, cheiro-oral paresthesias, and some degree of (primarily) unilateral paresis. Additionally, ataxia and cerebellar degeneration are frequently part of the FHM phenotype. Up to 50% of cases are caused by mutations in Ca_v2.1 encoded by *CACNA1A*. Current pathogenesis models of migraine with aura suggests cortical spreading depression which consists of an initial brief spike of increased neuronal activity followed by long-lasting suppression of excitability spreading across the cortex at 1–3 mm/min. The depression wave is associated with long-lasting depolarization associated with elevation of extracellular potassium and intracellular sodium. The progress of FHM correlates to the succession of symptoms during the aura initiating the migraine attacks. FHM1 includes sporadic hemiplegic migraine with progressive cerebellar ataxia. The aura may be prolonged and confusion and loss of consciousness may occur. In the interval, some families additionally present with epilepsy, retinal degeneration, hypacusis, and persistent cerebellar dysfunction with *Purkinje* cell atrophy. While migraine is mainly caused by gain-of-function, loss-of-function may lead to additional ataxia. Of the seven known S4 mutations in Ca_v2.1, there is functional data for only two. I-R0Q increases open probability and channel density *in vitro* (Kraus et al., 1998; Hans et al., 1999). In a knock-in mouse this mutation generates increased current density in cerebellar neurons, enhanced transmission at the neuromuscular junction, and reduced threshold and increased velocity of cortical spreading depression, effects that are compatible with an omega current (van den Maagdenberg et al., 2004; **Figure 3**). II-R1Q shifts activation to the left but decreases peak current (Kraus et al., 2000). Omega currents produced by either of these mutations have yet to be demonstrated.

SODIUM CHANNEL MYOTONIA AND PARAMYOTONIA

Myotonia is an involuntary slowed relaxation after a forceful voluntary muscle contraction, experienced by the patient as muscle stiffness. After making a forceful fist or eyelid closure, the patient cannot reopen their hand or eye. Repetition decreases the myotonia, a phenomenon called warm-up. Electrical hyperexcitability of the muscle fiber membrane is the basis for myotonia, apparent in the form of repetitive APs in the EMG. Needle insertions into the resting muscle elicit myotonic bursts, i.e., runs of APs with amplitude and frequency modulation that sound like dive bombers. Autosomal dominantly inherited myotonia can be caused among others by mutations in *SCN4A*, the gene encoding the alpha subunit of the voltage-gated sodium channel of skeletal muscle, Na_v1.4 (Heine et al., 1993), essential for generation of the muscle fiber AP. Most mutations destabilize the fast-inactivated state so that the channel inactivates slower and incompletely (Lerche et al., 1993). The resulting subthreshold membrane potential facilitates AP generation. I-R3W causes typical myotonia with warm-up phenomenon and transient weakness (Lee et al., 2009). However, no functional data are available.

Paramyotonia (PC) is also caused by dominant *SCN4A* missense mutations. The cardinal symptom is cold-induced muscle stiffness that increases with continued activity called paradoxical myotonia, or paramyotonia for short. In most families, on intensive cooling the stiffness gives way to flaccid weakness or even to paralysis which is caused by severe membrane depolarization (Lehmann-Horn et al., 1987; Lerche et al., 1996). Families with IV-R0H/C/S/L/P also have episodes of generalized periodic paralysis (Lehmann-Horn and Jurkat-Rott, 1999). Such attacks occur

spontaneously and can be triggered by rest or elevated serum potassium. They are of much shorter duration than the cold-induced weakness that usually lasts for several hours even after the muscles are re-warmed. During cooling, PC muscle fibers slowly depolarize to an extent greater than that observed in normal muscle fibers. The depolarization is associated with long-lasting bursts of APs which cease when the membrane potential reaches −55 mV. At this potential sodium channels inactivate so that muscle becomes inexcitable and paralyzed. Causative mutations generally slow the entry into, and accelerate recovery from, fast inactivation (Yang et al., 1994). IV-R0 mutations slow deactivation, in addition to destabilizing the fast-inactivated state (Fan et al., 1996; Lerche et al., 1996; Featherstone et al., 1998; Groome et al., 1999; Mitrovic et al., 1999). No omega current is observed (Francis et al., 2011), possibly because R0 is located outside of the canaliculus (**Figures 2** and **3**).

PERIODIC PARALYSIS

Autosomal dominant hypokalemic periodic paralysis (HypoPP) is characterized by episodes of flaccid generalized muscle weakness accompanied by low serum potassium levels. Triggers for the weakness are carbohydrates and insulin with subsequent hypokalemia, rest after exercise, and cooling. Oral potassium administration accelerates the recovery of muscle strength. Native patient muscle fibers show long-lasting membrane depolarization paradoxically triggered by lowering of extracellular potassium, resulting in an inactivation of sodium channels necessary for AP generation (Jurkat-Rott et al., 2000). This effect is exacerbated in the presence of insulin (Bond and Gordon, 1993; Ruff, 1999). Permanent progressive weakness is additionally found in ∼60% of patients whereby muscle degenerates and is increasingly replaced by fatty tissue. The causative mutations are located in the skeletal muscle calcium channel $Ca_v1.1$ encoded by *CACNA1S* (HypoPP-1) and the skeletal muscle sodium channel $Na_v1.4$ encoded by *SCN4A*. Given the finding that all but one of these mutations neutralize a positively charged S4 residue, it is not surprising that a role for omega currents as a causal factor in the pathogenesis of the channelopathies has been most clearly demonstrated for the periodic paralyzes.

Functional studies of the alpha currents of either of these channels do not satisfactorily explain the phenotype. In $Ca_v1.1$, II-R1H/G and IV-R2H/G (**Figure 3**) lead to loss-of-function in the sense of current amplitude reduction, slowing of activation, reduced open probability, left shift of steady-state inactivation, reduced amplitude and broadening of APs (Lehmann-Horn et al., 1995; Lapie et al., 1996; Jurkat-Rott et al., 1998; Morrill et al., 1998; Morrill and Cannon, 1999; Kuzmenkin et al., 2007). None of these gating defects are expected to lead to increased depolarization. Similarly, in $Na_v1.4$, II-R1H, II-R2H/G/S/C, and II-R3G/W/Q show reduced current amplitude, left shift of steady-state fast inactivation, enhanced fast and slow inactivation, slowed recovery after long depolarizations, and reduced AP amplitudes (Bulman et al., 1999; Jurkat-Rott et al., 2000; Struyk et al., 2000; Bendahhou et al., 2001; Kuzmenkin et al., 2002; Carle et al., 2006; Wu et al., 2008, 2011). These defects would not contribute to depolarization either.

In $Na_v1.4$, II-R1H, II-R2H/G/C/S, and III-R2Q mutations generate omega currents that are activated by hyperpolarization, are still active at the usual resting potential, but are closed by depolarizations large enough to activate and thus, move S4 (**Figure 3**). Their amplitude is about 1% of the alpha pore current. Substitution of these arginines by the bulky histidine residue enables proton transport only; other cations do not seem to have enough space to pass (Sokolov et al., 2007; Struyk and Cannon, 2007; Francis et al., 2011). Substitution of these arginines with uncharged resides such as glycine allow an inwardly rectifying flow of small monovalent cations whereby potassium and cesium are preferred over sodium or lithium (Sokolov et al., 2007; Struyk et al., 2008). **Figure 2C** shows current-voltage relationships for R222G/h$Na_V1.4$ channels from experiments performed in our lab as an example (Holzherr et al., 2010). Omega pores conduct currents that show an above-linear increase in amplitude with hyper- or depolarization although the electrical field is focused to a single amino acid (*Ohm* resistor) and not constantly increasing within the membrane (constant field theory). The non-linearity of the omega current reflects the stochastic process of a voltage-dependent open probability and follows a Boltzmann distribution.

Guanidinium, a derivative of arginine, has greater than 10 times the conductance through the omega pore than monovalent cations, while divalent and trivalent cations block the omega pore at mM concentrations (Sokolov et al., 2010). In that study, a screen of guanidine derivatives as potential blockers of the pathogenic omega current in HypoPP yielded one compound, 1-(2-4 xylyl) guanine that exhibited similar potency for block compared to the divalent cations tested. In addition, there is an inward cation leak current at hyperpolarized potentials in native muscle of R1H knock-in mice with omega features (Wu et al., 2011). The conclusion from these alternative approaches to study omega currents is that they contribute to the depolarization leading to inexcitability and weakness. Nevertheless, despite similarities of sodium channel omega currents with those in *Shaker* produced by R1H mutations, their blockade is quite different, suggesting differences in shape, size, and exact cation pathway along the canaliculi of these channels. Perhaps this phenomenon is related to the postulation that two adjacent mutated charges promote omega currents in voltage-gated potassium channels, a requisite that does not hold true for sodium channels.

In contrast to the hyperpolarization-induced omega currents from substitutions of II-R1 and II-R2, II-R3G/Q/W mutations generate $Na_v1.4$ cation currents that are activated by depolarization (**Figure 3**). This means that the omega currents are conducted when S4 is in the activated or inactivated state, but not in the resting state. This omega current is deactivated at hyperpolarized membrane potentials (Sokolov et al., 2008). The associated phenotype differs slightly in the ictal serum potassium levels which can be low or normal (normokalemic periodic paralysis, NormoPP). Also, the reaction to oral potassium administration may be different than for HypoPP – anything from amelioration to worsening of the weakness.

For II-R1H/Q and IV-R2H/G $Ca_v1.1$ channel mutations (**Figure 3**), no direct omega currents have been shown. However, in native patient muscle there is an inward cation leak current at hyperpolarized potentials with omega features (Jurkat-Rott et al., 2009). Also, based on these measurements, the periodic paralysis

episodes can be successfully modeled. The underlying idea is that depolarized muscle fibers will be paralyzed, and that polarized fibers will be fully functional. If transitions between these two situations are reversible, the membrane potential is bi-stable.

BI-STABILITY OF MEMBRANE POTENTIAL

P-states are the electrically stable resting membrane potentials of a cell in the nomenclature of Jurkat-Rott et al. (2009). Normal cells reveal a bimodal distribution around the stable membrane potentials P1 and P2. At physiological conditions, most fibers are highly negative polarized and in the excitable P1-state which follows the predictions of the Goldman–Hodgkin–Katz equation. Upon an increased sodium conductance, e.g., by omega pores, the fraction of cells in the (depolarized) P2-state is increased. With slow depolarization, voltage-gated sodium channels might inactivate via closed-state inactivation and render the cells inexcitable. In contrast, cells that remain in the P1-state are only slightly depolarized and thus still excitable. This bi-stability is the result of inwardly rectifying potassium channels (K_{ir}), which open with hyperpolarization and close with depolarization (**Figure 4A**). The bi-stability is the reason that only a small increase in sodium conductance, e.g., by an omega pore, is required to shift cells from the P1- to the P2-state (**Figure 4B**). Vice versa, a repolarizing conductance can shift the membrane back to the P1-state (**Figure 4**). Transitions between the P1- and P2-states can occur when any trigger drives the system closer to a limit point or shifts a limit point. If the limit points of both states (LP1 and LP2) are situated at different K^+ values, the system shows hysteresis (**Figure 4C**). If external K^+ is considered as a control parameter, it is shown to play an important role in driving the system to its limits, and set the stage during "physiological" hypokalemia, for the paradoxical depolarization triggered by a slight increase in sodium conductance provided by an omega current. A significant role for the activated omega pore as a causal factor in the pathogenesis of HypoPP is supported by the computer model whose details are given in the Appendix and whose parameters are given in **Table 2**.

A drop of serum K^+ will decrease K_{ir} conductance. Although the Nernst equation predicts hyperpolarization when external K^+ is reduced, the hypokalemia-induced reduction of K_{ir} conductance may shift the cells from the P1- to the P2-state (**Figure 4C**). Therefore, cells show a bimodal distribution of membrane potentials especially at low K^+. This phenomenon is called paradoxical depolarization (Jurkat-Rott and Lehmann-Horn, 2007; Struyk and Cannon, 2008; Jurkat-Rott et al., 2009). Not surprisingly, decreased conductance in mutant K_{ir} channels contributes to the pathogenesis of episodic paralysis associated with thyrotoxicosis (K_{ir} 2.6; Ryan et al., 2010; Cheng et al., 2011), periodic paralysis and cardiac arrhythmia in Tawil–Anderson's syndrome (K_{ir} 2.1; Plaster

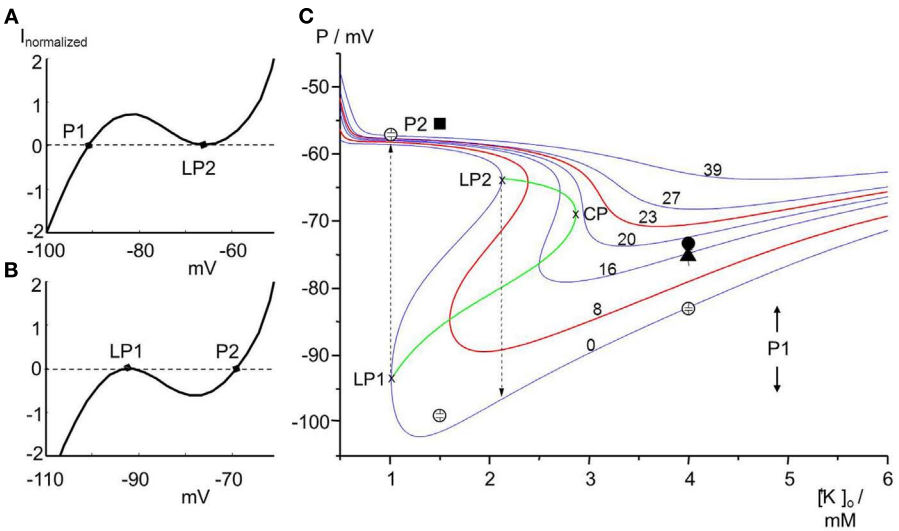

FIGURE 4 | Effects of omega currents schematically (A) and in a computer simulation (B). (A) The current-voltage relationship of K_{ir} potassium channels shows a voltage range characterized by a "negative" resistance. This negativity leads to membrane bi-stability. Whereas small instantaneous changes of P1 will be compensated for (P1 is therefore a stable membrane potential), larger depolarizing artifacts will cause a jump of P1 to the limit point LP2. P1 can be regained by substantial repolarizing influences like the Na/K pump. **(B)** The curve is downwardly shifted by an omega Na^+ current. Limit point LP1 is a very instable membrane potential that will be shifted to P2 by even smallest instantaneous changes. In the P2-state the cell membrane will be electrically stable. **(C)** Membrane potentials P for various $[K^+]_o$ values and for various omega pore conductances (in $\mu S/cm^2$). Reducing $[K^+]_o$ first leads to hyperpolarization until the limit point (LP1) is reached at which the membrane potential becomes instable and jumps to the depolarized state of about −58 mV. From there, increasing $[K^+]_o$ takes the potential along the curve until LP2 is reached. LP2 is the starting point for the repolarization. The curves of LP1 and LP2 meet in the cusp point, CP. The region inside the cusp (bounded by LP1, LP2, and CP) is bi-stable. In contrast omega pore conductances larger than 18 $\mu S/cm^2$ result in *gradual* depolarization without bi-stability. The model reveals that an omega pore shifts LP1 and LP2 (the cusp) to the right, i.e., less severe hypokalemia is required to shift cells from the P1- to the P2-state. The membrane potentials yielded by the computer simulation were compared with values measured for muscle fibers by use of microelectrodes: open symbols stand for human controls (−83 ± 5 mV in 95% of fibers at 4 mM K^+, −99 ± 3 mV for 87% at 1.5 mM K^+, and −58 mV for 91% at 1 mM K^+); filled symbols for HypoPP patients with either $Ca_v1.1$-R1239H (circle: −74 ± 5 mV in 76% of fibers at 4 mM K^+) or $Ca_v1.1$-R528H (triangle: −75 ± 5 mV in 91% of fibers at 4 mM K^+); at 1.5 mM K^+, 95% of the patients' fibers −56 mV (square; $n = 127$). Modified after Jurkat-Rott et al. (2010).

Table 2 | Parameters of the catastrophe model.

Parameter	Value	Unit
GATING PARAMETERS OF Na_V, K_V, AND CLC		
$\hat{E}_{omega}$	−110	mV
A_{omega}	34	mV
$\hat{g}_{Na_V}$	268	mS/cm^2
$\hat{g}_{NaL}$	2.75	μS/cm^2
$\hat{g}_{K_V}$	21.6	mS/cm^2
$\hat{g}_{ClC}$	0.5	mS/cm^2
$\hat{g}_{ir}$	0.0485	mS/cm^2
K_S	0.0475	mM^2
K_K	5	mM^2
δ	0.2	–
$\hat{J}_p$	8	Nmol cm^{-2} s^{-1}
K_{mK}	1	mM
K_{mNa}	8	mM
L_H	1.25×10^{-10}	l cm^{-2} N^{-1} s^{-1}
EXTRA AND INITIAL INTRACELLULAR CONCENTRATIONS		
$\hat{c}_e^{Na^+} + \hat{c}_e^{K^+}$	141.5	mM
$\hat{c}_e^{Cl^-}$	108	mM
$\hat{c}_e^{Fix^-}$	25.8	mM
$\hat{c}_e^{Neutral}$	10	mM
$\hat{c}_i^{Na^+}$	15.6	mM
$\hat{c}_i^{K^+}$	132.3	mM
$\hat{c}_i^{S}$	8.9	mM
$\hat{c}_i^{Cl^-}$	4.3	mM
$\hat{c}_i^{Fix-}$	124.1	mM
E_{H^+}	−18.5	mV
V_i	3.38	μl
$\bar{c}_{H_2O}$	55555	mM
PARAMETERS FOR ION AND WATER FLUXES		
$\hat{\alpha}_m$	0.288	ms^{-1}
$\hat{\beta}_m$	1.38	ms^{-1}
$\hat{E}_m$	−42	mV
$K_{\alpha m}$	10	mV
$K_{\beta m}$	18	mV
$\hat{\alpha}_h$	0.0081	ms^{-1}
$\hat{\beta}_h$	4.38	ms^{-1}
$\hat{E}_h$	−45	mV
$K_{\alpha h}$	14.7	mV
$K_{\beta h}$	9	mV
$\hat{E}_S$	−85	mV
A_S	6	mV
$\hat{\alpha}_n$	0.0131	ms^{-1}
$\hat{\beta}_n$	0.067	ms^{-1}
$\hat{E}_n$	−37	mV
$K_{\alpha n}$	7	mV
$K_{\beta n}$	40	mV
$\hat{E}_{h_K}$	−30	mV
$K_{\tau hK}$	25.75	mV
A_{h_K}	7.5	mV
$\hat{E}_a$	70	mV
A_a	150	mV
PHYSICAL AND STRUCTURAL PARAMETERS		
D_f	70	μm
η	2	–
$\bar{c}_m$	1	μF/cm^2
z_{Fix}	−1.3	–
R	8.3145	J mol^{-1} K^{-1}
T	311.15	K
F	96485	C/mol

(Continued)

et al., 2001) and underlies barium-induced augmentation of paradoxical depolarization of skeletal muscle fibers in low external K^+ (K_{ir} 2.1; Struyk and Cannon, 2008). Decreased conductance of the ATP-sensitive K channel in skeletal muscle may also be a causative factor in hypokalemic-induced depolarization, at least in response to insulin (Tricarico et al., 1998). It has been proposed that part of the therapeutic effect of acetazolamide in HypoPP is its action to promote the activation of several different types of skeletal muscle potassium channels, which may offset the decreased conductance of K_{ir} (for review see Matthews and Hanna, 2010).

If the omega pore conductance is >18 μS/cm^2 (for the conditions in **Figure 4C**), the bi-stability is replaced by a single stable resting potential. The value depends on the conductance ratio g_K/g_ω with g_K carried by additional (e.g., delayed rectifying) K_v channels which are less dependent on extracellular K^+ than are K_{ir} channels. In this monostable system, the membrane potential can vary between −74 and −58 mV (**Figure 4C**).

Usually the majority of normal cells do not become inexcitable in response to decreased serum K^+, because the limit points are located at very low K^+ that do not occur physiologically. However in the presence of an omega current, the limit points are shifted to higher K^+, and transitions between the states are possible under physiological conditions. HypoPP seems to be caused by such a shift. For instance, computer simulation of the effect of R669H on Vrest in response to low external K^+ predicts a decrease in the threshold for paradoxical depolarization of muscle fibers, similar to that observed experimentally with barium poisoning (Struyk and Cannon, 2008). Cation ionophores like amphotericin B and gramicidin can mimic the omega pore current and serve as a successful, pharmacological *in vitro* model for HypoPP (Jurkat-Rott et al., 2009). Based on the ionophore experiments, the fraction of fibers in the P2-state may correspond to the chronic weakness in HypoPP patients. Typical triggers such as glucose and insulin causing hypokalemia will further increase this fraction and precipitate a paralytic attack. The pharmacological computer model predicts that smaller omega currents require a more severe hypokalemia of the patients to shift cells into the P2-state than larger omega currents.

SODIUM OVERLOAD, CYTOTOXIC EDEMA, AND TISSUE DEGENERATION

By tackling the question as to whether sodium influx (e.g., through omega pores) increases the cytoplasmic sodium concentration, a ^{23}Na MR sequence was developed (Nielles-Vallespin et al., 2007)

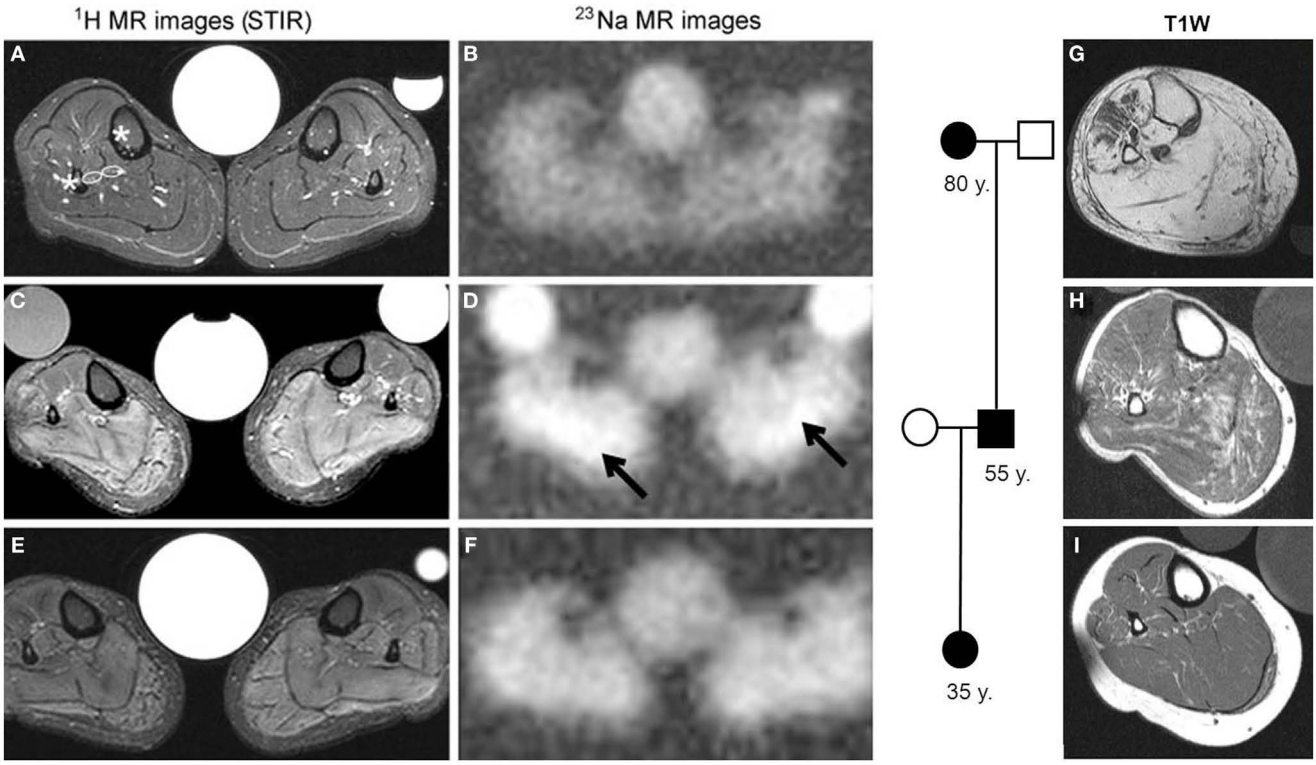

FIGURE 5 | ^{1}H and ^{23}Na measurements in the calf muscles of HypoPP patients. (A–F) T2-weighted STIR ^{1}H (left) and ^{23}Na-MR images (right) from a healthy control **(A,B)** and the propositus of a HypoPP family, a 37-year-old female harboring the Cav1.1-R1239H mutation **(C–F)**. The images in **(C,D)** were taken before treatment and the images in **(E,F)** were taken after treatment with 250 mg/d acetazolamide for 4 weeks. Note the very high proton intensities in STIR **(C)** and the elevated Na^{+} concentration before treatment **(D)**, arrows pointing at highest Na signal intensities) and their improvement after treatment. The central reference contains 0.3% NaCl solution; occasional side tubes containing 0.3% NaCl in 1% agarose (left) and 0.6% NaCl in H_2O (right) were additional standards. **(G–I)** Axial T1-weighted MR images from family members patients: the female's 80-year-old grandmother whose limb muscles were almost completely replaced with fat **(G)**, the female's 35-year-old sister **(I)**, and the 55-year-old uncle **(H,G)**. Modified after Jurkat-Rott et al. (2009).

that indeed revealed a muscle sodium overload in HypoPP patients (**Figure 5**). In addition, ^{1}H-MR images (MRI) with a short-tau inversion recovery (STIR) sequence displayed an edema in the muscles of these HypoPP patients (**Figures 5A–F**). Therefore the question arose as to whether the edema was caused by a cytoplasmic sodium accumulation and osmotic imbalance, or by an interstitial edema, e.g., by an inflammation. To answer this question the MRI technique was further improved to a ^{23}Na MRI inversion recovery sequence (Na-IR) which partially suppresses the signal raised by free sodium in the extracellular fluid and thus mainly represents cytoplasmic sodium (Nagel et al., 2011). In the HypoPP patients the nature of the edema was cytoplasmic. It seemed to be cytotoxic as all patients who showed the edema presented with a chronic weakness and muscle degeneration with age (**Figures 5G–I**).

In parallel with the concept of degeneration caused by sodium overload, ictal cytotoxic edema during the long-lasting depolarization (spreading depression) has been frequently reported in FHM (for example Chabriat et al., 2000; Butteriss et al., 2003) and has been suggested to sustain the long-lasting aura (Iizuka et al., 2006) and contribute to neurodegeneration (Carreño et al., 2011). Likewise, ictal edema is associated with neuronal degeneration and sclerosis of the hippocampus in FSs (Scott et al., 2003, 2006; Sokol et al., 2003). Therefore, it is possible that intracellular sodium overload may contribute to neuronal as well as muscle channelopathies.

REPOLARIZATION AND RELIEF OF THE CYTOTOXIC EDEMA

Guided by the experience that acetazolamide has favorable effects on the episodic weakness in the periodic paralyzes (Resnick et al., 1968), this agent was administered to HypoPP patients and reduced the chronic weakness of the patients as well as the sodium overload and edema in the MRI (**Figure 5**). In the pharmacological *in vitro* model of HypoPP using an ionophore, acetazolamide shifted many fibers from the P2- to the P1-state. This *in vitro* effect was considered to be responsible for the positive, *in vivo* effects (Jurkat-Rott et al., 2009). Thus, drugs that repolarize the fiber membrane may prevent progression of the cell degeneration by reducing the cytotoxic edema. Supporting the idea that FHM and epilepsy share similar pathomechanisms to HypoPP, it is not surprising that acetazolamide is standard treatment option for both epilepsy (Wolf, 2011) and FHM (Russell and Ducros, 2011).

ACKNOWLEDGMENTS

The work was supported by research grants from the Else Kröner-Fresenius-Stiftung and the BMBF (IonoNeurOnet), both to Karin Jurkat-Rott and Frank Lehmann-Horn (2010_A27), and by NIH 1R15NS064556-01 to James Groome. Frank Lehmann-Horn is endowed Senior Research Professor of the non-profit Hertie-Foundation. We thank M. Fauler and V. Winston (ISU) for their contributions to the computer models.

REFERENCES

Alekov, A., Rahman, M. M., Mitrovic, N., Lehmann-Horn, F., and Lerche, H. (2000). A sodium channel mutation causing epilepsy in man exhibits subtle defects in fast inactivation and activation in vitro. *J. Physiol. (Lond.)* 529, 533–539.

Alonso, I., Barros, J., Tuna, A., Seixas, A., Coutinho, P., Sequeiros, J., and Silveira, I. (2004). A novel R1347Q mutation in the predicted voltage sensor segment of the P/Q-type calcium-channel alpha-subunit in a family with progressive cerebellar ataxia and hemiplegic migraine. *Clin. Genet.* 65, 70–72.

Banderali, U., Juranka, P. F., Clark, R. B., Giles, W. R., and Morris, C. E. (2010). Impaired stretch modulation in potentially lethal cardiac sodium channel mutants. *Channels (Austin)* 4, 12–21.

Barela, A. J., Waddy, S. P., Lickfett, J. G., Hunter, J., Anido, A., Helmers, S. L., Goldin, A. L., and Escayg, A. (2006). An epilepsy mutation in the sodium channel SCN1A that decreases channel excitability. *J. Neurosci.* 26, 2714–2723.

Bartos, D. C., Duchatelet, S., Burgess, D. E., Klug, D., Denjoy, I., Peat, R., Lupoglazoff, J. M., Fressart, V., Berthet, M., Ackerman, M. J., January, C. T., Guicheney, P., and Delisle, B. P. (2011). R231C mutation in KCNQ1 causes long QT syndrome type 1 and familial atrial fibrillation. *Heart Rhythm* 8, 48–55.

Battistini, S., Stenirri, S., Piatti, M., Gelfi, C., Righetti, P. G., Rocchi, R., Giannini, F., Battistinin, N., Guazzi, C. G., Faerrarri, M., and Carrera, P. (1999). A new CACNA1A gene mutation in acetazolamide-responsive familial hemiplegic migraine and ataxia. *Neurology* 53, 38–43.

Bendahhou, S., Cummins, T. R., Griggs, R. C., Fu, Y. H., and Ptácek, L. J. (2001). Sodium channel inactivation defects are associated with acetazolamide-exacerbated hypokalemic periodic paralysis. *Ann. Neurol.* 50, 417–420.

Bezzina, C. R., Rook, M. B., Groenewegen, W. A., Herfst, L. J., van der Wal, A. C., Lam, J., Jongsma, H. J., Wilde, A. A., and Mannens, M. M. (2003). Compound heterozygosity for mutations (W156X and R225W) in SCN5A associated with severe cardiac conduction disturbances and degenerative changes in the conduction system. *Circ. Res.* 92, 159–168.

Bond, E. F., and Gordon, A. M. (1993). Insulin-induced membrane changes in (K+) depleted rat skeletal muscle. *Am. J. Physiol.* 265, C257–C265.

Bulman, D. E., Scoggan, K. A., van Oene, M. D., Nicolle, M. W., Hahn, A. F., Tollar, L. L., and Ebers, G. C. (1999). A novel sodium channel mutation in a family with hypokalemic periodic paralysis. *Neurology* 53, 1932–1936.

Butteriss, D. J., Ramesh, V., and Birchall, D. (2003). Serial MRI in a case of familial hemiplegic migraine. *Neuroradiology* 45, 300–303.

Cannon, S. C. (2010). Voltage-sensor mutations in channelopathies of skeletal muscle. *J. Physiol. (Lond.)* 588, 1887–1895.

Carle, T., Lhuillier, L., Luce, S., Strenberg, D., Devuyst, O., Fontaine, B., and Tabti, N. (2006). Gating defects of a novel Na+ channel mutant causing hypokalemic peiodic paralysis. *Biochem. Biophys. Res. Commun.* 348, 653.

Carreño, O., García-Silva, M. T., García-Campos, Ó., Martínez-de Aragón, A., Cormand, B., and Macaya, A. (2011). Acute striatal necrosis in hemiplegic migraine with de novo CACNA1A mutation. *Headache* 51, 1542–1546.

Catterall, W. A. (2010). Ion channel voltage sensors: structure, function, and pathophysiology. *Neuron* 67, 915–928.

Catterall, W. A., Kalume, F., and Oakley, J. C. (2010). NaV1.1 channels and epilepsy. *J. Physiol. (Lond.)* 588, 1849–1859.

Chabriat, H., Vahedi, K., Clark, C. A., Poupon, C., Ducros, A., Denier, C., Le Bihan, D., and Bousser, M. G. (2000). Decreased hemispheric water mobility in hemiplegic migraine related to mutation of CACNA1A gene. *Neurology* 54, 510–512.

Chabrier, S., Monnier, N., and Lunardi, J. (2008). Early onset of hypokalaemic periodic paralysis caused by a novel mutation of the CACNA1S gene. *J. Med. Genet.* 45, 686–688.

Cheng, C.-J., Lin, S.-H., Lo, Y.-F., Yang, S.-S., Hsu, Y.-J., Cannon, S. C., and Huang, C.-L. (2011). Identification and functional characterization of Kir2.6 mutations associated with non-familial hypokalemic periodic paralysis. *J. Biol. Chem.* 286, 27425–27435.

Chouabe, C., Neyroud, N., Richard, P., Denjoy, I., Hainque, B., Romey, G., Drici, M. D., Guicheney, P., and Barhanin, J. (2000). Novel mutations in KvLQT1 that affect Iks activation through interactions with Isk. *Cardiovasc. Res.* 45, 971–980.

Davies, N. P., Eunson, L. H., Samuel, M., and Hanna, M. G. (2001). Sodium channel gene mutations in hypokalemic periodic paralysis: an uncommon vause in the UK. *Neurology* 57, 1323–1325.

Dedek, K., Kunath, B., Kananura, C., Reuner, U., Jentsch, T. J., and Steinlein, O. K. (2001). Myokymia and neonatal epiepsy caused by a mutation in the voltage sensor of the KCNQ2 K+ channel. *Proc. Natl. Acad. Sci. U.S.A.* 98, 12272–12277.

Ducros, A., Denier, C., Joutel, A., Cecillon, M., Lescoat, C., Vahedi, K., Darcel, F., Vicaut, E., Bousser, M. G., and Tournier-Lasserve, E. (2001). The clinical spectrum of familial hemiplegic migraine associated with mutations in a neuronal calcium channel. *N. Engl. J. Med.* 345, 17–24.

Dumaine, R., Wang, Q., Keating, M. T., Hartmann, H. A., Schwartz, P. J., Brown, A. M., and Kirsch, G. E. (1996). Multiple mechanisms of Na+ channel – linked long-QT syndrome. *Circ. Res.* 78, 916–924.

Escayg, A., and Goldin, A. L. (2010). Sodium channel SCN1A and epilepsy: mutations and mechanisms. *Epilepsia* 51, 1650–1168.

Escayg, A., MacDonald, B. T., Meisler, M. H., Baulac, S., Huberfeld, G., An-Gourfinkel, I., Brice, A., LeGuern, E., Moulard, B., Chaigne, D., Buresi, C., and Malafosse, A. (2000). Mutations of SCN1A, encoding a neuronal sodium channel, in two families with GEFS+2. *Nat. Genet.* 24, 343–345.

Fan, Z., George, A. L. Jr., Kyle, J. W., and Makielski, J. C. (1996). Two human paramyotonia congenital mutations have opposite effects on lidocaine block of Na+ channels expressed in a mammalian cell line. *J. Physiol. (Lond.)* 496, 275–286.

Featherstone, D. E., Fujimoto, E., and Ruben, P. C. (1998). A defect in skeletal muscle sodium channel deactivation exacerbates hyperexcitability in human paramyotonia congenita. *J. Physiol. (Lond.)* 506, 627–638.

Fodstad, H., Swan, H., Laitinen, P., Piippo, K., Paavonen, K., Viitasalo, M., Toivonen, L., and Kontula, K. (2004). Four potassium channel mutations account for 73% of the genetic spectrum underlying long-QT syndrome (LQTS) and provide evidence for a strong founder effect in Finland. *Ann. Med.* 36, 53–63.

Francis, D. G., Rybalchenko, V., Struyk, A., and Cannon, S. C. (2011). Leaky sodium channels from voltage sensor mutations in periodic paralysis, but not paramyotonia. *Neurology* 76, 1635–1641.

Franqueza, L., Lin, M., Shen, J., Splawski, I., Keating, M. T., and Sanguinetti, M. C. (1999). Long QT syndrome-associated mutations in the S4-S5 linker of KvLQT1 potassium channels modify gating and interaction with minK subunits. *J. Biol. Chem.* 274, 21063–21070. [Erratum in: *J. Biol. Chem.* 274, 25188].

Friend, K. L., Crimmins, D., Phan, T. G., Sue, C. M., Colley, A., Fung, V. S., Morris, J. G., Sutherland, G. R., and Richards, R. I. (1999). Detection of a novel missense mutation and second recurrent mutation in the CACNA1A gene in individuals with EA-2 and FHM. *Hum. Genet.* 105, 261–265.

Frigo, G., Rampazzo, A., Bauce, B., Pilichou, K., Beffagna, G., Danieli, G. A., Nava, A., and Martini, B. (2007). Homozygous SCN5A mutation in Brugada syndrome with monomorphic ventricular tachycardia and structural heart abnormalities. *Europace* 9, 391–397.

Gamal El-Din, T. M., Heldstab, H., Lehmann, C., and Greeff, N. G. (2010). Double gaps along Shaker S4 demonstrate omega currents at three different closed states. *Channels (Austin)* 4, 93–100.

Groome, J. R., Fujimoto, E., George, A. L., and Ruben, P. C. (1999). Differential effects of homologous S4 mutations in human skeletal muscle sodium channels on deactivation gating from open and inactivated states. *J. Physiol. (Lond.)* 516, 687–698.

Groome, J. R., and Winston, V. (2012). Voltage sensor module in NaV1.4: S1-S3 charges regulate fast inactivation. *Biophys. Soc. Abstr.* 1655, Pos B425.

Hans, M., Luvisetto, S., Williams, M. E., Spagnolo, M., Urrutia, A., Tottene, A., Brust, P. F., Johnson, E. C., Harpold, M. M., Stauderman, K. A., and Pietrobon, D. (1999). Functional consequences of mutations in the human alpha1A calcium channel subunit linked to familial hemiplegic migraine. *J. Neurosci.* 19, 1610–1619.

Heine, R., Pika, U., and Lehmann-Horn, F. (1993). A novel SCN4A mutation causing myotonia aggravated by cold and potassium. *Hum. Mol. Genet.* 2, 1349–1353.

Holzherr, B. D., Groome, J. R., Fauler, M., Nied, E., Lehmann-Horn, F., and Jurkat-Rott, K. (2010). Characterization of a novel hNaV1.4 mutation causing hypokalemic periodic paralysis. *Biophys. Soc. Abstr.* LB201, Pos L201.

Hong, D., Luan, X., Chen, B., Zheng, R., Zhang, W., Wang, Z., and Yuan, Y. (2010). Both hypokalaemic and normokalaemic periodic paralysis in different members of a single family with novel R1129Q mutation in SCN4A gene. *J. Neurol. Neurosurg. Psychiatr.* 81, 703–704.

Iizuka, T., Sakai, F., Suzuki, K., Igarashi, H., and Suzuki, N. (2006). Implication of augmented vasogenic leakage in the mechanism of persistent aura in sporadic hemiplegic migraine. *Cephalgia* 26, 332–335.

Itoh, T., Tanaka, T., Nagai, R., Kamiya, T., Sawayama, T., Nakayama, T., Tomoike, H., Sakurada, H., Yazaki, Y., and Nakamura, Y. (1998). Genomic organization and mutational analysis of HERG, a gene responsible for familial long QT syndrome. *Hum. Genet.* 102, 435–439.

Jurkat-Rott, K., Holzherr, B., Fauler, M., and Lehmann-Horn, F. (2010). Sodium channelopathies of skeletal muscle result from gain or loss of function. *Pflugers Arch.* 460, 239–248.

Jurkat-Rott, K., and Lehmann-Horn, F. (2007). Do hyperpolarization-induced proton currents contribute to the pathogenesis of hypokalemic periodic paralysis, a voltage sensor channelopathy? *J. Gen. Physiol.* 130, 1–5.

Jurkat-Rott, K., Lehmann-Horn, F., Elbaz, A., Heine, R., Gregg, R. G., Hogan, K., Powers, P. A., Lapie, P., Vale-Santos, J. E., Weissenbach, J., and Fontaine, B. (1994). A calcium channel mutation causing hypokalemic periodic paralysis. *Hum. Mol. Genet.* 3, 1415–1419.

Jurkat-Rott, K., Mitrovic, N., and Lehmann-Horn, F. (2000). Voltage-sensor sodium channel mutations cause hypokalemic periodic paralysis type 2 by enhanced inactivation and reduced current. *Proc. Natl. Acad. Sci. U.S.A.* 97, 9549–9554.

Jurkat-Rott, K., Uetz, U., Pika-Hartlaub, U., Powell, J., Fontaine, B., Melzer, W., and Lehmann-Horn, F. (1998). Calcium currents and transients of native and heterologously expressed mutant skeletal muscle DHP receptor alpha1 subunits (R528H). *FEBS Lett.* 423, 198–204.

Jurkat-Rott, K., Weber, M. A., Fauler, M., Guo, X. H., Holzherr, B. D., Paczulla, A., Nordsborg, N., Joechle, W., and Lehmann-Horn, F. (2009). K+-dependent paradoxical membrane depolarization and Na+ overload, major and reversible contributors to weakness by ion channel leaks. *Proc. Natl. Acad. Sci. U.S.A.* 106, 4036–4041.

Kahlig, K. M., Lepist, I., Leung, K., Rajamani, S., and George, A. L. (2010). Ranolazine selectively blocks persistent current evoked by epilepsy-associated Nav1.1 mutations. *Br. J. Pharmacol.* 161, 1414–1426.

Kahlig, K. M., Misra, S. N., and George, A. L. Jr. (2006). Impaired inactivation gate stabilization predicts increased persistent current for an epilepsy-associated SCN1A mutation. *J. Neurosci.* 26, 10958–10966.

Kim, J. B., Kim, M. H., Lee, S. J., Kim, D. J., and Lee, B. C. (2007). The genotype and clinical phenotype of Korean patients with familial hypokalemic periodic paralysis. *J. Korean Med. Sci.* 22, 946–951.

Kraus, R. L., Sinnegger, M. J., Glossmann, H., Hering, S., and Striessnig, J. (1998). Familial hemiplegic migraine mutations change alpha1A Ca2+ channel kinetics. *J. Biol. Chem.* 273, 5586–5590.

Kraus, R. L., Sinnegger, M. J., Koschak, A., Glossmann, H., Stenirri, S., Carrera, P., and Striessnig, J. (2000). Three new familial hemiplegic migraine mutants affect P/Q-type Ca(2+) channel kinetics. *J. Biol. Chem.* 275, 9239–9243.

Kuzmenkin, A., Hang, C., Kuzmenkina, E., and Jurkat-Rott, K. (2007). Gating of the HypoPP-1 mutations: I. Mutant-specific effects and cooperativity. *Pflugers Arch.* 454, 495–505.

Kuzmenkin, A., Muncan, V., Jurkat-Rott, K., Hang, C., Lerche, H., Lehmann-Horn, F., and Mitrovic, N. (2002). Enhanced inactivation and pH sensitivity of Na+ channel mutations causing hypokalaemic periodic paralysis type II. *Brain* 125, 835–843.

Lapie, P., Goudet, C., Nargeot, J., Fontaine, B., and Lory, P. (1996). Electrophysiological properties of the hypokalaemic periodic paralysis mutation (R528H) of the skeletal muscle alpha 1s subunit as expressed in mouse L cells. *FEBS Lett.* 382, 244–248.

Lee, S. C., Kim, H. S., Park, Y. E., Choi, Y. C., Park, K. H., and Kim, D. S. (2009). Clinical diversity of SCN4A-mutation-associated skeletal muscle sodium channelopathy. *J. Clin. Neurol.* 5, 186–191.

Lehmann-Horn, F., and Jurkat-Rott, K. (1999). Voltage-gated ion channels and hereditary disease. *Physiol. Rev.* 79, 1317–1371.

Lehmann-Horn, F., Rüdel, R., and Ricker, K. (1987). Membrane defects in paramyotonia congenita (Eulenburg). *Muscle Nerve* 10, 633–641.

Lehmann-Horn, F., Sipos, I., Jurkat-Rott, K., Heine, R., Brinkmeier, H., Fontaine, B., Kovacs, L., and Melzer, W. (1995). Altered calcium currents in human hypokalemic periodic paralysis myotubes expressing mutant L-type calcium channels. *Soc. Gen. Physiol. Ser.* 50, 101–113.

Lerche, H., Heine, R., Pika, U., George, A. L., Mitrovic, N., Browatzki, M., Weiss, T., Bastide-Rivet, M., Franke, C., LoMonaco, M., Ricker, K., and Lehmann-Horn, F. (1993). Human sodium channel myotonia: slowed channel inactivation due to substitutions for a glycine within the III/IV linker. *J. Physiol. (Lond.)* 470, 13–22.

Lerche, H., Mitrovic, N., Dubowitz, V., and Lehmann-Horn, F. (1996). Paramyotonia congenita: the R1448P Na+ channel mutation in adult human skeletal muscle. *Ann. Neurol.* 39, 599–608.

Lossin, C., Rhodes, T. H., Desai, R. R., Vanoye, C. G., Wang, D., Carniciu, S., Devinsky, O., and George, A. L. Jr. (2003). Epilepsy-associated dysfunction in the voltage-gated neuronal sodium channel SCN1A. *J. Neurosci.* 23, 11289–11295.

Lupoglazoff, J. M., Denjoy, I., Villain, E., Fressart, V., Simon, F., Bozio, A., Berthet, M., Benammar, N., Hainque, B., and Guicheney, P. (2004). Long QT syndrome in neonates: conduction disorders associated with HERG mutations and sinus bradycardia with KCNQ1 mutations. *J. Am. Coll. Cardiol.* 43, 826–830.

Makita, N., Shirai, N., Magashima, M., Matsuoka, R., Yamada, Y., Tohse, N., and Kitabatake, A. (1998). A de novo missense mutation of human cardiac Na(+) channel exhibiting novel molecular mechanism of long QT syndrome. *FEBS Lett.* 423, 5–9.

Maljevic, S., Wuttke, T. V., and Lerche, H. (2008). Nervous system Kv7 disorders: breakdown of a subthreshold brake. *J. Physiol. (Lond.)* 586, 1791–1801.

Martin, M. S., Dutt, K., Papale, L. A., Dubé, C. M., Dutton, S. B., de Haan, G., Shankar, A., Tufik, S., Meisler, M. H., Baram, T. Z., Goldin, A. L., and Escayg, A. (2010). Altered function of the SCN1A voltage-gated sodium channel leads to gamma-aminobutyric acid-ergic (GABAergic) interneuron abnormalities. *J. Biol. Chem.* 285, 9823–9834.

Matthews, E., and Hanna, M. G. (2010). Muscle channelopathies: does the predicted gating pore offer new treatment insights for hypokalemic periodic paralysis? *J. Physiol. (Lond.)* 588, 1879–1886.

Matthews, E., Labrum, R., Sweeney, M. G., Sud, R., Haworth, A., Chinnery, P. F., Meola, G., Schorge, S., Kullmann, D. M., Davis, M. B., and Hanna, M. G. (2009). Voltage sensor charge loss accounts for most cases of hypokalemic periodic paralysis. *Neurology* 72, 1544–1547.

Matthews, E., Tan, S. V., Fialho, D., Sweeney, M. G., Sud, R., Haworth, A., Stanley, E., Cea, G., Davis, M. B., Hanna, M. G. (2008). What causes paramyotonia in the United Kingdom? Common and new SCN4A mutations revealed. *Neurology* 70, 50–53.

Miceli, F., Vargas, E., Bezanilla, F., and Taglialatela, M. (2012). Gating currents from K(v)7 channels carrying neuronal hyperexcitability mutations in the voltage-sensing domain. *Biophys. J.* 102, 1372–1382.

Millat, G., Chevalier, P., Restier-Miron, L., Da Costa, A., Bouvagnet, P., Kugener, B., Fayol, L., Gonzàlez Armengod, C., Oddou, B., Chanavat, V., Froidefond, E., Perraudin, R., Rousson, R., and Rodriguez-Lafrasse, C. (2006). Spectrum of pathogenic mutations and associated polymorphisms in a cohort of 44 unrelated patients with long QT syndrome. *Clin. Genet.* 70, 214–227.

Mitrovic, N., George, A. L. Jr., Rüdel, R., Lehmann-Horn, F., and Lerche, H. (1999). Mutant channels contribute <50% to Na+ current in paramyotonia congenita muscle. *Brain* 122, 1085–1092.

Mohammad-Panah, R., Demolombe, S., Neyroud, N., Guicheney, P., Kyndt, F., van den Hoff, M., Baró, I., and Escande, D. (1999). Mutations in a dominant-negative isoform correlate with phenotype in inherited cardiac arrhythmias. *Am. J. Hum. Genet.* 64, 1015–1023.

Morrill, J. A., Brown, R. H. Jr., and Cannon, S. C. (1998). Gating of the L-type Ca channel in human skeletal myotubes: an activation defect caused by the hypokalemic periodic paralysis mutation R528H. *J. Neurosci.* 18, 10320–10334.

Morrill, J. A., and Cannon, S. C. (1999). Effects of mutations causing hypokalaemic periodic paralysis on the skeletal muscle L-type Ca2+ channel expressed in *Xenopus laevis* oocytes. *J. Physiol. (Lond.)* 520, 321–336.

Mullen, S. A., and Scheffer, I. E. (2009). Translational research in epilepsy genetics. *Arch. Neurol.* 66, 21–26.

Nagel, A. M., Amarteifio, E., Lehmann-Horn, F., Jurkat-Rott, K., Semmler, W., Schad, L. R., and Weber, M. A. (2011). 3 Tesla sodium inversion recovery magnetic resonance imaging allows improved visualization of intracellular sodium content changes in muscular channelopathies. *Invest. Radiol.* 46, 759–766.

Nakajima, T., Furukawa, T., Hirano, Y., Tanaka, T., Sakurada, H., Takahashi, T., Nagai, R., Itoh, T., Katayama, Y., Nakamura, Y., and Hiraoka, M. (1999). Voltage-shift of the current activation in HERG S4 mutation (R534C) in LQT2. *Cardiovasc. Res.* 44, 283–293.

Nielles-Vallespin, S., Weber, M. A., Bock, M., Bongers, A., Speier, P., Combs, S. E., Wöhrle, J., Lehmann-Horn, F., Essig, M., and Schad, L. R. (2007). 3D radial projection technique with ultrashort echo times for sodium MRI: clinical applications in human brain and skeletal muscle. *Magn. Reson. Med.* 57, 74–81.

Oakley, J. C., Kalume, F., and Catterall, W. A. (2011). Insights into pathophysiology and therapy from a mouse model of Dravet syndrome. *Epilepsia* 52, 59–61.

Ophoff, R. A., Terwindt, G. M., Vergouwe, M. N., van Eijk, R., Oefner, P. J., Hoffman, S. M. G., Lamerdin, J. E., Mohrenweiser, H. W., Bulman, D. E., Ferrari, M., Haan, J., Lindhout, D., van Ommen, G.-J. B., Hofker, M. H., Ferrari, M. D., and Frants, R. R. (1996). Familial hemiplegic migraine and episodic ataxia type-2 are caused by mutations in the Ca(2+) channel gene CACNL1A4. *Cell* 87, 543–552.

Plaster, N. M., Tawil, R., Tristani-Firouzi, M., Canun, S., Bendahhou, S., Tsunoda, A., Donaldson, M. R., Iannaccone, S. T., Brunt, E., Barohn, R., Clark, J., Deymeer, F., George, A. L. Jr., Fish, F. A., Hahn, A., Nitu, A., Ozdemir, C., Serdaroglu, P., Subramony, S. H., Wolfe, G., Fu, Y.-H., and Ptacek, L. J. (2001). Mutations in Kir2.1 cause the developmental and episodic electrical phenotypes of Anderson's syndrome. *Cell* 105, 511–519.

Ptacek, L. J., George, A. L.Jr., Barchi, R. L., Griggs, R. C., Riggs, J. E., Robertson, M., and Leppert, M. F. (1992). Mutations in an S4 segment of the adult skeletal muscle sodium channel cause paramyotonia congenita. *Neuron* 8, 891–897.

Ptacek, L. J., Tawil, R., Griggs, R. C., Engel, A. G., Layzer, R. B., Kwiecinski, H., McManis, P. G., Santiago, L., Moore, M., Fouad, G., Bradley, P., and Leppert, M. F. (1994). Dihydropyridine receptor mutations cause hypokalemic periodic paralysis. *Cell* 77, 863–868.

Resnick, J. S., Engel, W. K., Griggs, R. C., and Stam, A. C. (1968). Acetazolamide prophylaxis in hypokalemic periodic paralysis. *N. Engl. J. Med.* 278, 582–586.

Rhodes, T. H., Lossin, C., Vanoye, C. G., Wang, D. W., and George, A. L. Jr. (2004). Noninactivating voltage-gated sodium channels in severe myoclonic epilepsy of infancy. *Proc. Natl. Acad. Sci. U.S.A.* 101, 11147–11152.

Ruan, Y., Liu, N., Bloise, R., Napolitano, C., and Priori, S. G. (2007). Gating properties of SCN5A mutations and the response to mexiletine in long-QT syndrome type 3 patients. *Circulation* 116, 1137–1144.

Ruff, R. L. (1999). Insulin acts in hypokalemic periodic paralysis by reducing inward rectifier K current. *Neurology* 53, 1556.

Russell, M. B., and Ducros, A. (2011). Sporadic and familial hemiplegic migraine: pathophysiological mechanisms, clinical characteristics, diagnosis, and management. *Lancet Neurol.* 10, 457–470.

Ryan, D. P., da Silva, M. R. D., Soong, T. W., Fontaine, B., Donaldson, M. R., Kung, A. W. C., Jongjaroenprasert, W., Liang, M. C., Khoo, D. H. C., Cheah, J. S., Ho, S. C., Bernstein, H. S., Maciel, R. M. B., Brown, R. H. Jr., and Ptacek, L. J. (2010). Mutations in potassium channel Kir2.6 cause susceptibility to thyrotoxic hypokalemic periodic paralysis. *Cell* 140, 88–98.

Scott, R. C., King, M. D., Gadian, D. G., Neville, B. G., and Connelly, A. (2003). Hippocampal abnormalities after prolonged febrile convulsion: a longitudinal MRI study. *Brain* 126, 2551–2557.

Scott, R. C., King, M. D., Gadian, D. G., Neville, B. G., and Connelly, A. (2006). Prolonged febrile seizures are associated with hippocampal vasogenic edema and developmental changes. *Epilepsia* 47, 1493–1498.

Sokol, D. K., Demyer, W. E., Edwards-Brown, M., Sanders, S., and Garg, B. (2003). From swelling to sclerosis: acute change in mesial hippocampus after prolonged febrile seizure. *Seizure* 12, 237–240.

Sokolov, S., Scheuer, T., and Catterall, W. A. (2005). Ion permeation through a voltage- sensitive gating pore in brain sodium channels having voltage sensor mutations. *Neuron* 47, 183–189.

Sokolov, S., Scheuer, T., and Catterall, W. A. (2007). Gating pore current in an inherited ion channelopathy. *Nature* 446, 76–78.

Sokolov, S., Scheuer, T., and Catterall, W. A. (2008). Depolarization-activated gating pore current conducted by mutant sodium channels in potassium-sensitive normokalemic periodic paralysis. *Proc. Natl. Acad. Sci. U.S.A.* 105, 19980–19985.

Sokolov, S., Scheuer, T., and Catterall, W. A. (2010). Ion permeation and block of the gating pore in the voltage sensor of NaV1.4 channels with hypokalemic periodic paralysis mutations. *J. Gen. Physiol.* 136, 225–236.

Spampanato, J., Escayg, A., Meisler, M. H., and Goldin, A. L. (2001). Functional effects of two voltage-gated sodium channel mutations that cause generalized epilepsy with febrile seizures plus type 2. *J. Neurosci.* 21, 7481–7490.

Splawski, I., Shen, J., Timothy, K. W., Lehmann, M. H., Priori, S., Robinson, J. L., Moss, A. J., Schwartz, P. J., Towbin, J. A., Vincent, G. M., and Keating, M. T. (2000). Spectrum of mutations in long-QT syndrome genes. KVLQT1, HERG, SCN5A, KCNE1, and KCNE2. *Circulation* 102, 1178–1185.

Starace, D. M., and Bezanilla, F. (2001). Histidine scanning mutagenesis of basic residues of the S4 segment of the Shaker K+ channel. *J. Gen. Physiol.* 117, 469–490.

Starace, D. M., and Bezanilla, F. (2004). A proton pore in a potassium channel voltage sensor reveals a focused electric field. *Nature* 427, 548–553.

Starace, D. M., Stefani, E., and Bezanilla, F. (1997). Voltage-dependent proton transport by the voltage sensor of the Shaker K+ channel. *Neuron* 19, 1319–1327.

Struyk, A. F., and Cannon, S. C. (2007). A Na+ channel mutation linked to hypokalemic periodic paralysis exposes a proton-selective gating pore. *J. Gen. Physiol.* 130, 11–20.

Struyk, A. F., and Cannon, S. C. (2008). Paradoxical depolarization of Ba2+-treated muscle exposed to low extracellular K+: insights into resting potential abnormalities in hypokalemic paralysis. *Muscle Nerve* 37, 326–337.

Struyk, A. F., Markin, V. S., Francis, D., and Cannon, S. (2008). Gating pore currents in DIIS4 mutations of NaV1.4 associated with periodic paralysis: saturation of ion flux and implications for disease pathogenesis. *J. Gen. Physiol.* 132, 447–464.

Struyk, A. F., Scoggan, K. A., Bulman, D. E., and Cannon, S. C. (2000). The human skeletal muscle Na channel mutation R669H associated with hypokalemic periodic paralysis enhances slow inactivation. *J. Neurosci.* 20, 8610–8617.

Tombola, F., Pathak, M. M., and Isacoff, E. Y. (2005). Voltage-sensing arginines in a potassium channel permeate and occlude cation-selective pores. *Neuron* 45, 379–388.

Tonelli, A., D'Angelo, M. G., Salati, R., Villa, L., Germinasi, C., Frattini, T., Meola, G., Turconi, A. C., Bresolin, N., and Bassi, M. T. (2006). Early onset, non fluctuating spinocerebellar ataxia and a novel missense mutation in CACNA1A gene. *J. Neurol. Sci.* 241, 13–17.

Tricarico, D., and Camerino, D. C. (2011). Recent advances in the pathogenesis and drug action in periodic paralyses and related channelopathies. *Front. Pharmacol.* 2:8. doi:10.3389/fphar.2011.00008

Tricarico, D., Pierno, S., Mallamaci, R., Brigiani, G. S., Capriulo, R., Santoro, G., and Camerino, D. C. (1998). The biophysical and pharmacological characteristics of skeletal muscle ATP-sensitive K+ channels are modified in K+-depleted rat, an animal model of hypokalemic periodic paralysis. *Mol. Pharmacol.* 54, 197–206.

van den Maagdenberg, A. M., Pietrobon, D., Pizzorusso, T., Kaja, S., Broos, L. A., Cesetti, T., van de Ven, R. C., Tottene, A., van der Kaa, J., Plomp, J. J., Frants, R. R., and Ferrari, M. D. (2004). A Cacna1a knockin migraine mouse model with increased susceptibility to cortical spreading depression. *Neuron* 41, 701–710.

Vanoye, C. G., Lossin, C., Rhodes, T. H., and George, A. L. Jr. (2006). Single-channel properties of human NaV1.1 and mechanism of channel

dysfunction in SCN1A-associated epilepsy. *J. Gen. Physiol.* 127, 1–14.

Vicart, S., Sternberg, D., Fournier, E., Ochsner, F., Laforet, P., Kuntzer, T., Eymard, B., Hainque, B., and Fontaine, B. (2004). New mutations of SCN4A cause a potassium-sensitive normokalemic periodic paralysis. *Neurology* 63, 2120–2127.

Wallinga, W., Meijer, S. L., Alberink, M. J., Vliek, M., Wienk, E. D., and Ypey, D. L. (1999). Modelling action potentials and membrane currents of mammalian skeletal muscle fibres in coherence with potassium concentration changes in the T-tubular system. *Eur. Biophys. J.* 28, 317–329.

Wolf, P. (2011). Acute drug administration in epilepsy: a review. *CNS Neurosci. Ther.* 17, 442–448.

Wu, F., Mi, W., Burns, D. K., Fu, Y., Gray, H. F., Struyk, A. F., and Cannon, S. C. (2011). A sodium channel knockin mutant (NaV1.4-R669H) mouse model of hypokalemic periodic paralysis. *J. Clin. Invest.* 121, 4082–4094.

Wu, L., Wu, W., Yan, G., Wang, X., and Liu, J. (2008). The construction and preliminary investigation of the cell model of a novel mutation R675Q in the SCN4A gene identified in a Chinese family with normokalemic periodic paralysis. *Zhonghua Yi Xue Yi Chuan Xue Za Zhi* 25, 629–632.

Wuttke, T. V., Jurkat-Rott, K., Paulus, W., Garncarek, M., Lehmann-Horn, F., and Lerche, H. (2007). Peripehral nerve hyperexcitability due to dominant-negative KCNQ2 mutations. *Neurology* 69, 2045–2053.

Yamagishi, H., Furutani, M., Kamisago, M., Morikawa, Y., Kojima, Y., Hino, Y., Furutani, Y., Kimura, M., Imamura, S., Takao, A., Momma, K., and Matsuoka, R. (1998). A de novo missense mutation (R1623Q) of the SCN5A gene in a Japanese girl with sporadic long QT sydrome. Mutations in brief no. 140. Online. *Hum. Mutat.* 11, 481.

Yang, N., Ji, S., Zhou, M., Ptacek, L. J., Barchi, R. L., Horn, R., and George, A. L. Jr. (1994). Sodium channel mutations in paramyotonia congenita exhibit similar biophysical phenotypes in vitro. *Proc. Natl. Acad. Sci. U.S.A.* 91, 12785–12789.

Conflict of Interest Statement: The authors declare that the research was conducted in the absence of any commercial or financial relationships that could be construed as a potential conflict of interest.

Received: 22 April 2012; accepted: 23 May 2012; published online: 11 June 2012.
Citation: Jurkat-Rott K, Groome J and Lehmann-Horn F (2012) Pathophysiological role of omega pore current in channelopathies. Front. Pharmacol. ***3****:112. doi: 10.3389/fphar.2012.00112*
This article was submitted to Frontiers in Pharmacology of Ion Channels and Channelopathies, a specialty of Frontiers in Pharmacology.

APPENDIX

PATHOGENESIS MODEL – CATASTROPHE ON THE CUSP

Using catastrophe theory, the effects of an omega current were simulated in a one-compartment computer model of skeletal muscle fibers. Both changes of ion concentrations and consecutive water shifts were considered. The size of the T-tubular system was accounted for by a specific factor. It was not considered a separate compartment since the low-resistance T-tubular openings justified the assumption of an equilibrium. Parameters of the catastrophe model are given in **Table 2**; notations and abbreviations at the end of the Appendix.

The membrane was equipped with the following conductances: a background Na^+ leak conductance (g_{NaL}), the omega pore conductance (g_{leak}), a voltage-gated Na^+ (g_{NaV}) and K^+ (g_{Kv}) conductance, an inward-rectifying K^+ (g_{IR}) and a voltage-dependent Cl^- (g_{Cl}) conductance, a hydraulic conductivity (L_H), and a Na^+/K^+ pump flux (J_p). The model was based on the charge-difference approach (3) in which the membrane potential E is calculated from the amount of charges in the intracellular compartment Q_i and the membrane area A_m:

$$E = \frac{Q_i}{\bar{c}_m \cdot A_m} \text{ with } A_m = 4 \cdot \eta \cdot \frac{V_i}{D_f}$$

$$Q_i = F \cdot \sum_{ion} n_{ion} \cdot z_{ion} \text{ ion} \in \{\text{Na}, K, \text{Cl}, \text{Fix}, S\}$$

V_i was the cell volume, D_f the fiber diameter and η a factor correcting the size of the T-tubular membrane. The cell was only permeable for Na, *K*, Cl, and H_2O. *Fix* are intracellular anions (e.g., proteins, phosphates), which – in this model – cannot pass through the membrane. Their overall charge valence z_{Fix} is set to −1.3. This was necessary to avoid very negative membrane potentials at low potassium concentrations. *S* are the positive charged ions, that block inward-rectifying K^+ channels from inside upon depolarization. Its valence z_S is set to +2, so they represent Mg^{2+}. Multiple positively charged polyamines that increase the strength of rectification were not considered.

The amounts of ions and water in the cell *n* are state variables in this model. They are integrated over time by numerically solving the differential equations that describe their fluxes *J*:

$$n_s = \hat{n}_s + \int_0^t J_s \cdot dt \; s \in \{Na, K, Cl, H_2O\}$$

$$J_s = \frac{dn_s}{dt} = \sum_c J_s^c + \sum_p J_s^p \quad \begin{matrix} c \in \{Na_V, K_V, K_{ir}, ClC, Aqua\} \\ p \in \{Na/K - pump\} \end{matrix}$$

The fluxes of ions through channels J_s^c and water through an aquaporin $J_{H_2O}^{Aqua}$ (modeled by a simple hydraulic conductivity) are computed by the following equations:

$$J_{ion}^c = -F^{-1} \cdot g_{ion}^c \cdot (E - E_{ion}) \quad \begin{matrix} ion \in \{Na^+, K^+, Cl^-\} \\ c \in \{Na_L, Leak, Na_V, K_V, K_{ir}, ClC\} \end{matrix}$$

$$J_{H_2O}^{Aqua} = L_H \cdot \hat{c}_{H_2O} \cdot \Delta\Pi$$

The driving forces for the fluxes were the electrochemical gradients ($E - E_{ion}$) for ions or the osmotic pressure difference $\Delta\Pi$ for water:

$$E_{ion} = \frac{R \cdot T}{z_{ion} \cdot F} \cdot \ln\left(\frac{c_e^{ion}}{c_i^{ion}}\right)$$

$$\Delta\Pi = R \cdot T \cdot \sum_{sol} \left(c_i^{sol} - c_e^{sol}\right) \text{ sol} \in \{\text{Na, K, Cl, Fix, } S\}$$

The Na/K pump was modeled by

$$J_p = \hat{J}_p \cdot \left(1 + K_{mK} \Big/ c_e^{K^+}\right)^{-2} \cdot \left(1 + K_{mNa} \Big/ c_i^{Na^+}\right)^{-3}, J_{Na^+}^p = -3 \cdot J_p \text{ and } J_{K^+}^p = 2 \cdot J_p$$

The parameters K_{mK} and K_{mNa} were taken from Wallinga et al. (1999). The maximum pump flux $\hat{J}_{\mathrm{p}}$ was chosen to get an intracellular Na^+ concentration $c_i^{Na^+}$ of 15 mM at control conditions. Intracellular ion concentrations were calculated from the cell volume V_{i} and the amount of ions:

$$Vi = \frac{\sum_s n_s}{\bar{c}_{H_2O}},\ \mathrm{s} \in \{\mathrm{Na, K, Cl, Fix, H_2O}\}$$

$$c_i^{\mathrm{ion}} = \frac{n_{\mathrm{ion}}}{Vi},\ \mathrm{ion} \in \{\mathrm{Na, K, Cl, Fix}\}$$

The voltage-gated Na^+ (Na_V), K^+ (K_V), and Cl^- (ClC1) conductances were based on the Hodgkin–Huxley type formalism; identifiers had their classical meaning. The equations taken from Wallinga et al. (1999) are given here for completeness:

$$g_{\mathrm{Na}_V}^{\mathrm{Na}^+} = \hat{g}_{\mathrm{Na}_V} \cdot m^3 \cdot h \cdot S,\ g_{\mathrm{K}_V}^{\mathrm{K}^+} = \hat{g}_{\mathrm{K}_V} \cdot n^4 \cdot h_K \text{ and } g_{\mathrm{ClC}}^{\mathrm{Cl}^-} = \hat{g}_{\mathrm{ClC}} \cdot a^4$$

The gating variables m, h, S (Na_V slow inactivation), n, and h_K (inactivation of K_V) were state variables and defined by the following differential equations

$$\frac{dy}{dt} = \alpha_y \cdot (1 - y) - \beta_y \cdot y\ y \in \{m,\ n,\ h\}$$

$$\alpha_m = \frac{\hat{\alpha}_m \cdot \left(E - \hat{E}_m\right)}{1 - e^{-\left(E - \hat{E}_m\right)/K_{\alpha m}}} \text{ and } \beta_m = \hat{\beta}_m \cdot e^{-\left(E - \hat{E}_m\right)/K_{\beta m}}$$

$$\alpha_h = \hat{\alpha}_h \cdot e^{-\left(E - \hat{E}_h\right)/K_{\alpha h}} \text{ and } \beta_h = \frac{\hat{\beta}_h}{1 + e^{-\left(E - \hat{E}_h\right)/K_{\beta h}}}$$

$$\frac{dS}{dt} = \frac{S_\infty - S}{\tau_S},\ \tau_S = \frac{60}{0.2 + 5.65 \cdot \left[(E + 90)/100\right]^2} \text{ and } S_\infty = \frac{1}{1 + e^{\left(E - \hat{E}_S\right)/A_S}}$$

$$\alpha_n = \frac{\hat{\alpha}_n \cdot \left(E - \hat{E}_n\right)}{1 - e^{-\left(E - \hat{E}_n\right)/K_{\alpha n}}} \text{ and } \beta_n = \hat{\beta}_n \cdot e^{-\left(E - \hat{E}_n\right)/K_{\beta n}}$$

$$\frac{dh_K}{dt} = \frac{h_{K\infty} - h_K}{\tau_{h_K}},\quad \tau_{h_K} = e^{-\left(E - E_{h_K}\right)/K_{h_K}} \text{ and } h_{K\infty} = \frac{1}{1 + e^{\left(E - \hat{E}_{h_K}\right)/A_{h_K}}}$$

The gating variable of ClC1 was assumed to reach the steady-state instantaneously

$$a = \frac{1}{1 + e^{\left(E - \hat{E}_a\right)/A_a}}$$

For the inward-rectifying potassium channels the same model as in Wallinga et al. (1999) was used, parameters were chosen to get appropriate values for the limit points at control conditions and a resting conductivity at $c_{\mathrm{e}}^{\mathrm{K}^+} = 3.5$ mM of 41 μS/cm^2. The equations were:

$$g_{\mathrm{IR}}^{\mathrm{K}^+} = g'_{\mathrm{IR}} \cdot y,\ g'_{\mathrm{IR}} = \frac{\hat{g}_{IR} \cdot \left(c_{\mathrm{R}}^{\mathrm{K}^+}\right)^2}{K_{\mathrm{IR}}^{\mathrm{K}^+} + \left(c_{\mathrm{R}}^{\mathrm{K}^+}\right)^2},\ c_{\mathrm{R}}^{\mathrm{K}^+} = c_{\mathrm{e}}^{\mathrm{K}^+} \cdot e^{-\delta \mathrm{E}_{\mathrm{K}^+} \mathrm{F}/RT}$$

$$y = 1 - \left[1 + \frac{K_{IR}^{S}}{c_i^S \cdot e^{2(1-\delta)EF/RT}} \cdot \left(1 + \frac{\left(c_R^{K^+}\right)^2}{K_{IR}^{K^+}} \right) \right]^{-1}$$

The constant background sodium leak conductance was then adapted to reach a K^+ to Na^+ permeability ratio between 0.01 and 0.02 and a membrane potential of approximately –86 mV (at $c_e^{K^+} = 3.5$ mM).

For modeling the H^+ leak conductance, it was assumed – based on the ^{31}P MR spectroscopy measurements (Jurkat-Rott et al., 2009) – that the H^+ equilibrium potential was constant and further, that every H^+ was exchanged by one Na^+ ion, presumably by a Na^+/H^+ exchanger. Thus the omega current was treated as a sodium current (indirectly) driven by the electrochemical gradient for protons. Its conductance was modeled as a pore with a voltage-dependent open probability that follows a Boltzmann distribution. The equation

$$g_{omega} = \hat{g}_{omega} \cdot \left(1 + e^{E - \hat{E}_{leak} / A_{leak}} \right)^{-1}$$

was fitted to the HypoPP muscle fiber results. The Na^+ flux (indirectly) mediated by the omega pore was calculated by

$$J_{omega}^{Na^+} = -F^{-1} \cdot g_{omega} \cdot \left(E - E_{H^+} \right) \text{ with } E_{H^+} = \frac{R \cdot T}{F} \cdot \ln \left(\frac{10^{pH_i}}{10^{pH_e}} \right)$$

The model was implemented in MatLab Version 7.3 (The Mathworks, Inc.). Initial-value problems were solved with ODE15s, a solver for sets of stiff ordinary differential equations. Then bifurcation analysis was done by using the continuation routines of the toolbox CL_MATCONT Version 2.4.

NOTATIONS AND ABBREVIATIONS

Indices

Aqua	water channel
c	channel like voltage-gated Na^+ channel, voltage-gated K^+ channel
ClC1	voltage-dependent Cl^- channel
e	extracellular
f	fiber
i	intracellular
ion	Ion: Na^+, K^+, Cl^-
IR	inwardly rectifying K^+ channel
K_V	voltage-gated K^+ channel
Omega	omega pore conductance
Na_L	background Na^+ channels
Na_V	voltage-gated Na^+ channel
p	Na^+/K^+-pump
s	substance: sodium, potassium, chloride, fixed anion, water
∞	steady-state

Identifiers

a	gating variable of the Cl^- channel
A_m	membrane area
c	concentration
Cl^-	chloride ion
c_m	specific membrane capacity

D_f	fiber diameter
δ	electrical distance from outside where binding site for K^+ and S^{2+} is localized in K_{ir}
E	membrane potential
E_{ion}	equilibrium potential (Nernst)
F	Faraday constant
Fix	intracellular fixed anions (e.g., proteinates, phosphates)
g	conductance
H^+	protons
η	scaling factor relating the size of T-tubular membrane to sarcolemma
J	flux
K^+	potassium ion
K_{mK}	sensitivity of the Na^+/K^+-pump for extracellular potassium
K_{mNa}	sensitivity of the Na^+/K^+-pump for intracellular sodium
K_K	dissociation constant of K^+ on K_{ir} channels
K_S	dissociation constant of S^{2+} on K_{ir} channels
L_H	hydraulic conductivity
m, h, S	gating variables of the voltage-gated Na^+ channel (activation, fast, slow inactivation)
n, h_K	gating variables of the voltage-gated K^+ channel (activation, inactivation)
n	amount of substance
Na^+	sodium ion
Π	osmotic pressure
Q	charge
R	gas constant
S^{2+}	intracellular fixed cation (cytoplasmic blocker of K_{ir} channels)
T	absolute temperature
t	time
V_i	cell volume

frontiers in
PHARMACOLOGY

REVIEW ARTICLE
published: 12 September 2012
doi: 10.3389/fphar.2012.00166

Mechanism of electromechanical coupling in voltage-gated potassium channels

Rikard Blunck [1,2,3] **** and Zarah Batulan*** [1,2]

[1] *Groupe d'étude des protéines membranaires, Montreal, QC, Canada*
[2] *Department of Physiology, Université de Montréal, Montreal, QC, Canada*
[3] *Department of Physics, Université de Montréal, Montreal, QC, Canada*

Edited by:
Gildas Loussouarn, University of Nantes, France

Reviewed by:
Baron Chanda, University of Wisconsin-Madison, USA
Matthew Perry, Victor Chang Cardiac Research Institute, Australia

****Correspondence:***
Rikard Blunck, Département de Physique, Université de Montréal, C.P. 6128 succ. Centre-Ville, Montreal, QC, Canada H3C 3J7.
e-mail: rikard.blunck@umontreal.ca

Voltage-gated ion channels play a central role in the generation of action potentials in the nervous system. They are selective for one type of ion – sodium, calcium, or potassium. Voltage-gated ion channels are composed of a central pore that allows ions to pass through the membrane and four peripheral voltage sensing domains that respond to changes in the membrane potential. Upon depolarization, voltage sensors in voltage-gated potassium channels (Kv) undergo conformational changes driven by positive charges in the S4 segment and aided by pairwise electrostatic interactions with the surrounding voltage sensor. Structure-function relations of Kv channels have been investigated in detail, and the resulting models on the movement of the voltage sensors now converge to a consensus; the S4 segment undergoes a combined movement of rotation, tilt, and vertical displacement in order to bring 3–4e^+ each through the electric field focused in this region. Nevertheless, the mechanism by which the voltage sensor movement leads to pore opening, the electromechanical coupling, is still not fully understood. Thus, recently, electromechanical coupling in different Kv channels has been investigated with a multitude of techniques including electrophysiology, 3D crystal structures, fluorescence spectroscopy, and molecular dynamics simulations. Evidently, the S4–S5 linker, the covalent link between the voltage sensor and pore, plays a crucial role. The linker transfers the energy from the voltage sensor movement to the pore domain via an interaction with the S6 C-termini, which are pulled open during gating. In addition, other contact regions have been proposed. This review aims to provide (i) an in-depth comparison of the molecular mechanisms of electromechanical coupling in different Kv channels; (ii) insight as to how the voltage sensor and pore domain influence one another; and (iii) theoretical predictions on the movement of the cytosolic face of the Kv channels during gating.

Keywords: voltage-gated potassium channels, electromechanical coupling, gating, HCN, HERG, BK_{Ca}

INTRODUCTION

Voltage-gated potassium channels (Kv) are a group of membrane proteins that regulate the flow of potassium ions into and out of cells in response to changes in the membrane potential. Kv channels are found throughout the body in different cell types. Their expression in neuronal and muscle tissues helps generate action potentials as well as maintain the resting membrane potential, thereby playing a critical role in cellular excitability in the central nervous and cardiac systems. Other roles of this class of proteins include regulation of hormone release such as the insulin secretion pathway (MacDonald and Wheeler, 2003) and implication in immune response (Koo et al., 1997; Beeton et al., 2001; Blunck et al., 2001; Thomas et al., 2011). Mutations in the genes encoding Kv channels lead to familial neuronal and cardiac diseases, including cardiac arrhythmias, episodic ataxia, epilepsy, and congenital deafness (Adelman et al., 1995; Neyroud et al., 1997; Jentsch, 2000; Tristani-Firouzi and Sanguinetti, 2003; Imbrici et al., 2006).

Kv channels assemble as symmetric tetramers, with each subunit consisting of six transmembrane α-helices (S1–S6) connected by five linker regions. The first four helices (S1–S4) of one monomer form a distinct voltage sensor at the periphery, whereas the S5–S6 of all four monomers collectively arrange into a single ion conducting pore in the center of the structure (**Figures 1A,B**, Long et al., 2005a). Access to the ion conducting pore is controlled by an intracellular gate comprised of the S6 C-terminal ends, which form a bundle crossing that obstructs the pore when the channel is closed (Armstrong, 1971; Holmgren et al., 1997; Doyle et al., 1998). The S5–S6 linker forms a re-entrant loop (p-loop), arranging at the extracellular funnel into a small pore helix and the selectivity filter responsible for the preference for potassium over sodium in K^+ channels (Doyle et al., 1998).

Each voltage sensor comprises a motif of four to six basic residues separated by two hydrophobic ones. This creates a positively charged surface along the S4 responsible for the sensitivity toward the membrane potential (**Figure 1C**). Driven by the positive charges in the S4 helix, the S4 transitions into the activated state (Liman et al., 1991; Papazian et al., 1991; Aggarwal and MacKinnon, 1996; Seoh et al., 1996). The S4 is partly accessible to the lipid environment, but the charged surface is directed toward the other helices of the voltage sensor S1–S3 (Long et al., 2005a).

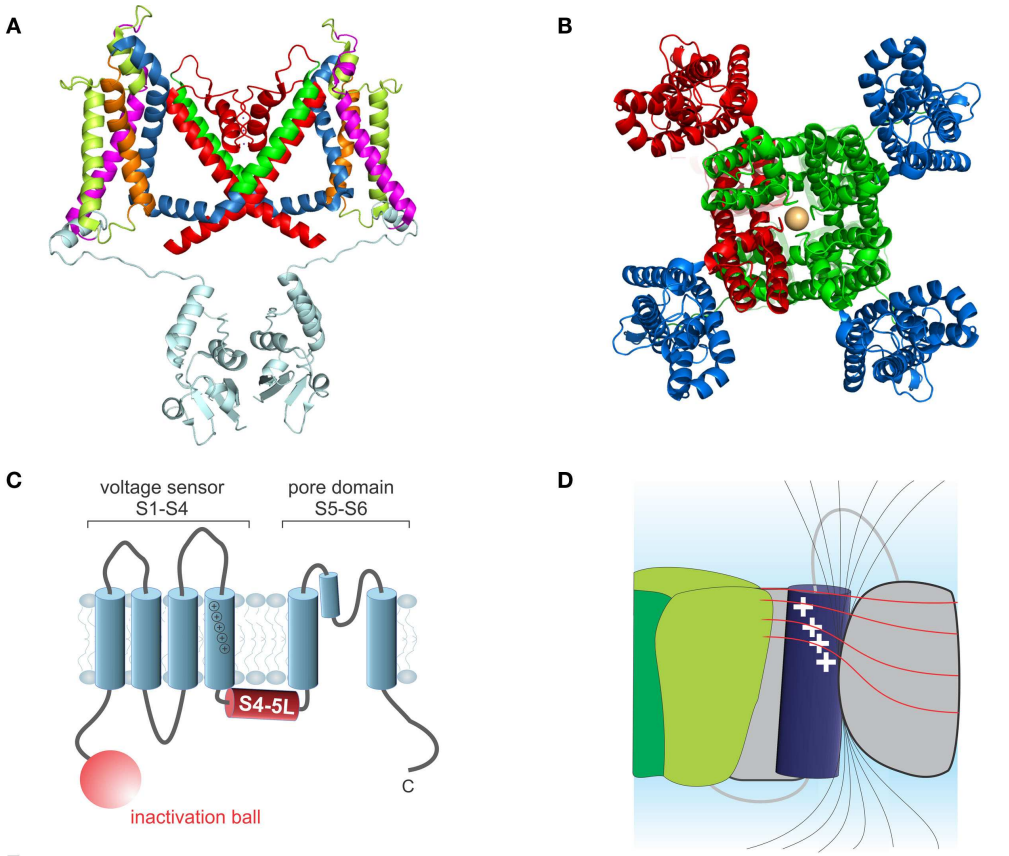

E

		S4-S5 linker	$S6_T$	
Shaker	378	HSKG**LQILGRT**LKASM**RELGLL**IFFLFIG	PVPVIVSN**FNYFY**HRETDQEE	493
Kv1.1		HSKG**LQILG**Q**T**LKASM**RELGLL**IFFLFIG	PVPVIVSN**FNYFY**HRETEGEE	
Kv1.2		HSKG**LQILG**Q**T**LKASM**RELGLL**IFFLFIG	PVPVIVSN**FNYFY**HRETEGEE	
Kv1.3		HSKG**LQILG**Q**T**LKASM**RELGLL**IFFLFIG	PVPVIVSN**FNYFY**HRETEGEE	
Kv1.4		HSKG**LQILG**H**T**LRASM**RELGLL**IFFLFIG	PVPVIVSN**FNYFY**HRETENEE	
Kv1.5		HSKG**LQILGKT**LQASM**RELGLL**IFFLFIG	PVPVIVSN**FNYFY**HRETDHEE	
Kv1.6		HSKG**LQILGKT**LQASM**RELGLL**IFFLFIG	PVPVIVSN**FNYFY**HRETEQEE	
Kv1.7		HSKG**LQILG**Q**T**LRASM**RELGLL**IFFLFIG	PVPVIVSN**F**S**YFY**HRETEGEE	
Kv1.8		HSKG**LQILG**Q**T**LKASM**RELGLL**IFFLFIG	PVPVIVSN**FNYFY**HRETENEE	
Kv2.1		HSTG**LQ**S**LG**F**T**LRRSYN**ELGLL**ILFLAMG	PIPIIVNN**F**S**EFY**KEQKRQEK	
Kv3.1		HFVG**L**RV**LG**H**T**LRASTN**E**FL**LL**IIFLALG	PVPVIVNN**F**GMY**Y**SLAMAKQK	
Kv4.1		HSQG**LR**I**LG**Y**T**LKSCAS**ELG**F**L**LFSLTMA	PVPVIVSN**F**SRI**Y**HQNQRADK	
Kv5.1		HSSG**LQ**T**L**TY**A**LKRSF**KELGLL**LMYLAVG	PIHPIINN**F**VRY**Y**NKQRVLET	
Kv6.1		HSLG**LQ**T**LG**L**T**ARRCT**RE**F**GLL**LLFLCVA	PVTSIFHT**F**SRS**Y**LELKQEQE	
HERG	538	KLDRYSEYGAAVLFLLMCTFALIAHWLAC	IFGNVSAIIQRLYSGTARYHT	675
HCN1	279	HQWEEIFHMTYDLASAVVRIFNLIGMMLL	FVGHATALIQSLDSSRRQYQE	409
HCN2	321	HQWEEIFHMTYDLASAVMRICNLISMMLL	FIGHATALIQSLDSSRRQYQE	451
BKCa	220	ILQFLNILKTSNSIKLVNLLSIFISTWLT	YVPEIIELIGNRKKYGGSYSA	338

FIGURE 1 | Structure of voltage-gated potassium channels. (A) *Side view* of the structure of Kv1.2/2.1 chimera (PDB: 2R9R, Long et al., 2007); in monomer A the segments S1–S6 are colored *magenta*, *lime*, *orange*, *blue*, *red*, and *green*, respectively. The T1 domain and the T1–S1 linker are shown in *light blue*. **(B)** Structure of Kv1.2/2.1 chimera (*top view*). One subunit is colored in *red*. For the other three voltage sensor domains are colored in *blue* and the pore domain in *green*. **(C)** Topology of Kv channels; S1–S4 form the voltage sensor, S5 and S6 together with the p-loop form the pore domain. The N-terminus contains the inactivation ball peptide. **(D)** The electric field inside the voltage sensor is concentrated on a few Ångström and is moving upon conformational change of the S4; *black* lines indicate the electric field and illustrate the concentration of the field, the *red* lines indicate equipotential planes (modified after Blunck et al., 2005; Chanda et al., 2005). **(E)** Sequence alignment of the S4–S5 linker and $S6_T$ of different Kv channels (HERG alignment according to Ng et al., 2012). Accession numbers: *Shaker-CAA29917*; *Kv1.1-NP_000208*; *Kv1.2-NP_004965*; *Kv1.3-NP_002223*; *Kv1.4-NP_002224*; *Kv1.5-NP_002225*; *Kv1.6-NP_002226*; *Kv1.7-NP_114092*; *Kv1.8-Q16322*; *Kv2.1-NP_004966*; *Kv3.1-NP_004967*; *Kv4.1-NP_004970*; *Kv5.1-NP_002227*; *Kv6.1-NP_002228*; *HERG-BAA37096*; *HCN1-NP_066550*; *HCN2-EDL31671*; *BKCa-AF118141*.

Voltage sensor and pore domain are covalently linked by the S4–S5 linker. The N-terminus forms a structure hanging below the ion channel pore ("hanging gondola," Kreusch et al., 1998; Bixby et al., 1999; Long et al., 2005a) called the T1 domain (**Figure 1A**), which is responsible for the correct assembly of the tetrameric channels (Li et al., 1992; Shen and Pfaffinger, 1995).

Kv CHANNEL GATING

Upon depolarization of the membrane potential, the voltage sensors driven by the positively charged S4 undergo a conformational change (Mannuzzu et al., 1996; Cha and Bezanilla, 1997), which subsequently leads to pore opening. It has been shown that the S4 traverses several closed states before entering the activated state (Perozo et al., 1994; Zagotta et al., 1994b). Once all four voltage sensors are activated, the pore opens in one cooperative step (Zagotta et al., 1994a). The voltage sensor movement may electrically be detected as *gating currents* caused by the rearrangement of its electrostatic charges with respect to the electric field. The activation transitions are reflected in the gating currents as two major components – the first associated with the early closed-state transitions and the second with the major conformational change of the voltage sensor (Perozo et al., 1994). A fraction of the gating charge (∼13%) was also associated to the final concerted activation (Smith-Maxwell et al., 1998a; Ledwell and Aldrich, 1999; Pathak et al., 2005). Major charge movement was separated from the final cooperative transition and pore opening by three conservative mutations in the non-basic residues of the lower[1] S4 (ILT mutation).

Combining the crystal structures of Kv1.2 and the Kv1.2/2.1 chimera (Long et al., 2005a, 2007) with a wealth of electrophysiological and voltage-clamp fluorometry results enabled to associate the kinetic transitions to structural features of the voltage sensor. One major landmark was the suggestion that the electric field does not homogenously drop off as it does within the membrane but that it reaches far into the voltage sensor along water-filled crevices from both faces in a manner that the field is concentrated onto a narrow span, a hydrophobic seal, between both sides (**Figure 1D**, Larsson et al., 1996; Starace and Bezanilla, 2001, 2004; Asamoah et al., 2003; Chanda et al., 2005; Tombola et al., 2005). Although a crystal structure is available only for the activated state, various models exist for the resting state and the gating movement of the voltage sensor. Starting from the sliding helix (Larsson et al., 1996; Yang et al., 1996) or helical screw model (Guy and Seetharamulu, 1986; Ahern and Horn, 2005), the transporter model (Starace and Bezanilla, 2001, 2004; Chanda et al., 2005), and the paddle model (Jiang et al., 2003; Ruta et al., 2005), the current understanding converges more and more toward a single consensus model for the gating movement of the voltage sensor (Khalili-Araghi et al., 2010; Vargas et al., 2011; Jensen et al., 2012; Yarov-Yarovoy et al., 2012). According to this consensus, the positive gating charges on the S4 are stabilized by pairwise interactions with anionic charges in S1–S3 aligned along the interface to S4 (Papazian et al., 1995; Tiwari-Woodruff et al., 2000; Yarov-Yarovoy et al., 2006). During activation, the positive charges "jump" from one negative charge to the following one leading to the conformational change of the voltage sensor. The movement of the S4 itself has been projected to be a combination of (i) a tilt of the S4 helix in the membrane, (ii) a rotation around the helix axis, and (iii) small vertical and radial translations. This movement will displace the S4–S5 linker and thus lead to pore opening (see below). In addition, it has been suggested that the S4 helix itself adopts a 3_{10} helical conformation permitting the helix to stretch and accommodate the continued stability of charged interactions (Long et al., 2007; Clayton et al., 2008; Villalba-Galea et al., 2008; Bjelkmar et al., 2009; Khalili-Araghi et al., 2010). The inner part of the S4 lengthens while the two ends twist around like a corkscrew. Whether the S4 adopts the 3_{10} conformation spontaneously or during activation is presently unknown. Upon prolonged stay in the activated state, S4 is then proposed to transform from a 3_{10} to an α-helix, which has been described as "relaxation" of the voltage sensor. (Villalba-Galea et al., 2008).

Pore opening itself is accomplished by a widening of the bundle crossing at the C-terminal S6. The S6 of many Kv channels contains a PVP motif leading to a kink of its axis (**Figures 1A,E**). It is assumed that, during pore opening, the S6 C-terminal to the PVP motif is moving away from the central axis thereby permitting entry into the central water-filled cavity. Opening of the pore, however, triggers inactivation of the channel. Two major types of inactivation have been described, N- and C-type inactivation. During the fast, N-type inactivation, a ball peptide tethered to the N-terminus of the Kv channels enters the open pore and blocks access to it (Armstrong and Bezanilla, 1977; Hoshi et al., 1990; Zagotta et al., 1990). During slow, C-type inactivation, the selectivity filter acts as a second gate and prevents ions from passing through (Yellen, 2002; Blunck et al., 2006; Cordero-Morales et al., 2006a,b). Opening of the lower gate directly triggers the slow entry into the C-type inactivated state (Cuello et al., 2010b,c), implying that the two gates of the ion conducting pore act diametrically – opening of the cytosolic gate triggers closing of the extracellular one.

ELECTROMECHANICAL COUPLING

As described above, the energy driving the opening of the pore is generated by the voltage sensor upon changes of the surrounding *electric field*. Accordingly, *electromechanical* coupling describes the process of transferring this energy from the voltage sensor to the pore domain, triggering the *mechanical* opening of the pore. By first approximation, the voltage sensor movement pulls the lower S5 helix outward via the only covalent link, the S4–S5 linker. However, a number of questions remain unanswered by this simplified view. First, the major voltage sensor movement seems to occur independently followed by a single cooperative step that is associated with pore opening (Zagotta et al., 1994a; Pathak et al., 2005); in other words, all four voltage sensors have to be activated before the final pore opening step is allowed. The major (charge) movement of the voltage sensor thus has to happen independently of pore domain opening, arguing against a direct coupling between both movements. Second, it is not clear how the conformational rearrangement of the S4 mechanically leads to a widening of the helical bundle crossing. Third and finally, while the S5 is covalently linked to the voltage sensor, it is the S6 that obstructs the ion

[1]Throughout the manuscript, "lower" and "upper" refer to the cytosolic and extracellular half of the transmembrane domains.

conduction pathway. How are both helices linked to one another? Some of these questions have already been answered to date; others remain the focus of research. Below, we will outline the results that led to the current understanding of the mechanisms of electromechanical coupling and discuss the open problems. Initially, we will concentrate on the Shaker-like Kv channels as the fundamental model system and compare the mechanism with results obtained in other voltage-dependent potassium channels.

ELECTROMECHANICAL COUPLING IN SHAKER-LIKE Kv CHANNELS

Early on, it was found that the covalent link between voltage sensor and pore, the S4–S5 linker plays a key role in the electromechanical coupling. Slesinger et al. (1993) already identified positions in the S4–S5 linker that influence the properties of the permeation pore, but at that time, the linker was still assumed to be part of the ion conducting pathway. Its involvement in the intermediate (coupling) transitions was first proposed by Schoppa and Sigworth (1998a,b) and, for HERG channels (Human ether-a-go-go related gene, see below), by Sanguinetti and Xu (1999). However, as it is the S6 – not the S5 helix that lines the pore (Liu et al., 1997; Doyle et al., 1998), it remained unanswered as to how movement of the S4–S5 linker led to pore opening itself. Lu et al. (2001, 2002) solved this problem by demonstrating that the S4–S5 linker directly interacts with the C-terminal S6 ($S6_T$) promoting pore opening. They constructed Shaker-KcsA chimeras by replacing the Shaker pore with the corresponding KcsA domain. These constructs were gating voltage dependently only if the corresponding S4–S5 linker and $S6_T$ were paired. The involvement of $S6_T$ in electromechanical coupling was corroborated by mutations in this region leading to altered coupling (Ding and Horn, 2002, 2003; Hackos et al., 2002; Soler-Llavina et al., 2006; Labro et al., 2008; Batulan et al., 2010; Haddad and Blunck, 2011). Lu et al. (2002) showed that both the motifs $_{483}$YFYH$_{486}$ in the $S6_T$ and $_{385}$LGRTLKAS$_{392}$ in the S4–S5 linker were essential, although these regions should probably be extended to $_{481}$FNYFY$_{485}$ and $_{382}$LQILGRT$_{388}$ (**Figure 1E**, McCormack et al., 1991; Schoppa and Sigworth, 1998a; Soler-Llavina et al., 2006; Labro et al., 2008; Haddad and Blunck, 2011). In the crystal structure of Kv1.2, these are also the regions that make the closest contact between both regions of the same subunit (Long et al., 2005b, **Figure 2A**). It is suggested that F481, Y483, and F484 form a hydrophobic pocket, into which the S4–S5 linker and in particular I384 and T388 insert (Labro et al., 2008; Haddad and Blunck, 2011). Sequence alignment of the S4–S5 linker and $S6_T$ regions shows that the motifs are conserved among Kv1 family members. In Kv2-6, few variations occur with L382, L385 in the S4–S5 linker and F481, Y485 in the $S6_T$ being strictly conserved (**Figure 1E**).

Lu et al. (2002) also found the C-terminal part of the S4–S5 linker ($_{393}$MRELGLL$_{399}$) to be essential although it does not make direct contact in the open state structure. However, it had been demonstrated that this region interacts with Y485 (in the $_{483}$YFYH$_{486}$ motif) of the neighboring subunit (Batulan et al., 2010). Three of the residues involved, E395, L399, and Y485 are strictly conserved throughout Kv1-6 (**Figure 1E**). Mutations in this region influence primarily the deactivation of off-gating kinetics, indicating that this interaction develops in the open state only. When looking at the three-dimensional arrangement of all four S4–S5 linker and the $S6_T$ (**Figure 2B**, Long et al., 2007), it becomes evident that the $_{481}$FNYFYH$_{486}$ motif of the $S6_T$ is nestled between the N-terminal part of the S4–S5 linker of the same subunit ($_{382}$LQILGRT$_{388}$) and the C-terminal part of the neighboring S4–S5 linker ($_{394}$RELGL$_{398}$). The formation of an intersubunit link between the S4 and S5 linker of one subunit with the $S6_T$ of the neighboring one (Batulan et al., 2010) has also very recently been proposed to develop after pore opening in the prokaryotic sodium channel Nav-Ab (Payandeh et al., 2012). In Nav-Ab, the interaction is located more toward the center of the S4–S5 linker possibly because Nav-Ab undergoes a different type of inactivation (see below).

ALTERNATIVE INTERACTION REGIONS

Despite the fact that the most profound interactions on the electromechanical coupling were found in the S4–S5 linker and $S6_T$ region, other contacts between the voltage sensors and the pore domain seem to influence electromechanical coupling as well. These may explain why still a voltage-dependent opening of the pores is observed in "uncoupled" mutants (Haddad and Blunck, 2011)[2]. Mutations in the region of N-terminal S5 (401–405) and the S6 in the region of the PVP kink (472–479) have a similar, although less pronounced, effect as uncoupling mutations (Kanevsky and Aldrich, 1999; Soler-Llavina et al., 2006). According to the crystal structure of the Kv1.2/2.1 chimera (Long et al., 2007), these positions are oriented toward the voltage sensor of the neighboring subunit, right at the area where the ILT mutations (V369I-I372L-S376T) are located (**Figure 2C**). Soler-Llavina et al. (2006) suggested therefore a direct annealing between the lower S4 and the S5 of the neighboring subunit. This is different from the suggestion of Batulan et al. (2010) of an intersubunit interaction between the S4–S5 linker and the S6 of the neighboring subunit. As the residues involved in the interaction between the S4 and the neighboring S5 are all hydrophobic, an influence of membrane lipids positioned at the interface of the voltage sensor and pore domain is also possible (Soler-Llavina et al., 2006).

The lipid composition had been shown to influence activation of the prokaryotic KvAP (Schmidt et al., 2006, 2009) and Shaker K^+ channels (Borjesson et al., 2008, 2010; Xu et al., 2008). In the bacterial voltage-gated KvAP channel, it has been proposed that the positively charged arginine residues along the voltage sensor interact with and are stabilized by negatively charged lipid phosphodiester groups (Schmidt et al., 2006). By changing the lipid environment from a phospholipid to a non-phospholipid make-up, the voltage sensor switches from an activated to a resting state. Similarly, enzymatic cleavage of the phospholipid head groups hinders Shaker K^+ activation (Ramu et al., 2006; Xu et al., 2008). Recently even binding sites for polyunsaturated fatty acids had been identified (Decher et al., 2010; Borjesson and Elinder, 2011). Nevertheless, these interactions seem to be electrostatic in nature and do not seem to target the coupling between voltage sensor and pore domain.

[2]Alternatively, this opening could be an intrinsic property of the selectivity filter, as observed in KcsA Cordero-Morales et al. (2006a).

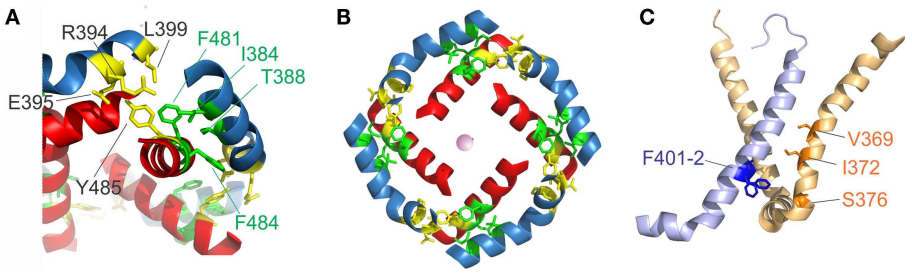

FIGURE 2 | S4–S5 linker and $S6_T$ interaction. (A) Region of annealing between the S4–S5 linker (*blue*) and the $S6_T$ (*red*). Residues identified in intrasubunit interaction (I381, T388, F481, and F484) are colored in *green*, residues involved in intersubunit interactions (R394, E395, L399, and Y485) are colored in *yellow*. **(B)** Coordination of the S4–S5 linker and the $S6_T$ in the crystal structure. The S4–S5 linkers form a ring and enclose the $S6_T$ between two S4–S5 linkers. [coloring as in **(A)**]. **(C)** Residues involved in direct contact of S4 (*light orange*) with the neighboring S5 (*light blue*) are shown in *blue* (F401, F402) and *orange* (ILT: V369, I372, S376).

Two other contact regions have been implicated in electromechanical coupling. First, the crystal structure predicts the upper S5 to be in close contact with the upper S4 of the neighboring subunit. Close proximity of these regions had been proposed earlier (Elinder et al., 2001a,b; Laine et al., 2003) although mutations in this region did not seem to energetically uncouple voltage sensor and pore. The interaction may therefore play a minor functional role, or have effects primarily on gating kinetics (Soler-Llavina et al., 2006).

The second contact area involves S1 and the pore helix (Lee et al., 2009). This was identified, in addition to the S4–S5 linker, based on a statistical coevolution analysis of Kv channels. Crosslinking of S1 to the pore helix in the prokaryotic KvAP channels prevented channel opening to a certain extent. The authors suggest that a S1-pore helix interaction acts as an anchor to facilitate coupling via the S4–S5 linker.

ENERGETIC CONSIDERATIONS IN ELECTROMECHANICAL COUPLING – ELASTICITY

As it is required for all four voltage sensors to have moved before the pore opens in a single cooperative step (Zagotta et al., 1994a), the system has to contain a certain amount of "elasticity," where the energy provided by the activation of a single voltage sensor is "stored" until all four voltage sensors have been activated. The structural basis for the elasticity remains unknown; it shows, however, in the energetics of the electromechanical coupling. Uncoupling by point mutations (Ledwell and Aldrich, 1999; Ding and Horn, 2003; Soler-Llavina et al., 2006; Haddad and Blunck, 2011) separates gating charge–voltage (*QV*, reflecting voltage sensor movement) and conductance–voltage (*GV*) relations (reflecting pore opening); while the *QV* is shifted to more negative potentials, the *GV* is shifted to more positive ones (**Figure 3A**). This is a distinct property of disturbed electromechanical coupling, as stabilizing or destabilizing either the voltage sensor in its resting state or the pore in its open state would lead to symmetric effects on *QV* and *GV* (Ding and Horn, 2003; Batulan et al., 2009; Muroi et al., 2009, 2010; Haddad and Blunck, 2011). The shift of the *QV* to more negative potentials means that less energy is required to activate the voltage sensors. In the wildtype channel, this energy is likely transferred to the pore, indicating that the pore itself prefers to remain in the closed state. A separation between *QV* and *GV* can only be achieved by modifying the energetic coupling between both modules (Batulan et al., 2009; Muroi et al., 2009, 2010; Haddad and Blunck, 2011).

If the system is considered as two entities, voltage sensor and pore, which can transit from resting to activated and closed to open, respectively, then a certain amount of energy (ΔG_{exc}) is exchanged between both systems (**Figure 3B**). Muroi et al. (2010) modeled the behavior of the two systems as cooperatively coupled. The cooperative models imply that the pore has a relatively high probability of opening in the voltage range where the voltage sensors become activated[3]. Uncoupled mutants, however, seem to have a very low open probability in that region (Ledwell and Aldrich, 1999; Soler-Llavina et al., 2006; Muroi et al., 2010; Haddad and Blunck, 2011). Considering, furthermore, the tight interaction between voltage sensor and pore discussed above, it is likely that their respective free energies are largely dependent on the presence of the other module. Thus, it is more prudent to describe the energetic states of the *entire* system in a sequential model (resting-activated-open; **Figure 3C**; Haddad and Blunck, 2011), where the charge *Q* is moved during the closed-activated transition. In this description, the energy exchanged between voltage sensor and pore domain will influence the energy level of the intermediate, "activated" state. As the energy required to open the pore has to be available prior to entering the activated state, the activated state becomes higher energetic (**Figure 3C**). It is important to note that the final opening transition in the models is inevitably voltage dependent in order to explain the voltage dependence of the "uncoupled" mutants' *GV* (Ledwell and Aldrich, 1999; Soler-Llavina et al., 2006; Haddad and Blunck, 2011). The default state of the pore in different Kv channels has in detail been discussed in Vardanyan and Pongs (2012, in this topic issue).

Interestingly, the separation of *QV* and *GV* can be inversed by a single point mutation (I384A) in the S4–S5 linker of the Shaker channel (Haddad and Blunck, 2011). In the I384A mutant, *QV* and *GV* superpose, indicating that voltage sensor movement is tightly

[3]If the probability for pore opening was negligible, the cooperative models would become identical to a three-state sequential model. In this case, the state with open pore and resting voltage sensor would never be occupied.

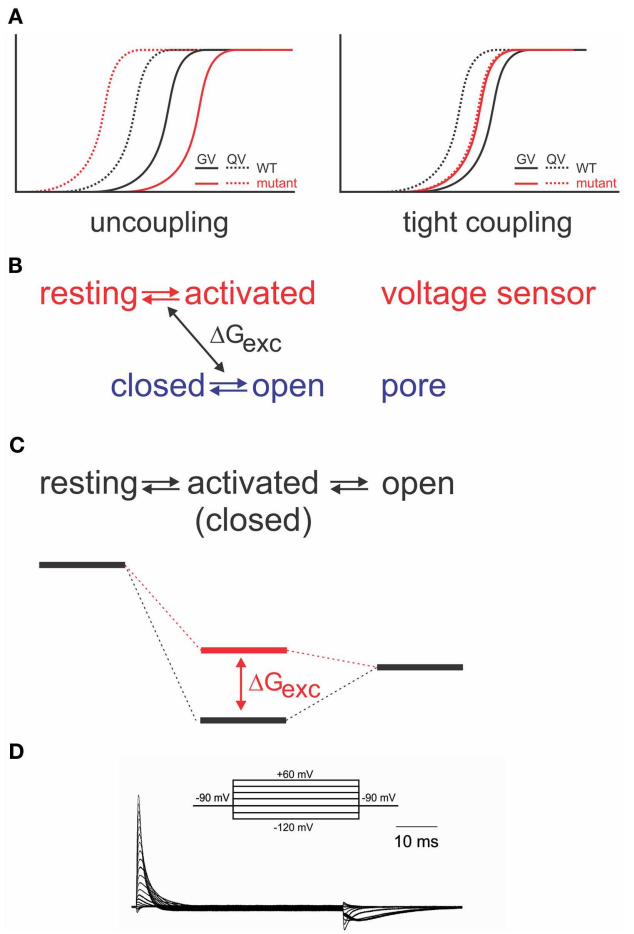

FIGURE 3 | Energetic coupling between voltage sensor and pore domain. (A) Change of gating charge–voltage (*QV*) and conductance–voltage (*GV*) relations for uncoupled (*left*) and tightly coupled (*right*) mutants (modified from Haddad and Blunck, 2011). **(B)** Relation between two separate models and exchange of free energy between voltage sensor and pore domain. **(C)** Analogous sequential model and associated energy diagram. Change of coupling energy ΔG alters energy level of activated state. Charges are moved during resting-activated transition. **(D)** Gating currents elicited from the Shaker-W434F mutant in response to pulses from −90 to potentials varying between −120 to +60 mV in 10 mV intervals.

coupled to pore opening (**Figure 3A**). In the energetic model, the transition from the activated to the open state occurs immediately. Physically, it means that a single subunit is no longer "permitted" to enter the activated state without opening the pore. It is likely that due to the tight coupling, more energy is transferred to the pore enabling it to open at lower potentials (Haddad and Blunck, 2011).

SPRING OR BOLT?

This leads us to the question about the nature of the link between the voltage sensor and pore. What can we say about the movement of S4–S5 linker and $S6_T$ relative to one another? In principle, two scenarios are possible. The first possible scenario is that the S4–S5 linker and $S6_T$ remain in close contact during activation. The S4 and/or the S4–S5 linker act as a spring that becomes strained or compressed by the activation of the voltage sensors. If sufficient energy is stored, the $S6_T$ is pushed or pulled open. In the second scenario, the S4–S5 linker acts as a bolt that prevents the pore from opening. Only once all four bolts are removed, i.e., the S4–S5 linkers have moved out of the way, the pore passively follows the opening. In the second scenario, the energy for opening of the pore is not provided by the voltage sensor; instead the voltage sensors "break" the interaction between S4–S5 linker and $S6_T$. As a consequence, only the *QV*, not the *GV* should be affected by uncoupling.

In both scenarios the interaction between S4–S5 linker and $S6_T$ has to occur in the closed state. An interaction that occurs in the open state would lead to an *increase* in the energy of the activated state and shift the voltage dependence (*QV*) to more *positive* potentials when disturbed, contrary to the experimental observations. The interaction has to occur thus in the closed state. The same conclusion has been found based on disulfide bridges in HERG channels (Ferrer et al., 2006) and by interaction with complementary peptides in KCNQ1 channels (Choveau et al., 2011), both of which are thought to have similar coupling mechanisms (see below, Labro et al., 2011).

The same two possibilities exist for channel deactivation as for activation; the S4–S5 linkers could return to the deactivated state leaving the $S6_T$ to follow passively or the $S6_T$ could be pulled or pushed back into its resting position by the S4–S5 linker. The question remains, therefore, whether the N-terminus of the S4–S5 linker keeps in close contact with the $S6_T$ throughout the gating process. Several results indicate that both regions are rather "loosely" coupled, as first suggested for HCN channels by Chen et al. (2001). First, the strength of the coupling varies considerably in response to small changes, e.g., I384N and I384A in Shaker lead to uncoupling and tight coupling, respectively. If the link would remain intact continuously, these effects should not be observed. A sliding or detaching between both helices is thus more likely. Accordingly, the HERG channel can be locked in the closed state by a disulfide bridge between S4–S5 linker and the $S6_T$ (Ferrer et al., 2006). Second, Choveau et al. (2011) showed that co-expressed peptides of the respective complementary helix influenced gating. Nevertheless, it cannot be excluded that this already occurred during protein folding. Third, in HCN channels (Chen et al., 2001) as in the Kv-KcsA chimera (Lu et al., 2001, 2002), disturbance of the coupling by mismatch of S4–S5 linker and $S6_T$ led to a fraction of the channels being constitutively open. In contrast, uncoupling in Shaker led to constitutively closed channels (Smith-Maxwell et al., 1998b; Ledwell and Aldrich, 1999; Soler-Llavina et al., 2006; Haddad and Blunck, 2011). The difference is likely found in the "preferred" state of the pore itself. KcsA, gated by protons (Heginbotham et al., 1999), is held closed by a series of pH-dependent interactions at the helical bundle crossing (Takeuchi et al., 2007; Thompson et al., 2008; Cuello et al., 2010a). Upon increase in proton concentration, release of the interactions and electrostatic repulsion of the charged residues leads to pore opening. As the transition to the open state occurs spontaneously devoid of additional energy sources, the pore opens by itself and the Kv-KcsA chimera need to push the pore closed. The negative shift of the *QV* in the uncoupled Shaker mutants, on the other

hand, demonstrates that energy is required to bring the channel into the open state. In addition, no voltage independent component is observed in Shaker channels even at open probabilities as low as 10^{-6} (Islas and Sigworth, 1999). Thus, although the pore is not locked in the closed state, it will not open spontaneously and needs to be pushed (or pulled) open. The structural basis for the inherently different behavior of the pores might be based on the PVP motif found in many Kv channels but not in HCN, HERG, or KcsA (**Figure 1E**). This is supported by the fact that mutation of the second proline in the PVP motif to an aspartate leads to a constitutively open channel with only fractional voltage dependence (Sukhareva et al., 2003). This must be seen in the context of the general pore architecture and cannot be generalized. As we will discuss below, the HCN channels' default state is closed despite the absence of a PVP motif. The other way around, HERG channels become constitutively open by introducing a PVP motif in the S6 (Fernandez et al., 2004; for a detailed discussion of constitutive conductance see also Vardanyan and Pongs, 2012).

Finally, in the tightly coupled mutant I384A, the voltage sensors are held back in their activated state during deactivation leading to very slow closing kinetics (Haddad and Blunck, 2011). All of the above suggest that during deactivation, the voltage sensors "separate" from the $S6_T$, and that the pore follows passively. While the Kv-KcsA chimeras need to be pushed closed (Lu et al., 2002), wildtype Shaker channels need to be pushed open (Haddad and Blunck, 2011).

STABILIZATION OF THE ACTIVATED STATE

Just like the annealing of the N-terminus of the S4–S5 linker to $S6_T$, also the interaction between the lower S4 and S5 of the neighboring subunit seem to follow a similar pattern and develop in the closed state (Smith-Maxwell et al., 1998a,b; Ledwell and Aldrich, 1999; Pathak et al., 2005; Soler-Llavina et al., 2006). Other influences on the voltage sensor movement, on the other hand, develop mainly in the open state. The gating currents of the non-conducting mutant W434F (Perozo et al., 1993; Bezanilla et al., 1994; Stefani et al., 1994) are asymmetric for the beginning and end of a depolarizing pulse (**Figure 3D**). The slow rising phase of the off-gating currents was attributed to an interaction developing between the C-terminus of the S4–S5 linker and the $S6_T$ of the neighboring subunit (Batulan et al., 2010). The interaction stabilizes the pore in the open position during the final transitions of activation. The pore thus "pushes" less onto the voltage sensors so that they require more energy to return to their resting state.

This effect is also one of the reasons for the shift of the voltage dependence during prolonged depolarizations (Fedida et al., 1996; Olcese et al., 1997, 2001; Haddad and Blunck, 2011; Lacroix et al., 2011). The voltage sensor no longer feels the pore pushing, so that it follows a voltage dependence shifted to more negative potentials. However, the structural implications are not restricted to the pore region but also lead to conformational changes in the voltage sensor (Bruening-Wright and Larsson, 2007; Villalba-Galea et al., 2008; Haddad and Blunck, 2011). The conformational change or "relaxation" of the voltage sensor has not been observed in uncoupled Shaker mutants (Gagnon and Bezanilla, 2010; Haddad and Blunck, 2011), and the related slowing of deactivation kinetics are not observed if pore opening is blocked (Batulan et al., 2010; Lacroix et al., 2011). Thus, through the electromechanical coupling, a conformational change is allosterically induced in the voltage sensor domain. On the other hand, the conformational changes are observed in the isolated voltage sensor of the voltage-gated phosphatase CiVSP (Villalba-Galea et al., 2008).

It is thought that the S4 adopts a 3_{10} helical structure in resting state or during activation in order to better pair the positive charges with the negatively charged counterparts in the S1–S3 and relaxes in the activated state to an α-helical structure (Clayton et al., 2008; Villalba-Galea et al., 2008; Catterall, 2010; Chakrapani et al., 2010). This is a mechanism similar to open state stabilization occurring in the pore described above (Batulan et al., 2010). In both cases, the channel when entering the activated open state is not immediately in its optimal coordination. The side chains have to reorient themselves and adapt to their new environment, and during this adjustment new links form stabilizing the open state of both pore and voltage sensor.

MODEL FOR MOVEMENT OF THE S4–S5 LINKER

Presently, only a crystal structure for the presumably open inactivated state of Kv channels is known (Long et al., 2005a, 2007). Several models have been proposed on the closed state (see above), which are constrained by biophysical data obtained from the extracellular face of the channel. The movement of the lower S4 and the S4–S5 linker is currently extrapolated in molecular dynamics simulations (Khalili-Araghi et al., 2010; Vargas et al., 2011; Jensen et al., 2012; Yarov-Yarovoy et al., 2012). Based on the open state crystal structure and the results presented above, one can make predictions about the mode of action of the S4–S5 linker and its interaction with the surrounding environment. **Figure 2B** shows the relative orientation and the interactions relevant to electromechanical coupling in the Kv1.2/2.1 chimera (Long et al., 2007). Starting from this conformation, the S4 will translate to a certain extent downwards combined with a tilt and rotation and will pull the S4–S5 linker with it. The slow component in the gating indicates that the intersubunit interaction between the S4–S5 linker and the neighboring S6T (**Figures 2A,B**, yellow, Batulan et al., 2010; Payandeh et al., 2012) will break during this movement and leave the $S6_T$ to follow the S4–S5 linker. Although the coupling between $S6_T$ and S4–S5 linker exists in the open and closed state, the "elastic" nature of it allows for a relative sliding or temporary separation between both helices. During closing the S6 will be straightened and the S4–S5 linker will push the $S6_T$ inwards as suggested by Yarov-Yarovoy et al. (2012). The movement will tilt the N-terminus of the S4–S5 linker inwards, which would mean that it would move close to the S5. In order to keep the S4–S5 interaction (**Figure 2C**, Smith-Maxwell et al., 1998b; Ledwell and Aldrich, 1999; Soler-Llavina et al., 2006) intact also in the closed state while achieving a horizontal tilt in the S4–S5 linker, both S4 and S5 have to rotate during closure. Similar movements had been suggested based on molecular dynamics simulations. However, in order to be confident about the movement of the internal face of the channel during gating, either a closed-state crystal structure or dynamic structural data as recently presented (Faure et al., 2012) are required.

RELATION TO OTHER VOLTAGE-GATED POTASSIUM CHANNELS

The above discussion evolved mainly around the electromechanical coupling of the Shaker Kv channels. Some questions remain however – first, in how far the mechanisms found in these channels are conserved in other voltage-gated potassium channels; second, how are they modulated in order to accommodate hyperpolarization-activated channels; third and finally, how does the voltage sensor machinery interact with other activators such as Ca^{2+} or cyclic nucleotides.

DELAYED RECTIFIER Kv CHANNELS

The sequences of the S4–S5 linker and the $S6_T$ (**Figure 1E**) do not significantly vary between the different delayed rectifier potassium channels. Accordingly, the close interaction between both regions has been demonstrated for several members of these families such as Kv1.5 (KCNA5, Labro et al., 2008), Kv2 (KCNB, Jara-Oseguera et al., 2011), Kv4 (KCND, Bhattacharji et al., 2006; Barghaan and Bahring, 2009), KvLQT (KCNQ, Choveau et al., 2011; Labro et al., 2011), and HERG (KCNH, see below, Sanguinetti and Xu, 1999; Tristani-Firouzi et al., 2002; Ferrer et al., 2006; Van Slyke et al., 2010). In contrast to Shaker-related Kv channels, Kv4 channels enter an inactivated state directly from the closed state at low potentials (Jerng and Covarrubias, 1997; Bahring et al., 2001; Bähring and Covarrubias, 2011). This so-called *closed-state inactivation* is distinct from both N- and C-type inactivation in Shaker-related Kv channels. It has been suggested by Barghaan and Bahring (2009) to be caused by the loose interaction between the S4–S5 linker and the $S6_T$. The $S6_T$ separates from the S4–S5 linker during opening or in the open state leading to reclosure of the pore. In this case, the pore's default state would be closed as in the other Kv channels containing a PVP motif. Accordingly, inactivation is prevented by the mutation of the PVP motif to PVA (Bhattacharji et al., 2006). The loss in contact between S4–S5 linker and S6T during inactivation has also been suggested for HCN channels (see below) and would be in accordance with the crystal structure of the inactivated state of NaV-Ab (Payandeh et al., 2012). It is therefore likely that Kv4 and NaV-Ab undergo the same type of inactivation where the cytosolic pore gate closes due to loss of contact to the $S6_T$ (**Figure 4B**).

HYPERPOLARIZATION-ACTIVATED CYCLIC NUCLEOTIDE-GATED CHANNELS

Hyperpolarization-activated cyclic nucleotide-gated (HCN) channels are expressed in pacemaker cells found in the heart and the nervous system. HCN channels are activated at hyperpolarized, rather than depolarized, potentials, and are selectively conducting cationic inward currents known as I_f in the heart (DiFrancesco, 1993) and I_h in neurons (Pape et al., 1996). These currents contribute to the slow depolarization of pacemaker cells, which is important for changes in heart rate and maintenance of neural oscillatory networks (Santoro and Tibbs, 1999). Although this group shares significant sequence homology and channel architecture with Kv channels (Santoro et al., 1998; Shin et al., 2001; Rothberg et al., 2002), they differ in that they contain a cytoplasmic cyclic nucleotide binding domain (CNBD) attached to the S6 C-terminus. Binding of cyclic nucleotide, primarily cyclic AMP, to this domain shifts HCN channel activation to more positive potentials (Gauss et al., 1998; Shin et al., 2001; Wainger et al., 2001).

Despite the absence of any similarity to the S4–S5 linker and the $S6_T$ region of Kv channels, HCN channel activation appears coupled to the movement of the voltage sensor via annealing of the S4–S5 linker to $S6_T$. Alanine-scanning mutagenesis of the S4–S5 linker identified three residues (E324, Y331, and R339)[4] that may be important in channel closing (Chen et al., 2001). Various mutations in these positions increased the minimal open probability when expressed in oocytes, thus channels stay open even at very large depolarizations. Later results suggested that one of these S4–S5 linker amino acids, R339, interacts with a residue on the C-terminal end of the S6, D443, forming a salt bridge, and that this interaction may be modified by a nearby residue, R447 (Decher et al., 2004). The findings indicated that, similar to Kv channels, electromechanical coupling in HCN channels is mediated from the S4–S5 linker to the $S6_T$. However, despite the similarities in the coupling mechanism, two properties of HCN channels distinguish them from Kv channels. First, the channel is closed rather than opened by the movement of the S4–S5 linker in response to depolarization. Second, the $S6_T$ is the covalent link to the CNBD, which means that both interaction partners, S4–S5 linker and $S6_T$, are linked to an activating module, the voltage sensor and the CNBD, respectively. $S6_T$ and the following C-linker enable the gating by cyclic nucleotides in cyclic nucleotide-gated channels (Wang et al., 2001; Zagotta et al., 2003).

Although the channel opens at hyperpolarized potentials, the voltage sensor movement itself shows all the characteristics of Shaker channels (Mannikko et al., 2002; Bruening-Wright et al., 2007). The voltage dependence of opening can even be reversed to open at depolarizing potentials by cross-bridging the distal C-linker with the S4–S5 linker (Prole and Yellen, 2006). Yellen and co-workers (Shin et al., 2001, 2004; Rothberg et al., 2002) therefore proposed that during "desensitization" of the channel, i.e., closing at depolarized potentials, the coupling between the voltage sensor and the pore "slips" or gets separated. Therefore, no energy is transferred any longer to the pore, and the pore closes. Despite its similarity, the process is different than the closed-state inactivation proposed for Kv4 channels (see above and Barghaan and Bahring, 2009; Bähring and Covarrubias, 2011; Payandeh et al., 2012). Kv4 channels first open and then inactivate with a temporal delay whereas the HCN channels are open and only close in response to depolarization. In both cases, the pore's default state is closed, and the voltage sensor brings it into the open state. In HCN channels, however, the resting state is already open, and the gating movement of the S4–S5 linker tries to open it even further, which leads to separation and closing of the pore (**Figures 4B,C**).

The second feature distinguishing HCN channels from most other Kv channels, the cytosolic CNBD, is linked to $S6_T$ via the C-linker. From the crystal structures of the C-linker and CNBD of several CNG channels (Zagotta et al., 2003; Xu et al., 2010; Lolicato et al., 2011; Brelidze et al., 2012), it is known that the CNBDs form a tetrameric ring below the transmembrane pore

[4]Numbering according to human HCN2 Acc. number EDL31671.

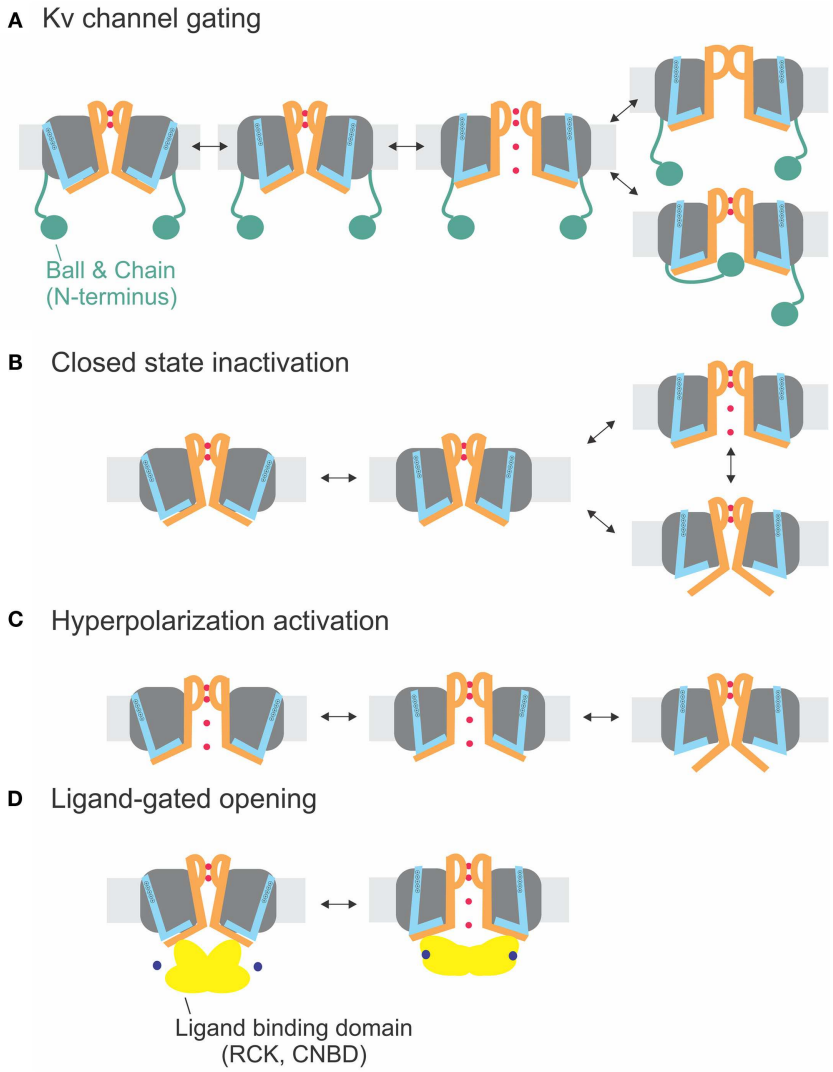

FIGURE 4 | Electromechanical coupling types. (A) Electromechanical coupling in Shaker channels. Activation of the S4 (*blue*) applies strain onto the link to the $S6_T$ (*S6 orange*), and finally leads to pore opening. Inactivation occurs by N-type inactivation (ball and chain; *bottom*) or C-type inactivation (selectivity filter; *top*). **(B)** Closed-state inactivation: Closed-state inactivation (*bottom*) is caused by a loose coupling between S4–S5 linker and $S6_T$; upon decoupling, the pore enters its default state (closed). **(C)** Coupling in hyperpolarization-activated channels: Activation of the S4 leads to decoupling between S4–S5 linker and $S6_T$ and closing of the pore. **(D)** Ligand-gated opening. The ligand binding domains are linked to the $S6_T$ directly and apply their energy directly to the S6.

that interacts via the C-linker onto the S4–S5 linker. This indicates that both voltage and cAMP-binding act upon the same gate (Shin et al., 2004), suggesting that cAMP-binding modulates the coupling efficiency between S4–S5 linker and $S6_T$. Binding of cAMP to HCN2 channels leads to a shift of channel closing to more depolarized potentials. Also cleaving the CNBD leads to a shift to more depolarized potentials (Wainger et al., 2001), indicating that the CNBD facilitates hyperpolarization-activated closing of the channel and that cAMP binding inhibited the closing (Wainger et al., 2001; Craven and Zagotta, 2006). Interpreting this in view of a separation between S4–S5 linker and $S6_T$, on the other hand, the separation occurs at higher potentials indicating that the strain between both modules is relieved by cAMP binding. Although the exact mechanism is not known, cAMP binding stabilizes the pore in its open position perhaps by "pulling" the S6 termini outwards (**Figure 4D**). Stabilization of the open pore would also explain the higher current induced by cAMP in HCN2 channels (Wainger et al., 2001).

HERG CHANNELS

Human ether-a-go-go related gene (HERG, KCNH1, Kv11.1) channels are expressed in heart, neurons, endocrine glands, and smooth muscle (reviewed in Perrin et al., 2008; Cheng and Claydon, 2012). Although initially identified by screening a human hippocampal cDNA library, HERG is actually important in regulating the heartbeat – in particular, the repolarization of the

cardiac action potential as well as pacemaking behavior of the nodes of the heart (Piper et al., 2005). Mutations in this gene cause chromosome 7-associated long QT syndrome, a condition which predisposes patients to cardiac arrhythmias (Curran et al., 1995). Unlike most Kv channels, HERG are inward rectifiers, which function to limit the outflow of potassium ions during an action potential. However, compared to other inward rectifiers which block potassium conductance via an intracellular polyamine block, HERG channels prevent potassium outflow by rapid inactivation (Schonherr and Heinemann, 1996; Smith et al., 1996; Spector et al., 1996; Wang et al., 1997). Another distinguishing feature is that these channels activate and deactivate slowly compared to other Kv channels and that the inactivation process is voltage-dependent (Spector et al., 1996; Wang et al., 1997). They are closely related to the HCN channels, but despite the similarities, fundamental differences exist in their coupling mechanism; first, in the role of the CNBD, and second in the inactivation mechanism.

Previous evidence from Sanguinetti and Xu (1999) has shown that movement of the voltage sensor is coupled to channel activation via interaction of the S4–S5 linker with $S6_T$. As in the HCN channels, this interaction seems to be mainly electrostatic; a single charge-reversal mutation of a residue on the S4–S5 linker, D540K, changed the channel's properties, allowing reopening by hyperpolarization. Tristani-Firouzi et al. (2002) showed that this mutant phenotype could be reversed by introducing a complementary mutation at one specific amino acid, R665D, located at the S6 cytosolic end, which suggested that a D540K – R665 interaction is required for hyperpolarization-induced channel activation and that an electrostatic repulsion between the lysine and arginine is likely to underlie this altered channel behavior. This premise was further supported in the mutants D540R and D540K – R665K, which like D540K were also activated at hyperpolarizing potentials and have basic residues at both positions that exert a repulsive force. Simple neutralization of D540 (D540A), however, did not seem to be sufficient to efficiently uncouple the channel but still had significant influence on gating kinetics (Ng et al., 2012).

These results alone, however, could not clarify whether in the wildtype HERG channel the D540 and R665 residues form an electrostatic interaction that stabilizes the closed state at hyperpolarized potentials (Tristani-Firouzi et al., 2002). Interestingly, the addition of either I662A or L666A into the D540K mutant reduced the hyperpolarization induced inward current and increased the rate of deactivation, indicating that these two residues may modify the interaction between D540 and R665. Later work confirmed the involvement of these residues in coupling the voltage sensor movement with channel activation via the S4–S5 linker since a disulfide bond formation locked the channel in the closed state (Ferrer et al., 2006).

More recent work, alternatively, proposes that hydrophobic interactions may play a role in the electromechanical coupling between the S4–S5 linker and the S6 in HERG channels (Wynia-Smith et al., 2008). Based on homology modeling, V659 was found nestled within a hydrophobic pocket formed by S6, S5, and the S4–S5 linker residues in the closed state. Various mutations in this position disrupted channel closing, suggesting that these hydrophobic residues may be implicated in coupling pore and voltage sensor activation (Wynia-Smith et al., 2008). Residues C-terminal to V659 are more likely involved in S6–S6 interactions. In particular mutating the residues Q664, Y667, and S668 led to a constitutive leak current suggesting that they are involved either in closed-state stabilization or directly form the occluding gate at the bundle crossing (Wynia-Smith et al., 2008).

The importance of the S4–S5 linker is also underlined by the recent finding that other residues therein (S543, Y545, G546, and A548) variably influence activation/deactivation kinetics and steady state activation although the mechanism is not as well understood (Wang et al., 1998; Van Slyke et al., 2010; Ng et al., 2012). It seems clear that the S4–S5 linker is responsible for the slow kinetics of the HERG channel (Van Slyke et al., 2010). Thus far, coupling between S4–S5 linker and $S6_T$ is conserved in HERG channels.

In contrast to HCN channel inactivation, however, HERG inactivation is not mediated by a loose coupling of S4–S5 linker and $S6_T$ but by conformational changes at the outer pore region (Smith et al., 1996; Spector et al., 1996; Vaid et al., 2008; Kopfer et al., 2012). The process is thus similar to C-type inactivation observed in other Kv channels. In HERG channels, independent processes for C-type inactivation and pore opening are required because they open during deactivation but remain closed at hyperpolarized potentials. In addition, HERG channels, although containing a CNBD[5] near the C-terminus (Warmke and Ganetzky, 1994), are not sensitive to cyclic nucleotides (Sanguinetti et al., 1995), which might be due to the low affinity ($>51\,\mu M$) of cAMP to the binding site (Brelidze et al., 2009); however, even at high concentrations (10 mM) no effect on the current was observed. Muskett et al. (2011) proposed that instead the N-terminus, known to influence deactivation times, keeps the CNBD in the activated position, thereby stabilizing the open pore. The underlying reason might also be a lack in coupling between the CNBD and the coupling region (S4–S5 linker/S6T).

The CNBD seems to play a role mainly for assembly and trafficking of HERG (Akhavan et al., 2005). Thus in spite of the close relation to HCN channels, the electromechanical coupling mechanism of HERG resembles rather that of other Kv channels (**Figure 4A**).

LARGE CONDUCTANCE CALCIUM-ACTIVATED POTASSIUM CHANNELS (BK_{ca})

Calcium and voltage-activated potassium channels (K_{Ca}) are categorized into three major groups[large (BK), intermediate (IK), and small (SK) conductances] all of which are activated by both membrane depolarization and increases in intracellular calcium. K_{Ca} channels are comprised of α-subunit tetramers which assemble with auxiliary β-subunits that function to regulate sensitivity to calcium. In this review, we will concentrate on the BK_{Ca} channels, as their structure-function relations have been most intensively studied. BK channels are similar to Kv channels in that they contain voltage sensing (S1–S4) and pore (S5–S6) transmembrane regions but also differ because of the presence of additional domains: (i) a transmembrane helix S0, which interacts with the β-subunit (Wallner et al., 1996), (ii) a cytosolic domain made up of two regulator

[5]Also called cyclic nucleotide binding homology domain, CNBHD, in HERG channels.

of potassium conductance (RCK) domains (RCK1 and RCK2) that contain high affinity calcium binding sites (Jiang et al., 2001), and finally (iii) a magnesium binding site, located at the interface between the cytosolic face of the voltage sensing domain and RCK1 (reviewed in Yang et al., 2008; Latorre et al., 2010; and Lee and Cui, 2010).

Although the gating mechanism is similar to other Kv channels (Diaz et al., 1998; Cui and Aldrich, 2000; Ma et al., 2006; Savalli et al., 2006), differences to the delayed rectifier Kv channels have been reported (Li and Aldrich, 2004, 2006; Zhou et al., 2011). The positive S4 residues do not as dominantly control the voltage dependence; instead charged residues throughout the voltage sensor domain lead to more global conformational changes (Ma et al., 2006; Savalli et al., 2006; Pantazis et al., 2009, 2010). Also the S0 segment has been suggested to be a functional part of the voltage sensor (Koval et al., 2007). Nevertheless, although it has not yet been shown directly, the structural similarities to the other Kv channels suggest that the coupling to the pore domain is mediated by the S4–S5 linker as in the other voltage-gated channels. Calcium dependence is modulated by mutations in the S4–S5 linker (Sullivan et al., 1997). In contrast, it has been shown that the intracellular RCK domain coordinates a magnesium ion not with the S4–S5 but the S0-S1 linker (Yang et al., 2008).

The RCK domains are responsible for modulating the voltage-dependent opening of BK_{Ca} by intracellular calcium (Jiang et al., 2001). Each monomer contains both RCK domains – specifically, a top ring consisting only of RCK1 and a bottom ring only consisting of RCK2 are formed (Yuan et al., 2010). Binding of Ca^{2+} to the RCK "gating ring" triggers a conformational change mainly in RCK1. The N-terminal lobe moves away from the central axis increasing the diameter by 12 Å. The N-terminus of the RCK domain is linked to the S6 via a 17 amino acid linker, leaving room to the possibility that the increased diameter of the gating ring pulls on the S6 decreasing the energy for the voltage sensor to open the pore. Implication of the S4–S5 linker in calcium dependent gating has been suggested early on based on mutagenesis data (Sullivan et al., 1997). Nevertheless, the interaction with the S0–S1 linker may also play a role (Yang et al., 2007, 2008). Coupling to voltage sensor and ligand binding site thus seems to be conserved also in BK_{Ca} channels. The distinct influence of the S0–S1 linker (which does not exist in other Kv channels) might reflect the more pronounced influence of the entire voltage sensor domain in BK_{Ca} channels.

A similar mechanism for channel opening by the RCK domains due to calcium binding has been proposed for opening of small calcium-activated potassium channels (SK_{Ca}), where Ca/calmodulin binds to the Cam-binding domain (Schumacher et al., 2001). This chemomechanical coupling (**Figure 4D**) is similar to CNG channels. The difference between electro- and chemomechanical coupling is the link of the activator to the S4–S5 linker and the $S6_T$, respectively.

CONCLUDING REMARKS

We reviewed the mechanism of electromechanical coupling in various potassium channels, and found that the transfer of energy via annealing of the S4–S5 linker to the $S6_T$ seems to be universally conserved throughout voltage-gated potassium channels (**Figure 4**). The manner of interaction (hydrophobic versus electrostatic) and the tightness of the coupling varies. "Decoupling" upon depolarization leads to hyperpolarization-activated channels (HCN) or to closed-state inactivation (Kv4, NavAB) according to whether the channel is open or closed at hyperpolarized potentials, respectively (**Figures 4B,C**). Another factor influencing the coupling is the pore's default state. In channels where decoupling is required for channel closing, the pore has to close by default whereas channels which do not have an external energy source, such as the chemically activated KcsA channels, require the pore to open by default.

Annealing between the S4–S5 linker and the $S6_T$ as part of electromechanical coupling also seems to be conserved among other voltage-gated ion channels and has been suggested for skeletal sodium channels (Muroi et al., 2010), a prokaryotic sodium channel (Payandeh et al., 2011, 2012; Yarov-Yarovoy et al., 2012), and voltage-gated calcium channels (Wall-Lacelle et al., 2011). It does not seem to be restricted to voltage-gated channels; some ligand-gated channels seem to follow a similar mechanism as has been shown, for instance, for the proton-gated KcsA channel (Thompson et al., 2008; Cuello et al., 2010a). Chemomechanical coupling involving a cytosolic ligand binding domain, however, is directly linked to the C-terminus of S6 (Schumacher et al., 2001; Zagotta et al., 2003; Taraska and Zagotta, 2010).

A number of familial diseases have been assigned to mutations located in the regions identified for electromechanical coupling including episodic ataxia (Rajakulendran et al., 2007), epilepsy (Escayg et al., 2000), long QT syndrome (Sanguinetti, 2010), and congenital deafness (Baig et al., 2011). Mutations in this region often do not eradicate channel function but rather modulate its voltage dependence, which might underlie the etiology of these non-fatal diseases. In this review, we saw that differences in the region of electromechanical coupling tune the channel, rendering it constitutively open, creating leaky channels or even reversing their voltage-dependence.

ACKNOWLEDGMENTS

We want to thank Élise Faure and Jennifer Shin for comments on the manuscript. Groupe d'étude des protéines membranaires (GÉPROM) is funded by the Fonds de recherché du Québec en santé (FRSQ). Rikard Blunck holds a Canada Research Chair in Molecular Mechanisms on Membrane Proteins.

REFERENCES

Adelman, J. P., Bond, C. T., Pessia, M., and Maylie, J. (1995). Episodic ataxia results from voltage-dependent potassium channels with altered functions. *Neuron* 15, 1449–1454.

Aggarwal, S. K., and MacKinnon, R. (1996). Contribution of the S4 segment to gating charge in the Shaker K+ channel. *Neuron* 16, 1169–1177.

Ahern, C. A., and Horn, R. (2005). Focused electric field across the voltage sensor of potassium channels. *Neuron* 48, 25–29.

Akhavan, A., Atanasiu, R., Noguchi, T., Han, W., Holder, N., and Shrier, A. (2005). Identification of the cyclic-nucleotide-binding domain as a conserved determinant of ion-channel cell-surface localization. *J. Cell Sci.* 118, 2803–2812.

Armstrong, C. M. (1971). Interaction of tetraethylammonium ion derivatives with the potassium channels

of giant axons. *J. Gen. Physiol.* 58, 413–437.

Armstrong, C. M., and Bezanilla, F. (1977). Inactivation of the sodium channel. II. Gating current experiments. *J. Gen. Physiol.* 70, 567–590.

Asamoah, O. K., Wuskell, J. P., Loew, L. M., and Bezanilla, F. (2003). A fluorometric approach to local electric field measurements in a voltage-gated ion channel. *Neuron* 37, 85–97.

Bahring, R., Boland, L. M., Varghese, A., Gebauer, M., and Pongs, O. (2001). Kinetic analysis of open- and closed-state inactivation transitions in human Kv4.2 A-type potassium channels. *J. Physiol. (Lond.)* 535, 65–81.

Bähring, R., and Covarrubias, M. (2011). Mechanisms of closed-state inactivation in voltage-gated ion channels. *J. Physiol. (Lond.)* 589, 461–479.

Baig, S. M., Koschak, A., Lieb, A., Gebhart, M., Dafinger, C., Nurnberg, G., Ali, A., Ahmad, I., Sinnegger-Brauns, M. J., Brandt, N., Engel, J., Mangoni, M. E., Farooq, M., Khan, H. U., Nurnberg, P., Striessnig, J., and Bolz, H. J. (2011). Loss of Cav1.3 (CACNA1D) function in a human channelopathy with bradycardia and congenital deafness. *Nat. Neurosci.* 14, 77–84.

Barghaan, J., and Bahring, R. (2009). Dynamic coupling of voltage sensor and gate involved in closed-state inactivation of kv4.2 channels. *J. Gen. Physiol.* 133, 205–224.

Batulan, Z., Haddad, G. A., and Blunck, R. (2010). An intersubunit interaction between S4-S5 linker and S6 is responsible for the slow off-gating component in Shaker K+ channels. *J. Biol. Chem.* 285, 14005–14019.

Batulan, Z., Haddad, G. A., Marsolais, M., and Blunck, R. (2009). Investigating the electromechanical coupling in voltage-gated K+ channels. *Biophys. J.* 96, 369a.

Beeton, C., Barbaria, J., Giraud, P., Devaux, J., Benoliel, A. M., Gola, M., Sabatier, J. M., Bernard, D., Crest, M., and Beraud, E. (2001). Selective blocking of voltage-gated K+ channels improves experimental autoimmune encephalomyelitis and inhibits T cell activation. *J. Immunol.* 166, 936–944.

Bezanilla, F., Perozo, E., and Stefani, E. (1994). Gating of Shaker K+ channels: II. The components of gating currents and a model of channel activation. *Biophys. J.* 66, 1011–1021.

Bhattacharji, A., Kaplan, B., Harris, T., Qu, X., Germann, M. W., and Covarrubias, M. (2006). The concerted contribution of the S4-S5 linker and the S6 segment to the modulation of a Kv channel by 1-alkanols. *Mol. Pharmacol.* 70, 1542–1554.

Bixby, K. A., Nanao, M. H., Shen, N. V., Kreusch, A., Bellamy, H., Pfaffinger, P. J., and Choe, S. (1999). Zn2+-binding and molecular determinants of tetramerization in voltage-gated K+ channels. *Nat. Struct. Biol.* 6, 38–43.

Bjelkmar, P., Niemela, P. S., Vattulainen, I., and Lindahl, E. (2009). Conformational changes and slow dynamics through microsecond polarized atomistic molecular simulation of an integral Kv1.2 ion channel. *PLoS Comput. Biol.* 5, e1000289. doi:10.1371/journal.pcbi.1000289

Blunck, R., Chanda, B., and Bezanilla, F. (2005). Nano to micro – fluorescence measurements of electric fields in molecules and genetically specified neurons. *J. Membr. Biol.* 208, 91–102.

Blunck, R., Cordero-Morales, J. F., Cuello, L. G., Perozo, E., and Bezanilla, F. (2006). Detection of the opening of the bundle crossing in KcsA with fluorescence lifetime spectroscopy reveals the existence of two gates for ion conduction. *J. Gen. Physiol.* 128, 569–581.

Blunck, R., Scheel, O., Muller, M., Brandenburg, K., Seitzer, U., and Seydel, U. (2001). New insights into endotoxin-induced activation of macrophages: involvement of a K+ channel in transmembrane signaling. *J. Immunol.* 166, 1009–1015.

Borjesson, S. I., and Elinder, F. (2011). An electrostatic potassium channel opener targeting the final voltage sensor transition. *J. Gen. Physiol.* 137, 563–577.

Borjesson, S. I., Hammarstrom, S., and Elinder, F. (2008). Lipoelectric modification of ion channel voltage gating by polyunsaturated fatty acids. *Biophys. J.* 95, 2242–2253.

Borjesson, S. I., Parkkari, T., Hammarstrom, S., and Elinder, F. (2010). Electrostatic tuning of cellular excitability. *Biophys. J.* 98, 396–403.

Brelidze, T. I., Carlson, A. E., Sankaran, B., and Zagotta, W. N. (2012). Structure of the carboxy-terminal region of a KCNH channel. *Nature* 481, 530–533.

Brelidze, T. I., Carlson, A. E., and Zagotta, W. N. (2009). Absence of direct cyclic nucleotide modulation of mEAG1 and hERG1 channels revealed with fluorescence and electrophysiological methods. *J. Biol. Chem.* 284, 27989–27997.

Bruening-Wright, A., Elinder, F., and Larsson, H. P. (2007). Kinetic relationship between the voltage sensor and the activation gate in spHCN channels. *J. Gen. Physiol.* 130, 71–81.

Bruening-Wright, A., and Larsson, H. P. (2007). Slow conformational changes of the voltage sensor during the mode shift in hyperpolarization-activated cyclic-nucleotide-gated channels. *J. Neurosci.* 27, 270–278.

Catterall, W. A. (2010). Ion channel voltage sensors: structure, function, and pathophysiology. *Neuron* 67, 915–928.

Cha, A., and Bezanilla, F. (1997). Characterizing voltage-dependent conformational changes in the Shaker K+ channel with fluorescence. *Neuron* 19, 1127–1140.

Chakrapani, S., Sompornpisut, P., Intharathep, P., Roux, B., and Perozo, E. (2010). The activated state of a sodium channel voltage sensor in a membrane environment. *Proc. Natl. Acad. Sci. U.S.A.* 107, 5435–5440.

Chanda, B., Asamoah, O. K., Blunck, R., Roux, B., and Bezanilla, F. (2005). Gating charge displacement in voltage-gated ion channels involves limited transmembrane movement. *Nature* 436, 852–856.

Chen, J., Mitcheson, J. S., Tristani-Firouzi, M., Lin, M., and Sanguinetti, M. C. (2001). The S4-S5 linker couples voltage sensing and activation of pacemaker channels. *Proc. Natl. Acad. Sci. U.S.A.* 98, 11277–11282.

Cheng, Y. M., and Claydon, T. W. (2012). Voltage-dependent gating of HERG potassium channels. *Front. Pharmacol.* 3:83. doi:10.3389/fphar.2012.00083

Choveau, F. S., Rodriguez, N., Abderemane Ali, F., Labro, A. J., Rose, T., Dahimene, S., Boudin, H., Le Henaff, C., Escande, D., Snyders, D. J., Charpentier, F., Merot, J., Baro, I., and Loussouarn, G. (2011). KCNQ1 channels voltage dependence through a voltage-dependent binding of the S4-S5 linker to the pore domain. *J. Biol. Chem.* 286, 707–716.

Clayton, G. M., Altieri, S., Heginbotham, L., Unger, V. M., and Morais-Cabral, J. H. (2008). Structure of the transmembrane regions of a bacterial cyclic nucleotide-regulated channel. *Proc. Natl. Acad. Sci. U.S.A.* 105, 1511–1515.

Cordero-Morales, J. F., Cuello, L. G., and Perozo, E. (2006a). Voltage-dependent gating at the KcsA selectivity filter. *Nat. Struct. Mol. Biol.* 13, 319–322.

Cordero-Morales, J. F., Cuello, L. G., Zhao, Y., Jogini, V., Cortes, D. M., Roux, B., and Perozo, E. (2006b). Molecular determinants of gating at the potassium-channel selectivity filter. *Nat. Struct. Mol. Biol.* 13, 311–318.

Craven, K. B., and Zagotta, W. N. (2006). CNG and HCN channels: two peas, one pod. *Annu. Rev. Physiol.* 68, 375–401.

Cuello, L. G., Cortes, D. M., Jogini, V., Sompornpisut, A., and Perozo, E. (2010a). A molecular mechanism for proton-dependent gating in KcsA. *FEBS Lett.* 584, 1126–1132.

Cuello, L. G., Jogini, V., Cortes, D. M., Pan, A. C., Gagnon, D. G., Dalmas, O., Cordero-Morales, J. F., Chakrapani, S., Roux, B., and Perozo, E. (2010b). Structural basis for the coupling between activation and inactivation gates in K(+) channels. *Nature* 466, 272–275.

Cuello, L. G., Jogini, V., Cortes, D. M., and Perozo, E. (2010c). Structural mechanism of C-type inactivation in K(+) channels. *Nature* 466, 203–208.

Cui, J., and Aldrich, R. W. (2000). Allosteric linkage between voltage and Ca(2+)-dependent activation of BK-type mslo1 K(+) channels. *Biochemistry* 39, 15612–15619.

Curran, M. E., Splawski, I., Timothy, K. W., Vincent, G. M., Green, E. D., and Keating, M. T. (1995). A molecular basis for cardiac arrhythmia: HERG mutations cause long QT syndrome. *Cell* 80, 795–803.

Decher, N., Chen, J., and Sanguinetti, M. C. (2004). Voltage-dependent gating of hyperpolarization-activated, cyclic nucleotide-gated pacemaker channels: molecular coupling between the S4-S5 and C-linkers. *J. Biol. Chem.* 279, 13859–13865.

Decher, N., Streit, A. K., Rapedius, M., Netter, M. F., Marzian, S., Ehling, P., Schlichthorl, G., Craan, T., Renigunta, V., Kohler, A., Dodel, R. C., Navarro-Polanco, R. A., Preisig-Muller, R., Klebe, G., Budde, T., Baukrowitz, T., and Daut, J. (2010). RNA editing modulates the binding of drugs and highly unsaturated fatty acids to the open pore of Kv potassium channels. *EMBO J.* 29, 2101–2113.

Diaz, L., Meera, P., Amigo, J., Stefani, E., Alvarez, O., Toro, L., and Latorre, R. (1998). Role of the S4 segment in a voltage-dependent calcium-sensitive potassium (hSlo)

channel. *J. Biol. Chem.* 273, 32430–32436.

DiFrancesco, D. (1993). Pacemaker mechanisms in cardiac tissue. *Annu. Rev. Physiol.* 55, 455–472.

Ding, S., and Horn, R. (2002). Tail end of the s6 segment: role in permeation in shaker potassium channels. *J. Gen. Physiol.* 120, 87–97.

Ding, S., and Horn, R. (2003). Effect of S6 tail mutations on charge movement in Shaker potassium channels. *Biophys. J.* 84, 295–305.

Doyle, D. A., Morais, C. J., Pfuetzner, R. A., Kuo, A., Gulbis, J. M., Cohen, S. L., Chait, B. T., and MacKinnon, R. (1998). The structure of the potassium channel: molecular basis of K+ conduction and selectivity. *Science* 280, 69–77.

Elinder, F., Arhem, P., and Larsson, H. P. (2001a). Localization of the extracellular end of the voltage sensor S4 in a potassium channel. *Biophys. J.* 80, 1802–1809.

Elinder, F., Mannikko, R., and Larsson, H. P. (2001b). S4 charges move close to residues in the pore domain during activation in a K channel. *J. Gen. Physiol.* 118, 1–10.

Escayg, A., MacDonald, B. T., Meisler, M. H., Baulac, S., Huberfeld, G., An-Gourfinkel, I., Brice, A., Leguern, E., Moulard, B., Chaigne, D., Buresi, C., and Malafosse, A. (2000). Mutations of SCN1A, encoding a neuronal sodium channel, in two families with GEFS+2. *Nat. Genet.* 24, 343–345.

Faure, E., McGuire, H., Marsolais, M., and Blunck, R. (2012). Movement of the S4-S5 linker of KvAP during gating. *Biophys. J.* 102, 13a.

Fedida, D., Bouchard, R., and Chen, F. S. (1996). Slow gating charge immobilization in the human potassium channel Kv1.5 and its prevention by 4-aminopyridine. *J. Physiol. (Lond.)* 494(Pt 2), 377–387.

Fernandez, D., Ghanta, A., Kauffman, G. W., and Sanguinetti, M. C. (2004). Physicochemical features of the HERG channel drug binding site. *J. Biol. Chem.* 279, 10120–10127.

Ferrer, T., Rupp, J., Piper, D. R., and Tristani-Firouzi, M. (2006). The S4-S5 linker directly couples voltage sensor movement to the activation gate in the human ether-a'-go-go-related gene (hERG) K+ channel. *J. Biol. Chem.* 281, 12858–12864.

Gagnon, D. G., and Bezanilla, F. (2010). The contribution of individual subunits to the coupling of the voltage sensor to pore opening in Shaker K channels: effect of ILT mutations in heterotetramers. *J. Gen. Physiol.* 136, 555–568.

Gauss, R., Seifert, R., and Kaupp, U. B. (1998). Molecular identification of a hyperpolarization-activated channel in sea urchin sperm. *Nature* 393, 583–587.

Guy, H. R., and Seetharamulu, P. (1986). Molecular model of the action potential sodium channel. *Proc. Natl. Acad. Sci. U.S.A.* 83, 508–512.

Hackos, D. H., Chang, T. H., and Swartz, K. J. (2002). Scanning the intracellular S6 activation gate in the shaker K+ channel. *J. Gen. Physiol.* 119, 521–532.

Haddad, G. A., and Blunck, R. (2011). Mode shift of the voltage sensors in Shaker K+ channels is caused by energetic coupling to the pore domain. *J. Gen. Physiol.* 137, 455–472.

Heginbotham, L., Lemasurier, M., Kolmakova-Partensky, L., and Miller, C. (1999). Single streptomyces lividans K(+) channels: functional asymmetries and sidedness of proton activation. *J. Gen. Physiol.* 114, 551–560.

Holmgren, M., Smith, P. L., and Yellen, G. (1997). Trapping of organic blockers by closing of voltage-dependent K+ channels: evidence for a trap door mechanism of activation gating. *J. Gen. Physiol.* 109, 527–535.

Hoshi, T., Zagotta, W. N., and Aldrich, R. W. (1990). Biophysical and molecular mechanisms of Shaker potassium channel inactivation. *Science* 250, 533–538.

Imbrici, P., D'Adamo, M. C., Kullmann, D. M., and Pessia, M. (2006). Episodic ataxia type 1 mutations in the KCNA1 gene impair the fast inactivation properties of the human potassium channels Kv1.4-1.1/Kvbeta1.1 and Kv1.4-1.1/Kvbeta1.2. *Eur. J. Neurosci.* 24, 3073–3083.

Islas, L. D., and Sigworth, F. J. (1999). Voltage sensitivity and gating charge in Shaker and Shab family potassium channels. *J. Gen. Physiol.* 114, 723–742.

Jara-Oseguera, A., Ishida, I. G., Rangel-Yescas, G. E., Espinosa-Jalapa, N., Perez-Guzman, J. A., Elias-Vinas, D., Le Lagadec, R., Rosenbaum, T., and Islas, L. D. (2011). Uncoupling charge movement from channel opening in voltage-gated potassium channels by ruthenium complexes. *J. Biol. Chem.* 286, 16414–16425.

Jensen, M. O., Jogini, V., Borhani, D. W., Leffler, A. E., Dror, R. O., and Shaw, D. E. (2012). Mechanism of voltage gating in potassium channels. *Science* 336, 229–233.

Jentsch, T. J. (2000). Neuronal KCNQ potassium channels: physiology and role in disease. *Nat. Rev. Neurosci.* 1, 21–30.

Jerng, H. H., and Covarrubias, M. (1997). K+ channel inactivation mediated by the concerted action of the cytoplasmic N- and C-terminal domains. *Biophys. J.* 72, 163–174.

Jiang, Y., Pico, A., Cadene, M., Chait, B. T., and MacKinnon, R. (2001). Structure of the RCK domain from the *E. coli* K+ channel and demonstration of its presence in the human BK channel. *Neuron* 29, 593–601.

Jiang, Y., Ruta, V., Chen, J., Lee, A., and MacKinnon, R. (2003). The principle of gating charge movement in a voltage-dependent K(+) channel. *Nature* 423, 42–48.

Kanevsky, M., and Aldrich, R. W. (1999). Determinants of voltage-dependent gating and open-state stability in the S5 segment of Shaker potassium channels. *J. Gen. Physiol.* 114, 215–242.

Khalili-Araghi, F., Jogini, V., Yarov-Yarovoy, V., Tajkhorshid, E., Roux, B., and Schulten, K. (2010). Calculation of the gating charge for the Kv1.2 voltage-activated potassium channel. *Biophys. J.* 98, 2189–2198.

Koo, G. C., Blake, J. T., Talento, A., Nguyen, M., Lin, S., Sirotina, A., Shah, K., Mulvany, K., Hora, D. Jr., Cunningham, P., Wunderler, D. L., McManus, O. B., Slaughter, R., Bugianesi, R., Felix, J., Garcia, M., Williamson, J., Kaczorowski, G., Sigal, N. H., Springer, M. S., and Feeney, W. (1997). Blockade of the voltage-gated potassium channel Kv1.3 inhibits immune responses in vivo. *J. Immunol.* 158, 5120–5128.

Kopfer, D. A., Hahn, U., Ohmert, I., Vriend, G., Pongs, O., De Groot, B. L., and Zachariae, U. (2012). Molecular determinants in K+ channel hERG inactivation gating. *Biophys. J.* 102, 529a–530a.

Koval, O. M., Fan, Y., and Rothberg, B. S. (2007). A role for the S0 transmembrane segment in voltage-dependent gating of BK channels. *J. Gen. Physiol.* 129, 209–220.

Kreusch, A., Pfaffinger, P. J., Stevens, C. F., and Choe, S. (1998). Crystal structure of the tetramerization domain of the Shaker potassium channel. *Nature* 392, 945–948.

Labro, A. J., Boulet, I. R., Choveau, F. S., Mayeur, E., Bruyns, T., Loussouarn, G., Raes, A. L., and Snyders, D. J. (2011). The S4-S5 linker of KCNQ1 channels forms a structural scaffold with the S6 segment controlling gate closure. *J. Biol. Chem.* 286, 717–725.

Labro, A. J., Raes, A. L., Grottesi, A., Van, H. D., Sansom, M. S., and Snyders, D. J. (2008). Kv channel gating requires a compatible S4-S5 linker and bottom part of S6, constrained by non-interacting residues. *J. Gen. Physiol.* 132, 667–680.

Lacroix, J. J., Labro, A. J., and Bezanilla, F. (2011). Properties of deactivation gating currents in Shaker channels. *Biophys. J.* 100, L28–L30.

Laine, M., Lin, M. C., Bannister, J. P., Silverman, W. R., Mock, A. F., Roux, B., and Papazian, D. M. (2003). Atomic proximity between S4 segment and pore domain in Shaker potassium channels. *Neuron* 39, 467–481.

Larsson, H. P., Baker, O. S., Dhillon, D. S., and Isacoff, E. Y. (1996). Transmembrane movement of the shaker K+ channel S4. *Neuron* 16, 387–397.

Latorre, R., Morera, F. J., and Zaelzer, C. (2010). Allosteric interactions and the modular nature of the voltage- and Ca2+-activated (BK) channel. *J. Physiol. (Lond.)* 588, 3141–3148.

Ledwell, J. L., and Aldrich, R. W. (1999). Mutations in the S4 region isolate the final voltage-dependent cooperative step in potassium channel activation. *J. Gen. Physiol.* 113, 389–414.

Lee, S. Y., Banerjee, A., and MacKinnon, R. (2009). Two separate interfaces between the voltage sensor and pore are required for the function of voltage-dependent K(+) channels. *PLoS Biol.* 7, e47. doi:10.1371/journal.pbio.1000047

Lee, U. S., and Cui, J. (2010). BK channel activation: structural and functional insights. *Trends Neurosci.* 33, 415–423.

Li, M., Jan, Y. N., and Jan, L. Y. (1992). Specification of subunit assembly by the hydrophilic amino-terminal domain of the Shaker potassium channel. *Science* 257, 1225–1230.

Li, W., and Aldrich, R. W. (2004). Unique inner pore properties of BK channels revealed by quaternary ammonium block. *J. Gen. Physiol.* 124, 43–57.

Li, W., and Aldrich, R. W. (2006). State-dependent block of BK channels by synthesized shaker ball peptides. *J. Gen. Physiol.* 128, 423–441.

Liman, E. R., Hess, P., Weaver, F., and Koren, G. (1991). Voltage-sensing residues in the S4 region of a mammalian K+ channel. *Nature* 353, 752–756.

Liu, Y., Holmgren, M., Jurman, M. E., and Yellen, G. (1997). Gated access

to the pore of a voltage-dependent K+ channel. *Neuron* 19, 175–184.

Lolicato, M., Nardini, M., Gazzarrini, S., Möller, S., Bertinetti, D., Herberg, F. W., Bolognesi, M., Martin, H., Fasolini, M., Bertrand, J. A., Arrigoni, C., Thiel, G., and Moroni, A. (2011). Tetramerization dynamics of C-terminal domain underlies isoform-specific cAMP gating in hyperpolarization-activated cyclic nucleotide-gated channels. *J. Biol. Chem.* 286, 44811–44820.

Long, S. B., Campbell, E. B., and MacKinnon, R. (2005a). Crystal structure of a mammalian voltage-dependent shaker family K+ channel. *Science* 309, 897–903.

Long, S. B., Campbell, E. B., and Mackinnon, R. (2005b). Voltage sensor of Kv1.2: structural basis of electromechanical coupling. *Science* 309, 903–908.

Long, S. B., Tao, X., Campbell, E. B., and MacKinnon, R. (2007). Atomic structure of a voltage-dependent K+ channel in a lipid membrane-like environment. *Nature* 450, 376–382.

Lu, Z., Klem, A. M., and Ramu, Y. (2001). Ion conduction pore is conserved among potassium channels. *Nature* 413, 809–813.

Lu, Z., Klem, A. M., and Ramu, Y. (2002). Coupling between voltage sensors and activation gate in voltage-gated K+ channels. *J. Gen. Physiol.* 120, 663–676.

Ma, Z., Lou, X. J., and Horrigan, F. T. (2006). Role of charged residues in the S1-S4 voltage sensor of BK channels. *J. Gen. Physiol.* 127, 309–328.

MacDonald, P. E., and Wheeler, M. B. (2003). Voltage-dependent K(+) channels in pancreatic beta cells: role, regulation and potential as therapeutic targets. *Diabetologia* 46, 1046–1062.

Mannikko, R., Elinder, F., and Larsson, H. P. (2002). Voltage-sensing mechanism is conserved among ion channels gated by opposite voltages. *Nature* 419, 837–841.

Mannuzzu, L. M., Moronne, M. M., and Isacoff, E. Y. (1996). Direct physical measure of conformational rearrangement underlying potassium channel gating. *Science* 271, 213–216.

McCormack, K., Tanouye, M. A., Iverson, L. E., Lin, J. W., Ramaswami, M., McCormack, T., Campanelli, J. T., Mathew, M. K., and Rudy, B. (1991). A role for hydrophobic residues in the voltage-dependent gating of Shaker K+ channels. *Proc. Natl. Acad. Sci. U.S.A.* 88, 2931–2935.

Muroi, Y., Arcisio-Miranda, M., and Chanda, B. (2009). Tryptophan scanning mutagenesis to identify the residues involved in coupling between the pore and DIII voltage-sensor of a sodium channel. *Biophys. J.* 96, 248a.

Muroi, Y., Arcisio-Miranda, M., Chowdhury, S., and Chanda, B. (2010). Molecular determinants of coupling between the domain III voltage sensor and pore of a sodium channel. *Nat. Struct. Mol. Biol.* 17, 230–237.

Muskett, F. W., Thouta, S., Thomson, S. J., Bowen, A., Stansfeld, P. J., and Mitcheson, J. S. (2011). Mechanistic insight into human ether-a-go-go-related gene (hERG) K+ channel deactivation gating from the solution structure of the EAG domain. *J. Biol. Chem.* 286, 6184–6191.

Neyroud, N., Tesson, F., Denjoy, I., Leibovici, M., Donger, C., Barhanin, J., Faure, S., Gary, F., Coumel, P., Petit, C., Schwartz, K., and Guicheney, P. (1997). A novel mutation in the potassium channel gene KVLQT1 causes the Jervell and Lange-Nielsen cardioauditory syndrome. *Nat. Genet.* 15, 186–189.

Ng, C. A., Perry, M. D., Tan, P. S., Hill, A. P., Kuchel, P. W., and Vandenberg, J. I. (2012). The S4-S5 linker acts as a signal integrator for HERG K+ channel activation and deactivation gating. *PLoS ONE* 7, e31640. doi:10.1371/journal.pone.0031640

Olcese, R., Latorre, R., Toro, L., Bezanilla, F., and Stefani, E. (1997). Correlation between charge movement and ionic current during slow inactivation in Shaker K+ channels. *J. Gen. Physiol.* 110, 579–589.

Olcese, R., Sigg, D., Latorre, R., Bezanilla, F., and Stefani, E. (2001). A conducting state with properties of a slow inactivated state in a shaker K(+) channel mutant. *J. Gen. Physiol.* 117, 149–163.

Pantazis, A., Gudzenko, V., Savalli, N., Kohanteb, A., Sigg, D., and Olcese, R. (2009). Cooperativity between voltage-sensing domains in the human BK channel revealed by voltage-clamp fluorometry. *Biophys. J.* 96, 481a. [Meeting Abstracts].

Pantazis, A., Kohanteb, A. P., and Olcese, R. (2010). Relative motion of transmembrane segments S0 and S4 during voltage sensor activation in the human BKCa channel. *J. Gen. Physiol.* 136, 645–657.

Papazian, D. M., Shao, X. M., Seoh, S. A., Mock, A. F., Huang, Y., and Wainstock, D. H. (1995). Electrostatic interactions of S4 voltage sensor in Shaker K+ channel. *Neuron* 14, 1293–1301.

Papazian, D. M., Timpe, L. C., Jan, Y. N., and Jan, L. Y. (1991). Alteration of voltage-dependence of Shaker potassium channel by mutations in the S4 sequence. *Nature* 349, 305–310.

Pape, P. C., Jong, D. S., and Chandler, W. K. (1996). A slow component of intramembranous charge movement during sarcoplasmic reticulum calcium release in frog cut muscle fibers. *J. Gen. Physiol.* 107, 79–101.

Pathak, M., Kurtz, L., Tombola, F., and Isacoff, E. (2005). The cooperative voltage sensor motion that gates a potassium channel. *J. Gen. Physiol.* 125, 57–69.

Payandeh, J., Gamal El-Din, T. M., Scheuer, T., Zheng, N., and Catterall, W. A. (2012). Crystal structure of a voltage-gated sodium channel in two potentially inactivated states. *Nature* 486, 135–139.

Payandeh, J., Scheuer, T., Zheng, N., and Catterall, W. A. (2011). The crystal structure of a voltage-gated sodium channel. *Nature* 475, 353–358.

Perozo, E., MacKinnon, R., Bezanilla, F., and Stefani, E. (1993). Gating currents from a nonconducting mutant reveal open-closed conformations in Shaker K+ channels. *Neuron* 11, 353–358.

Perozo, E., Santacruz-Toloza, L., Stefani, E., Bezanilla, F., and Papazian, D. M. (1994). S4 mutations alter gating currents of Shaker K channels. *Biophys. J.* 66, 345–354.

Perrin, M. J., Subbiah, R. N., Vandenberg, J. I., and Hill, A. P. (2008). Human ether-a-go-go related gene (hERG) K+ channels: function and dysfunction. *Prog. Biophys. Mol. Biol.* 98, 137–148.

Piper, D. R., Sanguinetti, M. C., and Tristani-Firouzi, M. (2005). Voltage sensor movement in the hERG K+ channel. *Novartis Found. Symp.* 266, 46–52; discussion 52-56, 95–99.

Prole, D. L., and Yellen, G. (2006). Reversal of HCN channel voltage dependence via bridging of the S4-S5 linker and Post-S6. *J. Gen. Physiol.* 128, 273–282.

Rajakulendran, S., Schorge, S., Kullmann, D. M., and Hanna, M. G. (2007). Episodic ataxia type 1: a neuronal potassium channelopathy. *Neurotherapeutics* 4, 258–266.

Ramu, Y., Xu, Y., and Lu, Z. (2006). Enzymatic activation of voltage-gated potassium channels. *Nature* 442, 696–699.

Rothberg, B. S., Shin, K. S., Phale, P. S., and Yellen, G. (2002). Voltage-controlled gating at the intracellular entrance to a hyperpolarization-activated cation channel. *J. Gen. Physiol.* 119, 83–91.

Ruta, V., Chen, J., and MacKinnon, R. (2005). Calibrated measurement of gating-charge arginine displacement in the KvAP voltage-dependent K+ channel. *Cell* 123, 463–475.

Sanguinetti, M. C. (2010). HERG1 channelopathies. *Pflugers Arch.* 460, 265–276.

Sanguinetti, M. C., Jiang, C., Curran, M. E., and Keating, M. T. (1995). A mechanistic link between an inherited and an acquired cardiac arrhythmia: HERG encodes the IKr potassium channel. *Cell* 81, 299–307.

Sanguinetti, M. C., and Xu, Q. P. (1999). Mutations of the S4-S5 linker alter activation properties of HERG potassium channels expressed in Xenopus oocytes. *J. Physiol. (Lond.)* 514(Pt 3), 667–675.

Santoro, B., Liu, D. T., Yao, H., Bartsch, D., Kandel, E. R., Siegelbaum, S. A., and Tibbs, G. R. (1998). Identification of a gene encoding a hyperpolarization-activated pacemaker channel of brain. *Cell* 93, 717–729.

Santoro, B., and Tibbs, G. R. (1999). The HCN gene family: molecular basis of the hyperpolarization-activated pacemaker channels. *Ann. N. Y. Acad. Sci.* 868, 741–764.

Savalli, N., Kondratiev, A., Toro, L., and Olcese, R. (2006). Voltage-dependent conformational changes in human Ca(2+)- and voltage-activated K(+) channel, revealed by voltage-clamp fluorometry. *Proc. Natl. Acad. Sci. U.S.A.* 103, 12619–12624.

Schmidt, D., Cross, S. R., and MacKinnon, R. (2009). A gating model for the archeal voltage-dependent K(+) channel KvAP in DPhPC and POPE:POPG decane lipid bilayers. *J. Mol. Biol.* 390, 902–912.

Schmidt, D., Jiang, Q. X., and MacKinnon, R. (2006). Phospholipids and the origin of cationic gating charges in voltage sensors. *Nature* 444, 775–779.

Schonherr, R., and Heinemann, S. H. (1996). Molecular determinants for activation and inactivation of HERG, a human inward rectifier potassium channel. *J. Physiol. (Lond.)* 493(Pt 3), 635–642.

Schoppa, N. E., and Sigworth, F. J. (1998a). Activation of Shaker potassium channels. II. Kinetics of the V2 mutant channel. *J. Gen. Physiol.* 111, 295–311.

Schoppa, N. E., and Sigworth, F. J. (1998b). Activation of Shaker potassium channels. III. An activation gating model for wild-type and V2

mutant channels. *J. Gen. Physiol.* 111, 313–342.

Schumacher, M. A., Rivard, A. F., Bachinger, H. P., and Adelman, J. P. (2001). Structure of the gating domain of a Ca2+-activated K+ channel complexed with Ca2+/calmodulin. *Nature* 410, 1120–1124.

Seoh, S. A., Sigg, D., Papazian, D. M., and Bezanilla, F. (1996). Voltage-sensing residues in the S2 and S4 segments of the Shaker K+ channel. *Neuron* 16, 1159–1167.

Shen, N. V., and Pfaffinger, P. J. (1995). Molecular recognition and assembly sequences involved in the subfamily-specific assembly of voltage-gated K+ channel subunit proteins. *Neuron* 14, 625–633.

Shin, K. S., Maertens, C., Proenza, C., Rothberg, B. S., and Yellen, G. (2004). Inactivation in HCN channels results from reclosure of the activation gate: desensitization to voltage. *Neuron* 41, 737–744.

Shin, K. S., Rothberg, B. S., and Yellen, G. (2001). Blocker state dependence and trapping in hyperpolarization-activated cation channels: evidence for an intracellular activation gate. *J. Gen. Physiol.* 117, 91–101.

Slesinger, P. A., Jan, Y. N., and Jan, L. Y. (1993). The S4-S5 loop contributes to the ion-selective pore of potassium channels. *Neuron* 11, 739–749.

Smith, P. L., Baukrowitz, T., and Yellen, G. (1996). The inward rectification mechanism of the HERG cardiac potassium channel. *Nature* 379, 833–836.

Smith-Maxwell, C. J., Ledwell, J. L., and Aldrich, R. W. (1998a). Role of the S4 in cooperativity of voltage-dependent potassium channel activation. *J. Gen. Physiol.* 111, 399–420.

Smith-Maxwell, C. J., Ledwell, J. L., and Aldrich, R. W. (1998b). Uncharged S4 residues and cooperativity in voltage-dependent potassium channel activation. *J. Gen. Physiol.* 111, 421–439.

Soler-Llavina, G. J., Chang, T. H., and Swartz, K. J. (2006). Functional interactions at the interface between voltage-sensing and pore domains in the Shaker K(v) channel. *Neuron* 52, 623–634.

Spector, P. S., Curran, M. E., Zou, A., Keating, M. T., and Sanguinetti, M. C. (1996). Fast inactivation causes rectification of the IKr channel. *J. Gen. Physiol.* 107, 611–619.

Starace, D. M., and Bezanilla, F. (2001). Histidine scanning mutagenesis of basic residues of the S4 segment of the shaker k+ channel. *J. Gen. Physiol.* 117, 469–490.

Starace, D. M., and Bezanilla, F. (2004). A proton pore in a potassium channel voltage sensor reveals a focused electric field. *Nature* 427, 548–553.

Stefani, E., Toro, L., Perozo, E., and Bezanilla, F. (1994). Gating of Shaker K+ channels: I. Ionic and gating currents. *Biophys. J.* 66, 996–1010.

Sukhareva, M., Hackos, D. H., and Swartz, K. J. (2003). Constitutive activation of the Shaker Kv channel. *J. Gen. Physiol.* 122, 541–556.

Sullivan, D. A., Holmqvist, M. H., and Levitan, I. B. (1997). Characterization of gating and peptide block of mSlo, a cloned calcium-dependent potassium channel. *J. Neurophysiol.* 78, 2937–2950.

Takeuchi, K., Takahashi, H., Kawano, S., and Shimada, I. (2007). Identification and characterization of the slowly exchanging pH-dependent conformational rearrangement in KcsA. *J. Biol. Chem.* 282, 15179–15186.

Taraska, J. W., and Zagotta, W. N. (2010). Fluorescence applications in molecular neurobiology. *Neuron* 66, 170–189.

Thomas, J., Epshtein, Y., Chopra, A., Ordog, B., Ghassemi, M., Christman, J. W., Nattel, S., Cook, J. L., and Levitan, I. (2011). Anthrax lethal factor activates K(+) channels to induce IL-1beta secretion in macrophages. *J. Immunol.* 186, 5236–5243.

Thompson, A. N., Posson, D. J., Parsa, P. V., and Nimigean, C. M. (2008). Molecular mechanism of pH sensing in KcsA potassium channels. *Proc. Natl. Acad. Sci. U.S.A.* 105, 6900–6905.

Tiwari-Woodruff, S. K., Lin, M. A., Schulteis, C. T., and Papazian, D. M. (2000). Voltage-dependent structural interactions in the Shaker K(+) channel. *J. Gen. Physiol.* 115, 123–138.

Tombola, F., Pathak, M. M., and Isacoff, E. Y. (2005). Voltage-sensing arginines in a potassium channel permeate and occlude cation-selective pores. *Neuron* 45, 379–388.

Tristani-Firouzi, M., Chen, J., and Sanguinetti, M. C. (2002). Interactions between S4-S5 linker and S6 transmembrane domain modulate gating of HERG K+ channels. *J. Biol. Chem.* 277, 18994–19000.

Tristani-Firouzi, M., and Sanguinetti, M. C. (2003). Structural determinants and biophysical properties of HERG and KCNQ1 channel gating. *J. Mol. Cell Cardiol.* 35, 27–35.

Vaid, M., Claydon, T. W., Rezazadeh, S., and Fedida, D. (2008). Voltage clamp fluorimetry reveals a novel outer pore instability in a mammalian voltage-gated potassium channel. *J. Gen. Physiol.* 132, 209–222.

Van Slyke, A. C., Rezazadeh, S., Snopkowski, M., Shi, P., Allard, C. R., and Claydon, T. W. (2010). Mutations within the S4-S5 linker alter voltage sensor constraints in hERG K+ channels. *Biophys. J.* 99, 2841–2852.

Vardanyan, V., and Pongs, O. (2012). Coupling of voltage sensors to the channel pore: a comparative view. *Front. Pharmacol.* 3:145. doi:10.3389/fphar.2012.00145

Vargas, E., Bezanilla, F., and Roux, B. (2011). In search of a consensus model of the resting state of a voltage-sensing domain. *Neuron* 72, 713–720.

Villalba-Galea, C. A., Sandtner, W., Starace, D. M., and Bezanilla, F. (2008). S4-based voltage sensors have three major conformations. *Proc. Natl. Acad. Sci. U.S.A.* 105, 17600–17607.

Wainger, B. J., Degennaro, M., Santoro, B., Siegelbaum, S. A., and Tibbs, G. R. (2001). Molecular mechanism of cAMP modulation of HCN pacemaker channels. *Nature* 411, 805–810.

Wall-Lacelle, S., Hossain, M. I., Sauve, R., Blunck, R., and Parent, L. (2011). Double mutant cycle analysis identified a critical leucine residue in the IIS4S5 linker for the activation of the Ca(V)2.3 calcium channel. *J. Biol. Chem.* 286, 27197–27205.

Wallner, M., Meera, P., and Toro, L. (1996). Determinant for beta-subunit regulation in high-conductance voltage-activated and Ca(2+)-sensitive K+ channels: an additional transmembrane region at the N terminus. *Proc. Natl. Acad. Sci. U.S.A.* 93, 14922–14927.

Wang, J., Chen, S., and Siegelbaum, S. A. (2001). Regulation of hyperpolarization-activated HCN channel gating and cAMP modulation due to interactions of COOH terminus and core transmembrane regions. *J. Gen. Physiol.* 118, 237–250.

Wang, J., Trudeau, M. C., Zappia, A. M., and Robertson, G. A. (1998). Regulation of deactivation by an amino terminal domain in human ether-a-go-go-related gene potassium channels. *J. Gen. Physiol.* 112, 637–647.

Wang, S., Liu, S., Morales, M. J., Strauss, H. C., and Rasmusson, R. L. (1997). A quantitative analysis of the activation and inactivation kinetics of HERG expressed in Xenopus oocytes. *J. Physiol. (Lond.)* 502(Pt 1), 45–60.

Warmke, J. W., and Ganetzky, B. (1994). A family of potassium channel genes related to eag in Drosophila and mammals. *Proc. Natl. Acad. Sci. U.S.A.* 91, 3438–3442.

Wynia-Smith, S. L., Gillian-Daniel, A. L., Satyshur, K. A., and Robertson, G. A. (2008). hERG gating microdomains defined by S6 mutagenesis and molecular modeling. *J. Gen. Physiol.* 132, 507–520.

Xu, X., Vysotskaya, Z. V., Liu, Q., and Zhou, L. (2010). Structural basis for the cAMP-dependent gating in the human HCN4 channel. *J. Biol. Chem.* 285, 37082–37091.

Xu, Y., Ramu, Y., and Lu, Z. (2008). Removal of phospho-head groups of membrane lipids immobilizes voltage sensors of K+ channels. *Nature* 451, 826–829.

Yang, H., Hu, L., Shi, J., Delaloye, K., Horrigan, F. T., and Cui, J. (2007). Mg2+ mediates interaction between the voltage sensor and cytosolic domain to activate BK channels. *Proc. Natl. Acad. Sci. U.S.A.* 104, 18270–18275.

Yang, H., Shi, J., Zhang, G., Yang, J., Delaloye, K., and Cui, J. (2008). Activation of Slo1 BK channels by Mg2+ coordinated between the voltage sensor and RCK1 domains. *Nat. Struct. Mol. Biol.* 15, 1152–1159.

Yang, N., George, A. L. Jr., and Horn, R. (1996). Molecular basis of charge movement in voltage-gated sodium channels. *Neuron* 16, 113–122.

Yarov-Yarovoy, V., Baker, D., and Catterall, W. A. (2006). Voltage sensor conformations in the open and closed states in ROSETTA structural models of K(+) channels. *Proc. Natl. Acad. Sci. U.S.A.* 103, 7292–7297.

Yarov-Yarovoy, V., Decaen, P. G., Westenbroek, R. E., Pan, C. Y., Scheuer, T., Baker, D., and Catterall, W. A. (2012). Structural basis for gating charge movement in the voltage sensor of a sodium channel. *Proc. Natl. Acad. Sci. U.S.A.* 109, E93–E102.

Yellen, G. (2002). The voltage-gated potassium channels and their relatives. *Nature* 419, 35–42.

Yuan, P., Leonetti, M. D., Pico, A. R., Hsiung, Y., and MacKinnon, R. (2010). Structure of the human BK channel Ca2+-activation apparatus at 3.0 a resolution. *Science* 329, 182–186.

Zagotta, W. N., Hoshi, T., and Aldrich, R. W. (1990). Restoration of inactivation in mutants of Shaker potassium channels by a peptide derived from ShB. *Science* 250, 568–571.

Zagotta, W. N., Hoshi, T., and Aldrich, R. W. (1994a). Shaker potassium channel gating. III: evaluation of kinetic models for activation. *J. Gen. Physiol.* 103, 321–362.

Zagotta, W. N., Hoshi, T., Dittman, J., and Aldrich, R. W. (1994b). Shaker potassium channel gating. II: transitions in the activation pathway. *J. Gen. Physiol.* 103, 279–319.

Zagotta, W. N., Olivier, N. B., Black, K. D., Young, E. C., Olson, R., and Gouaux, E. (2003). Structural basis for modulation and agonist specificity of HCN pacemaker channels. *Nature* 425, 200–205.

Zhou, Y., Xia, X. M., and Lingle, C. J. (2011). Cysteine scanning and modification reveal major differences between BK channels and Kv channels in the inner pore region. *Proc. Natl. Acad. Sci. U.S.A.* 108, 12161–12166.

Conflict of Interest Statement: The authors declare that the research was conducted in the absence of any commercial or financial relationships that could be construed as a potential conflict of interest.

Received: 30 May 2012; accepted: 24 August 2012; published online: 12 September 2012.

*Citation: Blunck R and Batulan Z (2012) Mechanism of electromechanical coupling in voltage-gated potassium channels. Front. Pharmacol. **3**:166. doi: 10.3389/fphar.2012.00166*

This article was submitted to Frontiers in Pharmacology of Ion Channels and Channelopathies, a specialty of Frontiers in Pharmacology.

frontiers in
PHARMACOLOGY

REVIEW ARTICLE
published: 23 May 2012
doi: 10.3389/fphar.2012.00100

Voltage sensor inactivation in potassium channels

Robert Bähring*, Jan Barghaan, Regina Westermeier and Jessica Wollberg

Institut für Zelluläre und Integrative Physiologie, Zentrum für Experimentelle Medizin, Universitätsklinikum Hamburg-Eppendorf, Hamburg, Germany

Edited by:
Gildas Loussouarn, University of Nantes, France

Reviewed by:
Harley Takatsuna Kurata, University of British Columbia, Canada
Keith Elmslie, AT Still University of Health Sciences, USA

****Correspondence:***
Robert Bähring, Institut für Zelluläre und Integrative Physiologie, Zentrum für Experimentelle Medizin, Universitätsklinikum Hamburg-Eppendorf, Martinistr. 52, 20246 Hamburg, Germany.
e-mail: r.baehring@uke.uni-hamburg.de

In voltage-gated potassium (Kv) channels membrane depolarization causes movement of a voltage sensor domain. This conformational change of the protein is transmitted to the pore domain and eventually leads to pore opening. However, the voltage sensor domain may interact with two distinct gates in the pore domain: the activation gate (A-gate), involving the cytoplasmic S6 bundle crossing, and the pore gate (P-gate), located externally in the selectivity filter. How the voltage sensor moves and how tightly it interacts with these two gates on its way to adopt a relaxed conformation when the membrane is depolarized may critically determine the mode of Kv channel inactivation. In certain Kv channels, voltage sensor movement leads to a tight interaction with the P-gate, which may cause conformational changes that render the selectivity filter non-conductive ("P/C-type inactivation"). Other Kv channels may preferably undergo inactivation from pre-open closed-states during voltage sensor movement, because the voltage sensor temporarily uncouples from the A-gate. For this behavior, known as "preferential" closed-state inactivation, we introduce the term "A/C-type inactivation". Mechanistically, P/C- and A/C-type inactivation represent two forms of "voltage sensor inactivation."

Keywords: Kv channels, P/C-type inactivation, closed-state inactivation, U-type inactivation

INTRODUCTION

Voltage-gated potassium (Kv) channels control excitability and discharge behavior of nerve and muscle cells (Hille, 2001). Kv channel activation may occur in response to strong membrane depolarization, which occurs when action potentials are generated. In this case, the voltage-dependent activation of a potassium conductance critically determines repolarization and afterhyperpolarization (Hodgkin and Huxley, 1952). Alternatively, Kv channels may be activated by subthreshold depolarization, and the resultant potassium conductance may prevent or delay action potential firing (Connor and Stevens, 1971). Notably, many Kv channels undergo inactivation when the membrane is depolarized, meaning that they adopt a non-conducting conformation, which is different from the resting state, and from which the channels can only recover when the membrane is re- or hyperpolarized (Hille, 2001). Whenever such inactivation occurs, the influence of potassium flow on the membrane potential is only transient and provided with refractoriness, which may be of physiological relevance: For instance, the transient nature of a potassium conductance in ventricular cardiomyocytes supports the spike-and-dome morphology of the action potential (Greenstein et al., 2000); in the nervous system brief inactivation of a subthreshold operating dendritic potassium conductance at postsynaptic sites, which normally suppresses dendritic excitation, may lead to local dendritic spike amplification (Hoffman et al., 1997; Magee and Johnston, 1997); and the slow and incomplete recovery of a presynaptic potassium conductance from inactivation may lead to frequency-dependent spike broadening, thereby enhancing calcium entry and transmitter release (Jackson et al., 1991). These are only a few examples showing that Kv channel inactivation may serve electrical signaling on the cellular level. Due to its critical role in cell physiology, the kinetics, voltage dependence, and structure-function relationships of Kv channel inactivation have been the focus of intense research for decades.

Three main mechanisms have been identified so far that may lead to the inactivation of Kv channels (Kurata and Fedida, 2006; Bähring and Covarrubias, 2011). (1) When the cloning of Kv channel genes made detailed structure-function analyses possible, the first inactivation mechanism to be identified was "N-type inactivation"; the name refers to the part of the channel protein involved: A tethered N-terminal inactivation domain of the channel protein plugs the open pore according to a ball-and-chain mechanism (Hoshi et al., 1990); N-type inactivation is usually very fast (on the time scale of few milliseconds). (2) Next, it was recognized that more C-terminal portions of the channel protein also play an important role in Kv channel inactivation. The fact that the pore domain is involved in this mechanism led to the term "P/C-type inactivation": Conformational changes at the external pore entrance near the selectivity filter (the P-gate) impair channel conductivity (Hoshi et al., 1991; Yellen et al., 1994). Like N-type inactivation, P/C-type inactivation has been classically viewed as an open state inactivation mechanism, however, P/C-type inactivation may also occur from closed-states (see below). (3) Finally, some Kv channels preferably inactivate from closed-states and not from the open state. Although the existence of such "preferential" closed-state inactivation (CSI) was recognized early on, the structural determinants involved have remained a mystery for a long time. It is now thought that temporary uncoupling of the voltage sensor from the S6 activation gate (A-gate) underlies preferential CSI (Barghaan and Bähring, 2009); P/C-type inactivation; and preferential CSI represent slower processes (usually on the time scale of tens to hundreds of milliseconds).

Fast N-type inactivation can be abolished by genetic or enzymatic removal of the N-terminal inactivation domain, and experimental application of the isolated inactivation peptide can restore inactivation (Hoshi et al., 1990; Zagotta et al., 1990). N-type inactivation may also be conferred to non- or slowly inactivating channels by their association with auxiliary β-subunits which for their part possess an N-terminal inactivation domain (Rettig et al., 1994; Wallner et al., 1999; Jerng et al., 2009). By contrast, the slower P/C-type inactivation and preferential CSI are more intrinsic to the channel. P/C-type inactivation can be prevented by external TEA, elevated external potassium concentrations and by a threonine to valine mutation at the external pore entrance (Choi et al., 1991; Lopez-Barneo et al., 1993). Preferential CSI is critically influenced by mutations located on the internal side of the pore; i.e., the S4–S5 linker and the S6 activation gate (Jerng et al., 1999; Barghaan and Bähring, 2009). Notably, both P/C-type inactivation and preferential CSI of Kv channels critically depend on conformational changes of the voltage sensor domain (Kurata and Fedida, 2006; Bähring and Covarrubias, 2011). Due to the fact that the voltage sensor is instrumental in both mechanisms, P/C-type inactivation and preferential CSI may be seen as two forms of "voltage sensor inactivation". Here we provide a brief overview of work, that has demonstrated and mechanistically examined preferential CSI and P/C-type inactivation in the *Shaker*-related Kv channel subfamilies Kv1–Kv4.

FORMAL DESCRIPTION OF Kv CHANNEL INACTIVATION

A mechanistic understanding of ion channel function requires the definition of different states which the protein complex may adopt. The formal description is then usually followed by the assignment of structural correlates based on experimental evidence. The basic features of Kv channel gating, including voltage-dependent activation, pore opening and channel inactivation, may be formally described by the simplified scheme shown in **Figure 1A** (Scheme 1). When the membrane is depolarized (ΔV) the channels go from a resting state (C_R), via an activated but still closed-state (C^*), to an open state (O). The channels may inactivate either from C^* (CSI) to adopt a closed-inactivated state (I_C) or from the open state to reach one of two different but interconnected open-inactivated states (I_N or $I_{P/C}$), representing the mechanisms of N-type and P/C-type inactivation, respectively. N-type inactivation is thought to favor entry into the P/C-type inactivated state ($I_{N,P/C}$) due to the prevention of ion flux and the resultant ion deprivation of the pore (Baukrowitz and Yellen, 1995). Scheme 1 does not account for the tetrameric arrangement which allows cooperativity of Kv channel gating. Also, Scheme 1 assumes that P/C-type inactivation requires channel opening, which represents a classical view but may not be appropriate. A more sophisticated kinetic scheme, suitable for global kinetic modeling (Kaulin et al., 2008), is shown in **Figure 1B** (Scheme 2). Here, during activation the channels go from a resting state (C_R), via several partially activated closed-states (C_1–C_4) and an opening-permissive pre-open closed-state (C_5), to an open state (O). The channels can inactivate from the partially activated and pre-open closed-states to adopt either one of the states $A_R - A_5$ (these transitions represent preferential CSI), or the channels may adopt one of the inactivated states $P_R - P_6$ (these transitions represent P/C-type inactivation). Translated into structural terms (see also **Figure 2**), the majority of transitions from left to right in Scheme 2 are associated with conformational changes of the voltage sensor (ΔV, **Figure 1B**). When the voltage sensor has adopted an activated conformation in all four subunits (states C_1–C_4) the channel goes to an opening-permissive conformation (C_5) from which it can undergo a concerted opening step (O). However, voltage sensor movement may also induce different forms of inactivation, as it either leads to an uncoupling from the A-gate (A-states) or to a tight interaction with the P-gate, thereby causing conformational changes in the selectivity filter which reduce conductivity (P-states). These structural determinants will be discussed in more detail. Notably, Scheme 2 allows P/C-type inactivation from both open and closed-states (see below). Similar to previously suggested models accounting for parallel pathways of P/C-type inactivation and preferential CSI (Klemic et al., 2001; Kurata et al., 2005), Scheme 2 does not account for N-type inactivation (**Figure 1B**), because it was originally developed for channels in which this form of inactivation plays a negligible role (Kaulin et al., 2008). Also, in the more detailed discussion of preferential CSI and P/C-type inactivation as two forms of voltage sensor inactivation below, we shall leave N-type inactivation unconsidered. We will first discuss indications and the mechanistic basis of preferential CSI in Kv channels, and

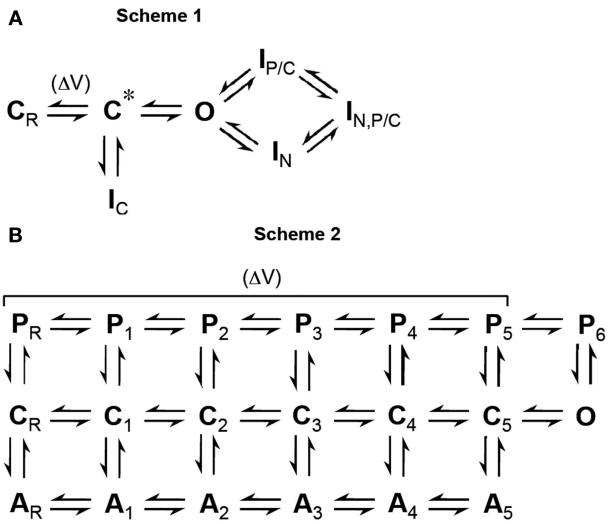

FIGURE 1 | Formal description of Kv channel gating. (A) Scheme 1: Simplified gating scheme which represents a classical view of inactivation from open and closed-states (C_R, resting state; C*, activated but still closed-state; O, open state; I_N, N-type inactivated state; $I_{P/C}$, P/C-type inactivated state; $I_{N,P/C}$, N-type and P/C-type inactivated state; I_C, closed-inactivated state). The voltage-sensitive transition is indicated (ΔV). **(B)** Scheme 2: Extended gating scheme adopted from Kaulin et al. (2008), which accounts for the activation pathway of a tetrameric channel accompanied by two inactivation pathways based on different mechanisms (C, closed-states; A, inactivated states involving the A-gate; P, inactivated states involving the P-gate; suffix R means "resting," suffixes 1–4 represent number of subunits in this state, suffix 5 denotes states which precede a concerted opening step; O, open state). The voltage-sensitive transitions are indicated (ΔV). Collectively, A-states represent preferential closed-state inactivation (CSI) or "A/C-type inactivation"; P-states represent P/C-type inactivation, P_1–P_5 from closed-states, P_6 from the open state.

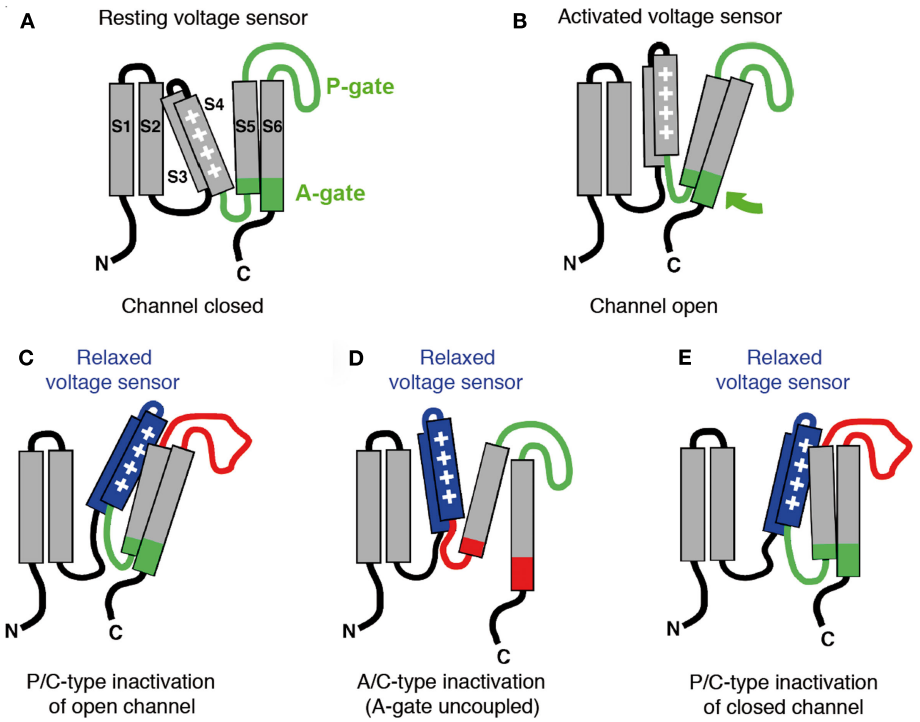

FIGURE 2 | Models of voltage-dependent activation and voltage sensor inactivation in Kv channels. Cartoons illustrate putative conformations a single Kv channel α-subunit may adopt in a subtype-specific manner when the membrane encounters prolonged depolarization. **(A)** Resting state; the voltage sensor is in its resting position (down) and the channel is closed (S1–S6, transmembrane segments; P-gate, pore gate with selectivity filter; A-gate, activation gate represented by the distal S6 segment, which is involved in the bundle crossing in the tetramer). **(B)** Open conducting state; the voltage sensor is activated (up) and the channel is open (green arrow denotes putative opening motion of the A-gate). **(C)** Open but non-conducting state; the voltage sensor has adopted a relaxed conformation (blue) which tightly interacts with the P-gate rendering the selectivity filter non-conducting (red). **(D)** Closed-inactivated state with the A-gate uncoupled (red); the voltage sensor has adopted a relaxed conformation (blue), and the A-gate is closed (A/C-type inactivation). **(E)** Closed-inactivated state with the P-gate in its non-conductive conformation (red); the voltage sensor has adopted a relaxed conformation (blue), the A-gate is still coupled to the voltage sensor but the channel has not opened (P/C-type inactivation of a closed channel).

then consider P/C-type inactivation as an alternative reflection of voltage sensor inactivation based on differences in the crosstalk between voltage sensor domain and pore domain.

INDICATIONS OF PREFERENTIAL CSI IN Kv CHANNELS

The first indication of a cumulative form of inactivation in Kv channels, which may involve pre-open closed-states, came from recordings done on molluscan neurons (Aldrich, 1981). In this study Aldrich noticed that, after a voltage pulse, the maximum current obtained with a second pulse was less than the current at the end of the first pulse. This finding indicated that, instead of recovery from inactivation, even more inactivation must have occurred during the interpulse interval at a negative voltage. Accordingly, Kv channels which preferentially inactivate from closed rather than open states show faster and stronger inactivation in response to a series of test pulses rather than to one long pulse. Furthermore, at steady-state Kv channels with preferential CSI show pronounced inactivation at intermediate voltages and less inactivation at more positive voltages where the open probability is increased. Such behavior produces U-shaped inactivation curves, which led to the term "U-type inactivation," with no reference to the structures involved. Kv2.1 (Klemic et al., 1998) and Kv3.1 channels (Klemic et al., 2001) undergo strong cumulative inactivation with repeated brief voltage pulses, and the inactivation curves of these channels exhibit a U-type profile, indicative of preferential CSI. U-type features of steady-state inactivation curves as an indication of preferential CSI have also been observed for N-terminally truncated *Shaker* channels (*Sh*Δ; Klemic et al., 2001) and a naturally occurring Kv1.5 N-terminal deletion mutant (Kv1.5ΔN209; Klemic et al., 2001; Kurata et al., 2001; Kurata et al., 2002; Kurata et al., 2005).

Computer modeling of non-*Shaker* A-type potassium currents in neurons from *Drosophila* (Solc and Aldrich, 1990) and of the transient outward current (I_{to}) in ferret ventricular myocytes (Campbell et al., 1993) suggested that inactivation coupled to the voltage-dependent activation pathway of the underlying channels is necessary to reproduce the experimentally observed gating behavior (Ic-state in Scheme 1, A-states in Scheme 2, **Figure 1**). Moreover, it was observed that prepulse inactivation of the ferret I_{to} occurred at voltages where no opening was detectable (Campbell et al., 1993). The pioneering study by Campbell and coworkers and the fact that I_{to} is mainly mediated by members of the Kv4 subfamily of Kv channels (Dixon et al., 1996), led to a focusing on Kv4 channels to learn more about the mechanism of preferential CSI. It is also important in this context that P/C-type mechanisms play a negligible role in Kv4 channel inactivation, as external TEA does

not influence (Jerng and Covarrubias, 1997) and high external potassium concentrations accelerate macroscopic current decay (Jerng and Covarrubias, 1997; Kirichok et al., 1998; Bähring et al., 2001; Shahidullah and Covarrubias, 2003; Kaulin et al., 2008). Notably, the homologous position where a threonine to valine mutation eliminates P/C-type inactivation in *Shaker*B channels (T449V; Lopez-Barneo et al., 1993), is already occupied by valine in Kv4 channels.

Just like native I_{to}, recombinant Kv4 channels in heterologous expression systems show the typical discrepancy between the voltage dependencies of macroscopic inactivation and activation, resulting in almost no overlap of the corresponding curves and a minimal conductance window (Jerng et al., 1999; Bähring et al., 2001; Patel et al., 2004; Dougherty et al., 2008; Kaulin et al., 2008; Barghaan and Bähring, 2009). This is a strong indication of preferential CSI as an intrinsic property of Kv4 channels. Notably, however, the inactivation curves of Kv4 channels do not show U-type features. But this is due to the fact that, even at strongly depolarized membrane voltages, which favor channel opening, occupancy of the open state is only transient in Kv4 channels and they rather tend to close and accumulate in closed-inactivated states (Jerng et al., 1999; Bähring et al., 2001; Barghaan et al., 2008; Kaulin et al., 2008). Thus, these channels exhibit preferential CSI at all relevant voltages. This assertion is based on the finding that the closing step plays a critical role in Kv4 channel inactivation. Experimentally this has been tested by the use of different permeant ions (high and identical concentrations of one ion species on either side of the membrane): Rubidium ions, which have a longer residency time in the pore than potassium ions not only slow Kv4 deactivation tail currents following brief activation pulses but also macroscopic inactivation during prolonged pulses (Bähring et al., 2001; Shahidullah and Covarrubias, 2003; Barghaan et al., 2008). Also, point mutations, which cause a slowing of deactivation tail current decay, at the same time slow macroscopic inactivation in Kv4 channels (Jerng et al., 1999). Any open state inactivation mechanism would be favored and macroscopic current decay accelerated when channel closing is delayed. Also, recovery from open-inactivated states is usually accompanied by re-opening tail currents before the channels close. The complete absence of such re-opening tail currents when the membrane potential is repolarized after a prolonged voltage pulse sufficiently depolarized to open Kv4 channels (Bähring et al., 2001), also reflects their final accumulation in closed-inactivated states at all relevant voltages.

MECHANISM OF CSI IN Kv4 CHANNELS

Recent studies have now shed light on what might happen mechanistically during CSI in Kv4 channels. In one study, mutational and thermodynamic analyses of putative coupling domains between the voltage sensor and the A-gate were correlated with CSI kinetics and steady-state inactivation in Kv4.2 channels (Barghaan and Bähring, 2009); in another study a detailed electrophysiological analysis of gating charge movement was performed and the results correlated with Kv4.2 channel inactivation (Dougherty et al., 2008).

Previous findings had already given a hint on the structural correlates that might be responsible for the finding that Kv channels can stay closed despite voltage sensor movement. For instance, in N-terminally truncated and L382I point-mutated *Shaker*B channels enhanced CSI had been observed relative to wild-type (Ayer and Sigworth, 1997). The L382I mutation lies at the S4 end of the S4–S5 linker. Notably, the S4–S5 linker is critically involved in the coupling of the voltage sensor to the A-gate in Kv channels (Lu et al., 2002; Yifrach and MacKinnon, 2002; Long et al., 2005). A physical model of CSI has been suggested (Shin et al., 2004; Barghaan and Bähring, 2009), in which S4–S5 linker residues may fail to make tight contact with their S6 counterparts. Barghaan and Bähring (2009) directly tested this hypothesis by applying scanning mutagenesis and double-mutant cycle analysis to the Kv4.2 S4–S5 linker and the distal S6 segment. Such double-mutant cycle analysis has previously identified pairs of amino acids within these two domains, which, by direct coupling, mediate the voltage-dependent opening of the A-gate in *Shaker*B channels (Yifrach and MacKinnon, 2002). In corresponding Kv4.2 single- and double-mutants, these sites were tested for their involvement in CSI by applying prepulse inactivation protocols. The results of these experiments suggested that pairs of amino acids, one in the S4–S5 linker and the other one in the distal S6 segment, not only interact with each other to open the A-gate, but are dynamic interaction partners in Kv4 channel CSI (Barghaan and Bähring, 2009). It was concluded that Kv4 channel CSI is based on the temporary uncoupling of the voltage sensor from the A-gate.

In voltage-dependent ion channels the movement of gating charge can be influenced by inactivation, as first characterized for voltage-dependent sodium channels (Armstrong and Bezanilla, 1977). In the absence of inactivation gating charges located in S4 may freely move across the membrane electric field (see **Figures 2A,B**), which can be detected as outward and inward gating currents (Armstrong and Bezanilla, 1973). However, if the return of the voltage sensor to its resting conformation is impeded and slowed ("gating charge immobilization") the detection of gating currents may be constricted or impossible ("loss of gating charge"). This may be the case if the voltage sensor adopts a stable ("relaxed") conformation in response to a prolonged depolarization (see **Figures 2C–E**). In Kv channels gating charge immobilization has been shown previously for both N-type (Bezanilla et al., 1991; Perozo et al., 1992; Roux et al., 1998) and P/C-type inactivation (Fedida et al., 1996; Olcese et al., 1997). Dougherty et al. (2008) tested whether gating charge immobilization also occurs in Kv4.2 channels known to preferentially undergo CSI. If the dynamic uncoupling model of CSI is correct and conformational changes of the voltage sensor represent the proximate cause of Kv4 channel CSI, electrophysiological manifestations of inactivation and gating charge immobilization should share the same voltage dependence and kinetics. The experiments by Dougherty et al. (2008) revealed profound gating charge immobilization over a narrow range of negative membrane potentials where CSI is expected to occur. Moreover, the kinetics of the loss of gating charge at positive and recovery of gating charge at negative voltages were identical to the kinetics of ionic current decay and macroscopic recovery from inactivation, respectively. These results showed that the loss of gating charge and the onset of inactivation reflect the same molecular mechanism, and they strongly suggested that the voltage sensor is directly involved in the mechanism of Kv4 channel CSI. The results also explained why CSI is critically influenced

by neutralizing positive charges (Skerritt and Campbell, 2007, 2009) or introducing non-native positive charges (Skerritt and Campbell, 2008) in the Kv4.3 S4 segment.

Obviously, CSI in Kv4 channels corresponds to the failure of the voltage sensors to actively open the A-gate. It is not known to date whether uncoupling allows the voltage sensor to adopt its relaxed conformation, or whether this slow conformational change of the voltage sensor actually causes uncoupling. Optical recording techniques, including voltage-clamp fluorimetry, may help to elucidate structural rearrangements during Kv4 channel CSI not accessible by electrophysiological measurements, thereby clarifying the cause-and-effect relationships of voltage sensor relaxation and A-gate uncoupling.

P/C- AND A/C-TYPE INACTIVATION: TWO VARIATIONS OF VOLTAGE SENSOR – PORE DOMAIN CROSSTALK

P/C-type inactivation involves conformational changes at the P-gate (Pardo et al., 1992; De Biasi et al., 1993; Lopez-Barneo et al., 1993; Kurata and Fedida, 2006) including the selectivity filter (Ogielska et al., 1995; Panyi et al., 1995; Liu et al., 1996; Kiss and Korn, 1998; Yellen, 1998; Zhou et al., 2001; Kurata and Fedida, 2006; Ahern et al., 2009). Electrostatic interactions involving H-bonds between the pore helix and the selectivity filter have been shown to promote these conformational changes (Cordero-Morales et al., 2006, 2007). Notably, gating charge immobilization (see above) has also been observed for P/C-type inactivation (Olcese et al., 1997; Loots and Isacoff, 1998; Larsson and Elinder, 2000; Wang and Fedida, 2001), suggesting that the voltage sensor may also adopt a stable relaxed conformation during prolonged depolarizations (Olcese et al., 1997). These older observations for P/C-type inactivation are highly similar to the more recent findings for Kv4.2 (Dougherty et al., 2008), a channel in which P/C-type inactivation is known to play a minor role (Kaulin et al., 2008).

Based on the results discussed above, a picture is beginning to evolve where the crosstalk between the voltage sensor domain and the pore domain, which is essential for Kv channel activation, also represents the structural framework for different manifestations of Kv channel inactivation. The voltage sensor domain has been shown to be able to directly communicate with two distinct gates in the pore domain: the P-gate in the selectivity filter and the A-gate involving the S6 bundle crossing (**Figure 2A**; Loots and Isacoff, 2000; Elinder et al., 2001; Lu et al., 2002; Lainé et al., 2003; Webster et al., 2004; Soler-Llavina et al., 2006; Barghaan and Bähring, 2009). When the membrane is depolarized the voltage sensor domain may adopt at least two distinct sets of conformations: First, it moves quickly and makes tight contact with the A-gate to open it (**Figure 2B**). Then, if the depolarization is sustained, the voltage sensor slowly adopts a more stable (relaxed) conformation (**Figures 2C,D**). The nature of the relaxed conformation depends on Kv channel subtype: In some Kv channels the voltage sensor may encounter favorable strong interactions with the P-gate stabilizing it in its non-conducting conformation (Loots and Isacoff, 2000; Elinder et al., 2001; **Figure 2C**). This mechanism corresponds to P/C-type inactivation as discussed above. Other Kv channels may have P-gates that are not permissive to inactivation, and thus, no inactivation (other than N-type, if a respective inactivation domain is present) will occur (**Figure 2B**). However, in some Kv channels with non-inactivating P-gates the voltage sensor domain may interact poorly with the A-gate. In these channels the voltage sensor also starts to move quickly, reaching for the A-gate, but the contact may fail or be short-lived due to a "slippery" A-gate. Nevertheless, the voltage sensor of these channels slowly drifts toward a relaxed conformation (**Figure 2D**). This corresponds to the preferential CSI mechanism discussed above for Kv4 channels. It may also apply to Kv channels with prominent U-type features of inactivation, like Kv2.1 and Kv3.1.

Although P/C-type inactivation is classically viewed as an open channel inactivation mechanism (see **Figures 1A** and **2C**), recent work has shown that the P-gate may also undergo inactivation when the channel is still closed. Claydon et al. (2007, 2008) have performed electrophysiological measurements combined with voltage-clamp fluorimetry to examine whether *Shaker*IR (N-type inactivation removed) channels may undergo P/C-type inactivation also from closed-states. Acidic pH, which promotes rearrangements at the P-gate, and the *Shaker* ILT triple-mutant (Smith-Maxwell et al., 1998), which segregates channel opening from voltage-dependent activation by shifting the respective curves apart, were exploited in this study. Conformational changes were inferred by fluorescence changes reported by fluorophores placed on the extracellular S3–S4 loop and an external pore site. The observed signals strongly indicated that the conformational changes involved in P/C-type inactivation also occur when the channels are far from opening (see **Figures 1B** and **2E**). Thus, we encounter a mechanism of CSI, which is of the P/C-type and totally different from the one discussed above for Kv4 channels. Accordingly, we introduce the term "A/C-type inactivation" to describe the mechanism of preferential CSI found in Kv4 channels, with a direct reference to the structures involved: A/C-type inactivation is non-N-type (i.e., C-type) and involves uncoupling of the voltage sensor from the A-gate. Currently there is no experimental evidence for the simultaneous occurrence of A/C- and P/C-type inactivation in one channel. Notably, however, an elegant study by Kurata et al. (2005) has shown previously that P/C-type and U-type inactivation can co-exist in Kv1.5 channels. It is currently unknown whether an A/C-type or a P/C-type mechanism is responsible for these U-type features.

"INTOXICATION" OF VOLTAGE SENSOR INACTIVATION

What tools do we have, other than, or in addition to, electrophysiological recordings and voltage-clamp fluorimetry combined with mutational analysis, to study voltage sensor inactivation? Targeting the structures involved with pharmacological tools may be a promising strategy. Intriguingly, gating modifier toxins isolated from tarantula spiders have been shown to act especially on Kv channels known to exhibit preferential CSI (A/C-type inactivation) including Kv2.1 and Kv4 channels (Swartz and MacKinnon, 1995; Sanguinetti et al., 1997; Diochot et al., 1999; Escoubas et al., 2002; Ebbinghaus et al., 2004). The action of Hanatoxin on Kv2.1/*drk1* channels has been mechanistically studied in great detail by Swartz and coworkers: The toxin directly interacts with the voltage sensor, even when it is in the resting (down) conformation; it stabilizes the resting conformation of the voltage sensor, thereby accelerating channel closure and shifting the voltage dependence of activation to more positive potentials (Swartz and

MacKinnon, 1997a,b; Lee et al., 2003). Based on these findings, it would be of considerable interest to know what the tarantula toxins do to voltage sensor inactivation? As to that, it has been found that the toxins more specific for Kv4 channels, including *Heteropoda* toxins, cause a slowing of macroscopic inactivation, an acceleration of recovery from inactivation and a shift of steady-state inactivation curves to more positive potentials (Sanguinetti et al., 1997; Diochot et al., 1999; Escoubas et al., 2002; Ebbinghaus et al., 2004; DeSimone et al., 2009, 2011). These findings are in accordance with a prevention of the relaxed conformation of the voltage sensor because it is stabilized in its resting conformation. Notably, the bacterial KvAP channel, the crystal structure of which has been solved (Lee et al., 2005), also shows clear indications of preferential CSI (Schmidt et al., 2009). As proposed earlier for HCN and Kv4 channels (Shin et al., 2004; Dougherty et al., 2008; Kaulin et al., 2008; Barghaan and Bähring, 2009), an A/C-type inactivation mechanism has been considered in the case of KvAP (Schmidt et al., 2009). Like Kv2.1 and Kv4 channels, KvAP can be modulated by a voltage sensor toxin (VSTx1) via a membrane-access mechanism and direct binding to the voltage sensor (Lee and MacKinnon, 2004; Ruta and MacKinnon, 2004). However, VSTx1 favors the inactivated state of KvAP, probably by binding to the activated and/or relaxed (up) conformation of the voltage sensor. Thus, although gating modifier toxins appear to be valuable tools for further investigations of voltage sensor inactivation, the questions to be answered first are: Do gating modifier toxins differ in their mode of action, or does the effect of gating modifier toxins critically depend on Kv channel subtype, or both? Doubtlessly, crystallization of a Kv channel in the absence and presence of a ligand that influences the likelihood of an A/C- or P/C-type inactivated state would significantly advance structural analysis of voltage sensor inactivation.

CONCLUDING REMARKS

The purpose of this review was to focus on intrinsic mechanisms of inactivation in Kv channels that involve conformational changes of the voltage sensor (i.e., voltage sensor inactivation). In particular, we pointed out that subtype-specific variations in the crosstalk between voltage sensor domain and pore domain play a decisive role for the mode of Kv channel inactivation. Furthermore, in order to up-date current nomenclature of inactivation mechanisms in a useful manner, we introduced the term "A/C-type inactivation." Based on the finding that P/C-type inactivation can also occur from closed-states, the term "CSI" for a dynamic coupling between voltage sensor and A-gate seems no longer appropriate.

ACKNOWLEDGMENTS

Our research on Kv channel gating mechanisms is supported by grant Ba 2055/1-2 from the Deutsche Forschungsgemeinschaft to Robert Bähring.

REFERENCES

Ahern, C. A., Eastwood, A. L., Dougherty, D. A., and Horn, R. (2009). An electrostatic interaction between TEA and an introduced pore aromatic drives spring-in-the-door inactivation in Shaker potassium channels. *J. Gen. Physiol.* 134, 461–469.

Aldrich, R. W. (1981). Inactivation of voltage-gated delayed potassium current in molluscan neurons. A kinetic model. *Biophys. J.* 36, 519–532.

Armstrong, C. M., and Bezanilla, F. (1973). Currents related to movement of the gating particles of the sodium channels. *Nature* 242, 459–461.

Armstrong, C. M., and Bezanilla, F. (1977). Inactivation of the sodium channel. II. Gating current experiments. *J. Gen. Physiol.* 70, 567–590.

Ayer, R. K. Jr., and Sigworth, F. J. (1997). Enhanced closed-state inactivation in a mutant Shaker K^+ channel. *J. Membr. Biol.* 157, 215–230.

Bähring, R., Boland, L. M., Varghese, A., Gebauer, M., and Pongs, O. (2001). Kinetic analysis of open- and closed-state inactivation transitions in human Kv4.2 A-type potassium channels. *J. Physiol. (Lond.)* 535, 65–81.

Bähring, R., and Covarrubias, M. (2011). Mechanisms of closed-state inactivation in voltage-gated ion channels. *J. Physiol. (Lond.)* 589, 461–479.

Barghaan, J., and Bähring, R. (2009). Dynamic coupling of voltage sensor and gate involved in closed-state inactivation of Kv4.2 channels. *J. Gen. Physiol.* 133, 205–224.

Barghaan, J., Tozakidou, M., Ehmke, H., and Bähring, R. (2008). Role of N-terminal domain and accessory subunits in controlling deactivation-inactivation coupling of Kv4.2 channels. *Biophys. J.* 94, 1276–1294.

Baukrowitz, T., and Yellen, G. (1995). Modulation of K^+ current by frequency and external $[K^+]$: a tale of two inactivation mechanisms. *Neuron* 15, 951–960.

Bezanilla, F., Perozo, E., Papazian, D. M., and Stefani, E. (1991). Molecular basis of gating charge immobilization in Shaker potassium channels. *Science* 254, 679–683.

Campbell, D. L., Rasmusson, R. L., Qu, Y., and Strauss, H. C. (1993). The calcium-independent transient outward potassium current in isolated ferret right ventricular myocytes. I. Basic characterization and kinetic analysis. *J. Gen. Physiol.* 101, 571–601.

Choi, K. L., Aldrich, R. W., and Yellen, G. (1991). Tetraethylammonium blockade distinguishes two inactivation mechanisms in voltage-activated K^+ channels. *Proc. Natl. Acad. Sci. U.S.A.* 88, 5092–5095.

Claydon, T. W., Kehl, S. J., and Fedida, D. (2008). Closed-state inactivation induced in KV1 channels by extracellular acidification. *Channels (Austin)* 2, 139–142.

Claydon, T. W., Vaid, M., Rezazadeh, S., Kwan, D. C., Kehl, S. J., and Fedida, D. (2007). A direct demonstration of closed-state inactivation of K^+ channels at low pH. *J. Gen. Physiol.* 129, 437–455.

Connor, J. A., and Stevens, C. F. (1971). Prediction of repetitive firing behaviour from voltage clamp data on an isolated neuron soma. *J. Physiol. (Lond.)* 213, 31–53.

Cordero-Morales, J. F., Cuello, L. G., Zhao, Y., Jogini, V., Cortes, D. M., Roux, B., and Perozo, E. (2006). Molecular determinants of gating at the potassium-channel selectivity filter. *Nat. Struct. Mol. Biol.* 13, 311–318.

Cordero-Morales, J. F., Jogini, V., Lewis, A., Vasquez, V., Cortes, D. M., Roux, B., and Perozo, E. (2007). Molecular driving forces determining potassium channel slow inactivation. *Nat. Struct. Mol. Biol.* 14, 1062–1069.

De Biasi, M., Hartmann, H. A., Drewe, J. A., Taglialatela, M., Brown, A. M., and Kirsch, G. E. (1993). Inactivation determined by a single site in K^+ pores. *Pflügers Arch.* 422, 354–363.

DeSimone, C. V., Lu, Y., Bondarenko, V. E., and Morales, M. J. (2009). S3b amino acid substitutions and ancillary subunits alter the affinity of *Heteropoda venatoria* toxin 2 for Kv4.3. *Mol. Pharmacol.* 76, 125–133.

DeSimone, C. V., Zarayskiy, V. V., Bondarenko, V. E., and Morales, M. J. (2011). *Heteropoda* toxin 2 interaction with Kv4.3 and Kv4.1 reveals differences in gating modification. *Mol. Pharmacol.* 80, 345–355.

Diochot, S., Drici, M. D., Moinier, D., Fink, M., and Lazdunski, M. (1999). Effects of phrixotoxins on the Kv4 family of potassium channels and implications for the role of Ito1 in cardiac electrogenesis. *Br. J. Pharmacol.* 126, 251–263.

Dixon, J. E., Shi, W., Wang, H. S., McDonald, C., Yu, H., Wymore, R. S., Cohen, I. S., and McKinnon, D. (1996). Role of the Kv4.3 K^+ channel in ventricular muscle. A molecular correlate for the transient outward current. *Circ. Res.* 79, 659–668.

Dougherty, K., De Santiago-Castillo, J. A., and Covarrubias, M. (2008). Gating charge immobilization in Kv4.2 channels: the basis of closed-state inactivation. *J. Gen. Physiol.* 131, 257–273.

Ebbinghaus, J., Legros, C., Nolting, A., Guette, C., Celerier, M. L., Pongs, O., and Bähring, R. (2004). Modulation of Kv4.2 channels by a peptide isolated from the venom of the giant bird-eating tarantula *Theraphosa leblondi*. *Toxicon* 43, 923–932.

Elinder, F., Männikkö, R., and Larsson, H. P. (2001). S4 charges move close to residues in the pore domain during activation in a K channel. *J. Gen. Physiol.* 118, 1–10.

Escoubas, P., Diochot, S., Celerier, M. L., Nakajima, T., and Lazdunski, M. (2002). Novel tarantula toxins for subtypes of voltage-dependent potassium channels in the Kv2 and Kv4 subfamilies. *Mol. Pharmacol.* 62, 48–57.

Fedida, D., Bouchard, R., and Chen, F. S. (1996). Slow gating charge immobilization in the human potassium channel Kv1.5 and its prevention by 4-aminopyridine. *J. Physiol. (Lond.)* 494, 377–387.

Greenstein, J. L., Wu, R., Po, S., Tomaselli, G. F., and Winslow, R. L. (2000). Role of the calcium-independent transient outward current Ito1 in shaping action potential morphology and duration. *Circ. Res.* 87, 1026–1033.

Hille, B. (2001). *Ion Channels of Excitable Membranes.* Sunderland, MA: Sinauer Associates, Inc.

Hodgkin, A. L., and Huxley, A. F. (1952). A quantitative description of membrane current and its application to conduction and excitation in nerve. *J. Physiol. (Lond.)* 117, 500–544.

Hoffman, D. A., Magee, J. C., Colbert, C. M., and Johnston, D. (1997). K^+ channel regulation of signal propagation in dendrites of hippocampal pyramidal neurons. *Nature* 387, 869–875.

Hoshi, T., Zagotta, W. N., and Aldrich, R. W. (1990). Biophysical and molecular mechanisms of Shaker potassium channel inactivation. *Science* 250, 533–538.

Hoshi, T., Zagotta, W. N., and Aldrich, R. W. (1991). Two types of inactivation in Shaker K^+ channels: effects of alterations in the carboxy-terminal region. *Neuron* 7, 547–556.

Jackson, M. B., Konnerth, A., and Augustine, G. J. (1991). Action potential broadening and frequency-dependent facilitation of calcium signals in pituitary nerve terminals. *Proc. Natl. Acad. Sci. U.S.A.* 88, 380–384.

Jerng, H. H., and Covarrubias, M. (1997). K^+ channel inactivation mediated by the concerted action of the cytoplasmic N- and C-terminal domains. *Biophys. J.* 72, 163–174.

Jerng, H. H., Dougherty, K., Covarrubias, M., and Pfaffinger, P. J. (2009). A novel N-terminal motif of dipeptidyl peptidase-like proteins produces rapid inactivation of KV4.2 channels by a pore-blocking mechanism. *Channels (Austin)* 3, 448–461.

Jerng, H. H., Shahidullah, M., and Covarrubias, M. (1999). Inactivation gating of Kv4 potassium channels: molecular interactions involving the inner vestibule of the pore. *J. Gen. Physiol.* 113, 641–660.

Kaulin, Y. A., De Santiago-Castillo, J. A., Rocha, C. A., and Covarrubias, M. (2008). Mechanism of the modulation of Kv4:KChIP-1 channels by external K^+. *Biophys. J.* 94, 1241–1251.

Kirichok, Y. V., Nikolaev, A. V., and Krishtal, O. A. (1998). $[K^+]$out accelerates inactivation of Shal-channels responsible for A-current in rat CA1 neurons. *Neuroreport* 9, 625–629.

Kiss, L., and Korn, S. J. (1998). Modulation of C-type inactivation by K^+ at the potassium channel selectivity filter. *Biophys. J.* 74, 1840–1849.

Klemic, K. G., Kirsch, G. E., and Jones, S. W. (2001). U-type inactivation of Kv3.1 and Shaker potassium channels. *Biophys. J.* 81, 814–826.

Klemic, K. G., Shieh, C. C., Kirsch, G. E., and Jones, S. W. (1998). Inactivation of Kv2.1 potassium channels. *Biophys. J.* 74, 1779–1789.

Kurata, H. T., Doerksen, K. W., Eldstrom, J. R., Rezazadeh, S., and Fedida, D. (2005). Separation of P/C- and U-type inactivation pathways in Kv1.5 potassium channels. *J. Physiol. (Lond.)* 568, 31–46.

Kurata, H. T., and Fedida, D. (2006). A structural interpretation of voltage-gated potassium channel inactivation. *Prog. Biophys. Mol. Biol.* 92, 185–208.

Kurata, H. T., Soon, G. S., Eldstrom, J. R., Lu, G. W., Steele, D. F., and Fedida, D. (2002). Amino-terminal determinants of U-type inactivation of voltage-gated K^+ channels. *J. Biol. Chem.* 277, 29045–29053.

Kurata, H. T., Soon, G. S., and Fedida, D. (2001). Altered state dependence of C-type inactivation in the long and short forms of human Kv1.5. *J. Gen. Physiol.* 118, 315–332.

Lainé, M., Lin, M. C., Bannister, J. P., Silverman, W. R., Mock, A. F., Roux, B., and Papazian, D. M. (2003). Atomic proximity between S4 segment and pore domain in Shaker potassium channels. *Neuron* 39, 467–481.

Larsson, H. P., and Elinder, F. (2000). A conserved glutamate is important for slow inactivation in K^+ channels. *Neuron* 27, 573–583.

Lee, H. C., Wang, J. M., and Swartz, K. J. (2003). Interaction between extracellular Hanatoxin and the resting conformation of the voltage-sensor paddle in Kv channels. *Neuron* 40, 527–536.

Lee, S. Y., Lee, A., Chen, J., and MacKinnon, R. (2005). Structure of the KvAP voltage-dependent K^+ channel and its dependence on the lipid membrane. *Proc. Natl. Acad. Sci. U.S.A.* 102, 15441–15446.

Lee, S. Y., and MacKinnon, R. (2004). A membrane-access mechanism of ion channel inhibition by voltage sensor toxins from spider venom. *Nature* 430, 232–235.

Liu, Y., Jurman, M. E., and Yellen, G. (1996). Dynamic rearrangement of the outer mouth of a K^+ channel during gating. *Neuron* 16, 859–867.

Long, S. B., Campbell, E. B., and MacKinnon, R. (2005). Voltage sensor of Kv1.2: structural basis of electromechanical coupling. *Science* 309, 903–908.

Loots, E., and Isacoff, E. Y. (1998). Protein rearrangements underlying slow inactivation of the Shaker K^+ channel. *J. Gen. Physiol.* 112, 377–389.

Loots, E., and Isacoff, E. Y. (2000). Molecular coupling of S4 to a K^+ channel's slow inactivation gate. *J. Gen. Physiol.* 116, 623–636.

Lopez-Barneo, J., Hoshi, T., Heinemann, S. H., and Aldrich, R. W. (1993). Effects of external cations and mutations in the pore region on C-type inactivation of Shaker potassium channels. *Receptors Channels* 1, 61–71.

Lu, Z., Klem, A. M., and Ramu, Y. (2002). Coupling between voltage sensors and activation gate in voltage-gated K^+ channels. *J. Gen. Physiol.* 120, 663–676.

Magee, J. C., and Johnston, D. (1997). A synaptically controlled, associative signal for Hebbian plasticity in hippocampal neurons. *Science* 275, 209–213.

Ogielska, E. M., Zagotta, W. N., Hoshi, T., Heinemann, S. H., Haab, J., and Aldrich, R. W. (1995). Cooperative subunit interactions in C-type inactivation of K channels. *Biophys. J.* 69, 2449–2457.

Olcese, R., Latorre, R., Toro, L., Bezanilla, F., and Stefani, E. (1997). Correlation between charge movement and ionic current during slow inactivation in Shaker K^+ channels. *J. Gen. Physiol.* 110, 579–589.

Panyi, G., Sheng, Z., and Deutsch, C. (1995). C-type inactivation of a voltage-gated K^+ channel occurs by a cooperative mechanism. *Biophys. J.* 69, 896–903.

Pardo, L. A., Heinemann, S. H., Terlau, H., Ludewig, U., Lorra, C., Pongs, O., and Stühmer, W. (1992). Extracellular K^+ specifically modulates a rat brain K^+ channel. *Proc. Natl. Acad. Sci. U.S.A.* 89, 2466–2470.

Patel, S. P., Parai, R., and Campbell, D. L. (2004). Regulation of Kv4.3 voltage-dependent gating kinetics by KChIP2 isoforms. *J. Physiol. (Lond.)* 557, 19–41.

Perozo, E., Papazian, D. M., Stefani, E., and Bezanilla, F. (1992). Gating currents in Shaker K^+ channels. Implications for activation and inactivation models. *Biophys. J.* 62, 160–171.

Rettig, J., Heinemann, S. H., Wunder, F., Lorra, C., Parcej, D. N., Dolly, J. O., and Pongs, O. (1994). Inactivation properties of voltage-gated K^+ channels altered by presence of β-subunit. *Nature* 369, 289–294.

Roux, M. J., Olcese, R., Toro, L., Bezanilla, F., and Stefani, E. (1998). Fast inactivation in Shaker K^+ channels. Properties of ionic and gating currents. *J. Gen. Physiol.* 111, 625–638.

Ruta, V., and MacKinnon, R. (2004). Localization of the voltage-sensor toxin receptor on KvAP. *Biochemistry* 43, 10071–10079.

Sanguinetti, M. C., Johnson, J. H., Hammerland, L. G., Kelbaugh, P. R., Volkmann, R. A., Saccomano, N. A., and Mueller, A. L. (1997). *Heteropoda* toxins: peptides isolated from spider venom that block Kv4.2 potassium channels. *Mol. Pharmacol.* 51, 491–498.

Schmidt, D., Cross, S. R., and MacKinnon, R. (2009). A gating model for the archeal voltage-dependent K^+ channel KvAP in DPhPC and POPE:POPG decane lipid bilayers. *J. Mol. Biol.* 390, 902–912.

Shahidullah, M., and Covarrubias, M. (2003). The link between ion permeation and inactivation gating of Kv4 potassium channels. *Biophys. J.* 84, 928–941.

Shin, K. S., Maertens, C., Proenza, C., Rothberg, B. S., and Yellen, G. (2004). Inactivation in HCN channels results from reclosure of the activation gate: desensitization to voltage. *Neuron* 41, 737–744.

Skerritt, M. R., and Campbell, D. L. (2007). Role of S4 positively charged residues in the regulation of Kv4.3 inactivation and recovery. *Am. J. Physiol. Cell Physiol.* 293, C906–C914.

Skerritt, M. R., and Campbell, D. L. (2008). Non-native R1 substitution in the S4 domain uniquely alters Kv4.3 channel gating. *PLoS ONE* 3, e3773. doi:10.1371/journal.pone.0003773

Skerritt, M. R., and Campbell, D. L. (2009). Contribution of electrostatic and structural properties of Kv4.3 S4 arginine residues to the regulation

of channel gating. *Biochim. Biophys. Acta* 1788, 458–469.

Smith-Maxwell, C. J., Ledwell, J. L., and Aldrich, R. W. (1998). Uncharged S4 residues and cooperativity in voltage-dependent potassium channel activation. *J. Gen. Physiol.* 111, 421–439.

Solc, C. K., and Aldrich, R. W. (1990). Gating of single non-Shaker A-type potassium channels in larval *Drosophila* neurons. *J. Gen. Physiol.* 96, 135–165.

Soler-Llavina, G. J., Chang, T. H., and Swartz, K. J. (2006). Functional interactions at the interface between voltage-sensing and pore domains in the Shaker Kv channel. *Neuron* 52, 623–634.

Swartz, K. J., and MacKinnon, R. (1995). An inhibitor of the Kv2.1 potassium channel isolated from the venom of a *Chilean tarantula*. *Neuron* 15, 941–949.

Swartz, K. J., and MacKinnon, R. (1997a). Hanatoxin modifies the gating of a voltage-dependent K^+ channel through multiple binding sites. *Neuron* 18, 665–673.

Swartz, K. J., and MacKinnon, R. (1997b). Mapping the receptor site for hanatoxin, a gating modifier of voltage- dependent K^+ channels. *Neuron* 18, 675–682.

Wallner, M., Meera, P., and Toro, L. (1999). Molecular basis of fast inactivation in voltage and Ca^{2+}-activated K^+ channels: a transmembrane β-subunit homolog. *Proc. Natl. Acad. Sci. U.S.A.* 96, 4137–4142.

Wang, Z., and Fedida, D. (2001). Gating charge immobilization caused by the transition between inactivated states in the Kv1.5 channel. *Biophys. J.* 81, 2614–2627.

Webster, S. M., Del Camino, D., Dekker, J. P., and Yellen, G. (2004). Intracellular gate opening in Shaker K^+ channels defined by high-affinity metal bridges. *Nature* 428, 864–868.

Yellen, G. (1998). The moving parts of voltage-gated ion channels. *Q. Rev. Biophys.* 31, 239–295.

Yellen, G., Sodickson, D., Chen, T. Y., and Jurman, M. E. (1994). An engineered cysteine in the external mouth of a K^+ channel allows inactivation to be modulated by metal binding. *Biophys. J.* 66, 1068–1075.

Yifrach, O., and MacKinnon, R. (2002). Energetics of pore opening in a voltage-gated K^+ channel. *Cell* 111, 231–239.

Zagotta, W. N., Hoshi, T., and Aldrich, R. W. (1990). Restoration of inactivation in mutants of Shaker potassium channels by a peptide derived from ShB. *Science* 250, 568–571.

Zhou, Y., Morais-Cabral, J. H., Kaufman, A., and MacKinnon, R. (2001). Chemistry of ion coordination and hydration revealed by a K^+ channel-Fab complex at 2.0 Å resolution. *Nature* 414, 43–48.

Conflict of Interest Statement: The authors declare that the research was conducted in the absence of any commercial or financial relationships that could be construed as a potential conflict of interest.

Received: 16 March 2012; accepted: 04 May 2012; published online: 23 May 2012.

*Citation: Bähring R, Barghaan J, Westermeier R and Wollberg J (2012) Voltage sensor inactivation in potassium channels. Front. Pharmacol. **3**:100. doi: 10.3389/fphar.2012.00100*

This article was submitted to Frontiers in Pharmacology of Ion Channels and Channelopathies, a specialty of Frontiers in Pharmacology.

frontiers in
PHARMACOLOGY

REVIEW ARTICLE
published: 27 July 2012
doi: 10.3389/fphar.2012.00145

Coupling of voltage-sensors to the channel pore: a comparative view

***Vitya Vardanyan*[1,2]* *and Olaf Pongs*[2,3]**

[1] *Ion Channel Research Group, Institute of Molecular Biology, National Academy of Sciences of the Republic of Armenia, Yerevan, Armenia*
[2] *Zentrum für Molekulare Neurobiologie Hamburg, Hamburg, Germany*
[3] *Physiologisches Institut, Universität des Saarlandes, Homburg, Germany*

Edited by:
Gildas Loussouarn, University of Nantes, France

Reviewed by:
Manuel L. Covarrubias, Thomas Jefferson University, USA
Geoff Abbott, University of California Irvine, USA

***Correspondence:**
Vitya Vardanyan, Ion Channel Research Group, Institute of Molecular Biology, National Academy of Sciences of the Republic of Armenia, Yerevan, Armenia.
e-mail: v_vardanyan@mb.sci.am

The activation of voltage-dependent ion channels is initiated by potential-induced conformational rearrangements in the voltage-sensor domains that propagates to the pore domain (PD) and finally opens the ion conduction pathway. In potassium channels voltage-sensors are covalently linked to the pore via S4–S5 linkers at the cytoplasmic site of the PD. Transformation of membrane electric energy into the mechanical work required for the opening or closing of the channel pore is achieved through an electromechanical coupling mechanism, which involves local interaction between residues in S4–S5 linker and pore-forming alpha helices. In this review we discuss present knowledge and open questions related to the electromechanical coupling mechanism in most intensively studied voltage-gated *Shaker* potassium channel and compare structure-functional aspects of coupling with those observed in distantly related ion channels. We focus particularly on the role of electromechanical coupling in modulation of the constitutive conductance of ion channels.

Keywords: ion channels, voltage-sensors, electromechanical coupling

INTRODUCTION

Voltage-dependent ion channels are important components of excitable biological membranes responsible for initiation, propagation, and shaping of action potentials (Hille, 2001). In non-excitable cells they are in charge of electrolyte transport into and out of cells. Numerous gene mutations of ion channels are implicated in human inherited diseases, pathologies of which are often associated with impaired voltage control of channels (Ashcroft, 1999). Discovery of new therapeutic agents targeting ion channels requires a solid knowledge of structure-function correlation of these complex membrane proteins.

In recent decades the molecular mechanisms of permeation, selectivity and conductance in many ion channels have been revealed with unprecedented precision by combination of electrophysiological, biochemical, and crystallographic methods. In this respect, potassium (K) channels are the best understood ion channels, which are integral membrane proteins typically formed by the association of four identical subunits (Doyle et al., 1998). The Pore Domain (PD) of K channels represents a tetramer of two membrane-spanning alpha helixes that are connected with each other via a P-loop, which is responsible for potassium selectivity. The PD contains a channel gate, which controls ion permeation (Holmgren et al., 1998; del Camino and Yellen, 2001; Swartz, 2004; Webster et al., 2004; del Camino et al., 2005). The structural correlate of the gate is a bundle of overcrossing alpha helixes at the cytoplasmatic entryway of the channel pore (Holmgren et al., 1998). These alpha helices correspond to the M2 helix of the non-voltage-gated (Doyle et al., 1998) and to the S6 helix of voltage-gated potassium (Kv) channels. To close the gate, the pore constricts and forms a hydrophobic seal by side-chains of converging S6 pore helices (Doyle et al., 1998; Holmgren et al., 1998; del Camino and Yellen, 2001; Hackos et al., 2002). Opening and closing of Kv channel gate is under the stringent control of the membrane electric potential (Islas and Sigworth, 1999). In Kv channels the pore is covalently linked to four specialized membrane-embedded peripheral functional modules, Voltage Sensing Domains (VSDs) that are comprised of S1–S4 membrane-spanning segments. VSDs are capable of sensing changes in membrane potential and respond with conformational changes that propagate to the PD (Bezanilla, 2000; Jiang et al., 2003; Catterall, 2010). Available crystal structures along with functional data suggest that VSDs are semi-independent functional units (Long et al., 2005a, 2007; Alabi et al., 2007). In recent years, a significant progress has been made toward the elucidation of the molecular architecture and functional principles of these specialized domains (Bezanilla, 2008; Catterall, 2010; Tao et al., 2010). VSDs are connected to the PD by a linker, known as S4–S5 linker at the cytoplasmic side of the membrane. The VSD-PD assembly represents an exquisite molecular electromechanical coupling device, which converts potential energy of the membrane electric field into the mechanical work needed to control the selective permeation of potassium ions. Several functional studies indicate that concordance between the S4–S5 linker and distal S6 region of the PD is important for transmission of conformational changes from VSDs to PD (Chen et al., 2001; Lu et al., 2001, 2002; Decher et al., 2004; Long et al., 2005b; Soler-Llavina et al., 2006; Labro et al., 2008; Lee et al., 2009; Choveau et al., 2011). How the conformational changes originating in VSDs are transferred to the PD and how they influence the functional state of the channel gate remains an unresolved issue.

In this review we summarize current knowledge and open questions concerning to the molecular and structural aspects of electromechanical coupling. The *Shaker* Kv channel is the most

intensively investigated voltage-gated channel in terms of electromechanical coupling. Here, we highlight similarities and key differences of electromechanical coupling process in *Shaker* and in some distantly related ion channels.

CURRENT VIEW OF ELECTROMECHANICAL COUPLING

It is well established that voltage-sensors are semi-independent membrane-embedded modules (Alabi et al., 2007; Long et al., 2007) that undergo conformational changes upon alterations of membrane potential (Bezanilla, 2000, 2008; Villalba-Galea et al., 2008). The details of conformational changes that actually take place in VSDs are a subject of much debate (Campos et al., 2007; Borjesson and Elinder, 2008; Broomand and Elinder, 2008; Villalba-Galea et al., 2008; Tao et al., 2010; Vargas et al., 2011). It is not completely understood how and to which extent positive charges of S4 helix move upon a change in membrane potential (Campos et al., 2007; Bezanilla, 2008). It is also unclear how homogeneous is the electric field that membrane-embedded VSDs experience (Bezanilla, 2008; Catterall, 2010).

Transmission of conformational changes from each voltage-sensors to the pore was thought to occur primarily through S4–S5 linker, since the latter directly connects dynamic S4 segment of the VSDs to S5 segment of the PD. A decade ago Lu et al. (2002) first demonstrated that interaction between S4–S5 linker and distal S6 segment of the PD is also essential for coupling. The molecular and structural aspects of this phenomenon remained obscure until crystal structures of *Shaker*-related channels were resolved with remarkable resolution (Long et al., 2005a,b, 2007). Two non-covalent interaction interfaces between VSDs and PD were observed in crystal structures of *Shaker*-related channels. An extensive interface was observed at the cytoplasmatic side of the membrane involving side-chains of S4–S5 linker and side-chains of the distal S6 segment (Long et al., 2005b, 2007). The second, comparably small interface was found at the extracellular side of the pore formed by interaction of side-chains of S1 segment of VSDs with side-chains of S5 in the pore (Long et al., 2005a, 2007; Lee et al., 2009). It has been suggested that latter interface plays a role in effective translocation of charged S4 helix during membrane voltage changes (Lee et al., 2009). An essential role for transmission of conformational changes from VSDs to the channel gate was given to the interactions between S4–S5 linker and distal S6 (Labro et al., 2005; Long et al., 2005b).

S4–S5 linkers in *Shaker*-related channels adopt an amphipathic alpha helical conformation (Long et al., 2005a, 2007) both in crystals and in solution (Ohlenschlager et al., 2002). The functional mutagenesis data suggest that changes in the amphipathic configuration of S4–S5 helix disturb the electromechanical coupling process (Labro et al., 2008). In the activated Kv channel, the S4–S5 helix runs parallel to the intracellular side of the lipid bilayer (Long et al., 2005b, 2007) with its hydrophobic side facing the lipid membrane. The hydrophilic face of S4–S5 linker is exposed to the cytoplasm (Long et al., 2007). Currently, it is unknown whether the hydrophilic side is involved in specific interactions with other parts of the ion channel. The interaction between S6 helix with its "receptor" site on the S4–S5 linker requires the pore helices to bend or kink (Long et al., 2005b). Most likely, this is associated with the occurrence of a conserved PXP motif and a "gating hinge" glycine in S6 helix (Ding et al., 2005; Long et al., 2005b). The molecular interactions between the side-chains of S4–S5 helix and side-chains of the distal S6 segment (Long et al., 2005b) apparently play a key role for transmission of conformational changes during channel gating. It is likely that interaction between S4–S5 linker and distal S6 takes place also at the closed state of the channel. Molecular dynamic simulations studies predict the movement pattern of S4–S5 linker as well as its interaction with S6 during the voltage gating process of *Shaker*-related channels (Yarov-Yarovoy et al., 2006; Jensen et al., 2012). Summarizing experimental and theoretical studies Blunck and Batulan discuss two alternative scenarios where S4–S5 linker functions (1) as a spring and (2) as a bolt (see current review issue).

In spite of available nice models, the essential questions need to be addressed experimentally in order to understand the electromechanical coupling mechanism in detail. For example, which channel states are predominantly influenced by interaction of S4–S5 linker and S6? Are these interactions the only determinants of electromechanical coupling or other factors (interactions) play a significant role (see for example Lee et al., 2009; Batulan et al., 2010)? Do similar molecular and structural principles govern electromechanical coupling in ion channels distantly related to *Shaker*? Of note is that mutagenesis experiments have shown that the interactions between S4–S5 linker and the distal S6 play a key role in electromechanical coupling also in hERG- (Ferrer et al., 2006), KCNQ1- (Choveau et al., 2011), HCN- (Chen et al., 2001), and KAT1-channels (Ferrer et al., 2006; Grabe et al., 2007). In Kv4 channels coupling strength determines the inactivation properties of channels (Barghaan and Bahring, 2009; Bahring et al., 2012). Nevertheless, electrophysiological analysis of S4–S5 linker mutants revealed some essential differences between *Shaker* and more distantly related channels that we will describe below. Elucidation of these differences will help us to further our knowledge about the electromechanical coupling process and design new comprehensive studies in future.

UNCOUPLING VOLTAGE-SENSORS FROM THE PORE IN *SHAKER*

In voltage-dependent ion channels the effectiveness of converting electrical energy into mechanical work that influences the state of the channel gate is dependent on the strength of electromechanical coupling. If the coupling is strong, the gate will be under the tight control of VSDs. If the electromechanical coupling between VSDs and the PD is markedly weaker or absent, the conformational changes in VSDs will no longer be able to influence the opening or the closing of channel gate. Mutations or chimeric replacements localized in S4–S5 linker and/or S6 region significantly affect the gating properties of voltage-gated ion channels (Sullivan et al., 1997; Lu et al., 2001, 2002; Tristani-Firouzi et al., 2002; Ferrer et al., 2006; Labro et al., 2008; Barghaan and Bahring, 2009; Haddad and Blunck, 2011). Moreover, a fractional voltage-dependent and voltage-independent conductance was observed in some mutants, indicating that modulation of the coupling strength can markedly influence also the stability of the resting-closed state of channels. In **Figure 1** we have highlighted the localization of mutations having a drastic influence on the functional properties of channels.

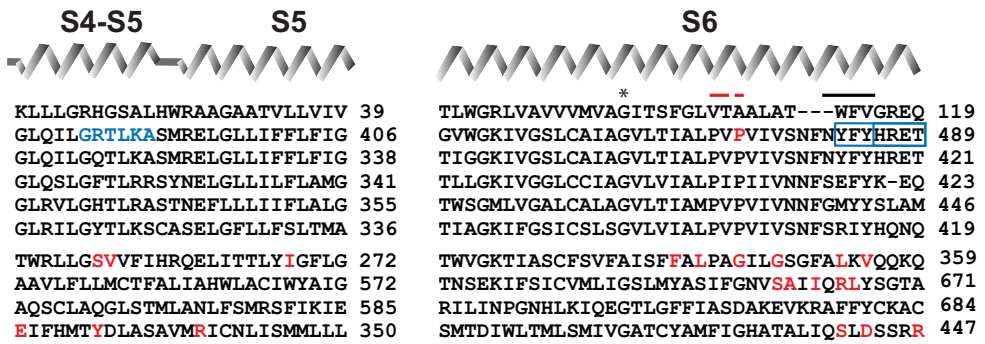

FIGURE 1 | Sequence alignment of relevant Kv channels in the S4–S5 linker and in S6 segment. Diagram above the sequences represents secondary structure elements corresponding to the recent crystal structure of Kv1.2–Kv2.1 chimeric channel in lipid-like environment (Long et al., 2007). Residues indicated by red letters show localization of the mutations involved in constitutive conductance of corresponding channels. Residues shown with blue letters and blue frames indicate position of mutations, which render *Shaker*-KcsA chimeras (carrying distal S6 starting from I477, as well as S4–S5 linker from *Shaker*, but the rest of the pore from KcaA) non-functional (Lu et al., 2002). Red bar indicates the position of PXP motive of Kv channels; black bar indicates localization of the gate. Asterisk shows gating hinge glycine. Sequence identification numbers are as follows: KcsA, GI 612269090; *Shaker*, GI 288442; rat Kv1.2, GI 24418849; human Kv2.1, GI 4826784; human Kv3.1, GI 163792201; human Kv4.1, GI 27436981; human KCNQ1, GI 32479527; mouse HCN2, GI 6680189; hERG, GI 4156239; rat BK, GI 13929184.

The first comprehensive mutagenesis studies, focusing on the molecular aspects of the electromechanical coupling were started by Lu et al. (2001, 2002). The results indicated that two large segments, one corresponding to the S4–S5 linker and the other to the distal part of S6, should be preserved in *Shaker* in order to maintain full voltage control over *Shaker* channel gating (Lu et al., 2002). Mismatches between S4–S5 linker and distal S6 by replacement of corresponding segments of *Shaker* by KcsA resulted in channels with a partial constitutive conductance. Single channel analysis revealed that the constitutive conductance in these channels reflects spontaneous fluctuations of the channel between open and closed states (Lu et al., 2002) at resting voltage-sensor conditions. In wild type *Shaker* channels spontaneous channel openings at hyperpolarized potentials are rare events with an estimated open probability of 10^{-9} (Islas and Sigworth, 1999). Results indicated that the constitutive conductance in *Shaker*-KcsA chimeras can be explained by a weakening of coupling between VSDs and PD. Hydrophilic substitutions at residue Pro475 in *Shaker* also caused a constitutive conductance, in spite of the fact that P475 is located within the conduction pathway of the channel (Hackos et al., 2002; Sukhareva et al., 2003). Thus, it has been proposed that coupling strength plays a significant role for constitutive conductance in P475 hydrophilic mutants too (Sukhareva et al., 2003).

Haddad and Blunck (2011) recently proposed an alternative explanation of uncoupling in *Shaker* studying the mode shift of gating charge translocation in VSDs (Haddad and Blunck, 2011). They suggest that a marked reduction in coupling strength, or complete uncoupling, will result in permanently closed *Shaker* channels. This proposal was based on thorough electrophysiological analysis of S4 segment translocation and voltage-dependent conductance of two *Shaker* mutations I384N and F484G (Haddad and Blunck, 2011). The choice of the mutations was based on recent crystal structures of Kv channels (Long et al., 2005b, 2007). One mutation was localized at S4–S5 linker (I384N) and the other within distal S6 (F484G). Uncoupling in these two mutants was characterized by a significant leftward shift in the gating charge (Q) – voltage (V) relation (QV curve) accompanied with rightward shift in conductance (G) – voltage (V) relationship (GV curve). A shift of QV curve to more negative potentials indicates that less energy is required for translocation of VSDs from a resting to an activated position in mutant. I384N and F484G *Shaker* channels were expressed robustly on plasma membrane but only a small fraction of channels could be opened even by extreme depolarization pulses (Haddad and Blunck, 2011). This indicates that the channel gate remained mostly closed although voltage-sensors could be easily translocated from the resting state to an activated state. Conversely, I384A *Shaker* mutation considerably detained the voltage-sensor movement judged by a large positive shift in the QV curve. Taking into consideration that the GV relation is almost unchanged in I384A, authors suggested that mutant channels display a stronger coupling than wild type (Haddad and Blunck, 2011). In summary, it was suggested that at the resting state the *Shaker* pore applies a mechanical load onto VSDs. The uncoupling mutations I384N and F484G take this mechanical load off, thereby facilitating the translocation of gating charges, but arresting the channel pore in a closed state. Strengthening of coupling between VSDs and the pore in the I348A mutant constrains S4 segment translocation but facilitates channel opening. Similar considerations were made in earlier studies regarding to the gating current kinetics of F484 *Shaker* mutants (Ding and Horn, 2003).

At first glance, abovementioned two explanations for uncoupling in *Shaker* seem somewhat contradictory. The first states that uncoupling in *Shaker* promotes the formation of channels with constitutively open pore, whereas the second hypothesis proposes that *Shaker* channels with uncoupled voltage-sensors are permanently closed. Analysis of voltage-sensor movement and plasma membrane expression of constitutively conducting *Shaker*-KcsA channels may shed a light on this ambiguity.

ELECTROMECHANICAL COUPLING IN CHANNELS DISTANTLY RELATED TO *SHAKER*

Principles of electromechanical coupling were elucidated on the basis of functional and structural studies carried out predominantly on *Shaker* or related potassium channels. To substantiate the generality of these principles, the electromechanical coupling was investigated also in channels distantly related to *Shaker*, e.g., KCNQ1, HERG, and HCN2 channels (Sanguinetti and Xu, 1999; Chen et al., 2001; Tristani-Firouzi et al., 2002; Decher et al., 2004; Macri and Accili, 2004; Ferrer et al., 2006; Prole and Yellen, 2006; Boulet et al., 2007; Labro et al., 2008, 2011; Choveau et al., 2011). The low sequence homology of these channels with *Shaker* makes it difficult to correlate the mutational data with currently available structural models of K channels (Long et al., 2005a, 2007; Jensen et al., 2012). In spite of low sequence homology, it is remarkable that gating properties of KCNQ1, HERG, and HCN2 channels change similarly when mutating the corresponding S4–S5 linker and distal S6 regions (**Figure 1**). Electrophysiological analysis of KCNQ1, HERG, and HCN2 channels carrying mutations or chimeric replacements in S4–S5 linker and S6 showed three main phenotypes: (1) GV relations exhibit significant shifts to both positive and negative potentials; (2) some mutants were non-functional in heterologous expression systems; (3) a significant number of point mutants gave rise to constitutively conducting channels. Constitutive conductance in *Shaker* was observed only upon substitution of P475 pore residue with amino acids having hydrophilic side-chains, which we will discuss below in detail. At this point, we will briefly summarize the main findings of studies related to the electromechanical coupling in KCNQ1, HERG, and HCN2 channels.

Exchange of the entire S6 segment of hERG potassium channel with its counterpart from bovine ether-a-go-go (bEAG) resulted in hERG/bEAG chimeric channel with a partial constitutive conductance (Ficker et al., 1998). In order to restore complete voltage-gated features of the chimeric channel, it was necessary to reconstitute the distal S6 hERG sequence (SAIIQRL) in the hERG/bEAG chimera. Furthermore, transfer of bEAG S4–S5 linker to the hERG disrupted the complete hERG channel closure (Ferrer et al., 2006). Substitution of distal S6 region with corresponding bEAG segment in this chimera fully restored the channel closure at hyperpolarized potentials (Ferrer et al., 2006). Further mutational analysis showed that an exchange of five amino acids (colored red in **Figure 1**) sufficed to restore fully voltage-gated properties. These results accentuate the concordance between S4–S5 linker and S6 sequences for complete closure of hERG channel at hyperpolarized potentials (Ferrer et al., 2006). Data are also in agreement with an earlier suggestion that S4–S5 linker and distal S6 in HCN2 channel are in close proximity at hyperpolarized membrane potentials (Tristani-Firouzi et al., 2002). This proposal was based on electrophysiological analysis of channels carrying mutations at D540 (S4–S5 linker) and R665 (S6) residues.

Recent scanning mutagenesis of KCNQ1 channel revealed that S4–S5 linker and distal S6 are the most sensitive regions for mutational gating perturbations (Ma et al., 2011). A significant number of mutants in these regions drastically affected KCNQ1 channel function by shifting GV relations toward positive and, respectively, negative directions. Boulet et al. (2007) and Choveau et al. (2011) obtained similar results for KCNQ1 channel. Moreover, analysis of double-mutant, constructed by combination of two point mutants, one located on S4–S5 linker (V254A), the other on S6 (L353A), confirmed the hypothesis that S4–S5 linker and S6 interact with each other to ensure the voltage-dependent gating of KCNQ1 (Choveau et al., 2011). This interaction, however, appears to be state-dependent, i.e., it only takes place in the closed state of the channel (Choveau et al., 2011).

Electromechanical coupling is well investigated also in hyperpolarization-activated cyclic nucleotide gated cation (HCN) channels. HCN channels are particularly interesting from this point of view, since they have an inverse voltage-dependent gating mode, i.e., hyperpolarization activates, whereas depolarization deactivates HCN channels (Brown et al., 1979; Gauss et al., 1998; Biel et al., 2009). Alanine scanning mutagenesis of the S4–S5 linker region in HCN2 revealed several amino acid residues, mutation of which gave rise to a channel with partial constitutive conductance (Chen et al., 2001). Mutations causing a constitutively open HCN2 channel were also identified in its distal S6 region (Decher et al., 2004). Based on the functional analysis of double mutants, it has been proposed that electrostatic interaction between side-chains of S4–S5 linker and distal S6 mediate electromechanical coupling in HCN2 channels (Decher et al., 2004). The coupling, however, is thought to be completely disrupted at depolarized potentials which leads to the closure of channel gate also known as voltage desensitization (Shin et al., 2004).

EVALUATING THE SIMILARITIES AND DIFFERENCES

A significant number of mutations in S4–S5 linker and distal S6 markedly alter the gating properties of *Shaker* and related channels (Isacoff et al., 1991; McCormack et al., 1991; Schoppa et al., 1992; Li-Smerin et al., 2000; Hackos et al., 2002; Yifrach and MacKinnon, 2002; Ding and Horn, 2003; Soler-Llavina et al., 2006). Similar observations have been made upon mutations of the corresponding regions of KCNQ1, hERG, and HCN2 channels (Donger et al., 1997; Chen et al., 2000; Decher et al., 2004; Ferrer et al., 2006; Boulet et al., 2007; Ma et al., 2011). Yet, there are noteworthy differences. Examination of available mutational data revealed that point mutations rarely cause a constitutive conductance in *Shaker* (Yifrach and MacKinnon, 2002; Soler-Llavina et al., 2006). By contrast, analysis of KCNQ1 and HCN2 channels carrying comparable point mutations in their S4–S5 linker and distal S6 regions showed that quite a significant number of mutant KCNQ1 and HCN2 channels demonstrate a large constitutively open component (Chen et al., 2001; Decher et al., 2004; Ma et al., 2011). These data indicate that KCNQ1, HCN2, and hERG channels are more susceptible to constitutive conductance than the *Shaker* channel.

Two different mechanisms are discussed in literature as possible cause of partial or complete constitutive conductance in voltage-gated ion channels. A leak of the ions through the channel pore due to incomplete closure of the gate at resting voltage-sensor conditions is one possible mechanism. Single channel measurements of mutant *Shaker* channels (Islas and Sigworth, 1999; Sukhareva et al., 2003) as well as BK channel (Horrigan and Aldrich, 2002) indicated that the pore is able to completely prevent the ion flow. This suggests that the constitutively open component of conductance is due to spontaneous fluctuations of channel between the open

and the closed states in resting voltage-sensor conditions (Horrigan and Aldrich, 2002; Sukhareva et al., 2003; Niu et al., 2004). Thus, the resting sate of KCNQ1 as well as HCN2 channels allows significant spontaneous transitions to the open state independent of changes in membrane voltage (Decher et al., 2004; Ma et al., 2011). Significant number of point mutations in S4–S5 linker and distal S6 in these two channels even more destabilized the resting-closed state, in exceptional cases leading to constitutively open phenotype.

Evaluating the energetics of pore opening by a double-mutant cycle analysis, it has been proposed that the *Shaker* pore is intrinsically closed, i.e., the closed state is energetically favored in virtual absence of VSDs (Yifrach and MacKinnon, 2002). Analysis of *Shaker* mutants with respect to gating charge movement (Ding and Horn, 2003) and mode shift in VSDs translocation (Haddad and Blunck, 2011) were in agreement with this conclusion. Considering VSDs and PD as two separate elements of the VSD-PD bimodular system, in current issue Blunck and Batulan describe the electromechanical coupling from thermodynamic point of view. Analysis suggests that strong electromechanical coupling will require less energy for opening of the channel pore with a given probability. It follows, that complete uncoupling of the gate from VSDs will lead to permanently closed channels, since energy provided by VSDs will no longer reach to the PD.

If channel possesses an intrinsically open pore, uncoupling would lead to constitutively open channels. In these channels, VSDs must exert a mechanical work to close the pore. This hypothesis reasons that various degrees of constitutive conductance in KCNQ1, HCN2, and hERG mutants are caused by alteration in coupling strength. In extreme cases, when coupling between VSDs and PD is lost, channels open constitutively as observed in some mutant KCNQ1 and HCN2 channels (Chen et al., 2000; Ma et al., 2011). Nevertheless, *Shaker* hydrophobic mutations at P475 position (Hackos et al., 2002; Sukhareva et al., 2003) and *Shaker*-KcsA chimeras (Lu et al., 2001, 2002) also show various degrees of constitutive conductance. How can these results be reconciled with our hypothesis?

P475 position in *Shaker* corresponds to the second proline of the PXP motif of K channel pores. The PXP motif may provide flexibility to the inner S6 helixes in most of Kv channels (del Camino et al., 2000) and allow the bending of S6 helixes at the cytoplasmic side of the pore (del Camino and Yellen, 2001). Studies investigating the constitutive conductance in *Shaker* suggested that hydrophilic substitutions at P475 position change the electromechanical coupling between VSDs and the gate (Hackos et al., 2002; Sukhareva et al., 2003). P475 is localized in the pore of the *Shaker* channel, quite far away from the putative coupling interface proposed by MacKinnon and colleagues (Long et al., 2005b). Recent crystal structures indicate that the bending of the S6 helices makes the interaction between S4–S5 linker helix and distal S6 region topologically possible (Long et al., 2005b, 2007). Thus, one possible explanation is, that the hydrophilic P475 mutations change the electromechanical coupling strength by influencing the bending properties of pore helixes. Since other P475 substitutions, which also influence the flexibility of S6 helices, do not cause a constitutive conductance (Li-Smerin et al., 2000; Sukhareva et al., 2003; Soler-Llavina et al., 2006), bending of S6 seems insufficient to explain the data. Significant changes in voltage gating properties observed in P457 hydrophilic mutants hint toward a more complex picture of mutational influence (Sukhareva et al., 2003). Weakening the strength of electromechanical coupling accompanied by alteration in intrinsic pore properties it the likely cause of partial constitutive conductance phenotype in *Shaker* P475 hydrophilic mutants.

We reexamined the results of Shaker-KcsA chimeric replacements studied by Lu et al. (2002) in the light of the structural data that became available after the work was published (Long et al., 2005a, 2007). According to our analysis the mutational manipulations causing a partial constitutive conductance in *Shaker*-KcsA and Kv2.1-KcsA chimeras (Lu et al., 2002) are located in proximal S5 (SMRELGL sequence in *Shaker*) and in distal S6 (PVPVIVSN sequence in *Shaker*; **Figure 2**). Careful assessment also indicates that mutations restricted to S4–S5 linker are not able to produce constitutively open channels. Apparently, changes outside of the S4–S5 linker are required to generate constitutively open *Shaker* channels.

The distal S6 segments of KscA and *Shaker* channels differ significantly in sequence as well as in structural organization (Doyle et al., 1998; Long et al., 2007). Therefore, it is possible that chimeric replacements of *Shaker* S6 segment with the corresponding KcsA sequence (Lu et al., 2002) markedly influence the intrinsic properties of the *Shaker* pore. Thus, we propose that *Shaker*-KcsA chimeras and P475 hydrophilic substitutions affect two important features in *Shaker*: (1) coupling strength between VSDs and the PD is decreased and (2) intrinsic properties of pore are altered.

It follows that the pores of wild type KCNQ1 and HCN2 channels are likely to be thermodynamically more stable at their open state in the absence of the voltage-sensors, i.e., intrinsically more stable at the opened state. Two important features observed in these channels corroborate this notion. (1) Wild type KCNQ1 and HCN2 channels demonstrate a significant constitutive conductance at resting voltage-sensor conditions (Decher et al., 2004; Ma et al., 2011). (2) A large number of S4–S5 linker mutants significantly alter the constitutively open component in these channels (Chen et al., 2001; Decher et al., 2004; Boulet et al., 2007; Choveau et al., 2011). The reverse voltage-gated mode of HCN2 channel makes the comparison of HCN2 with KCNQ1 fairly difficult. Let us first briefly describe the reverse voltage gating of the HCN2 channel. It has been hypothesized that depolarization of HCN channels uncouples the channel pore from VSDs, which leads to the channel closure (Shin et al., 2004). According to this hypothesis, at hyperpolarized potentials the coupling between S4–S5 linker with S6 reestablishes itself resulting in stabilized open state. This assumes, that mutations disabling the association of VSDs with the PD at hyperpolarized potentials will drive the HCN channels into permanently desensitized state, i.e., channels will be closed at all voltages. Mutagenesis of S4–S5 linker and the end of S6 segment of HCN2 channels, however, indicated that the vast majority of mutants were functional (Chen et al., 2001; Decher et al., 2004). Moreover, large number of mutants exhibited constitutively open component. S4–S5 linker mutants Y331 and R339 demonstrated a complete constitutive conductance (Chen et al., 2001). Therefore, Sanguinetti and colleagues suggested that a significant reduction of the coupling strength in HCN2 is a likely reason for partial

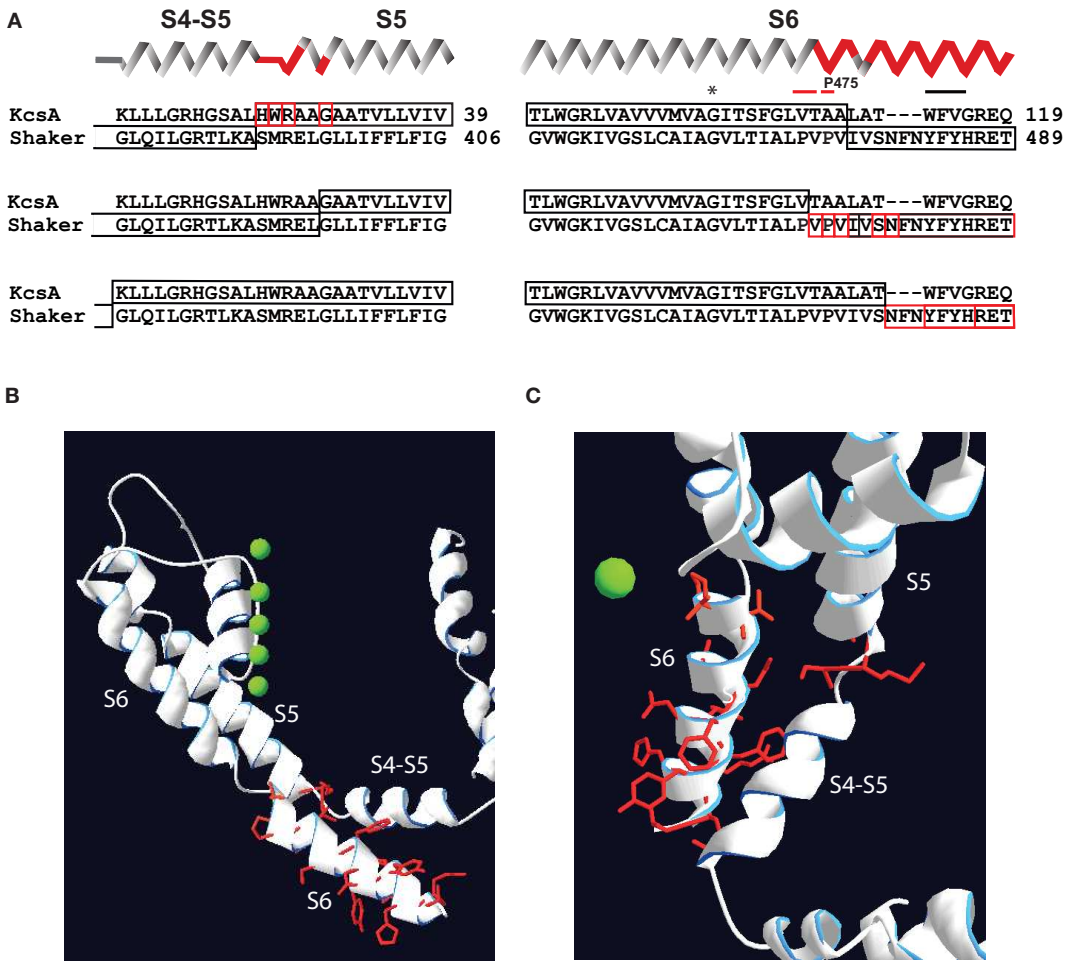

FIGURE 2 | Localization of mutations susceptible for constitutive conductance in *Shaker*-KcsA chimeric channels according to recent Kv crystals. (A) Three groups of KcsA-*Shaker* chimeras that demonstrated partial or almost complete constitutive activation are shown separately. Secondary structure succession pattern on the top of sequence alignments corresponds to the recent crystal structure of the Kv1.2–Kv2.1 chimera (Long et al., 2007). Red-framed residues indicate the extension of the chimeric link (one residue at a time) causing constitutive conductance. **(B)** Localization of residues susceptible for constitutive conductance mapped on crystal structure of Kv1.2–Kv2.1. The side-chains of these residues are represented as red sticks. Only one subunit is shown for simplicity. **(C)** Top view of same structure shown in **(B)**.

or complete constitutive conductance of mutant channels (Chen et al., 2001; Decher et al., 2004). Thus, the mechanism of HCN2 gating is apparently more complex than it is originally thought. A systematic analysis of the voltage-sensor movement in mutant channels by measuring the gating current or fluorescence properties of labeled residues can help us to reveal more about the role of coupling in HCN2 channel gating in future. Nevertheless, since a large number of mutant HCN2 channels are characterized in the literature, we were interested whether the fraction of constitutive conductance is dependent on voltage-gated properties of HCN2 channel as we previously revealed for KCNQ1.

CONSTITUTIVE CONDUCTANCE IN KCNQ1 AND HCN2 IS LINKED TO VOLTAGE-DEPENDENT CLOSED-OPEN EQUILIBRIUM OF THE PORE

Large-scale mutagenesis of S4–S5 linker and PD residues of KCNQ1 revealed a strong correlation between the fraction of constitutive conductance (G_{min}) and the midpoint of the voltage-dependent conductance ($V_{1/2}$; Ma et al., 2011). The $V_{1/2}$–G_{min} correlation in KCNQ1 could be well described by an Eq. 1, which is based on a simple allosteric gating scheme (**Scheme 1**) involving a voltage-dependent and a voltage-independent closed to open transition as shown below (Ma et al., 2011).

Kv·exp(ZFV/RT) component describes the voltage-dependent equilibrium constant. Z, F, and R have their usual meanings, T is the absolute temperature; K_a is equilibrium constant of voltage-independent transitions; b is an allosteric factor. The mathematical relationship between constitutively open component – G_{min} and the midpoint of potential-sensitive fraction – $V_{1/2}$ is given by equation:

$$G_{min} = \frac{1 + Kv \cdot e^{\frac{ZF}{RT} \cdot V_{1/2}}}{(b-1) \cdot Kv \cdot e^{\frac{ZF}{RT} \cdot V_{1/2}}} \quad (1)$$

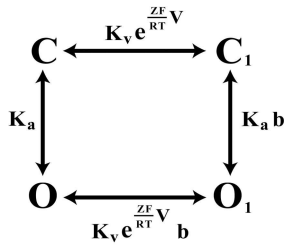

SCHEME 1 | The four-state allosteric gating scheme, illustrating the voltage-dependent (horizontal) and voltage-independent (vertical) channel transitions. C and C1 signify the closed-states of the channel, O and O1 the open states, correspondingly.

We were interested whether the G_{min}–$V_{1/2}$ correlation observed with KCNQ1 mutants might be seen also for HCN2 mutants. The estimation method for constitutive conductance component in HCN2 mutants was the same as we previously described for KCNQ1 (Ma et al., 2011). Analyzing mutagenesis data of HCN2 channel (Chen et al., 2001; Decher et al., 2004) we observed that many mutations in HCN2 induce large shifts in GV relationship. Next we plotted G_{min} versus $V_{1/2}$ for HCN2 channel. The resulting G_{min}–$V_{1/2}$ correlation was well described quantitatively by the allosteric gating model developed for KCNQ1 (**Figure 3**). The analysis indicates that KCNQ1 and HCN2 channels share a common feature – the equilibrium between voltage-dependent and voltage-independent transitions can be characterized by parameter **b**.

Unfortunately, the quantity of available mutational data for hERG channel was insufficient for a $V_{1/2}$–G_{min} correlation analysis. It is, however, noteworthy that hERG-bEAG chimeras with negatively shifted $V_{1/2}$ parameter also demonstrate an increase in G_{min} (Ferrer et al., 2006). In contrast, *Shaker* mutants remain tightly closed at hyperpolarized potentials (Yifrach and MacKinnon, 2002; Soler-Llavina et al., 2006; Ma et al., 2011) in spite of large shifts in their GV curve toward more negative potentials. Exceptions are P475 mutations that we discussed above.

A small constitutively conducting component was observed in single channel recordings of wild type HCN2 and BK channels (Gauss et al., 1998; Chen et al., 2001; Ma et al., 2011). The constitutive conduction in these channels reflects spontaneous fluctuations between open and closed states, which are observable even at the absence of their respective ligands (Proenza and Yellen, 2006; Yang et al., 2010). Earlier reports of constitutive association of the Ca^{2+}-binding protein calmodulin (CaM) with the C-terminus of KCNQ1 (Yus-Najera et al., 2002; Ghosh et al., 2006; Shamgar et al., 2006; Ciampa et al., 2011) prompted us to consider intracellular Ca^{2+} as a putative ligand for KCNQ1-CaM complex. Our preliminary data indicate that Ca^{2+} could act as an allosteric effector for KCNQ1 channel. The data are analogous to what has been observed for HCN2 (Proenza and Yellen, 2006; Biel et al., 2009; Kusch et al., 2010) and BK channels (Horrigan and Aldrich, 2002; Biel et al., 2009; Lee and Cui, 2010). In this context, it is of note that a recent analysis of VSD-movement of KCNQ1 suggested that the channel gating follows to the allosteric mechanism (Osteen et al., 2012).

Taken together, our analysis suggests that depending on channel type, the electromechanical coupling strength differentially influences the gating properties of ion channels. Particularly, if the channel pore prefers the closed state in absence of VSDs, as in case of *Shaker*, uncoupling would lead a tightly closed pore. Conversely, if the open state of channel pore is intrinsically more stable, uncoupling would lead to channels with partial or complete constitutively conductance. This seems to be the case for voltage-gated channels that possess C-terminal ligand-binding domains, e.g., KCNQ1, HCN2, and BK channels. From this point of view ligand-binding domains could be seen as "additional" gating machineries attached to the C-terminal part of S6 in HCN2, BK, and KCNQ1 channels that significantly influence the intrinsic pore properties. Consistent with this idea is the observation that the frequency of spontaneous openings in BK channels at resting state are dependent on the length of C-linker connecting S6 segment to RCK domains (Niu et al., 2004). Interestingly, the recent analysis of BK channel pore by cysteine modification experiments revealed that the inner BK channel pore at rest is significantly larger than the one in *Shaker* (Zhou et al., 2011). On the other hand modulation of channel gating by ligand-binding is likely to occur only if coupling between VSDs and the gate is not as dominant as in *Shaker*. Weaker coupling strength would enables fine-tuning of voltage-activated ion channels by their corresponding ligands.

FUTURE PERSPECTIVES

Finding answers to the following two conceptually important questions will significantly broaden our understanding about electromechanical coupling in voltage-gated ion channels.

1) What molecular forces determine the stability of the closed state in *Shaker* and in other potassium channels? An important step toward answering this question is the determination of closed Kv channel structures at defined membrane potential. Ideally, one may investigate channel structure in a distinct membranous environment at different membrane potentials in order to follow the activation process *in situ*. This seems particularly important in the light of recent observations suggesting that in some Kv channels interaction of S4–S5 linker with the distal S6 is dependent on channel state (Grabe et al., 2007; Barghaan and Bahring, 2009; Choveau et al., 2011). It is noteworthy that currently available crystal structures of Kv channels were obtained in a non-membranous environment, i.e., in the absence of an electric field (Long et al., 2005a, 2007). Though it is unclear what kind of channel state is generated under the conditions of crystallization, it can be argued that the conditions drive VSDs into a state described as closed-relaxed state (Villalba-Galea et al., 2008; Jensen et al., 2012). However, further structural and functional studies are required to correlate functional channel state with appropriate structure.
2) Which state is the thermodynamically preferred state of the pore in the absence of voltage-sensors in *Shaker* and in distantly related ion channels? Finding a clear-cut answer to this question is important for understanding the nature of constitutive conductance of ion channels.

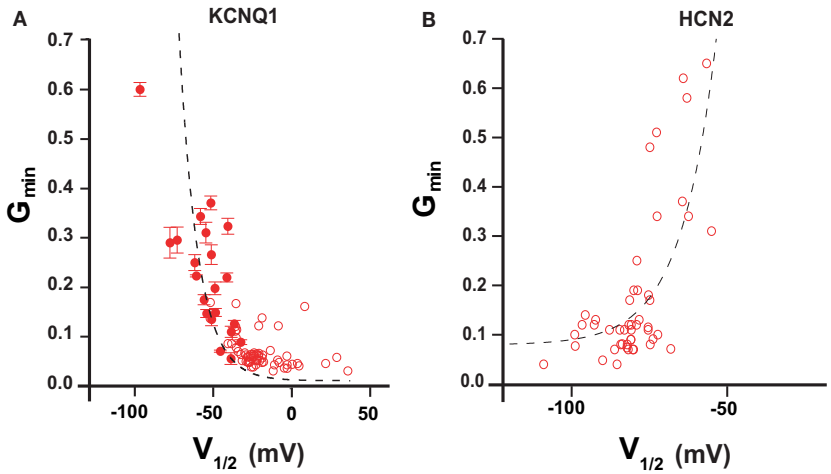

FIGURE 3 | G_{min}–$V_{1/2}$ relationship in KCNQ1 and HCN2 channels. **(A)** $V_{1/2}$–G_{min} correlation according to mutation-induced gating perturbations analysis of KCNQ1 (Ma et al., 2011) **(B)** $V_{1/2}$–G_{min} correlation for HCN2 channel calculated from published studies (Chen et al., 2001; Decher et al., 2004). Mutant channels showing G_{min} values larger than 0.7 are omitted (see restriction G_{min} <1; Ma et al., 2011). Dashed lines correspond to a theoretical calculation based on a simple allosteric gating scheme proposed earlier (Ma et al., 2011). Parameters are as follows: HCN2 Kv = 1.2×10^{-3}; Z = 2.27; b = 13.6, KCNQ1 Kv = 4.2×10^{-2}; Z = 2.37; $b = 1.59 \times 10^{3}$.

Extending the scanning mutagenesis studies to the single channel level will allow a more profound evaluation of coupling properties. Single channel recordings will provide us with valuable information on single channel conductance, duration of closed and opened states, maximal open probability and open probability at hyperpolarized potentials. Ideally, single channel measurements can be combined with structural studies (Sonnleitner et al., 2002). Applying novel techniques, such as solid-state NMR spectroscopy on Kv channels will certainly provide answers as well as raise new questions about the molecular mechanisms underling the electromechanical coupling and about its role in shaping voltage-gated properties of ion channels.

ACKNOWLEDGMENTS

Authors thank Dr. J. Schwarz for comments on the manuscript. Vitya Vardanyan is thankful to Volkswagen Foundation and to Institute for Molecular Biology NAS RA for support. Olaf Pongs is indebted to the Deutsche Forschungsgemeinschaft (Po137/37-1,2) and to German-Israeli DIP program (Po137/41-1; At 119/1-1) for support.

REFERENCES

Alabi, A. A., Bahamonde, M. I., Jung, H. J., Kim, J. I., and Swartz, K. J. (2007). Portability of paddle motif function and pharmacology in voltage sensors. *Nature* 450, 370–375.

Ashcroft, F. M. (1999). *Ion Channels and Disease: Channelopathies.* London: Academic Press, 481.

Bahring, R., Barghaan, J., Westermeier, R., and Wollberg, J. (2012). Voltage sensor inactivation in potassium channels. *Front. Pharmacol.* 3:100. doi:10.3389/fphar.2012.00100

Barghaan, J., and Bahring, R. (2009). Dynamic coupling of voltage sensor and gate involved in closed-state inactivation of kv4.2 channels. *J. Gen. Physiol.* 133, 205–224.

Batulan, Z., Haddad, G. A., and Blunck, R. (2010). An intersubunit interaction between S4-S5 linker and S6 is responsible for the slow off-gating component in Shaker K+ channels. *J. Biol. Chem.* 285, 14005–14019.

Bezanilla, F. (2000). The voltage sensor in voltage-dependent ion channels. *Physiol. Rev.* 80, 555–592.

Bezanilla, F. (2008). Ion channels: from conductance to structure. *Neuron* 60, 456–468.

Biel, M., Wahl-Schott, C., Michalakis, S., and Zong, X. (2009). Hyperpolarization-activated cation channels: from genes to function. *Physiol. Rev.* 89, 847–885.

Borjesson, S. I., and Elinder, F. (2008). Structure, function, and modification of the voltage sensor in voltage-gated ion channels. *Cell Biochem. Biophys.* 52, 149–174.

Boulet, I. R., Labro, A. J., Raes, A. L., and Snyders, D. J. (2007). Role of the S6 C-terminus in KCNQ1 channel gating. *J. Physiol. (Lond.)* 585, 325–337.

Broomand, A., and Elinder, F. (2008). Large-scale movement within the voltage-sensor paddle of a potassium channel-support for a helical-screw motion. *Neuron* 59, 770–777.

Brown, H. F., Difrancesco, D., and Noble, S. J. (1979). How does adrenaline accelerate the heart? *Nature* 280, 235–236.

Campos, F. V., Chanda, B., Roux, B., and Bezanilla, F. (2007). Two atomic constraints unambiguously position the S4 segment relative to S1 and S2 segments in the closed state of Shaker K channel. *Proc. Natl. Acad. Sci. U.S.A.* 104, 7904–7909.

Catterall, W. A. (2010). Ion channel voltage sensors: structure, function, and pathophysiology. *Neuron* 67, 915–928.

Chen, J., Mitcheson, J. S., Lin, M., and Sanguinetti, M. C. (2000). Functional roles of charged residues in the putative voltage sensor of the HCN2 pacemaker channel. *J. Biol. Chem.* 275, 36465–36471.

Chen, J., Mitcheson, J. S., Tristani-Firouzi, M., Lin, M., and Sanguinetti, M. C. (2001). The S4-S5 linker couples voltage sensing and activation of pacemaker channels. *Proc. Natl. Acad. Sci. U.S.A.* 98, 11277–11282.

Choveau, F. S., Rodriguez, N., Abderemane Ali, F., Labro, A. J., Rose, T., Dahimene, S., Boudin, H., Le Henaff, C., Escande, D., Snyders, D. J., Charpentier, F., Merot, J., Baro, I., and Loussouarn, G. (2011). KCNQ1 channels voltage dependence through a voltage-dependent binding of the S4-S5 linker to the pore domain. *J. Biol. Chem.* 286, 707–716.

Ciampa, E. J., Welch, R. C., Vanoye, C. G., and George, A. L. Jr. (2011). KCNE4 juxtamembrane region is required for interaction with calmodulin and for functional suppression of KCNQ1. *J. Biol. Chem.* 286, 4141–4149.

Decher, N., Chen, J., and Sanguinetti, M. C. (2004). Voltage-dependent gating of hyperpolarization-activated, cyclic nucleotide-gated pacemaker channels: molecular coupling between the S4-S5 and C-linkers. *J. Biol. Chem.* 279, 13859–13865.

del Camino, D., Holmgren, M., Liu, Y., and Yellen, G. (2000). Blocker protection in the pore of a voltage-gated K+ channel and its structural implications. *Nature* 403, 321–325.

del Camino, D., Kanevsky, M., and Yellen, G. (2005). Status of the intracellular gate in the activated-not-open state of shaker K+ channels. *J. Gen. Physiol.* 126, 419–428.

del Camino, D., and Yellen, G. (2001). Tight steric closure at the intracellular activation gate of a voltage-gated K+ channel. *Neuron* 32, 649–656.

Ding, S., and Horn, R. (2003). Effect of S6 tail mutations on charge movement in Shaker potassium channels. *Biophys. J.* 84, 295–305.

Ding, S., Ingleby, L., Ahern, C. A., and Horn, R. (2005). Investigating the putative glycine hinge in Shaker potassium channel. *J. Gen. Physiol.* 126, 213–226.

Donger, C., Denjoy, I., Berthet, M., Neyroud, N., Cruaud, C., Bennaceur, M., Chivoret, G., Schwartz, K., Coumel, P., and Guicheney, P. (1997). KVLQT1 C-terminal missense mutation causes a forme fruste long-QT syndrome. *Circulation* 96, 2778–2781.

Doyle, D. A., Morais Cabral, J., Pfuetzner, R. A., Kuo, A., Gulbis, J. M., Cohen, S. L., Chait, B. T., and MacKinnon, R. (1998). The structure of the potassium channel: molecular basis of K+ conduction and selectivity. *Science* 280, 69–77.

Ferrer, T., Rupp, J., Piper, D. R., and Tristani-Firouzi, M. (2006). The S4-S5 linker directly couples voltage sensor movement to the activation gate in the human ether-a'-go-go-related gene (hERG) K+ channel. *J. Biol. Chem.* 281, 12858–12864.

Ficker, E., Jarolimek, W., Kiehn, J., Baumann, A., and Brown, A. M. (1998). Molecular determinants of dofetilide block of HERG K+ channels. *Circ. Res.* 82, 386–395.

Gauss, R., Seifert, R., and Kaupp, U. B. (1998). Molecular identification of a hyperpolarization-activated channel in sea urchin sperm. *Nature* 393, 583–587.

Ghosh, S., Nunziato, D. A., and Pitt, G. S. (2006). KCNQ1 assembly and function is blocked by long-QT syndrome mutations that disrupt interaction with calmodulin. *Circ. Res.* 98, 1048–1054.

Grabe, M., Lai, H. C., Jain, M., Jan, Y. N., and Jan, L. Y. (2007). Structure prediction for the down state of a potassium channel voltage sensor. *Nature* 445, 550–553.

Hackos, D. H., Chang, T. H., and Swartz, K. J. (2002). Scanning the intracellular S6 activation gate in the shaker K+ channel. *J. Gen. Physiol.* 119, 521–532.

Haddad, G. A., and Blunck, R. (2011). Mode shift of the voltage sensors in Shaker K+ channels is caused by energetic coupling to the pore domain. *J. Gen. Physiol.* 137, 455–472.

Hille, B. (2001). *Ion Channels of Excitable Membranes*, 3rd Edn. Sunderland: Sinauer Associates, Inc.

Holmgren, M., Shin, K. S., and Yellen, G. (1998). The activation gate of a voltage-gated K+ channel can be trapped in the open state by an intersubunit metal bridge. *Neuron* 21, 617–621.

Horrigan, F. T., and Aldrich, R. W. (2002). Coupling between voltage sensor activation, Ca2+ binding and channel opening in large conductance (BK) potassium channels. *J. Gen. Physiol.* 120, 267–305.

Isacoff, E. Y., Jan, Y. N., and Jan, L. Y. (1991). Putative receptor for the cytoplasmic inactivation gate in the Shaker K+ channel. *Nature* 353, 86–90.

Islas, L. D., and Sigworth, F. J. (1999). Voltage sensitivity and gating charge in Shaker and Shab family potassium channels. *J. Gen. Physiol.* 114, 723–742.

Jensen, M. O., Jogini, V., Borhani, D. W., Leffler, A. E., Dror, R. O., and Shaw, D. E. (2012). Mechanism of voltage gating in potassium channels. *Science* 336, 229–233.

Jiang, Y., Ruta, V., Chen, J., Lee, A., and MacKinnon, R. (2003). The principle of gating charge movement in a voltage-dependent K+ channel. *Nature* 423, 42–48.

Kusch, J., Biskup, C., Thon, S., Schulz, E., Nache, V., Zimmer, T., Schwede, F., and Benndorf, K. (2010). Interdependence of receptor activation and ligand binding in HCN2 pacemaker channels. *Neuron* 67, 75–85.

Labro, A. J., Boulet, I. R., Choveau, F. S., Mayeur, E., Bruyns, T., Loussouarn, G., Raes, A. L., and Snyders, D. J. (2011). The S4-S5 linker of KCNQ1 channels forms a structural scaffold with the S6 segment controlling gate closure. *J. Biol. Chem.* 286, 717–725.

Labro, A. J., Raes, A. L., Grottesi, A., Van Hoorick, D., Sansom, M. S., and Snyders, D. J. (2008). Kv channel gating requires a compatible S4-S5 linker and bottom part of S6, constrained by non-interacting residues. *J. Gen. Physiol.* 132, 667–680.

Labro, A. J., Raes, A. L., and Snyders, D. J. (2005). Coupling of voltage sensing to channel opening reflects intrasubunit interactions in kv channels. *J. Gen. Physiol.* 125, 71–80.

Lee, S. Y., Banerjee, A., and MacKinnon, R. (2009). Two separate interfaces between the voltage sensor and pore are required for the function of voltage-dependent K+ channels. *PLoS Biol.* 7, e1000047. doi:10.1371/journal.pbio.1000047

Lee, U. S., and Cui, J. (2010). BK channel activation: structural and functional insights. *Trends Neurosci.* 33, 415–423.

Li-Smerin, Y., Hackos, D. H., and Swartz, K. J. (2000). A localized interaction surface for voltage-sensing domains on the pore domain of a K+ channel. *Neuron* 25, 411–423.

Long, S. B., Campbell, E. B., and MacKinnon, R. (2005a). Crystal structure of a mammalian voltage-dependent Shaker family K+ channel. *Science* 309, 897–903.

Long, S. B., Campbell, E. B., and MacKinnon, R. (2005b). Voltage sensor of Kv1.2: structural basis of electromechanical coupling. *Science* 309, 903–908.

Long, S. B., Tao, X., Campbell, E. B., and MacKinnon, R. (2007). Atomic structure of a voltage-dependent K+ channel in a lipid membrane-like environment. *Nature* 450, 376–382.

Lu, Z., Klem, A. M., and Ramu, Y. (2001). Ion conduction pore is conserved among potassium channels. *Nature* 413, 809–813.

Lu, Z., Klem, A. M., and Ramu, Y. (2002). Coupling between voltage sensors and activation gate in voltage-gated K+ channels. *J. Gen. Physiol.* 120, 663–676.

Ma, L. J., Ohmert, I., and Vardanyan, V. (2011). Allosteric features of KCNQ1 gating revealed by alanine scanning mutagenesis. *Biophys. J.* 100, 885–894.

Macri, V., and Accili, E. A. (2004). Structural elements of instantaneous and slow gating in hyperpolarization-activated cyclic nucleotide-gated channels. *J. Biol. Chem.* 279, 16832–16846.

McCormack, K., Tanouye, M. A., Iverson, L. E., Lin, J. W., Ramaswami, M., Mccormack, T., Campanelli, J. T., Mathew, M. K., and Rudy, B. (1991). A role for hydrophobic residues in the voltage-dependent gating of Shaker K+ channels. *Proc. Natl. Acad. Sci. U.S.A.* 88, 2931–2935.

Niu, X., Qian, X., and Magleby, K. L. (2004). Linker-gating ring complex as passive spring and Ca(2+)-dependent machine for a voltage- and Ca(2+)-activated potassium channel. *Neuron* 42, 745–756.

Ohlenschlager, O., Hojo, H., Ramachandran, R., Gorlach, M., and Haris, P. I. (2002). Three-dimensional structure of the S4-S5 segment of the Shaker potassium channel. *Biophys. J.* 82, 2995–3002.

Osteen, J. D., Barro-Soria, R., Robey, S., Sampson, K. J., Kass, R. S., and Larsson, H. P. (2012). Allosteric gating mechanism underlies the flexible gating of KCNQ1 potassium channels. *Proc. Natl. Acad. Sci. U.S.A.* 109, 7103–7108.

Proenza, C., and Yellen, G. (2006). Distinct populations of HCN pacemaker channels produce voltage-dependent and voltage-independent currents. *J. Gen. Physiol.* 127, 183–190.

Prole, D. L., and Yellen, G. (2006). Reversal of HCN channel voltage dependence via bridging of the S4-S5 linker and Post-S6. *J. Gen. Physiol.* 128, 273–282.

Sanguinetti, M. C., and Xu, Q. P. (1999). Mutations of the S4-S5 linker alter activation properties of HERG potassium channels expressed in Xenopus oocytes. *J. Physiol. (Lond.)* 514(Pt 3), 667–675.

Schoppa, N. E., Mccormack, K., Tanouye, M. A., and Sigworth, F. J. (1992). The size of gating charge in wild-type and mutant Shaker potassium channels. *Science* 255, 1712–1715.

Shamgar, L., Ma, L., Schmitt, N., Haitin, Y., Peretz, A., Wiener, R., Hirsch, J., Pongs, O., and Attali, B. (2006). Calmodulin is essential for cardiac IKS channel gating and assembly: impaired function in long-QT mutations. *Circ. Res.* 98, 1055–1063.

Shin, K. S., Maertens, C., Proenza, C., Rothberg, B. S., and Yellen, G. (2004). Inactivation in HCN channels results from reclosure of the activation gate: desensitization to voltage. *Neuron* 41, 737–744.

Soler-Llavina, G. J., Chang, T. H., and Swartz, K. J. (2006). Functional interactions at the interface between voltage-sensing and pore domains in the Shaker K(v) channel. *Neuron* 52, 623–634.

Sonnleitner, A., Mannuzzu, L. M., Terakawa, S., and Isacoff, E. Y. (2002). Structural rearrangements in single ion channels detected optically in living cells. *Proc. Natl. Acad. Sci. U.S.A.* 99, 12759–12764.

Sukhareva, M., Hackos, D. H., and Swartz, K. J. (2003). Constitutive activation of the Shaker Kv channel. *J. Gen. Physiol.* 122, 541–556.

Sullivan, D. A., Holmqvist, M. H., and Levitan, I. B. (1997). Characterization of gating and peptide block of

mSlo, a cloned calcium-dependent potassium channel. *J. Neurophysiol.* 78, 2937–2950.

Swartz, K. J. (2004). Opening the gate in potassium channels. *Nat. Struct. Mol. Biol.* 11, 499–501.

Tao, X., Lee, A., Limapichat, W., Dougherty, D. A., and MacKinnon, R. (2010). A gating charge transfer center in voltage sensors. *Science* 328, 67–73.

Tristani-Firouzi, M., Chen, J., and Sanguinetti, M. C. (2002). Interactions between S4-S5 linker and S6 transmembrane domain modulate gating of HERG K+ channels. *J. Biol. Chem.* 277, 18994–19000.

Vargas, E., Bezanilla, F., and Roux, B. (2011). In search of a consensus model of the resting state of a voltage-sensing domain. *Neuron* 72, 713–720.

Villalba-Galea, C. A., Sandtner, W., Starace, D. M., and Bezanilla, F. (2008). S4-based voltage sensors have three major conformations. *Proc. Natl. Acad. Sci. U.S.A.* 105, 17600–17607.

Webster, S. M., Del Camino, D., Dekker, J. P., and Yellen, G. (2004). Intracellular gate opening in Shaker K+ channels defined by high-affinity metal bridges. *Nature* 428, 864–868.

Yang, J., Krishnamoorthy, G., Saxena, A., Zhang, G., Shi, J., Yang, H., Delaloye, K., Sept, D., and Cui, J. (2010). An epilepsy/dyskinesia-associated mutation enhances BK channel activation by potentiating Ca2+ sensing. *Neuron* 66, 871–883.

Yarov-Yarovoy, V., Baker, D., and Catterall, W. A. (2006). Voltage sensor conformations in the open and closed states in ROSETTA structural models of K+ channels. *Proc. Natl. Acad. Sci. U.S.A.* 103, 7292–7297.

Yifrach, O., and MacKinnon, R. (2002). Energetics of pore opening in a voltage-gated K+ channel. *Cell* 111, 231–239.

Yus-Najera, E., Santana-Castro, I., and Villarroel, A. (2002). The identification and characterization of a noncontinuous calmodulin-binding site in noninactivating voltage-dependent KCNQ potassium channels. *J. Biol. Chem.* 277, 28545–28553.

Zhou, Y., Xia, X. M., and Lingle, C. J. (2011). Cysteine scanning and modification reveal major differences between BK channels and Kv channels in the inner pore region. *Proc. Natl. Acad. Sci. U.S.A.* 108, 12161–12166.

Conflict of Interest Statement: The authors declare that the research was conducted in the absence of any commercial or financial relationships that could be construed as a potential conflict of interest.

Received: 31 March 2012; accepted: 07 July 2012; published online: 27 July 2012. Citation: Vardanyan V and Pongs O (2012) Coupling of voltage-sensors to the channel pore: a comparative view. Front. Pharmacol. ***3****:145. doi: 10.3389/fphar.2012.00145*

This article was submitted to Frontiers in Pharmacology of Ion Channels and Channelopathies, a specialty of Frontiers in Pharmacology.

frontiers in
PHARMACOLOGY

REVIEW ARTICLE
published: 13 September 2012
doi: 10.3389/fphar.2012.00168

Being flexible: the voltage-controllable activation gate of Kv channels

Alain J. Labro* and Dirk J. Snyders*

Department of Biomedical Sciences, University of Antwerp, Antwerp, Belgium

Edited by:
Gildas Loussouarn, Université de Nantes, France

Reviewed by:
Gea-Ny Tseng, Virginia Commonwealth University, USA
Adam Hill, Victor Chang Cardiac Research Institute, Australia

****Correspondence:***
Alain J. Labro and Dirk J. Snyders, Department of Biomedical Sciences, University of Antwerp, Universiteitsplein 1, 2610 Antwerp, Belgium.
e-mail: alain.labro@ua.ac.be; dirk.snyders@ua.ac.be

Kv channels form voltage-dependent potassium selective pores in the outer cell membrane and are composed out of four α-subunits, each having six membrane-spanning α-helices (S1–S6). The α-subunits tetramerize such that the S5–S6 pore domains co-assemble into a centrally located K^+ pore which is surrounded by four operational voltage-sensing domains (VSD) that are each formed by the S1–S4 segments. Consequently, each subunit is capable of responding to changes in membrane potential and dictates whether the pore should be conductive or not. K^+ permeation through the pore can be sealed off by two separate gates in series: (a) at the inner S6 bundle crossing (BC gate) and (b) at the level of the selectivity filter (SF gate) located at the extracellular entrance of the pore. Within the last years a general consensus emerged that a direct communication between the S4S5-linker and the bottom part of S6 ($S6_c$) constitutes the coupling with the VSD thus making the BC gate the main voltage-controllable activation gate. While the BC gate listens to the VSD, the SF changes its conformation depending on the status of the BC gate. Through the eyes of an entering K^+ ion, the operation of the BC gate apparatus can be compared with the iris-like motion of the diaphragm from a camera whereby its diameter widens. Two main gating motions have been proposed to create this BC gate widening: (1) tilting of the helix whereby the S6 converts from a straight α-helix to a tilted one or (2) swiveling of the $S6_c$ whereby the S6 remains bent. Such motions require a flexible hinge that decouples the pre- and post-hinge segment. Roughly at the middle of the S6 there exists a highly conserved glycine residue and a tandem proline motif that seem to fulfill the role of a gating hinge which allows for tilting/swiveling/rotations of the post-hinge S6 segment. In this review we delineate our current view on the operation of the BC gate for controlling K^+ permeation in Kv channels.

Keywords: bundle crossing gate, glycine and PXP hinge point, pore opening and closure, selectivity filter, shaker potassium channel, voltage-dependent gating

INTRODUCTION

Potassium (K) channels form transmembrane permeation pathways (pores) with a high selectivity for K^+ over other monovalent ions like Na^+. *In vivo*, these channels are responsible for repolarizing the membrane potential back to its resting condition following an action potential, to set the resting membrane potential of the cell and to determine the action potential firing rate (Hille, 2001). The biophysical properties and abundance of these channels shape the time course of the action potential, and constitute a critical determining factor of cellular excitability. To serve their *in vivo* role, the flow of K^+ needs to be strictly controlled and channels need to be able to actively open or close their pore in response to varying stimuli such as changes in pH or Ca^{2+}/ligand concentration. In the case of voltage-gated potassium (Kv) channels, which are the predominant K channels shaping the action potential duration, this stimulus is a change in membrane potential.

A typical Kv channel is composed of four individual α-subunits (MacKinnon, 1991), each containing six membrane spanning helices (S1–S6) organized to form a central K^+ pore with the S5 and S6 segments (**Figures 1A,B**; Doyle et al., 1998; Long et al., 2005). The S4 segment is positively charged and assembles with the S1–S3 segments into a voltage-sensing domain (VSD) that detects changes in membrane potential. Since each subunit has its own VSD, a functional channel consists out of one centrally located K^+ pore that is surrounded by four operational VSDs. Membrane re- or depolarization creates a force on the VSD causing its movement. This molecular rearrangement is transmitted via an electromechanical coupling to the channel's activation gate(s) that seals off the K^+ pore. K^+ permeation can be sealed off by two separate gates in series: (a) at the inner S6 bundle crossing (BC; Liu et al., 1997; del Camino and Yellen, 2001) and (b) at the level of the selectivity filter (SF; Liu et al., 1996; Loots and Isacoff, 1998; Cuello et al., 2010b). An in depth review on the operation of the VSD and electromechanical coupling has been given by others in this research topic of Frontiers in Pharmacology (Blunck and Batulan, 2012; Delemotte et al., 2012; Vardanyan and Pongs, 2012). Here we delineate the current view on the operation of the channel's activation gate for which most of our understanding comes from studies in the prototypical *Shaker* Kv channel. Therefore the

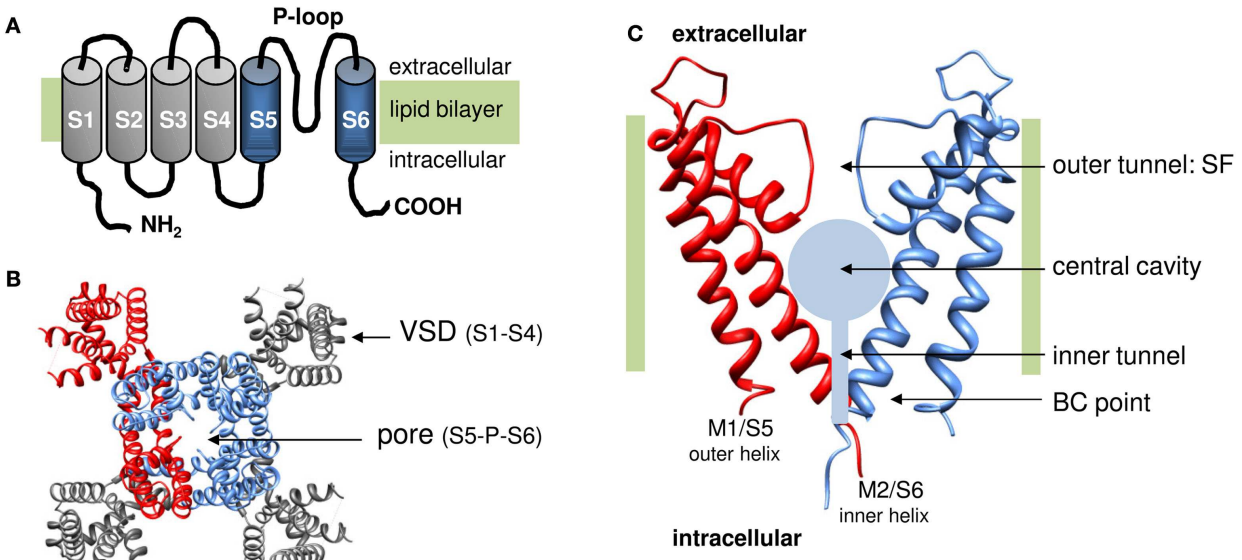

D

	P-loop (SF-gate)	S6 (M2 in KcsA/MthK)	
Shaker	FWWAVVTMT**TVGYG**DMTPVGFWGKIVGSLCVVA**G**VLTIAL**PVP**VIVSNFNYFY		485
Kv1.2	FWWAVVSMT**TVGYG**DMVPTTIGGKIVGSLCAIA**G**VLTIAL**PVP**VIVSNFNYFY		417
KCSA	LWWSVETAT**TVGYG**DLYPVTLWGRLVAVVVMVA**G**ITSFGLVTAALATWFVQRE		118
KirBac1.1	FFFSVETLA**TVGYG**DMHPQTVYAHAIATLEIFV**G**MSGIALST**G**LVFARFARPR		153
MthK	LYWTFVTIA**TVGYG**DYSPSTPLGMYFTVTLIVL**G**IGTFAVAVERLLEFLINRE		102
KvAP	LWWAVVTAT**TVGYG**DVVPATPIGKVIGIAVMLT**G**ISALTLLI**G**TVSNMFQKIL		239
Kv2.1	FWWATITMT**TVGYG**DIYPKTLLGKIVGGLCCIA**G**VLVIAL**PIP**IIVNNFSEFY		420
Kv3.1	FWWAVVTMT**TLGYG**DMYPQTW-GMLVGALCALA**G**VLTIAM**PVP**VIVNNFGMYY		443
Kv4.1	FWYTIVTMT**TLGYG**DMVPSTIAGKIFGSICSLS**G**VLVIAL**PVP**VIVSNFSRIY		415
KvS(Kv6.2)	YWWAVISMT**TVGYG**DMVPRSLPGQVVALSSILS**G**ILLMAF**PVT**SIFHTFSRSY		412
KCNQ1(Kv7.1)	LWWGVVTVT**TIGYG**DKVPQTWVGKTIASCFSVFAISFFAL**PAG**ILGSGFALKV		360
hERG(Kv11.1)	LYFTFSSLT**SVGFG**NVSPNTNSEKIFSICVMLI**G**SLMYASIFG**G**NVSAIIQRLY		667

FIGURE 1 | Topology of K channels. (A) Cartoon of the six transmembrane segment (S1–S6) one P-loop (6Tm-1P) topology of a Kv channel α-subunit with both amino (NH_2) and carboxyl (COOH) terminus located intracellular. The S1–S4 segments form the VSD (represented in gray) and the S5-P-loop-S6 region assembles with three other pore domains into the K^+ permeation pathway. **(B)** Top view (from the extracellular side) of the 3D structure of the Kv1.2 channel (protein data bank accession code 2A79; Long et al., 2005). To illustrate the fourfold symmetrical assembly of the α-subunits into a functional channel, one α-subunit is represented in red. In the other subunits the pore region (S5-P-loop-S6) is colored blue and the VSD (S1–S4) is represented in gray. Note that the pore regions form a centrally located K^+ pore that is surrounded by four independent VSDs. **(C)** Side view of the pore module of the 2Tm-1P K channel KcsA that was crystallized in the closed state (protein data bank accession code 1BL8; Doyle et al., 1998). The first transmembrane segment M1 (which resembles S5 in Kv channels) locates at the periphery and faces the lipid bilayer whereas the second transmembrane segment M2 (corresponding to S6) forms the inner pore helix. The front and back α-subunit are omitted to illustrate the layout of the K^+ permeation pathway that – from the intracellular to the extracellular side – can be divided in three recognizable sections; (1) a water filled inner tunnel, (2) a wider 12 Å in diameter water filled cavity, and (3) a narrower outer tunnel that forms the ion selectivity filter (SF) that dictates K^+ selectivity. Both the inner tunnel and the central cavity are formed by the inner pore helices that cross the membrane under an angle of ∼25° making the resemblance with an inverted teepee (Doyle et al., 1998). The K^+ pathway contains two energy barriers for K^+ that function as a gate: (1) at the bundle crossing (BC) of the M2/S6 helices (BC gate) that forms a barrier for hydrated K^+ and (2) the SF that allows passage of K^+ ions which have shed their hydration shell. **(D)** Sequence alignment of the inner pore helix of the pore module (S6 and M2 segment, respectively), and the P-loop that forms the channels SF which contains the TVGYGD signature sequence (highlighted in brown) for a K^+ selective channel (Heginbotham et al., 1994). Highlighted in red is the highly conserved glycine residue in the middle of the inner pore helix. The PXP motif present in Kv channels is highlighted in yellow. Note that in the "silent" Kv channels (KvS, with the Kv6.2 member represented) the second proline of the PXP motif is lacking. The residues proposed to seal off the K^+ pore in *Shaker* (gate residues V478 and F484) are highlighted in blue and the residues at the level of the BC in KcsA are highlighted in purple.

detailed findings and residue numbering are from *Shaker* unless mentioned otherwise.

LOCATION OF THE BUNDLE CROSSING GATE

The first evidence for the presence of a voltage-controllable gate that seals off K^+ permeation at the intracellular entrance of the channel pore came from blocking experiments in giant squid axons using quaternary ammonium (QA) derivatives such as tetraethylammonium (TEA). These seminal studies showed that intracellularly applied QA derivatives blocked the K^+ current only after opening of the channels (Armstrong, 1966, 1971; Armstrong and Hille, 1972). Furthermore, when the QA derivatives were bound and induced current block, they impeded the closure of the intracellular gate during membrane repolarization making the resemblance with a foot in the door mechanism. About 20 years later the first *Shaker* Kv channel was cloned (Papazian et al., 1987; Timpe et al., 1988), and the drug blocking experiments were repeated yielding similar results (K^+ permeation through these *Shaker* channels behaved like the K^+ currents in giant squid axons) strengthening the hypothesis of a gate at the intracellular entrance of the K^+ pore (Choi et al., 1993). With a growing number of cloned Kv channels and improved molecular biology techniques, structure-function mutagenesis studies indicated that residues within the S6 transmembrane segment affected the binding affinity for these QA derivatives (Hartmann et al., 1991; Yellen et al., 1991; Choi et al., 1993; Shieh and Kirsch, 1994; Taglialatela et al., 1994). These results provided the first evidence for the S6 segment being involved in lining the K^+ permeation pathway and housing the intracellularly located activation gate.

The location of this intracellular S6 activation gate was determined by investigating the chemical modification rate of introduced cysteine residues by organic derivates (MTS reagents) and Cd^{2+} (Liu et al., 1997). Comparison of the state-dependent accessibility of several S6 residues (closed vs. open) revealed that the residues above I477 were only modified by MTS reagents or Cd^{2+} – and thus accessible – when the channel gate was open. Residues below I477 were always accessible and no difference was observed between a closed or open gate conformation. The fact that modification of all tested residues was prevented by larger QA derivatives indicated that these residues effectively line the K^+ permeation pathway. From the different residues tested, V474C showed the highest difference in modification rate between the closed and open conformation (Liu et al., 1997; del Camino and Yellen, 2001). Although Cd^{2+} binding to V474C and channel block occurred irreversibly, the unblock could be monitored using reducing reagents (e.g., DTT) and appeared to be highly voltage-dependent suggesting that residue V474 is located above the gate residue(s) that seal off the K^+ pore. The observation that the Cd^{2+} block did not affect the voltage-dependent gating kinetics of the channel led the authors to propose, based on testing different gating schemes, that the position of the cysteine does not change much between the closed and open gate conformation. This supported the hypothesis that the voltage-dependent accessibility to this residue was not because it lies buried within the channel protein in the closed state but because it effectively lines the K^+ permeation pathway and access to it is controlled by the intracellular S6 activation gate below this level (Liu et al., 1997; Webster et al., 2004).

Since the access of Cd^{2+}, that is smaller in size than K^+, was well controlled by this intracellular S6 activation gate it was conceivable that also K^+ would be retained. However, Cd^{2+} is a divalent and has a stronger hydration shell than K^+ making it not a perfect substitute. Repeating the accessibility studies with the monovalent silver Ag^+ ion (that serves as a better substitute for K^+ than Cd^{2+}; Lue and Miller, 1995) showed a 700-fold difference in the modification rate of V474C between the closed and open channel conformation. These data showed that the K^+ flow can be sealed off at the level of his intracellular S6 activation gate (del Camino and Yellen, 2001). However, since also the access of much bigger QA derivatives is controlled, this intracellular S6 activation gate is most likely not involved in determining K^+ selectivity and its sole role would be to control the K^+ flow.

THE INTRACELLULAR CHANNEL GATE WORKS AS A HYDROPHOBIC SEAL

The studies detailed above strongly supported the notion for the presence of an activation gate for K^+ ions in the bottom part of the S6 segment (around or below residue I477) at the intracellular entrance of the channel pore (Liu et al., 1997). In an extensive mutagenesis scan of the S6 to pinpoint the gate residue, all residues were mutated to either a tryptophan or alanine (Hackos et al., 2002). Tryptophan was used to increase side-chain volume substantially as to narrow the gate and promote the closed state. On the contrary, an alanine would reduce side-chain volume and might increase the gate radius which would promote channel opening. The scan revealed residues V478 and F484 as strong candidates to be the effective gate residue(s) (**Figure 1D**; Hackos et al., 2002). In agreement, substituting P475 by a charged aspartate (that results in charge-charge repulsion and thus promotes gate widening) resulted in a constitutive conducting K^+ pore (Sukhareva et al., 2003). Mutating F484 to a cysteine reduced not only the open probability but also the single-channel conductance supporting that this residue forms an energy barrier for electrodiffusion of K^+ ions (Ding and Horn, 2002). The fact that both candidates for being the gate residue(s) were not charged or strongly polarized, favored the idea that the nature of the gate relied on creating a hydrophobic barrier for K^+ ions instead of an electrostatic field effect (del Camino and Yellen, 2001). Accordingly, the channel gate could be trapped in the closed conformation by a tryptophan substitution for residue V478 that resulted in the formation of a hydrophobic seal, strengthening the idea that the gate residue(s) form(s) a steric hindrance for K^+ permeation (Kitaguchi et al., 2004). Energy calculations indicated that with a strong constriction and small pore radii (<2 Å) the energy barrier for K^+ to pass indeed originates from Van der Waals interactions (i.e., a hydrophobic seal; Tai et al., 2009).

The elucidation of the 3D crystal structure of the two transmembrane one pore (2Tm-1P) K channel KcsA, a prokaryotic K channel that is not gated by voltage, provided the first detailed picture of a channel pore and greatly advanced our understanding of ion permeation (Doyle et al., 1998). The two transmembrane segments (M1 and M2) of KcsA correspond to the S5 and S6 segments of the *Shaker* Kv channel and could even substitute them (Lu et al., 2001). The initial suggestion that the KcsA structure represents a well conserved outline of a K^+ pore found in many types of K channels has been confirmed by the crystallization of

other K channels (Jiang et al., 2002a; Tao et al., 2009) including the voltage-gated bacterial KvAP channel (Jiang et al., 2003) and more recently the *Shaker*-related Kv1.2 channel (Long et al., 2005, 2007). The pore, formed by either the M1–M2 or S5–S6 segments and the P-loop between them, shows a fourfold symmetry whereby the individual α-subunits arrange themselves around the ion-conducting pathway that can be divided in three regions. From the intracellular to the extracellular side, the pathway starts with (1) a water filled tunnel which opens into (2) a wider water filled cavity. Both these regions are delineated by the four inner hydrophobic pore helices (the M2 or S6 segments) that cross the membrane under an angle of ∼25° (**Figure 1C**). At the end of the cavity starts (3) a second narrower outer tunnel that is formed by the P-loops and forms the channel's SF that dictates K^+ selectivity.

Since the M2 helices in KcsA traverse the plasma membrane under an angle of ∼25° and cross each other at the intracellular entrance of the pore, the resemblance was made with the supporting rods of an inverted teepee (Doyle et al., 1998). At the BC point of the four helices the channel pore is constricted such that it would be impossible for K^+ to pass, indicating that the initial KcsA structure represented the closed conformation. Based on sequence alignment (**Figure 1D**), the residues that appeared in *Shaker* to be accessible only in the open channel conformation are indeed located above this BC point. Therefore, this BC of the M2 (S6) helices most likely forms the intracellular activation or BC gate. As previously suggested, this BC gate controls the K^+ flow but does not dictate K^+ selectivity which is limited to the SF.

Later, another 2Tm-1P prokaryotic K channel (KirBac1.1) was crystallized in the closed state showing a similar pore architecture as KcsA (Kuo et al., 2003): the M2 helices formed a BC gate and a central cavity that could house hydrated K^+ ions lowering the energetic cost for putting a charged ion in the middle of the lipid bilayer (Doyle et al., 1998; Roux and MacKinnon, 1999). Both structures suggested that closure of the BC gate does not involve a large scale collapse of the permeation pore but is limited to a pore constriction at the level of the BC point. This is further evidenced by the observation that QA derivatives could be trapped behind the intracellular activation (BC) gate upon channel closure in the *Shaker* pore mutant I470C (Holmgren et al., 1997). This indicated that in the I470C mutant there is sufficient room behind the BC gate to house QA derivatives up to a diameter of 8–10 Å. Bigger derivatives do not fit completely and by sticking out they function as a foot in the door keeping the BC gate open upon membrane repolarization that normally promotes channel closure. In the hERG (Kv11.1) Kv channel the space behind the BC gate is even larger than in *Shaker* as also bigger components could be trapped (Mitcheson et al., 2000). Consequently, the BC gate acts as a trap door mechanism for QA derivatives and small blockers such that they are retained within the central cavity behind the closed BC gate (Holmgren et al., 1997; Liu et al., 1997). The crystallization of KcsA in the presence of tetrabutylammonium and subsequent structure determination showed that QA derivates can indeed occupy the central cavity when the channel is closed (Zhou et al., 2001).

Such a trap door mechanism for BC gate operation strengthens the concept that channel closure does not involve mayor rearrangements of the permeation pathway, i.e., a full collapse of the central cavity. However, recent MD simulation studies pointed to the role of hydrophobic changes and dewetting (water leaving) of the pore and cavity for controlling the K^+ flow in Kv channels (Jensen et al., 2010, 2012). Previous simulations on simple nanopores showed that a hydrophobic pore with a diameter of 6 Å forms already a considerable energy barrier for water and consequently hydrated K^+ ions. This indicates that the BC gate does not need to physically occlude completely to a diameter smaller than the size of a K^+ ion (2.66 Å diameter) in order to be functionally closed and shut off the K^+ flow (Beckstein et al., 2003, 2004). In the recently proposed hydrophobic gating mechanism for Kv channels, BC gate closure is preceded by dewetting the pore which is sufficient to terminate the K^+ flow. Conversely, BC gate opening proceeds after rehydration of the pore. These dewetting and rehydration processes involve effective rearrangements of the pore and a partial collapse of the central cavity (Jensen et al., 2010, 2012). Therefore, the hypothesis that the cavity is structurally different between the closed and the open channel state is quite conceivable but a full collapse seems unlikely as it would be inconsistent with the trapping of QA derivatives and other drugs behind the BC gate.

BC GATE MOVEMENT IS UNDER CONTROL OF THE VSD

The BC gate appears to comprise the V478 and/or F484 residues that seal off the permeation pathway by forming a hydrophobic constriction (**Figure 1D**). The observation that (a) accessibility of an introduced cysteine at residue position 474, located above this hydrophobic seal, followed the voltage-dependence of channel opening and (b) mutations in the BC gate region affected the VSD movement (Ding and Horn, 2003) strongly indicated that the BC gate communicates directly with the VSD and forms the channel's main voltage-controllable activation gate.

The conductance for K^+ in the closed state was estimated to be about 100,000 times lower than that of the open state showing tight closure of the ion pore (Soler-Llavina et al., 2003). It has been well established that the channel traverses multiple closed states before reaching the "activated-not-open" state followed by a final transition that results in BC gate opening (Bezanilla et al., 1994; Zagotta et al., 1994; Schoppa and Sigworth, 1998; Zandany et al., 2008). Most of these states reflect different VSD conformations but also the status of the BC gate is different between the activated and the open state (del Camino et al., 2005). This raises the question whether conformational changes of the BC gate in the pre-open states are sufficient to allow ion permeation and result in different conducting states. Due to its fourfold symmetry each channel has four S6 gate regions that each communicate with their own VSD (Labro et al., 2005). For *Shaker* it is generally assumed that the four S6 gate regions operate in a cooperative manner and that BC gate opening occurs in a concerted step (Zandany et al., 2008) when all four VSDs have reached their activated state. However, this does not need to be a universal rule and pre-open BC gate movements might be sufficient to allow passage of K^+ ions in certain K channels. In the case of the Kv2.1 channel (previously named drk1), that has a higher single-channel conductance than *Shaker*, subconductance levels for K^+ have indeed been observed in the early steps of channel opening and during channel closure (Chapman et al., 1997; Chapman and VanDongen, 2005). This suggests that, at least for Kv2.1, the movement of one S6 helix is sufficient to

have partial pore opening which results in subconductance levels. Accordingly, occupancy of the first subconductance state was linked to the movement of the first of the four VSDs (Chapman and VanDongen, 2005).

Possibly, these independent S6 movements can only be observed directly as subconductance states in K^+ channels with a relative high single-channel conductance: in channels with lower single-channel conductance the amplitude of the subconductance states would be too low and hidden within the noise. Alternatively, a tight packing of the S6 helices at the BC imposes a high cooperativity in the movement of the S6 helices and BC gate making the subconductance states too short lived to be detected (Gagnon and Bezanilla, 2010). In *Shaker* the BC gate constriction (S6 bundle packing) in the closed state is probably very tight and BC gate opening occurs in a concerted step that could be isolated by introduction of the ILT mutations in the channel's gating machinery (Ledwell and Aldrich, 1999). Using a mutant *Shaker* construct that displays an increased single-channel conductance and an open state stabilization, subconductance levels were observed during both channel activation and deactivation supporting that subconductance states also exist in *Shaker* but are too short lived or too small to be detected directly (Zheng and Sigworth, 1997, 1998). When the channel opens, the BC gate widens and the S6 BC becomes less packed. Using hidden Markov model analysis subconductance states could indeed be resolved during deactivation of Wild-Type *Shaker* channels (Zheng et al., 2001). Since these subconductance states reflect the behavior of individual subunits, this predicts that ionic current deactivation should follow VSD return. Detailed studies on the movement of the VSD of *Shaker* indeed revealed such a correlation and full BC gate closure (shutting off the K^+ flow) occurred only when the last VSD had returned to its rested state (Bezanilla et al., 1991). Although these data suggest the presence of subconductance levels, shutting down the K^+ flow is most likely not a gradual process that develops with each subunit moving as the largest decay in ionic current deactivation (more than 3/4 of the total amplitude) precedes full gating charge return (Varga et al., 2002). Recent MD modeling studies showed that closure of the S6 gate region from one subunit is sufficient to prevent almost any hydrated K^+ from passing the BC gate indicating that the VSD return of one subunit causes the largest drop in K^+ flow through the pore (Jensen et al., 2010, 2012).

THE BC DIAMETER AS POTENTIAL BASIS FOR SINGLE-CHANNEL CONDUCTANCE AND SUBCONDUCTANCE LEVELS

The underlying structural basis for these subconductance levels in Kv2.1 channels has not been unequivocally determined but most likely they find their origin in individual S6 movements. However, since K^+ conduction in the closed state is about 100,000 times lower than in the open one (Soler-Llavina et al., 2003) but Ag^+ and Cd^{2+} modification of residue V474C displays only a 700-fold difference between both states (del Camino and Yellen, 2001), one may question whether the BC gate is solely responsible for controlling the K^+ flow. Within the mechanism of hydrophobic pore gating (discussed above) these contradicting data could be reconciled if K^+ flow is halted by dewetting the pore which does not require a fully closed BC gate (Jensen et al., 2012). On the other hand, it has been shown that the subconductance levels in the T442S *Shaker* chimera have a different ion selectivity suggesting that also the SF is involved (Zheng and Sigworth, 1997). Since S6 undergoes overall structural changes upon BC gate opening that are transmitted upward along the S6 helix and can trigger the closure of the SF during the process of C-type inactivation (Cuello et al., 2010a,b), it is possible that the conformation of the SF also differs when the BC gate is open or closed. In this speculative scenario the SF would have three main conformations; (1) the SF is in an intermediate conducting state when the BC gate is closed but converts to (2) a higher conducting state upon BC gate opening and finally (3) collapses during C-type inactivation (**Figure 2A**). The observed changes in ion selectivity are in support of this scenario that implies the presence of two activation gates. Fluorescence lifetime spectroscopy in KcsA channels showed indeed a discrepancy between BC gate opening and actual K^+ conduction pointing to a role of the SF as a second gate (Blunck et al., 2006). Interestingly, in several 2Tm-1P K channels (Claydon et al., 2003; Clarke et al., 2010) and in 6Tm-1P cyclic nucleotide gated and Ca^{2+} gated eukaryotic K channels, K^+ permeation seems to be fully controlled at the level of the SF (Sun et al., 1996; Flynn and Zagotta, 2001; Contreras et al., 2008; Thompson and Begenisich, 2012). Although in Kv channels K^+ permeation appears to be mainly controlled by the BC gate, there is strong evidence for a direct communication between the BC gate and the SF (Panyi and Deutsch, 2006; Cuello et al., 2010a,b). Since in most Kv channels full BC gate opening develops during a final concerted step, intra-subunit pre-open S6 movements might already result in rearrangements of both the central cavity and the SF. It has been shown that the conformation of the BC gate (and consequently S6) in the pre-open state differs from the closed and the open one (del Camino et al., 2005). Furthermore, MD simulations show that subtle motions in the side chains of S6 residues can alter the behavior of the subunits and affect larger scale rearrangements (Denning and Woolf, 2010). Such a mechanism of pre-open S6 movements can form the basis for closed state inactivation in certain types of Kv channels (Barghaan and Bahring, 2009; Bahring and Covarrubias, 2011; Bahring et al., 2012) and might explain the modulating role of individual Kv α-subunits in a heterotetrameric configuration as in Kv6.4/Kv2.1 channels (Bocksteins et al., 2012).

Although the exact gate movements remain largely undefined, they must involve movement of the S6 helices relative to each other because a metal bridge between V476C and H486 in adjacent subunits can lock the BC gate in the open state (Holmgren et al., 1998). This strongly suggests that the opening and closure of the BC gate involves larger scale movements of the bottom part of the S6 ($S6_c$) segment. This brings us to the question, does the diameter of BC gate opening determines the single-channel conductance? Residue substitutions in the BC gate vicinity indeed affected the single-channel conductance of Kv channels supporting that the BC gate forms an energy barrier that can affect the K^+ flow rate (Lopez et al., 1994; Shieh and Kirsch, 1994; Ding and Horn, 2002). Substituting the S6 in *Shaker* by Kv3.1 sequence, which has a higher single-channel conductance, indeed resulted in a *Shaker* chimera that displayed an increased single-channel conductance compared to WT channels (Lopez et al., 1994; Taglialatela et al., 1994). Within this chimera the sequence of the SF was conserved and exchanging the SF region between *Shaker* and Kv3.1 had

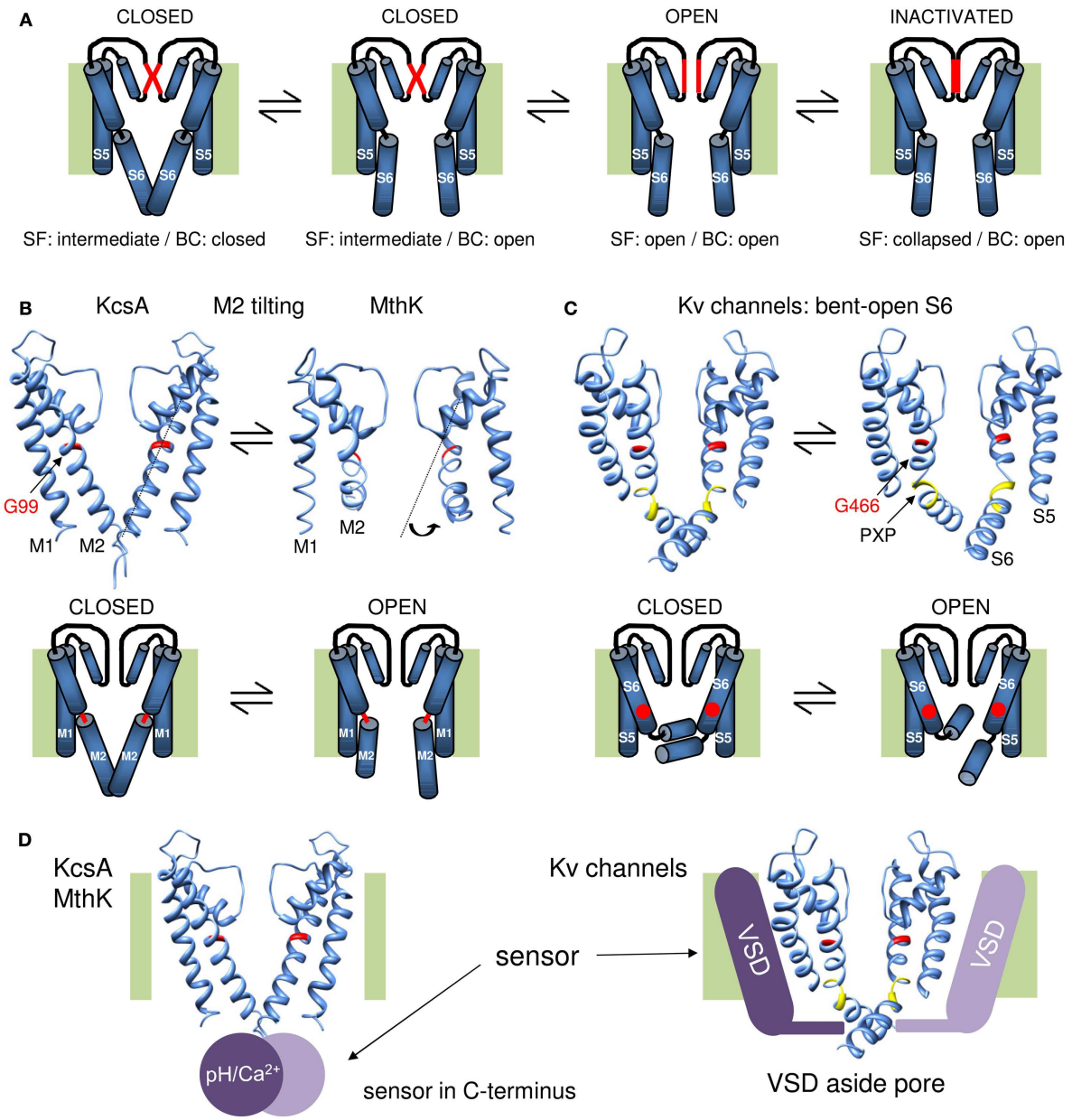

FIGURE 2 | Overview of the gating mechanisms for pore opening in K channels. (A) Cartoon representation of a gating mechanism involving the sequential opening of two gates: the BC and SF gate. Assuming that the SF is in an intermediate conducting state in the closed channel conformation, the channel has both its SF and BC gate closed. Upon membrane depolarization (or other stimulus that triggers channel opening) the BC gate opens but the SF remains in its intermediate conducting state. This BC gate opening subsequently triggers the SF to open and results in full channel opening. Upon prolonged depolarization (or other stimulus) the SF collapses and the channel enters the inactivated state. **(B)** KcsA/MthK gating mechanism that involves conversion of a straight inner M2 pore helix (closed conformation) into a conformation whereby the M2 helix splays open at the level of a conserved glycine residue (G99 in KcsA). On top the 3D crystal structures of KcsA on the left (closed state) and MthK on the right (open conformation, protein data bank accession code 1LNQ; Doyle et al., 1998; Jiang et al., 2002a). Note the different conformation of the M2 helix that tilts at the level of a glycine residue in the middle of the helix (indicated in red). Below a cartoon representation of the proposed gating mechanism whereby the glycine forms a hinge point (indicated in red) and opening of the BC gate requires tilting of the post-hinge M2 segment. **(C)** Proposed gating mechanism for *Shaker*-type Kv channels. On the right the 3D crystal structure of the Kv1.2 channel in the open conformation and on the left a model for the closed state built by Pathak et al. (2007). Note that the inner S6 pore helix remains bent in both closed and open conformation resulting in the "bent-open S6 model" for channel gating. The glycine counterpart that forms the hinge in KcsA/MthK is G466 (indicated in red). However, the bend in S6 is not at this glycine residue but at the conserved PXP motif (colored yellow) located seven residues further downstream. Below a cartoon representation of the proposed gating mechanism whereby G466 is indicated with a red dot. In contrast to the mechanism in **(B)**, most of the reorientations in S6 occur in the vicinity of the PXP motif. **(D)** Illustration for the location of the stimulus sensor in KcsA/MthK vs. Kv channels. Left: the 3D structure of KcsA with the pH sensor (Ca^{2+} sensor in case of MthK) indicated with a purple sphere that locates in the C-terminus underneath the inner M2 pore helix. Right: the Kv1.2 structure with the VSD indicated with a purple bar situated besides/adjacent to the K^+ pore. The different location of the stimulus sensor that controls the status of the BC gate may explain their different gating mechanism proposed in **(B,C)**.

indeed no impact on the single-channel conductance (Taglialatela et al., 1994). Accordingly, the different types of K channels crystallized to date display a very similar SF structure although they have quite different single-channel conductances. Therefore, the SF is most likely not involved in tuning the conductance to this extent, but its configuration is mainly conserved and optimized to highly discriminate K^+ over Na^+ at a 1000:1 ratio and at the same time allowing K^+ flow at a high rate ($\sim 10^7$ ions s^{-1}; Morais-Cabral et al., 2001). Although more experimental support is needed, it appears that the BC gate not only seals off the pore when closed but also controls the K^+ flow rate when open (i.e., the single-channel conductance). Consequently, an alternative and more speculative explanation for the presence of subconductance levels is the existence of intermediate conducting BC gate conformations that originate from non-concerted S6 movements of individual subunits. Indeed, recent studies on the gating mechanism of Kv7.1 (KCNQ1) channels showed that BC gate opening in this type of Kv channels does not require that all four VSDs have moved to their activated state (Ma et al., 2011; Osteen et al., 2012). Although Kv7.1 may be an isolated case, such gating mechanism yields several "intermediate" open states of the BC gate that originate from individual VSD movements.

Although the SF may function as a second gate in series to the BC gate and may undergo conformational changes during activation, most likely the BC gate remains the main activation gate in Kv channels that is under tight control of the VSD. Over the past years a general consensus arose that in most Kv channels the electromechanical coupling that links the BC gate region with the VSD originates from a molecular communication between the S4S5-linker ($S4S5_L$) and $S6_c$ (see Blunck and Batulan, 2012; Vardanyan and Pongs, 2012 in this research topic of Frontiers in Pharmacology). Subsequently, these $S6_c$ movements that lead to BC gate opening are also transmitted along the entire six helix up to the level of the SF that can respond by changing its conformation. The induced conformational change might destabilize the SF and trigger C-type inactivation that results in a full collapse of the SF when all the K^+ ions have left the SF (Baukrowitz and Yellen, 1996; Ogielska and Aldrich, 1999). Consequently, altering the K^+ concentration in the extracellular or intracellular milieu (affecting the K^+ flow through the channel pore) affects the speed of C-type inactivation (Lopez-Barneo et al., 1993; Baukrowitz and Yellen, 1995). Interestingly, these K^+-dependent effects on SF gating and C-type inactivation in general are reflected in the speed of BC gate opening and closure (Starkus et al., 1997; Ader et al., 2009). This indicates that the communication between both gates is mutual and that molecular motions within the SF (i.e., during C-type inactivation) may modulate the behavior of the BC gate which is controlled by the VSD.

MOVEMENTS OF THE BC GATE IN THE TRANSITION FROM CLOSED TO OPEN

The observation that the BC gate could be locked open by the formation of an inter-subunit Cd^{2+} bridge between an introduced cysteine at position V476 (located above the BC) and H483 (located below it) indicated that BC gate opening required movements around the BC point (Holmgren et al., 1998). Electron paramagnetic resonance (EPR) studies of spin-labeled introduced cysteine residues in the vicinity of the BC region in KcsA showed translations and counterclockwise rotations of the M2 helices during BC gate opening. From these distance measurements a gating mechanism was proposed whereby the M2 helices tilt away from the central pore axis and the BC forms an apparatus that from a top view opens and closes like the diaphragm of a camera (Perozo et al., 1999; Liu et al., 2001).

In 2002 the prokaryotic 2Tm-1P Ca^{2+}-activated K channel MthK was the first K channel to be crystallized in the open conformation. This structure showed indeed a tilted M2 helix that splays open below the level of a highly conserved glycine residue (G466 in *Shaker*; Jiang et al., 2002a). Comparing this "bent open" MthK structure with KcsA supported a gating mechanism whereby the M2 helices convert from an almost straight α-helical closed conformation to a bent-open one (Jiang et al., 2002b; **Figure 2B**). Mass tagging experiments in KcsA support this gating model as substantial movements of the intracellular half of the M2 helix were observed during BC gate opening (Kelly and Gross, 2003). An open KcsA model based on the MthK structure suggested that the bottom part of the M2 segment tilts away from the central axis such that the BC point widens up to a 12 Å pore diameter allowing large drug molecules to access the central cavity (Jiang et al., 2002b). Resolving the open state structure of both KcsA (Cuello et al., 2010a,b) and the KirBac3.1 (Bavro et al., 2012) channel showed indeed the bending of the M2 helix whereby the BC widens to a diameter of about 10 Å, which is somewhat smaller than the pore widening in MthK (Liu et al., 2001; Uysal et al., 2011).

While this M2 tilting away from the central pore axis is a very elegant gating mechanism, the question remained whether the BC gate in Kv channels operates in a similar way. The first question is whether the original KcsA and KirBac1.1 structures resemble the closed state of the BC gate in *Shaker*. The finding that the modification of cysteine residues within $S6_c$ is protected by application of pore blockers strongly dispelled this idea and suggested that the S6 helix in *Shaker* remains partly bent even in the closed state (del Camino et al., 2000). Second, Cd^{2+} bridging studies of accessible cysteine residues provided distance constraints and suggested that the $S6_c$ after the BC point remains closer together in the open conformation than in MthK (Webster et al., 2004). This view was confirmed with the 3D crystal structure of the Kv1.2 channel in the open state, but the BC constriction still widens up to 12 Å in diameter which easily allows access of QA derivatives (8–12 Å in diameter; Long et al., 2005). These results resulted to a bent S6 model of the BC gate in *Shaker* for both the open and closed conformation excluding a mechanism whereby the $S6_c$ switched between a straight α-helix and a bent-open situation (del Camino et al., 2000; Webster et al., 2004). Furthermore, this bending of S6 does not occur at G466 but at a conserved PXP motif (P473-X-P475) located further down in S6 (**Figure 1**; del Camino et al., 2000; Long et al., 2005).

Thus while in all K channels investigated to date, an increase in diameter at the level of the BC explains channel opening, the molecular rearrangements appear different. Whereas BC gate opening in the 2Tm-1P channels appears to involve conversion of the M2 helix from a straight to a bent conformation, the S6 helix in Kv channels remains kinked at the level of a conserved PXP motif

resulting in a bent-open S6 conformation in both the open and closed state (**Figures 2B,C**). One notable exception might be the Kv11.1 (hERG) channel that similar as the 2TM-1P channels lacks these proline residues in $S6_c$ making its BC gate structure and gating mechanism different (Cheng and Claydon, 2012). Nevertheless, in both mechanisms of BC gate opening the molecular movements at the $S6_c$ are most likely detected by the SF gate. Crystallographic studies of the KcsA channel indicated that the central located S6 residue F103 (which is the counterpart of I470 in *Shaker*) forms a key residue in the molecular coupling between the BC gate and the SF (Cuello et al., 2010a,b). However, KcsA belongs to the 2TM-1P K channels and although the communication appears to traverse mainly along the S6 segment, the molecular coupling between BC gate and SF may be more complicated in Kv channels with a 6Tm-1P topology. Indeed, investigating the communication between BC gate and C-type inactivation at the SF in the Kv11.1 channel showed that in addition to the S6 segment also other channel regions are involved (Wang et al., 2011). Although these findings do not necessarily apply to all types of Kv channels, they highlight that the coupling between BC gate and SF might be more complex.

OPERATION OF THE BC GATE: REQUIREMENT OF A HINGE REGION

Within either gating mechanism, the opening and closure of the BC gate requires a flexible hinge that decouples the pre- and post-hinge portion of the M2 or S6 helix, respectively. In the context of their propensity to break an α-helix, both glycine and proline residues are the obvious candidates to destabilize the helix and to form a hinge that allows tilting or swiveling motions (Tieleman et al., 2001; Bright and Sansom, 2003). The open pore structure of the prokaryotic channels KcsA (Cuello et al., 2010a,b), KirBac3.1 (Bavro et al., 2012), MthK (Jiang et al., 2002a), and KvAP (Jiang et al., 2003) showed that the bending point of the inner pore helix is at a highly conserved glycine residue in the middle of the helix (Guda et al., 2007). Extrapolating this to *Shaker* (and other Kv channels) suggested that glycine residue 466 (**Figure 1D**) located about eight residues above the BC region would act as the gating hinge (Jiang et al., 2002a,b, 2003; Yifrach and MacKinnon, 2002; Magidovich and Yifrach, 2004). Substituting G466 in *Shaker* by an α-helix promoting alanine residue indeed resulted in non-functional channels that could be rescued by introducing a glycine one position upstream (at residue 465). This highlights the requirement of a glycine in the middle of the S6 segment for voltage-dependent gating in Kv channels (Ding et al., 2005).

Besides this conserved glycine, *Shaker* and other Kv channels contain a tandem proline (PXP) motif seven residues more downstream (**Figure 1D**) that kinks the S6 helix and creates the bent S6 model. In contrast to KcsA, the KirBac1.1 channel has a glycine residue (G143) at the equivalent position of the second proline residue of the PXP motif and it was proposed to form a pivoting point for gating while the centrally conserved G134 (equivalent of G466 in *Shaker*) might be more important for protein packing (Kuo et al., 2003). However, MD simulations showed that the M2 helix displays bending motions at both glycine positions (Domene et al., 2005; Grottesi et al., 2005). In the *Shaker*-type Kv1.5 channel, functional data underscored the need of S6-helix destabilizing proline residues for voltage-dependent channel gating (Labro et al., 2003) and also in other Kv channels alanine substitutions for the prolines of the PXP motif were not well tolerated (Hackos et al., 2002; Yifrach and MacKinnon, 2002; Harris et al., 2003; Bhattacharji et al., 2006; Seebohm et al., 2006). Furthermore, exchanging the pore module of *Shaker* by its KcsA counterpart that contained the glycine but not the PXP motif resulted in electrically silent channels (Caprini et al., 2001) but a voltage-dependent chimera was obtained when the PXP sequence was re-introduced (Lu et al., 2002; Caprini et al., 2005). These data underscored the importance of this PXP motif for voltage-dependent channel gating which was further supported by the 3D crystal structure of Kv1.2 showing that the S6 helix indeed bends open at this PXP motif (Long et al., 2005). Interestingly, the so-called "silent" Kv channels (that are unable to form functional homotetrameric Kv channels) all lack the second proline of the PXP motif (**Figure 1D**; Bocksteins and Snyders, 2012).

Does this PXP motif forms a rigid kink or does it function as a flexible hinge? The observation that mutations of this motif affect the channel's gating kinetics (Hackos et al., 2002; Labro et al., 2003) and that substituting the PXPV sequence in Kv1.5 by AXPP resulted in channels that switched between a fast and a slow activation mode, strongly support the notion that this region reorients during BC gate opening and closure (Labro et al., 2008). In addition to these functional studies, several MD simulations showed an increased flexibility of the S6 helix in the vicinity of the PXP motif and support the formation of a gating hinge at this level (Mashl and Jakobsson, 2008; Imbrici et al., 2009; Denning and Woolf, 2010). These simulations also strengthen the difference in the mechanism of BC gate opening in channels that only possess the central glycine (KcsA/MthK) and the PXP containing Kv channels (Choe and Grabe, 2009).

Metal-bridging studies of the V474C mutant (which is the central residue of the PXP motif) showed that the position of the side chain does not change much with opening suggesting that the residue remains quite stationary during gating (Webster et al., 2004). Although speculative, this suggests that the largest part of the machinery that moves for opening or closing the BC gate is around or downstream of this valine residue. Thus in *Shaker*-type channels the PXP motif would form the main gating hinge or at least creates a second one in addition to the conserved glycine (G466 in *Shaker)* that is flexible in channels like KcsA, MthK, KvAP, and GIRK4 (Jiang et al., 2002a,b, 2003; Jin et al., 2002). In KCNQ1 (Kv7.1) channels the central glycine is missing and the PAG motif (homologous to the *Shaker* PXP motif, **Figure 1D**) is most important for channel gating (Seebohm et al., 2006). In contrast, its closest relative KCNQ2 does possess the central glycine and mutation to an alanine is not tolerated making firm conclusions based on sequence similarities difficult (Seebohm et al., 2006). Studies in Kir3.4 showed that pivoting does not occur at the glycine itself but one residue upstream (Rosenhouse-Dantsker and Logothetis, 2006). Although glycine and proline are the residues that have the highest intrinsic propensity for destabilizing an α-helix, the effective degree of destabilization and helix rigidity is determined by the overall residue composition of the helix (Rosenhouse-Dantsker and Logothetis, 2006).

In contrast to the other Kv channels, the hERG channel does not contain a PXP motif in the $S6_C$ suggesting that its closed state resembles more the straight α-helix KcsA conformation than the bent-open Kv model. However, besides the centrally located glycine, hERG contains also a glycine at the level of the PXP motif (**Figure 1D**). Remarkably, both glycine residues are not important for voltage-dependent channel gating which led to the idea that the S6 helix of hERG is indeed more rigid than that of other Kv channels (Hardman et al., 2007). Such a difference in rigidity might result in a different mechanistic operation of the BC gate (Cheng and Claydon, 2012). Depending on the preferred conformation of the BC gate, the work performed by the VSD is either to open the gate or to close it. It is quite possible that the preferred (lowest energy) conformational state of the BC gate differs between the different types of Kv channels. For *Shaker* it has been proposed that the BC gate prefers the closed conformation because mutations more often promote the open state than the closed one indicating that the latter is harder to affect and thus represents the intrinsic lower state (Yifrach and MacKinnon, 2002). However, some caution is needed because if the mutation distorts the coupling with the VSD then the opposite is true which might be the scenario in the hERG and KCNQ1 channels (Tristani-Firouzi et al., 2002; Ferrer et al., 2006; Choveau et al., 2011; Labro et al., 2011). Furthermore, the work performed by the VSD might also be dual since both the open and closed conformations of the BC gate represent an energetic minimum. Indeed, it has been shown that BC gate opening stabilizes the VSD in the open conformation (Batulan et al., 2010). Consequently, the VSD needs to pull the BC gate open, but once the gate is fully open the VSD needs to push actively to close it again (Jensen et al., 2012).

In conclusion, K channels contain two gates in series: (1) the BC gate located at the intracellular BC of the inner pore helix (M2 or S6) and (2) the SF gate at the extracellular end of the pore (**Figure 1C**). Consequently, upon membrane depolarization the K^+ pore traverses a sequence of events that most likely includes the following conformations (excluding closed state inactivation): (1) BC-closed/SF-intermediate, (2) BC-open/SF-intermediate, (3) BC-open/SF-open, and (4) BC-open/SF-inactivated (**Figure 2**). In Kv channels, and most likely also the other types of K channels, the BC gate is the main activation gate that is under control of various environmental stimuli such as the membrane potential. From the point of view of the K^+ ion, the BC gate apparatus displays an iris-like motion at the level where the inner helices cross similar to the opening or closure of the diaphragm from a camera. Two main gating mechanisms have been proposed, in case of the 2TM-1P K channels KcsA and MthK the inner M2 pore helix tilts away from the central K^+ permeation pathway and converts from an almost straight α-helix conformation (BC gate closed) to a bent one (BC gate open; **Figure 2B**). In Kv channels the inner S6 pore helix remains bent in both the open and the closed state (bent-open S6 model) displaying most likely more swiveling motions (**Figure 2C**). The difference between inner pore (BC gate) movements may find its origin in their mechanism of channel opening/closure: BC gate opening in KcsA or MthK relies on pH or Ca^{2+} sensing that involves structural changes in the C-terminally located pH/Ca^{2+} sensing domain (Jiang et al., 2002a; Thompson et al., 2008; Uysal et al., 2009, 2011); in contrast, the BC gate in Kv channels is under direct control of the VSD that is located next to it (Long et al., 2005), and the $S6_C$ probably needs to remain bent to maintain contact with the VSD in the closed state (**Figure 2D**). However, while the VSD directly controls the status of the BC gate, it is not the sole modulator for the overall channel status and conformational changes in NH_2- and COOH-terminal domains can modulate the gating kinetics (Barros et al., 2012).

ACKNOWLEDGMENTS

This work was supported by the Research Foundation Flanders (FWO, Fonds voor Wetenschappelijk Onderzoek Vlaanderen) grants G.0449.11 (to Dirk J. Snyders) and 1.5.087.11N (to Alain J. Labro).

REFERENCES

Ader, C., Schneider, R., Hornig, S., Velisetty, P., Vardanyan, V., Giller, K., Ohmert, I., Becker, S., Pongs, O., and Baldus, M. (2009). Coupling of activation and inactivation gate in a K^+-channel: potassium and ligand sensitivity. *EMBO J.* 28, 2825–2834.

Armstrong, C. M. (1966). Time course of TEA^+-induced anomalous rectification in squid giant axon. *J. Gen. Physiol.* 50, 491–503.

Armstrong, C. M. (1971). Interaction of tetraethylammonium ion derivatives with the potassium channels of giant axons. *J. Gen. Physiol.* 58, 413–437.

Armstrong, C. M., and Hille, B. (1972). The inner quaternary ammonium ion receptor in potassium channels of the node of Ranvier. *J. Gen. Physiol.* 59, 388–400.

Bahring, R., Barghaan, J., Westermeier, R., and Wollberg, J. (2012). Voltage sensor inactivation in potassium channels. *Front. Pharmacol.* 3:100. doi:10.3389/fphar.2012.00100

Bahring, R., and Covarrubias, M. (2011). Mechanisms of closed-state inactivation in voltage-gated ion channels. *J. Physiol. (Lond.)* 589, 461–479.

Barghaan, J., and Bahring, R. (2009). Dynamic coupling of voltage sensor and gate involved in closed-state inactivation of kv4.2 channels. *J. Gen. Physiol.* 133, 205–224.

Barros, F., Dominguez, P., and de la Pena, P. (2012). Cytoplasmic domains and voltage-dependent potassium channel gating. *Front. Pharmacol.* 3:49. doi:10.3389/fphar.2012.00049

Batulan, Z., Haddad, G. A., and Blunck, R. (2010). An intersubunit interaction between S4–S5 linker and S6 is responsible for the slow off-gating component in Shaker K^+ channels. *J. Biol. Chem.* 285, 14005–14019.

Baukrowitz, T., and Yellen, G. (1995). Modulation of K current by frequency and external $[K^+]$: a tale of two inactivation mechanisms. *Neuron* 15, 951–960.

Baukrowitz, T., and Yellen, G. (1996). Use-dependent blockers and exit rate of the last ion from the multi-ion pore of a K^+ channel. *Science* 271, 653–656.

Bavro, V. N., De, Z. R., Schmidt, M. R., Muniz, J. R., Zubcevic, L., Sansom, M. S., Venien-Bryan, C., and Tucker, S. J. (2012). Structure of a KirBac potassium channel with an open bundle crossing indicates a mechanism of channel gating. *Nat. Struct. Mol. Biol.* 19, 158–163.

Beckstein, O., Biggin, P. C., Bond, P., Bright, J. N., Domene, C., Grottesi, A., Holyoake, J., and Sansom, M. S. (2003). Ion channel gating: insights via molecular simulations. *FEBS Lett.* 555, 85–90.

Beckstein, O., Tai, K., and Sansom, M. S. (2004). Not ions alone: barriers to ion permeation in nanopores and channels. *J. Am. Chem. Soc.* 126, 14694–14695.

Bezanilla, F., Perozo, E., Papazian, D. M., and Stefani, E. (1991). Molecular basis of gating charge immobilization in *Shaker* potassium channels. *Science* 254, 679–683.

Bezanilla, F., Perozo, E., and Stefani, E. (1994). Gating of *Shaker* K^+ channels: II. The components of gating currents and a model of channel activation. *Biophys. J.* 66, 1011–1021.

Bhattacharji, A., Kaplan, B., Harris, T., Qu, X., Germann, M. W., and Covarrubias, M. (2006). The concerted contribution of the S4–S5 linker and the S6 segment to the modulation of a Kv channel by 1-alkanols. *Mol. Pharmacol.* 70, 1542–1554.

Blunck, R., and Batulan, Z. (2012). Mechanism of electromechanical coupling in voltage-gated potassium channels. *Front. Pharmacol.* 3:166. doi:10.3389/fphar.2012.00166

Blunck, R., Cordero-Morales, J. F., Cuello, L. G., Perozo, E., and Bezanilla, F. (2006). Detection of the opening of the bundle crossing in KcsA with fluorescence lifetime spectroscopy reveals the existence of two gates for ion conduction. *J. Gen. Physiol.* 128, 569–581.

Bocksteins, E., Labro, A. J., Snyders, D. J., and Mohapatra, D. P. (2012). The electrically silent kv6.4 subunit confers hyperpolarized gating charge movement in kv2.1/kv6.4 heterotetrameric channels. *PLoS ONE* 7, e37143. doi:10.1371/journal.pone.0037143

Bocksteins, E., and Snyders, D. J. (2012). Electrically silent kv subunits: their molecular and functional characteristics. *Physiology (Bethesda)* 27, 73–84.

Bright, J. N., and Sansom, M. S. P. (2003). The flexing/twirling helix: exploring the flexibility about molecular hinges formed by proline and glycine motifs in transmembrane helices. *J. Phys. Chem. B* 107, 627–636.

Caprini, M., Fava, M., Valente, P., Fernandez-Ballester, G., Rapisarda, C., Ferroni, S., and Ferrer-Montiel, A. (2005). Molecular compatibility of the channel gate and the N terminus of S5 segment for voltage-gated channel activity. *J. Biol. Chem.* 280, 18253–18264.

Caprini, M., Ferroni, S., Planells-Cases, R., Rueda, J., Rapisarda, C., Ferrer-Montiel, A., and Montal, M. (2001). Structural compatibility between the putative voltage sensor of voltage-gated K^+ channels and the prokaryotic KcsA channel. *J. Biol. Chem.* 276, 21070–21076.

Chapman, M. L., and VanDongen, A. M. (2005). K channel subconductance levels result from heteromeric pore conformations. *J. Gen. Physiol.* 126, 87–103.

Chapman, M. L., VanDongen, H. M., and VanDongen, A. M. (1997). Activation-dependent subconductance levels in the drk1 K channel suggest a subunit basis for ion permeation and gating. *Biophys. J.* 72, 708–719.

Cheng, Y. M., and Claydon, T. W. (2012). Voltage-dependent gating of HERG potassium channels. *Front. Pharmacol.* 3:83. doi:10.3389/fphar.2012.00083

Choe, S., and Grabe, M. (2009). Conformational dynamics of the inner pore helix of voltage-gated potassium channels. *J. Chem. Phys.* 130, 215103.

Choi, K. L., Mossman, C., Aube, J., and Yellen, G. (1993). The internal quaternary ammonium receptor site of *Shaker* potassium channels. *Neuron* 10, 533–541.

Choveau, F. S., Rodriguez, N., Ali, F. A., Labro, A. J., Rose, T., Dahimene, S., Boudin, H., Le, H. C., Escande, D., Snyders, D. J., Charpentier, F., Merot, J., Baro, I., and Loussouarn, G. (2011). KCNQ1 channels voltage dependence through a voltage-dependent binding of the S4–S5 linker to the pore domain. *J. Biol. Chem.* 286, 707–716.

Clarke, O. B., Caputo, A. T., Hill, A. P., Vandenberg, J. I., Smith, B. J., and Gulbis, J. M. (2010). Domain reorientation and rotation of an intracellular assembly regulate conduction in Kir potassium channels. *Cell* 141, 1018–1029.

Claydon, T. W., Makary, S. Y., Dibb, K. M., and Boyett, M. R. (2003). The selectivity filter may act as the agonist-activated gate in the G protein-activated Kir3.1/Kir3.4 K+ channel. *J. Biol. Chem.* 278, 50654–50663.

Contreras, J. E., Srikumar, D., and Holmgren, M. (2008). Gating at the selectivity filter in cyclic nucleotide-gated channels. *Proc. Natl. Acad. Sci. U.S.A.* 105, 3310–3314.

Cuello, L. G., Jogini, V., Cortes, D. M., Pan, A. C., Gagnon, D. G., Dalmas, O., Cordero-Morales, J. F., Chakrapani, S., Roux, B., and Perozo, E. (2010a). Structural basis for the coupling between activation and inactivation gates in K(+) channels. *Nature* 466, 272–275.

Cuello, L. G., Jogini, V., Cortes, D. M., and Perozo, E. (2010b). Structural mechanism of C-type inactivation in K(+) channels. *Nature* 466, 203–208.

del Camino, D., Holmgren, M., Liu, Y., and Yellen, G. (2000). Blocker protection in the pore of a voltage-gated K^+ channel and its structural implications. *Nature* 403, 321–325.

del Camino, D., Kanevsky, M., and Yellen, G. (2005). Status of the intracellular gate in the activated-not-open state of Shaker K+ channels. *J. Gen. Physiol.* 126, 419–428.

del Camino, D., and Yellen, G. (2001). Tight steric closure at the intracellular activation gate of a voltage-gated K(+) channel. *Neuron* 32, 649–656.

Delemotte, L., Klein, M. L., and Tarek, M. (2012). Molecular dynamics simulations of voltage-gated cation channels: insights on voltage-sensor domain function and modulation. *Front. Pharmacol.* 3:97. doi:10.3389/fphar.2012.00097

Denning, E. J., and Woolf, T. B. (2010). Cooperative nature of gating transitions in K(+) channels as seen from dynamic importance sampling calculations. *Proteins* 78, 1105–1119.

Ding, S., and Horn, R. (2002). Tail end of the s6 segment: role in permeation in Shaker potassium channels. *J. Gen. Physiol.* 120, 87–97.

Ding, S., and Horn, R. (2003). Effect of S6 tail mutations on charge movement in Shaker potassium channels. *Biophys. J.* 84, 295–305.

Ding, S., Ingleby, L., Ahern, C. A., and Horn, R. (2005). Investigating the putative glycine hinge in Shaker potassium channel. *J. Gen. Physiol.* 126, 213–226.

Domene, C., Doyle, D. A., and Venien-Bryan, C. (2005). Modeling of an ion channel in its open conformation. *Biophys. J.* 89, L01–L03.

Doyle, D. A., Cabral, J. M., Pfuetzner, R. A., Kuo, A., Gulbis, J. M., Cohen, S. L., Chait, B. T., and MacKinnon, R. (1998). The structure of the potassium channel: molecular basis of K^+ conduction and selectivity. *Science* 280, 69–77.

Ferrer, T., Rupp, J., Piper, D. R., and Tristani-Firouzi, M. (2006). The S4-S5 linker directly couples voltage sensor movement to the activation gate in the human ether-a-go-go-related gene (hERG) K+ channel. *J. Biol. Chem.* 281, 12858–12864.

Flynn, G. E., and Zagotta, W. N. (2001). Conformational changes in S6 coupled to the opening of cyclic nucleotide-gated channels. *Neuron* 30, 689–698.

Gagnon, D. G., and Bezanilla, F. (2010). The contribution of individual subunits to the coupling of the voltage sensor to pore opening in Shaker K channels: effect of ILT mutations in heterotetramers. *J. Gen. Physiol.* 136, 555–568.

Grottesi, A., Domene, C., Hall, B., and Sansom, M. S. (2005). Conformational dynamics of M2 helices in KirBac channels: helix flexibility in relation to gating via molecular dynamics simulations. *Biochemistry* 44, 14586–14594.

Guda, P., Bourne, P. E., and Guda, C. (2007). Conserved motifs in voltage-sensing and pore-forming modules of voltage-gated ion channel proteins. *Biochem. Biophys. Res. Commun.* 352, 292–298.

Hackos, D. H., Chang, T. H., and Swartz, K. J. (2002). Scanning the intracellular s6 activation gate in the Shaker K(+) channel. *J. Gen. Physiol.* 119, 521–532.

Hardman, R. M., Stansfeld, P. J., Dalibalta, S., Sutcliffe, M. J., and Mitcheson, J. S. (2007). Activation gating of hERG potassium channels: S6 glycines are not required as gating hinges. *J. Biol. Chem.* 282, 31972–31981.

Harris, T., Graber, A. R., and Covarrubias, M. (2003). Allosteric modulation of a neuronal K+ channel by 1-alkanols is linked to a key residue in the activation gate. *Am. J. Physiol. Cell Physiol.* 285, C788–C796.

Hartmann, H. A., Kirsch, G. E., Drewe, J. A., Taglialatela, M., Joho, R. H., and Brown, A. M. (1991). Exchange of conduction pathways between two related K^+ channels. *Science* 251, 942–944.

Heginbotham, L., Lu, Z., Abramson, T., and MacKinnon, R. (1994). Mutations in the K^+ channel signature sequence. *Biophys. J.* 66, 1061–1067.

Hille, B. (2001). *Ion Channels of Excitable Membranes.* Sunderland, MA: Sinauer.

Holmgren, M., Shin, K. S., and Yellen, G. (1998). The activation gate of a voltage-gated K^+ channel can be trapped in the open state by an intersubunit metal bridge. *Neuron* 21, 617–621.

Holmgren, M., Smith, P. L., and Yellen, G. (1997). Trapping of organic blockers by closing of voltage-dependent K^+ channels: evidence for a trap door mechanism of activation gating. *J. Gen. Physiol.* 109, 527–535. [see comments].

Imbrici, P., Grottesi, A., D'Adamo, M. C., Mannucci, R., Tucker, S. J., and Pessia, M. (2009). Contribution of the central hydrophobic residue in the PXP motif of voltage-dependent K+ channels to S6 flexibility and gating properties. *Channels (Austin)* 3, 39–45.

Jensen, M. O., Borhani, D. W., Lindorff-Larsen, K., Maragakis, P., Jogini, V., Eastwood, M. P., Dror, R. O., and Shaw, D. E. (2010). Principles of conduction and hydrophobic gating in K+ channels. *Proc. Natl. Acad. Sci. U.S.A.* 107, 5833–5838.

Jensen, M. O., Jogini, V., Borhani, D. W., Leffler, A. E., Dror, R. O., and Shaw, D. E. (2012). Mechanism of voltage gating in potassium channels. *Science* 336, 229–233.

Jiang, Y., Lee, A., Chen, J., Cadene, M., Chait, B. T., and MacKinnon, R. (2002a). Crystal structure and mechanism of a calcium-gated potassium channel. *Nature* 417, 515–522.

Jiang, Y., Lee, A., Chen, J., Cadene, M., Chait, B. T., and MacKinnon, R. (2002b). The open pore conformation of potassium channels. *Nature* 417, 523–526.

Jiang, Y., Lee, A., Chen, J., Ruta, V., Cadene, M., Chait, B. T., and MacKinnon, R. (2003). X-ray structure of a voltage-dependent K(+) channel. *Nature* 423, 33–41.

Jin, T., Peng, L., Mirshahi, T., Rohacs, T., Chan, K. W., Sanchez, R., and Logothetis, D. E. (2002). The (beta)gamma subunits of G proteins gate a K(+) channel by pivoted bending of a transmembrane segment. *Mol. Cell* 10, 469–481.

Kelly, B. L., and Gross, A. (2003). Potassium channel gating observed with site-directed mass tagging. *Nat. Struct. Biol.* 10, 280–284.

Kitaguchi, T., Sukhareva, M., and Swartz, K. J. (2004). Stabilizing the closed S6 gate in the Shaker Kv channel through modification of a hydrophobic seal. *J. Gen. Physiol.* 124, 319–332.

Kuo, A., Gulbis, J. M., Antcliff, J. F., Rahman, T., Lowe, E. D., Zimmer, J., Cuthbertson, J., Ashcroft, F. M., Ezaki, T., and Doyle, D. A. (2003). Crystal structure of the potassium channel KirBac1.1 in the closed state. *Science* 300, 1922–1926.

Labro, A. J., Boulet, I. R., Choveau, F. S., Mayeur, E., Bruyns, T., Loussouarn, G., Raes, A. L., and Snyders, D. J. (2011). The S4-S5 linker of KCNQ1 channels forms a structural scaffold with the S6 segment controlling gate closure. *J. Biol. Chem.* 286, 717–725.

Labro, A. J., Grottesi, A., Sansom, M. S., Raes, A. L., and Snyders, D. J. (2008). A Kv channel with an altered activation gate sequence displays both "fast" and "slow" activation kinetics. *Am. J. Physiol. Cell Physiol.* 294, C1476–C1484.

Labro, A. J., Raes, A. L., Bellens, I., Ottschytsch, N., and Snyders, D. J. (2003). Gating of Shaker-type channels requires the flexibility of S6 caused by prolines. *J. Biol. Chem.* 278, 50724–50731.

Labro, A. J., Raes, A. L., and Snyders, D. J. (2005). Coupling of voltage sensing to channel opening reflects intrasubunit interactions in kv channels. *J. Gen. Physiol.* 125, 71–80.

Ledwell, J. L., and Aldrich, R. W. (1999). Mutations in the S4 region isolate the final voltage-dependent cooperative step in potassium channel activation. *J. Gen. Physiol.* 113, 389–414.

Liu, Y., Holmgren, M., Jurman, M. E., and Yellen, G. (1997). Gated access to the pore of a voltage-dependent K^+ channel. *Neuron* 19, 175–184.

Liu, Y., Jurman, M. E., and Yellen, G. (1996). Dynamic rearrangement of the outer mouth of a K^+ channel during gating. *Neuron* 16, 859–867.

Liu, Y. S., Sompornpisut, P., and Perozo, E. (2001). Structure of the KcsA channel intracellular gate in the open state. *Nat. Struct. Biol.* 8, 883–887.

Long, S. B., Campbell, E. B., and MacKinnon, R. (2005). Crystal structure of a mammalian voltage-dependent *Shaker* family K^+ channel. *Science* 309, 897–903.

Long, S. B., Tao, X., Campbell, E. B., and MacKinnon, R. (2007). Atomic structure of a voltage-dependent K+ channel in a lipid membrane-like environment. *Nature* 450, 376–382.

Loots, E., and Isacoff, E. Y. (1998). Protein rearrangements underlying slow inactivation of the *Shaker* K^+ channel. *J. Gen. Physiol.* 112, 377–389.

Lopez, G. A., Jan, Y. N., and Jan, L. Y. (1994). Evidence that the S6 segment of the *Shaker* voltage-gated K^+ channel comprises part of the pore. *Nature* 367, 179–182.

Lopez-Barneo, J., Hoshi, T., Heinemann, S. H., and Aldrich, R. W. (1993). Effects of external cations and mutations in the pore region on C-type inactivation of *Shaker* potassium channels. *Recept. Channels* 1, 61–71.

Lu, Z., Klem, A. M., and Ramu, Y. (2001). Ion conduction pore is conserved among potassium channels. *Nature* 413, 809–813.

Lu, Z., Klem, A. M., and Ramu, Y. (2002). Coupling between voltage sensors and activation gate in voltage-gated K^+ channels. *J. Gen. Physiol.* 120, 663–676.

Lue, Q., and Miller, C. (1995). Silver as a probe of pore-forming residues in a potassium channel. *Science* 268, 304–307.

Ma, L. J., Ohmert, I., and Vardanyan, V. (2011). Allosteric features of KCNQ1 gating revealed by alanine scanning mutagenesis. *Biophys. J.* 100, 885–894.

MacKinnon, R. (1991). Determination of the subunit stoichiometry of a voltage-activated K channel. *Nature* 350, 232–235.

Magidovich, E., and Yifrach, O. (2004). Conserved gating hinge in ligand- and voltage-dependent K+ channels. *Biochemistry* 43, 13242–13247.

Mashl, R. J., and Jakobsson, E. (2008). End-point targeted molecular dynamics: large-scale conformational changes in potassium channels. *Biophys. J.* 94, 4307–4319.

Mitcheson, J. S., Chen, J., and Sanguinetti, M. C. (2000). Trapping of a methanesulfonanilide by closure of the HERG potassium channel activation gate. *J. Gen. Physiol.* 115, 229–240.

Morais-Cabral, J. H., Zhou, Y., and MacKinnon, R. (2001). Energetic optimization of ion conduction rate by the K^+ selectivity filter. *Nature* 414, 37–42.

Ogielska, E. M., and Aldrich, R. W. (1999). Functional consequences of a decreased potassium affinity in a potassium channel pore. Ion interactions and C-type inactivation. *J. Gen. Physiol.* 113, 347–358.

Osteen, J. D., Barro-Soria, R., Robey, S., Sampson, K. J., Kass, R. S., and Larsson, H. P. (2012). Allosteric gating mechanism underlies the flexible gating of KCNQ1 potassium channels. *Proc. Natl. Acad. Sci. U.S.A.* 109, 7103–7108.

Panyi, G., and Deutsch, C. (2006). Cross talk between activation and slow inactivation gates of Shaker potassium channels. *J. Gen. Physiol.* 128, 547–559.

Papazian, D. M., Schwarz, T. L., Tempel, B. L., Jan, Y. N., and Jan, L. Y. (1987). Cloning of genomic and complementary DNA from *Shaker*, a putative potassium channels gene from Drosophila. *Science* 237, 749–753.

Pathak, M. M., Yarov-Yarovoy, V., Agarwal, G., Roux, B., Barth, P., Kohout, S., Tombola, F., and Isacoff, E. Y. (2007). Closing in on the resting state of the *Shaker* K channel. *Neuron* 56, 124–140.

Perozo, E., Cortes, D. M., and Cuello, L. G. (1999). Structural rearrangements underlying K^+-channel activation gating. *Science* 285, 73–78.

Rosenhouse-Dantsker, A., and Logothetis, D. E. (2006). New roles for a key glycine and its neighboring residue in potassium channel gating. *Biophys. J.* 91, 2860–2873.

Roux, B., and MacKinnon, R. (1999). The cavity and pore helices in the KcsA K^+ channel: electrostatic stabilization of monovalent cations. *Science* 285, 100–102.

Schoppa, N. E., and Sigworth, F. J. (1998). Activation of Shaker potassium channels. III. An activation gating model for wild-type and V2 mutant channels. *J. Gen. Physiol.* 111, 313–342.

Seebohm, G., Strutz-Seebohm, N., Ureche, O. N., Baltaev, R., Lampert, A., Kornichuk, G., Kamiya, K., Wuttke, T. V., Lerche, H., Sanguinetti, M. C., and Lang, F. (2006). Differential roles of S6 domain hinges in the gating of KCNQ potassium channels. *Biophys. J.* 90, 2235–2244.

Shieh, C. C., and Kirsch, G. E. (1994). Mutational analysis of ion conduction and drug binding sites in the inner mouth of voltage-gated K^+ channels. *Biophys. J.* 67, 2316–2325.

Soler-Llavina, G. J., Holmgren, M., and Swartz, K. J. (2003). Defining the conductance of the closed state in a voltage-gated K^+ channel. *Neuron* 38, 61–67.

Starkus, J. G., Kuschel, L., Rayner, M. D., and Heinemann, S. H. (1997). Ion conduction through C-type inactivated *Shaker* channels. *J. Gen. Physiol.* 110, 539–550.

Sukhareva, M., Hackos, D. H., and Swartz, K. J. (2003). Constitutive activation of the *Shaker* Kv channel. *J. Gen. Physiol.* 122, 541–556.

Sun, Z. P., Akabas, M. H., Goulding, E. H., Karlin, A., and Siegelbaum, S. A. (1996). Exposure of residues in the cyclic nucleotide-gated channel pore: P region structure and function in gating. *Neuron* 16, 141–149.

Taglialatela, M., Champagne, M. S., Drewe, J. A., and Brown, A. M. (1994). Comparison of H5, S6, and H5-S6 exchanges on pore properties of voltage-dependent K^+ channels. *J. Biol. Chem.* 269, 13867–13873.

Tai, K., Haider, S., Grottesi, A., and Sansom, M. S. (2009). Ion channel gates: comparative analysis of energy barriers. *Eur. Biophys. J.* 38, 347–354.

Tao, X., Avalos, J. L., Chen, J., and MacKinnon, R. (2009). Crystal structure of the eukaryotic strong inward-rectifier K+ channel Kir2.2 at 3.1 A resolution. *Science* 326, 1668–1674.

Thompson, A. N., Posson, D. J., Parsa, P. V., and Nimigean, C. M. (2008). Molecular mechanism of pH sensing in KcsA potassium channels. *Proc. Natl. Acad. Sci. U.S.A.* 105, 6900–6905.

Thompson, J., and Begenisich, T. (2012). Selectivity filter gating in large-conductance Ca^{2+}-activated K+ channels. *J. Gen. Physiol.* 139, 235–244.

Tieleman, D. P., Shrivastava, I. H., Ulmschneider, M. R., and Sansom, M. S. (2001). Proline-induced hinges in transmembrane helices: possible roles in ion channel gating. *Proteins* 44, 63–72.

Timpe, L. C., Schwarz, T. L., Tempel, B. L., Papazian, D. M., Jan, Y. N., and Jan, L. Y. (1988). Expression of functional potassium channels from *Shaker* cDNA in Xenopus oocytes. *Nature* 331, 143–145.

Tristani-Firouzi, M., Chen, J., and Sanguinetti, M. C. (2002). Interactions between S4–S5 linker and S6 transmembrane domain modulate gating of HERG K^+ channels. *J. Biol. Chem.* 277, 18994–19000.

Uysal, S., Cuello, L. G., Cortes, D. M., Koide, S., Kossiakoff, A. A., and Perozo, E. (2011). Mechanism of activation gating in the full-length KcsA K^+ channel. *Proc. Natl. Acad. Sci. U.S.A.* 108, 11896–11899.

Uysal, S., Vasquez, V., Tereshko, V., Esaki, K., Fellouse, F. A., Sidhu, S. S., Koide, S., Perozo, E., and Kossiakoff, A. (2009). Crystal structure of full-length KcsA in its closed conformation. *Proc. Natl. Acad. Sci. U.S.A.* 106, 6644–6649.

Vardanyan, V., and Pongs, O. (2012). Coupling of voltage-sensors to the channel pore: a comparative view. *Front. Pharmacol.* 3:145. doi: 10.3389/fphar.2012.00145

Varga, Z., Rayner, M. D., and Starkus, J. G. (2002). Cations affect the rate of gating charge recovery in wild-type and W434F Shaker channels through a variety of mechanisms. *J. Gen. Physiol.* 119, 467–485.

Wang, D. T., Hill, A. P., Mann, S. A., Tan, P. S., and Vandenberg, J. I. (2011). Mapping the sequence of conformational changes underlying selectivity filter gating in the K(v)11.1 potassium channel. *Nat. Struct. Mol. Biol.* 18, 35–41.

Webster, S. M., Del Camino, D., Dekker, J. P., and Yellen, G. (2004). Intracellular gate opening in Shaker K+ channels defined by high-affinity metal bridges. *Nature* 428, 864–868.

Yellen, G., Jurman, M. E., Abramson, T., and MacKinnon, R. (1991). Mutations affecting internal TEA blockade identify the probable pore-forming region of a K^+ channel. *Science* 251, 939–942.

Yifrach, O., and MacKinnon, R. (2002). Energetics of pore opening in a voltage-gated k(+) channel. *Cell* 111, 231–239.

Zagotta, W. N., Hoshi, T., Dittman, J., and Aldrich, R. W. (1994). *Shaker* potassium channel gating II: transitions in the activation pathway. *J. Gen. Physiol.* 103, 279–319.

Zandany, N., Ovadia, M., Orr, I., and Yifrach, O. (2008). Direct analysis of cooperativity in multisubunit allosteric proteins. *Proc. Natl. Acad. Sci. U.S.A.* 105, 11697–11702.

Zheng, J., and Sigworth, F. J. (1997). Selectivity changes during activation of mutant Shaker potassium channels. *J. Gen. Physiol.* 110, 101–117.

Zheng, J., and Sigworth, F. J. (1998). Intermediate conductances during deactivation of heteromultimeric Shaker potassium channels. *J. Gen. Physiol.* 112, 457–474.

Zheng, J., Vankataramanan, L., and Sigworth, F. J. (2001). Hidden Markov model analysis of intermediate gating steps associated with the pore gate of Shaker potassium channels. *J. Gen. Physiol.* 118, 547–564.

Zhou, M., Morais-Cabral, J. H., Mann, S., and MacKinnon, R. (2001). Potassium channel receptor site for the inactivation gate and quaternary amine inhibitors. *Nature* 411, 657–661.

Conflict of Interest Statement: The authors declare that the research was conducted in the absence of any commercial or financial relationships that could be construed as a potential conflict of interest.

Received: 08 May 2012; accepted: 26 August 2012; published online: 13 September 2012.

Citation: Labro AJ and Snyders DJ (2012) Being flexible: the voltage-controllable activation gate of Kv channels. Front. Pharmacol. ***3****:168. doi: 10.3389/fphar.2012.00168*

This article was submitted to Frontiers in Pharmacology of Ion Channels and Channelopathies, a specialty of Frontiers in Pharmacology.

frontiers in
PHARMACOLOGY

REVIEW ARTICLE
published: 23 March 2012
doi: 10.3389/fphar.2012.00049

Cytoplasmic domains and voltage-dependent potassium channel gating

Francisco Barros*, Pedro Domínguez and Pilar de la Peña

Departamento de Bioquímica y Biología Molecular, Universidad de Oviedo, Oviedo, Asturias, Spain

Edited by:
Gildas Loussouarn, University of Nantes, France

Reviewed by:
Bernard Attali, Tel Aviv University, Israel
Martin Tristani, University of Utah, USA

****Correspondence:***
Francisco Barros, Departamento de Bioquímica y Biología Molecular, Universidad de Oviedo, Edificio Santiago Gascón, Campus del Cristo, 33006 Oviedo, Asturias, Spain.
e-mail: fbarros@uniovi.es

The basic architecture of the voltage-dependent K^+ channels (Kv channels) corresponds to a transmembrane protein core in which the permeation pore, the voltage-sensing components and the gating machinery (cytoplasmic facing gate and sensor–gate coupler) reside. Usually, large protein tails are attached to this core, hanging toward the inside of the cell. These cytoplasmic regions are essential for normal channel function and, due to their accessibility to the cytoplasmic environment, constitute obvious targets for cell-physiological control of channel behavior. Here we review the present knowledge about the molecular organization of these intracellular channel regions and their role in both setting and controlling Kv voltage-dependent gating properties. This includes the influence that they exert on Kv rapid/N-type inactivation and on activation/deactivation gating of *Shaker*-like and *eag*-type Kv channels. Some illustrative examples about the relevance of these cytoplasmic domains determining the possibilities for modulation of Kv channel gating by cellular components are also considered.

Keywords: potassium channel, voltage-dependent gating, cytoplasmic domains, structure–function relationships, inactivation gating, activation/deactivation gating

Ion channels are integral membrane proteins allowing for the passive passage of specific inorganic ions across cell membranes, propelled by their electrochemical gradients. Voltage-dependent or voltage-gated channels are proteins in which some parts of the molecule change their conformation in response to alterations of the electric field within the membrane (i.e., the transmembrane voltage), shifting the conformational equilibrium back and forth from closed to open (and inactivated) states (**Figure 1**; for an overview see Hille, 1992; Coetze et al., 1999; Swartz, 2004, 2008; Yu et al., 2005; Ashcroft, 2006; Bezanilla, 2008). Inactivation is a process by which an open channel enters a stable non-conducting state after a maintained depolarizing change in membrane potential.

Voltage-dependent potassium channels (Kv channels; Gutman et al., 2005) belong to a family of proteins (**Figure 2**) characterized by the presence of a pore-forming subunit with a six transmembrane segment (S1–S6) topology in which the last two segments, linked by a pore loop, constitute the ion-permeation pore. The voltage-sensing domain is formed by the S1–S4 segments, in which S4 contains a high density of positively charged residues and is the main transmembrane voltage-sensing component (Yellen, 1998, 2002; Swartz, 2004, 2008; Yu et al., 2005; Ashcroft, 2006; Bezanilla, 2008). Aside from the possible presence of accessory subunits (see below), in the Kv channels four pore subunits form a tetrameric structure surrounding a central conduction pathway (**Figure 2**). This oligomeric organization is also shared by other members of the family (not all of them activated by voltage) including cyclic nucleotide-activated channels, hyperpolarization-activated cation channels, Ca^{2+}-activated K^+ channels, and TRP channels. Voltage-gated Ca^{2+} and Na^+ channels share this overall organization, but instead contain four similar repeats with six transmembrane segments in a single polypeptide, mimicking the Kv tetramers (Yellen, 1998, 2002; Swartz, 2004, 2008; Yu et al., 2005; Ashcroft, 2006; Bezanilla, 2008).

At least three functional elements are found in the Kv channels: an ion conduction pore in which the ionic selectivity resides, a voltage sensor that detects changes in the electric transmembrane field, subsequently coupling its conformational states to the operation of the gate(s) (i.e., to channel gating), and one or more gates that open and close in response to voltage. Three possible gates have been recognized in Kv channels (Yellen, 1998, 2002): (i) an activation gate located at the cytoplasmic face of the permeation pore at the end of the S6 transmembrane helix, (ii) a pore or selectivity filter gate at the level of the selectivity filter itself, and (iii) an inactivation gate capable of plugging the pore from the cytoplasmic face. The first two gating mechanisms are linked to conformational rearrangements of the voltage sensors, providing the activation and C-type inactivation properties to the Kv channels, and the third mechanism confers the rapid/N-type inactivation behavior (**Figure 1**).

Selectivity filters, voltage sensors, and most gating elements of the Kv channels are located within the transmembranal portion of the channel core, except for the cytoplasmic gates themselves and the sensor–gate coupler(s) (e.g., the S4–S5 linker) that are located at the cytoplasmic channel surface and therefore can also be considered cytoplasmic (**Figure 2**). Whereas this basic architecture pertains to the whole voltage-dependent cation channel superfamily, additional elements exist in the form of intracellular domains and/or accessory subunits, able to strongly influence the gating properties (Minor, 2001; Varshney and Mathew, 2003; Roosild et al., 2004) and thus regulate channel functionality, either directly or in response to exogenous modulators. The contribution

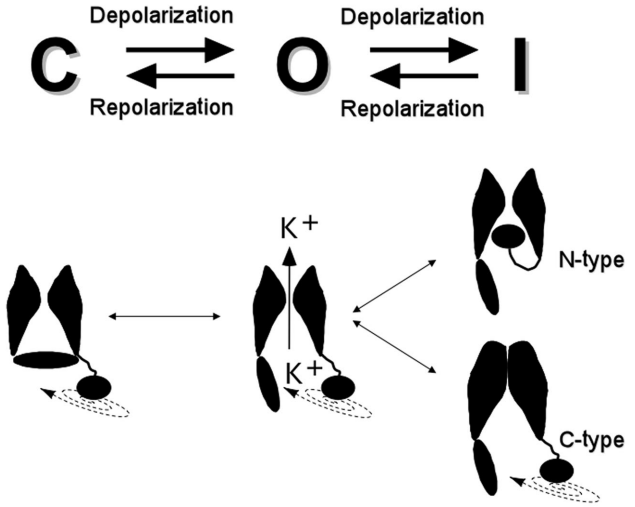

FIGURE 1 | Schematic cartoon of the conformational states and voltage-driven gating modifications of Kv channels. The drawings at the bottom represent two α-subunits and a symbolic cytoplasmic gate, with one diffusible ball-and-chain structure attached to their cytoplasmic face. N-type inactivation as a consequence of plugging of the pore after opening the cytoplasmic activation gate, and C-type inactivation by collapsing of the selectivity filter gate, are represented on the right.

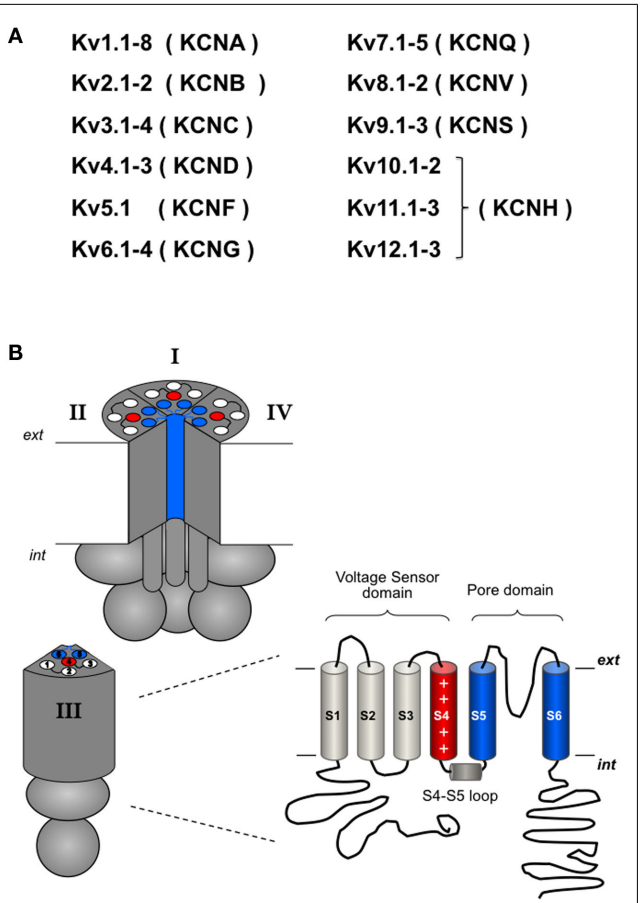

FIGURE 2 | (A) Overview of the Kv channels subfamilies. **(B)** Schematic representation of the tetrameric organization of a Kv channel. A structural folding model of one of the four α subunits is shown on the *right*. Note that in contrast to the considerable homogeneity in the transmembranal core and the loops linking the transmembrane helices, large variations in the relative size and positioning of the amino and carboxy terminals are found in the different Kv channels. For more explanations, see text.

of additional accessory β-subunits to channel behavior (reviewed in Li et al., 2006; Bett and Rasmusson, 2008; Pongs and Schwarz, 2010; Vacher and Trimmer, 2011) will not be considered here. In order to review the current knowledge about the participation of cytoplasmic structures in the gating behavior of Kv channels, we will consider first the structural organization of these channel domains. Then, using well studied examples (e.g., *Shaker*-like and *eag* channels), we will focus on the role of cytoplasmic regions in determining channel gating properties. Recent data about the interactions between the N- and C-terminal cytoplasmic regions and/or between them and components of the gating machinery in the channel core (e.g., the S4–S5 linker or the gate) will also be considered. Finally, we will review some cases illustrating the modulation of gating properties through signal transduction elements such as calmodulin or protein kinases and/or phosphatases.

STRUCTURAL ORGANIZATION OF THE Kv CHANNEL CYTOPLASMIC DOMAINS

The tridimensional structure of the transmembrane core of some Kv channels has been solved at high resolution (Jian et al., 2003; Long et al., 2005a, 2007). Given the overall identity and primary structure conservation of these protein segments, it is reasonable to assume that all of the Kv family members would share a common arrangement in these regions. However, solving the high-resolution structure of a complete Kv channel still remains a major challenge and the tridimensional structure and/or complete architecture of the cytoplasmic domains of the Kv channels are unknown. In fact, these regions show far more divergence than the rest of the molecule does, even among closely related channels. Nevertheless, specific regions of these domains have been structurally characterized using a "divide and conquer" approach (Gaudet, 2009), thus providing partial information to be joined together and integrated with biochemical and electrophysiological data to yield a better picture of the channel organization on a domain by domain basis (Biggin et al., 2000). This approach has led to the proposal of two general assemblies for the Kv channel cytoplasmic components (**Figure 3**; Yellen, 2002): (a) The pattern typically exhibited by the Kv1–Kv4 cluster (Yu et al., 2005; Pischalnikova and Sokolova, 2009), in which, hanging centrally below the transmembranal core there is an N-terminal T1 "tetramerization domain" that determines, among other functional characteristics, the specificity of subunit assembly. (b) The pattern shared by the Kv7 and Kv10–Kv12 channels, characterized by the absence of a T1 domain and the presence of a C-terminal domain located centrally below the transmembrane channel core. Interestingly, this second overall organization also pertains to other relatives from the voltage-gated ion channel superfamily (Gutman et al., 2005; Yu et al., 2005), including those gated coordinately by voltage and ligand binding [such as the hyperpolarization-activated and cyclic

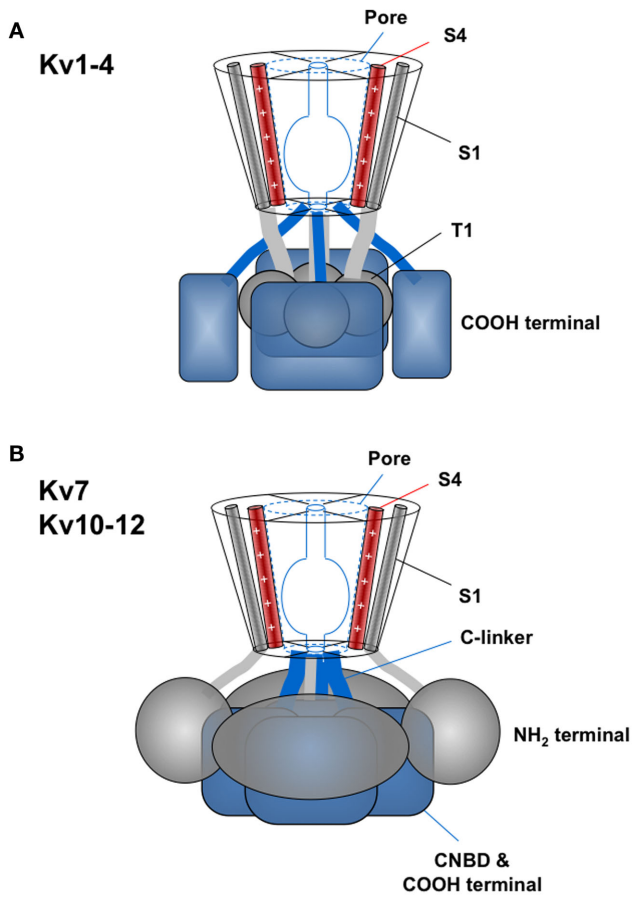

FIGURE 3 | Basic patterns of Kv channel cytoplasmic domains structural organization. (A) General organization of the Kv1–Kv4 channels group with the T1 "tetramerization domains" hanging centrally below the transmembranal core and attached to it through four linkers continued from the first transmembrane helices. In this case the C-terminal structures probably track to the periphery surrounding T1 and extending to its bottom. **(B)** General cytoplasmic architecture of the Kv7 and Kv10–Kv12 channels characterized by a carboxy terminus (i.e., the C-linker/CNBD region of the Kv10–Kv12 channels or the A–D helical regions of the Kv7 channels) forming a compact tetrameric structure in a central position immediately below the cytoplasmic pore opening. In this case the amino terminus probably surrounds the C-terminus and extends to its bottom establishing extensive contacts with its top and side surfaces. Note that in both models the initial amino terminal structures (ball-like and *eag*/PAS domains for Kv1–Kv4 and Kv10–Kv12, respectively) are likely to interact with the gate surroundings in the transmembrane core. S4 segment is also depicted as a reference. See text for details.

nucleotide-gated (HCN) and BK/K_{Ca}1 channels] and those gated exclusively by intracellular ligands [cyclic nucleotide-gated (CNG) and SK/K_{Ca}2]. Besides these "cytoplasmic cores," a panoply of protein domains and motifs (**Figure 4**) can be present in the cytoplasmic regions that, in addition to some accessory subunits, add diversification in structure, function, and regulation to the different channel subfamilies and even to different members of the same subfamily.

Examples of cytoplasmic domains for which the tridimensional structure has been solved, include the cited T1 domain (Kreusch et al., 1998; Bixby et al., 1999; Gulbis et al., 2000; Minor et al., 2000; Scannevin et al., 2004; Long et al., 2005a; Pioletti et al., 2006), the distal N-terminus inactivation structures from Kv3.4, *ShakerB*, and Kv1.4 (Antz et al., 1997; Schott et al., 1998; Wissmann et al., 2003), the N-terminal PAS domain and its initial distal segments from Kv11.1 (Morais-Cabral et al., 1998; Li et al., 2010; Muskett et al., 2011; Ng et al., 2011), and the C-terminal coiled-coil segment from Kv7.4 and Kv7.1 (Howard et al., 2007; Wiener et al., 2008). It is also interesting to note the current availability of high-resolution tridimensional structures for the C-terminal C-linker/cNBD regions of the Kv-related HCN and CNG channels (Zagotta et al., 2003; Schünke et al., 2011), providing a valuable reference for homologous regions present in some Kv channels such as those of the *eag* family.

Additionally, several regions putatively involved in different aspects of channel behavior other than gating (e.g., oligomerization and assembly, trafficking, surface expression, protein–protein interactions, modulation, or drug–channel interactions) have been recognized in the Kv cytoplasmic channel regions (**Figure 4**; Hopkins et al., 1994; Xu et al., 1995; Ponce et al., 1997; Kupershmidt et al., 1998; Schulteis et al., 1998; Bentley et al., 1999; Cukovic et al., 2001; Yang et al., 2001; Leung et al., 2003; Kunjilwar et al., 2004; Callsen et al., 2005; Choi et al., 2005; Xu et al., 2010; Zheng et al., 2010), that in many cases have not been associated to a known tridimensional structure. Finally, the availability of low-resolution images for some voltage-dependent K^+ channels yields interesting possibilities to fit with partial X-ray data, and provides significant new insights into the overall architecture of the channel molecule (Sokolova et al., 2001, 2003; Orlova et al., 2003; Parcej and Eckhardt-Strelau, 2003; Kim et al., 2004; Adair et al., 2008; Pischalnikova and Sokolova, 2009; Wang and Sigworth, 2009).

ROLE OF CYTOPLASMIC DOMAINS IN INACTIVATION GATING

A pioneering indication that some cytoplasmic region(s) could participate in the control of gating behavior was provided by analyzing the process of inactivation. Thus, the specific abolition of voltage-dependent Na^+ current inactivation by intracellular treatment with proteolytic enzymes (Armstrong et al., 1973) subsequently led to the proposal of a "ball-and-chain" mechanism as the determinant of this inactivation process (Armstrong and Bezanilla, 1977). However, a better molecular explanation of this mechanism, in which a cytoplasmic blocking particle tethered to the channel protein (the "ball," see **Figures 1** and **4**) binds rapidly to the pore and plugs it after the activation gate opens, was obtained in 1990 by studying the fast/N-type-inactivation of the Kv-type *Shaker* K^+ channel of *Drosophila*. Thus, deletion of the first ≈20 amino acids of the amino terminus eliminated rapid inactivation (Hoshi et al., 1990), whereas a soluble peptide containing that sequence restored inactivation in a concentration-dependent manner (Zagotta et al., 1990). It was subsequently observed that the soluble peptide (or N-terminal inactivation domain) competes with intracellularly applied channel blockers (e.g., quaternary amines, Choi et al., 1991), that it is expelled to the cytoplasm by potassium flow from the extracellular side of the membrane (Demo and Yellen, 1991), and that the inactivation process traps the channel in an open-inactivated state that prevents it from closing, making the recovery of inactivation typically via the open state

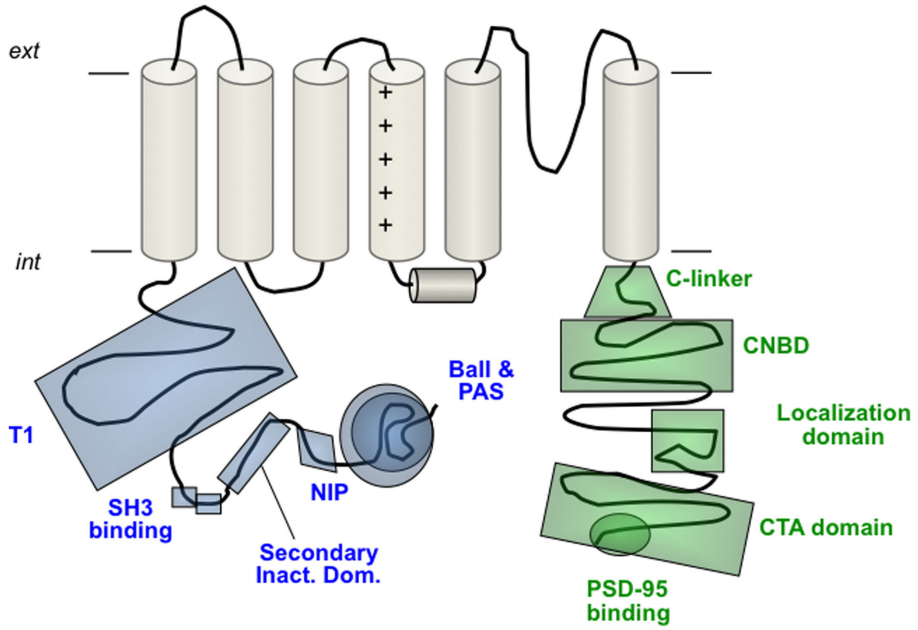

FIGURE 4 | Schematic view of different structural and/or functional domains recognized at the cytoplasmic ends of Kv channels. In the amino terminus these include the ball-like structure responsible for fast N-type inactivation, the *eag*/PAS domain of the *eag*-like channels, the NIP domain that protects Kv1.6 channels against rapid inactivation, the secondary inactivation domain reported for Kv1.4 channels, the double SH3 binding domain of Kv1.5, and the T1 tetramerization domain (also called NAB) of the Kv1–Kv4 channels. In the carboxy terminus the domains shown correspond to the C-linker and cNBD encountered in the *eag*-like channels, the localization domain and the C-terminal activation (CTA) domain of Kv2.1 and the post-synaptic density protein (PSD-95)-binding domain of some Kv1 channels. A more detailed view of the Kv7 channels carboxy terminus organization is shown schematically in **Figure 6**. For more explanations, see text. Note that not all the depicted domains pertain to the same Kv channel.

(Demo and Yellen, 1991; Ruppersberg et al., 1991). Moreover, the inactivation domain was shown to interact with a binding site in the pore cavity, which overlaps with the binding site for quaternary amine blockers (Zhou et al., 2001; Gonzalez et al., 2011).

Some aspects of the ball-and-chain inactivation mechanism are worthy of further consideration, since the structural arrangements of the "chain" are not as clear as those of the "ball." Thus, shortening the length of the *Shaker* chain accelerated inactivation rates (Hoshi et al., 1990) as if this region were acting as a flexible linker to tether the ball to the channel. However, some Kv1.4 deletions that reduce the length of the "chain" not only do not increase the rate of inactivation, but actually slow inactivation as if the specific structure of this region could affect the movement and/or orientation of the inactivating particle (Rasmusson et al., 1998). It has also been suggested that rather than being a simple tether, this "chain" region may act in concert with other cytoplasmic structures to orientate and constrain the movement of the inactivation particle (Isacoff et al., 1991; Jern and Covarrubias, 1997; Sankaranarayanan et al., 2005; Baker et al., 2006). In this sense, it has been proposed that interactions of the Kv1.1 T1 domain with the more distal N-terminal structures play an important role in defining the strength of the ball-triggered N-type inactivation (Baker et al., 2006) and it has also been recognized that ball interaction(s) with the T1 domain and the S4–S5 linker seem to be crucial for proper development of the fast/N-type inactivation (Isacoff et al., 1991; Holmgren et al., 1996; Baker et al., 2006). Thus, in contrast with the well defined position of the ball plugging the conduction pathway inside the pore to inactivate the channel, the resting position of the chain segments and their dynamic rearrangements during the closed to open and inactive transitions are not well known. There is indirect evidence supporting the interpretation that these structures might wrap around the scaffold provided by the T1 tetramer hanging below the channel core (**Figure 3A**), so that upon depolarization they would snake through the windows lined by the S1–T1 linkers to reach a pocket on the upper T1 domain surface and subsequently the channel cavity below the selectivity filter (Gulbis et al., 2000; Kobertz et al., 2000; Zhou et al., 2001; Baker et al., 2006). However, it has also been proposed that the ball-and-chain combination is confined to the space between the T1 domain and the transmembrane portion of the channel (Varhsney et al., 2004).

In addition to the ball, a second inactivating domain with the ability to endow the channel with rapid inactivation has been identified in a more proximal part of the N-terminus of some Kv channels (e.g., Kv1.4; Kondoh et al., 1997; Höllerer-Beitz et al., 1999; Wissmann et al., 2003), and an N-type inactivation-prevention (NIP) domain (**Figure 4**) has been mapped close to the Kv1.6 N-terminal end (Roeper et al., 1998). As an alternative to the ball and length-dependent chain mechanism, a fast inactivation mechanism has been proposed for Kv1.4, based on electrostatic interactions between oppositely charged N-terminal segments and between the positively charged inactivation ball and acidic residues of the T1–S1 linker, that shorten the distance between the inactivating particle and its binding site, helping to orientate the ball

and causing the channel to inactivate more efficiently (Fan et al., 2012).

It is important to mention that even though a similar architecture is maintained around the gating machinery, the functional effects of the cytoplasmic domains can vary among channels even belonging to the same subfamily. This is the case of the fast inactivating A-type Kv4 channels, in which the existence of a N-type inactivation mechanism and a ball-like inactivating peptide at the N-terminus have been recognized (Gebauer et al., 2004), although it seems to play a minor role since the Kv4 most prominent inactivation is based in a temporary loss of coupling between the voltage sensor and the cytoplasmic gate (Barghaan et al., 2008; Barghaan and Bähring, 2009). Remarkably, the development of Kv4 inactivation is determined by the presence of amphipathic N-terminal sequences and a positively charged domain at the C-terminus, that may interact with each other (Jern and Covarrubias, 1997; Hatano et al., 2004).

As indicated above (see **Figure 1**), collapsing of the selectivity filter during depolarization steps can lead to a second type of inactivation named "C-type inactivation" (or "selectivity filter gating"; Wang et al., 2011). Recent data from some prototypical K^+ channels (e.g., KcsA and Kir) have provided a structural basis for allosteric coupling between activation at the level of the internal membrane surface and this type of inactivation at the channel selectivity filter, and about the influence exerted on them by intracellular domains (Uysal et al., 2011; Clarke et al., 2010; Cuello et al., 2010; Zhou and Jan, 2010). This yields some new ideas about how the structural modifications in the cytosolic domains can be allosterically transmitted to the intracellular gate and even to more distant gating elements in the channel core. It is important to note that selectivity filter gating not only pertains to KcsA and Kir voltage-independent K^+ channels containing exclusively a pore domain (Norton and Gulbis, 2010), but also to a wide range of Kv channels, to other highly selective K^+ channels such as SK and BK_{Ca}, and to non-selective cation channels (e.g., CNG channels) related to the Kv family (Bruening-Wright et al., 2007; Cox and Hoshi, 2011; Wang et al., 2011) in which the gating motions around the S6 bundle cross and hence the coupled selectivity filter rearrangements, can also be influenced by conformational changes in the cytoplasmic domains.

IMPLICATION OF CYTOPLASMIC DOMAINS IN ACTIVATION/DEACTIVATION GATING OF T1-CONTAINING Kv CHANNELS

The Kv channel's activation gate is located at the intracellular end of the pore at the C-terminus of the S6 transmembrane segment (Armstrong, 1971; Holmgren et al., 1997, 1998; Liu et al., 1997; Perozo et al., 1999; del Camino et al., 2000; del Camino and Yellen, 2001; Hackos et al., 2002; Webster et al., 2004; Wynia-Smith et al., 2008). Although other contacts and interactions between different domains could be involved (Ding and Horn, 2003; Li et al., 2008; Labro et al., 2011), coupling of the voltage sensor movement to operation of the gate mainly involves the S4–S5 linker which seems to act as a structural link, influencing gate dynamics via physical interaction(s) with the intracellular end of S6 and/or the cytoplasmic "C-linker" region (**Figure 4**) following it (Lu et al., 2002; Tristani-Firouzi et al., 2002; Ding and Horn, 2003; Long et al., 2005b; Ferrer et al., 2006; Boulet et al., 2007; Labro et al., 2008, 2011; Nishizawa and Nishizawa, 2009; Choveau et al., 2011). Interestingly, a similar coupling via S4–S5 linker interaction with the cytoplasmic end of S6 has been proposed for HCN and KAT1 channels (Chen et al., 2001; Decher et al., 2004; Prole and Yellen, 2006), that show an overall structure very similar to that of Kv channels, but in which opening is triggered by membrane hyperpolarization rather than depolarization (Männikkö et al., 2002; Latorre et al., 2003; Vemana et al., 2004; Grabe et al., 2007). This opposite polarity of gating is perhaps achieved by a different binding of the S4–S5 linker to the extreme of S6 only in the open state whereas in the Kv channels this interaction takes place in the closed state (Choveau et al., 2011).

Since the gate and the sensor–gate coupler (i.e., the S4–S5 linker) locate at the cytoplasmic channel surface, these structures become accessible targets for modulation from the cytoplasmic milieu, providing attractive means of channel activity regulation not only by amino- and /or carboxy-located channel domains but also by soluble products of signal transduction cascades. One example of channel gating modulation by cytoplasmic domains is that of Kv2.1. Early work with Kv2.1 indicated that the activation gating could be strongly affected by the cytoplasmic amino and carboxyl termini (VanDongen et al., 1990), and the influence of the channel amino terminus in voltage-dependent gating and modulation has been subsequently confirmed (Pascual et al., 1997). It has been demonstrated that interactions between the N- and C-terminal regions of Kv2.1 lacking auxiliary β subunits determine its activation properties, trafficking, and phosphorylation-dependent modulation (Ju et al., 2003; Scholle et al., 2004; Mohapatra et al., 2008), in a way that resembles the interaction between the α and the auxiliary β subunits in other Kv channels (Mohapatra et al., 2008). Another case is that of Kv1.2, in which an interaction between the C-terminus and the S4–S5 linker of a neighboring subunit which is able to regulate channel activation has also been suggested (Zhao et al., 2009). It has also been reported that the polar T1 surfaces of the mammalian Kv1.2 and the *Aplysia* Kv1.1 channels play a key role in the conformational changes that lead to channel opening (Cushman et al., 2000; Minor et al., 2000). More recently, use of fluorescence resonance energy transfer (FRET) microscopy combined with voltage-clamp recording has allowed the detection of conformational rearrangements in the relative orientation of Kv1.2 N- and C-termini upon depolarization (Kobrinsky et al., 2006; Lvov et al., 2009), a mechanism that could be related to gating regulation and that may also pertain to other Kv channels. Interestingly, similar gating-related motions of the N- and C-termini have been detected in Kv7.1 and the CNGA1 channel using an equivalent approach (Taraska and Zagotta, 2007; Haitin et al., 2009), although both channels belong to the subgroup characterized by the absence of the T1 domain (see above). Finally, in the case of Kv4 channels, it has been demonstrated that the T1–T1 interface is functionally active and dynamic during gating (Wang et al., 2005) and, based on work with Kv4.1 channels, it has been concluded that the complex voltage-dependent gating rearrangements of eukaryotic Kv channels are not limited to the membrane-spanning core, but must include the intracellular T1–T1 interface (Wang and Covarrubias, 2006).

CYTOPLASMIC DOMAINS AND ACTIVATION/DEACTIVATION GATING OF *eag*-TYPE Kv CHANNELS

An interesting contribution to the topic of gating control by cytoplasmic domains is provided by members of the *eag* family, that comprises the Kv10–Kv12 subfamilies (Warmke and Ganetzky, 1994). Overall sequence similarity between *eag*- and *Shaker*-type Kv1–Kv4 channels is quite low except for the pore region, but a much higher degree of homology is found between *eag*-type channels and CNG, HCN, and inwardly rectifying plant K^+ channels (Anderson et al., 1992; Sentenac et al., 1992; Warmke and Ganetzky, 1994; Yu et al., 2005).

Kv10 (*ether-á-go-go* or *eag*) channels are involved in setting the membrane potential in several cell types and appear to be related to processes like cell-cycle, proliferation, and tumor progression (Felipe et al., 2006; Arcangeli et al., 2009; Wulff et al., 2009; Asher et al., 2010). Several studies have demonstrated the involvement of cytoplasmic domains in the control of *eag* channel gating. Thus, it has been observed that the most distal region and the PAS domain at the N-terminus of the *eag* channels are involved in determining gating kinetics (Terlau et al., 1997; Stevens et al., 2009; Wray, 2009), and that alterations in *eag* gating following truncation of the initial portion of the N-terminus can be compensated by mutation of the voltage sensor S4 segment (Terlau et al., 1997). It has also been shown that the voltage dependence of *eag* currents is not determined solely by the membrane-spanning domains (Lörinczi et al., 2009), and that the N- and C-terminal regions could be involved in controlling a gating step after movement of the voltage sensor, as well as in regulating biophysical properties of the channel (Li et al., 2011). Also, voltage-dependent gating characteristics of plant KAT1 channels seem to be influenced by the N- and C-termini of the protein (Marten and Hoshi, 1997, 1998).

The relationship between cytoplasmic structures and gating properties has been exhaustively investigated in the Kv11.1 (human *ether-á-go-go*-related gene or hERG) channel, a remarkable entity both from the pathophysiological and the biophysical points of view. hERG mediates the cardiac delayed rectifier potassium current I_{Kr} (Sanguinetti et al., 1995; Trudeau et al., 1995) and mutations in the hERG gene and drug inhibition of hERG channels underlie inherited and acquired type 2 long-QT syndrome (Sanguinetti et al., 1995; Viskin, 1999; Keating and Sanguinetti, 2001; Redfern et al., 2002; Thomas et al., 2003; Finlayson et al., 2004; Roden and Viswanathan, 2005; Goldenberg and Moss, 2008). On the other hand, hERG channels play a key role in setting the electrical behavior of a variety of non-cardiac cell types (Barros et al., 1994, 1997; Bauer et al., 1999; Schäfer et al., 1999; Cherubini et al., 2000; Emmi et al., 2000; Overholt et al., 2000; Rosati et al., 2000; Arcangeli et al., 2009). These physiological roles of hERG derive from its unusual gating properties, characterized by slow activation kinetics and a very fast inactivation on depolarization. Thus, hERG currents increase during repolarization due to a fast recovery from inactivation followed by a much slower deactivation for which the channels remain open for longer periods of time at negative voltages, giving rise to the typical hERG tail currents. In the case of the heart, this contributes to the repolarization of the cardiac action potential and to the prevention of arrhythmias induced by early after-depolarizations or ectopic beats (Smith et al., 1996; Lu et al., 2001).

As for other voltage-gated potassium channels, voltage sensors and gating elements have been mapped to the transmembrane core of hERG (Smith and Yellen, 2002; Liu et al., 2003; Piper et al., 2003; Subbiah et al., 2004, 2005; Zhang et al., 2004, 2005; Saenen et al., 2006). In the case of hERG a volume larger than the core region hangs toward the cytoplasm since the cytoplasmic regions account for around 80% of the channel protein (**Figure 5**), but details about the structural architecture of these extensive regions are still lacking (Miranda et al., 2008). What has been clearly demonstrated is that the distinctive gating properties of hERG are strongly influenced by some cytoplasmic protein domains. Thus, the conserved *eag* N-terminal domain at the beginning of the hERG N-terminus and the exclusive proximal domain following it up to the S1 segment (**Figure 5**) were identified as important determinants of the remarkably slow deactivation and activation gating kinetics, respectively (Schönherr and Heinemann, 1996; Spector et al., 1996; Morais-Cabral et al., 1998; Wang et al., 1998; Chen et al., 1999; Viloria et al., 2000; Aydar and Palmer, 2001; Alonso-Ron et al., 2008; Gustina and Trudeau, 2009; Ng et al., 2011). In these studies, it has been repeatedly demonstrated that the N-terminal *eag* domain determines the slow hERG deactivation, since channels with particular deletions of the amino terminus, or with point mutations in the *eag* domain, show rapid deactivation kinetics. The fact that short deletions at the beginning of the N-terminus mimic the effect of more extensive amino terminal removal, points to the initial segment of the *eag* domain (residues 1–26) as the essential regulator of hERG deactivation gating (Wang et al., 1998, 2000; Ng et al., 2011).

Functional reconstitution of mutant channels with a recombinant eag N-terminal fragment, combined with TIRF–FRET spectroscopy, have recently been used to provide some additional insights into the regulation of hERG deactivation (Gustina and Trudeau, 2009; Fernández-Trillo et al., 2011). Thus, it has been recognized that normal slow deactivation gating involves an interaction between the initial N-terminal flexible segment (**Figure 5B**; Li et al., 2010; Muskett et al., 2011; Ng et al., 2011) and the gating machinery, likely at the level of the S4–S5 linker (Fernández-Trillo et al., 2011). Indeed, it has been shown that physical proximity exists between that unstructured and flexible segment of the hERG amino terminus and the N-terminal portion of the S4–S5 linker (De la Peña et al., 2011), further supporting this interpretation. In this context, the PAS sub-domain from the hERG *eag* domain and the amphipathic α-helix (residues 13–23) could act as a scaffold and a spacer helping to correctly orientate the initial flexible tail of the amino end (residues 2–9) toward the S4–S5 linker to modulate hERG gating (De la Peña et al., 2011; Fernández-Trillo et al., 2011; Ng et al., 2011). Additionally, the extensive contacts of these structures with the top and side surfaces of the C-linker/cNBD domains, that hang centrally below the pore domain in this type of channel (**Figures 3B** and **5B**), could help to allosterically modulate the operation of the cytoplasmic gate at the C-terminus of the S6 segment, which is directly attached to the C-linker (Muskett et al., 2011; Gustina and Trudeau, 2011). In fact, the involvement of some residues of the C-linker/cNBD regions of the hERG carboxy terminus in the control of deactivation gating through their interaction with the N-terminal-most region has also been proposed (Al-Owais et al., 2009; Kolbe et al., 2010; Muskett et al., 2011).

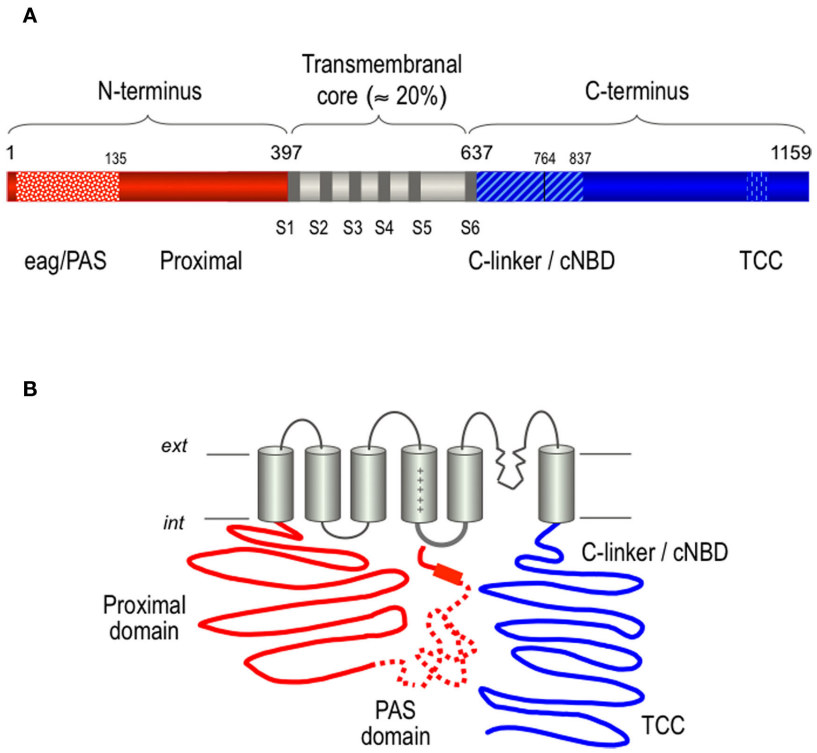

FIGURE 5 | Structural organization of the hERG K^+ channel. (A) Schematic linear diagram of the hERG channel protein. The regions corresponding to the eag/PAS (residues 1–135) and the proximal domains up to the first transmembrane helix are shown as striped and solid red bars, respectively. The transmembranal core region containing the six transmembrane helices and the carboxy terminus are shown colored in gray and blue, respectively. TCC indicates the proposed location of a tetramerization coiled-coil at the C-terminus. The size of every domain is represented on a horizontal scale proportional to the total length of the protein. **(B)** Schematic representation of a hERG channel α-subunit showing the proposed relative positioning of the PAS region in the amino terminus (dotted line), and the flexible tail of the amino end (initial solid red line segment) and the amphipathic α-helix separating them (red rectangle) pointing toward the S4–S5 linker on the cytoplasmic surface of the channel core. The proximity between the initial regions of the N-terminus and the C-linker/cNBD domains that are directly linked to the cytoplasmic gate at the bottom of helix S6 is also used to illustrate the possible existence of additional interactions between these channel structures. For more explanations, see text.

On the other hand, it has also been demonstrated that the hERG proximal domain (**Figure 5**) plays an important role in the activation channel properties and their modulation by hormones (Viloria et al., 2000; Gómez-Varela et al., 2002, 2003; Alonso-Ron et al., 2008, 2009). A small cluster of basic residues within this proximal domain close to the S1 segment has been subsequently recognized as a determinant of the hERG activation behavior through an electrostatic influence on the gating machinery (Saenen et al., 2006). However, although the modulation of hERG activation gating by a G protein-coupled hormone receptor is impaired after deletion of the proximal domain, it is observed in the absence of the cluster of basic residues (Gómez-Varela et al., 2003; Alonso-Ron et al., 2009). Interestingly, kinetic measurements of hERG activation under steady-state conditions, indicated that the initial region of the *eag* domain also affects the activation behavior (Alonso-Ron et al., 2008), suggesting that an interaction of this region with the channel core may also be involved in the modifications of gating caused by the deletion of the proximal domain (Viloria et al., 2000; Alonso-Ron et al., 2008). Nevertheless, the exact regions of the gating machinery at which the regulatory effects on activation are exerted remain to be established, although the bottom part of S4, the S4–S5 linker, the C-terminal portion of S6 and the C-linker/cNBD regions have been considered as possible candidates (Viloria et al., 2000; Tristani-Firouzi et al., 2002; Saenen et al., 2006; Alonso-Ron et al., 2008; De la Peña et al., 2011; Gustina and Trudeau, 2011).

Therefore, the long cytoplasmic domains of hERG exert important contributions to its unusual gating properties, supporting the interpretation that physical interactions between cytoplasmic domains and/or between them and the transmembrane channel core may also constitute an essential component of the gating machinery in other Kv channels.

ROLE OF CYTOPLASMIC Kv DOMAINS IN MODULATION OF CHANNEL GATING BY SIGNAL TRANSDUCTION ELEMENTS

Due to their accessibility to inner cell components, the cytoplasmic domains of Kv channels are obvious targets for cell-physiological control of channel function. Some illustrative cases are the regulation of Kv1.1 inactivation by concurrent direct binding of syntaxin and G protein βγ subunits (Michaelevski et al., 2002), the inhibition of human Kv10.1 channels by Ca/calmodulin binding to the N- and C-terminal structures (Ziechner et al., 2006),

the dependence of Kv11.1 rERG hormonal modulation on the presence of the N-terminal splicing variant *erg1b* (Kirchberger et al., 2006), and the modulation of Kv2.1 gating by binding of the SNARE complex components to the cytoplasmic channel tails (He et al., 2006). Also, two paradigmatic examples, the calmodulin modulation of Kv7 channels via their C-terminus, and the widespread regulation of channel function by protein phosphorylation, are considered next.

Kv7 (KCNQ) channels are a subfamily of Kv channels of great physiological importance in the kidney, gastro-intestinal tract, brain, and heart. In fact, there are several mutations in human Kv7 genes that lead to cardiac and neurological disorders such as long-QT syndrome and neonatal epilepsy (reviewed in Ashcroft, 2006; Haitin and Attali, 2008; Maljevic et al., 2010). Kv7 channels exhibit, as a distinctive feature, a C-terminus much longer than that of other Kv channels, which is critical for Kv7 assembly and trafficking, and also gating (reviewed in Haitin and Attali, 2008), and thus some Kv7 associated channelopathies involve mutations or alterations in this domain (Wen and Levitan, 2002; Haitin and Attali, 2008; Zheng et al., 2010). The Kv7 C-terminus contains several structural motifs including coiled-coils, calmodulin-binding structures, and basic amino acid clusters (**Figure 6**). Also, calmodulin interacts with the C-terminus of Kv7.1–Kv7.5 (Yus-Nájera et al., 2002; Haitin and Attali, 2008), an association that has also been demonstrated by TIRF/FRET techniques to take place in living mammalian cells (Bal et al., 2008). Although calmodulin can be constitutively tethered to Kv7 channels both in the absence or presence of Ca^{2+} (Wen and Levitan, 2002; Shahidullah et al., 2005), these interactions are likely to have Ca^{2+}-dependent and Ca^{2+}-independent components (Bal et al., 2008; Alaimo et al., 2009). Thus, it has been proposed that the calmodulin-binding module at the Kv7 C-terminus is endowed with a dual regulatory function: a Ca^{2+} sensor function that affects gating, and a second role in folding and trafficking mediated by a binding site with high affinity for calmodulin (Haitin and Attali, 2008). Interestingly, the calmodulin-binding module at the Kv7 C-termini seems to physically and functionally overlap with a phosphatidylinositol 4,5-bisphosphate (PIP_2)-binding site, allowing a more complex and sophisticated modulation of channel properties (Haitin and Attali, 2008; Hernandez et al., 2008; Bal et al., 2010). Thus, in Kv7.2/Kv7.3 heteromers that mediate the neuronal "M current," channel activity is enhanced by PIP_2 and suppressed by Ca^{2+}/calmodulin (Gamper and Shapiro, 2003, 2007; Zhang et al., 2003; Gamper et al., 2005; Suh and Hille, 2005; Hernandez et al., 2008). In contrast, both PIP_2 and Ca^{2+}/calmodulin seem to activate Kv7.1 channels mediating the cardiac I_{Ks} current (Loussouarn et al., 2003; Shamgar et al., 2006). Remarkably, disruption of Ca^{2+}/calmodulin binding to Kv7.2 is associated with neonatal epilepsy (Etxeberria et al., 2007; Haitin and Attali, 2008), and mutations impairing PIP_2 or calmodulin binding to Kv7.1 lead to certain forms of cardiac long-QT syndrome (Park et al., 2005; Ghosh et al., 2006; Shamgar et al., 2006).

Phosphorylation constitutes the most common covalent post-translational modification in eukaryotes (Cohen, 2001) and it can be an important modulatory mechanism for ion channel function, since the presence of phosphorylation targets for one or more kinases potentially allows for sensitive, dynamic, and reversible tuning of the structural and functional status of the protein (Levitan, 1994; Jonas and Kaczmarek, 1996; Park et al., 2008; Cerda and Trimmer, 2010). The exposure of the cytoplasmic domains to the internal cell environment makes them suitable molecular targets for phosphorylation-mediated modulation of channel activity. They can also act as sites of interaction with modulatory partners able to recruit targeting proteins such as phosphatases and kinases leading to the phosphorylation-dependent regulation of gating (Kass et al., 2003). Among those motifs, a C-terminally located leucine zipper is involved in recruiting, via an adaptor protein, a signaling complex including protein kinase A (PKA) and protein phosphatase 1, that are required for β-adrenergic receptor modulation of cardiac Kv7.1 (Marx et al., 2002). Indeed, several phosphorylated residues located in the N- and C-termini have been recognized as targets for regulation of Kv gating properties. Thus, the C-terminal Kv2.1 cytoplasmic domain can act as an autonomous domain sufficient to transfer Kv2.1-like clustering, voltage-dependent activation, and cholinergic modulation to diverse Kv channels (Mohapatra and Trimmer, 2006), and direct phosphorylation of its distal end alters channel voltage-dependent activation (Murakoshi et al., 1997). Interestingly, differential phosphorylation at a specific subset of sites, instead of the utilization of cell-specific phosphorylation sites, can explain differences in gating properties of Kv2.1 in different cell types under basal conditions, and in the same cell type under basal versus stimulated conditions (Park et al., 2007). Some other cases of gating regulation by phosphorylation of cytoplasmic domains have been less studied but are also illustrative: (i) Tyrosine kinase-dependent suppression of Kv1.2 by phosphorylation of an N-terminal residue has been observed, and antagonization of this effect by recruiting a protein tyrosine phosphatase to the N- and C-termini of the channel has also been shown (Huang et al., 1993; Tsai et al., 1999). (ii) Inactivation gating parameters of *Shaker* and Kv3.4 channels have been reported to be modulated by PKA-dependent phosphorylation of the C-terminus and protein kinase C (PKC)-dependent phosphorylation of the N-terminal inactivation particle, respectively (Covarrubias et al., 1994; Drain et al., 1994; Beck et al., 1998; Antz et al., 1999). (iii) It is known that some N- and C-terminal Kv4.2 residues can be phosphorylated by PKA and MAPK, respectively, and that some cross-talk between these phosphorylation loci can exist (Adams et al., 2000; Anderson et al., 2000; Schrader et al., 2009), but the functional consequences of such an interaction still remain obscure. (iv) Ca/calmodulin-dependent protein kinase II phosphorylates C-terminally located sites of *Drosophila eag* channels and modulates their function (Whang et al., 2002). (v) It has been shown that phosphorylation of the S4–S5 linker of neuronal KCNQ (Kv7) channels inhibits them (Surti et al., 2005). (vi) The state of phosphorylation of the Kv1.1 C-terminus regulates the extent of inactivation conferred by the Kvβ1.1 subunit through a mechanism related to the interaction of the αβ channel complex with the microfilaments via a PSD-like protein (Jing et al., 1997). All these data constitute overwhelming evidence that phosphorylation of cytoplasmic domains is a widespread mechanism of reversible gating modulation in Kv channels.

A promising addition to the study of channel modulation by phosphorylation is the use of phosphoproteomic approaches to identify the channel target residues of the phosphorylation events

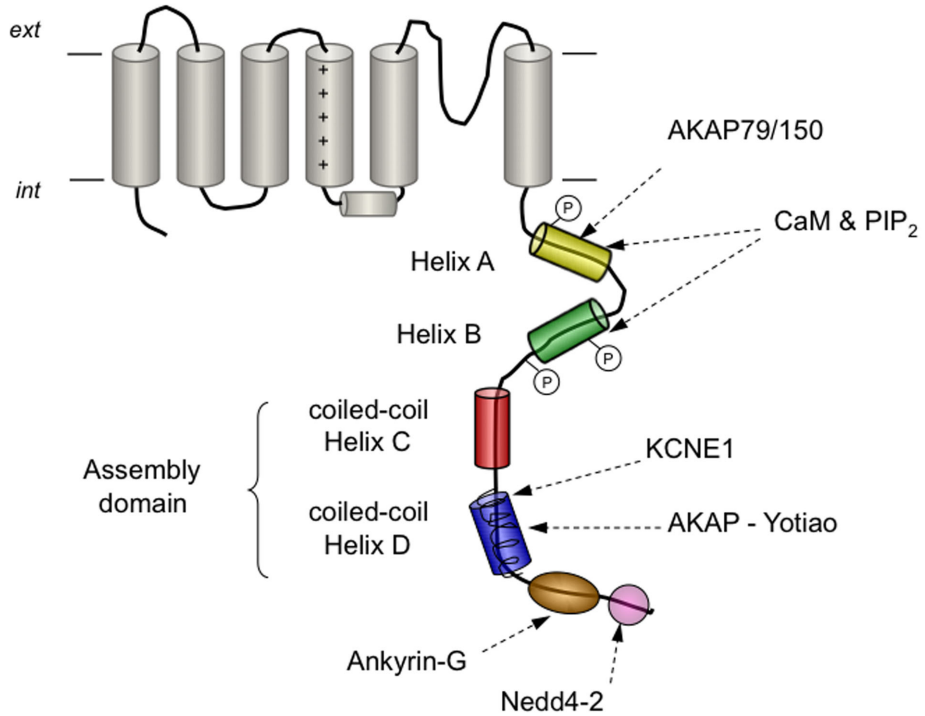

FIGURE 6 | Schematic representation of the carboxy-terminal tail structures and/or interaction sites present in Kv7 channels. The four helical regions (helices A–D) conserved in all family members are shown as cylinders. Formation of coiled-coil assemblies at the level of helices C and D is indicated. The proposed location of the conserved interaction sites with calmodulin (CaM) and phosphatidylinositol 4,5-bisphosphate (PIP_2), with A-kinase anchoring protein 79/150 (AKAP79/150) in Kv7.2, with the auxiliary β subunit KCNE1 in Kv7.1, with AKAP-Yotiao in Kv7.1, with ankyrin-G in Kv7.2–Kv7.3 and with ubiquitin-protein ligase Nedd4-2 in Kv7.1 and Kv7.2–Kv7.3, are also shown. Phosphorylation sites by Src kinase in helix A and by protein kinase C in helix B are indicated by an encircled P.

(reviewed in Cerda and Trimmer, 2010; Cerda et al., 2010; Baek et al., 2011). This method has allowed identification of N- and C-terminal phosphosites on α subunits of Kv1.1–Kv1.6, Kv2.1–Kv2.2, Kv3.1–Kv3.4, Kv4.1–Kv4.3, and Kv7.2–Kv7.5, although the functional significance of most of these phosphosites has not yet been determined. This aspect is quite relevant, since even though a phosphorylation mechanism may be involved in channel regulation, it is possible that the phosphate modification does not take place in the channel protein itself (Vacher and Trimmer, 2011). On the other hand, an agonist-dependent change in the basal phosphorylation level of the channel molecule may not cause a concomitant modification of the gating or other channel properties. An illustrative case of some of these concerns is provided by the hormonal modulation of the Kv11.1 (ERG) channel gating. Thus, early studies about the mechanism of ERG channels inhibition by thyrotropin-releasing hormone in adenohypophysial cells, pointed to a phosphorylation event as determinant of the hormonal induced response (Delgado et al., 1992; Barros et al., 1993, 1998). Further work demonstrated that the cytoplasmic N-terminal proximal domain was required for hormonal modulation of hERG gating (Gómez-Varela et al., 2003). Subsequently, it has been proposed that the PKC-dependent modulation of hERG is exerted either independently of direct phosphorylation of the channel protein itself in *Xenopus* oocytes (Thomas et al., 2003, 2004), or via a direct phosphorylation of the pore forming hERG subunits in mammalian cells (Cockerill et al., 2007). In this sense, the possibility that the cell types differentially supply molecular components of the signaling pathways involved in the channel modulation (Miranda et al., 2005), should also be considered. Interestingly, a direct phosphorylation of the hERG cytoplasmic domains by PKA is involved in the regulation triggered by activation of β-adrenergic receptors (Thomas et al., 1999; Cui et al., 2000, 2001; Kiehn, 2000; Kagan et al., 2002; Karle et al., 2002), and some signaling cross-talk between PKC and PKA cannot be excluded.

In summary, either by directly affecting the gating machinery or by influencing it in response to cellular modulators, Kv cytoplasmic regions constitute important regulators of voltage-dependent channel gating. Unfortunately, the striking advances characterizing the tridimensional structures of some channel core constituents have not been paralleled by similar success regarding the architecture of the cytoplasmic regions. Whereas physical interactions between the cytoplasmic domains and/or between them and the transmembranal channel core clearly constitute essential components of the gating machinery, details about dynamic conformational rearrangements in these regions during channel functionality remain mostly unknown. Combining structural studies with other fluorimetric, spectroscopic, and biophysical functional approaches could provide a better understanding of the dynamic steps connecting the discrete conformations resolved in the crystallographic structures.

ACKNOWLEDGMENTS

This work was supported by the Spanish Ministerio de Ciencia e Innovación (MICINN) by grant BFU2009-11262 and a Consolider-Ingenio project (SICI; CSD2008-00005). The authors thank the members of the Hormone Receptors and Ion Channels Group of the University of Oviedo for their scientific and technical contribution and Dr. Kevin Dalton for proofreading the text.

REFERENCES

Adair, B., Nunn, R., Lewis, S., Dukes, I, Philipson, L., and Yeager, M. (2008). Single particle image reconstruction of the human recombinant Kv2.1 channel. *Biophys. J.* 94, 2106–2114.

Adams, J. P., Anderson, A. E., Varga, A. W., Dineley, K. T., Cook, R. G., Pfaffinger, P. J., and Sweatt, J. D. (2000). The A-type potassium channel Kv4.2 is a substrate for the mitogen-activated protein kinase ERK. *J. Neurochem.* 75, 2277–2287.

Alaimo, A., Gómez-Posada, J. C., Aivar, P., Etxeberría, A., Rodriguez-Alfaro, J. A., Areso, P., and Villarroel, A. (2009). Calmodulin activation limits the rate of KCNQ2 K^+ channel exit from the endoplasmic reticulum. *J. Biol. Chem.* 284, 20668–20675.

Alonso-Ron, C., Barros, F., Manso, D. G., Gómez-Varela, D., Miranda, P., Carretero, L., Domínguez, P., and de la Peña, P. (2009). Participation of HERG channel cytoplasmic structures on regulation by the G protein-coupled TRH receptor. *Pflügers Arch.* 457, 1237–1252.

Alonso-Ron, C., de la Peña, P., Miranda, P., Domínguez, P., and Barros, F. (2008). Thermodynamic and kinetic properties of amino-terminal and S4–S5 loop HERG channel mutants under steady-state conditions. *Biophys. J.* 94, 3893–3911.

Al-Owais, M., Bracey, K., and Wray, D. (2009). Role of intracellular domains in the function of the herg potassium channel. *Eur. Biophys. J.* 38, 569–576.

Anderson, A. E., Adams, J. P., Qian, Y., Cook, R. G., Pfaffinger, P. J., and Sweatt, J. D. (2000). Kv4.2 phosphorylation by cyclic AMP-dependent protein kinase. *J. Biol. Chem.* 275, 5337–5346.

Anderson, J. A., Huprikar, S. S., Kochian, L. V., Lucas, W. J., and Gaber, R. F. (1992). Functional expression of a probable *Arabidopsis thaliana* potassium channel in *Saccharomyces cerevisiae*. *Proc. Natl. Acad. Sci. U.S.A.* 89, 3736–3740.

Antz, C., Bauer, T., Kalbacher, H., Frank, R., Covarrubias, M., Kalbitzer, H. R., Ruppersberg, J. P., Baukrowitz, T., and Fakler, B. (1999). Control of K^+ channel gating by protein phosphorylation: structural switches of the inactivation gate. *Nat. Struct. Biol.* 6, 146–150.

Antz, C., Geyer, M., Fakler, B., Schott, M. K., Guy, H. R., Frank, R., Ruppersberg, J. P., and Kalbitzer, H. R. (1997). NMR structure of inactivation gates from mammalian voltage-dependent potassium channels. *Nature* 385, 272–275.

Arcangeli, A., Crociani, O., Lastraioli, E., Masi, A., Pilozzi, S., and Becchetti, A. (2009). Targeting ion channels in cancer: a novel frontier in antineoplastic therapy. *Curr. Med. Chem.* 16, 66–93.

Armstrong, C. M. (1971). Interaction of tetraethylammonium ion derivatives with the potassium channels of giant axons. *J. Gen. Physiol.* 58, 413–437.

Armstrong, C. M., and Bezanilla, F. (1977). Inactivation of the sodium channel. II. Gating current experiments. *J. Gen. Physiol.* 70, 567–590.

Armstrong, C. M., Bezanilla, F., and Rojas, E. (1973). Destruction of sodium conductance inactivation in squid axons perfused with pronase. *J. Gen. Physiol.* 62, 375–391.

Ashcroft, F. M. (2006). From molecule to malady. *Nature* 440, 440–447.

Asher, V., Sowter, H., Shaw, R., Bali, A., and Khan, R. (2010). Eag and HERG potassium channels as novel therapeutic targets in cancer. *World J. Surg. Oncol.* 8, 113.

Aydar, E., and Palmer, C. (2001). Functional characterization of the C-terminus of the human ether-à-go-go-related gene K^+ channel (HERG). *J. Physiol.* 534, 1–14.

Baek, J.-H., Cerda, O., and Trimmer, J. S. (2011). Mass spectrometry-based phosphoproteomics reveals multisite phosphorylation of mammalian brain voltage-gated sodium and potassium channels. *Semin. Cell Dev. Biol.* 22, 153–159.

Baker, K. A., Hilty, C., Peti, W., Prince, A., Pfaffinger, P. J., Wider, G., Wüthrich, K., and Choe, S. (2006). NMR-derived dynamic aspects of N-type inactivation of a Kv channel suggest a transient interaction with the T1 domain. *Biochemistry* 45, 1663–1672.

Bal, M., Zaika, O., Martin, P., and Shapiro, M. S. (2008). Calmodulin binding to M-type K^+ channels assayed by TIRF/FRET in living cells. *J. Physiol.* 586, 2307–2320.

Bal, M., Zhang, J., Hernandez, C. C., Zaika, O., and Shapiro, M. S. (2010). Ca^{2+}/calmodulin disrupts AKAP79/150 interactions with KCNQ (M-type) K^+ channels. *J. Neurosci.* 30, 2311–2323.

Barghaan, J., and Bähring, R. (2009). Dynamic coupling of voltage sensor and gate involved in closed-state inactivation of Kv4.2 channels. *J. Gen. Physiol.* 133, 205–224.

Barghaan, J., Tozakidou, M., Ehmke, H., and Bähring, R. (2008). Role of N-terminal domain and accessory subunits in controlling deactivation–inactivation coupling of Kv4.2 channels. *Biophys. J.* 94, 1276–1294.

Barros, F., del Camino, D., Pardo, L. A., Palomero, T., Giráldez, T., and de la Peña, P. (1997). Demonstration of an inwardly rectifying K^+ current component modulated by thyrotropin-releasing hormone and caffeine in GH3 rat anterior pituitary cells. *Pflügers Arch.* 435, 119–129.

Barros, F., Gomez-Varela, D., Viloria, C. G., Palomero, T., Giráldez, T., and de la Peña, P. (1998). Modulation of human erg K^+ channel gating by activation of a G protein-coupled receptor and protein kinase C. *J. Physiol.* 511, 333–346.

Barros, F., Mieskes, G., del Camino, D., and de la Peña, P. (1993). Protein phosphatase 2A reverses inhibition of inward rectifying K^+ currents by thyrotropin-releasing hormone in GH3 pituitary cells. *FEBS Lett.* 336, 433–439.

Barros, F., Villalobos, C., García-Sancho, J., del Camino, D., and de la Peña, P. (1994). The role of the inwardly rectifying K^+ current in resting potential and thyrotropin-releasing hormone-induced changes in cell excitability of GH3 rat anterior pituitary cells. *Pflügers Arch.* 426, 221–230.

Bauer, C. K., Schäfer, R., Schiemann, D., Reid, G., Hanganu, I., and Schwarz, J. R. (1999). A functional role of the erg-like inward-rectifying K^+ current in prolactin secretion from rat lactotrophs. *Mol. Cell. Endocrinol.* 148, 37–45.

Beck, E. J., Sorensen, R. G., Slater, S. J., and Covarrubias, M. (1998). Interactions between multiple phosphorylation sites in the inactivation particle of a K^+ channel: insights into the molecular mechanism of protein kinase C action. *J. Gen. Physiol.* 112, 71–84.

Bentley, G. N., Brooks, M. A., O'Neill, C. A., and Findlay, J. B. (1999). Determinants of potassium channel assembly localized within the cytoplasmic C-terminal domain of Kv2.1. *Biochim. Biophys. Acta* 1418, 176–184.

Bett, G. C. L., and Rasmusson, R. L. (2008). Modification of K^+ channel-drug interactions by ancillary subunits. *J. Physiol.* 586, 929–950.

Bezanilla, F. (2008). How membrane proteins sense voltage. *Nat. Rev. Mol. Cell Biol.* 9, 323–332.

Biggin, P. C., Roosild, T., and Choe, S. (2000). Potassium channel structure: domain by domain. *Curr. Opin. Struct. Biol.* 10, 456–461.

Bixby, K. A., Nanao, M. H., Shen, N. V., Kreusch, A., Bellamy, H., Pfaffinger, P. J., and Choe, S. (1999). Zn^{2+}-binding and molecular determinants of tetramerization in voltage-gated K^+ channels. *Nat. Struct. Biol.* 6, 38–43.

Boulet, I. R., Labro, A. J., Raes, A. L., and Snyders, D. J. (2007). Role of the S6 C-terminus in KCNQ1 channel gating. *J. Physiol.* 585, 325–337.

Bruening-Wright, A., Lee, W.-S., Adelman, J. P., and Maylie, J. (2007). Evidence for a deep pore activation gate in small conductance Ca^{2+}-activated K^+ channels. *J. Gen. Physiol.* 130, 601–610.

Callsen, B., Isbrandt, D., Sauter, K., Hartmann, L. S., Pongs, O., and Bähring, R. (2005). Contribution of N- and C-terminal Kv4.2 channel domains to KChIP interaction. *J. Physiol.* 568, 397–412.

Cerda, O., Baek, J.-Y., and Trimmer, J. S. (2010). Mining recent brain proteomic databases for ion channel phosphosite nuggets. *J. Gen. Physiol.* 137, 3–16.

Cerda, O., and Trimmer, J. S. (2010). Analysis and functional implications of phosphorylation of neuronal voltage-gated potassium channels. *Neurosci. Lett.* 486, 60–67.

Chen, J., Mitcheson, J. S., Tristani-Firouzi, M., Lin, M., and Sanguinetti, M. C. (2001). The S4–S5 linker couples voltage sensing and activation of pacemaker channels. *Proc. Natl. Acad. Sci. U.S.A.* 98, 11277–11282.

Chen, J., Zou, A., Splawski, I., Keating, M. T., and Sanguinetti, M. C. (1999). Long QT syndrome-associated mutations in the Per-Arnt-sim (PAS) domain of HERG potassium channels accelerate deactivation. *J. Biol. Chem.* 274, 10113–10118.

Cherubini, A., Taddei, G. L., Crociani, O., Paglierani, M., Buccoliero, A. M., Fontana, L., Noci, I., Borri, P., Borrani, E., Giachi, M., Becchetti, A., Rosati, B., Wanke, E., Olivotto, M., and Arcangeli, A. (2000). HERG potassium channels are more frequently expressed in human endometrial cancer as compared to non-cancerous endometrium. *Br. J. Cancer* 83, 1722–1729.

Choi, K. L., Aldrich, R. W., and Yellen, G. (1991). Tetraethylammonium blockade distinguishes two inactivation mechanisms in voltage-activated K^+ channels. *Proc. Natl. Acad. Sci. U.S.A.* 88, 5092–5095.

Choi, W. S., Khurana, A., Mathur, R., Viswanathan, V., Steele, D. F., and Fedida, D. (2005). Kv1.5 surface expression is modulated by retrograde trafficking of newly endocytosed channels by the dynein motor. *Circ. Res.* 97, 363–371.

Choveau, F. S., Rodriguez, N., Ali, F. A., Labro, A. J., Rose, T., Dahimene, S., Boudin, H., Le Henaff, C., Escande, D., Snyders, D. J., Charpentier, F., Merot, J., Baro, I., and Loussouarn, G. (2011). KCNQ1 channels voltage dependency through a voltage-dependent binding of the S4–S5 linker to the pore domain. *J. Biol. Chem.* 286, 707–716.

Clarke, O. B., Caputo, A. T., Hill, A. P., Vandenberg, J. I., Smith, B. J., and Gulbis, J. M. (2010). Domain reorientation and rotation of an intracellular assembly regulate conduction in Kir potassium channels. *Cell* 141, 1018–1029.

Cockerill, S. L., Tobin, A. B., Torrecilla, I., Willars, G. B., Standen, N. B., and Mitcheson, J. S. (2007). Modulation of hERG potassium currents in HEK-293 cells by protein kinase C. Evidence for direct phosphorylation of pore forming subunits. *J. Physiol.* 581, 479–493.

Coetze, W. A., Amarillo, Y., Chiu, J., Chow, A., Lau, D., McCormack, T., Moreno, H., Nadal, M. S., Ozaita, A., Poutney, D., Saganich, M., Vega-Saenz de Miera, E., and Rudy, B. (1999). Molecular diversity of K^+ channels. *Ann. N. Y. Acad. Sci.* 868, 233–2865.

Cohen, P. (2001). The role of protein phosphorylation in human health and disease. *Eur. J. Biochem.* 268, 5001–5010.

Covarrubias, M., Wei, A., Salkoff, L., and Vyas, T. B. (1994). Elimination of rapid potassium channel inactivation by phosphorylation of the inactivation gate. *Neuron* 13, 1403–1412.

Cox, D. H., and Hoshi, T. (2011). Where's the gate? Gating in the deep pore of the BKCa channel. *J. Gen. Physiol.* 238, 133–136.

Cuello, L. G., Joginin, V., Cortes, D. M., Pan, A. C., Gagnon, D. G., Dalmas, O., Cordero-Morales, J. F., Chakrapani, S., Roux, B., and Perozo, E. (2010). Structural basis for the coupling between activation and inactivation gates in K^+ channels. *Nature* 466, 272–275.

Cui, J., Kagan, A., Qin, D., Mathew, J., Melman, Y., and McDonald, T. V. (2001). Analysis of the cyclic nucleotide binding domain on the HERG potassium channel and interactions with KCNE2. *J. Biol. Chem.* 276, 17244–17251.

Cui, J., Melman, Y. F., Palma, E., Fishman, G. I., and McDonald, T. V. (2000). Cyclic AMP regulates the HERG K^+ channel by dual pathways. *Curr. Biol.* 10, 671–674.

Cukovic, D., Lu, G. W., Wible, B., Steele, D. F., and Fedida, D. (2001). A discrete amino terminal domain of Kv1.5 and Kv1.4 potassium channels interacts with the spectrin repeats of alpha-actinin-2. *FEBS Lett.* 498, 87–92.

Cushman, S. J., Nanao, M. H., Jahng, A. W., DeRubeis, D., Choe, S., and Pfaffinger, P. J. (2000). Voltage dependent activation of potassium channels is coupled to T1 domain structure. *Nat. Struct. Biol.* 7, 403–407.

De la Peña, P., Alonso-Ron, C., Machín, A., Fernández-Trillo, J., Carretero, L., Domínguez, P., and Barros, F. (2011). Demonstration of physical proximity between the amino terminus and the S4–S5 linker of the hERG potassium channel. *J. Biol. Chem.* 286, 19065–19075.

Decher, N., Chen, J., and Sanguinetti, M. C. (2004). Voltage-dependent gating of hyperpolarization-activated, cyclic nucleotide-gated pacemaker channels. molecular coupling between the S4–S5 and C-linkers. *J. Biol. Chem.* 279, 13859–13865.

del Camino, D., Holmgren, M., Liu, Y., and Yellen, G. (2000). Blocker protection in the pore of a voltage-gated K^+ channel and its structural implications. *Nature* 403, 321–325.

del Camino, D., and Yellen, G. (2001). Tight steric closure of the intracellular activation gate of a voltage-gated K^+ channel. *Neuron* 32, 649–656.

Delgado, L. M., de la Peña, P., del Camino, D., and Barros, F. (1992). Okadaic acid and calyculin A enhance the effect of thyrotropin-releasing hormone on GH3 rat anterior pituitary cells excitability. *FEBS Lett.* 311, 41–45.

Demo, S. D., and Yellen, G. (1991). The inactivation gate of the Shaker K^+ channel behaves like an open-channel blocker. *Neuron* 7, 743–753.

Ding, S., and Horn, R. (2003). Effect of S6 tail mutations on charge movement in Shaker potassium channels. *Biophys. J.* 84, 295–305.

Drain, P., Dubin, A. E., and Aldrich, R. W. (1994). Regulation of Shaker K^+ channel inactivation gating by the cAMP-dependent protein kinase. *Neuron* 12, 1097–1109.

Emmi, A., Wenzel, H. J., Schwartzkroin, P. A., Taglialatela, M., Castaldo, P., Bianchi, L., Nerbonne, J., Robertson, G. A., and Janigro, D. (2000). Do glia have heart? Expression and functional role for ether-a-go-go currents in hippocampal astrocytes. *J. Neurosci.* 20, 3915–3925.

Etxeberria, A., Aivar, P., Rodriguez-Alfaro, J. A., Alaimo, A., Villacé, P., Gómez-Posada, J. C., Areso, P., and Villarroel, A. (2007). Calmodulin regulates the trafficking of KCNQ2 potassium channels. *FASEB J.* 22, 1135–1143.

Fan, Z., Ji, X., Zhang, D., and Xiao, Z. (2012). Electrostatic interaction between inactivation ball and T1–S1 linker region of Kv1.4 channel. *Biochim. Biophys. Acta* 1818, 55–63.

Felipe, A., Vicente, R., Villalonga, N., Roura-Ferrer, M., Martínez-Mármol, R., Solé, L., Ferreres, J. C., and Condom, E. (2006). Potassium channels: new targets in cancer therapy. *Cancer Detect. Prev.* 30, 375–385.

Fernández-Trillo, J., Barros, F., Machín, A., Carretero, L., Domínguez, P., and de la Peña, P. (2011). Molecular determinants of interactions between the N-terminal domain and the transmembrane core that modulate hERG K^+ channel gating. *PLoS ONE* 6, e24674. doi:10.1371/journal.pone.0024674

Ferrer, T., Rupp, J., Piper, D. R., and Tristani-Firouzi, M. (2006). The S4–S5 linker directly couples voltage sensor movement to the activation gate in the human ether-a-go-go-related gene (hERG) K^+ channel. *J. Biol. Chem.* 281, 12858–12864.

Finlayson, K., Witchel, H. J., McCulloch, J., and Sharkey, J. (2004). Acquired QT interval prolongation and HERG: implications for drug discovery and development. *Eur. J. Pharmacol.* 500, 129–142.

Gamper, N., Li, Y., and Shapiro, M. S. (2005). Structural requirements for differential sensitivity of KCNQ K^+ channels to modulation by Ca^{2+}/calmodulin. *Mol. Biol. Cell* 16, 3538–3551.

Gamper, N., and Shapiro, M. S. (2003). Calmodulin mediates Ca^{2+}-dependent modulation of M-type K^+ channels. *J. Gen. Physiol.* 122, 17–31.

Gamper, N., and Shapiro, M. S. (2007). Regulation of ion transport proteins by membrane phosphoinositides. *Nat. Rev. Neurosci.* 8, 921–934.

Gaudet, R. (2009). Divide and conquer: high resolution structural information on TRP channel fragments. *J. Gen. Physiol.* 133, 231–237.

Gebauer, M., Isbrandt, D., Sauter, K., Callsen, B., and Nolting, A. (2004). N-type inactivation features of Kv2.4 channel gating. *Biophys. J.* 86, 210–223.

Ghosh, S., Nunziato, D. A., and Pitt, G. S. (2006). KCNQ1 assembly and function is blocked by long-QT syndrome mutations that disrupt interaction with calmodulin. *Circ. Res.* 98, 1048–1054.

Goldenberg, I., and Moss, A. J. (2008). Long QT syndrome. *J. Am. Coll. Cardiol.* 51, 2291–2300.

Gómez-Varela, D., Barros, F., Viloria, C. G., Giráldez, T., Manso, D. G., Dupuy, S. G., Miranda, P., and de la Peña, P. (2003). Relevance of the proximal domain in the amino-terminus of HERG channels for regulation by a phospholipase C-coupled hormone receptor. *FEBS Lett.* 535, 125–130.

Gómez-Varela, D., de la Peña, P., García, J., Giráldez, T., and Barros, F. (2002). Influence of amino-terminal structures on kinetic transitions between several closed and open states in human erg K^+ channels. *J. Membr. Biol.* 187, 117–133.

Gonzalez, C., Lopez-Rodriguez, A., Srikumar, D., Rosenthal, J. J. C., and Holmgren, M. (2011). Editing of human Kv1.1 channel mRNAs disrupts binding of the N-terminus tip at the intracellular cavity. *Nat. Commun.* 2:436. doi:10.1038/ncomms1446

Grabe, M., Lai, H. C., Jain, M., Jan, Y. N., and Jan, L. Y. (2007). Structure prediction for the down state of a potassium channel voltage sensor. *Nature* 445, 550–553.

Gulbis, J. M., Zhou, M., Mann, S., and MacKinnon, R. (2000). Structure of

the cytoplasmic β subunit-T1 assembly of voltage-dependent K^+ channels. *Science* 289, 123–127.

Gustina, A. S., and Trudeau, M. C. (2009). A recombinant N-terminal domain fully restores deactivation gating in N-truncated and long QT syndrome mutant hERG potassium channels. *Proc. Natl. Acad. Sci. U.S.A.* 106, 13082–13087.

Gustina, A. S., and Trudeau, M. C. (2011). hERG potassium channel gating is mediated by N- and C-terminal region interactions. *J. Gen. Physiol.* 137, 315–325.

Gutman, G. A., Chandy, K. G., Grissmer, S., Lazdunski, M., McKinnon, D., Pardo, L. A., Robertson, G. A., Rudy, B., Sanguinetti, M. C., Stühmer, W., and Wang, X. (2005). International Union of Pharmacology. LIII. Nomenclature and molecular relationships of voltage-gated potassium channels. *Pharmacol. Rev.* 57, 473–508.

Hackos, D. A., Chang, T.-H., and Swartz, K. J. (2002). Scanning the intracellular S6 activation gate in the Shaker K^+ channel. *J. Gen. Physiol.* 119, 521–532.

Haitin, Y., and Attali, B. (2008). The C-terminus of Kv7 channels: a multifunctional module. *J. Physiol.* 586, 1803–1810.

Haitin, Y., Wiener, R., Shaham, D., Peretz, A., Cohen, E. B., Shamgar, L., Pongs, O., Hirsch, J. A., and Attali, B. (2009). Intracellular domains interactions and gated motions of IKS potassium channel subunits. *EMBO J.* 28, 1994–2005.

Hatano, N., Ohya, S., Muraki, K., Clark, R. B., Giles, W. R., and Imaizumi, Y. (2004). Two arginines in the cytoplasmic C-terminal domain are essential for voltage-dependent regulation of A-type K^+ current in the Kv4 channel subfamily. *J. Biol. Chem.* 279, 5450–5459.

He, Y., Kang, Y., Leung, Y., Xia, F., Gao, X., Xie, H., Gaisano, H. Y., and Tsushima, R. G. (2006). Modulation of Kv2.1 channel gating and TEA sensitivity by distinct domains of SNAP-25. *Biochem. J.* 396, 363–369.

Hernandez, C. C., Zaika, O., Tolstykh, G. P., and Shapiro, M. S. (2008). Regulation of neural KCNQ channels: signalling pathways, structural motifs and functional implications. *J. Physiol.* 586, 1811–1821.

Hille, B. (1992). *Ionic Channels of Excitable Membranes.* Sunderland, MA: Sinauer.

Höllerer-Beitz, G., Schönherr, R., Koenen, M., and Heinemann, S. H. (1999). N-terminal deletions of rKv1.4 channels affect the voltage dependence of channel availability. *Pflügers Arch.* 438, 141–146.

Holmgren, M., Jurman, M. E., and Yellen, G. (1996). N-type inactivation and the S4–S5 region of the Shaker channel. *J. Gen. Physiol.* 108, 195–206.

Holmgren, M., Shin, K. S., and Yellen, G. (1998). The activation gate of a voltage-gated K^+ channel can be trapped in the open state by an intersubunit metal bridge. *Neuron* 21, 617–621.

Holmgren, M., Smith, P. L., and Yellen, G. (1997). Trapping of organic blockers by closing of voltage-dependent K^+ channels: evidence for a trap door mechanism of activation gating. *J. Gen. Physiol.* 109, 527–535.

Hopkins, W. F., Demas, V., and Tempel, B. L. (1994). Both N- and C-terminal regions contribute to the assembly and functional expression of homo- and heteromultimeric voltage-gated K^+ channels. *J. Neurosci.* 14, 1385–1393.

Hoshi, T., Zagotta, W. N., and Aldrich, R. W. (1990). Biophysical and molecular mechanisms of Shaker potassium channel inactivation. *Science* 250, 533–538.

Howard, R. J., Clark, K., Holton, J. M., and Minor, D. L. Jr. (2007). Structural insight into KCNQ (Kv7) channel assembly and channelopathy. *Neuron* 53, 663–675.

Huang, X.-Y., Morielli, A. D., and Peralta, E. G. (1993). Tyrosine kinase-dependent suppression of a potassium channel by the G protein-coupled m1 muscarinic acetylcholine receptor. *Cell* 75, 1145–1156.

Isacoff, E. Y., Jan, Y. N., and Jan, L. Y. (1991). Putative receptor for the cytoplasmic inactivation gate in the Shaker K^+ channel. *Nature* 353, 86–90.

Jern, H. H., and Covarrubias, M. (1997). K^+ channel inactivation mediated b the concerted action of the cytoplasmic N- and C-terminal domains. *Biophys. J.* 72, 163–174.

Jian, Y., Lee, A., Chen, J., Ruta, V., Cadene, M., Chait, B. T., and MacKinnon, R. (2003). X-ray structure of a voltage-dependent K^+ channel. *Nature* 423, 33–41.

Jing, J., Peretz, T., Singer-Lahat, D., Chikvashvili, D., Thornhill, W. B., and Lotan, I. (1997). Inactivation of a voltage-dependent K^+ channel by β subunit: modulation by a phosphorylation-dependent interaction between the distal C terminus of α subunit and cytoskeleton. *J. Bio. Chem.* 272, 14021–14024.

Jonas, E. A., and Kaczmarek, L. K. (1996). Regulation of potassium channels by protein kinases. *Curr. Opin. Neurobiol.* 6, 318–323.

Ju, M., Stevens, L., Leadbitter, E., and Wray, D. (2003). The roles of N- and C-terminal determinants in the activation of the Kv2.1 potassium channel. *J. Biol. Chem.* 278, 12769–12778.

Kagan, A., Melman, Y., Krumerman, A., and McDonald, T. V. (2002). 14-3-3 amplifies and prolongs adrenergic stimulation of HERG K^+ channel activity. *EMBO J.* 21, 1889–1898.

Karle, C. A., Zitron, E., Zhang, W., Kathöfer, S., Schoels, W., and Kiehn, J. (2002). Rapid component IKr of the guinea-pig cardiac delayed rectifier K^+ current is inhibited by beta1-adrenoreceptor activation, via protein kinase A-dependent pathways. *Cardiovasc. Res.* 53, 355–362.

Kass, R. S., Kurokawa, J., Marx, S. O., and Marks, A. R. (2003). Leucine/isoleucine zipper coordination of ion channel macromolecular signaling complexes in the heart: roles in inherited arrhythmias. *Trends Cardiovasc. Med.* 13, 52–56.

Keating, M. T., and Sanguinetti, M. C. (2001). Molecular and cellular mechanisms of cardiac arrhythmias. *Cell* 104, 569–580.

Kiehn, J. (2000). Regulation of the cardiac repolarizing HERG potassium channel by protein kinase A. *Trends Cardiovasc. Med.* 10, 205–209.

Kim, L. A., Furat, J., Gutierrez, D., Butler, M. H., Xu, S., Golstein, S. A. N., and Grigorieff, N. (2004). Three-dimensional structure of Ito: Kv4.2-KChIP2 ion channels by electron microscopy at 21 Å resolution. *Neuron* 41, 513–519.

Kirchberger, N. M., Wulfsen, I., Schwarz, J. R., and Bauer, C. K. (2006). Effects of TRH on heteromeric rat erg1a/1b K^+ channels are dominated by the rerg1b subunit. *J. Physiol.* 571, 27–42.

Kobertz, W. R., Williams, C., and Miller, C. (2000). Hanging gondola structure of the T1 domain in a voltage-gated K^+ channel. *Biochemistry* 39, 10347–10352.

Kobrinsky, E., Stevens, L., Kazmi, Y., and Soldatov, N. M. (2006). Molecular rearrangements of the Kv2.1 potassium channel termini associated with voltage gating. *J. Biol. Chem.* 281, 19233–19240.

Kolbe, K., Schönherr, R., Gessner, G., Sahoo, N., Hoshi, T., and Heinemann, S. H. (2010). Cysteine 723 in the C-linker segment confers oxidative inhibition of hERG1 potassium channels. *J. Physiol.* 588, 2999–3009.

Kondoh, S., Ishii, K., Nakamura, Y., and Taira, N. (1997). A mammalian transient type K^+ channel, rat Kv1.4, has two potential domains that could produce rapid inactivation. *J. Biol. Chem.* 272, 19333–19338.

Kreusch, A., Pfaffinger, P. J., Stevens, C. F., and Choe, S. (1998). Crystal structure of the tetramerization domain of the Shaker potassium channel. *Nature* 392, 945–948.

Kunjilwar, K., Strang, C., DeRubeis, D., and Pfaffinger, P. J. (2004). KChIP3 rescues the functional expression of Shal channel tetramerization mutants. *J. Biol. Chem.* 279, 54542–54551.

Kupershmidt, S., Snyders, D. J., Raes, A., and Roden, D. M. (1998). A K^+ channel splice variant common in human heart lacks a C-terminal domain required for expression of rapidly activating delayed rectifier current. *J. Biol. Chem.* 273, 27231–27235.

Labro, A. J., Boulet, I. R., Choveau, F., Mayeur, E., Bruyns, T., Loussouarn, G., Raes, A. L., and Snyders, D. J. (2011). The S4–S5 linker of KCNQ1 channels forms a structural scaffold with the S6 segment controlling gate closure. *J. Biol. Chem.* 286, 717–725.

Labro, A. J., Raes, A. L., Grottesi, A., Van Hoorick, D., Sansom, M. S. P., and Snyders, D. J. (2008). Kv channel gating requires a compatible S4–S5 linker and bottom part of S6, constrained by non-interacting residues. *J. Gen. Physiol.* 132, 667–680.

Latorre, R., Olcese, R., Basso, C., Gonzalez, C., Muñoz, F., Cosmelli, D., and Alvarez, O. (2003). Molecular coupling between voltage sensor and pore opening in the *Arabidopsis* inward rectifier K^+ channel. *J. Gen. Physiol.* 122, 459–469.

Leung, Y. M., Kang, Y., Gao, X., Xia, F., Xie, H., Sheu, L., Tsuk, S., Lotan, I., Tsushima, R. G., and Gaisano, H. Y. (2003). Syntaxin 1A binds to the cytoplasmic C terminus of Kv2.1 to regulate channel gating and trafficking. *J. Biol. Chem.* 278, 17532–17538.

Levitan, I. B. (1994). Modulation of ion channels by protein phosphorylation and de phosphorylation. *Annu. Rev. Physiol.* 56, 193–212.

Li, L., Liu, K., Hu, Y., Li, D., and Luan, S. (2008). Single mutations convert an outward K^+ channel into an inward K^+ channel. *Proc. Natl. Acad. Sci. U.S.A.* 105, 2871–2876.

Li, Q., Gayen, S., Chen, A. S., Huang, Q., Raida, M., and Kang, C. (2010). NMR solution structure of the N-terminal domain of hERG and its interaction with the S4–S5 linker.

Biochem. Biophys. Res. Commun. 403, 126–132.

Li, Y., Liu, X., Wu, Y., Xu, Z., Li, H., Griffith, L. C., and Zhou, Y. (2011). Intracellular regions of the eag potassium channel play a critical role in generation of voltage-dependent currents. *J. Biol. Chem.* 286, 1389–1399.

Li, Y., Um, S. Y., and McDonald, T. V. (2006). Voltage-gated potassium channels: regulation by accessory subunits. *Neuroscientist.* 12, 199–210.

Liu, J., Zhang, M., Jiang, M., and Tseng, G.-N. (2003). Negative charges in the transmembrane domains of the HERG K channel are involved in the activation and deactivation gating processes. *J. Gen. Physiol.* 121, 599–614.

Liu, Y., Holmgren, M., Jurman, M. E., and Yellen, G. (1997). Gated access to the pore of a voltage-gated K^+ channel. *Neuron* 19, 175–184.

Long, S. B., Campbell, E. B., and MacKinnon, R. (2005a). Crystal structure of a mammalian voltage-dependent Shaker family K^+ channel. *Science* 309, 897–902.

Long, S. B., Campbell, E. B., and Mackinnon, R. (2005b). Voltage sensor of Kv1.2: structural basis of electromechanical coupling. *Science* 309, 903–908.

Long, S. B., Tao, X., Campbell, E. B., and MacKinnon, R. (2007). Atomic structure of a voltage-dependent K^+ channel in a lipid membrane-like environment. *Nature* 450, 376–382.

Lörinczi, E., Napp, J., Contreras-Jurado, C., Pardo, L. A., and Stühmer, W. (2009). The voltage dependence of hEag currents is not determined solely by membrane-spanning domains. *Eur. Biophys. J.* 38, 279–284.

Loussouarn, G., Park, K.-H., Bellocq, C., Baró, I., Charpentier, F., and Escande, D. (2003). Phosphatidylinositol 4,5-bisphosphate, PIP2, controls KCNQ1/KCNE1 voltage-gated potassium channels: a functional homology between voltage-gated and inward rectifier K^+ channels. *EMBO J.* 22, 5412–5421.

Lu, Y., Mahaut-Smith, M. P., Varghese, A., Huang, C. L., Kemp, P. R., and Vandenberg, J. I. (2001). Effects of premature stimulation on HERG K^+ channels. *J. Physiol.* 537, 843–851.

Lu, Z., Klem, A. M., and Ramu, Y. (2002). Coupling between voltage sensors and activation gate in voltage-gated K^+ channels. *J. Gen. Physiol.* 120, 663–676.

Lvov, A., Greitzer, D., Berlin, S., Chikvashvili, D., Tsuk, S., and Lotan, I. (2009). Rearrangements in the relative orientation of cytoplasmic domains induced by a membrane-anchored protein mediate modulations in Kv channel gating. *J. Biol. Chem.* 284, 28276–28291.

Maljevic, S., Wuttke, T. V., Seebohm, G., and Lerche, H. (2010). Kava7 channelopathies. *Pflügers Arch.* 460, 277–288.

Männikkö, R., Elinder, F., and Larsson, H. P. (2002). Voltage-sensing mechanism is conserved among ion channels gated by opposite voltages. *Nature* 419, 837–841.

Marten, I., and Hoshi, T. (1997). Voltage-dependent gating characteristics of the K^+ channel KAT1 depend on the N and C termini. *Proc. Natl. Acad. Sci. U.S.A.* 94, 3448–3453.

Marten, I., and Hoshi, T. (1998). The N-terminus of the K channel KAT1 controls its voltage-dependent gating by altering the membrane electric field. *Biophys. J.* 74, 2953–2962.

Marx, S. O., Kurokawa, J., Reiken, S., Motoike, H., D'Armiento, J., Marks, A. R., and Kass, R. S. (2002). Requirement of a macromolecular signaling complex for b-adrenergic receptor modulation of the KCNQ1-KCNE1 potassium channel. *Science* 295, 496–499.

Michaelevski, I., Chikvashvili, D., Tsuk, S., Fili, O., Lohse, M. J., Singer-Lahat, D., and Lotan, I. (2002). Modulation of a brain voltage-gated K^+ channel by syntaxin 1A requires the physical interaction of $G\beta\gamma$ with the channel. *J. Biol. Chem.* 277, 34909–34917.

Minor, D. L. Jr. (2001). Potassium channels: life in the post-structural world. *Curr. Opin. Struct. Biol.* 11, 408–414.

Minor, D. L., Lin, Y.-F., Mobley, B. C., Avelar, A., Jan, Y. N., Jan, L. Y., and Berger, J. M. (2000). The polar T1 interface is linked to conformational changes that open the voltage-gated potassium channel. *Cell* 102, 657–670.

Miranda, P., Giráldez, T., de la Peña, P., Manso, D. G., Alonso-Ron, C., Gómez-Varela, D., Domínguez, P., and Barros, F. (2005). Specificity of TRH receptor coupling to G-proteins for regulation of ERG K^+ channels in GH3 rat anterior pituitary cells. *J. Physiol.* 566, 717–736.

Miranda, P., Manso, D. G., Barros, F., Carretero, L., Hughes, T. E., Alonso-Ron, C., Domínguez, P., and de la Peña, P. (2008). FRET with multiply labeled HERG K^+ channels as a reporter of the in vivo coarse architecture of the cytoplasmic domains. *Biochim. Biophys. Acta* 1783, 1681–1699.

Mohapatra, D. P., Siino, D. F., and Trimmer, J. S. (2008). Interdomain cytoplasmic interactions govern the intracellular trafficking, gating, and modulation of the Kv2.1 channel. *J. Neurosci.* 28, 4982–4994.

Mohapatra, D. P., and Trimmer, J. S. (2006). The Kv2.1 C terminus can autonomously transfer Kv2.1-like phosphorylation-dependent localization, voltage-dependent gating, and muscarinic modulation to diverse Kv channels. *J. Neurosci.* 26, 685–695.

Morais-Cabral, J. H., Lee, A., Cohen, S. L., Chait, B. T., Li, M., and MacKinnon, R. (1998). Crystal structure and functional analysis of the HERG potassium channel N terminus: a eukaryotic PAS domain. *Cell* 95, 649–655.

Murakoshi, H., Shi, G., Scannevin, R. H., and Trimmer, J. S. (1997). Phosphorylation of the Kv2.1 channel alters voltage-dependent activation. *Mol. Pharmacol.* 52, 821–828.

Muskett, F. W., Thouta, S., Thomson, S. J., Bowen, A., Stansfeld, P. J., and Mitcheson, J. S. (2011). Mechanistic insight into hERG K^+ channel deactivation gating from the solution structure of the eag domain. *J. Biol. Chem.* 286, 6184–6191.

Ng, C. A., Hunter, M. J., Perry, M. D., Mobli, M., Ke, Y., Kuchel, P. W., King, G. F., Stock, D., and Vandenberg, J. I. (2011). The N-terminal tail of hERG contains an amphipathic α-helix that regulates channel deactivation. *PLoS ONE* 6, e16191. doi:10.1371/journal.pone.0016191

Nishizawa, M., and Nishizawa, K. (2009). Coupling of S4 helix translocation and S6 gating analyzed by molecular-dynamics simulations and mutated Kv channels. *Biophys. J.* 97, 90–100.

Norton, R. S., and Gulbis, J. M. (2010). Potassium channel gating: not an open and shut case. *Proc. Natl. Acad. Sci. U.S.A.* 107, 7623–7624.

Orlova, E. V., Papakosta, M., Booy, F. P., Van Heel, M., and Dolly, J. O. (2003). Voltage-gated K^+ channel from mammalian brain: 3D structure at 18 Å of the complete $(\alpha)4(\beta)4$ complex. *J. Mol. Biol.* 326, 1005–1012.

Overholt, J. L., Ficker, E., Yang, T., Shams, H., Bright, G. R., and Prabhakar, N. R. (2000). HERG-like potassium current regulates the resting membrane potential in glomus cells of the rabbit carotid body. *J. Neurophysiol.* 83, 1150–1157.

Parcej, D. N., and Eckhardt-Strelau, L. (2003). Structural characterisation of neuronal voltage-sensitive K^+ channels heterologously expressed in *Pichia pastoris*. *J. Mol. Biol.* 333, 103–116.

Park, K. H., Piron, J., Dahimene, S., Merot, J., Baro, I., Escande, D., and Loussouarn, G. (2005). Impaired KCNQ1-KCNE1 and Phosphatidylinositol-4,5-bisphosphate interaction underlies the long QT syndrome. *Circ. Res.* 96, 730–739.

Park, K.-S., Mohapatra, D. P., and Trimmer, J. S. (2007). Proteomic analysis of Kv2.1 channel phosphorylation sites determining cell background specific differences in function. *Channels* 1, 59–61.

Park, K.-S., Yang, J.-W., Seikel, E., and Trimmer, J. S. (2008). Potassium channel phosphorylation in excitable cells: providing dynamic functional variability to a diverse family of ion channels. *Physiology* 23, 49–57.

Pascual, J. M., Shieh, C.-C. Kirsch, G. E., and Brown, A. M. (1997). Contribution of the NH2 terminus of Kv2.1 to channel activation. *Am. J. Physiol.* 273, C1849–C1858.

Perozo, E., Cortes, D. M., and Cuello, L. G. (1999). Structural rearrangements underlying K^+ channel activation gating. *Science* 285, 73–78.

Pioletti, M., Findeisen, F., Hura, G. L., and Minor, D. L. Jr. (2006). Three-dimensional structure of the KchIP1-Kv4.3 T1 complex reveals a cross-shaped octamer. *Nat. Struct. Mol. Biol.* 13, 987–995.

Piper, D. R., Varghese, A., Sanguinetti, M. C., and Tristani-Firouzi, M. (2003). Gating currents associated with intramembrane charge displacement in HERG potassium channels. *Proc. Natl. Acad. Sci. U.S.A.* 100, 10534–10539.

Pischalnikova, A. V., and Sokolova, O. S. (2009). The domain and conformational organization in potassium voltage-gated ion channels. *J. Neuroimmune Pharmacol.* 4, 71–82.

Ponce, A., Vega-Saenz de Miera, E., Kentros, C., Moreno, H., Thornhill, B., and Rudy, B. (1997). K^+ channel subunit isoforms with divergent carboxy-terminal sequences carry distinct membrane targeting signals. *J. Membr. Biol.* 159, 149–159.

Pongs, O., and Schwarz, J. R. (2010). Ancillary subunits associated with voltage-dependent K^+ channels. *Physiol. Rev.* 90, 755–796.

Prole, D. L., and Yellen, G. (2006). Reversal of HCN channel voltage dependence via bridging of the S4–S5 linker and post-S6. *J. Gen. Physiol.* 128, 273–282.

Rasmusson, R. L., Morales, M. J., Wang, S., Liu, S., Campbell, D. L., Brahmajothi, M. V., and Strauss, H. C. (1998). Inactivation of voltage-gated cardiac K^+ channels. *Circ. Res.* 82, 739–750.

Redfern, W. S., Carlsson, L., Davis, A. S., Lynch, W. G., MacKenzie, I., Palethorpe, S., Siegl, P. K. S., Strang, I., Sullivan, A. T., Wallis, R., Camm, A. J., and Hammond, T. G. (2002). Relationships between preclinical cardiac electrophysiology, clinical QT interval prolongation and torsade de pointes for a broad range of drugs: evidence for a provisional safety margin in drug development. *Cardiovasc. Res.* 58, 32–45.

Roden, D. M., and Viswanathan, P. C. (2005). Genetics of acquired long QT syndrome. *J. Clin. Invest.* 115, 2025–2032.

Roeper, J., Sewing, S., Zhang, Y., Sommer, T., Wanner, S. G., and Pongs, O. (1998). NIP domain prevents N-type inactivation in voltage-gated potassium channels. *Nature* 391, 390–393.

Roosild, T. P., Le, K.-T., and Choe, S. (2004). Cytoplasmic gatekeepers of K^+-channel flux: a structural perspective. *Trends Biochem. Sci.* 29, 39–45.

Rosati, B., Marchetti, P., Crociani, O., Lecchi, M., Lupi, R., Arcangeli, A., Olivotto, M., and Wanke, E. (2000). Glucose- and arginine-induced insulin secretion by human pancreatic β-cells: the role of HERG K^+ channels in firing and release. *FASEB J.* 14, 2601–2610.

Ruppersberg, J. P., Frank, R., Pongs, O., and Stocker, M. (1991). Cloned neuronal IK(A) channels reopen during recovery from inactivation. *Nature* 353, 657–660.

Saenen, J. B., Labro, A. J., Raes, A., and Snyders, D. J. (2006). Modulation of HERG gating by a charge cluster in the N-terminal proximal domain. *Biophys. J.* 91, 4381–4391.

Sanguinetti, M. C, Jiang, C, Curran, M. E., and Keating, M. T. (1995). A mechanistic link between an inherited and an acquired cardiac arrhythmia. *Cell* 81, 299–307.

Sankaranarayanan, K., Varshney, A., and Mathew, M. K. (2005). N type rapid inactivation in human Kv1.4 channels: functional role of a putative C-terminal helx. *Mol. Membr. Biol.* 22, 389–400.

Scannevin, R. H., Wang, K., Jow, F., Megules, J., Kopsco, D. C., Edris, W., Carroll, K. C., Lü, Q., Xu, W., Xu, Z., Katz, A. H., Olland, S., Lin, L., Taylor, M., Stahl, M., Malakian, K., Somers, W., Mosyak, L., Bowlby, M. R., Chanda, P., and Rhodes, K. J. (2004). Two N-terminal domains of Kv4 K^+ channels regulate binding to and modulation by KchIP1. *Neuron* 41, 587–598.

Schäfer, R., Wulfsen, I., Behrens, S., Weinsberg, F., Bauer, C. K., and Schwarz, J. R. (1999). The erg-like current in rat lactotrophs. *J. Physiol.* 518, 401–416.

Scholle, A., Zimmer, T., Koopmann, R., Engeland, B., Pongs, O., and Benndorf, K. (2004). Effects of Kv1.2 intracellular regions on activation of Kv2.1 channels. *Biophys. J.* 87, 873–882.

Schönherr, R., and Heinemann, S. H. (1996). Molecular determinants for activation and inactivation of HERG, a human inward rectifier potassium channel. *J. Physiol.* 493, 635–642.

Schott, M. K., Antz, C., Frank, R., Ruppersberg, J. P., and Kalbitzer, H. R. (1998). Structure of the inactivation gate from the Shaler voltage-gated K^+ channel analyzed by NMR spectroscopy. *Eur. Biophys. J.* 27, 99–104.

Schrader, L. A., Ren, Y., Cheng, F., Bui, D., Sweatt, J. D., and Anderson, A. E. (2009). Kv4.2 is a locus for PKC and ERK/MAPK cross-talk. *Biochem. J.* 417, 705–715.

Schulteis, C. T., Nagaya, N., and Papazian, D. M. (1998). Subunit folding and assembly steps are interspersed during Shaker potassium channel biogenesis. *J. Biol. Chem.* 273, 26210–26217.

Schünke, S., Stoldt, M., Lecher, J., Kaupp, U. B., and Willbold, D. (2011). Structural insights into conformational changes of a cyclic nucleotide-binding domain in solution from Mesorhizobium loti K1 channel. *Proc. Natl. Acad. Sci. U.S.A.* 108, 6121–6126.

Sentenac, H., Bonneaud, N., Minet, M., Lacroute, F., Salmon, J. M., Gaymard, F., and Grignon, C. (1992). Cloning and expression in yeast of a plant potassium ion transport system. *Science* 256, 663–665.

Shahidullah, M., Santarelli, L. C., Wen, H., and Levitan, I. B. (2005). Expression of a calmodulin-binding KCNQ2 potassium channel fragment modulates neuronal M-current and membrane excitability. *Proc. Natl. Acad. Sci. U.S.A.* 102, 16454–16459.

Shamgar, L., Ma, L., Schmitt, N., Haitin, Y., Peretz, A., Wiener, R., Hirsch, J., Pongs, O., and Atali, B. (2006). Calmodulin is essential for cardiac IKS channel gating and assembly: impaired function in long-QT mutations. *Circ. Res.* 98, 1055–1063.

Smith, P. L., Baukrowitz, T., and Yellen, G. (1996). The inward rectification mechanism of the HERG cardiac potassium channel. *Nature* 379, 833–836.

Smith, P. L., and Yellen, G. (2002). Fast and slow voltage sensor movements in HERG potassium channels. *J. Gen. Physiol.* 119, 275–293.

Sokolova, O., Accardi, A., Gutierrez, D., Lau, A., Rigney, M., and Grigorieff, N. (2003). Conformational changes in the C terminus of Shaker K^+ channel bound to the rat Kvβ2-subunit. *Proc. Natl. Acad. Sci. U.S.A.* 100, 12607–12612.

Sokolova, O., Kolmakova-Partensky, L., and Grigorieff, N. (2001). Three-dimensional structure of a voltage-gated potassium channel at 2.5 nm resolution. *Structure* 9, 215–220.

Spector, P. S., Curran, M. E., Zou, A., Keating, M. T., and Sanguinetti, M. C. (1996). Fast inactivation causes rectification of the IKr channel. *J. Gen. Physiol.* 107, 611–619.

Stevens, L., Ju, M., and Wray, D. (2009). Roles of surface residues of intracellular domains of heag potassium channels. *Eur. Biophys. J.* 38, 523–532.

Subbiah, R. N., Clarke, C. E., Smith, D. J., Zhao, J., Campbell, T. J., and Vandenberg, J. I. (2004). Molecular basis of slow activation of the human ether-á-go-go related gene potassium channel. *J. Physiol.* 558, 417–431.

Subbiah, R. N., Kondo, M., Campbell, T. J., and Vandenberg, J. I. (2005). Tryptophan scanning mutagenesis of the HERG K^+ channel: the S4 domain is loosely packed and likely to be lipid exposed. *J. Physiol.* 569, 367–379.

Suh, B., and Hille, B. (2005). Regulation of ion channels by phosphatidylinositol 4,5-bisphosphate. *Curr. Opin. Neurobiol.* 15, 1–9.

Surti, T. S., Huang, L., Jan, Y. N., Jan, L. Y., and Cooper, E. C. (2005). Identification by mass spectrometry and functional characterization of two phosphorylation sites of KCNQ2/KCNQ3 channels. *Proc. Natl. Acad. Sci. U.S.A.* 102, 17828–17833.

Swartz, K. J. (2004). Towards a structural view of gating in potassium channels. *Nat. Rev. Neurosci.* 5, 905–916.

Swartz, K. J. (2008). Sensing voltage across lipid membranes. *Nature* 456, 891–897.

Taraska, J. W., and Zagotta, W. N. (2007). Structural dynamics in the gating ring of cyclic nucleotide-gated ion channels. *Nat. Struct. Mol. Biol.* 14, 854–860.

Terlau, H., Heinemann, S. H., Stühmer, W., Pongs, O., and Ludwig, J. (1997). Amino terminal-dependent gating of the potassium channel rat eag is compensated by a mutation in the S4 segment. *J. Physiol.* 502, 537–543.

Thomas, D., Wu, K., Wimmer, A.-B., Zitron, E., Hammerling, B. C., Kathöfer, S., Lueck, S., Bloehs, R., Kreye, V. A. W., Kiehn, J., Katus, H. A., Schoels, W., and Karle, C. A. (2004). Activation of cardiac human ether-a-go-go related gene potassium currents is regulated by α1A-adrenoreceptors. *J. Mol. Med.* 82, 826–837.

Thomas, D., Zhang, W., Karle, C. A., Kathöfer, S., Schöls, W., Kübler, W., and Kiehn, J. (1999). Deletion of protein kinase A phosphorylation sites in the HERG potassium channel inhibits activation shift by protein kinase A. *J. Biol. Chem.* 274, 27457–27462.

Thomas, D., Zhang, W., Wu, K., Wimmer, A.-B., Gut, B., Wendt-Nordahl, G., Kathöfer, S., Kreye, V. A. W., Katus, H. A., Schoels, W., Kiehn, J., and Karle, C. A. (2003). Regulation of potassium channel activation by protein kinase C independent of direct phosphorylation of the channel protein. *Cardiovasc. Res.* 59, 14–26.

Tristani-Firouzi, M., Chen, J., and Sanguinetti, M. C. (2002). Interactions between S4–S5 linker and S6 transmembrane domain modulate gating of HERG K^+ channels. *J. Biol. Chem.* 277, 18994–19000.

Trudeau, M. C., Warmke, J. W., Ganetzky, B., and Robertson, G. A. (1995). HERG, a human inward rectifier in the voltage-gated potassium channel family. *Science* 269, 92–95.

Tsai, W., Morielli, A. D., Cachero, T. G., and Peralta, E. G. (1999). Receptor protein tyrosine phosphatase α participates in the m1 muscarinic acetylcholine receptor-dependent regulation of Kv1.2 channel activity. *EMBO J.* 18, 109–118.

Uysal, S., Cuello, L. G., Cortes, D. M., Koide, S., Kossiakoff, A. A., and Perozo, E. (2011). Mechanism of activation gating in the full-length KcsA K^+ channel. *Proc. Natl. Acad. Sci. U.S.A.* 108, 11896–11899.

Vacher, H., and Trimmer, J. S. (2011). Diverse roles for auxiliary subunits in phosphorylation-dependent regulation of mammalian brain voltage-gated potassium channels. *Pflügers Arch.* 462, 631–643.

VanDongen, A. M. J., Frech, G. C., Drewe, J. A., Joho, R. H., and Brown, A. M. (1990). Alteration and restoration of K^+ channel function by deletions at the N- and C-termini. *Neuron* 5, 433–443.

Varhsney, A., Chanda, B., and Mathew, M. K. (2004). Arranging the elements of the potassium channel: the T1 domain occludes the cytoplasmic face of the channel. *Eur. Biophys. J.* 33, 370–376.

Varshney, A., and Mathew, M. K. (2003). A tale of two tails: cytosolic termini and K^+ channel function. *Prog. Biophys. Mol. Biol.* 83, 153–170.

Vemana, S., Pandey, S., and Larsson, H. P. (2004). S4 movement in a mammalian HCN channel. *J. Gen. Physiol.* 123, 21–32.

Viloria, C. G., Barros, F., Giráldez, T., Gómez-Varela, D., and de la Peña, P. (2000). Differential effects of amino-terminal distal and proximal domains in the regulation of human erg K^+ channel gating. *Biophys. J.* 79, 231–246.

Viskin, S. (1999). Long QT syndromes and torsade de pointes. *Lancet* 354, 1625–1633.

Wang, D. T., Hill, A. P., Mann, S. A., Tan, P. S., and Vandenberg, J. I. (2011). Mapping the sequence of conformational changes underlying selectivity filter gating in the Kv11.1 potassium channel. *Nat. Struct. Mol. Biol.* 18, 35–41.

Wang, G., and Covarrubias, M. (2006). Voltage-dependent gating rearrangements in the intracellular T1–T1 interface of a K^+ channel. *J. Gen. Physiol.* 127, 391–400.

Wang, G., Shahidullah, M., Rocha, C. A., Strang, C., Pfaffinger, P. J., and Covarrubias, M. (2005). Functionally active T1–T1 interfaces revealed by the accessibility of intracellular thiolate groups in Kv4 channels. *J. Gen. Physiol.* 126, 55–69.

Wang, J., Myers, C. D., and Robertson, G. A. (2000). Dynamic control of deactivation gating by a soluble amino-terminal domain in HERG K^+ channels. *Biophys. J.* 115, 749–758.

Wang, J., Trudeau, M. C., Zappia, A. M., and Robertson, G. A. (1998). Regulation of deactivation by an amino terminal domain in human ether-a-go-go-related gene potassium channels. *J. Gen. Physiol.* 112, 637–647.

Wang, L., and Sigworth, F. J. (2009). Structure of the BK potassium channel in a lipid membrane from electron cryomicroscopy. *Nature* 461, 242–245.

Warmke, J. W., and Ganetzky, B. (1994). A family of potassium channel genes related to eag in *Drosophila* and mammals. *Proc. Natl. Acad. Sci. U.S.A.* 91, 3438–3442.

Webster, S. M., del Camino, D., Dekker, J. P., and Yellen, G. (2004). Intracellular gate opening in Shaker K^+ channels defined by high-affinity metal bridges. *Nature* 428, 864–868.

Wen, H., and Levitan, I. B. (2002). Calmodulin is an auxiliary subunit of KCNQ2/3 potassium channels. *J. Neurosci.* 22, 7991–8001.

Whang, Z., Wilson, G. F., and Griffith, L. C. (2002). Calcium/calmodulin-dependent protein kinase II phosphorylates and regulates the *Drosophila* eag potassium channel. *J. Biol. Chem.* 277, 24022–24029.

Wiener, R., Haitin, Y., Shamgar, L., Fernández-Alonso, M. C., Martos, A., Chomsky-Hecht, O., Rivas, G., Attali, B., and Hirsch, J. A. (2008). The KCNQ1 (Kv7.1) COOH terminus, a multitiered scaffold for subunit assembly and protein interaction. *J. Biol. Chem.* 283, 5815–5830.

Wissmann, R., Bildl, W., Oliver, D., Beyermann, M., Kalbitzer, H. R., Bentrop, D., and Fakler, B. (2003). Solution structure and function of the "tandem inactivation domain" of the neuronal A-type potassium channel Kv1.4. *J. Biol. Chem.* 278, 16142–16150.

Wray, D. (2009). Intracellular regions of potassium channels: Kv2.1 and heag. *Eur. Biophys. J.* 38, 285–292.

Wulff, H., Castle, N. A., and Pardo, L. A. (2009). Voltage-gated potassium channels as therapeutic targets. *Nat. Rev. Drug Disc.* 8, 982–1001.

Wynia-Smith, S. L., Gillian-Daniel, A. L., Satyshur, K. A., and Robertson, G. A. (2008). hERG gating micro domains defined by S6 mutagenesis and molecular modeling. *J. Gen. Physiol.* 132, 507–520.

Xu, J., Yu, W., Jan, Y. N., Jan, L. Y., and Li, M. (1995). Assembly of voltage-gated potassium channels. Conserved hydrophilic motifs determine subfamily-specific interactions between the alpha-subunits. *J. Biol. Chem.* 270, 24761–24768.

Xu, M., Gu, Y., Barry, J., and Gu, C. (2010). Kinesin I transports tetramerized Kv3 channels through the axon initial segment via direct binding. *J. Neurosci.* 30, 15987–16001.

Yang, E. K., Alvira, M. R., Levitan, E. S., and Takimoto, K. (2001). Kvbeta subunits increase expression of Kv4.3 channels by interacting with their C termini. *J. Biol. Chem.* 276, 4839–4844.

Yellen, G. (1998). The moving parts of voltage-gated ion channels. *Q. Rev. Biophys.* 31, 239–295.

Yellen, G. (2002). The voltage-gated potassium channels and their relatives. *Nature* 419, 35–42.

Yu, F. H., Yarov-Yarovoy, V., Gutman, G. A., and Catterall, W. A. (2005). Overview of molecular relationships in the voltage-gated ion channel superfamily. *Pharmacol. Rev.* 57, 387–395.

Yus-Nájera, E., Santana-Castro, I., and Villarroel, A. (2002). The identification and characterization of noncontinuous calmodulin-binding site in noninactivating voltage-dependent KCNQ potassium channels. *J. Biol. Chem.* 277, 28545–28553.

Zagotta, W. N., Hoshi, T., and Aldrich, R. W. (1990). Restoration of inactivation in mutants of Shaker K^+ channels by a peptide derived from ShB. *Science* 250, 568–571.

Zagotta, W. N., Olivier, N. B., Black, K. D., Young, E. C., Olson, R., and Gouaux, E. (2003). Structural basis for modulation and agonist specificity of HCN pacemaker channels. *Nature* 425, 200–205.

Zhang, H., Craciun, L. C., Mirshahi, T., Rohács, T., Lopes, C. M. B., Jin, T., and Logothetis, D. E. (2003). PIP2 activates KCNQ channels, and its hydrolysis underlies receptor-mediated inhibition of M currents. *Neuron* 37, 963–975.

Zhang, M., Liu, J., Jiang, M., Wu, D.-M., Sonawane, K., Guy, H. R., and Tseng, G.-N. (2005). Interactions between charged residues in the transmembrane segments of the voltage-sensing domain in the hERG channel. *J. Membr. Biol.* 207, 169–181.

Zhang, M., Liu, J., and Tseng, G.-N. (2004). Gating charges in the activation and inactivation processes of the HERG channel. *J. Gen. Physiol.* 124, 703–718.

Zhao, L.-L., Wu, A., Bi, L.-J., Liu, P., Zhang, X.-E., Jiang, T., Jin, G., and Qi, Z. (2009). Length-dependent regulation of the Kv1.2 channel activation by its C-terminus. *Mol. Membr. Biol.* 26, 186–193.

Zheng, R., Thompson, K., Obeng-Gymah, E., Alessi, D., Chen, J., Cheng, H., and McDonald, T. V. (2010). Analysis of the interactions between the C-terminal cytoplasmic domains of KCNQ1 and KCNE1 channel subunits. *Biochem. J.* 428, 75–84.

Zhou, M., Morais-Cabral, J. H., Mann, S., and MacKinnon, R. (2001). Potassium channel receptor site for the inactivation gate and quaternary amine inhibitors. *Nature* 411, 657–661.

Zhou, W., and Jan, L. (2010). A twist on potassium channel gating. *Cell* 141, 920–922.

Ziechner, U., Schönherr, R., Born, A., Gavrilova-Ruch, O., Glaser, R. W., Malesevic, M., Küllertz, G., and Heinemann, S. H. (2006). Inhibition of human ether á go-go potassium channels by Ca^{2+}/calmodulin binding to the cytosolic N- and C-termini. *FEBS J.* 273, 1074–1086.

Conflict of Interest Statement: The authors declare that the research was conducted in the absence of any commercial or financial relationships that could be construed as a potential conflict of interest.

Received: 24 October 2011; accepted: 05 March 2012; published online: 23 March 2012.

Citation: Barros F, Domínguez P and de la Peña P (2012) Cytoplasmic domains and voltage-dependent potassium channel gating. Front. Pharmacol. ***3****:49. doi: 10.3389/fphar.2012.00049*

This article was submitted to Frontiers in Pharmacology of Ion Channels and Channelopathies, a specialty of Frontiers in Pharmacology.

frontiers in
PHARMACOLOGY

REVIEW ARTICLE
published: 08 May 2012
doi: 10.3389/fphar.2012.00083

Voltage-dependent gating of hERG potassium channels

Yen May Cheng and Tom W. Claydon*

Department of Biomedical Physiology and Kinesiology, Simon Fraser University, Burnaby, BC, Canada

Edited by:
Gildas Loussouarn, University of Nantes, France

Reviewed by:
Zeineb Es-Salah-Lamoureux, INSERM, France
Medha M. Pathak, University of California Irvine, USA

****Correspondence:***
Tom W. Claydon, Department of Biomedical Physiology and Kinesiology, Simon Fraser University, 8888 University Drive, Burnaby, BC, Canada V5A 1S6.
e-mail: thomas_claydon@sfu.ca

The mechanisms by which voltage-gated channels sense changes in membrane voltage and energetically couple this with opening of the ion conducting pore has been the source of significant interest. In voltage-gated potassium (Kv) channels, much of our knowledge in this area comes from *Shaker*-type channels, for which voltage-dependent gating is quite rapid. In these channels, activation and deactivation are associated with rapid reconfiguration of the voltage-sensing domain unit that is electromechanically coupled, via the S4–S5 linker helix, to the rate-limiting opening of an intracellular pore gate. However, fast voltage-dependent gating kinetics are not typical of all Kv channels, such as Kv11.1 (human ether-à-go-go related gene, hERG), which activates and deactivates very slowly. Compared to *Shaker* channels, our understanding of the mechanisms underlying slow hERG gating is much poorer. Here, we present a comparative review of the structure–function relationships underlying activation and deactivation gating in *Shaker* and hERG channels, with a focus on the roles of the voltage-sensing domain and the S4–S5 linker that couples voltage sensor movements to the pore. Measurements of gating current kinetics and fluorimetric analysis of voltage sensor movement are consistent with models suggesting that the hERG activation pathway contains a voltage independent step, which limits voltage sensor transitions. Constraints upon hERG voltage sensor movement may result from loose packing of the S4 helices and additional intra-voltage sensor counter-charge interactions. More recent data suggest that key amino acid differences in the hERG voltage-sensing unit and S4–S5 linker, relative to fast activating *Shaker*-type Kv channels, may also contribute to the increased stability of the resting state of the voltage sensor.

Keywords: hERG, gating, voltage sensor, gating charge transfer center, potassium channel, S4-S5 linker, *Shaker*

INTRODUCTION

OVERVIEW

The finely tuned voltage-dependence of ion channels has long been a topic of interest for ion channel biophysicists. For voltage-gated K^+ (Kv) channels, much of the knowledge gathered to date on voltage-dependent gating has focused on structure–function relationships in the archetypal *Shaker* channel and other closely related members of the Kv1 family. However, the fast voltage-dependent activation (opening) and deactivation (closing) gating kinetics of *Shaker* are not typical of all Kv channels. For example, Kv11.1 (human ether-à-go-go related gene, hERG) channels activate and deactivate very slowly. hERG channels underlie the cardiac delayed rectifier current, I_{Kr}, and their unique voltage-dependent gating properties are critical to normal repolarization during the cardiac action potential. This highlights the importance of understanding the processes involved in hERG function. However, compared to *Shaker*-like channels, the processes regulating the gating of hERG channels are much less clear. This review focuses on the molecular determinants of the unique voltage-dependent activation and deactivation kinetics of hERG channels. To begin, the rest of this section provides a brief review of general Kv channel structure and function and an introduction to the differences between hERG and *Shaker* gating kinetics. The following sections will then focus on the roles of the S4 voltage sensor and S4–S5 linker in the slow gating of hERG channels. As part of this discussion potentially important structural differences between hERG and *Shaker* channels within these regions will be highlighted.

BASIC Kv CHANNEL ARCHITECTURE

In their simplest form, Kv channels consist of a tetrameric assembly of identical α-subunits around a central pore. Each α-subunit has six α-helical transmembrane segments, S1–S6, and cytoplasmic N- and C-terminal domains (**Figure 1A**). The voltage-sensing domain of each α-subunit is comprised of segments S1–S4. Importantly, the S4 segment has the distinction of containing four to eight basic residues (Arg or Lys), spaced apart by pairs of hydrophobic residues, that allow it to act as the primary voltage sensor. The S1–S3 segments, which possess a number of negatively charged residues (Papazian et al., 1987), complete the voltage-sensing domain and are thought to help stabilize the positively charged S4 segment in the lipid bilayer and to define the pathway for its movement through the electric field (reviewed in Börjesson and Elinder, 2008; Chanda and Bezanilla, 2008; Catterall, 2010).

The pore domain of an α-subunit is formed by the S5 and S6 segments, which are joined by a re-entrant pore helix and loop (P-loop). The X-ray crystal structures of selected bacterial and eukaryotic Kv channels have been solved (Jiang et al., 2003; Long et al., 2005a, 2007; Chen et al., 2010) and show that the pore domains are arranged with four-fold symmetry around the ion conduction pathway, while the voltage-sensing domains lie at the periphery (**Figure 1B**; Long et al., 2005a; Chen et al., 2010).The

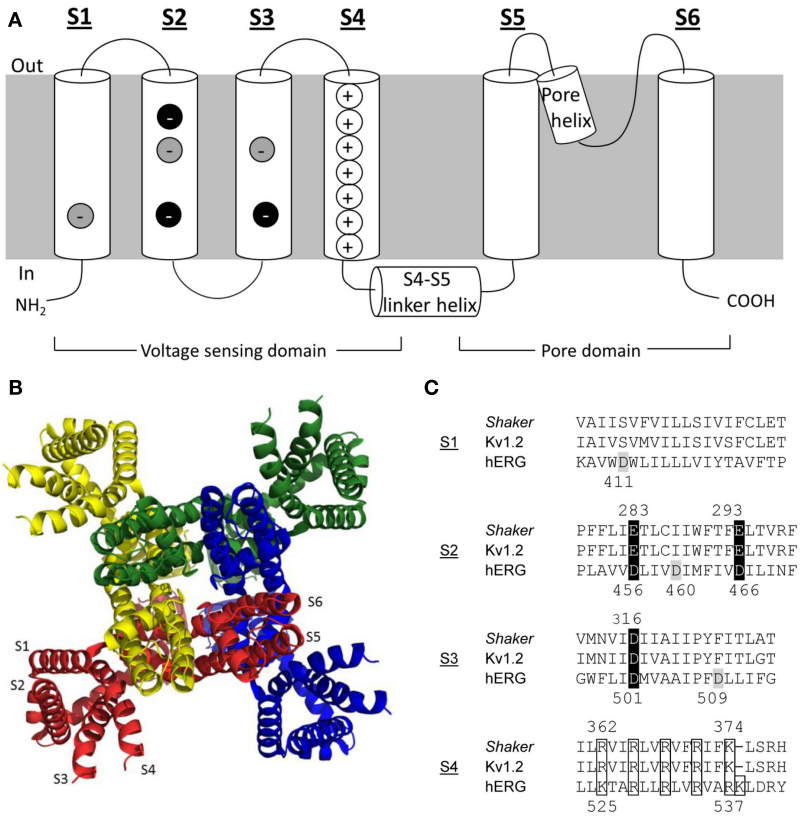

FIGURE 1 | Kv channel structure. (A) Cartoon representation of the membrane topology of a Kv channel α-subunit. Key charged residues within the voltage-sensing domain are highlighted. Negative charges highlighted in black are highly conserved, whereas those in gray are conserved only in the eag channel family. **(B)** Ribbon representation of the Kv channel tetrameric assembly based on the Kv1.2 crystal structure (Long et al., 2005a). Each subunit has been highlighted a different color for clarity. The model shows a view from the top of the channel looking down along the permeation pathway (at center). **(C)** Alignments of primary S1–S4 sequences in *Shaker,* Kv1.2, and hERG channels. Key charged residues are highlighted with the same color scheme as in panel A.

crystal structures of bacterial KcsA and MthK channels (Doyle et al., 1998; Jiang et al., 2002a,b) suggested that the convergence of the bottom of the M2 helices (analogous to S6 in eukaryotic Kv channels) at a "bundle crossing" forms an activation gate to control access between the pore and the cytoplasm. A conserved glycine residue has been proposed to serve as the "hinge" that allows the activation gate to open and close (Jiang et al., 2002a). Eukaryotic channels typically also have a PxP motif that lies distal to the glycine hinge, which is thought to introduce a sharp bend in the S6 helix that may contribute to opening and closing of the activation gate (del Camino et al., 2000; del Camino and Yellen, 2001) and/or coupling of the pore to the voltage-sensing domain (Lu et al., 2002; Long et al., 2005b). Although the X-ray crystal structures present only a static view and cannot alone show the dynamics of Kv channel gating, they have provided the structural framework necessary to describe the processes underlying Kv channel gating in response to changes in membrane voltage.

THE ELECTROMECHANICAL BASIS OF VOLTAGE-DEPENDENT Kv CHANNEL GATING

The culmination of Kv channel activation in response to depolarization is the opening of the intracellular gate allowing passage of K^+ ions through the channel pore. Subsequent membrane repolarization causes channel deactivation and the closure of the activation gate. It is instructive to consider the electromechanical processes of activation and deactivation in two parts, where (i) the change in membrane potential is first "sensed" by the channel and then (ii) translated into opening or closing of the activation gate.

Prior to any structural information, Hodgkin and Huxley (1952) proposed that voltage-dependent K^+ and Na^+channels possessed four charged particles that resided in the membrane electric field and served as voltage sensors, moving between activated and deactivated positions in response to changes in voltage. Membrane depolarization increased the probability that all four voltage sensors would be in the activated position, which was necessary for channel opening. When any of the sensors were in a deactivated position, the channel would be in one of several possible closed states. Evidence in support of this model was provided some 22 years later by measurements of the movement of gating charges across the membrane electric field, showing a capacitive gating current associated with channel activation (e.g., Armstrong and Bezanilla, 1974; Gilly and Armstrong, 1980). The S4 transmembrane segment was proposed to serve as the voltage sensor when it was found that Kv channel α-subunits and Nav

channel domains contain a conserved sequence of repeating positively charged residues (Noda et al., 1984; Papazian et al., 1987). While the role of S4 as the primary voltage sensor for Nav and Kv channels is now widely accepted, the dynamics of sensor movement through the electric field, which trigger opening and closing of channel, remain to be precisely defined.

Three general models of voltage-dependent S4 movement have been proposed: (i) the helical-screw or sliding helix model, where S4 rotates along its axis while being translated across the membrane to move gating charges across the electric field (Durell et al., 1998; Keynes and Elinder, 1999); (ii) the transporter-like model, where a mostly rotational movement of S4 (and perhaps a rearrangement of the membrane) essentially flips S4 charges from one side of the membrane to the other (Papazian and Bezanilla, 1997), and; (iii) the paddle model, initially based on the crystal structure of KvAP, in which a voltage sensor paddle comprised of S4 and the C-terminal half of S3 form a rigid structure that moves through the membrane and in close proximity to S1 and S2 (Jiang et al., 2003). While there has been significant debate over which model is most accurate, in recent years the models show some consensus. These models suggest that the series of gating charges is moved 6–15 Å across the membrane by S4 rotation and translation. A more detailed discussion concerning models of voltage sensor movement can be found in several recent reviews (Börjesson and Elinder, 2008; Chanda and Bezanilla, 2008; Catterall, 2010).

Movement of the voltage-sensing unit in response to changes in membrane potential is translated into the concerted opening or closing of the activation gate within the pore domain. Solution of the high resolution Kv1.2 crystal structure shows that within the same α-subunit the voltage-sensing domain lies away from the pore domain (**Figure 1B**), such that the top of S4 is actually in closer proximity with the pore domain of a neighboring subunit (Long et al., 2005a; Chen et al., 2010). On the cytoplasmic face of the channel the α-helical S4–S5 linker appears to lie across the distal S6 helix below the PxP motif within the same subunit, suggestive of a possible coupling mechanism between the two domains. Such structural observations are consistent with functional studies showing that specific interactions between the S4–S5 linker and the lower S6 segment are critical for voltage-dependent gating (e.g., Chen et al., 2001; Ding and Horn, 2002, 2003; Lu et al., 2002; Tristani-Firouzi et al., 2002; Labro et al., 2008; Nishizawa and Nishizawa, 2009). In the light of this evidence, it is proposed that the outward movement of S4 upon depolarization may create tension in the S4–S5 linker, which would allow the C-terminal end of S6 to pivot away from the central axis of the pore to open the activation gate. Conversely, repolarization and inward movement of S4 would tend to push the S4–S5 linker radially inward and exert a force on the internal end of S6 so that the activation gate closes.

hERG CHANNELS HAVE UNIQUELY SLOW ACTIVATION AND DEACTIVATION KINETICS

Compared to most other Kv channels, hERG channel gating kinetics are unusually slow (**Figure 2**). While archetypal *Shaker* channels activate with time constants of a few milliseconds, hERG channels activate and deactivate over *hundreds* of milliseconds (Sanguinetti and Tristani-Firouzi, 2006). Voltage-clamp fluorimetry (VCF) and gating current data have been purported to show that hERG slow activation and deactivation are due, at least in part, to rate-limiting voltage sensor movement (Smith and Yellen, 2002; Piper et al., 2003). In stark contrast, S4 movement in *Shaker* and other Kv channels is very rapid (e.g., Bezanilla et al., 1994; Zagotta et al., 1994b; Mannuzzu et al., 1996; Cha and Bezanilla, 1997; Loots and Isacoff, 1998; Kanevsky and Aldrich, 1999) and the rate-limiting step for channel opening and closing lies further along the activation pathway and most likely involves the final concerted opening (or closing) of the activation gate (Ledwell and Aldrich, 1999; Bezanilla, 2000; Fedida and Hesketh, 2001). The comparatively slower voltage sensor movement in hERG channels points to additional barriers or constraints to outward S4 movement that must be overcome before hERG channels can open.

In addition to putative slow S4 movement, there may be other mechanisms underlying slow hERG activation and deactivation gating. For example, we have shown that electromechanical coupling between the voltage-sensing domain and the pore domain by the S4–S5 linker helix is less efficient in hERG when compared

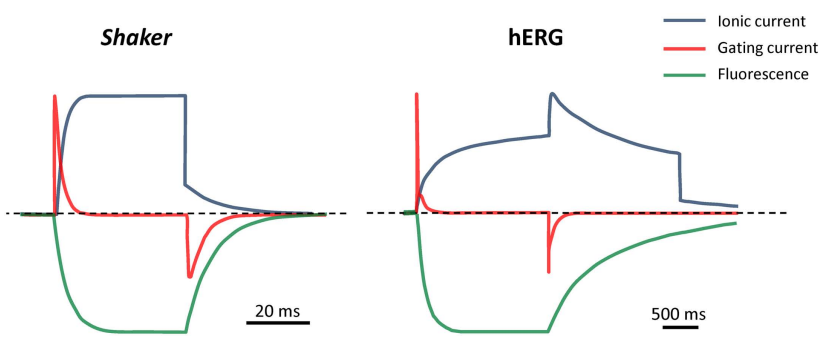

FIGURE 2 | Comparison of gating and kinetics in *Shaker* and hERG channels. Cartoon representation of ionic current, gating current and fluorescence reports for *Shaker* (fast-inactivation removed) and hERG channels in response to a depolarizing step from -80 to 0 mV, followed by a repolarizing step to -60 mV. Fluorescence traces represent reports from fluorophores attached at the outer end of S4, to *Shaker* A359C or hERG L520C. Note the different timescales and step durations for the fast-activating *Shaker* and slow-activating hERG channels. Schematics were generated based on data from primary sources cited in the text (see Does Slow S4 Voltage Sensor Movement Underlie Slow hERG Gating Kinetics?").

to *Shaker* channels (e.g., Van Slyke et al., 2010) and this could contribute to slow responses to changes in membrane potential. hERG deactivation also appears to be more complex than that of *Shaker* channels, in that additional modulation of deactivation may come from the interaction of an N-terminal Per-Arnt-Sim (PAS) domain with other regions of the channel, perhaps the S4–S5 linker and/or the C-terminus (Morais Cabral et al., 1998; Wang et al., 1998; Gustina and Trudeau, 2009, 2011; Fernández-Trillo et al., 2011).

Following activation, and with continued depolarization, many Kv channels undergo an additional gating process of inactivation where they enter into a non-conducting inactivated state that is distinct from the closed state occupied at negative potentials. Typically, inactivation is voltage-independent and relatively slow compared to channel activation, such that significant outward current may be observed before inactivation is observed as a decay in current (reviewed in Kurata and Fedida, 2006). hERG inactivation is unique in that both its onset and recovery (1–10 ms timecourses) are much faster than the kinetics for activation and deactivation (Wang et al., 1997). This is important for its physiological role conducting repolarizing current during the late phase of the cardiac action potential (Sanguinetti and Tristani-Firouzi, 2006). In further contrast to inactivation in channels such as *Shaker*, hERG inactivation also appears to depend directly on the membrane potential and the S4 segment has been proposed to serve as the voltage sensor for both the inactivation and activation processes (Piper et al., 2003). A thorough discussion of the voltage-dependent features of hERG (and other Kv channel) inactivation is beyond the scope of this review, and will not be discussed in further detail here.

In sum, compared to other members of the K^+ channel superfamily, hERG channels exhibit uniquely slow activation and deactivation kinetics. The remainder of this review turns attention to the structure–function relationships underlying these slow gating kinetics, with particular focus on the interactions involving the charged S4 voltage sensor and the S4–S5 linker helix that couples the voltage-sensing domain to the pore. A comparison between these structures in hERG and *Shaker* channels will be presented, along with a discussion of the extent to which differences in the amino acid sequences of these regions account for the differences in the voltage-dependent gating kinetics of these two channel types. Finally, the question of whether a gating charge transfer center like that recently described for *Shaker* channels is present in hERG channels is addressed.

REGULATION OF VOLTAGE SENSOR MOVEMENT IN hERG AND *SHAKER* CHANNELS

IDENTITY AND LOCATION OF CHARGE-CARRYING RESIDUES IN THE VOLTAGE-SENSING DOMAIN

As we do not yet have X-ray crystal structures for hERG or *Shaker* channels, much of the structural information for these and other Kv channels derives from comparisons of the primary sequences and alignment with the Kv1.2 X-ray crystal structures (Long et al., 2005a; Chen et al., 2010). Based on the high sequence homology between Kv1.2 and *Shaker* channels, as well as the Kv1.2 crystal structure, the S4 helix in *Shaker* contains six basic residues (R1-R4, K5, R6; **Figure 1**), consistent with earlier predictions (Papazian et al., 1987). Early mutagenesis studies (Liman et al., 1991; Papazian et al., 1991) had shown that neutralization of R1–K5 resulted in a reduced voltage-dependence of activation, which suggested that they, and consequently the S4 segment, were involved in voltage sensing. Direct measurements of gating charge from gating current experiments in *Shaker* have shown that channel opening is associated with the movement of ∼12–13 e_0 charges across the electric field (Schoppa et al., 1992; Aggarwal and Mackinnon, 1996; Noceti et al., 1996; Seoh et al., 1996). Gating current measurements from charge neutralization mutants confirmed that the gating charge associated with activation was indeed carried by the S4 charges, with the largest contributions made from the four outermost arginine residues (R1–R4) and perhaps a smaller contribution from K5 (Aggarwal and Mackinnon, 1996; Seoh et al., 1996). The potential contributions to the gating charge of three negatively charged residues in S2 (E283, E293) and S3 (D316) that are highly conserved among Kv channels (**Figure 1A,C**) have similarly been assessed; with a significant contribution coming from E293 in S2 and a much smaller contribution from D316 (Seoh et al., 1996).

In addition to these charge neutralization studies, other studies were conducted to determine the extent of S4 translocation across the membrane. Some used the substituted cysteine accessibility method, which involves mutating a specific residue to a cysteine and determining its state-dependent accessibility to externally or internally applied cysteine-reactive compounds such as methanethiosulfonate (MTS) reagents or *p*-chloromercuribenzenesulfonate (pCMBS). After accounting for methodological differences, the results of these studies (Larsson et al., 1996; Yusaf et al., 1996; Baker et al., 1998; Wang et al., 1999) suggested that the S4 charged residues reside in an intracellularly accessible water-filled crevice at negative resting potentials and that depolarization results in the first two (R1, R2) and perhaps the third (R3) positively charged residues moving to an externally accessible position. In a different approach, Starace et al. (1997), Starace and Bezanilla (2001), Starace and Bezanilla (2004) substituted the S4 charges with histidine residues and determined their accessibility by examining the state-dependent titration of gating charge by intra- and extracellular pH. The results of these studies also suggested that at resting potentials, the *Shaker* S4 charges reside in a narrow, intracellularly accessible water-filled crevice and membrane depolarization results in the translocation of R1-R3, and most likely R4, but not K5 or R6, across the membrane to an extracellularly accessible crevice (Starace et al., 1997; Starace and Bezanilla, 2001). Compared to the substituted cysteine accessibility method, the potentially charge-conserving nature of histidine substitutions may contribute to a more native conformation of the voltage-sensing domain, as it has been reported that cysteine substitutions can affect the S4 topology such that the membrane spanning portion is reduced (Wang et al., 1999). Intriguingly, histidine substitution at R1 or R4 resulted in the formation of a proton pore at hyperpolarized and depolarized potentials, respectively (Starace and Bezanilla, 2001, 2004). This suggests that the substituted histidine residue at position 1 and 4 bridges a very narrow gap between the external and internal crevices in the resting and activated states, respectively (Starace and Bezanilla, 2001, 2004). Compared to the substituted cysteine accessibility method,

the ability of the histidine scanning mutagenesis to show translocation of R3 and R4 likely arises from the small size and improved mobility of protons relative to MTS and pCMBS. To sum, activation of *Shaker* channels results in the translocation of R1-R3 and probably R4 across the membrane, consistent with the conclusion from gating current measurements showing that much of the gating charge is carried by these four residues (reviewed in detail in Bezanilla, 2000; Catterall, 2010).

The primary sequence homology of hERG channels with *Shaker* and Kv1.2 channels is considerably poorer than that observed within the Kv1 channel family (**Figure 1C**). There has been little consensus on how the sequences of hERG and *Shaker* channels should be aligned and, thus, how to define exactly where the transmembrane segment borders (i.e., extracellular and intracellular limits) are in hERG channels. Within the voltage-sensing domain of hERG, the S4 segment has, depending on the alignment used, up to seven basic residues (K1, R2–R5, K6, R7), although the repeating sequence of a positive residue at every third position separated by two hydrophobic residues capitulates after the fifth arginine residue (**Figure 1C**). The amount of gating charge moved with hERG activation has been estimated to be ∼6 e_0 using limiting slope analysis of the voltage-dependence of channel open probability (P_o); even after correction to 8 e_0 by factoring in the underestimation of total charge by the limiting slope method (Zhang et al., 2004), this is still less than the ∼12 e_0 observed for *Shaker*. Cysteine substitution of only the three outermost hERG S4 positive charges (K1, R2, R3) resulted in significant decreases in the total gating charge, which suggests that they transfer most of the charge moved during activation (Zhang et al., 2004), compared to the first four charges in *Shaker* (see above). Similar to E293 in *Shaker*, hERG D466 in S2 also appears to have a role in gating charge transfer (Zhang et al., 2004). The contributions of the other two conserved negative residues in S2 (D456) and S3 (D501), as well as three additional non-conserved negative charges in the voltage-sensing domain (Liu et al., 2003) to gating charge have not been assessed. To account for the ∼1 e_0 per subunit difference in gating charge between hERG and *Shaker,* Zhang et al. (2004) aligned the first positive charge in hERG (K1; i.e., K525) with the second positively charged residue in *Shaker* (R2; i.e., R365) and rKv1.2 (R297). This was supported by the finding that hERG K1 but not R2 was accessible to externally applied MTSET (Subbiah et al., 2004; Zhang et al., 2004), which the authors interpreted to be consistent with similar experiments showing inaccessibility of the equivalent *Shaker* R3 residue to external MTSET (Larsson et al., 1996; Baker et al., 1998). A recent study using ROSETTA modeling and molecular dynamics to generate a hERG structural model based on the available Kv1.2, KvAP, and Kv1.2–Kv2.1 chimera X-ray crystal structures is also supportive of this hERG K1:*Shaker* R2 alignment (Subbotina et al., 2010).

The S4 alignment for hERGK1 and *Shaker* R2 presented by Zhang et al. (2004) had been proposed before, based on the results of alignment software (Liu et al., 2003; Subbiah et al., 2004), and has since been used by others to interpret their findings (Subbiah et al., 2005; Zhang et al., 2005; Es-Salah-Lamoureux et al., 2010). As alluded to above, however, an alternative alignment where hERG K1 aligns with *Shaker* R1 has also frequently been used (Wang et al., 1997; Smith and Yellen, 2002; Silverman et al., 2003; Piper et al., 2005; Elliott et al., 2009), based primarily on computer-generated alignments of the hERG and *Shaker* sequences. Support for this second alignment comes from a recent report that a stretch of hERG S4 residues (523–529) encompassing the two outermost positive charges (K525, R528) becomes accessible to external pCMBS with depolarization (Elliott et al., 2009). The region of external pCMBS accessible *Shaker* S4 residues (I360–L366) also includes the first two charged residues (R362, R365; Yusaf et al., 1996), which suggests that the extent of S4 movement is very similar in both hERG and *Shaker* channels. These results, along with the finding that both hERG L523 and *Shaker* I360 correspond to the interface between the extracellular solution and the cell membrane at rest (Wang et al., 1999; Elliott et al., 2009), support an alignment of hERG K1 with *Shaker* R1. Furthermore, comparison of the shifts in the voltage-dependence of activation caused by cysteine substitution along the hERG and *Shaker* S4 segments also agrees with a hERG K1:*Shaker* R1 alignment (Elliott et al., 2009). The disagreement of these results obtained with pCMBS with those showing that hERG R528C was inaccessible to MTSET (Zhang et al., 2004) were reconciled by demonstrating that MTSET can react with externally accessible cysteines in hERG and *Shaker* without producing an appreciable effect on channel function and may therefore give a less reliable report on cysteine accessibility (Wang et al., 1999; Elliott et al., 2009). A consequence of a hERG K1:*Shaker* R1 alignment is that the reasons for the 4 e_0 difference in gating charge between the two channels remains unclear.

DOES SLOW S4 VOLTAGE SENSOR MOVEMENT UNDERLIE SLOW hERG GATING KINETICS?

In the previous section, we have discussed the structure of the voltage-sensing domain and showed that the locations of the charge-carrying residues in the hERG voltage-sensing domain are similar to those for *Shaker* and Kv1.2 channels. Furthermore, the extent of S4 translocation across the membrane with depolarization appears to be comparable in each of these channels. Thus, gross structural differences between the voltage-sensing domains are unlikely to be the underlying reason for the much slower activation and deactivation kinetics of hERG compared to *Shaker* channels. We now turn attention toward the rate at which the S4 voltage sensor moves in response to changes in membrane potential. VCF measurements on hERG S4 movement were first performed a decade ago when three consecutive residues (E518, E519, and L520) in the extracellular S3–S4 linker were individually mutated to cysteines and labeled with a fluorescent probe (tetramethylrhodamine-5-maleimide, TMRM); changes in the fluorescent report from these positions were correlated with the voltage- and time-dependence of the ionic current to provide a "picture" of S4 movement (Smith and Yellen, 2002). Fluorophores attached to E518 and E519 showed both fast and slow voltage-dependent changes in fluorescence, while L520 gave a single slow report (**Figure 2**). The slow fluorescence report from all three positions correlated well with the voltage-dependent and temporal properties of ionic current activation and deactivation and responded in parallel to maneuvers that altered the kinetics of channel deactivation. In *Shaker* channels, fluorescent reports from similar positions indicated that S4 movement occurs *prior to* and *at lower potentials* than channel opening (Mannuzzu et al., 1996;

Cha and Bezanilla, 1997; Loots and Isacoff, 1998). The overlap of the voltage- and time-dependence of the hERG slow fluorescence and ionic current signals suggested that S4 movement reported by the probe is slow and likely the rate-limiting step in the activation process (Smith and Yellen, 2002). Although the fast fluorescence report from probes at E518 and E519 had kinetics and a voltage-dependence that were well correlated with those of channel inactivation, manipulations that affected inactivation did not alter the fast fluorescence (Smith and Yellen, 2002) suggesting that the fast fluorescence component is unlikely to represent a direct report on inactivation gating dynamics.

Shortly after Smith and Yellen's (2002) VCF measurements, the first hERG gating currents were recorded and showed that the kinetics of the movement of the majority of gating charge were remarkably slower ($\tau \approx 50$ ms) than that reported for other Kv channels, such as *Shaker* (**Figure 2**). Thus, these electrical measurements supported the conclusion from the fluorescence measurements that slow S4 movement underlies hERG gating kinetics. hERG gating currents are unique among those of Kv channels in that they have two components: (i) an initial very rapid transient ($\tau \approx 0.5$ ms) and (ii) a slowly decaying component ($\tau \approx 50$ ms) that carries the majority of the gating charge (**Figure 2**; Piper et al., 2003). In contrast to the VCF data, which suggested that S4 movement occurred with a similar voltage-dependence to channel activation, the voltage-dependence of total gating charge (Q–V) movement was left-shifted relative to the conductance–voltage (G–V) relationship. This is more in line with Q–V and G–V relationships previously described for *Shaker* channels (Bezanilla, 2000) and would appear to indicate that the majority of hERG gating charge movement precedes channel opening. Interestingly, the Q–V for the fast component was right-shifted compared to the G–V and very similar to the fluorescence–voltage relationship for the fast fluorescence component reports from E518 and E519 (Smith and Yellen, 2002). Also consistent with the reported fluorescence data, the fast gating charge component did not correlate well with hERG inactivation properties (other than its kinetics), indicating that the fast gating charge movement did not reflect charge movement associated with hERG inactivation. Instead, based on the observation that the fast gating charge component contributed to the majority of charge moved at potentials below the activation threshold, Piper et al. (2003) concluded that the fast gating charge transient corresponded to transitions between closed states early in the activation pathway. In sum, the results of early VCF and gating current experiments in hERG channels suggested that gating charge and S4 movement occurs prior to channel opening, but that it is slow and therefore contributes to the slow activation process characteristic of hERG.

The view that the slow fluorescence reports from E518C, E519C, and L520C is correlated to S4 movement during activation has recently been questioned. It had previously been reported that labeling of wild-type (WT) hERG with TMRM did not result in any voltage-dependent changes in fluorescence, which was interpreted to indicate that native cysteine residues did not contribute to the fluorescence observed from the mutant channels (Smith and Yellen, 2002; Van Slyke et al., 2010). Es-Salah-Lamoureux et al. (2010) found that TMRM binding to two native cysteine residues in the S1–S2 linker resulted in fluorescence reports that modified the report from E519C in the S3–S4 linker. When the native cysteine residues were substituted with valine, the fluorescence report from E519C was augmented and the fast fluorescence report had a voltage-dependence (F–V) that was left-shifted from the G–V relationship and consistent with the voltage-dependence of total gating charge in hERG movement (Piper et al., 2003). The authors proposed that the fast fluorescence component from E519C reports on rapid S4 movement while the slow component reports on subsequent rearrangements associated with pore opening and closing. Instead, it may be that the fast fluorescence change from E519C reports on the early rapid gating charge movements reported by Piper et al. (2003). Further investigation is required to determine precisely which reconfigurations of the channel the VCF measurements from the hERG S3-S4 linker are reporting on.

hERG ACTIVATION MAY INVOLVE A RATE-LIMITING STEP THAT IS VOLTAGE-INDEPENDENT

In addition to the results of VCF and gating current experiments that suggest the rate of hERG activation is limited by slow S4 movement, analysis of macroscopic ionic currents and kinetic simulations have led to predictions that the hERG activation pathway involves a voltage-independent, rate-limiting step. Characterization of the voltage-dependence of the activation time constant (τ_{act}) showed that hERG channels activate in a sigmoidal fashion (Trudeau et al., 1995; Liu et al., 1996; Wang et al., 1997), which suggests that the activation pathway is a multi-step process, similar to other Kv channels, such as *Shaker* (Zagotta et al., 1994a; Fedida and Hesketh, 2001). Detailed analysis of the late phase of activation (sometimes measured as the last 50% of the activation time course) suggested that τ_{act} nears saturation at strongly depolarized potentials (15 ms at +160 mV), which is indicative of a voltage-independent step that becomes rate-limiting at positive potentials (Liu et al., 1996; Wang et al., 1997; Subbiah et al., 2004). The strong voltage-dependence of the deactivation rate implies that the final closed to open (and open to closed) transition must be voltage-dependent, thereby requiring that the voltage-independent transition precede the final opening transition (Liu et al., 1996; Wang et al., 1997). Thus, the final linear kinetic model (**Figure 3A**) for hERG gating proposed by Wang et al. (1997) has three closed states preceding the final open state with a voltage-independent transition between the second and third closed states, immediately before the final opening step. Several other gating schemes have also been proposed, with the major variations having only two closed states (Oehmen et al., 2002) or with the addition of a direct transition from the final closed state to the inactivated state (i.e., channel opening is not required for inactivation; Clancy and Rudy, 2001; Mazhari et al., 2001). All of these models retain a voltage-independent transition prior to the final opening step. A recent comparison of the above kinetic models found that the simple linear model first proposed by Wang et al. (1997) is best able to reproduce the qualitative and quantitative behavior of hERG channels under voltage-clamp and action potential simulations (Bett et al., 2011).

The model for hERG gating proposed by Wang et al. (1997) is limited in that it does not correlate transitions in the model with changes in individual α-subunits, in contrast to gating schemes such as the Zagotta Hoshi Aldrich (ZHA; Zagotta et al., 1994a)

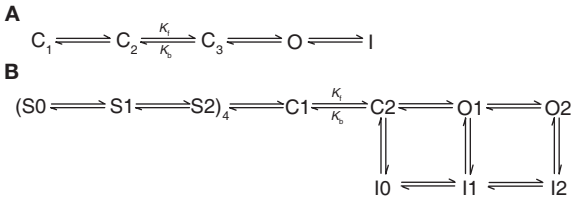

FIGURE 3 | Proposed schemes to describe hERG channel gating. **(A)** the three closed state model proposed by Wang et al. (1997). Kf and Kb represent voltage independent transitions that are rate limiting for opening at strongly depolarized potentials. **(B)** The modified gating scheme proposed by Piper et al. (2003) to account for the biphasic nature of hERG gating currents and multiple sequential voltage-dependent transitions of the voltage sensor.

and Schoppa and Sigworth (S–S; Schoppa and Sigworth, 1998a) models for *Shaker* channel gating that were based on combined gating current, macroscopic ionic current and single channel current data. For example, the S–S model suggests that each subunit independently proceeds through three voltage-dependent gating steps, followed by two concerted transitions to a final closed state and then to the open state (Schoppa and Sigworth, 1998a; Fedida and Hesketh, 2001). Following the first records of hERG gating currents, Piper et al. (2003) proposed an updated Markov model that incorporated the Wang et al. (1997) hERG model as well as the ZHA and S–S *Shaker* models (**Figure 3B**). This model takes into account the biphasic nature of the hERG gating currents and, similar to the ZHA and S–S models, assumes that each subunit independently undergoes two sequential, voltage-dependent transitions before the channel proceeds in a concerted fashion through two sequential closed states from where the channel may then open. Also like the S–S model, the early independent transitions were thought to correspond to movement of gating charge and were rate-limiting at lower membrane potentials. The voltage-independent transition between the last two closed states that is rate-limiting at strongly depolarized potentials is maintained, although the rate of the reverse transition is several-fold higher than in the original Wang et al. model. The expanded model presented by Piper et al. (2003) is reasonably able to simulate ionic and gating currents of WT and inactivation-deficient mutant hERG channels under voltage-clamp conditions, although its ability to accurately predict currents under action potential simulation has not been assessed.

S4 MOVEMENT AND GATING ARE REGULATED BY INTRA-SUBUNIT INTERACTIONS

The sections above have focused primarily on the location and motion of positively charged residues in the S4 segment of the voltage-sensing domain. We now turn attention toward the potential interactions between the S4 segment and the three other transmembrane segments that make up the voltage-sensing domain (i.e., S1, S2, and S3), which may contribute to the regulation of voltage-dependent S4 movement.

Early charge neutralization studies of the S4 segment in *Shaker* channels, showed that two S4 mutants, K5Q (K374Q) and R6Q (R377Q), did not produce functional channels (Papazian et al., 1991). Expression and function of K5Q, and to a lesser extent R6Q, could be rescued when paired with the neutralization of highly conserved negative charges at the intracellular ends of S2 (E293Q) or S3 (D316N), which suggests that interactions between these charged residues are important for protein folding and maturation (Papazian et al., 1995). Using a similar charge reversal approach (i.e., K5E, E293K, D316K), Tiwari-Woodruff et al. (1997, 2000) suggested that specific interactions occur between K5, E293, and D316 in the same subunit and that these interactions may be electrostatic in nature (but see below). Potential electrostatic interactions were also shown between E283 at the extracellular end of S2 and R3 and R4 in S4 (Tiwari-Woodruff et al., 1997, 2000). As E283 did not exhibit state-dependent accessibility to external MTS reagents (Wang et al., 1999; Tiwari-Woodruff et al., 2000), it likely does not move relative to the electric field during channel activation. Thus, this latter result suggests that E283 interacts sequentially with the charge-carrying R3 and R4 residues as they move through the electric field (Tiwari-Woodruff et al., 2000). The stabilization of partially activated and/or open states of the channel by interactions of E283 with R3 and R4 is further supported by the observation that disrupting these interactions, by mutation of E283, caused a depolarizing shift in the *G–V* relationship (Papazian et al., 1995). In sum, the above findings, in combination with previous data on gating charge movement and accessibility are consistent with the hypothesis that R3 and R4 interact with E283 near the extracellular surface of the channel during activation, while interactions at the intracellular face of the channel between E293, K5, and D316 tend to stabilize the closed state. More recently, experiments with neutral unnatural amino acid homologs for E283, E293, and D316 have suggested that, while the interactions involving E283 are indeed electrostatic in nature, E293 and D316 do not participate in electrostatic interactions with S4 and are instead important in maintaining the water-filled crevice at the base of the voltage-sensing domain (Pless et al., 2011). Mutation of E293, D316, and/or K5 may thus change the local dielectric within the water-filled vestibule, which could result in an altered electric field and the observed effects of these mutations on voltage-dependent *Shaker* gating. Determination of the X-ray crystal structures for Kv1.2, the Kv1.2–Kv2.1 paddle chimera and KvAP in the activated conformation confirm the close proximities of E283 to R4 and of K5 to E293 and D316 (Jiang et al., 2003; Long et al., 2005a, 2007; Chen et al., 2010).

Compared to the interactions occurring in the voltage-sensing domain in the activated conformation, for which there is high resolution structural information, the nature of the interactions occurring in the resting closed state are less clear. The ability of R1 and R4 *Shaker* mutants to conduct protons or monovalent cations through the voltage-sensing domain at hyperpolarized and depolarized potentials, respectively (Starace and Bezanilla, 2004; Tombola et al., 2005), suggests that these residues occupy similar positions in the resting and activated states. Mutation of E283 modulated these "gating pore" currents, suggesting that, like R4, R1 approaches E283 during gating (Tombola et al., 2005). Disulfide bond formation between R1C and I241C in S1 or I287C in S2 in the closed state (Campos et al., 2007) also supports close proximity of R1 and E283 in the resting state. Several structural models

of *Shaker*, Kv1.2 and KvAP channels in the resting state have been developed using these experimental data to constrain the position of R1 close to E283 (Yarov-Yarovoy et al., 2006; Campos et al., 2007; Pathak et al., 2007; Nishizawa and Nishizawa, 2008; Schow et al., 2010; Vargas et al., 2011). Using molecular dynamics simulations to calculate the gating charge transferred when the Kv1.2 S4 segment moves from a resting position, where R1 and E283 interact, to an activated conformation, where R4 and E283 interact, resulted in a value of ∼12–12.7 e_0 (Khalili-Araghi et al., 2010), which is in good agreement with experimental findings (Bezanilla, 2000).

In contrast to the data discussed above, other experimental evidence suggests that *Shaker* R1 does not interact with E283 at rest and is instead located in a "gating charge transfer center" formed by F290 further down in the S2 segment, in the intracellularly accessible water-filled crevice defined by E293 in S2 and D316 in S3 (**Figure 4A**; Tao et al., 2010; Lin et al., 2011). In the Kv1.2 and Kv1.2–Kv2.1 chimera crystal structures the highly conserved F233 residue (analogous to *Shaker* F290) forms part of the 10 Å thick hydrophobic layer in the voltage-sensing domain that focuses the transmembrane electric field and also separates the intracellular and extracellularly accessible water-filled crevices in the voltage-sensing domain. Based on this, F233 has been described as a "hydrophobic plug" and "Phe gap" (Long et al., 2007; Chen et al., 2010). The crystal structures, which depict S4 in its activated conformation, show that F233 separates K5 (i.e., *Shaker* K374) from the extracellular crevice and it was proposed that the S4 charges move across the electric field by sequentially flipping past the phenylalanine residue, such that R1 occupies this position at rest, consistent with a translocation of the S4 segment of 10 Å (Long et al., 2007; Chen et al., 2010; Tao et al., 2010). It was recently shown that the F290W mutation in *Shaker* increased the affinity of the gating charge transfer center for lysine residues, presumably due to an induced cation–π relationship (Tao et al., 2010; Pless et al., 2011). In support of a resting R1–F290 interaction, the charge-conserving R1K mutation (in the F290W background) resulted in a right-shifted G-V relationship indicative of a stabilized resting conformation and increased interaction between the substituted K1 charge and the tryptophan residue at 290 (Tao et al., 2010). A recent assessment of the ability of I287H and R1H in *Shaker* to form a binding site for extracellular Zn^{2+} has also shown that, at −80 mV, only a fraction of channels have voltage sensors where I287H and R1H are in close enough proximity to bind Zn^{2+} and this proportion decreases with changes in potential in either direction (Lin et al., 2011). This is consistent with voltage-dependent translocation of S4 that moves R1 further away from I287, and supports the idea of an inward movement of R1 away from I287 and, thus, E283 upon hyperpolarization. I287H can form a Zn^{2+} binding site when paired with A359H in the S3–S4 linker and Zn^{2+} binding to this site stabilizes the resting state (Lin et al., 2011). These findings lend strong support to the hypothesis that R1 does not interact with E283 in the fully closed state, but is instead located further toward the intracellular space, perhaps in the vicinity of the gating charge transfer center. It is possible to reconcile these data with previous studies if one considers that interactions with the gating charge transfer center do not preclude R1 from approaching I287 and interacting with E283 during transitions through partially activated states.

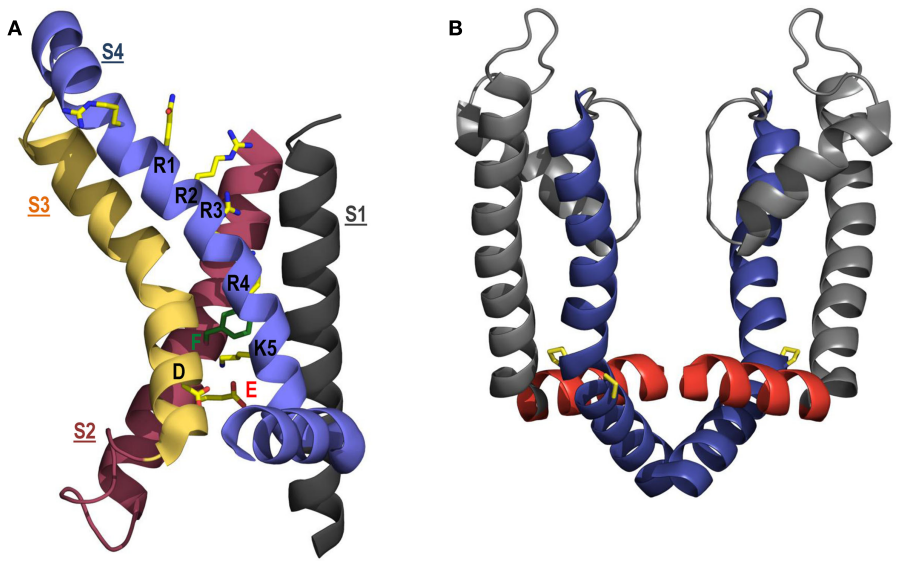

FIGURE 4 | Structural models of the voltage-sensing domain and pore domain. (A) ribbon representation of the voltage-sensing domain (S1, black; S2, red; S3, yellow; S4, blue) in an open conformation based on the Kv1.2–Kv2.1 chimera crystal structure (Long et al., 2007). Side chains found in the proposed gating charge transfer center (D316, E283, and F290) and along S4 (R1, R2, R3, R4, K5) are colored according to atom type: C, yellow; N, blue; O, red; phenylalanine, green. For clarity, the S1–S2 linker has been omitted. **(B)** Ribbon representation of the open pore domain (S5, gray; S6, blue) and S4–S5 linker (red), based on the Kv1.2–Kv2.1 chimera crystal structure, showing the close apposition of the S4–S5 linker and distal S6 helices. Proline residues that form the highly conserved PxP motif in the distal S6 helix and allow electromechanical coupling via the S4–S5 linker are highlighted in yellow. Only two subunits of the tetramer are shown (two subunits have been removed for clarity).

As discussed above, the S4 segment of hERG contains a lysine residue at the extracellular (K1; K525) and intracellular extremes (K6; K538), while *Shaker*-type channels have an arginine at the top of S4 (**Figure 1C**). The presence of both K1and K6 have been reported to stabilize the closed state of hERG: mutations at these positions caused a hyperpolarizing shift of the *G–V* relationship and accelerated activation (Liu et al., 2003; Subbiah et al., 2004, 2005; Zhang et al., 2004, 2005; Piper et al., 2005; Subbotina et al., 2010). Given that substitution of K1 or K6 with neutral (Q, C, W, or A) and/or charged (D or E) residues caused destabilization of the closed state, the lysine interactions are unlikely to be electrostatic in nature. The stabilization of the hERG closed state by K6 at the bottom of S4 is in stark contrast to the proposed role played by K5 at the bottom of the *Shaker* S4 in stabilizing the open state (see above, Tao et al., 2010; Lacroix and Bezanilla, 2011; Pless et al., 2011). Importantly, K6 is one of two consecutive positively charged residues at the bottom of the hERG S4 (R5 or R537 being the other) and either could potentially act as the analogous residue to *Shaker* K5. Although not yet formally assessed, the proximity of these two consecutive basic residues may contribute to the differential effects of substituting K6 in hERG, compared to K5 in *Shaker*. In contrast to the closed-state stabilization of K1 and K6, neutralization or charge reversal of the hERG S4 arginines (R2, R3, R4, R5) generally caused a moderate depolarizing shift of the *G–V* relationship (Subbiah et al., 2004, 2005; Zhang et al., 2004, 2005; Piper et al., 2005). Intriguingly, the arginine mutants often also affected the time constants for channel activation and deactivation (Subbiah et al., 2004, 2005; Zhang et al., 2005). Together, these results suggest that the arginines in the middle of S4 may be involved in interactions that stabilize the open state or, alternatively, in facilitating transitions leading to the open state. Overall, R2 and R3 were shown to have the largest effects on both the voltage-dependence and rate of channel opening (Subbiah et al., 2004, 2005; Piper et al., 2008). As the analogous residues in Kv1.2 have been suggested to form salt-bridges within the activated conformation of the voltage-sensing domain seen in the Kv1.2 crystal structure (Long et al., 2005a), these observations have been considered to suggest that interactions involving R2 and R3 are particularly important in stabilizing partially activated states and the slow activation of hERG (Piper et al., 2005; Subbiah et al., 2005). Similar parallels can also be drawn with the roles of *Shaker* R3 and R4 in stabilization of partially activated conformations (see above).

As with *Shaker* channels, the potential interaction partners for the S4 basic residues in hERG channels have been studied, albeit less extensively. The voltage-sensing domains of hERG and other eag family members possess three conserved negative charges in S2 (D456, D466) and S3 (D501), as well as three additional acidic residues not conserved across other Kv channel families: D411 (S1), D460 (S2) and D509 (S3), and an extra lysine at the base of S1 (K407; **Figure 1A,C**). It is conceivable that the presence of these non-conserved negative charges in hERG may result in additional electrostatic interactions with S4 basic residues and perhaps contribute to the uniquely slow gating of hERG channels. Using double mutant cycle analysis and charge reversal mutations, Zhang et al. (2005) found evidence for interactions between K1 and D456 (equivalent to the proposed R1–E283 interaction in *Shaker*) and between K6 and D411 at the base of S1, both of which were proposed to stabilize the closed state and contribute to slow hERG activation. The latter interaction would be absent in *Shaker* channels, which do not possess a D411 equivalent in S1. The same study showed that D456 also interacts with R2 during partially activated states and that this interaction facilitates activation. The same approach was used more recently with charge neutralization mutants to show that R3 is energetically coupled during activation to all of the acidic residues in the voltage-sensing domain (Piper et al., 2008), although note that a R3–D411 interaction is inconsistent with the results of Zhang et al. (2005), which specifically showed that R3 did not interact with D411. The sum of these findings is a picture of hERG activation that involves a voltage sensor that is stabilized at the top and bottom by interactions involving K525 and K538, respectively. Depolarization would provide sufficient energy to break these interactions and new interactions of R528 and R531 with D456 would form as the S4 segment is extruded. Based on findings in closely related eag channels, R534 also likely interacts with D456 in the activated state (Silverman et al., 2003), consistent with the salt-bridges observed between the analogous residues in the Kv1.2 crystal structure (Long et al., 2005a). Support for an R534–D546 interaction is also provided by the observation that Mg^{2+} binding to the pocket of negative charges in hERG formed by D456 and the non-conserved D460 and D501 residues accelerated deactivation, presumably by disrupting the ability of R534 to interact with D456 and, thus, destabilizing the activated state (Lin and Papazian, 2007). Thus, the sequential coupling of the S4 arginines to D456 at the top of S2 during hERG activation is very similar to the model for *Shaker* channel activation proposed by Papazian and colleagues (see above). This is in good agreement with the observation that the extent of *Shaker* and hERG S4 extrusion appears to be quite similar (as discussed above, Elliott et al., 2009).

IS THE GATING CHARGE TRANSFER CENTER DESCRIBED FOR *SHAKER* CONSERVED IN hERG?

Recently there has been considerable renewed interest in the regulation of the movement of S4 charges across the electric field in response to changes in voltage. In large part, interest has focused on the potential role of a highly conserved phenylalanine residue in S2 (F290) that forms part of a hydrophobic plug at the base of the voltage-sensing domain (Chen et al., 2010). As mentioned above, it was recently suggested that F290 acts as a gating charge transfer center in *Shaker* channels (Tao et al., 2010). Introduction of a tryptophan residue at position 290 resulted in preferential interaction of the gating charge transfer center with lysine (over arginine residues), such that the closed or open conformations of the voltage sensor could be stabilized depending on whether a lysine occupied the first or fifth charged position in S4, respectively (Tao et al., 2010). Although a cation–π interaction between lysines and the native phenylalanine residue was ruled out (Tao et al., 2010; Lacroix and Bezanilla, 2011), the increased affinity for lysine caused by the F290W mutation is likely due to a preferential cation–π interaction with the indole ring of the substituted tryptophan residue (Pless et al., 2011). Currently, there

is still debate over whether F290 regulates the movement of each individual S4 gating charge across the electric field in WT *Shaker* (Tao et al., 2010) or if this interaction is limited to only the fourth arginine (R4; Lacroix and Bezanilla, 2011). Nevertheless, it seems clear that in the F290W mutant, the open state of the channel is stabilized and activation is rapid with an arginine at the top of S4 and a lysine at the bottom (i.e., R1, K5; Tao et al., 2010).

To date, there is little published information regarding the importance of the gating charge transfer center in voltage-gated ion channels other than *Shaker*. The phenylalanine residue in S2 thought to form the gating charge transfer center in *Shaker* (F290) is conserved in hERG channels (F463; see **Figure 1C**). We have examined the effects of charge-conserving mutations in the S4 segments of hERG channels to address the question of whether a gating charge transfer center also regulates S4 movement and channel activation in hERG channels. In *Shaker*, switching the position of the arginine at the top of S4 and the lysine at the bottom (i.e., R1K–K5R) in the F290W background caused a dramatic slowing of channel activation, deactivation, and gating charge movement, consistent with the stabilization of the closed state by the presence of a lysine at the top, but not the bottom, of S4 (Tao et al., 2010). Intriguingly, WT hERG channels, which present slow activation, deactivation, and gating charge movement, have a lysine (K1) as the outermost S4 charge and the arginine residue immediately adjacent to K6, R5, aligns better with the repeating sequence of S4 charges (i.e., KxxRxxRxxR^{537}K^{538}) and, thus, with *Shaker* K5 (see **Figure 1C**). We have asked whether the different nature of the charged residues at the ends of the S4 helix (i.e., lysine vs. arginine) contribute to the unique voltage-dependent gating properties of hERG channels. We found that the charge-conserving K1R mutation in hERG causes a large left-shift of the *G–V* relationship (Cheng et al., 2012), consistent with previous reports that hERG K1 is important in stabilization of the closed state of the channel (Zhang et al., 2004, 2005; Subbiah et al., 2005). This finding is also in agreement with the observation in *Shaker* channels that a lysine at the outer end of the S4 segment imparts greater resting-state stability than an arginine residue (Tao et al., 2010) and is therefore supportive of a gating charge transfer center mechanism. Investigating interactions at the bottom of S4, we found that both R5K and K6R mutations exhibited a right-shifted voltage-dependence of activation (Cheng et al., 2012). These data suggest that a lysine at position 5 (i.e., R5K) destabilizes the open state, but at position 6 a lysine stabilizes the open state. Although the latter is in line with the finding in *Shaker* that a lysine residue at the bottom of S4 stabilizes the open state, the finding that a lysine at position 5 *destabilizes* the open state is in contrast to the results in *Shaker* (Tao et al., 2010). These data raise the question as to which residue, R5 or K6, occupies the gating charge transfer center in the activated state. Furthermore, it is apparent that the putative interactions between the proposed gating charge transfer center and the charged residues at the base of S4 in hERG appear to be more complex than those described in *Shaker* channels. The different identities (i.e., lysine or arginine) of the charged residues at the extreme ends of the S4 segments in hERG and *Shaker* channels and their resulting interactions with the putative gating charge transfer center may contribute to the characteristically slow gating of hERG channels.

ROLE OF THE S4–S5 LINKER IN hERG AND *SHAKER* CHANNEL GATING

THE S4–S5 LINKER COUPLES THE VOLTAGE-SENSING AND PORE DOMAINS

As mentioned above, the S4–S5 linker plays a pivotal role in Kv channel gating. This short connecting linker lies at the internal lipid interface and couples translation of the S4 voltage sensor segment to opening and closing of the intracellular pore gate. Crystal structure representations of the Kv1.2 channel open state show that the S4–S5 linker lies in close apposition to the distal S6 segment of the same subunit (**Figure 4B**) and have led to the proposal that the S4–S5 linker electromechanically couples voltage sensing with channel opening (Long et al., 2005a; Chen et al., 2010). This critical role of the S4–S5 linker in Kv channels is also supported by functional evidence. Chimeric constructs of *Shaker* and KcsA channels demonstrated that voltage dependent gating requires the distal S4–S5 linker of *Shaker* from L385 to L399 (Lu et al., 2002). Replacement of the *Shaker* S4–S5 linker, along with a portion of the distal S6 helix, with the corresponding sequence from the voltage insensitive KcsA channel specifically abolished voltage dependent gating in *Shaker* channels. A similar chimeric approach using voltage-gated Kv1.5 and Kv2.1 channels showed that voltage-dependent gating required specific contacts between the S4 and S5 linker with the distal S6 helix, which allow for mechanical translation of voltage sensor movement to the S6 pore gate (Labro et al., 2008). More recently, gating current and VCF measurements of voltage sensor dynamics in *Shaker* channels showed that direct coupling between R394, E395, and L398 in the S4–S5 linker and Y485 in the distal S6 segment stabilizes the open state of channels (Batulan et al., 2010). A similar coupling role for the S4–S5 linker has been reported in hERG channels. Charge reversal of D540 in the S4–S5 linker destabilized the closed state of hERG causing channels to re-open upon hyperpolarization (Sanguinetti and Xu, 1999). Alanine substitution of R665, but not other neighboring residues, in the distal S6 segment prevented re-opening in D540K channels, suggesting that electrostatic repulsion between D540K and R665 causes re-opening of the intracellular activation gate at hyperpolarized potentials (Tristani-Firouzi et al., 2002). Subsequent studies showed that cross-linking of cysteine residues engineered at D540 in the S4–S5 linker and L666 in the distal S6 segment stabilized the closed conformation of the hERG activation gate (Ferrer et al., 2006). Interestingly, cross-linking of these residues also immobilized a portion of voltage sensor gating charge, consistent with a role of the S4–S5 linker in electromechanical coupling in hERG channels.

Outward movement of the S4 helices is translated, via the S4–S5 linkers, into a pivoted bending of the lower portion of the S6 helices that opens the aperture of an intracellular gate to permit ion permeation. Comparison of channel structures crystallized in the open state, such as Kv1.2, KvAP, and MthK (Jiang et al., 2002b, 2003; Long et al., 2005a; Chen et al., 2010), with those in the closed state, such as KcsA, (Doyle et al., 1998) suggest that the intracellular

gate in Kv channels is formed by the convergence of the S6 helices near a highly conserved PxP motif that introduces a kink in the α-helical structure to allow for electromechanical coupling with the S4–S5 linker (**Figure 4B**). Upon depolarization, movement of the S4–S5 linker is predicted to cause radial displacement of the lower S6 helices in a manner that is dependent on the flexibility of a conserved "glycine hinge" higher up in S6. This model of activation is supported by substituted cysteine accessibility studies showing that residues below the activation gate are accessible to chemical modification by MTS reagents in both closed and open states, while residues above are only accessible in the open state (Liu et al., 1997). Furthermore, sites above the activation gate were protected from MTS modification by binding of pore blockers, such as tetrabutylammonium (TBA), tetraethylammonium (TEA), and the N-terminal inactivation particle (Liu et al., 1997; del Camino et al., 2000). A scanning mutagenesis study pinpointed V478 and F481 as sites that occlude ion permeation in the closed state (Hackos et al., 2002), the former of which has been described as a hydrophobic seal that prevents K^+ access to the inner cavity of the channel (Kitaguchi et al., 2004). This putative hydrophobic seal in *Shaker* lies approximately one helical turn below the PVP motif-induced kink in S6 and two turns above the S4–S5 linker contact point in S6 (Y485) described by Batulan et al. (2010). Based on these structural and functional data, a mechanism by which S4–S5 linker coupling of voltage sensor movement displaces the distal S6 helices to dilate an intracellular pore aperture around V478 (in *Shaker*) presents a compelling model to describe Kv channel activation gating.

A MISSING PxP MOTIF IN hERG MAY CONTRIBUTE TO ITS UNIQUE GATING

Interestingly, hERG channels lack the well conserved PxP motif in S6. This has raised questions as to the location of the intracellular gate in hERG channels and how it is coupled to S4 movement. Introduction of the PVP motif into hERG channels (substituting the $I^{655}F^{656}G^{657}$ triplet) apparently locked channels in the open state (Fernandez et al., 2004). This suggests that the structure of the hERG activation gate and its coupling to the voltage-sensing unit is different from that in Kv channels such as *Shaker*. Robertson and co-workers performed a cysteine scan of the distal portion of S6 in hERG in an attempt to determine the structural elements that define the intracellular pore gate (Wynia-Smith et al., 2008). Cysteine substitution at Q664, Y667, and S668 induced slow deactivation and constitutive channel opening at negative potentials. Mapping these sites onto models of the open and closed states of the channel (based on Kv1.2 and MlotiK1 crystal structures, respectively) suggested that they form a gating ring that occludes the permeation pathway in the closed state. Interestingly, this occlusion site is positioned in the vicinity of the S4–S5 linker contact point in S6 (L666) described by Ferrer et al. (2006) and approximately two helical turns below the location of the gate (V478) in *Shaker* channels. This suggests that the position of the pore gate in hERG channels may be different from that described in *Shaker*. If this is the case, the mechanism by which S4–S5 linker interactions with S6 drive opening and closing of the gate is an important issue that will require further investigation in order to fully understand hERG's unusual gating characteristics.

CRITICAL STRUCTURAL FEATURES OF THE hERG AND *SHAKER* S4–S5 LINKERS

Analysis of the Kv1.2 channel structure in the open configuration shows that the S4–S5 linker spans residues S311-A323 and forms three turns of an amphipathic helix (Long et al., 2005a). Similar findings were reported from NMR structures of the *Shaker* channel S4–S5 linker isolated and incorporated into lipid micelles (Ohlenschlager et al., 2002). The amphipathic nature of the helix is consistent with a position approximately parallel to the plane of the membrane, and suggests that the short helix lies at the interface of the internal phospholipid layer. NMR structures have also been reported for the S4–S5 linker of hERG channels (Gayen et al., 2012; Ng et al., 2012). These structures of isolated S4–S5 linker peptide fragments formed in the presence of dodecylphosphocholine (DPC) phospholipid demonstrate that the linker forms a 3_{10}-helix from S543 to Y545 (Gayen et al., 2012) or an amphipathic α-helix from L539 to L550 (Ng et al., 2012). The structural discrepancy may simply result from determination of structures using peptide fragments of different length; the S4–S5 linker fragment used by Gayen et al. was shorter (L539–A548) than that used by Ng et al. (L532–F551). Indeed, residues 539–541 appear to adopt a near helical configuration in the structure presented by Gayen et al. However, as Ng et al. discuss, this discrepancy may also reflect the dynamic nature of the S4–S5 linker structure. Both studies are somewhat limited in this regard, in that the linker structure is analyzed in an isolated peptide removed from both S4 and S5, which tether the linker at either end, and also from steric interactions with the S6 helices. Despite this limitation, these structures represent the best available structural representations of the S4–S5 linker in hERG channels to date.

In *Shaker* channels a highly conserved leucine heptad repeat runs from the distal S4 to the proximal S5, spanning the S4–S5 linker. Leucine zippers are important structural motifs that function as dimerization domains for protein–protein and protein–DNA interactions. The role of the putative leucine zipper motif in *Shaker* channels is unclear, but disruption of the hydrophobic domain sequence was shown to destabilize the open state of the channel (McCormack et al., 1991). In particular, mutation of the 2nd leucine residue (L382V) within the heptad repeat shifted activation gating of *Shaker* channels by ∼+70 mV and reduced the voltage-sensitivity. Gating current analysis in this "V2" mutant showed no change in the amount of charge during activation, but found that the on-gating charge movement became separated into two components. In the V2 mutant, most of the charge moved at negative potentials with a voltage dependence similar to that in WT channels, but a small component of charge moved only at more strongly depolarized potentials that correlates with the voltage dependence of opening of the mutant channels (Schoppa et al., 1992). Subsequent kinetic analysis supported the generation of a model in which the V2 mutation destabilized the open state of the channel by disrupting late cooperative gating transitions without greatly altering voltage sensor transitions earlier in the activation pathway (Schoppa and Sigworth, 1998a,b). Consistent with this idea, 4-aminopyridine, a drug shown to specifically inhibit late gating transitions associated with final concerted channel opening rearrangements, was shown to act on the same component of charge movement altered by the V2 mutation (McCormack

et al., 1994). Taken together, these data suggest a critical role of the hydrophobic leucine heptad repeat residues within the S4–S5 linker in coupling voltage sensor transitions to the opening of the intracellular pore gate.

Alignment of the S4, S4–S5, and S5 linker regions in *Shaker* and hERG suggests that an isoleucine/leucine heptad repeat may exist in hERG as in *Shaker*, but that the repeat is naturally disrupted by the presence of a glycine (G546) at the 2nd leucine position. Given that substitution of the 2nd heptad leucine in *Shaker* (by the V2 mutation) destabilized the open state of the channel, we have proposed that the presence of a glycine at position 546 may contribute to the slow gating kinetics that are peculiar to the hERG channel (Van Slyke et al., 2010). We showed that restoration of the leucine heptad (by the mutation G546L) destabilized the closed state relative to the open state and accelerated channel activation kinetics. VCF measurements suggested that this was due to faster voltage sensor movement, from which it was inferred that the S4–S5 linker glycine residue may constrain voltage sensor transitions. Interestingly, when G546 was substituted by a number of other different amino acids, the effects on gating were very similar to those of the G546L mutation suggesting that the native glycine residue contributed an additional energy barrier to activation of 1.9–4.3 kcal/mol (the energy equivalent to 1–2 H-bonds). These data suggested that the helical content of the S4–S5 linker is critical to the relative stability of the open and closed states in hERG channels, rather than the presence of a leucine heptad repeat. A "stiffer" helix produced by substitutions of G546 with helix-forming residues, or perhaps by interaction of cytoplasmic domains, biases the channel toward the open state, destabilizing the closed state.

Resolvable helical NMR structures of the S4–S5 linker in *Shaker* and hERG channels could only be detected in the presence of DPC (Ohlenschlager et al., 2002; Gayen et al., 2012; Ng et al., 2012). It is therefore important to consider whether the functional consequences of S4–S5 linker mutations, such as those of G546, are due to altered interactions between the side-chain at the position of interest and the surrounding lipid environment. Interestingly, although the S4–S5 linker is an amphipathic helix, both NMR structures of the S4–S5 linker of hERG channels place Y542 and G546 on the same face of the helix (Gayen et al., 2012; Ng et al., 2012). Both of these sites have been implicated in interactions of the S4–S5 linker with the N-terminus. Y542C was shown to cross-link with V3C in the N-terminal domain (de la Peña et al., 2011) and *N*-ethylmaleimide-labeled G546C prevented access of the N-terminus to its interaction site (Wang et al., 1998). This functional evidence suggests that although these residues align along the hydrophobic surface of the helix in the NMR structures, this face may be exposed to solvent in the full-length channel. Further evidence against lipid interaction altering effects of G546 mutations is that the G546A mutation (which does not significantly alter the side chain structure nor, therefore, lipid interactions) had just as dramatic an effect on gating as the introduction of bulky hydrophobic residues that would be expected to alter lipid interactions dramatically. In its native configuration within the channel, the extent to which the S4–S5 linker interacts with the surrounding lipid remains to be determined. The short S4–S5 linker, tethered at either end by S4 and S5 and crossing over and interacting with S6 clearly resides, at least partially, within a proteinaceous environment forming multiple protein–protein interactions. Furthermore, the presence of internally accessible canaliculi that have been proposed to project along the internal length of S4 (Bezanilla, 2000), confer additional complexity when considering the manner in which the channel protein interacts with its lipid environment at this critical location. A recent LRET study of the structural dynamics of the S4–S5 linker in response to voltage sensor gating in KvAP channels showed that the linker is highly dynamic, experiencing both translational and rotational motions (Faure et al., 2012). Such dynamics are consistent with the linker's role in electromechanical coupling, and will need to be taken into account when evaluating its involvement in potential protein–lipid interactions.

CYTOPLASMIC DOMAINS MAY INTERACT WITH THE S4–S5 LINKER TO MODULATE GATING

Deletion of the majority of the N-terminus, from residues 2-354 or 2-373, dramatically accelerated hERG channel deactivation (Schonherr and Heinemann, 1996; Spector et al., 1996). Subsequent studies showed that residues 2–16 were responsible for regulating the rate of deactivation (Wang et al., 1998) and that slow deactivation could be restored in N-terminal deleted channels by the application of an N-terminal peptide corresponding to this sequence (Wang et al., 2000) or to residues 1–135 (Morais Cabral et al., 1998). These data demonstrated that the distal N-terminus stabilizes the open state of the hERG channel. A high resolution crystal structure of the N-terminus of hERG from residue 26–135 was solved by Morais Cabral et al. (1998). Onto this, the authors mapped the functional effects of individual mutations, which demonstrated that residues F29 and Y43 had a particularly large effect on deactivation gating and showed that these residues were located within a hydrophobic patch that may form a complex interaction surface. Recently, the NMR structure of the distal N-terminus was reported (Li et al., 2010; Muskett et al., 2011; Ng et al., 2011). This structure contains residues 1–135 and therefore includes the first 25 amino acids missing from the previous crystal structure. Driven by the NMR structure of the distal portion of the N-terminus, along with mutational analysis, Vandenberg and co-workers have suggested that residues R5 and G6 are essential for slow deactivation of hERG gating and that the remainder of the N-terminus contributes to deactivation gating by orienting the distal N-terminal tail in such a manner as to promote interaction with the core of the channel (Ng et al., 2011).

Interestingly, deletion of regions of the proximal N-terminus (residues 138–373) have the opposite effect to distal deletions, shifting the voltage dependence of activation in the hyperpolarizing direction (Viloria et al., 2000; Gómez-Varela et al., 2002) and accelerating the time course of activation (Alonso-Ron et al., 2008), suggesting that this region is important in stabilizing the closed state of the channel. This is supported by the observation that a cluster of charged residues (three positive and one negative between residues 362 and 372) in the proximal N-terminus strongly stabilized the closed state of the channel (Saenen et al., 2006). Thus, it is clear that the N-terminus plays a key role in dictating the unusual activation and deactivation gating of hERG channels.

hERG channel deactivation is also modified by deletions of the C-terminus. Deactivation was markedly accelerated following deletion of the distal 236 residues of the C-terminus and was not further accelerated by deletion of the N-terminal 2-354 residues (Aydar and Palmer, 2001). These data suggest that the C- and N-termini act in concert to modify deactivation behavior of hERG channels. Subsequent studies support such a functional interaction. A strategy of introducing positively charged lysine residues within the C-terminus was used to discover putative functional interaction sites (Al-Owais et al., 2009). This study showed that a number of lysine substitutions within the cyclic nucleotide binding homology domain (cNBHD) accelerated deactivation gating. The authors mapped these sites onto a homology model of the cNBHD and described a banded pattern of distribution suggesting a broad interaction surface similar to that identified in the N-terminus (Morais Cabral et al., 1998). Recently, the NMR structure of the N-terminal 1–26 residues of hERG channels was mapped onto a structural model of the cNBHD (Muskett et al., 2011). This study highlighted the presence of several negatively charged patches on the surface of the cNBHD that align well with the docked N-terminal structure, which presents positive charges along one face of an amphipathic helix formed by residues 13–23. Charge reversal of a number of these negative acidic residues accelerated deactivation suggesting that charge–charge interactions occur with the N-terminus and a model was generated predicting electrostatic interactions of R4, R5, and H7 in the N-terminus with D843, E847, and D850 in the cNBHD. Consistent with a functional interaction between N- and C-termini, application of an N-terminal peptide could not restore slow deactivation in N-terminally truncated channels that lacked the cNBHD (Gustina and Trudeau, 2011). Taken together, these data suggest that the N- and C-termini of hERG channels interact to modify deactivation behavior. Additional discussion of this topic may also be found in a companion review by Barros et al. (2012).

In *Shaker* channels mutations within the S4–S5 linker alter interactions with an N-terminal domain that binds within and occludes the intracellular pore conferring rapid N-type inactivation (Isacoff et al., 1991; Holmgren et al., 1996; del Camino et al., 2000). A mutagenic scan of the S4–S5 linker revealed five sites (L385, T388, S392, E395, and L396) that, when mutated, altered N-type inactivation of *Shaker* channels (Isacoff et al., 1991) and a subsequent study showed that chemical modification of A391C altered binding of a soluble N-terminal inactivation domain peptide (Holmgren et al., 1996). These data suggest that the N-terminal inactivation domain comes into close proximity with the S4–S5 linker in *Shaker* channels. Similarly, numerous reports have suggested that the hERG N-terminus impacts gating transitions via interactions with the S4–S5 linker. Modification of a cysteine residue substituted at G546 in the S4–S5 linker with N-ethylmaleimide interfered with the action of the N-terminus, suggesting that a bulky adjunct attached to the S4–S5 linker impedes binding of the N-terminus (Wang et al., 1998). Using VCF, we have shown that truncation of the N-terminus (Δ2-354) accelerated the fluorescence report of S4 return (Van Slyke et al., 2010), suggesting that the N-terminus directly modifies voltage sensor configurations. Further support for a functional interaction between the S4–S5 linker and the N-terminus comes from a study showing that a cysteine residue introduced at Y542 in the S4–S5 linker prevented the restoration of slow deactivation induced by the application of a 1–135 peptide fragment in N-terminal truncated channels (Fernández-Trillo et al., 2011). Moreover, Y542C could cross-link with a cysteine substituted at residue V3 in the N-terminus (de la Peña et al., 2011). This interaction occurred preferentially in the closed state and could be reversed under reducing conditions. This provides strong evidence that the distal N-terminus is within close proximity of the S4–S5 linker, at least in closed channels, and builds upon previous reports from the same research group that a number of S4–S5 linker mutations seem to mimic the acceleration of deactivation observed in N-terminal mutant constructs (Alonso-Ron et al., 2008). Structural evidence also points to a direct interaction of the N-terminus with the S4–S5 linker. Li et al. (2010) presented the NMR structure of amino acids 1–135 of the N-terminus of hERG and reported chemical shifts of several residues within the N-terminal region after the addition of an S4–S5 linker peptide that included residues R541–V549. Such perturbations were interpreted to indicate a direct interaction between the S4–S5 linker and N-terminus peptides, and residues 86–94 were predicted to be key candidates for binding. This interaction site is different from other N-terminal interaction sites shown from functional studies, which describe key roles for F29 and Y43 (Morais Cabral et al., 1998), V3 (de la Peña et al., 2011), and R5 and G6 (Ng et al., 2011). This suggests that multiple contact points may govern the functional interaction between the N-terminus and the S4–S5 linker. Alternatively, since the S4–S5 linker is integral to the dynamics of electromechanical coupling, S4–S5 linker interactions with the N-terminus may be state-dependent and this may account for some of the differences observed. Additional functional studies by Ng et al. (2012) identified a complex pattern of gating modifying behaviors in channels in which S4–S5 linker residues were mutated. This was interpreted to suggest that the S4–S5 linker not only couples voltage sensor movement to pore opening in hERG channels, but also takes part in complex interactions as the channel transitions between closed and open states. In particular, S543, Y545, G546, and A548 were identified as key residues participating in interactions with other channel domains. This observation is consistent with previous studies that identified G546 as a critical site for hERG gating that is within proximity with the N-terminal domain (Wang et al., 1998; Van Slyke et al., 2010). It is conceivable that these contact points (S543, Y545, G546, and A548) mediate multi-site interactions with a complex formed by the N- and C-termini that modulate the open state stability of hERG channels. Our VCF data suggest that this may occur via alterations to the relative stability of resting/active voltage sensor configurations (Van Slyke et al., 2010). Furthermore, our evidence that flexibility of the S4–S5 linker may be a key determinant of rate-limiting voltage sensor gating could suggest that such cytoplasmic domain interactions with the S4–S5 linker may alter gating by altering the flexibility of linker. Taken together, this series of structural and functional evidence provides strong support for a model in which the N- and perhaps also the C-terminus modifies transitions between the open and closed states by direct interactions with the S4–S5 linker that may modify the stability of the activated configuration of the hERG channel voltage sensor.

SUMMARY

Despite significant attention, the mechanistic basis of the physiologically and pharmacologically important slow activation and deactivation processes in hERG channels remain unclear. Here, we have taken a comparative approach to evaluate possible mechanisms responsible by discussing the role of sequence divergence in hERG and the archetypal Kv channel, *Shaker*. Structurally speaking, the available data suggest that the voltage-sensing domain in hERG channels is not significantly different from that in *Shaker*. Functionally speaking, the intra-voltage-sensing domain charge–charge interactions also seem quite similar in hERG and *Shaker* channels. This leads the search for the mechanistic basis underlying hERG's unique gating processes elsewhere. Recent evidence suggests that a gating charge transfer center may exist within the voltage sensor domain of hERG, as in *Shaker* channels, and that key differences in the nature of the charges at the inner and outer margins of the S4 segment are important in regulating gating differences between these two channels. In addition, sequence divergence at the level of the S4–S5 linker also contributes to the slow gating in hERG channels. Data suggest that S4–S5 linker flexibility changes may be a key determinant of hERG gating, enabling integration of cytoplasmic domain interactions with the stability of the voltage sensor domain in resting and activated states. Although many questions remain concerning the intriguingly unique gating characteristics of hERG channels, these new observations provide a tantalizing view of how Kv channel functional diversity may have evolved via subtle alterations in the primary sequence.

ACKNOWLEDGMENTS

This work was supported by a Heart and Stroke Foundation of Canada New Investigator Award and a Michael Smith Foundation for Health Research Career Scholar Award held by Tom W. Claydon.

REFERENCES

Aggarwal, S. K., and Mackinnon, R. (1996). Contribution of the S4 segment to gating charge in the shaker K^+ channel. *Neuron* 16, 1169–1177.

Alonso-Ron, C., de la Peña, P., Miranda, P., Dominguez, P., and Barros, F. (2008). Thermodynamic and kinetic properties of amino-terminal and S4-S5 loop HERG channel mutants under steady-state conditions. *Biophys. J.* 94, 3893–3911.

Al-Owais, M., Bracey, K., and Wray, D. (2009). Role of intracellular domains in the function of the herg potassium channel. *Eur. Biophys. J.* 38, 569–576.

Armstrong, C. M., and Bezanilla, F. (1974). Charge movement associated with the opening and closing of the activation gates of the Na channels. *J. Gen. Physiol.* 63, 533–552.

Aydar, E., and Palmer, C. (2001). Functional characterization of the C-terminus of the human ether-a-go-go-related gene K^+ channel (HERG). *J. Physiol. (Lond.)* 534, 1–14.

Baker, O. S., Larsson, H. P., Mannuzzu, L. M., and Isacoff, E. Y. (1998). Three transmembrane conformations and sequence-dependent displacement of the S4 domain in shaker K^+ channel gating. *Neuron* 20, 1283–1294.

Barros, F., Domínguez, P., and de la Peña, P. (2012). Cytoplasmic domains and voltage-dependent potassium channel gating. *Front. Pharmacol.* 3:49. doi:10.3389/fphar.2012.00049

Batulan, Z., Haddad, G. A., and Blunck, R. (2010). An intersubunit interaction between S4-S5 linker and S6 is responsible for the slow off-gating component in shaker K^+ channels. *J. Biol. Chem.* 285, 14005–14019.

Bett, G. C., Zhou, Q., and Rasmusson, R. L. (2011). Models of HERG gating. *Biophys. J.* 101, 631–642.

Bezanilla, F. (2000). The voltage sensor in voltage-dependent ion channels. *Physiol. Rev.* 80, 555–592.

Bezanilla, F., Perozo, E., and Stefani, E. (1994). Gating of shaker K^+ channels: II. The components of gating currents and a model of channel activation. *Biophys. J.* 66, 1011–1021.

Börjesson, S. I., and Elinder, F. (2008). Structure, function, and modification of the voltage sensor in voltage-gated ion channels. *Cell Biochem. Biophys.* 52, 149–174.

Campos, F. V., Chanda, B., Roux, B., and Bezanilla, F. (2007). Two atomic constraints unambiguously position the S4 segment relative to S1 and S2 segments in the closed state of shaker K channel. *Proc. Natl. Acad. Sci. U.S.A.* 104, 7904–7909.

Catterall, W. A. (2010). Ion channel voltage sensors: structure, function, and pathophysiology. *Neuron* 67, 915–928.

Cha, A., and Bezanilla, F. (1997). Characterizing voltage-dependent conformational changes in the shaker K^+ channel with fluorescence. *Neuron* 19, 1127–1140.

Chanda, B., and Bezanilla, F. (2008). A common pathway for charge transport through voltage-sensing domains. *Neuron* 57, 345–351.

Chen, J., Mitcheson, J. S., Tristani-Firouzi, M., Lin, M., and Sanguinetti, M. C. (2001). The S4-S5 linker couples voltage sensing and activation of pacemaker channels. *Proc. Natl. Acad. Sci. U.S.A.* 98, 11277–11282.

Chen, X., Wang, Q., Ni, F., and Ma, J. (2010). Structure of the full-length shaker potassium channel Kv1.2 by normal-mode-based X-ray crystallographic refinement. *Proc. Natl. Acad. Sci. U.S.A.* 107, 11352–11357.

Cheng, Y. M., Hull, C. M., Niven, C. M., Allard, C. R., and Claydon, T. W. (2012). Molecular determinants of voltage-dependent gating in hERG potassium channels. *Biophys. J.* 102, 329a.

Clancy, C. E., and Rudy, Y. (2001). Cellular consequences of HERG mutations in the long QT syndrome: precursors to sudden cardiac death. *Cardiovasc. Res.* 50, 301–313.

de la Peña, P., Alonso-Ron, C., Machin, A., Fernández-Trillo, J., Carretero, L., Dominguez, P., and Barros, F. (2011). Demonstration of physical proximity between the N terminus and the S4-S5 linker of the human ether-a-go-go-related gene (hERG) potassium channel. *J. Biol. Chem.* 286, 19065–19075.

del Camino, D., Holmgren, M., Liu, Y., and Yellen, G. (2000). Blocker protection in the pore of a voltage-gated K^+ channel and its structural implications. *Nature* 403, 321–325.

del Camino, D., and Yellen, G. (2001). Tight steric closure at the intracellular activation gate of a voltage-gated K^+ channel. *Neuron* 32, 649–656.

Ding, S., and Horn, R. (2002). Tail end of the S6 segment: role in permeation in shaker potassium channels. *J. Gen. Physiol.* 120, 87–97.

Ding, S., and Horn, R. (2003). Effect of S6 tail mutations on charge movement in shaker potassium channels. *Biophys. J.* 84, 295–305.

Doyle, D. A., Morais-Cabral, J. H., Pfuetzner, R. A., Kuo, A., Gulbis, J. M., Cohen, S. L., Chait, B. T., and Mackinnon, R. (1998). The structure of the potassium channel: molecular basis of K^+ conduction and selectivity. *Science* 280, 69–77.

Durell, S. R., Hao, Y., and Guy, H. R. (1998). Structural models of the transmembrane region of voltage-gated and other K^+ channels in open, closed, and inactivated conformations. *J. Struct. Biol.* 121, 263–284.

Elliott, D. J., Dondas, N. Y., Munsey, T. S., and Sivaprasadarao, A. (2009). Movement of the S4 segment in the hERG potassium channel during membrane depolarization. *Mol. Membr. Biol.* 26, 435–447.

Es-Salah-Lamoureux, Z., Fougere, R., Xiong, P. Y., Robertson, G. A., and Fedida, D. (2010). Fluorescence-tracking of activation gating in human ERG channels reveals rapid S4 movement and slow pore opening. *PLoS ONE* 5, e10876. doi:10.1371/journal.pone.0010876

Faure, E., McGuire, H., Marsolais, M., and Blunck, R. (2012). Movement of the S4-S5 linker of KvAP during gating. *Biophys. J.* 102, 13a.

Fedida, D., and Hesketh, J. C. (2001). Gating of voltage-dependent potassium channels. *Prog. Biophys. Mol. Biol.* 75, 165–199.

Fernandez, D., Ghanta, A., Kauffman, G. W., and Sanguinetti, M. C. (2004). Physicochemical features of the hERG channel drug binding site. *J. Biol. Chem.* 279, 10120–10127.

Fernández-Trillo, J., Barros, F., Machín, A., Carretero, L., Domínguez, P., and de la Peña, P. (2011). Molecular determinants of interactions between the N-terminal domain and the transmembrane core that modulate hERG K^+ channel gating. *PLoS ONE* 6, e24674. doi:10.1371/journal.pone.0024674

Ferrer, T., Rupp, J., Piper, D. R., and Tristani-Firouzi, M. (2006). The S4-S5 linker directly couples voltage sensor movement to the activation gate in the human ether-a'-go-go-related gene (hERG) K^+ channel. *J. Biol. Chem.* 281, 12858–12864.

Gayen, S., Li, Q., and Kang, C. (2012). The solution structure of the S4-S5 linker of the hERG potassium channel. *J. Pept. Sci.* 18, 140–145.

Gilly, W. F., and Armstrong, C. M. (1980). Gating current and potassium channels in the giant axon of the squid. *Biophys. J.* 29, 485–492.

Gómez-Varela, D., de la Peña, P., García, J., Giráldez, T., and Barros, F. (2002). Influence of amino-terminal structures on kinetic transitions between several closed and open states in human erg K^+ channels. *J. Membr. Biol.* 187, 117–133.

Gustina, A. S., and Trudeau, M. C. (2009). A recombinant N-terminal domain fully restores deactivation gating in N-truncated and long QT syndrome mutant hERG potassium channels. *Proc. Natl. Acad. Sci. U.S.A.* 106, 13082–13087.

Gustina, A. S., and Trudeau, M. C. (2011). hERG potassium channel gating is mediated by N- and C-terminal region interactions. *J. Gen. Physiol.* 137, 315–325.

Hackos, D. H., Chang, T. H., and Swartz, K. J. (2002). Scanning the intracellular S6 activation gate in the shaker K^+ channel. *J. Gen. Physiol.* 119, 521–532.

Hodgkin, A. L., and Huxley, A. F. (1952). A quantitative description of membrane current and its application to conduction and excitation in nerve. *J. Physiol. (Lond.)* 117, 500–544.

Holmgren, M., Jurman, M. E., and Yellen, G. (1996). N-type inactivation and the S4-S5 region of the shaker K^+ channel. *J. Gen. Physiol.* 108, 195–206.

Isacoff, E. Y., Jan, Y. N., and Jan, L. Y. (1991). Putative receptor for the cytoplasmic inactivation gate in the shaker K^+ channel. *Nature* 353, 86–90.

Jiang, Y., Lee, A., Chen, J., Cadene, M., Chait, B. T., and MacKinnon, R. (2002a). The open pore conformation of potassium channels. *Nature* 417, 523–526.

Jiang, Y., Lee, A., Chen, J., Cadene, M., Chait, B. T., and MacKinnon, R. (2002b). Crystal structure and mechanism of a calcium-gated potassium channel. *Nature* 417, 515–522.

Jiang, Y., Lee, A., Chen, J., Ruta, V., Cadene, M., Chait, B. T., and MacKinnon, R. (2003). X-ray structure of a voltage-dependent K^+ channel. *Nature* 423, 33–41.

Kanevsky, M., and Aldrich, R. W. (1999). Determinants of voltage-dependent gating and open-state stability in the S5 segment of shaker potassium channels. *J. Gen. Physiol.* 114, 215–242.

Keynes, R. D., and Elinder, F. (1999). The screw-helical voltage gating of ion channels. *Proc. Biol. Sci.* 266, 843–852.

Khalili-Araghi, F., Jogini, V., Yarov-Yarovoy, V., Tajkhorshid, E., Roux, B., and Schulten, K. (2010). Calculation of the gating charge for the Kv1.2 voltage-activated potassium channel. *Biophys J* 98, 2189–2198.

Kitaguchi, T., Sukhareva, M., and Swartz, K. J. (2004). Stabilizing the closed S6 gate in the shaker Kv channel through modification of a hydrophobic seal. *J. Gen. Physiol.* 124, 319–332.

Kurata, H. T., and Fedida, D. (2006). A structural interpretation of voltage-gated potassium channel inactivation. *Prog. Biophys. Mol. Biol.* 92, 185–208.

Labro, A. J., Raes, A. L., Grottesi, A., Van, H. D., Sansom, M. S., and Snyders, D. J. (2008). Kv channel gating requires a compatible S4-S5 linker and bottom part of S6, constrained by non-interacting residues. *J. Gen. Physiol.* 132, 667–680.

Lacroix, J. J., and Bezanilla, F. (2011). Control of a final gating charge transition by a hydrophobic residue in the S2 segment of a K^+ channel voltage sensor. *Proc. Natl. Acad. Sci. U.S.A.* 108, 6444–6449.

Larsson, H. P., Baker, O. S., Dhillon, D. S., and Isacoff, E. Y. (1996). Transmembrane movement of the shaker K^+ channel S4. *Neuron* 16, 387–397.

Ledwell, J. L., and Aldrich, R. W. (1999). Mutations in the S4 region isolate the final voltage-dependent cooperative step in potassium channel activation. *J. Gen. Physiol.* 113, 389–414.

Li, Q., Gayen, S., Chen, A. S., Huang, Q., Raida, M., and Kang, C. (2010). NMR solution structure of the N-terminal domain of hERG and its interaction with the S4-S5 linker. *Biochem. Biophys. Res. Commun.* 403, 126–132.

Liman, E. R., Hess, P., Weaver, F., and Koren, G. (1991). Voltage-sensing residues in the S4 region of a mammalian K^+ channel. *Nature* 353, 752–756.

Lin, M. C., Hsieh, J. Y., Mock, A. F., and Papazian, D. M. (2011). R1 in the shaker S4 occupies the gating charge transfer center in the resting state. *J. Gen. Physiol.* 138, 155–163.

Lin, M. C., and Papazian, D. M. (2007). Differences between ion binding to eag and HERG voltage sensors contribute to differential regulation of activation and deactivation gating. *Channels (Austin)* 1, 429–437.

Liu, J., Zhang, M., Jiang, M., and Tseng, G. N. (2003). Negative charges in the transmembrane domains of the HERG K channel are involved in the activation- and deactivation-gating processes. *J. Gen. Physiol.* 121, 599–614.

Liu, S., Rasmusson, R. L., Campbell, D. L., Wang, S., and Strauss, H. C. (1996). Activation and inactivation kinetics of an E-4031-sensitive current from single ferret atrial myocytes. *Biophys. J.* 70, 2704–2715.

Liu, Y., Holmgren, M., Jurman, M. E., and Yellen, G. (1997). Gated access to the pore of a voltage-dependent K^+ channel. *Neuron* 19, 175–184.

Long, S. B., Campbell, E. B., and MacKinnon, R. (2005a). Crystal structure of a mammalian voltage-dependent shaker family K^+ channel. *Science* 309, 897–903.

Long, S. B., Campbell, E. B., and MacKinnon, R. (2005b). Voltage sensor of Kv1.2: structural basis of electromechanical coupling. *Science* 309, 903–908.

Long, S. B., Tao, X., Campbell, E. B., and MacKinnon, R. (2007). Atomic structure of a voltage-dependent K^+ channel in a lipid membrane-like environment. *Nature* 450, 376–382.

Loots, E., and Isacoff, E. Y. (1998). Protein rearrangements underlying slow inactivation of the shaker K^+ channel. *J. Gen. Physiol.* 112, 377–389.

Lu, Z., Klem, A. M., and Ramu, Y. (2002). Coupling between voltage sensors and activation gate in voltage-gated K^+ channels. *J. Gen. Physiol.* 120, 663–676.

Mannuzzu, L. M., Moronne, M. M., and Isacoff, E. Y. (1996). Direct physical measure of conformational rearrangement underlying potassium channel gating. *Science* 271, 213–216.

Mazhari, R., Greenstein, J. L., Winslow, R. L., Marban, E., and Nuss, H. B. (2001). Molecular interactions between two long-QT syndrome gene products, HERG and KCNE2, rationalized by in vitro and in silico analysis. *Circ. Res.* 89, 33–38.

McCormack, K., Joiner, W. J., and Heinemann, S. H. (1994). A characterization of the activating structural rearrangements in voltage-dependent shaker K^+ channels. *Neuron* 12, 301–315.

McCormack, K., Tanouye, M. A., Iverson, L. E., Lin, J. W., Ramaswami, M., McCormack, T., Campanelli, J. T., Mathew, M. K., and Rudy, B. (1991). A role for hydrophobic residues in the voltage-dependent gating of Shaker K^+ channels. *Proc. Natl. Acad. Sci. U.S.A.* 88, 2931–2935.

Morais Cabral, J. H., Lee, A., Cohen, S. L., Chait, B. T., Li, M., and Mackinnon, R. (1998). Crystal structure and functional analysis of the HERG potassium channel N terminus: a eukaryotic PAS domain. *Cell* 95, 649–655.

Muskett, F. W., Thouta, S., Thomson, S. J., Bowen, A., Stansfeld, P. J., and Mitcheson, J. S. (2011). Mechanistic insight into human ether-a-go-go-related gene (hERG) K^+ channel deactivation gating from the solution structure of the EAG domain. *J. Biol. Chem.* 286, 6184–6191.

Ng, C. A., Hunter, M. J., Perry, M. D., Mobli, M., Ke, Y., Kuchel, P. W., King, G. F., Stock, D., and Vandenberg, J. I. (2011). The N-terminal tail of hERG contains an amphipathic alpha-helix that regulates channel deactivation. *PLoS ONE* 6, e16191. doi:10.1371/journal.pone.0016191

Ng, C. A., Perry, M. D., Tan, P. S., Hill, A. P., Kuchel, P. W., and Vandenberg, J. I. (2012). The s4-s5 linker acts as a signal integrator for HERG k channel activation and deactivation gating. *PLoS ONE* 7, e31640. doi:10.1371/journal.pone.0031640

Nishizawa, M., and Nishizawa, K. (2008). Molecular dynamics simulation of Kv channel voltage sensor helix in a lipid membrane with applied electric field. *Biophys. J.* 95, 1729–1744.

Nishizawa, M., and Nishizawa, K. (2009). Coupling of S4 helix translocation and S6 gating analyzed by molecular-dynamics simulations of mutated Kv channels. *Biophys. J.* 97, 90–100.

Noceti, F., Baldelli, P., Wei, X., Qin, N., Toro, L., Birnbaumer, L., and Stefani, E. (1996). Effective gating charges per channel in voltage-dependent K^+ and $Ca2^+$ channels. *J. Gen. Physiol.* 108, 143–155.

Noda, M., Shimizu, S., Tanabe, T., Takai, T., Kayano, T., Ikeda, T., Takahashi, H., Nakayama, H., Kanaoka, Y., Minamino, N., Kangawa, K., Matsuo, H., Raftery, M., Hirose, T., Inayama, S., Hayashida, H., Miyata, T., and Numa, S. (1984). Primary structure of electrophorus electricus sodium channel deduced from cDNA sequence. *Nature* 312, 121–127.

Oehmen, C. S., Giles, W. R., and Demir, S. S. (2002). Mathematical model of

the rapidly activating delayed rectifier potassium current I(Kr) in rabbit sinoatrial node. *J. Cardiovasc. Electrophysiol.* 13, 1131–1140.

Ohlenschlager, O., Hojo, H., Ramachandran, R., Gorlach, M., and Haris, P. I. (2002). Three-dimensional structure of the S4-S5 segment of the shaker potassium channel. *Biophys. J.* 82, 2995–3002.

Papazian, D. M., and Bezanilla, F. (1997). How does an ion channel sense voltage? *News Physiol. Sci.* 12, 203–210.

Papazian, D. M., Schwarz, T. L., Tempel, B. L., Jan, Y. N., and Jan, L. Y. (1987). Cloning of genomic and complementary DNA from shaker, a putative potassium channel gene from *Drosophila*. *Science* 237, 749–753.

Papazian, D. M., Shao, X. M., Seoh, S. A., Mock, A. F., Huang, Y., and Wainstock, D. H. (1995). Electrostatic interactions of S4 voltage sensor in shaker K^+ channel. *Neuron* 14, 1293–1301.

Papazian, D. M., Timpe, L. C., Jan, Y. N., and Jan, L. Y. (1991). Alteration of voltage-dependence of shaker potassium channel by mutations in the S4 sequence. *Nature* 349, 305–310.

Pathak, M. M., Yarov-Yarovoy, V., Agarwal, G., Roux, B., Barth, P., Kohout, S., Tombola, F., and Isacoff, E. Y. (2007). Closing in on the resting state of the shaker K^+ channel. *Neuron* 56, 124–140.

Piper, D. R., Hinz, W. A., Tallurri, C. K., Sanguinetti, M. C., and Tristani-Firouzi, M. (2005). Regional specificity of human ether-a'-go-go-related gene channel activation and inactivation gating. *J. Biol. Chem.* 280, 7206–7217.

Piper, D. R., Rupp, J., Sachse, F. B., Sanguinetti, M. C., and Tristani-Firouzi, M. (2008). Cooperative interactions between R531 and acidic residues in the voltage sensing module of hERG1 channels. *Cell. Physiol. Biochem.* 21, 37–46.

Piper, D. R., Varghese, A., Sanguinetti, M. C., and Tristani-Firouzi, M. (2003). Gating currents associated with intramembrane charge displacement in HERG potassium channels. *Proc. Natl. Acad. Sci. U.S.A.* 100, 10534–10539.

Pless, S. A., Galpin, J. D., Niciforovic, A. P., and Ahern, C. A. (2011). Contributions of counter-charge in a potassium channel voltage-sensor domain. *Nat. Chem. Biol.* 7, 617–623.

Saenen, J. B., Labro, A. J., Raes, A., and Snyders, D. J. (2006). Modulation of HERG gating by a charge cluster in the N-terminal proximal domain. *Biophys. J.* 91, 4381–4391.

Sanguinetti, M. C., and Tristani-Firouzi, M. (2006). hERG potassium channels and cardiac arrhythmia. *Nature* 440, 463–469.

Sanguinetti, M. C., and Xu, Q. P. (1999). Mutations of the S4-S5 linker alter activation properties of HERG potassium channels expressed in *Xenopus oocytes*. *J. Physiol. (Lond.)* 514, 667–675.

Schonherr, R., and Heinemann, S. H. (1996). Molecular determinants for activation and inactivation of HERG, a human inward rectifier potassium channel. *J. Physiol. (Lond.)* 493, 635–642.

Schoppa, N. E., McCormack, K., Tanouye, M. A., and Sigworth, F. J. (1992). The size of gating charge in wild-type and mutant shaker potassium channels. *Science* 255, 1712–1715.

Schoppa, N. E., and Sigworth, F. J. (1998a). Activation of shaker potassium channels. III. An activation gating model for wild-type and V2 mutant channels. *J. Gen. Physiol.* 111, 313–342.

Schoppa, N. E., and Sigworth, F. J. (1998b). Activation of shaker potassium channels. II. Kinetics of the V2 mutant channel. *J. Gen. Physiol.* 111, 295–311.

Schow, E. V., Freites, J. A., Gogna, K., White, S. H., and Tobias, D. J. (2010). Down-state model of the voltage-sensing domain of a potassium channel. *Biophys. J.* 98, 2857–2866.

Seoh, S. A., Sigg, D., Papazian, D. M., and Bezanilla, F. (1996). Voltage-sensing residues in the S2 and S4 segments of the shaker K^+ channel. *Neuron* 16, 1159–1167.

Silverman, W. R., Roux, B., and Papazian, D. M. (2003). Structural basis of two-stage voltage-dependent activation in K^+ channels. *Proc. Natl. Acad. Sci. U.S.A.* 100, 2935–2940.

Smith, P. L., and Yellen, G. (2002). Fast and slow voltage sensor movements in HERG potassium channels. *J. Gen. Physiol.* 119, 275–293.

Spector, P. S., Curran, M. E., Zou, A., Keating, M. T., and Sanguinetti, M. C. (1996). Fast inactivation causes rectification of the IKr channel. *J. Gen. Physiol.* 107, 611–619.

Starace, D. M., and Bezanilla, F. (2001). Histidine scanning mutagenesis of basic residues of the S4 segment of the shaker K^+ channel. *J. Gen. Physiol.* 117, 469–490.

Starace, D. M., and Bezanilla, F. (2004). A proton pore in a potassium channel voltage sensor reveals a focused electric field. *Nature* 427, 548–553.

Starace, D. M., Stefani, E., and Bezanilla, F. (1997). Voltage-dependent proton transport by the voltage sensor of the shaker K^+ channel. *Neuron* 19, 1319–1327.

Subbiah, R. N., Clarke, C. E., Smith, D. J., Zhao, J., Campbell, T. J., and Vandenberg, J. I. (2004). Molecular basis of slow activation of the human ether-a-go-go related gene potassium channel. *J. Physiol. (Lond.)* 558, 417–431.

Subbiah, R. N., Kondo, M., Campbell, T. J., and Vandenberg, J. I. (2005). Tryptophan scanning mutagenesis of the HERG K^+ channel: the S4 domain is loosely packed and likely to be lipid exposed. *J. Physiol. (Lond.)* 569, 367–379.

Subbotina, J., Yarov-Yarovoy, V., Lees-Miller, J., Durdagi, S., Guo, J., Duff, H. J., and Noskov, S. Y. (2010). Structural refinement of the hERG1 pore and voltage-sensing domains with ROSETTA-membrane and molecular dynamics simulations. *Proteins* 78, 2922–2934.

Tao, X., Lee, A., Limapichat, W., Dougherty, D. A., and Mackinnon, R. (2010). A gating charge transfer center in voltage sensors. *Science* 328, 67–73.

Tiwari-Woodruff, S. K., Lin, M. A., Schulteis, C. T., and Papazian, D. M. (2000). Voltage-dependent structural interactions in the Shaker K^+ channel. *J. Gen. Physiol.* 115, 123–138.

Tiwari-Woodruff, S. K., Schulteis, C. T., Mock, A. F., and Papazian, D. M. (1997). Electrostatic interactions between transmembrane segments mediate folding of Shaker K^+ channel subunits. *Biophys. J.* 72, 1489–1500.

Tombola, F., Pathak, M. M., and Isacoff, E. Y. (2005). Voltage-sensing arginines in a potassium channel permeate and occlude cation-selective pores. *Neuron* 45, 379–388.

Tristani-Firouzi, M., Chen, J., and Sanguinetti, M. C. (2002). Interactions between S4-S5 linker and S6 transmembrane domain modulate gating of HERG K^+ channels. *J. Biol. Chem.* 277, 18994–19000.

Trudeau, M. C., Warmke, J. W., Ganetzky, B., and Robertson, G. A. (1995). HERG, a human inward rectifier in the voltage-gated potassium channel family. *Science* 269, 92–95.

Van Slyke, A. C., Rezazadeh, S., Snopkowski, M., Shi, P., Allard, C. R., and Claydon, T. W. (2010). Mutations within the S4-S5 linker alter voltage sensor constraints in hERG K^+ channels. *Biophys. J.* 99, 2841–2852.

Vargas, E., Bezanilla, F., and Roux, B. (2011). In search of a consensus model of the resting state of a voltage-sensing domain. *Neuron* 72, 713–720.

Viloria, C. G., Barros, F., Giráldez, T., Gómez-Varela, D., and de la Peña, P. (2000). Differential effects of amino-terminal distal and proximal domains in the regulation of human erg K^+ channel gating. *Biophys. J.* 79, 231–246.

Wang, J., Myers, C. D., and Robertson, G. A. (2000). Dynamic control of deactivation gating by a soluble amino-terminal domain in HERG K^+ channels. *J. Gen. Physiol.* 115, 749–758.

Wang, J., Trudeau, M. C., Zappia, A. M., and Robertson, G. A. (1998). Regulation of deactivation by an amino terminal domain in human ether-a-go-go-related gene potassium channels. *J. Gen. Physiol.* 112, 637–647.

Wang, M. H., Yusaf, S. P., Elliott, D. J., Wray, D., and Sivaprasadarao, A. (1999). Effect of cysteine substitutions on the topology of the S4 segment of the shaker potassium channel: implications for molecular models of gating. *J. Physiol. (Lond.)* 521(Pt 2), 315–326.

Wang, S., Liu, S., Morales, M. J., Strauss, H. C., and Rasmusson, R. L. (1997). A quantitative analysis of the activation and inactivation kinetics of HERG expressed in *Xenopus oocytes*. *J. Physiol. (Lond.)* 502(Pt 1), 45–60.

Wynia-Smith, S. L., Gillian-Daniel, A. L., Satyshur, K. A., and Robertson, G. A. (2008). hERG gating microdomains defined by S6 mutagenesis and molecular modeling. *J. Gen. Physiol.* 132, 507–520.

Yarov-Yarovoy, V., Baker, D., and Catterall, W. A. (2006). Voltage sensor conformations in the open and closed states in ROSETTA structural models of K^+ channels. *Proc. Natl. Acad. Sci. U.S.A.* 103, 7292–7297.

Yusaf, S. P., Wray, D., and Sivaprasadarao, A. (1996). Measurement of the movement of the S4 segment during the activation of a voltage-gated potassium channel. *Pflugers Arch.* 433, 91–97.

Zagotta, W. N., Hoshi, T., and Aldrich, R. W. (1994a). Shaker potassium channel gating. III: evaluation of kinetic models for activation. *J. Gen. Physiol.* 103, 321–362.

Zagotta, W. N., Hoshi, T., Dittman, J., and Aldrich, R. W. (1994b). Shaker potassium channel gating. II: transitions in the activation pathway. *J. Gen. Physiol.* 103, 279–319.

Zhang, M., Liu, J., Jiang, M., Wu, D. M., Sonawane, K., Guy, H. R., and Tseng, G. N. (2005). Interactions between charged residues in the transmembrane segments of the voltage-sensing domain in the hERG channel. *J. Membr. Biol.* 207, 169–181.

Zhang, M., Liu, J., and Tseng, G. N. (2004). Gating charges in the activation and inactivation processes of the HERG channel. *J. Gen. Physiol.* 124, 703–718.

Conflict of Interest Statement: The authors declare that the research was conducted in the absence of any commercial or financial relationships that could be construed as a potential conflict of interest.

Received: 16 March 2012; accepted: 16 April 2012; published online: 08 May 2012.

Citation: Cheng YM and Claydon TW (2012) Voltage-dependent gating of hERG potassium channels. Front. Pharmacol. ***3****:83. doi: 10.3389/fphar.2012.00083*

This article was submitted to Frontiers in Pharmacology of Ion Channels and Channelopathies, a specialty of Frontiers in Pharmacology.

frontiers in
PHARMACOLOGY

REVIEW ARTICLE
published: 10 September 2012
doi: 10.3389/fphar.2012.00163

Polyunsaturated fatty acids modify the gating of Kv channels

Cristina Moreno, Alvaro Macias, Angela Prieto, Alicia De La Cruz and Carmen Valenzuela*

Instituto de Investigaciones Biomédicas "Alberto Sols," Consejo Superior de Investigaciones Científicas-Universidad Autónoma de Madrid, Madrid, Spain

Edited by:
Gildas Loussouarn, Université de Nantes, France

Reviewed by:
Zeineb Es-Salah-Lamoureux, INSERM, France
James Huettner, Washington University School of Medicine, USA

****Correspondence:***
Carmen Valenzuela, Instituto de Investigaciones Biomédicas "Alberto Sols," Consejo Superior de Investigaciones Científicas-Universidad Autónoma de Madrid, Arturo Duperier 4, 28029 Madrid, Spain.
e-mail: cvalenzuela@iib.uam.es

Polyunsaturated fatty acids (PUFAs) have been reported to exhibit antiarrhythmic properties, which are attributed to their capability to modulate ion channels. This PUFAs ability has been reported to be due to their effects on the gating properties of ion channels. In the present review, we will focus on the role of PUFAs on the gating of two Kv channels, Kv1.5 and Kv11.1. Kv1.5 channels are blocked by *n*−3 PUFAs of marine [docosahexaenoic acid (DHA) and eicosapentaenoic acid] and plant origin (alpha-linolenic acid, ALA) at physiological concentrations. The blockade of Kv1.5 channels by PUFAs steeply increased in the range of membrane potentials coinciding with those of Kv1.5 channel activation, suggesting that PUFAs-channel binding may derive a significant fraction of its voltage sensitivity through the coupling to channel gating. A similar shift in the activation voltage was noted for the effects of *n*–6 arachidonic acid (AA) and DHA on Kv1.1, Kv1.2, and Kv11.1 channels. PUFAs-Kv1.5 channel interaction is time-dependent, producing a fast decay of the current upon depolarization. Thus, Kv1.5 channel opening is a prerequisite for the PUFA-channel interaction. Similar to the Kv1.5 channels, the blockade of Kv11.1 channels by AA and DHA steeply increased in the range of membrane potentials that coincided with the range of Kv11.1 channel activation, suggesting that the PUFAs-Kv channel interactions are also coupled to channel gating. Furthermore, AA regulates the inactivation process in other Kv channels, introducing a fast voltage-dependent inactivation in non-inactivating Kv channels. These results have been explained within the framework that AA closes voltage-dependent potassium channels by inducing conformational changes in the selectivity filter, suggesting that Kv channel gating is lipid dependent.

Keywords: *n*−3 PUFAs, Kv1.5, Kv11.1, gating, voltage-sensor

INTRODUCTION

The polyunsaturated fatty acids (PUFAs) present in nature belong to two main classes: the *n*−6 class and *n*−3 class. Both *n*−3 and *n*−6 PUFAs are essential nutrients that must be acquired from diet and are required for normal development and cellular function. In addition, mammals cannot convert *n*−6 into *n*−3 PUFAs. Certain vegetables can be a source for *n*−3 PUFAs, such as α-linolenic acid (ALA; 18:3 *n*−3), whereas other *n*−3 PUFAs, including eicosapentaenoic acid (EPA; 20:5 *n*−3) and docosahexaenoic acid (DHA; 22:6 *n*−3), can be obtained from marine sources (Holman, 1998). ALA is found in some vegetable oils (i.e., flaxseed, canola, and soybean) and walnuts, whereas marine *n*−3 PUFAs are found in fish and seafood. ALA is the precursor of EPA and DHA, but the conversion is limited and inefficient in organisms (Brenna, 2002). After ingestion, *n*−3 PUFAs are widely distributed to the cells and have effects on the membrane composition and function, eicosanoid synthesis, signaling, and the regulation of gene expression (Jump, 2002). A high dietary intake of *n*−3 PUFAs has also been linked to favorable physiological alterations, including reductions in the triglyceride levels, antithrombotic effects, enhanced immune function, and antiarrhythmic actions, which together may contribute to a lower risk of cardiovascular disease (Calder, 2004).

The dramatic increase in the *n*−6/*n*−3 ratio in the diet of the Western population after the industrial revolution has contributed to the rise in cardiovascular disease (Sinclair, 1953, 1956; De Caterina et al., 2003; Leaf et al., 2003). Moreover, there is a growing body of evidence that dietary *n*−3 PUFAs have an important role in the prevention of coronary heart disease by decreasing the risk of sudden cardiac death and, in particular, in preventing fatal ventricular arrhythmias (Burr et al., 1989; de Lorgeril et al., 1994; Singh et al., 1997; GISSI-Prevenzione Investigators, 1999; Albert et al., 2002; Leaf et al., 2003; Tanaka et al., 2008; Tavazzi et al., 2008). Finally, *n*−3 and *n*−6 PUFAs are metabolized to lipoxins, resolvins, and maresins (Serhan et al., 2008; Bannenberg and Serhan, 2010). These EPA- and DHA-derived lipid mediators (collectively termed Specific Pro-resolving Mediators; SPMs) are active, as anti-inflammatory agents, at very low concentrations (picomolar to nanomolar range), and are degraded locally by specific inactivating enzymes, characteristic for the bioactivity of autacoids. These SPMs can also slow the progression of diabetic onset, cardiovascular disease, and aging-associated pathologies through the regulation of innate and adaptive immune responses. The antiarrhythmic properties of *n*−3 PUFAs have been attributed to their ability to modulate the ion channels involved in the genesis and/or maintenance of cardiac action potentials. PUFAs

inhibit the I_{Na}, I_{Kur}, $I_{TO,IKr}$, and I_{Ca} voltage-gated ion channels and increase I_{Ks} (Honoré et al., 1994; Xiao et al., 1995, 1997; Doolan et al., 2002; Jude et al., 2003; Guizy et al., 2005, 2008; Verkerk et al., 2006; Dujardin et al., 2008), all of which are critical for biological signaling and regulating ion flux on a millisecond time scale.

In addition to their effects on the magnitude of the ionic currents, it has been demonstrated that membrane lipids can convert the Kv A-type channels into delayed rectifiers and vice versa. Within this framework, phosphoinositides (PIPs) remove the N-type inactivation, whereas AA converts the Kv delayed rectifiers into A-type rectifier channels (Oliver et al., 2004). Moreover, PIP_2 modulates ion channel gating and the interaction between the Kv channels and β subunits (Loussouarn et al., 2003; Decher et al., 2008; Rodriguez et al., 2010; David et al., 2012). In the present review, we will focus on the effects of PUFAs on the gating of Kv1.5 and Kv11.1, the cloned counterparts of I_{Kur} and I_{Kr}, respectively.

EFFECTS OF n−3 PUFAs ON THE GATING OF Kv1.5 CHANNELS

Kv1.5 channels consist of four subunits, each containing six transmembrane segments (S1–S6). The voltage sensor of the channel is formed by the S1–S4 segments, and the segments S5 and S6, together with the P-loop form the ion conduction pathway. In the human heart, these subunits are expressed mainly in the atria (Roberds and Tamkun, 1991; Tamkun et al., 1991; Fedida et al., 1993). To sense changes in the membrane voltage, each ion channel is equipped with four voltage-sensor domains (S1–S4) connected to a central ion-conducting pore domain. It has been described that the bilayer-forming lipids interact with the S3 and S4 helices more strongly than with the S1 and S2 segments. Indeed, there are several reports indicating an important role of the lipid bilayer in the channel voltage-sensor (Butterwick and MacKinnon, 2010).

Regarding the pathophysiological roles of these channels, I_{Kur} and I_{TO} comprise the main human atrial repolarizing current. Moreover, I_{Kur} has not been recorded in the human ventricle. During chronic atrial fibrillation, there is an electrical remodeling that comprises shortening of the action potential duration and a lack of adaptation of the action potential duration to an accelerated heartbeat (Dobrev and Ravens, 2003; Wettwer et al., 2004). Because the Kv1.5 channels are mostly expressed in the atria, they have been proposed as pharmacological targets for antiarrhythmic drugs that are effective on supraventricular arrhythmias, such as atrial fibrillation (Varro et al., 2004; Wettwer, 2007; Dobrev et al., 2012). In fact, it has been proposed that the blockade of I_{TO} and/or I_{Kur} prolongs the atrial action potential at the plateau but not at the terminal phase of repolarization, leading to rotor termination (Pandit et al., 2005; Decher et al., 2006; Dobrev and Nattel, 2010).

The first study dealing with the effects of PUFAs on Kv1.5 channels was performed by Honoré et al. (1994) who analyzed two different PUFAs, AA and DHA. These authors reported the AA- and DHA-induced time-dependent blockade of these channels, the existence of an external binding site for $n-3$ PUFAs and also a change in the gating of Kv1.5 channels that appeared as a negative shift in the activation curve.

The effects of ALA were qualitatively similar to those previously reported for DHA and AA (Honoré et al., 1994; Guizy et al., 2008). This study also showed that ALA both decreases the magnitude of the Kv1.5 current in a time-dependent manner and also modifies the gating of the channel (**Figure 1**). In fact, ALA shifts the activation curve toward negative membrane potentials, and an acceleration of the activation kinetics was observed in the range of the activation of the channels, a result that was likely due to the negative voltage shift (Guizy et al., 2008). A similar shift in the activation voltage was reported for the effects of AA and DHA on the Kv1.1 (Gubitosi-Klug and Gross, 1996), Kv1.2, and Kv11.1 channels (Poling et al., 1995; Guizy et al., 2005). Similar to what was previously described for AA and DHA, the blocking effects of ALA on the Kv1.5 channels only appeared when the PUFA was added from the external side of the membrane. In contrast, when it was applied from the inner side of the cell membrane, the magnitude of the current was not modified, but a hyperpolarizing shift of the activation curve and a slower deactivation time course of the current were observed (**Figure 1**). This finding indicated that the blocking effects produced by ALA on the Kv1.5 channels were due to the interaction with an external domain of the channel or, alternatively, an external domain of another molecule interacting with the ion channel. However, ALA modified the gating of the channel when it was applied from both sides of the membrane. Block of the Kv1.5 channels induced by ALA increased in the range of the membrane potentials that coincided with those of Kv1.5 channel activation, suggesting that the ALA-Kv1.5 interaction is voltage-dependent and likely coupled to the channel gating.

The flanking S5 and S6 segments are considered to contribute to the presumably wider intracellular mouth of the ion channel (Aiyar et al., 1994; Lopez et al., 1994) and contain binding sites for quaternary ammonium open-channel blockers and similarly acting drugs, such as quinidine or bupivacaine (Choi et al., 1993; Valenzuela et al., 1995, 1996; Yeola et al., 1996; Arias et al., 2007), and the Kvβ1.3 regulatory subunit (Decher et al., 2008; David et al., 2012). Block of Kv1.5 channels by $n-3$ and $n-6$ PUFAs resembles the effects of open-channel blockers and Kvβ1.3 regulatory subunits (Snyders et al., 1992; Valenzuela et al., 1995; Yeola et al., 1996; Franqueza et al., 1997; Gonzalez et al., 2002b; Decher et al., 2005, 2008; Arias et al., 2007; David et al., 2012). However, although these open-channel blockers interact with the inner part of the ion pore (Yeola et al., 1996; Franqueza et al., 1997; Decher et al., 2004), the PUFAs blockade appeared to be the consequence of their interaction with an external binding site in the channel. This issue concerning to the action mechanisms by which PUFAs modify ion channel activity has been a matter of debate. In fact, there are several pieces of evidence suggesting direct effects on ion channels (Xiao et al., 2000, 2001), whereas others reports claim that the effects of PUFAs represent the consequence of their effects on the physical properties of the lipid bilayer (Girshman et al., 1997; Bruno et al., 2007; Lundbaek, 2008). In fact, the $n-3$ and $n-6$ PUFAs are amphiphilic substances that may modulate the ion channel function by one of the following mechanisms: (a) changing the biophysical characteristics of the lipid bilayer; (b) modifying the hydrophobic interactions between the channel protein and the lipid bilayer, or (c) interacting specifically with an amino acid involved in the gating or the permeation of the channel (Oliver et al., 2004; Boland and Drzewiecki, 2008; Lundbaek,

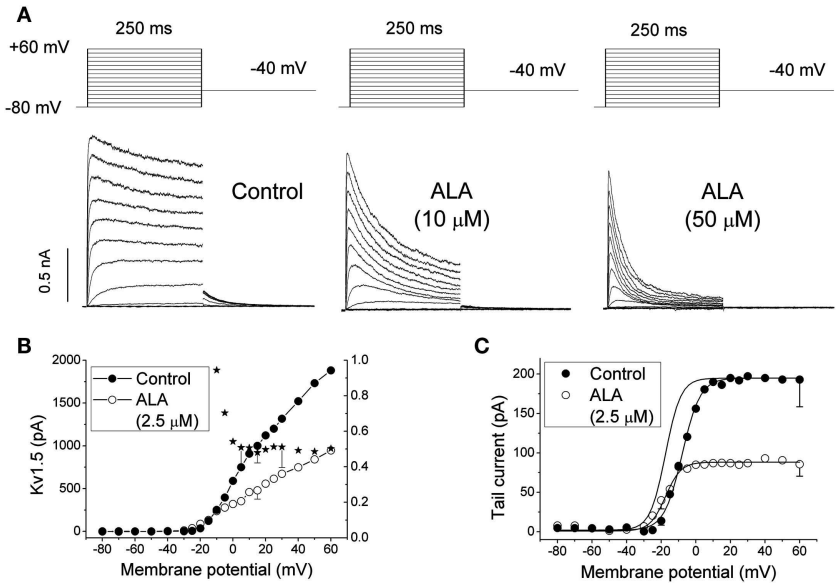

FIGURE 1 | (A) Original traces of Kv1.5 channels obtained after applying the pulse protocol shown in the upper part of the figure in the absence (Control) and in the presence of 10 and 50 μM α-linolenic acid (ALA). **(B)** Current-voltage (IV) relationship of Kv1.5 in the absence and in the presence of 2.5 μM ALA. The plot also shows the mean relative current ($I_{ALA/Control}$) at each membrane potential. **(C)** Kv1.5 activation curves obtained in the absence and in the presence of 2.5 μM ALA. The dotted line shows the activation curve obtained in the presence of ALA normalized to the matching control values. The data were obtained from Guizy et al. (2008).

2008; Meves, 2008). Recently, Decher et al. (2010) performed a study to elucidate the mechanism by which PUFAs modify the Kv1.x gating and the effects of AA and DHA on "edited" Kv1.x channels. Kv1.1 belongs to the increasing number of proteins having an amino acid sequence that is altered by RNA editing (Hoopengardner et al., 2003). In the "edited" Kv1.1 channels, an isoleucine facing the inner cavity of the pore is replaced by valine (I400V). This study shows that the effects of AA or other PUFAs (such as DHA) were strongly reduced in the "edited" Kv1.1 channels and also that, in heteromeric channels, the presence of only one "edited" Kv1.1 subunit was sufficient to decrease the affinity of PUFAs (Decher et al., 2010). This study concludes that the endogenous lipids AA and DHA produce an open-channel block of Kv channels, mimicking an increase in the rate of inactivation. These lipid effects are direct and can be antagonized by RNA editing of the Kv1.1 channels. However, the existence of "edited" Kv1.5 channels has not been demonstrated in the heart, brain, or other tissues. It is known that the isoleucine at position 400 is highly conserved in the Kv1.x channels and is located at the middle of the S6 helix, forming part of the wall of the central cavity of the ion channel (Long et al., 2005, 2007). In Kv1.5, the equivalent I400V position corresponds to I508, and the blocking effects of AA were also decreased in Kv1.5 I508A mutant channels. When the Kv1.1 channels were co-expressed with Kvβ1.1, the fractional block of the steady-state current by AA was strongly reduced (Decher et al., 2010). These data are consistent with the idea that Kvβ1.1 and AA compete for the same or overlapping binding sites located in the inner pore cavity, similar to the mode of action of quinidine and bupivacaine on Kvβ1.3 (Arias et al., 2007). Thus, the molecular mechanism of inactivation by AA might be analogous to the N-type inactivation by the Kvβ1 subunits (Decher et al., 2010). These results strongly suggest that, in contrast to the external binding site proposed by other authors (Honoré et al., 1994; Guizy et al., 2008), PUFAs seem to bind to an internal binding site that overlaps with the Kvβ1.3 and bupivacaine-binding site (Arias et al., 2007; Decher et al., 2008, 2010).

Why do PUFAs induce Kv1.5 block from the external side of the cell membrane? A possible explanation might be that when externally applied, PUFAs rapidly cross the lipid bilayer and bind to their internal receptor in the ion channel (Decher et al., 2010). Moreover, is it possible that no blocking effects are observed when PUFAs are applied from the internal side of the membrane. We may explain this unexpected behavior on the basis that, under these experimental conditions, PUFAs diffuse through the cell membrane into the bath faster than from the pipette to the membrane, as has been reported for other agents (DeCoursey, 1995; Brock et al., 2001; Macias et al., 2010).

EFFECTS OF PUFAs ON THE GATING OF Kv11.1 CHANNELS

Kv11.1 channels are encoded by the human ether-à-go-go-related gene (KCNH2), and the ionic current generated after their activation is responsible for the rapid delayed rectifier potassium current (I_{Kr}) in the heart and several other cell types. These channels are homotetramers of a protein formed by six membrane-spanning domains with intracellular N- and C-termini. I_{Kr} is characterized by a rapid activation at −30 mV and a strong inward rectification at positive potentials, which is due to the rapid voltage-dependent C-type inactivation. Inward rectification results from the fact that channel inactivation develops faster than channel activation at

positive potentials and limits the amount of time that channels exist in the open state (Smith et al., 1996; Spector et al., 1996).

The KCNH2 gene has been identified as the locus of mutations associated with type 2 long QT syndrome (LQTS2; Splawski et al., 2000; Roden et al., 2002; Kass and Moss, 2003). LQTS is a complex disease characterized by a marked QT interval prolongation and polymorphic ventricular tachycardia called torsades de pointes (TdP), causing syncope, seizures, and sudden death (Splawski et al., 2000; Roden et al., 2002; Kass and Moss, 2003; Shimizu, 2005). More than 290 mutations in the KCNH2 gene have been described, including frameshifts, insertions, deletions, and missense and nonsense mutations (Splawski et al., 2000; Roden et al., 2002; Kass and Moss, 2003; Shimizu, 2005). Mutant Kv11.1 channels producing LQTS2 generate reduced outward potassium currents that can be due to (a) the generation of non-functional channels, (b) altered channel gating, and/or (c) abnormal protein membrane trafficking (Thomas et al., 2003; Shimizu, 2005).

There is only one study in which the effects of acute PUFAs were studied in Kv11.1 channels (Guizy et al., 2005), reporting that the effects of AA and DHA block the Kv11.1 channels in a manner consistent with an open-channel block mechanism. The blockade induced by both of these PUFAs steeply increased in the range of the membrane potentials coinciding with the range of Kv11.1 channel activation, suggesting (similar to that reported for the Kv1.5 channels) that their binding may derive a significant fraction of its voltage sensitivity by coupling to the channel gating. Unfortunately, at strong depolarizing voltages, the open and inactivated conformations of the Kv11.1 channels are in rapid equilibrium, making it difficult to unequivocally identify the state(s) with which these two PUFAs interact.

Although AA induced a similar inhibition of the Kv11.1 current when measured at the end of depolarizing pulses and at the maximum tail currents, DHA inhibited this current to a higher extent when measured at the maximum tail current, suggesting an open-channel interaction mechanism (**Figure 2**). During depolarization, the Kv11.1 channels inactivate faster than they activate, and, thus, the amplitude of the current is reduced. Upon repolarization, the closed channels recover from inactivation with a very fast kinetics, resulting in tail currents with higher amplitudes than the maximum activated current (Smith et al., 1996; Spector et al., 1996). Experiments in which the transition from the closed to the inactivated state was removed demonstrated that both AA and DHA bind to the open state of the Kv11.1 channels in a time- and use-dependent manner, as previously described for cocaine and bupivacaine-type local anesthetics (Zhang et al., 2001; Gonzalez et al., 2002a). In agreement with these results, the blockade of Kv11.1 channels induced by AA and DHA measured after the recovery from fast inactivation was similar (for AA) or higher (for DHA) than that measured after a long depolarizing pulse in which most of the Kv11.1 channels were in the inactivated state (Snyders and Chaudhary, 1996; Spector et al., 1996; Guizy et al., 2005).

The time-dependent interaction with the ion channel was also evident in the deactivation process of the Kv11.1 channels that was accelerated in the presence of both AA and DHA. However, AA and DHA did not modify the onset kinetics of the inactivation process or the recovery process (Guizy et al., 2005). The faster deactivation induced by both of the PUFAs, together with their lack of effect on the recovery kinetics, are consistent with an open-channel block mechanism, as has been proposed for propafenone (Arias et al., 2003). Therefore, the time-, use-, and voltage-dependent interaction with Kv11.1 channels suggest that both AA and DHA preferentially bind to the open state of these channels and that DHA exhibits a higher affinity for this state of the channel (Guizy et al., 2005).

It was also reported that AA and DHA produced a positive shift of the inactivation curve, which was interpreted to be the consequence of PUFAs binding to a closed state of the channel. This interaction is likely to influence the apparent steady-state inactivation and maybe the activation process (Guizy et al., 2005). All of these results suggest that AA and DHA preferentially block the open state of Kv11.1 channels but also that they interact with a closed state, thus producing changes in the channel gating (**Figure 2**). However, the similar degree of AA-induced inhibition of the current at the end of long depolarizing pulses (when most channels are inactivated), at the maximum tail current or at the maximum peak current after the recovery of C-type inactivation cannot permit us to rule out an interaction between AA and the inactivated state of the Kv11.1 channels. Similarly, AA has also been reported to inhibit Kv11.1, Kv11.2, and Kv11.3 currents recorded from clonal somatomammotrophic GH_3/B_6 cells (Schledermann et al., 2001). These results show a decrease of the current and a marked acceleration of the deactivation. All of these results that involve a shift of the activation and inactivation curves, together with a modification of the deactivation kinetics, may suggest changes in the channel gating.

As stated above, it has been described that AA regulates the inactivation process in other potassium channels, introducing a fast voltage-dependent inactivation into non-inactivating Kv channels (Oliver et al., 2004). These results are in agreement with those reported by Guizy et al. (2005). Oliver et al. (2004) explain these results by proposing that AA inserts into the cell membrane from either side, interacts with the channel protein and allosterically induces a rapid closure of the open Kv channel pore through conformational modifications in the selectivity filter.

EFFECTS OF PUFAs ON Kv4 AND Kv7.1 + KCNE1 CHANNELS

As stated above, PUFAs are also able to modulate other cardiac ion channels present in the heart. Focusing on the outward K^+ currents, it has been reported that DHA and AA block I_{TO}, whereas DHA increases I_{Ks} (Singleton et al., 1999; Doolan et al., 2002; Boland et al., 2009; Xu et al., 2010). These studies show that both AA and DHA decrease the magnitude of Kv4.3 and also that AA shifts the activation curve, but not the inactivation curve, in the presence of KChiP1b but not in the absence of this accessory subunit. However, DHA shifts the activation curve both in the absence and in the presence of KChiP1b (Boland et al., 2009). In contrast, it has been reported that DHA increases I_{Ks} when Kv7.1 + KCNE1 was transfected into *Xenopus* oocytes (Doolan et al., 2002). Taking all of the effects of DHA on all of the outward potassium currents together, we can expect small changes in the duration of the cardiac action potential, as the blocking effects on I_{Kr}, I_{Kur}, I_{TO} can be counteracted by the effects on I_{Ks}.

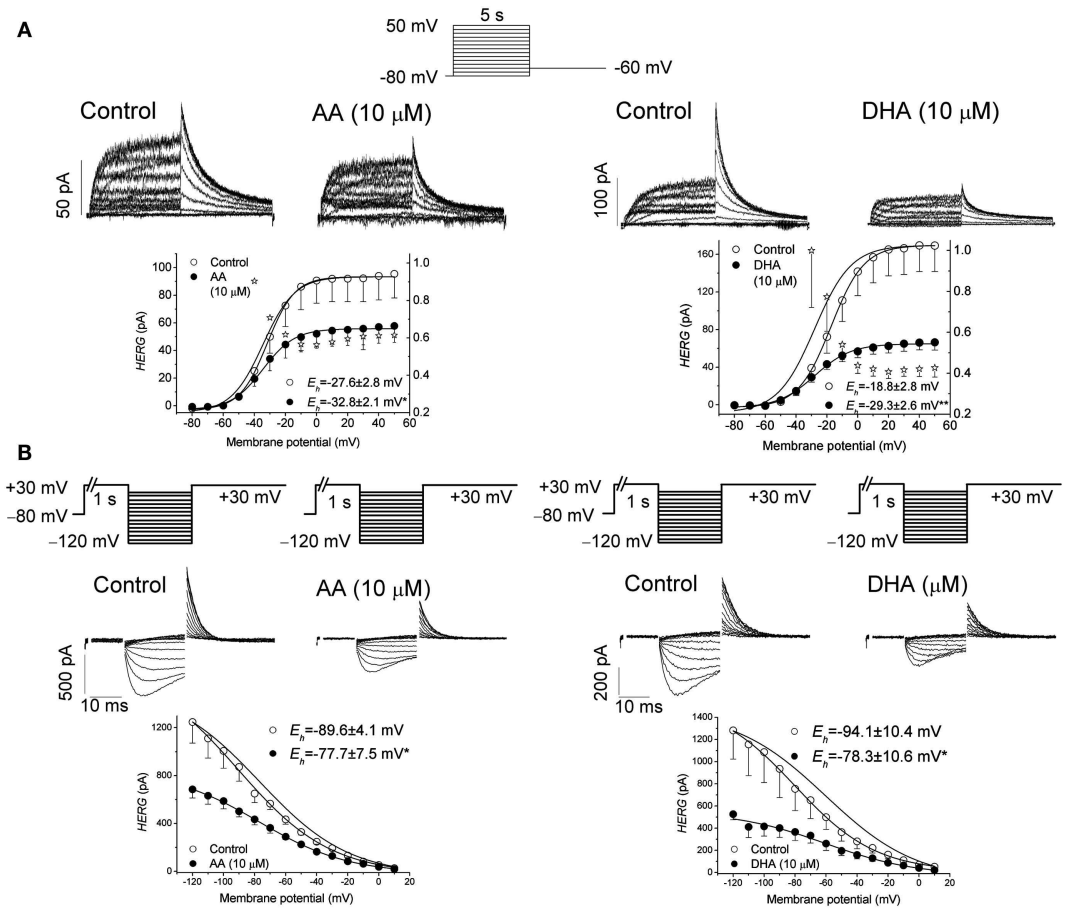

FIGURE 2 | (A) Original traces of Kv11.1 channels obtained after applying the pulse protocol shown in the upper part of the figure in the absence (Control) and in the presence of arachidonic acid (AA) and docohexaenoic acid (DHA) at 10 μM. This panel also shows the activation curves of the Kv11.1 channels in the absence and in the presence of AA and DHA. **(B)** Apparent voltage dependence of channel availability. The pulse protocol used to obtain each data point is shown at the top. Original traces obtained after applying such a pulse protocol in the absence and in the presence of 10 μM AA and DHA. Corrected data for the deactivation together with the Boltzmann fit. The data were obtained from Guizy et al. (2005).

CONCLUDING REMARKS

PUFAs have diverse effects on cardiac ion currents. All of the reports in which PUFA effects have been studied on Kv channels demonstrate that these molecules modify the channel gating, indicating that the gating of Kv channels can be modified by lipids. This is not a surprising result, as it has been previously described that the S3 and S4 helices of the voltage-sensor domain of KvAP channels exhibit specific interactions with phospholipids. Conversely, the S1 and S2 helices might present a generic hydrophobic surface that is more equally satisfied by detergents and long-chain lipids (Bond and Sansom, 2007; Butterwick and MacKinnon, 2010). It has also been described that a diet rich in PUFAs is able to modify the lipid bilayer composition. The effects of PUFAs can be different and even opposite when they are acutely or chronically applied. In fact, *n*−3 PUFAs decrease Kv1.5 channels under both experimental conditions (Guizy et al., 2008). However, PUFAs decreased the magnitude of the Kv11.1 current after an acute exposure, whereas they did not modify this potassium current recorded in myocytes obtained from animal fed with a diet rich in *n*−3 PUFAs (Verkerk et al., 2006; Den Ruijter et al., 2012). These apparent discrepant results may be explained by two different effects of PUFAs on ion channels: a direct effect on the ion channel and another produced after changing the membrane biophysical properties. Both mechanisms can modify the gating of the ion channel; however, the effects on the ion current magnitude will likely derive from direct PUFA-channel interactions. Further lipidomic and electrophysiological studies using mutant Kv11.1 channels are necessary for a better understanding of the effects of PUFAs on the gating of Kv channels.

ACKNOWLEDGMENTS

The authors want to express their thanks to Dr. Teresa Gonzalez for her helpful comments. This work was supported by SAF2010-14916 and FIS-RECAVA RD06/0014/0025. RECAVA is funded by the Instituto de Salud Carlos III. Cristina Moreno and Angela Prieto hold FPI fellowships. Alvaro Macias is a JAE-predoctoral fellow. Alicia De La Cruz held an RECAVA contract. We thank the editorial assistance of American Journal Experts.

REFERENCES

Aiyar, J., Nguyen, A. N., Chandy, K. G., and Grissmer, S. (1994). The P-region and S6 of Kv3.1 contribute to the formation of the ion conduction pathway. *Biophys. J.* 67, 2261–2264.

Albert, C. M., Campos, H., Stampfer, M. J., Ridker, P. M., Manson, J. E., Willett, W. C., and Ma, J. (2002). Blood levels of long-chain n-3 fatty acids and the risk of sudden death. *N. Engl. J. Med.* 346, 1113–1118.

Arias, C., Gonzalez, T., Moreno, I., Caballero, R., Delpon, E., Tamargo, J., and Valenzuela, C. (2003). Effects of propafenone and its main metabolite, 5-hydroxypropafenone, on HERG channels. *Cardiovasc. Res.* 57, 660–669.

Arias, C., Guizy, M., David, M., Marzian, S., Gonzalez, T., Decher, N., and Valenzuela, C. (2007). Kvβ1.3 reduces the degree of stereoselective bupivacaine block of Kv1.5 channels. *Anesthesiol.* 107, 641–651.

Bannenberg, G., and Serhan, C. N. (2010). Specialized pro-resolving lipid mediators in the inflammatory response: an update. *Biochim. Biophys. Acta* 1801, 1260–1273.

Boland, L. M., and Drzewiecki, M. M. (2008). Polyunsaturated fatty acid modulation of voltage-gated ion channels. *Cell Biochem. Biophys.* 52, 59–84.

Boland, L. M., Drzewiecki, M. M., Timoney, G., and Casey, E. (2009). Inhibitory effects of polyunsaturated fatty acids on Kv4/KChIP potassium channels. *Am. J. Physiol. Cell Physiol.* 296, C1003–C1014.

Bond, P. J., and Sansom, M. S. (2007). Bilayer deformation by the Kv channel voltage sensor domain revealed by self-assembly simulations. *Proc. Natl. Acad. Sci. U.S.A.* 104, 2631–2636.

Brenna, J. T. (2002). Efficiency of conversion of alpha-linolenic acid to long chain n-3 fatty acids in man. *Curr. Opin. Clin. Nutr. Metab. Care* 5, 127–132.

Brock, M. W., Mathes, C., and Gilly, W. F. (2001). Selective open-channel block of Shaker (Kv1) potassium channels by s-nitrosodithiothreitol (SNDTT). *J. Gen. Physiol.* 118, 113–134.

Bruno, M. J., Koeppe, R. E., and Andersen, O. S. (2007). Docosahexaenoic acid alters bilayer elastic properties. *Proc. Natl. Acad. Sci. U.S.A.* 104, 9638–9643.

Burr, M. L., Fehily, A. M., Gilbert, J. F., Rogers, S., Holliday, R. M., Sweetnam, P. M., Elwood, P. C., and Deadman, N. M. (1989). Effects of changes in fat, fish, and fibre intakes on death and myocardial reinfarction: diet and reinfarction trial (DART). *Lancet* 2, 757–761.

Butterwick, J. A., and MacKinnon, R. (2010). Solution structure and phospholipid interactions of the isolated voltage-sensor domain from KvAP. *J. Mol. Biol.* 403, 591–606.

Calder, P. C. (2004). n-3 Fatty acids and cardiovascular disease: evidence explained and mechanisms explored. *Clin. Sci.* 107, 1–11.

Choi, K. L., Mossman, C., Aube, J., and Yellen, G. (1993). The internal quaternary ammonium receptor site of shaker potassium channels. *Neuron* 10, 533–541.

David, M., Macias, A., Moreno, C., Prieto, A., Martinez-Marmol, R., Vicente, R., Felipe, A., Gonzalez, T., Tamkun, M. M., and Valenzuela, C. (2012). PKC activity regulates functional effects of KVβ1.3 on KV1.5 channels. Identification of a cardiac KV1.5 channelosome. *J. Biol. Chem.* 287, 21416–21428.

De Caterina, R., Madonna, R., Zucchi, R., and La Rovere, M. T. (2003). Antiarrhythmic effects of omega-3 fatty acids: from epidemiology to bedside. *Am. Heart J.* 146, 420–430.

de Lorgeril, M., Renaud, S., Mamelle, N., Salen, P., Martin, J. L., Monjaud, I., Guidollet, J., Touboul, P., and Delaye, J. (1994). Mediterranean alpha-linolenic acid-rich diet in secondary prevention of coronary heart disease. *Lancet* 343, 1454–1459.

Decher, N., Gonzalez, T., Streit, A. K., Sachse, F. B., Renigunta, V., Soom, M., Heinemann, S. H., Daut, J., and Sanguinetti, M. C. (2008). Structural determinants of Kvbeta1.3-induced channel inactivation: a hairpin modulated by PIP2. EMBO J. 27, 3164–3174.

Decher, N., Kumar, P., Gonzalez, T., Pirard, B., and Sanguinetti, M. C. (2006). Binding site of a novel Kv1.5 blocker: a "foot in the door" against atrial fibrillation. *Mol. Pharmacol.* 70, 1204–1211.

Decher, N., Kumar, P., Gonzalez, T., Renigunta, V., and Sanguinetti, M. C. (2005). Structural basis for competition between drug binding and Kvbeta1.3 accessory subunit-induced N-type inactivation of Kv1.5 channels. *Mol. Pharmacol.* 68, 995–1005.

Decher, N., Pirard, B., Bundis, F., Peukert, S., Baringhaus, K. H., Busch, A. E., Steinmeyer, K., and Sanguinetti, M. C. (2004). Molecular basis for Kv1.5 channel block: conservation of drug binding sites among voltage-gated K+ channels. *J. Biol. Chem.* 279, 394–400.

Decher, N., Streit, A. K., Rapedius, M., Netter, M. F., Marzian, S., Ehling, P., Schlichthorl, G., Craan, T., Renigunta, V., Kohler, A., Dodel, R. C., Navarro-Polanco, R. A., Preisig-Müller, R., Klebe, G., Budde, T., Baukrowitz, T., and Daut, J. (2010). RNA editing modulates the binding of drugs and highly unsaturated fatty acids to the open pore of Kv potassium channels. *EMBO J.* 29, 2101–2113.

DeCoursey, T. E. (1995). Mechanism of K+ channel block by verapamil and related compounds in rat alveolar epithelial cells. *J. Gen. Physiol.* 106, 745–779.

Den Ruijter, H. M., Verkerk, A. O., Schumacher, C. A., Houten, S. M., Belterman, C. N., Baartscheer, A., Brouwer, I. A., van, B. M., de, R. B., and Coronel, R. (2012). A diet rich in unsaturated fatty acids prevents progression toward heart failure in a rabbit model of pressure and volume overload. *Circ. Heart Fail.* 5, 376–384.

Dobrev, D., Carlsson, L., and Nattel, S. (2012). Novel molecular targets for atrial fibrillation therapy. *Nat. Rev. Drug Discov.* 11, 275–291.

Dobrev, D., and Nattel, S. (2010). New antiarrhythmic drugs for treatment of atrial fibrillation. *Lancet* 375, 1212–1223.

Dobrev, D., and Ravens, U. (2003). Remodeling of cardiomyocyte ion channels in human atrial fibrillation. *Basic Res. Cardiol.* 98, 137–148.

Doolan, G. K., Panchal, R. G., Fonnes, E. L., Clarke, A. L., Williams, D. A., and Petrou, S. (2002). Fatty acid augmentation of the cardiac slowly activating delayed rectifier current (IKs) is conferred by hminK. *FASEB J.* 16, 1662–1664.

Dujardin, K. S., Dumotier, B., David, M., Guizy, M., Valenzuela, C., and Hondeghem, L. M. (2008). Ultrafast sodium channel block by dietary fish oil prevents dofetilide-induced ventricular arrhythmias in rabbit hearts. *Am. J. Physiol. Heart Circ. Physiol.* 295, H1414–H1421.

Fedida, D., Wible, B., Wang, Z., Fermini, B., Faust, F., Nattel, S., and Brown, A. M. (1993). Identity of a novel delayed rectifier current from human heart with a cloned K^+ channel current. *Circ. Res.* 73, 210–216.

Franqueza, L., Longobardo, M., Vicente, J., Delpon, E., Tamkun, M. M., Tamargo, J., Snyders, D. J., and Valenzuela, C. (1997). Molecular determinants of stereoselective bupivacaine block of hKv1.5 channels. *Circ. Res.* 81, 1053–1064.

Girshman, J., Greathouse, D. V., Koeppe, R. E., and Andersen, O. S. (1997). Gramicidin channels in phospholipid bilayers with unsaturated acyl chains. *Biophys. J.* 73, 1310–1319.

GISSI-Prevenzione Investigators. (1999). Dietary supplementation with n-3 polyunsaturated fatty acids and vitamin E after myocardial infarction: results of the GISSI-prevenzione trial. Gruppo italiano per lo studio della sopravvivenza nell'infarto miocardico. *Lancet* 354, 447–455.

Gonzalez, T., Arias, C., Caballero, R., Moreno, I., Delpon, E., Tamargo, J., and Valenzuela, C. (2002a). Effects of levobupivacaine, ropivacaine and bupivacaine on HERG channels: stereoselective bupivacaine block. *Br. J. Pharmacol.* 137, 1269–1279.

Gonzalez, T., Navarro-Polanco, R., Arias, C., Caballero, R., Moreno, I., Delpon, E., Tamargo, J., Tamkun, M. M., and Valenzuela, C. (2002b). Assembly with the Kvβ1.3 subunit modulates drug block of hKv1.5 channels. *Mol. Pharmacol.* 62, 1456–1463.

Gubitosi-Klug, R. A., and Gross, R. W. (1996). Fatty acid ethyl esters, nonoxidative metabolites of ethanol, accelerate the kinetics of activation of the human brain delayed rectifier K^+ channel, Kv1.1. *J. Biol. Chem.* 271, 32519–32522.

Guizy, M., Arias, C., David, M., Gonzalez, T., and Valenzuela, C. (2005). ω-3 and ω-6 polyunsaturated fatty acids block HERG channels. *Am. J. Physiol. Cell Physiol.* 289, C1251–C1260.

Guizy, M., David, M., Arias, C., Zhang, L., Cofan, M., Ruiz-Gutierrez, V., Ros, E., Lillo, M. P., Martens, J. R., and Valenzuela, C. (2008). Modulation of the atrial specific Kv1.5 channel by the n-3 polyunsaturated fatty acid, alpha-linolenic acid. *J. Mol. Cell Cardiol.* 44, 323–335.

Holman, R. T. (1998). The slow discovery of the importance of omega 3 essential fatty acids in human health. *J. Nutr.* 128, 427S–433S.

Honoré, E., Barhanin, J., Attali, B., Lesage, F., and Lazdunski, M. (1994). External blockade of the major cardiac delayed-rectifier K^+ channel (Kv1.5) by polyunsaturated fatty acids. *Proc. Natl. Acad. Sci. U.S.A.* 91, 1937–1941.

Hoopengardner, B., Bhalla, T., Staber, C., and Reenan, R. (2003). Nervous system targets of RNA editing identified by comparative genomics. *Science* 301, 832–836.

Jude, S., Bedut, S., Roger, S., Pinault, M., Champeroux, P., White, E., and Le

Guennec, J. Y. (2003). Peroxidation of docosahexaenoic acid is responsible for its effects on I TO and I SS in rat ventricular myocytes. *Br. J. Pharmacol.* 139, 816–822.

Jump, D. B. (2002). The biochemistry of n-3 polyunsaturated fatty acids. *J. Biol. Chem.* 277, 8755–8758.

Kass, R. S., and Moss, A. J. (2003). Long QT syndrome: novel insights into the mechanisms of cardiac arrhythmias. *J. Clin. Invest.* 112, 810–815.

Leaf, A., Kang, J. X., Xiao, Y. F., and Billman, G. E. (2003). Clinical prevention of sudden cardiac death by n-3 polyunsaturated fatty acids and mechanism of prevention of arrhythmias by n-3 fish oils. *Circulation* 107, 2646–2652.

Long, S. B., Campbell, E. B., and MacKinnon, R. (2005). Voltage sensor of Kv1.2: structural basis of electromechanical coupling. *Science* 309, 903–908.

Long, S. B., Tao, X., Campbell, E. B., and MacKinnon, R. (2007). Atomic structure of a voltage-dependent K+ channel in a lipid membrane-like environment. *Nature* 450, 376–382.

Lopez, G. A., Jan, Y. N., and Jan, L. Y. (1994). Evidence that the S6 segment of the shaker voltage-gated K^+ channel comprises part of the pore. *Nature* 367, 179–182.

Loussouarn, G., Park, K. H., Bellocq, C., Baro, I., Charpentier, F., and Escande, D. (2003). Phosphatidylinositol-4,5-bisphosphate, PIP2, controls KCNQ1/KCNE1 voltage-gated potassium channels: a functional homology between voltage-gated and inward rectifier K+ channels. *EMBO J.* 22, 5412–5421.

Lundbaek, J. A. (2008). Lipid bilayer-mediated regulation of ion channel function by amphiphilic drugs. *J. Gen. Physiol.* 131, 421–429.

Macias, A., Moreno, C., Moral-Sanz, J., Cogolludo, A., David, M., Alemanni, M., Perez-Vizcaino, F., Zaza, A., Valenzuela, C., and Gonzalez, T. (2010). Celecoxib blocks cardiac Kv1.5, Kv4.3, and Kv7.1 (KCNQ1) channels: effects on cardiac action potentials. *J. Mol. Cell Cardiol.* 49, 984–992.

Meves, H. (2008). Arachidonic acid and ion channels: an update. *Br. J. Pharmacol.* 155, 4–16.

Oliver, D., Lien, C. C., Soom, M., Baukrowitz, T., Jonas, P., and Fakler, B. (2004). Functional conversion between A-type and delayed rectifier K^+ channels by membrane lipids. *Science* 304, 265–270.

Pandit, S. V., Berenfeld, O., Anumonwo, J. M., Zaritski, R. M., Kneller, J., Nattel, S., and Jalife, J. (2005). Ionic determinants of functional reentry in a 2-D model of human atrial cells during simulated chronic atrial fibrillation. *Biophys. J.* 88, 3806–3821.

Poling, J. S., Karanian, J. W., Salem, N. Jr., and Vicini, S. (1995). Time- and voltage-dependent block of delayed rectifier potassium channels by docosahexaenoic acid. *Mol. Pharmacol.* 47, 381–390.

Roberds, S. L., and Tamkun, M. M. (1991). Cloning and tissue-specific expression of five voltage-gated potassium channel cDNAs expressed in rat heart. *Proc. Natl. Acad. Sci. U.S.A.* 88, 1798–1802.

Roden, D. M., Balser, J. R., George, A. L. Jr., and Anderson, M. E. (2002). Cardiac ion channels. *Annu. Rev. Physiol.* 64, 431–475.

Rodriguez, N., Amarouch, M. Y., Montnach, J., Piron, J., Labro, A. J., Charpentier, F., Merot, J., Baro, I., and Loussouarn, G. (2010). Phosphatidylinositol-4,5-bisphosphate (PIP(2)) stabilizes the open pore conformation of the Kv11.1 (hERG) channel. *Biophys. J.* 99, 1110–1118.

Schledermann, W., Wulfsen, I., Schwarz, J. R., and Bauer, C. K. (2001). Modulation of rat erg1, erg2, erg3, and HERG K+ currents by thyrotropin-releasing hormone in anterior pituitary cells via the native signal cascade. *J. Physiol.* 532, 143–163.

Serhan, C. N., Yacoubian, S., and Yang, R. (2008). Anti-inflammatory and proresolving lipid mediators. *Annu. Rev. Pathol.* 3, 279–312.

Shimizu, W. (2005). The long QT syndrome: therapeutic implications of a genetic diagnosis. *Cardiovasc. Res.* 67, 347–356.

Sinclair, H. M. (1953). The diet of Canadian Indian Eskimos. *Proc. Nutr. Soc.* 12, 69–82.

Sinclair, H. M. (1956). Deficiency of essential fatty acids and atherosclerosis, etcetera. *Lancet* 270, 381–383.

Singh, R. B., Niaz, M. A., Sharma, J. P., Kumar, R., Rastogi, V., and Moshiri, M. (1997). Randomized, double-blind, placebo-controlled trial of fish oil and mustard oil in patients with suspected acute myocardial infarction: the Indian experiment of infarct survival–4. *Cardiovasc. Drugs Ther.* 11, 485–491.

Singleton, C. B., Valenzuela, S. M., Walker, B. D., Tie, H., Wyse, K. R., Bursill, J. A., Qiu, M. R., Breit, S. N., and Campbell, T. J. (1999). Blockade by N-3 polyunsaturated fatty acid of the Kv4.3 current stably expressed in Chinese hamster ovary cells. *Br. J. Pharmacol.* 127, 941–948.

Smith, P. L., Baukrowitz, T., and Yellen, G. (1996). The inward rectification mechanism of the HERG cardiac potassium channel. *Nature* 379, 833–836.

Snyders, D. J., and Chaudhary, A. C. (1996). High affinity open-channel block by dofetilide of HERG, expressed in a human cell line. *Mol. Pharmacol.* 49, 949–955.

Snyders, D. J., Knoth, K. M., Roberds, S. L., and Tamkun, M. M. (1992). Time-, voltage-, and state-dependent block by quinidine of a cloned human cardiac potassium channel. *Mol. Pharmacol.* 41, 322–330.

Spector, P. S., Curran, M. E., Zou, A., Keating, M. T., and Sanguinetti, M. C. (1996). Fast inactivation causes rectification of the IKr channel. *J. Gen. Physiol.* 107, 611–619.

Splawski, I., Shen, J., Timothy, K. W., Lehmann, M. H., Priori, S., Robinson, J. L., Moss, A. J., Schwartz, P. J., Towbin, J. A., and Vincent, G. M. et al. (2000). Spectrum of mutations in long-QT syndrome genes. KVLQT1, HERG, SCN5A, KCNE1, and KCNE2. *Circulation* 102, 1178–1185.

Tamkun, M. M., Knoth, K. M., Walbridge, J. A., Kroemer, H., Roden, D. M., and Glover, D. M. (1991). Molecular cloning and characterization of two voltage-gated K+ channel cDNAs from human ventricle. *FASEB J.* 5, 331–337.

Tanaka, K., Ishikawa, Y., Yokoyama, M., Origasa, H., Matsuzaki, M., Saito, Y., Matsuzawa, Y., Sasaki, J., Oikawa, S., Hishida, H., Itakura, H., Kita, T., Kitabatake, A., Nakaya, N., Sakata, T., Shimada, K., and Shirato, K. (2008). Reduction in the recurrence of stroke by eicosapentaenoic acid for hypercholesterolemic patients: subanalysis of the JELIS trial. *Stroke* 39, 2052–2058.

Tavazzi, L., Maggioni, A. P., Marchioli, R., Barlera, S., Franzosi, M. G., Latini, R., Lucci, D., Nicolosi, G. L., Porcu, M., and Tognoni, G. (2008). Effect of n-3 polyunsaturated fatty acids in patients with chronic heart failure (the GISSI-HF trial): a randomised, double-blind, placebo-controlled trial. *Lancet* 372, 1223–1230.

Thomas, D., Kiehn, J., Katus, H. A., and Karle, C. A. (2003). Defective protein trafficking in hERG-associated hereditary long QT syndrome (LQT2): molecular mechanisms and restoration of intracellular protein processing. *Cardiovasc. Res.* 60, 235–241.

Valenzuela, C., Delpon, E., Franqueza, L., Gay, P., Perez, O., Tamargo, J., and Snyders, D. J. (1996). Class III antiarrhythmic effects of zatebradine. Time-, state-, use-, and voltage-dependent block of hKv1.5 channels. *Circulation* 94, 562–570.

Valenzuela, C., Delpon, E., Tamkun, M. M., Tamargo, J., and Snyders, D. J. (1995). Stereoselective block of a human cardiac potassium channel (Kv1.5) by bupivacaine enantiomers. *Biophys. J.* 69, 418–427.

Varro, A., Biliczki, P., Iost, N., Virag, L., Hala, O., Kovacs, P., Matyus, P., and Papp, J. G. (2004). Theoretical possibilities for the development of novel antiarrhythmic drugs. *Curr. Med. Chem.* 11, 1–11.

Verkerk, A. O., van Ginneken, A. C., Berecki, G., Den Ruijter, H. M., Schumacher, C. A., Veldkamp, M. W., Baartscheer, A., Casini, S., Opthof, T., Hovenier, R., Fiolet, J. W., Zock, P. L., and Coronel, R. (2006). Incorporated sarcolemmal fish oil fatty acids shorten pig ventricular action potentials. *Cardiovasc. Res.* 70, 509–520.

Wettwer, E. (2007). Is there a functional correlate of Kv1.5 in the ventricle of canine heart and what would it mean for the use of I(Kur) blockers? *Br. J. Pharmacol.* 152, 835–837.

Wettwer, E., Hala, O., Christ, T., Heubach, J. F., Dobrev, D., Knaut, M., Varro, A., and Ravens, U. (2004). Role of IKur in controlling action potential shape and contractility in the human atrium: influence of chronic atrial fibrillation. *Circulation* 110, 2299–2306.

Xiao, Y. F., Gomez, A. M., Morgan, J. P., Lederer, W. J., and Leaf, A. (1997). Suppression of voltage-gated L-type Ca2+ currents by polyunsaturated fatty acids in adult and neonatal rat ventricular myocytes. *Proc. Natl. Acad. Sci. U.S.A.* 94, 4182–4187.

Xiao, Y. F., Kang, J. X., Morgan, J. P., and Leaf, A. (1995). Blocking effects of polyunsaturated fatty acids on Na+ channels of neonatal rat ventricular myocytes. *Proc. Natl. Acad. Sci. U.S.A.* 92, 11000–11004.

Xiao, Y. F., Ke, Q., Wang, S. Y., Auktor, K., Yang, Y., Wang, G. K., Morgan, J. P., and Leaf, A. (2001). Single point mutations affect fatty acid block of human myocardial sodium

channel alpha subunit Na+ channels. *Proc. Natl. Acad. Sci. U.S.A.* 98, 3606–3611.

Xiao, Y. F., Wright, S. N., Wang, G. K., Morgan, J. P., and Leaf, A. (2000). Coexpression with beta(1)-subunit modifies the kinetics and fatty acid block of hH1(alpha) Na(+) channels. *Am. J. Physiol. Heart Circ. Physiol.* 279, H35–H46.

Xu, X., Jiang, M., Wang, Y., Smith, T., Baumgarten, C. M., Wood, M. A., and Tseng, G. N. (2010). Long-term fish oil supplementation induces cardiac electrical remodeling by changing channel protein expression in the rabbit model. *PLoS. ONE.* 5, e10140. doi:10.1371/journal.pone.0010140

Yeola, S. W., Rich, T. C., Uebele, V. N., Tamkun, M. M., and Snyders, D. J. (1996). Molecular analysis of a binding site for quinidine in a human cardiac delayed rectifier K^+ channel. Role of S6 in antiarrhythmic drug binding. *Circ. Res.* 78, 1105–1114.

Zhang, S., Rajamani, S., Chen, Y., Gong, Q., Rong, Y., Zhou, Z., Ruoho, A., and January, C. T. (2001). Cocaine blocks HERG, but not KvLQT1+ minK, potassium channels. *Mol. Pharmacol.* 59, 1069–1076.

Conflict of Interest Statement: The authors declare that the research was conducted in the absence of any commercial or financial relationships that could be construed as a potential conflict of interest.

Received: 30 May 2012; accepted: 20 August 2012; published online: 10 September 2012.

Citation: Moreno C, Macias A, Prieto A, De La Cruz A and Valenzuela C (2012) Polyunsaturated fatty acids modify the gating of Kv channels. Front. Pharmacol. ***3****:163. doi: 10.3389/fphar.2012.00163*

This article was submitted to Frontiers in Pharmacology of Ion Channels and Channelopathies, a specialty of Frontiers in Pharmacology.

frontiers in
PHARMACOLOGY

REVIEW ARTICLE
published: 25 September 2012
doi: 10.3389/fphar.2012.00170

Dual regulation of voltage-sensitive ion channels by PIP_2

Aldo A. Rodríguez-Menchaca†, Scott K. Adney, Lei Zhou and Diomedes E. Logothetis*

Department of Physiology and Biophysics, School of Medicine, Virginia Commonwealth University, Richmond, VA, USA

Edited by:
Gildas Loussouarn, University of Nantes, France

Reviewed by:
Mark S. Shapiro, The University of Texas Health Science Center at San Antonio, USA
Show-Ling Shyng, Oregon Health and Science University, USA

***Correspondence:**
Diomedes E. Logothetis, Department of Physiology and Biophysics, School of Medicine, Virginia Commonwealth University, Richmond, VA 23298, USA. e-mail: delogothetis@vcu.edu

†***Present address:***
Aldo A. Rodríguez-Menchaca, Departamento de Fisiología y Biofísica, Facultad de Medicina, Universidad Autónoma de San Luis Potosí, San Luis Potosí 78210, México.

Over the past 16 years, there has been an impressive number of ion channels shown to be sensitive to the major phosphoinositide in the plasma membrane, phosphatidylinositol 4,5-bisphosphate (PIP_2). Among them are voltage-gated channels, which are crucial for both neuronal and cardiac excitability. Voltage-gated calcium (Cav) channels were shown to be regulated bidirectionally by PIP_2. On one hand, PIP_2 stabilized their activity by reducing current rundown but on the other hand it produced a voltage-dependent inhibition by shifting the activation curve to more positive voltages. For voltage-gated potassium (Kv) channels PIP_2 was first shown to prevent N-type inactivation regardless of whether the fast inactivation gate was part of the pore-forming α subunit or of an accessory β subunit. Careful examination of the effects of PIP_2 on the activation mechanism of Kv1.2 has shown a similar bidirectional regulation as in the Cav channels. The two effects could be distinguished kinetically, in terms of their sensitivities to PIP_2 and by distinct molecular determinants. The rightward shift of the Kv1.2 voltage dependence implicated basic residues in the S4–S5 linker and was consistent with stabilization of the inactive state of the voltage sensor. A third type of a voltage-gated ion channel modulated by PIP_2 is the hyperpolarization-activated cyclic nucleotide-gated (HCN) channel. PIP_2 has been shown to enhance the opening of HCN channels by shifting their voltage-dependent activation toward depolarized potentials. The sea urchin HCN channel, SpIH, showed again a PIP_2-mediated bidirectional effect but in reverse order than the depolarization-activated Cav and Kv channels: a voltage-dependent potentiation, like the mammalian HCN channels, but also an inhibition of the cGMP-induced current activation. Just like the Kv1.2 channels, distinct molecular determinants underlied the PIP_2 dual effects on SpIH, with the proximal C-terminus implicated in the inhibitory effect. The dual regulation of these very different ion channels, all of which are voltage-dependent, points to conserved mechanisms of regulation of these channels by PIP_2.

Keywords: PIP2, voltage sensor, voltage-gated channels, gating, S4–S5 linker

INTRODUCTION

Voltage-gated ion channels regulate the flow of different ions across the membrane in response to changes in membrane potential. These channels are composed of four subunits (or four linked domains) symmetrically arranged around a central ion-conducting pore. Voltage-gated ion channels open in response to depolarization or hyperpolarization. The change in membrane potential induces a conformational change in the voltage sensor domain located in the periphery of the ion channel; this conformational change is coupled to the ion-conducting pore, and leads to channel opening (Long et al., 2005; Bezanilla, 2008; Borjesson and Elinder, 2008).

Voltage-gated ion channels can be modulated by numerous factors including free fatty acids (Xiao et al., 2005; Borjesson et al., 2008; Xu et al., 2008a), toxins (Catterall et al., 2007; Swartz, 2007), metal ions (Elinder and Arhem, 2003), glycosylation (Fozzard and Kyle, 2002; Watanabe et al., 2003, 2007), palmitoylation (Gubitosi-Klug et al., 2005; Jindal et al., 2008), phosphorylation (Davis et al., 2001; Mohapatra and Trimmer, 2006; Mohapatra et al., 2007; Li et al., 2008), and phospholipids (Ramu et al., 2006; Schmidt et al., 2006; Xu et al., 2008b). Modulation by phospholipids includes phosphatidylinositol 4,5-bisphosphate (PIP_2), the lipid component of the inner membrane leaflet that modulates the activity of most ion channels and transporters tested (Suh and Hille, 2005, 2008; Logothetis et al., 2010).

PIP_2 plays an important role as an intermediate molecule in multiple receptor signaling pathways. PIP_2 hydrolysis by PLC produces 1,4,5-trisphosphate (IP_3) and diacylglycerol (DAG; Berridge, 1984). IP_3 mobilizes Ca^{2+} from the endoplasmic reticulum, while DAG activates PKC. However, PIP_2 itself acts as a signaling molecule through direct interactions with target proteins. Our review focuses on the effects of PIP_2 on voltage-dependent ion channels, particularly those showing bidirectional regulation.

VOLTAGE-GATED CALCIUM CHANNELS

Voltage-gated calcium (Cav) channels mediate calcium influx in response to membrane depolarization and regulate intracellular processes such as contraction, secretion, neurotransmission, and gene expression in many different cell types. There are five types of Cav channels: the high voltage-activated L- (Cav1), P/Q- (Cav2.1), N- (Cav2.2), and R- (Cav2.3), and the low voltage-activated T- (Cav3; Catterall, 2011). Cav channels are complexes of α1, α2, β, γ,

and δ subunits. It is in the α1 subunit that the conduction pore and voltage sensor apparatus are located. The α1 subunit is composed of four homologous domains (I–IV), with six transmembrane segments (S1–S6) in each. Similar to Kv and voltage-gated sodium (Nav) channels, the S1–S4 segments serve as the "voltage sensor" and the S5–S6 segments form the "pore domain" (Catterall et al., 2005).

Voltage-gated Ca^{2+} channels of the Cav2 subfamily (N- and P/Q-type) are regulated by G protein coupled receptors via two distinct pathways in sympathetic neurons (Ikeda and Dunlap, 1999). The first is the faster pathway, voltage-dependent, and membrane delimited, induced by direct interaction of the G protein βγ subunit with the channel protein (Herlitze et al., 1996; Ikeda, 1996; Dolphin, 2003). The second is the slower pathway that is voltage-independent. It uses signals that stimulate the $G_{q/11}$ type of G proteins to activate phospholipase C (PLC), which hydrolyzes PIP_2 into inositol triphosphate (IP_3) and diacylglycerol (DAG; Bernheim et al., 1991; Brown et al., 1997). This slower pathway was later attributed to depletion of PIP_2 by the activation of PLC (Wu et al., 2002; Gamper et al., 2004). The faster pathway has also been related to PIP_2. Rousset et al. (2004) reported that decreasing PIP_2 levels suppressed the constitutive inhibition of Cav2.1 channels by endogenous Gβγ subunits. These authors proposed that stabilization of the Gβγ sensitive state of Cav2.1 channels may require direct interaction with PIP_2. However, additional studies are needed to firmly establish the importance of PIP_2 in this pathway.

The first study on Cav channel modulation by PIP_2 reported that this phosphoinositide induces two opposing modulatory effects on Cav2.1 channels (Wu et al., 2002). Rundown of Cav2.1 channels in inside-out patches of *Xenopus* oocytes was greatly slowed and even reversed by the application of exogenous PIP_2 or Mg-ATP to the patch. Conversely, the application of PIP_2-antibody accelerated rundown, suggesting that PIP_2 stabilizes the activity of Cav2.1 channels and its depletion induces rundown. PIP_2 also exerted a voltage-dependent inhibitory effect by shifting the voltage dependence of activation toward depolarized potentials. This effect was antagonized by activation of protein kinase A (PKA; Wu et al., 2002). Modulation of Cav2.1 channels by PIP_2 has also been reported to occur in neostriatal projection neurons. Stimulation of muscarinic M1 receptors inhibited Cav2.1 channels in these neurons, an effect that could be abolished by inhibition of PLC. Consistent with these results, intracellular application of PIP_2 inhibited all muscarinic modulation of Cav2.1 channels (Perez-Burgos et al., 2010).

In subsequent studies, Cav2.2 modulation by PIP_2 was also reported (Gamper et al., 2004). In inside-out *Xenopus* oocytes patches expressing Cav2.2 channels, PIP_2 significantly slowed or reversed the rundown of these channels. In native Cav2.2 channels from sympathetic neurons, the current inhibition by muscarinic M1 receptor activation was diminished by intracellular application of diC8-PIP_2, and the current recovery was abolished when PIP_2 synthesis was blocked. Interestingly, activation of bradykinin receptors, which also activate PLC and induce PIP_2 hydrolysis, failed to inhibit Cav2.2 currents in the same neurons in which muscarinic M1 receptor activation was effective, an effect attributed to a probable concurrent Ca^{2+}-mediated stimulation of PIP_2 synthesis (Gamper et al., 2004). In a different study with the same type of neurons, bradykinin-induced voltage-independent inhibition of Ca^{2+} channels was reported and this effect could be abolished by inhibiting PLC, but it was not altered by inhibiting its downstream effectors (Lechner et al., 2005). The discrepancies with the previous study (i.e., Gamper et al., 2004) were attributed by the authors to differences in experimental conditions, such as the use of different cell culture media, differences in the buffering of intracellular Ca^{2+} concentrations, differences in intracellular Mg^{2+}, and differences in the voltage protocols used.

Another hypothesis for the slow $G_{q/11}$ mediated inhibition of L-, N-, and P/Q calcium channels involves arachidonic acid (AA). $G_{q/11}$ coupled receptor stimulation can acutely activate PLA_2 with the subsequent production of AA, which is proposed as the main signal mediating Cav channels inhibition (Roberts-Crowley et al., 2009). Thus, the same receptors that induce PIP_2 depletion can cause concurrent release of AA and modulate Cav channels according to the AA hypothesis.

A recent elegant study used two strategies to deplete PIP_2 without the production of the PLC downstream products (Suh et al., 2010). PIP_2 was depleted by rapamycin-induced translocation of an inositol lipid 5-phosphatase and a voltage-sensitive 5-phosphatase (VSP). These systems convert $PI(4,5)P_2$ to PI(4)P in the plasma membrane of intact cells, without activation of G protein-coupled receptors. Both systems suppressed Cav1.2, Cav1.3, Cav2.1, and Cav2.2 channels. Irreversible depletion of endogenous PIP_2 by rapamycin-induced translocation of INP54p 5-phosphatase to the plasma membrane irreversibly inhibited whole-cell Cav currents. On the other hand, reversible depletion of PIP_2 by the activation of the zebrafish voltage-sensitive phosphatase *Danio rerio* (Dr-VSP) reversibly inhibited Cav channels in whole-cell recordings, suggesting that PIP_2 is a cofactor required for channel activity. These results with intact cells (whole-cell experiments) did not completely recapitulate the effects reported in inside-out patches with Cav2.1 and Cav2.2 channels (Wu et al., 2002; Gamper et al., 2004). While in excised patches currents ran down almost completely, in intact cells PIP_2 depletion inhibited Cav2.1 currents by 29% and Cav2.2 by 55%. In addition, the inhibitory actions of PIP_2 were not observed. These differences as suggested by the authors could potentially reflect preservation in the whole-cell recordings of phosphorylation in some channels or cytoplasmic factors that make channels less PIP_2 sensitive or preserving PIP_2 synthesis that prevents full PIP_2 depletion (Suh et al., 2010).

Recently, it was demonstrated that the β subunits of voltage-gated Ca^{2+} channels also influence regulation by PIP_2 (Suh et al., 2012). Cav channels co-expressed with the β3 subunit could be partially inhibited by activating a voltage-sensitive lipid phosphatase to deplete PIP_2 (Suh et al., 2010). However, when these channels were co-expressed with the β2a subunit, the inhibition was smaller (Suh et al., 2012). The palmitoylation of two cysteine residues in the N terminus of the β2a subunit was responsible for this decrease in inhibition of Cav channel activity. When the palmitoylation sites were mutated, the β2a subunit behaved more like a β3 subunit. Furthermore, addition of a lipidation motif to β3 subunits reduced the inhibitory effects of Cav channels, similar to the palmitoylated β2a subunit (Suh et al., 2012). Thus, Cav channel

regulation by PIP_2 is dependent on both the α and β subunits. Previously, a similar pattern of β subunit effects on arachidonic acid modulation of Cav channels was reported (Heneghan et al., 2009; Mitra-Ganguli et al., 2009).

VOLTAGE-GATED POTASSIUM CHANNELS

Voltage-gated potassium (Kv) channels are involved in diverse physiological processes, including action potential repolarization, secretion of hormones and neurotransmitters, contraction of skeletal muscle, and others. Kv channels are homotetrameric, with each subunit containing the S1–S4 voltage sensor domain and the S5–S6 central pore domain (Yellen, 2002). As with Cav channels, the movement of the voltage sensor domain in response to membrane depolarization initiates conformational changes that lead to the pore opening. After channel opening, Kv channels undergo a time-dependent loss of conductivity by a mechanism termed inactivation. Two distinct mechanisms of inactivation have been described, N-type (or "ball and chain") inactivation, in which the N-terminal domain of certain α or β subunits of Kv channels plugs the open channel pore from the cytoplasmic side (Hoshi et al., 1991), and C-type inactivation, which appears to result from constriction of the selectivity filter (Yellen, 1998).

Only a few studies have demonstrated PIP_2 involvement in the regulation of voltage-dependent K^+ channels. PIP_2 shows remarkable effects on the N-type inactivation of certain voltage-gated K^+ channels, specifically, Kv1.4 and Kv3.4 (in which the "ball domain" is located in the N terminus of the α pore-forming subunit) and Kv1.1 co-expressed with the "ball domain"-containing Kvβ1.1 accessory subunit (Oliver et al., 2004). Application of exogenous PIP_2 to the intracellular side of the membrane expressing these channels removed the rapid N-type inactivation, regardless of whether the "ball domain" resided at the N terminus of the channel α or β subunit. It was proposed that PIP_2 insertion into the plasma membrane immobilized the positively charged "ball domain" through its negatively charged head-group and thereby prevented it from accessing the open pore. In this study a cluster of positive residues formed by Arg^{13} and Lys^{14} in the "ball domain" of Kv3.4 were proposed as the place where the electrostatic interaction between the PIP_2 and "ball domain" occurs (Oliver et al., 2004). Later, these findings were repeated for Kv1.5 channels co-expressed with the Kvβ1.3 accessory subunit. PIP_2 eliminated the Kvβ1.3 induced inactivation of Kv1.5 channels by immobilization of its "ball domain" as reported previously. An Arginine residue (Agr^5) in the N terminus of Kvβ1.3 subunit was identified as a critical residue for PIP_2 binding to the channel (Decher et al., 2008). Thus, changes in intracellular PIP_2 levels might be important for the inactivation of Kv channels and this would profoundly alter electrical signaling.

Shab channels, a prototypical member of the Kv2 channels subfamily (Wei et al., 1990) are also modulated by PIP_2. It was shown that standard light stimulation of *Drosophila* photoreceptors increased Shab currents (Krause et al., 2008). After light stimulation, the voltage dependence of activation of Shab channels was shifted to hyperpolarized potentials about 10 mV, with a small decrease on the current amplitude at depolarized potentials. The mechanism proposed for this modulation of Shab channels involves the activation of PLCβ4 and the resulting hydrolysis of PIP_2. Interestingly, a point mutation (R435Q) in the N terminus of the Shab channel abolished the PIP_2 hydrolysis effect. The same results were obtained expressing recombinant Shab channels in *Drosophila* S2 cells and recording currents in inside-out patches. Within a few minutes of patch excision the threshold for activation was left-shifted about 10 mV, an effect that was almost completely reversed by application of diC8-PIP_2 to the patch. These results led Krause et al. (2008) to suggest that PIP_2 may interact directly with the Shab channel and modulate its activity.

Kv1.3 is another voltage-gated K^+ channel reported to be modulated by PIP_2. The Kv1.3 channel is important in the activation and function of effector memory T cells (Gilhar et al., 2011). Recently, it was reported that PIP_2 applied through patch pipettes in whole-cell recordings significantly reduced Kv1.3 currents in Jurkat T cells and this regulation may be significant for the maintenance of T lymphocyte activation in immune responses (Matsushita et al., 2009). However, the mechanisms of this modulation need to be further explored.

Contrary to previous reports on Kv channel modulation by PIP_2, Kruse et al. (2012) recently tested a long list of Kv channels and found most of them insensitive to PIP_2; this list includes Kv1.1/Kvβ1.1, Kv1.3, Kv1.4, Kv1.5/Kvβ1.3, Kv2.1, Kv3.4, Kv4.2, and Kv4.3 (with different KChIPs). To test the effect of PIP_2 on Kv channels this group used three different strategies to deplete PIP_2 in intact cells, activation of the G protein-coupled muscarinic receptor M1, a zebrafish voltage-sensitive lipid 5-phosphatase (Dr-VSP), or an engineered fusion protein carrying both lipid 4-phosphatase and 5-phosphatase activity (pseudojanin). Kruse and colleagues offer some explanations for the discrepancy between previous experiments and their results, principally relying on the different strategies used to modulate the PIP_2 concentrations in the membrane. While previous groups applied exogenous PIP_2 to inside-out excised patches risking to increase PIP_2 concentration to supramaximal levels, this group transiently depleted PIP_2 in the membrane of intact cells maintaining all the constituents of the cell near normal conditions (Hilgemann, 2012; Kruse et al., 2012).

Recently, we also examined the effects of PIP_2 depletion on the voltage-dependent Kv1.2 channel using different approaches not only in inside-out patches but also in intact cells, using the voltage-sensitive phosphatase Ci-VSP. We obtained similar results to the Cav channels, namely a bidirectional regulation, where PIP_2 depletion left-shifted the voltage dependence of activation, increasing current at the same time it decreased the open probability causing an overall decrease in the current level (**Figure 1C**; Rodriguez-Menchaca et al., 2012). These two effects were kinetically distinct and exhibited distinct molecular determinants and sensitivities to PIP_2. The effect on the voltage dependence of activation proceeded through interactions of the S4–S5 linker that links the voltage sensor to the channel pore with PIP_2 (**Figure 1A**). Gating current measurements revealed that PIP_2 constrains the movement of the sensor via specific interactions of basic residues with PIP_2 in the closed state. In summary, using a similar strategy as Kruse et al. (2012) to transiently deplete PIP_2 in intact cells namely a voltage-sensitive phosphatase, we obtained contrasting results showing a dual effect on Kv1.2 and Shaker channels after PIP_2 depletion. In contrast, Kruse et al. did not observe any effect on the current

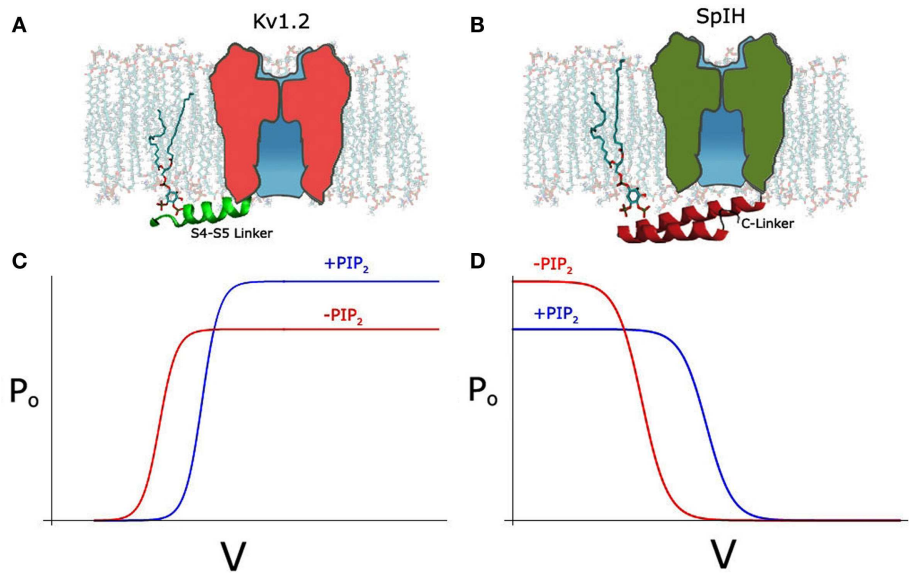

FIGURE 1 | (A) Schematic depicting PIP_2 interacting with S4–S5 linker (green) in the Kv1.2 channel, with linker shown in cartoon representation. **(B)** Schematic depicting PIP_2 interacting with A′ helix of C-linker (red) in the SpIH channel, adapted from Flynn and Zagotta (2011). **(C)** Hypothetical Po-V curve of Kv1.2 showing depolarizing shift and increase in Po after PIP_2 (blue line). **(D)** Hypothetical Po-V curve of SpIH showing depolarizing shift and decrease in Po after PIP_2.

amplitude of several Kv channels after PIP_2 depletion and did not test for changes in voltage dependency.

Consistent with our results, Abderemane-Ali et al. (2012) also reported a dual effect of PIP_2 on Shaker potassium channels; PIP_2 exerts a gain-of-function effect on the maximal current amplitude and a positive shift in the voltage dependence of activation, through an effect on the voltage sensor movement.

HYPERPOLARIZATION-ACTIVATED HCN CHANNELS

Hyperpolarization-activated Cyclic nucleotide-gated (HCN) channels unlike most voltage-gated channels open only in response to membrane hyperpolarization (Gauss et al., 1998; Ludwig et al., 1998; Santoro et al., 1998). The S1–S4 domain constitutes the voltage sensor again but with HCN channels the S4 segment moves inward upon membrane hyperpolarization (Mannikko et al., 2002; Bell et al., 2004). The coupling mechanism between this inward movement of the S4 and the opening of the gate, which is presumably located near the intracellular end of S6, is not clear. The cytoplasmic domain of HCN channels possesses a canonical cyclic nucleotide binding domain (CNBD). The CNBD is connected to the S6 segment through a 90-aa sequence called the C-linker (CL). Direct binding of cAMP or cGMP (cNMP) to the CNBD facilitates channel opening. At the macroscopic current level, the cNMP-dependent gating right shifts the voltage dependence of activation and increases the current amplitude (Robinson and Siegelbaum, 2003; Craven and Zagotta, 2006; Biel et al., 2009). The CL plays a dominant role in the coupling of cNMP binding to the channel opening.

Hyperpolarization-activated cyclic nucleotide-gated channel activity is also under the control of PIP_2. PIP_2 right shifts the hyperpolarization-dependent HCN channel activation, making the channel easier to open (Pian et al., 2006; Zolles et al., 2006; Flynn and Zagotta, 2011; Ying et al., 2011). This effect is remarkable – about 20 mV for mammalian HCN channels (HCN1, 2, and 4) and independent from the regulation by cAMP and cGMP. Direct evidence supporting these conclusions came from the experiments on inside-out membrane patches. Applying either native PIP_2 or the soluble diC_8-PIP_2 produced a depolarizing shift in HCN channel activation (Pian et al., 2006; Zolles et al., 2006; Flynn and Zagotta, 2011). The right shift in the I–V relationship could be reproduced separately under conditions of saturating concentrations of cAMP, in mutant channels that do not bind to cNMP, or in the HCN ΔC channels, in which the CL-CNBD has been deleted. Therefore, the interaction between PIP_2 and the transmembrane domains with their connecting loops of HCN channels are likely to be responsible for the voltage-dependent effect rather than the CL and CNBD, which are essential for cAMP-dependent gating. It has been suggested that most likely, PIP_2 exerts its effect on voltage dependence by stabilizing the activated state of the voltage sensor, which could be through either a generalized effect on the local electrostatic environment by PIP_2 or a specific interaction between the negatively charged head-group of PIP_2 with positively charged residues in the S4 or its surroundings (Flynn and Zagotta, 2011).

SpIH, a HCN channel cloned from Sea Urchin, can be fully activated by cAMP but only partially by cGMP (Flynn et al., 2007). Unlike the mammalian HCN channels, SpIH shows a bidirectional regulation by PIP_2 (Flynn and Zagotta, 2011). Like mammalian HCN channels it shows a right shift of the voltage dependence of activation (∼10 mV) in the presence or PIP_2, albeit half the magnitude of that in the mammalian channels (**Figure 1D**). Unlike the mammalian HCN channels, SpIH inactivates quickly in response

to a hyperpolarizing voltage step (Gauss et al., 1998). Binding of cAMP or cGMP relieves this voltage-dependent inactivation and markedly increases the macroscopic current amplitude. Independent from the positive effect on the voltage-dependent activation, PIP_2 seems to have an inhibitory effect on the cGMP-induced current (**Figure 1D**). This inhibitory effect is clearly related with the efficacy of the agonists. The maximal current under saturating concentration of cGMP is only about half of that of cAMP. Consistently, PIP_2 strongly inhibits the cGMP-dependent current but has a minimal effect on the cAMP-induced current.

Noticeably, as reported more than a decade ago, PIP_2 has a strong inhibitory effect on CNG channels, which is homologous to HCN channel and the cNMP binding is obligatory for its opening (Womack et al., 2000; Kaupp and Seifert, 2002). Several studies have produced atomic resolution structures of the HCN cytoplasmic C-terminal domains including that from SpIH channel (Zagotta et al., 2003; Flynn et al., 2007; Xu et al., 2010). Mutagenesis studies of the SpIH channel have identified several positively charged residues in the CL that contribute to the inhibitory effect by PIP_2 (**Figure 1B**). It has been suggested that through these specific electrostatic interactions, PIP_2 inhibits the channel opening by stabilizing the conformation of the CL that underlies the closed channel state in the absence of agonists (Flynn and Zagotta, 2011).

CONCLUDING REMARKS

The bidirectional effects of PIP_2 in three very different voltage-sensitive channels is quite remarkable. In the depolarization-activated Cav2.1 (Wu et al., 2002) and Kv1.2 (Rodriguez-Menchaca et al., 2012) studies, PIP_2 right-shifted the voltage dependence of activation (inhibitory) while it prevented rundown by stabilizing the open probability of the channel (stimulatory). In the hyperpolarization-activated HCN channel from the sea urchin (SpIH) PIP_2 right-shifted the voltage dependence of activation (stimulatory), while it inhibited the cGMP-induced activation (inhibitory). In Kv1.2, PIP_2 stabilized the inactive state of the voltage sensor by binding basic residues in the S4–S5 linker and the N terminus that could only coordinate PIP_2 in the closed state of the channel. In the SpIH HCN channel it was CL basic residues that accounted for the non-voltage-dependent effects of PIP_2. In both cases these molecular determinants affected only one or the other of the dual effects of PIP_2. These results from these very different channels (Cav, Kv, and HCN) suggest that the mechanism by which PIP_2 regulates channels sensitive to voltage may be conserved.

What might be the physiological significance of the dual regulation of certain voltage-gated ion channels that we have highlighted in this review? We speculate that in channels that are dependent on voltage but also to other modulatory intracellular signals, a balance needs to be achieved to regulate gating in a coordinated manner. PIP_2 and the S4–S5 linker are both perfectly positioned at the interface of the membrane to the cytosol to integrate cytosolic signals (e.g., cyclic nucleotides, Ca^{2+}, etc.) with the movement of the transmembrane voltage sensor.

REFERENCES

Abderemane-Ali, F., Es-Salah-Lamoureux, Z., Delemotte, L., Kasimova, M. A., Labro, A. J., Snyders, D. J., Tarek, M., Baró, I., and Loussouarn, G. (2012). Dual effect of PIP2 on Shaker K^+ channels. *J. Biol. Chem.* doi: 10.1074/jbc.M112.382085

Bell, D. C., Yao, H., Saenger, R. C., Riley, J. H., and Siegelbaum, S. A. (2004). Changes in local S4 environment provide a voltage-sensing mechanism for mammalian hyperpolarization-activated HCN channels. *J. Gen. Physiol.* 123, 5–19.

Bernheim, L., Beech, D. J., and Hille, B. (1991). A diffusible second messenger mediates one of the pathways coupling receptors to calcium channels in rat sympathetic neurons. *Neuron* 6, 859–867.

Berridge, M. J. (1984). Inositol trisphosphate and diacylglycerol as second messengers. *Biochem. J.* 220, 345–360.

Bezanilla, F. (2008). How membrane proteins sense voltage. *Nat. Rev. Mol. Cell Biol.* 9, 323–332.

Biel, M., Wahl-Schott, C., Michalakis, S., and Zong, X. (2009). Hyperpolarization-activated cation channels: from genes to function. *Physiol. Rev.* 89, 847–885.

Borjesson, S. I., and Elinder, F. (2008). Structure, function, and modification of the voltage sensor in voltage-gated ion channels. *Cell Biochem. Biophys.* 52, 149–174.

Borjesson, S. I., Hammarström, S., and Elinder, F. (2008). Lipoelectric modification of ion channel voltage gating by polyunsaturated fatty acids. *Biophys. J.* 95, 2242–2253.

Brown, D. A., Abogadie, F. C., Allen, T. G., Buckley, N. J., Caulfield, M. P., Delmas, P., Haley, J. E., Lamas, J. A., and Selyanko, A. A. (1997). Muscarinic mechanisms in nerve cells. *Life Sci.* 60, 1137–1144.

Catterall, W. A. (2011). Voltage-gated calcium channels. *Cold Spring Harb. Perspect. Biol.* 3, a003947.

Catterall, W. A., Cestèle, S., Yarov-Yarovoy, V., Yu, F. H., Konoki, K., and Scheuer, T. (2007). Voltage-gated ion channels and gating modifier toxins. *Toxicon* 49, 124–141.

Catterall, W. A., Perez-Reyes, E., Snutch, T. P., and Striessnig, J. (2005). International Union of Pharmacology. XLVIII. Nomenclature and structure-function relationships of voltage-gated calcium channels. *Pharmacol. Rev.* 57, 411–425.

Craven, K. B., and Zagotta, W. N. (2006). CNG and HCN channels: two peas, one pod. *Annu. Rev. Physiol.* 68, 375–401.

Davis, M. J., Wu, X., Nurkiewicz, T. R., Kawasaki, J., Gui, P., Hill, M. A., and Wilson, E. (2001). Regulation of ion channels by protein tyrosine phosphorylation. *Am. J. Physiol. Heart Circ. Physiol.* 281, 1835–1862.

Decher, N., Gonzalez, T., Streit, A. K., Sachse, F. B., Renigunta, V., Soom, M., Heinemann, S. H., Daut, J., and Sanguinetti, M. C. (2008). Structural determinants of Kvbeta1.3-induced channel inactivation: a hairpin modulated by PIP2. *EMBO J.* 27, 3164–3174.

Dolphin, A. C. (2003). G protein modulation of voltage-gated calcium channels. *Pharmacol. Rev.* 55, 607–627.

Elinder, F., and Arhem, P. (2003). Metal ion effects on ion channel gating. *Q. Rev. Biophys.* 36, 373–427.

Flynn, G. E., Black, K. D., Islas, L. D., Sankaran, B., and Zagotta, W. N. (2007). Structure and rearrangements in the carboxy-terminal region of SpIH channels. *Structure* 15, 671–682.

Flynn, G. E., and Zagotta, W. N. (2011). Molecular mechanism underlying phosphatidylinositol 4,5-bisphosphate-induced inhibition of SpIH channels. *J. Biol. Chem.* 286, 15535–15542.

Fozzard, H. A., and Kyle, J. W. (2002). Do defects in ion channel glycosylation set the stage for lethal cardiac arrhythmias? *Sci. STKE* 130, pe19.

Gamper, N., Reznikov, V., Yamada, Y., Yang, J., and Shapiro, M. S. (2004). Phosphatidylinositol [correction] 4,5-bisphosphate signals underlie receptor-specific Gq/11-mediated modulation of N-type Ca^{2+} channels. *J. Neurosci.* 24, 10980–10992.

Gauss, R., Seifert, R., and Kaupp, U. B. (1998). Molecular identification of a hyperpolarization-activated channel in sea urchin sperm. *Nature* 393, 583–587.

Gilhar, A., Bergman, R., Assay, B., Ullmann, Y., and Etzioni, A. (2011). The beneficial effect of blocking Kv1.3 in the psoriasiform SCID mouse model. *J. Invest. Dermatol.* 131, 118–124.

Gubitosi-Klug, R. A., Mancuso, D. J., and Gross, R. W. (2005). The human Kv1.1 channel is palmitoylated, modulating voltage sensing: identification of a palmitoylation consensus sequence. *Proc. Natl. Acad. Sci. U.S.A.* 102, 5964–5968.

Heneghan, J. F., Mitra-Ganguli, T., Stanish, L. F., Liu, L., Zhao, R., and Rittenhouse, A. R. (2009). The Ca^{2+} channel beta subunit determines whether stimulation of Gq-coupled receptors enhances or inhibit N current. *J. Gen. Physiol.* 134, 369–384.

Herlitze, S., Garcia, D. E., Mackie, K., Hille, B., Scheuer, T., and Catterall, W. A. (1996). Modulation of Ca^{2+} channels by G-protein beta gamma subunits. *Nature* 380, 258–262.

Hilgemann, D. W. (2012). Fitting Kv potassium channels into the PIP2 puzzle: Hille group connects dots between illustrious HH groups. *J. Gen. Physiol.* 140, 245–248.

Hoshi, T., Zagotta, W. N., and Aldrich, R. W. (1991). Two types of inactivation in Shaker K^+ channels: effects of alterations in the carboxy-terminal region. *Neuron* 7, 547–556.

Ikeda, S. R. (1996). Voltage-dependent modulation of N-type calcium channels by G-protein beta gamma subunits. *Nature* 380, 255–258.

Ikeda, S. R., and Dunlap, K. (1999). Voltage-dependent modulation of N-type calcium channels: role of G protein subunits. *Adv. Second Messenger Phosphoprotein Res.* 33, 131–151.

Jindal, H. K., Folco, E. J., Liu, G. X., and Koren, G. (2008). Posttranslational modification of voltage-dependent potassium channel Kv1.5:COOH-terminal palmitoylation modulates its biological properties. *Am. J. Physiol. Heart Circ. Physiol.* 294, 2012–2121.

Kaupp, U. B., and Seifert, R. (2002). Cyclic nucleotide-gated ion channels. *Physiol. Rev.* 82, 769–824.

Krause, Y., Krause, S., Huang, J., Liu, C. H., Hardie, R. C., and Weckström, M. (2008). Light-dependent modulation of Shab channels via phosphoinositide depletion in *Drosophila* photoreceptors. *Neuron* 59, 596–607.

Kruse, M., Hammond, G. R., and Hille, B. (2012). Regulation of voltage-gated potassium channels by PI(4,5)P2. *J. Gen. Physiol.* 140, 189–205.

Lechner, S. G., Hussl, S., Schicker, K. W., Drobny, H., and Boehm, S. (2005). Presynaptic inhibition via a phospholipase C- and phosphatidylinositol bisphosphate-dependent regulation of neuronal Ca^{2+} channels. *Mol. Pharmacol.* 68, 1387–1396.

Li, C. H., Zhang, Q., Teng, B., Mustafa, S. J., Huang, J. Y., and Yu, H. G. (2008). Src tyrosine kinase alters gating of hyperpolarization-activated HCN4 pacemaker channel through Tyr531. *Am. J. Physiol. Cell Physiol.* 294, 355–362.

Logothetis, D. E., Petrou, V. I., Adney, S. K., and Mahajan, R. (2010). Channelopathies linked to plasma membrane phosphoinositides. *Pflugers Arch.* 460, 321–341.

Long, S. B., Campbell, E. B., and Mackinnon, R. (2005). Voltage sensor of Kv1.2: structural basis of electromechanical coupling. *Science* 309, 903–908.

Ludwig, A., Zong, X., Jeglitsch, M., Hofmann, F., and Biel, M. (1998). A family of hyperpolarization-activated mammalian cation channels. *Nature* 393, 587–591.

Mannikko, R., Elinder, F., and Larsson, H. P. (2002). Voltage-sensing mechanism is conserved among ion channels gated by opposite voltages. *Nature* 419, 837–841.

Matsushita, Y., Ohya, S., Suzuki, Y., Itoda, H., Kimura, T., Yamamura, H., and Imaizumi, Y. (2009). Inhibition of Kv1.3 potassium current by phosphoinositides and stromal-derived factor-1alpha in Jurkat T cells. *Am. J. Physiol. Cell Physiol.* 296, 1079–1085.

Mitra-Ganguli, T., Vitko, I., Perez-Reyes, E., and Rittenhouse, A. R. (2009). Orientation of palmitoylated CaV-beta2a relative to CaV2.2 is critical for slow pathway modulation of N. type Ca^{2+} current by tachykinin receptor activation. *J. Gen. Physiol.* 134, 385–396.

Mohapatra, D. P., Park, K. S., and Trimmer, J. S. (2007). Dynamic regulation of the voltage-gated Kv2.1 potassium channel by multisite phosphorylation. *Biochem. Soc. Trans.* 35, 1064–1068.

Mohapatra, D. P., and Trimmer, J. S. (2006). The Kv2.1 C terminus can autonomously transfer Kv2.1-like phosphorylation-dependent localization, voltage-dependent gating, and muscarinic modulation to diverse Kv channels. *J. Neurosci.* 26, 685–695.

Oliver, D., Lien, C. C., Soom, M., Baukrowitz, T., Jonas, P., and Fakler, B. (2004). Functional conversion between A-type and delayed rectifier K^+ channels by membrane lipids. *Science* 304, 265–270.

Perez-Burgos, A., Prieto, G. A., Galarraga, E., and Bargas, J. (2010). CaV2.1 channels are modulated by muscarinic M1 receptors through phosphoinositide hydrolysis in neostriatal neurons. *Neuroscience* 165, 293–299.

Pian, P., Bucchi, A., Robinson, R. B., and Siegelbaum, S. A. (2006). Regulation of gating and rundown of HCN hyperpolarization-activated channels by exogenous and endogenous PIP2. *J. Gen. Physiol.* 128, 593–604.

Ramu, Y., Xu, Y., and Lu, Z. (2006). Enzymatic activation of voltage-gated potassium channels. *Nature* 442, 696–699.

Roberts-Crowley, M. L., Mitra-Ganduli, T., Liu, L., and Rittenhouse, A. R. (2009). Regulation of voltage-gated Ca^{2+} channels by lipids. *Cell Calcium* 45, 589–601.

Robinson, R. B., and Siegelbaum, S. A. (2003). Hyperpolarization-activated cation currents: from molecules to physiological function. *Annu. Rev. Physiol.* 65, 453–480.

Rodriguez-Menchaca, A. A., Adney, S. K., Tang, Q. Y., Meng, X. Y., Rosenhouse-Dantsker, A., Cui, M., and Logothetis, D. E. (2012). PIP2 controls voltage sensor movement and pore opening of Kv channels through the S4-S5 linker. *Proc. Natl. Acad. Sci. U.S.A.* 109, E2399–E2408.

Rousset, M., Cens, T., Gouin-Charnet, A., Scamps, F., and Charnet, P. (2004). Ca^{2+} and phosphatidylinositol 4,5-bisphosphate stabilize a Gbeta gamma-sensitive state of Ca V2 Ca^{2+} channels. *J. Biol. Chem.* 279, 14619–14630.

Santoro, B., Liu, D. T., Bartsch, D., Kandel, E. R., Siegelbaum, S. A., and Tibbs, G. R. (1998). Identification of a gene encoding a hyperpolarization-activated pacemaker channel of brain. *Cell* 93, 717–729.

Schmidt, D., Jiang, Q. X., and MacKinnon, R. (2006). Phospholipids and the origin of cationic gating charges in voltage sensors. *Nature* 444, 775–779.

Suh, B. C., and Hille, B. (2005). Regulation of ion channels by phosphatidylinositol 4,5-bisphosphate. *Curr. Opin. Neurobiol.* 15, 370–378.

Suh, B. C., and Hille, B. (2008). PIP2 is a necessary cofactor for ion channel function: how and why? *Annu. Rev. Biophys.* 37, 175–195.

Suh, B. C., Kim, D. I., Falkenburger, B. H., and Hille, B. (2012). Membrane-localized β-subunits alter the PIP2 regulation of high-voltage activated Ca^{2+} channels. *Proc. Natl. Acad. Sci. U.S.A.* 109, 3161–3166.

Suh, B. C., Leal, K., and Hille, B. (2010). Modulation of high-voltage activated Ca^{2+} channels by membrane phosphatidylinositol 4,5-bisphosphate. *Neuron* 67, 224–238.

Swartz, K. J. (2007). Tarantula toxins interacting with voltage sensors in potassium channels. *Toxicon* 49, 213–230.

Watanabe, I., Wang, H. G., Sutachan, J. J., Zhu, J., Recio-Pinto, E., and Thornhill, W. B. (2003). Glycosylation affects rat Kv1.1 potassium channel gating by a combined surface potential and cooperative subunit interaction mechanism. *J. Physiol.* 550, 51–66.

Watanabe, I., Zhu, J., Sutachan, J. J., Gottschalk, A., Recio-Pinto, E., and Thornhill, W. B. (2007). The glycosylation state of Kv1.2 potassium channels affects trafficking, gating, and simulated action potentials. *Brain Res.* 1144, 1–18.

Wei, A., Covarrubias, M., Butler, A., Baker, K., Pak, M., and Salkoff, L. (1990). K^+ current diversity is produced by an extended gene family conserved in *Drosophila* and mouse. *Science* 248, 599–603.

Womack, K. B., Gordon, S. E., He, F., Wensel, T. G., Lu, C. C., and Hilgemann, D. W. (2000). Do phosphatidylinositides modulate vertebrate phototransduction? *J. Neurosci.* 20, 2792–2799.

Wu, L., Bauer, C. S., Zhen, X. G., Xie, C., and Yang, J. (2002). Dual regulation of voltage-gated calcium channels by PtdIns(4,5)P2. *Nature* 419, 947–952.

Xiao, Y. F., Sigg, D. C., and Leaf, A. (2005). The antiarrhythmic effect of n-3 polyunsaturated fatty acids: modulation of cardiac ion channels as a potential mechanism. *J. Membr. Biol.* 206, 141–154.

Xu, X., Vysotskaya, Z. V., Liu, Q., and Zhou, L. (2010). Structural basis for the cAMP-dependent gating in the human HCN4 channel. *J. Biol. Chem.* 285, 37082–37091.

Xu, X. P., Erichsen, D., Börjesson, S. I., Dahlin, M., Amark, P., and Elinder, F. (2008a). Polyunsaturated fatty acids and cerebrospinal fluid from children on the ketogenic diet open a voltage-gated K channel: a putative mechanism of antiseizure action. *Epilepsy Res.* 80, 57–66.

Xu, Y., Ramu, Y., and Lu, Z. (2008b). Removal of phospho-head groups of membrane lipids immobilizes voltage sensors of K^+ channels. *Nature* 451, 826–829.

Yellen, G. (1998). The moving parts of voltage-gated ion channels. *Q. Rev. Biophys.* 31, 239–295.

Yellen, G. (2002). The voltage-gated potassium channels and their relatives. *Nature* 419, 35–42.

Ying, S. W., Tibbs, G. R., Picollo, A., Abbas, S. Y., Sanford, R. R., Accardi, A., Hofmann, F., Ludwig, A., and Goldstein, P. A. (2011). PIP2-mediated HCN3 channel gating is crucial for rhythmic burst firing in thalamic intergeniculate leaflet neurons. *J. Neurosci.* 31, 10412–10423.

Zagotta, W. N., Olivier, N. B., Black, K. D., Young, E. C., Olson, R., and Gouaux, E. (2003). Structural basis

for modulation and agonist specificity of HCN pacemaker channels. *Nature* 425, 200–205.

Zolles, G., Klocker, N., Wenzel, D., Weisser-Thomas, J., Fleischmann, B. K., Roeper, J., and Fakler, B. (2006). Pacemaking by HCN channels requires interaction with phosphoinositides. *Neuron* 52, 1027–1036.

Conflict of Interest Statement: The authors declare that the research was conducted in the absence of any commercial or financial relationships that could be construed as a potential conflict of interest.

Received: 12 May 2012; accepted: 04 September 2012; published online: 25 September 2012.

Citation: Rodríguez-Menchaca AA, Adney SK, Zhou L and Logothetis DE (2012) Dual regulation of voltage-sensitive ion channels by PIP_2. Front. Pharmacol. ***3****:170. doi: 10.3389/fphar.2012.00170*

This article was submitted to Frontiers in Pharmacology of Ion Channels and Channelopathies, a specialty of Frontiers in Pharmacology.

frontiers in
PHARMACOLOGY

REVIEW ARTICLE
published: 18 June 2012
doi: 10.3389/fphar.2012.00114

Contributions of intracellular ions to Kv channel voltage sensor dynamics

Samuel J. Goodchild and David Fedida*

Department of Anesthesiology, Pharmacology and Therapeutics, University of British Columbia, Vancouver, BC, Canada

Edited by:
Gildas Loussouarn, University of Nantes, France

Reviewed by:
Riccardo Olcese, University of California Los Angeles, USA
Michael E. Green, The City College of the City University of New York, USA

****Correspondence:***
David Fedida, Department of Anesthesiology, Pharmacology and Therapeutics, University of British Columbia, 217-2176 Health Sciences Mall, Vancouver, BC, Canada V6T1Z3.
e-mail: fedida@interchange.ubc.ca

Voltage-sensing domains (VSDs) of Kv channels control ionic conductance through coupling of the movement of charged residues in the S4 segment to conformational changes at the cytoplasmic region of the pore domain, that allow K^+ ions to flow. Conformational transitions within the VSD are induced by changes in the applied voltage across the membrane field. However, several other factors not directly linked to the voltage-dependent movement of charged residues within the voltage sensor impact the dynamics of the voltage sensor, such as inactivation, ionic conductance, intracellular ion identity, and block of the channel by intracellular ligands. The effect of intracellular ions on voltage sensor dynamics is of importance in the interpretation of gating current measurements and the physiology of pore/voltage sensor coupling. There is a significant amount of variability in the reported kinetics of voltage sensor deactivation kinetics of Kv channels attributed to different mechanisms such as open state stabilization, immobilization, and relaxation processes of the voltage sensor. Here we separate these factors and focus on the causal role that intracellular ions can play in allosterically modulating the dynamics of Kv voltage sensor deactivation kinetics. These considerations are of critical importance in understanding the molecular determinants of the complete channel gating cycle from activation to deactivation.

Keywords: ion channel, potassium channel, gating current, immobilization, inactivation

INTRODUCTION

Voltage-gated potassium channels (Kv) sense membrane voltage and underlie the repolarization of electrically excitable cells (Hille, 2001). This task is achieved by the division of the function of the channels into **voltage-sensing domain** (VSD) and ion conducting pore domain as shown in **Figure 1A** (Long et al., 2005b). Charged residues in the S4 transmembrane segment of the VSD move in response to changes in the membrane electrical field and this motion is translated through a coupling mechanism involving S4–S5 linker contacts with the bottom of S6-lined pore domain to open or close the intracellular gate of ionic conductance (Lee et al., 2009). The tight coupling between the two domains allows movements in one domain to be translated rapidly into movements in the other thus creating highly sensitive voltage-gated channels.

Once K^+ conductance has been activated the process must be reversed once the membrane is restored back to resting potentials so that excitable cell membranes do not become permanently hyperpolarized and unable to generate action potentials again. This is accomplished by deactivation and inactivation mechanisms, both of which serve to shut down channel conductance. Deactivation specifically refers to the voltage-dependent closure of the pore intracellular gate, whereas inactivation can occur under the conditions of continued depolarization and typically involves conformational changes in other regions of the channel. Inactivation can be broadly classed kinetically into fast inactivation, conferred by inactivation peptides either attached to the N-terminus of the channel protein or an accessory subunit that can enter the open channel at the intracellular gate and block conductance or slow inactivation which is caused by conformational rearrangements in the outer pore and selectivity filter region of the channel. Both inactivation and pore gating have effects on voltage sensor dynamics. Because there are several mechanisms that can impact on voltage sensor deactivation kinetics, the objective of this review is to present a clear description of these different factors which can overlap in their functional effects, and expand on the mechanism by which intracellular ions can influence these kinetics and thus the physiology of voltage sensing in Kv channels.

BASIS FOR VOLTAGE SENSING IN Kv CHANNELS

Kv channels are tetrameric transmembrane proteins with each subunit consisting of six transmembrane segments (S1–S6). The VSD of each subunit comprises of S1–S4, with the key determinant of voltage sensing being a series of positively charged arginine residues that line S4 (**Figure 1A**). The VSD is coupled to the pore domain, shown in **Figure 1B**, which comprises S5–S6 of each subunit, and comes together to form a S6-lined conduit for K^+ ions to flow across the membrane (Long et al., 2005a). At the extracellular end of the pore, selectivity for K^+ ions is conferred by a highly conserved structural element in the pore, the selectivity filter, that allows efficient dehydration and stabilization of dehydrated K^+ ions over Na^+ ions as the ions transport across the membrane (Heginbotham et al., 1994). On the cytosolic side of the selectivity filter a water filled central cavity is found where hydrated ions can reside before entering the filter (Zhou et al., 2001). **Figure 1B** highlights the locations of two ions (purple) occupying two of four possible binding sites in the SF and an ion residing in the inner cavity (blue) of the Kv1.2 channel crystal structure, which is in the

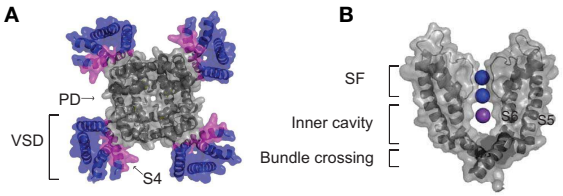

FIGURE 1 | Overview of Kv channel structure. (A) A top down view of the Kv1.2 open state channel tetramer (PDB: 2A79) with the voltage-sensing domains (S1–S4) in color. The charge carrying S4 segment of the voltage sensor domain is highlighted magenta and the pore domain S5–S6 segments are gray. **(B)** Side view of two pore forming subunits of the Kv1.2 illustrating the selectivity filter containing two K^+ ions of a possible four in positions 2 and 4 shown in blue and a K^+ ion residing in the intracellular cavity in magenta.

open state (Long et al., 2005b). In the closed state of the channel this cavity is isolated from the bulk cytosol by a constriction formed by a narrow bundle crossing of the pore-lining S6 helices (**Figure 1B**), which does not allow hydrated ions to permeate (Liu et al., 1997). Opening of this gate is initiated by depolarization of the membrane. This drives the positively charged S4 segment outward and induces a conformational shift at the bottom of the S6 segments to dilate the bundle crossing. Hydrated ions can then diffuse freely into the cavity and through the selectivity filter (Lu et al., 2002; Long et al., 2005b).

Much progress in understanding voltage gating has relied upon the fact that voltage sensor movement can be examined separately from pore opening and closing by recording the transient currents (gating currents), that are associated with the charged residues in the S4 segment moving within the applied field (for review, see Bezanilla, 2000). Kv channel gating currents are of the order of 1% or less of the magnitude of ionic currents, and therefore can only be resolved when recorded from channels in the absence of larger contaminating ionic currents (Armstrong and Bezanilla, 1974). Experimentally, ionic conductance can be eliminated by the removal of permeant ions from the recording solutions (Zagotta et al., 1994b), block of conductance (Bezanilla et al., 1991; Schoppa et al., 1992), or mutation of channels to render them non-conductive (Perozo et al., 1993; Wang et al., 1999).

MECHANISMS OF VOLTAGE SENSOR IMMOBILIZATION

Early studies of gating currents revealed that intracellular applied quaternary ammonium (QA) ions severely slow the recovery of ionic and gating currents by preventing pore gate closure (Armstrong, 1971; Choi et al., 1993; Melishchuk and Armstrong, 2001). This phenomenon was also observed to result from the fast inactivation process in Na^+ channels and was referred to as "charge immobilization" (Armstrong and Bezanilla, 1977). Because all the charge that has been moved by depolarization eventually returns if given an adequate recovery period the term immobilization really refers to a slowing of gating charge return.

For the purposes of the review we have used an established model of *Shaker*IR gating to simulate typical ionic and gating currents from a channel to illustrate typical immobilized gating charge. **Figure 2** illustrates currents simulated using an established model of shaker gating (Zagotta et al., 1994a). **Figure 2A** shows a simplified shaker gating scheme in which voltage sensors in the each four subunits undergo transitions between resting and activated states upon depolarization, followed by a sequential opening step that represents the pore opening. The transitions between resting and active carry the majority of gating charge. In **Figure 2B** the simulated ionic currents show a rapid increase in the open probability of the channel at depolarizing potentials more positive than −40 mV. The gating currents correlating to the same gating model are displayed in **Figure 2C** and show a mild immobilization of gating charge return, which is a typical feature of *Shaker* gating currents. The immobilization is seen in the return of gating charge (OFF gating currents) that display a rapid return after depolarizations to potentials where the channel has not opened (<-40 mV) followed by a slowing of the gating charge return after openings to potentials with significant channel probability of opening (>-20 mV). This slowing of OFF gating currents observed experimentally can be clearly linked to the channel opening process as it occurs only after the channel has opened.

In early studies with cloned *Shaker* channels it was found that the N-terminus fast inactivating peptide caused slowing of gating charge return when opened channels were bound with the inactivation peptide (Bezanilla et al., 1991). As the binding site for internal QA ions and the *Shaker* inactivation peptide has been identified as residing deep in the inner cavity region of the channel pore these observations demonstrate that occupancy of this site can cause voltage sensor immobilization through the prevention of pore closure (Choi et al., 1993; Gonzalez et al., 2011). To illustrate a more severe immobilization, such as that observed when intracellular QA ions or N-terminus inactivation peptides are present, an extra blocked state O:B was added to the open state of the model shown in **Figure 2A**. The gating currents from this model in the presence of a blocking particle (B) are shown in **Figure 2D**. The OFF gating currents show a severe slowing of charge return after depolarization to potentials that open the channel significantly, which equates to a strong immobilization due to the occupancy of the open pore by B preventing the first open to closed transition and the subsequent voltage sensor return to its resting state. In this case the degree of immobilization will be dependent upon the affinity of the blocker for the pore of the channel where high affinity blockers would induce a stronger immobilization. This type of immobilization is not limited to channels such as *Shaker* that posses N-terminus inactivation peptides as Kv channels often associate with β-subunits that can confer inactivation properties to the channel. For example, Kv1.2 associates with the Kvβ1.2 subunit which confers N-type inactivation and has also been shown to slow voltage sensor return (Peters et al., 2009).

The slow return of gating charges is structurally mediated through the coupling of the pore to the voltage sensor S4 through inter-subunit interactions between the S4–S5 linker of one subunit and the inner end of the S6 from a neighboring subunit (Batulan et al., 2010). This observation indicates that an open pore can slow voltage sensor return from the activated state as a result of the tight coupling between the two domains.

A summary of the mechanism by which pore occupancy by QA ions or N-terminus peptides can occupy the pore is shown in **Figure 2E**. Depolarization that is sufficiently positive to open the channel are usually associated with an mild immobilization of the voltage sensors in the open state and has been postulated to

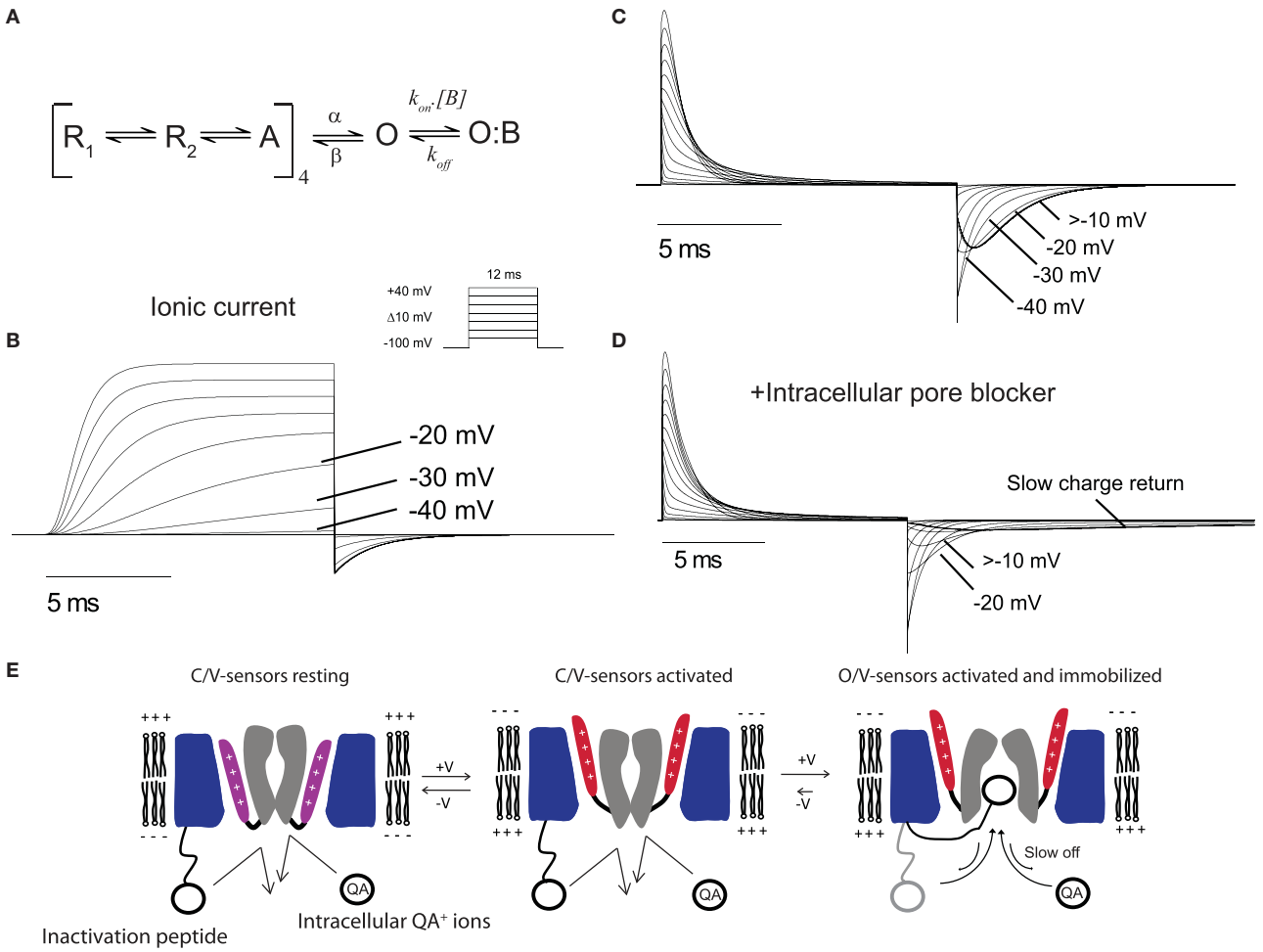

FIGURE 2 | Gating currents demonstrating immobilization. (A) A model of Shaker gating used to simulate currents (Zagotta et al., 1994a). The transitions from R to A carry the majority of gating charge and the channel opens once all four subunits have transitioned to A. The extra state O:B represents the an intracellular blocking particle as discussed in the text. Ionic **(B)** and gating **(C)** currents generated from the model in response to 12 ms depolarization from a holding potential of −100 mV with the program Ionchannellab (De Santiago-Castillo et al., 2010). **(D)** Gating currents display severe immobilization when the model is run in the presence of an intracellular blocker [B] according to the scheme shown in **(A)**. **(E)** Cartoon representation of the mechanism by which the N-terminus inactivation peptide or QA ions can cause an immobilization of gating charges. The S1–S3 segments of the VSD is colored blue, S4 shown in purple (resting) or red (activated), and the pore domain S5–S6 grey. At resting negative membrane potentials the pore is closed at the bundle crossing and the S4 charge carrying segments of the VSD are in a resting state. Upon depolarization the S4 segments move outwards into the activated position before the pore opens at the intracellular gate. Once the pore is opened the N-terminus inactivation peptide or QA ions can enter the cavity. The pore is unable to close when these particles in the cavity and has the effect of slowing the voltage sensors return from the activated state.

reflect an intrinsic stability of the pore in the open confirmation but could also result from the occupancy of the pore by the particular ions used in the internal solution. This effect is very dramatic in the presence of intracellular blockers or fast inactivation peptides which can occupy the inner pore cavity with a high affinity and stabilize the open state thus limiting the rate of return of the voltage sensors and associated gating charge.

INACTIVATION AND IMMOBILIZATION

In the absence of fast inactivation peptides or QA ions, immobilization of charge is still observed in Kv channels. This indicates that there are mechanisms other than pore block that underlie the process of immobilization. Gating currents have been recorded in the presence of K^+ ions from mutant *Shaker* channels that have been rendered non-conducting by a mutation W434F in the pore helix that causes the collapse of the selectivity filter (Perozo et al., 1993). These experiments were conducted using the non-conducting channel that also contained an N-terminus deletion of residues 6–46 that removes any fast inactivation process (named inactivation removed, *Shaker*IR), which causes voltage sensor immobilization (Bezanilla et al., 1991), yet gating currents from the *Shaker*IR-W434F recorded with K^+ internal solutions still displayed a slowing of gating current return after depolarization to potentials at which the channels open (Perozo et al., 1993). In addition, wild-type (WT) channels recorded with solutions using ion replacement to deplete conductive intracellular ions with non-permeant cationic molecules such as NMG^+ (Zagotta et al., 1994b) or $Tris^+$ (Varga et al., 2002) also display a slowing of voltage sensor return after depolarization to potentials where channels open. These studies clearly implicate the open pore as

a critical determinant in the slowing of charge return, however it is not the only determinant. In experiments with Kv1.5 channels using NMG^+ to replace K^+ and Na^+ and reveal gating currents it was demonstrated that long depolarizations that persist past the full activation time course of the channels induced a greater slowing of the charge return upon repolarization than shorter pulses (Fedida et al., 1996). This indicated that an immobilization process was occurring that was not only mediated by the pore opening. To further examine this effect the authors used the drug 4AP, which stabilizes the closed pore conformation. 4AP was found to remove the development of immobilization, along with the slow inactivation properties of the channel, suggesting that the immobilization of the gating charge was linked to slow inactivation (Fedida et al., 1996). This pointed to inactivation processes directly mediating an immobilization of the voltage sensors in Kv1.5. Similarly, in the *Shaker* channel lacking fast inactivation (*Shaker*IR) prolonged depolarization was found to immobilize the voltage sensor (Olcese et al., 1997). The immobilization in these experiments was reflected by a left shift of the voltage dependence of charge return compared with charge activation which indicated that more energy was required to return the voltage sensor to its resting configuration (Olcese et al., 1997). Interestingly, immobilization occurred in *Shaker*IR channels recorded in cut-open oocyte configuration where the conducting ions were replaced with NMG^+ as well as in the non-conducting mutant channels *Shaker*IR-W434F recorded in the presence of intracellular K^+ ions, suggesting the effect was not just related to open pore occupancy by the intracellular ions. Furthermore, the time course of the development of charge immobilization in the *Shaker*IR-W434F channel correlated with the time course of inactivation of *Shaker*IR channels (Olcese et al., 1997). These experiments implied an important distinction between inactivated states – that the W434F channel represents a pore inactivated state (P-type), thought to be due to a localized collapse of the selectivity filter, that can still undergo further conformational rearrangements that stabilize the voltage sensor on the same time scale as slow inactivation. This observation indicated that the W434F mutation, whilst collapsing the selectivity filter and preventing conductance, had not prevented other conformational rearrangements that involved the voltage sensor and correlated with slow inactivation. Despite these correlations the study could not conclude whether the P-type inactivation was causally linked with the conformational changes that immobilized the voltage sensors. A separate study investigated *Shaker*IR gating using voltage-clamp fluorometry, in which an environmentally sensitive fluorophore was attached to an engineered cysteine residue at the top of the S4 or the pore region to track conformational rearrangements of the two regions (Loots and Isacoff, 1998). It was found that the fluorescent probes in both regions tracked the onset and recovery of slow inactivation which suggested that pore inactivation alters the interaction between the two domains. Specifically, the study found two conformational rearrangements during *Shaker*IR channel inactivation – the first shuts the channel at the selectivity filter and represents the transition into the inactivated state found in the W434F P-type inactivated channel whereas the second rearrangement involves changes around S4 having the effect of stabilizing the inactivated state and making it more difficult for the voltage sensor to return to its resting position (Loots and Isacoff, 1998).

INTRACELLULAR ION EFFECTS ON IMMOBILIZATION

The experimental conditions required for the resolution of gating currents (mutations, block, and permeant ion depletion) create a significant hurdle when attempting to interpret the relevance of these measurements to physiological gating, in which conducting channels permeate small ions unimpeded. A significant advance came with the development of methodology using the patch clamp technique that enabled precise control of intracellular ionic concentrations and enabled Kv1.5 gating currents to be recorded in the presence of permeating ions Cs^+ and K^+ (Chen et al., 1997). OFF gating currents at −100 mV were recorded in the presence of a low concentration of internal K^+ or the poorly permeant Cs^+ ion which avoided contamination of the gating currents by large ionic conductance. These experiments uncovered that the rate of gating charge return was accelerated by the presence of permeant ions in these channels when compared with recordings in the absence of permeant ions using NMG^+ as a replacement cation (Chen et al., 1997). This implied that the very presence of permeating ions can influence the voltage sensor dynamics and led to the proposition of an allosteric modulatory site where permeant ions may interact to slow entry into a state from which gating charge is slow to return or to impair the entry into a slow inactivated state. Following this study the authors utilized a non-conducting Kv1.5-W472F mutant channel and found that replacing extracellular and intracellular NMG^+ with small group 1 intracellular cations also had the effect of relieving the charge immobilization, with intracellular effects being 10-fold more prominent (Wang et al., 1999). The differences in rates of charge recovery were apparent after depolarization more positive than −20 mV consistent with voltages at which the channel open probability rapidly increases. These studies implied that the effect was strongly dependent upon an intracellular site that was accessible when the channel opens and was hypothesized to regulate entry of the channel into the slow inactivated state which caused immobilization of charge. These two studies combined indicated that the role of ions was not intrinsically linked to their fluxing through the channel as the non-conducting mutant Kv1.5-W472F could also be modulated by varying intracellular ionic composition, but did not precisely locate the ion interaction sites involved.

Insight into the location of the intracellular interaction site for ions to modulate charge return came from studies on *Shaker*IR channels in which the size of the internal cavity was increased by a mutation at isoleucine 470 (Melishchuk and Armstrong, 2001). This residue is located approximately mid way along the S6 helix lining the intracellular cavity. Mutation from isoleucine to cysteine had the effect of accelerating charge return of gating currents recorded with intracellular Cs^+ or NMG^+. This observation led the authors to propose that the limiting step in charge return was pore closure, which in turn was rate limited by the exit rate of ions from inner cavity binding sites. In this case, because the study utilized short (15 ms) depolarizations, the charge immobilization was considered separately from any conformational changes in the tertiary structure of the protein that occurs over the time course of slow inactivation processes which are typically of a much longer time constant. This model proposed by Melishchuk and Armstrong (2001) was consistent with and further supported the classical "occupancy hypothesis" that was based on the observation that increasing the external concentration of permeant ions such

as K^+, Cs^+, and Rb^+ ions slows the deactivation kinetics of Kv channels as the pore is prevented from closing when occupied (Swenson and Armstrong, 1981; Matteson and Swenson, 1986).

An insightful study using a variety of different permeant and non-permeant ions that compared *Shaker*IR conducting and *Shaker*IR-W4343F non-conducting channels attempted to clarify the mechanistic differences in immobilization in these channels (Varga et al., 2002). The study first sought to examine the relationship between ionic deactivation and gating charge return in the WT channel. To achieve this without masking the gating currents the experiments were recorded with low concentrations of permeant ions on either side of the membrane (mM) 1 K^+, 1 Rb^+, or a higher concentration of the poorly permeant Cs^+ (115 mM). The gating currents under these conditions displayed ionic deactivation kinetics that were faster than charge recovery. This indicated that ion occupancy at these concentrations did not rate limit the voltage sensor return. However, because low concentrations of the highly permeant ions K^+ and Rb^+ had to be used to avoid contamination of the charge recovery measurements (this was not necessary for Cs^+ due to its lower permeability allowing it to be used at 115 mM) the result was not directly informative of more physiological conditions. To enable the comparisons to be made with high internal concentrations (115 mM) of K^+ and Rb^+ the experiments were conducted using the non-conducting W434F channel. These recordings using W434F displayed a slower rate of charge recovery than the WT channel with low concentrations of K^+ and Rb^+. This indicated a potential concentration dependent effect, where higher concentrations of ions had the effect of slowing charge recovery, consistent with occupancy slowing pore closure. Further insight came as a byproduct of the interesting observation that "non-conducting" W434F channels can in fact conduct K^+ in specific ionic conditions. When the extracellular solution was set at 115 mM K^+ and the internal contained 115 mM $Tris^+$, a K^+ conductance was observed. This K^+ conductance had the effect of slowing charge return more than when W434F was recorded in the absence of any permeating ions. This suggested that increasing the occupancy of the inner cavity with permeating K^+ ions lowered the rate of pore closure, also supporting the occupancy hypothesis. Taken together, these results suggested that gate closure was not rate-limiting for voltage sensor return in the WT channel in the presence of low concentrations of permeant ions, and that the gate could close before the voltage sensors returned to resting. Conversely, in high concentrations of intracellular permeant ions occupancy of the cavity was rate-limiting pore closure in the W434F channel.

A further observation from this study was that a slow component of charge return was also present in almost all conditions, and was dependent upon the ion species present. The authors postulated that this slowing of gating charge return was caused by the presence of varying degrees of inactivation accumulating over the depolarizing pulses used to evoke gating currents. Because inactivation is associated with conformational processes that slow charge return (Olcese et al., 1997; Loots and Isacoff, 1998), the varied effects with different ion species is likely to be partly due to the different occupancy of a site that slows entry into the inactivated states consistent with previous studies on immobilization that develops after the channel pore is open (Fedida et al., 1999; Wang et al., 1999).

From the studies discussed up to this point it is apparent that occupancy of the cavity is a critical factor in regulating voltage sensor immobilization. The main factors determining the dwell time of an ion in a binding site at a constant membrane potential are the interactions of the ion with the binding site and the potential electrostatic interaction with other ions nearby. Experiments using the divalent ion Ba^{2+} have been used to probe some of the electrostatic effects of ion–ion interactions. A key feature of Ba^{2+} ions in these studies is the deep binding site they occupy in the SF of K^+ channels, adjacent to the inner cavity site highlighted in **Figure 1B** (Neyton and Miller, 1988; Jiang and MacKinnon, 2000). The application of external Ba^{2+} was shown to accelerate charge return in *Shaker*IR-WT and -W434F, specifically after depolarizations to potentials where the channel opens, leading to the hypothesis that Ba^{2+} binding was destabilizing the open state of the channel (Hurst et al., 1997). This effect could well be mediated through a repulsive effect of the Ba^{2+} ions in the deep SF site with the positively charged K^+ ions residing in inner cavity sites. Some experimental support for this hypothesis also came from the detailed study by Varga et al. It was hypothesized that external Ba^{2+} ions would have effects on ions in the cavity from the deep site and influence the occupancy and thus exit rate of intracellular ions in the cavity. To test this hypothesis they applied external Ba^{2+} and observed an accelerated charge return in the W434F channel, which was faster when K^+ ions were in the cavity than with internal Na^+ ions, and had little effect with $Tris^+$ internal (Varga et al., 2002). These data indicated that K^+ ions interacted strongly and repulsively with Ba^{2+} but that the Na^+ and $Tris^+$ ions were sufficiently different in size and physico-chemical structure that they did not occupy a site that was directly affected by Ba^{2+} binding in the filter. The implication of this experiment was that K^+ occupancy of the inner cavity binding site could be destabilized by the Ba^{2+} ion binding presumably at a deep site in the SF (correlated with the lower blue sphere in **Figure 1B**), close enough to exert a significant electrostatic destabilization. This is however likely a simplified picture as it is likely that there is more than one binding site for ions within the intracellular cavity and that these sites can exert influence on each other (Thompson and Begenisich, 2001, 2003).

When discussing the intracellular ion binding sites it should be noted that these sites will be occupied by hydrated K^+ ions as the cavity also contains water molecules. Because a hydrated K^+ ion has a diameter of around 5 Å, with a hydration energy of −85 kcal/mol (Hille, 2001), it is likely that the steric bulk of the hydration sphere of the ion significantly contributes to an energetic barrier to channel pore closure. Generally the effects of ions in the cavity described have been considered to be steric, and the bulk of hydrated K^+ ions support this kind of hypothesis, as does the observation that large ions such as QA ions immobilize charge more severely than small ions. In addition, recent high level studies using all atom molecular dynamics simulations to simulate a complete gating cycles indicated that the open cavity dewetted before the pore collapses due to the hydrophobic nature of the cavity (Jensen et al., 2010, 2012). Hydrated ions must therefore exit before the pore can dewet fully before shutting, supporting the hypothesis that ionic occupancy in the cavity slows pore closure.

VOLTAGE SENSOR RELAXATION – A THIRD MECHANISM OF CHARGE IMMOBILIZATION?

Stabilization of the voltage sensor in the activated state after depolarization has also been observed in non-inactivating channels such as HCN channels (Bruening-Wright and Larsson, 2007), and the voltage-sensing phosphatase, ciVSP which has no pore (Villalba-Galea et al., 2008). Slowing of charge return in a voltage sensor without a pore is clearly a different process that cannot be dependent upon pore inactivation or ionic occupancy and suggests that the voltage sensor might possess an intrinsic property to "relax," representing the adoption of a distinct stable conformational state (Villalba-Galea et al., 2008, 2009). This process has also been proposed to occur in *Shaker*IR channels during prolonged depolarizing pulses as tracked by the entry into a state from which charge return is slow (Lacroix et al., 2011). Although relaxation may represent an intrinsic property of the voltage sensor, it is currently difficult to separate the observed slowing of charge return from those related to inactivation discussed above, that also show ion dependence (Shirokov, 2011). It follows that if voltage sensor relaxation is independent of pore-related inactivation processes then it should have little dependence on ionic conditions. Future studies that advance the structural information available for these states will ultimately allow the clear separation of inactivation and relaxation. Because relaxation of voltage sensors occurs over a much longer time scale than the slowing of charge return that can be observed developing with channel opening kinetics it is certainly not likely to impact directly on the rapid immobilization of charge caused by ions occupying the inner cavity.

CONCLUSION

The studies reviewed here have shown that charge immobilization can be caused by a combination of ion occupancy of the pore and conformational rearrangements associated with inactivation or relaxation, which can be broadly classed as intrinsic (related to protein tertiary structural rearrangements) and extrinsic (caused by external factors such as ion block of pore closure or inactivation) factors.

The various pathways affected by intracellular ions have been summarized by the simplified state scheme shown in **Figure 3**. The scheme assigns the majority of the charge carrying transitions of all the four subunits voltage sensors to the transition between R (resting) and A (activated). Depolarization causes the voltage sensors to shift from R to A, a transition which accounts for the gating charge measured on activation. After activation the pore domain opens sequentially and must shut before the reverse transition from A to R representing charge recovery. Slowing the transition from O to A will have the effect of slowing charge return. After opening, ions may enter the pore and occupy a site ($O{:}Ion_{S1}$) that prevents closure of the pore and will have the knock-on effect of slowing deactivation kinetics and, if slower than the A to R transition, the rate of charge return will also be slower. The rate of slowing of charge return is subject to modulation of the stability of $O{:}Ion_{S1}$, which is dependent upon the proximity of other ions and the intrinsic affinity for the pore cavity that the specific ion may have which will be dependent upon size, charge, and solvation. Once opened, or bound with an ion at S1, the channel might also enter an inactivated state (I) associated with a conformational rearrangement that stabilizes the voltage sensor and causes immobilization. The rate of entry into this inactivated state may be impaired by intracellular ions occupying a site that antagonizes inactivation ($O{:}Ion_{S2}$) – probably through a mechanism similar to the "foot in the door" attenuation of inactivation described for conducting channels (Baukrowitz and Yellen, 1995, 1996). The off rate for each ion site are modified by the multipliers α and β where α (β, which results in occupancy of S2 impairing the entry into the inactivated state without affecting the return of charge significantly. Alternatively, the entry into the inactivated state could be accelerated by reducing binding at the "foot in the door" site S2 through the depletion of appropriate binding ions by non-permeant cations which favor site S1; an experimental condition necessary to record gating currents from conducting channels which would increase the degree of immobilization observed.

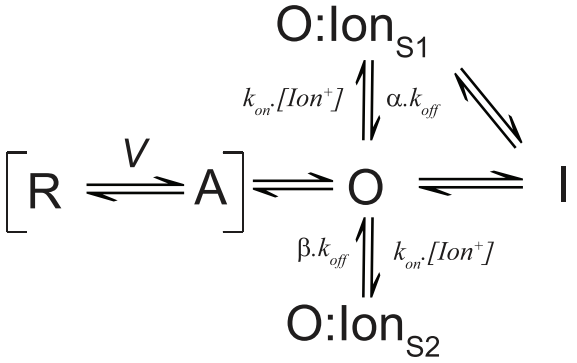

FIGURE 3 | State model summarizing the effects of intracellular ions on voltage sensor dynamics. The model is described in the text.

In this review we have attempted to identify and separate some important mechanisms that can contribute to voltage sensor immobilization and the ways in which those processes are subject to modulation by intracellular ions. It is apparent that these effects are not always easily separated and that often simultaneous immobilizing mechanisms are operating at the same time, dependent upon the particular recording solutions used and the durations of the depolarizing pulses. Despite these uncertainties it is clear that, especially after short depolarizations, that would not be considered to induce significant inactivation or relaxation, occupancy of the intracellular cavity by ions does affect the dynamics of the voltage sensor. This effect of intracellular ions could be thought of as allosteric in the sense that ion binding at pore sites influences the stability of the voltage sensor, a structurally distinct entity (**Figure 1A**). Considering that ions fluxing through the pore exert an influence on the deactivation voltage gating it is of physiological significance to understand the precise mechanisms by which these effects are mediated. It is conceivable that different channel subtypes have evolved around the ion species they carry and that ion occupancy effects on deactivation kinetics could have exerted some selective pressure depending on the particular channel subtype, which contributes to their particular deactivation gating phenotype. As more channels are investigated and high resolution structures are solved for Kv channels in different states a clearer picture will emerge of the ions role in gating as well as permeation.

REFERENCES

Armstrong, C. M. (1971). Interaction of tetraethylammonium ion derivatives with the potassium channels of giant axons. *J. Gen. Physiol.* 58, 413–437.

Armstrong, C. M., and Bezanilla, F. (1974). Charge movement associated with the opening and closing of the activation gates of the Na channels. *J. Gen. Physiol.* 63, 533–552.

Armstrong, C. M., and Bezanilla, F. (1977). Inactivation of the sodium channel. II. Gating current experiments. *J. Gen. Physiol.* 70, 567–590.

Batulan, Z., Haddad, G. A., and Blunck, R. (2010). An intersubunit interaction between S4–S5 linker and S6 is responsible for the slow off-gating component in Shaker K+ channels. *J. Biol. Chem.* 285, 14005–14019.

Baukrowitz, T., and Yellen, G. (1995). Modulation of K+ current by frequency and external [K+]: a tale of two inactivation mechanisms. *Neuron* 15, 951–960.

Baukrowitz, T., and Yellen, G. (1996). Use-dependent blockers and exit rate of the last ion from the multi-ion pore of a K+ channel. *Science* 271, 653–656.

Bezanilla, F. (2000). The voltage sensor in voltage-dependent ion channels. *Physiol. Rev.* 80, 555–592.

Bezanilla, F., Perozo, E., Papazian, D. M., and Stefani, E. (1991). Molecular basis of gating charge immobilization in Shaker potassium channels. *Science* 254, 679–683.

Bruening-Wright, A., and Larsson, H. P. (2007). Slow conformational changes of the voltage sensor during the mode shift in hyperpolarization-activated cyclic-nucleotide-gated channels. *J. Neurosci.* 27, 270–278.

Chen, F. S., Steele, D., and Fedida, D. (1997). Allosteric effects of permeating cations on gating currents during K+ channel deactivation. *J. Gen. Physiol.* 110, 87–100.

Choi, K. L., Mossman, C., Aubé, J., and Yellen, G. (1993). The internal quaternary ammonium receptor site of Shaker potassium channels. *Neuron* 10, 533–541.

De Santiago-Castillo, J. A., Covarrubias, M., Sánchez-Rodríguez, J. E., Perez-Cornejo, P., and Arreola, J. (2010). Simulating complex ion channel kinetics with IonChannelLab. *Channels (Austin)* 4, 422–428.

Fedida, D., Bouchard, R., and Chen, F. S. (1996). Slow gating charge immobilization in the human potassium channel Kv1.5 and its prevention by 4-aminopyridine. *J. Physiol. (Lond.)* 494(Pt 2), 377–387.

Fedida, D., Maruoka, N. D., and Lin, S. (1999). Modulation of slow inactivation in human cardiac Kv1.5 channels by extra- and intracellular permeant cations. *J. Physiol. (Lond.)* 515(Pt 2), 315–329.

Gonzalez, C., Lopez-Rodriguez, A., Srikumar, D., Rosenthal, J. J., and Holmgren, M. (2011). Editing of human K(V)1.1 channel mRNAs disrupts binding of the N-terminus tip at the intracellular cavity. *Nat. Commun.* 2, 436.

Heginbotham, L., Lu, Z., Abramson, T., and MacKinnon, R. (1994). Mutations in the K+ channel signature sequence. *Biophys. J.* 66, 1061–1067.

Hille, B. (2001). *Ionic Channels of Excitable Membranes.* Sunderland, MA: Sinauer Associates Inc.

Hurst, R. S., Roux, M. J., Toro, L., and Stefani, E. (1997). External barium influences the gating charge movement of Shaker potassium channels. *Biophys. J.* 72, 77–84.

Jensen, M. O., Borhani, D. W., Lindorff-Larsen, K., Maragakis, P., Jogini, V., Eastwood, M. P., Dror, R. O., and Shaw, D. E. (2010). Principles of conduction and hydrophobic gating in K+ channels. *Proc. Natl. Acad. Sci. U.S.A.* 107, 5833–5838.

Jensen, M. O., Jogini, V., Borhani, D. W., Leffler, A. E., Dror, R. O., and Shaw, D. E. (2012). Mechanism of voltage gating in potassium channels. *Science* 336, 229–233.

Jiang, Y., and MacKinnon, R. (2000). The barium site in a potassium channel by x-ray crystallography. *J. Gen. Physiol.* 115, 269–272.

Lacroix, J. J., Labro, A. J., and Bezanilla, F. (2011). Properties of deactivation gating currents in Shaker channels. *Biophys. J.* 100, L28–L30.

Lee, S. Y., Banerjee, A., and MacKinnon, R. (2009). Two separate interfaces between the voltage sensor and pore are required for the function of voltage-dependent K(+) channels. *PLoS Biol.* 7, e47. doi:10.1371/journal.pbio.1000047

Liu, Y., Holmgren, M., Jurman, M. E., and Yellen, G. (1997). Gated access to the pore of a voltage-dependent K+ channel. *Neuron* 19, 175–184.

Long, S. B., Campbell, E. B., and Mackinnon, R. (2005a). Crystal structure of a mammalian voltage-dependent Shaker family K+ channel. *Science* 309, 897–903.

Long, S. B., Campbell, E. B., and Mackinnon, R. (2005b). Voltage sensor of Kv1.2: structural basis of electromechanical coupling. *Science* 309, 903–908.

Loots, E., and Isacoff, E. Y. (1998). Protein rearrangements underlying slow inactivation of the Shaker K+ channel. *J. Gen. Physiol.* 112, 377–389.

Lu, Z., Klem, A. M., and Ramu, Y. (2002). Coupling between voltage sensors and activation gate in voltage-gated K+ channels. *J. Gen. Physiol.* 120, 663–676.

Matteson, D. R., and Swenson, R. P. Jr. (1986). External monovalent cations that impede the closing of K channels. *J. Gen. Physiol.* 87, 795–816.

Melishchuk, A., and Armstrong, C. M. (2001). Mechanism underlying slow kinetics of the OFF gating current in Shaker potassium channel. *Biophys. J.* 80, 2167–2175.

Neyton, J., and Miller, C. (1988). Discrete Ba2+ block as a probe of ion occupancy and pore structure in the high-conductance Ca2+ -activated K+ channel. *J. Gen. Physiol.* 92, 569–586.

Olcese, R., Latorre, R., Toro, L., Bezanilla, F., and Stefani, E. (1997). Correlation between charge movement and ionic current during slow inactivation in Shaker K+ channels. *J. Gen. Physiol.* 110, 579–589.

Perozo, E., MacKinnon, R., Bezanilla, F., and Stefani, E. (1993). Gating currents from a nonconducting mutant reveal open-closed conformations in Shaker K+ channels. *Neuron* 11, 353–358.

Peters, C. J., Vaid, M., Horne, A. J., Fedida, D., and Accili, E. A. (2009). The molecular basis for the actions of KVbeta1.2 on the opening and closing of the KV1.2 delayed rectifier channel. *Channels (Austin)* 3, 314–322.

Schoppa, N. E., McCormack, K., Tanouye, M. A., and Sigworth, F. J. (1992). The size of gating charge in wild-type and mutant Shaker potassium channels. *Science* 255, 1712–1715.

Shirokov, R. (2011). What's in gating currents? Going beyond the voltage sensor movement. *Biophys. J.* 101, 512–514; discussion 515–516.

Swenson, R. P. Jr., and Armstrong, C. M. (1981). K+ channels close more slowly in the presence of external K+ and Rb+. *Nature* 291, 427–429.

Thompson, J., and Begenisich, T. (2001). Affinity and location of an internal K+ ion binding site in shaker K channels. *J. Gen. Physiol.* 117, 373–384.

Thompson, J., and Begenisich, T. (2003). Functional identification of ion binding sites at the internal end of the pore in Shaker K+ channels. *J. Physiol. (Lond.)* 549(Pt 1), 107–120.

Varga, Z., Rayner, M. D., and Starkus, J. G. (2002). Cations affect the rate of gating charge recovery in wild-type and W434F Shaker channels through a variety of mechanisms. *J. Gen. Physiol.* 119, 467–485.

Villalba-Galea, C. A., Sandtner, W., Dimitrov, D., Mutoh, H., Knöpfel, T., and Bezanilla, F. (2009). Charge movement of a voltage-sensitive fluorescent protein. *Biophys. J.* 96, L19–L21.

Villalba-Galea, C. A., Sandtner, W., Starace, D. M., and Bezanilla, F. (2008). S4-based voltage sensors have three major conformations. *Proc. Natl. Acad. Sci. U.S.A.* 105, 17600–17607.

Wang, Z., Zhang, X., and Fedida, D. (1999). Gating current studies reveal both intra- and extracellular cation modulation of K+ channel deactivation. *J. Physiol. (Lond.)* 515(Pt 2), 331–339.

Zagotta, W. N., Hoshi, T., and Aldrich, R. W. (1994a). Shaker potassium channel gating. III: evaluation of kinetic models for activation. *J. Gen. Physiol.* 103, 321–362.

Zagotta, W. N., Hoshi, T., Dittman, J., and Aldrich, R. W. (1994b). Shaker potassium channel gating. II: transitions in the activation pathway. *J. Gen. Physiol.* 103, 279–319.

Zhou, Y., Morais-Cabral, J. H., Kaufman, A., and MacKinnon, R. (2001). Chemistry of ion coordination and hydration revealed by a K+ channel-Fab complex at 2.0 A resolution. *Nature* 414, 43–48.

Conflict of Interest Statement: The authors declare that the research was conducted in the absence of any commercial or financial relationships that could be construed as a potential conflict of interest.

Received: 30 March 2012; accepted: 25 May 2012; published online: 18 June 2012.

*Citation: Goodchild SJ and Fedida D (2012) Contributions of intracellular ions to Kv channel voltage sensor dynamics. Front. Pharmacol. **3**:114. doi: 10.3389/fphar.2012.00114*

This article was submitted to Frontiers in Pharmacology of Ion Channels and Channelopathies, a specialty of Frontiers in Pharmacology.

frontiers in
PHARMACOLOGY

REVIEW ARTICLE
published: 17 April 2012
doi: 10.3389/fphar.2012.00063

Regulation of voltage-activated K^+ channel gating by transmembrane β subunits

***Xiaohui Sun*[1,2,3†], *Mark A. Zaydman*[1,2,3†] *and Jianmin Cui*[1,2,3*]**

[1] *Department of Biomedical Engineering, Washington University, Saint Louis, MO, USA*
[2] *Center for the Investigation of Membrane Excitability Disorders, Washington University, Saint Louis, MO, USA*
[3] *Cardiac Bioelectricity and Arrhythmia Center, Washington University, Saint Louis, MO, USA*

Edited by:
Gildas Loussouarn, University of Nantes, France

Reviewed by:
Peter Larsson, University of Miami School of Medicine, USA
William R. Kobertz, UMass Medical School, USA

***Correspondence:**
Jianmin Cui, Department of Biomedical Engineering, Washington University, One Brookings Drive, Saint Louis, MO 63130, USA.
e-mail: jcui@wustl.edu

†*Xiaohui Sun and Mark A. Zaydman have contributed equally to this work.*

Voltage-activated K^+ (K_V) channels are important for shaping action potentials and maintaining resting membrane potential in excitable cells. K_V channels contain a central pore-gate domain (PGD) surrounded by four voltage-sensing domains (VSDs). The VSDs will change conformation in response to alterations of the membrane potential thereby inducing the opening of the PGD. Many K_V channels are heteromeric protein complexes containing auxiliary β subunits. These β subunits modulate channel expression and activity to increase functional diversity and render tissue specific phenotypes. This review focuses on the K_V β subunits that contain transmembrane (TM) segments including the KCNE family and the β subunits of large conductance, Ca^{2+}- and voltage-activated K^+ (BK) channels. These TM β subunits affect the voltage-dependent activation of K_V α subunits. Experimental and computational studies have described the structural location of these β subunits in the channel complexes and the biophysical effects on VSD activation, PGD opening, and VSD–PGD coupling. These results reveal some common characteristics and mechanistic insights into K_V channel modulation by TM β subunits.

Keywords: channel, β subunit, K_v, KCNQ1, BK, KCNE, KCNMB, LRRC

INTRODUCTION

Cellular electrical signals organize and control activity in the nervous, muscular, and hormonal tissues. The voltage-activated K^+ (K_V) channels are a large group of transmembrane (TM) proteins that open in response to membrane depolarization to permit the selective efflux of potassium ions across the membrane. K_V channels play an important role in shaping the electric signals of excitable tissues and also contribute to the maintenance of ion homeostasis. Although K_V channels vary greatly in their activity, conductance and pharmacology, the basic structure of the channel and the mechanism of voltage-dependent activation are well conserved across the K_V family. K_V channels share a common topology of six TM α helices (S1–S6) that are organized into two structural domains, the voltage-sensing domain (VSD, S1–S4) and the pore-gate domain (PGD, S5 and S6). As seen in the available K_V channel crystal structures, four α-subunits coassemble to form a tetrameric complex with a central pore built from the PGDs of all four subunits and with the four VSDs located peripheral to the central pore (**Figure 1**).

Voltage-dependent activation of K_V channels involves three general molecular events (Zagotta et al., 1994). First, depolarization of the membrane potential drives the outward movement of the S4 segment of the VSD that contains conserved basic residues positioned within the electric field (Tombola et al., 2005; Bezanilla, 2008). Second, the conformational change during VSD activation is propagated to the PGD through interactions between the S4/S5 linker and the cytosolic side of S6 (Lu et al., 2001; Tristani-Firouzi et al., 2002; Long et al., 2005), the S4 and S5 helices (Ledwell and Aldrich, 1999; Soler-Llavina et al., 2006; Grabe et al., 2007), and the extracellular side of the S1 and the pore helix (Lee et al., 2009); this event is known as coupling. The third event of K_V channel activation is the opening of the PGD to allow ion permeation (Yellen, 1998).

Voltage-activated K^+ channel function is modulated by auxiliary β subunits (Pongs and Schwarz, 2010). Of particular interest to this review are the TM β subunits due to their ability to regulate the voltage-dependent activation of K_V channels. Here we review the major TM β subunits including the KCNE family and the β subunits of voltage- and Ca^{2+}-activated K^+ (BK) channels to summarize our current understanding of the location of β subunits in the channel complex and their impact on the three molecular events of K_V channel voltage-dependent activation.

KCNE β SUBUNITS

The KCNE family of β subunits consists of five members (KCNE1–5, also known as minK and minK related peptides 1–4) that all contain a single TM domain with an intracellular COOH terminus and an extracellular NH_2 terminus (Takumi et al., 1988; Abbott et al., 1999; Piccini et al., 1999; **Figure 1A**). KCNE subunits coassemble with and modulate K_V α subunits resulting in a diverse set of K_V channel phenotypes. Not only can one member of the KCNE family regulate multiple different K_V channels,

Abbreviations: AF, atrial fibrillation; CTD, cytosolic domain; *F–V*, fluorescence–voltage relationship; *G–V*, conductance–voltage relationship; K_V channels, voltage-activated K^+ channels; LQTS, long QT syndrome; PGD, pore-gate domain; P_o–*V*, open probability–voltage relationship; SQTS, short QT syndrome; TM, transmembrane; VCF, voltage-clamp fluorometry; VSD, voltage-sensing domain.

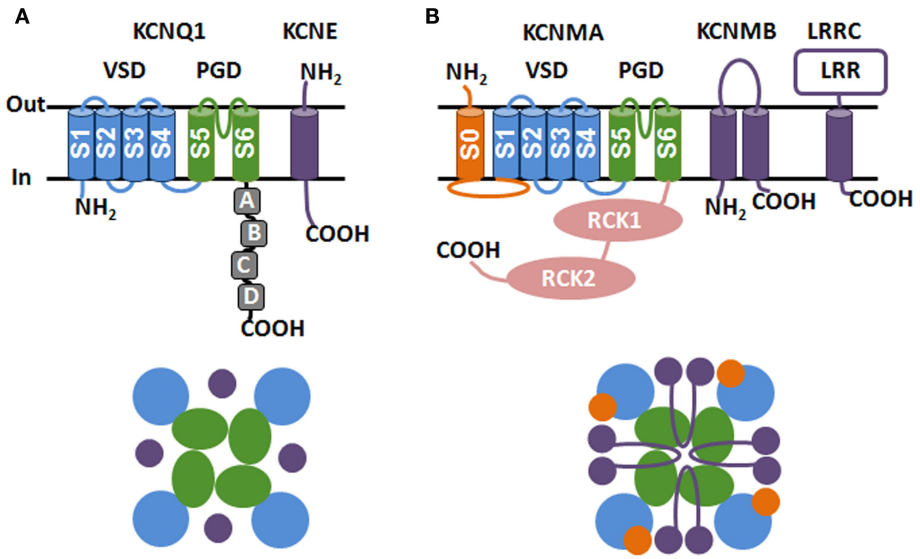

FIGURE 1 | Topology (top) and coassembly (bottom) of KCNQ1 (A) and BK channel (B) α subunits and β subunits. The voltage-sensing domain (VSD, S1–S4), pore-gate domain (PGD, S5 and S6), cytosolic domain (RCK1 and RCK2), S0 segment, and β subunits are colored as blue, green, pink, orange, and purple, respectively. The COOH terminal α-helices (A–D) of KCNQ1 and the leucine-rich-repeat domain (LRR) for LRRC are indicated. The coassembly of the heteromeric channel complex are illustrated as viewed from the extracellular face of the membrane (bottom).

but one K_V family member can be regulated by different KCNEs. For example, KCNQ1 (K_V7.1) can coassemble with all five of the KCNE family peptides; however, the effects of the different KCNEs on KCNQ1 function are very different (Barhanin et al., 1996; Sanguinetti et al., 1996; Schroeder et al., 2000; Tinel et al., 2000; Angelo et al., 2002; Grunnet et al., 2002). These effects range from constitutive, voltage-independent activation with KCNE3 (Schroeder et al., 2000), a shift of voltage-dependent activation to more positive voltages with KCNE1 (Barhanin et al., 1996; Sanguinetti et al., 1996) to inhibition of the ionic current by KCNE4 (Grunnet et al., 2002). Promiscuity in coassembly and diversity of functional regulation allows different tissues to carry unique electrophysiological phenotypes by expressing different KCNE–K_V combinations.

KCNE1 MODULATION OF KCNQ1

Of the many KCNE–K_V pairs, the channel formed by coassembly of KCNE1 with the KCNQ1 is the best studied due to the physiological importance of this channel, the dramatic effects of KCNE1 on the function of KCNQ1, and the fact that it was the first identified KCNE–K_V partnership. In the heart the heteromeric assembly of KCNQ1 + KCNE1 subunits generates the slow delayed-rectifier current (Barhanin et al., 1996; Sanguinetti et al., 1996), I_{Ks}, that is important for termination of the cardiac action potential (Sanguinetti and Jurkiewicz, 1990; Jost et al., 2007). In the inner ear KCNQ1 + KCNE1 channels play a role in the maintenance of endolymph potassium homeostasis (Vetter et al., 1996). Mutations in KCNQ1 (Wang et al., 1996b) or KCNE1 (Splawski et al., 1997) that compromise I_{Ks} function can cause long QT syndrome (LQTS) that manifests as prolongation of the QT interval on the surface electrocardiogram and a high risk of ventricular arrhythmias and sudden death. In some cases, the cardiac phenotype can be accompanied by congenital deafness (for review see Hedley et al., 2009). In contrast, I_{Ks} gain of function mutations cause premature repolarization and are associated with short QT syndrome (SQTS; Bellocq et al., 2004) and atrial fibrillation (AF; Chen et al., 2003; Hong et al., 2005; Lundby et al., 2007; Das et al., 2009).

The functional importance of KCNE1 effects on KCNQ1 channels is demonstrated by the existence of LQTS mutations in KCNE1 and by the remarkable modulation of KCNQ1 activity by KCNE1 in heterologous expression systems. Exogenous expression of KCNQ1 alone is sufficient to generate voltage-dependent potassium channels; however, coexpression of KCNE1 with KCNQ1 shifts the voltage-dependence of activation toward more depolarized potentials, slows activation and deactivation kinetics (Barhanin et al., 1996; Sanguinetti et al., 1996), removes inactivation (Pusch et al., 1998; Tristani-Firouzi and Sanguinetti, 1998), increases single channel conductance (Sesti and Goldstein, 1998; Yang and Sigworth, 1998), increases PIP_2 sensitivity (Li et al., 2011), renders the channel functionally sensitive to PKA phosphorylation (Kurokawa et al., 2003, 2009), and alters the channel pharmacology (Busch et al., 1997; Lerche et al., 2000). These functional changes result in a current that closely recapitulates the properties of the cardiac I_{Ks} current that are key to myocyte function *in vivo* (Silva and Rudy, 2005). In this brief review we will discuss the current evidence regarding the mechanism by which KCNE1 regulates the voltage-dependent activation of KCNQ1 as the best understood example of KCNE regulation of K_V channel gating. The study of KCNE3 and KCNE4 regulation of KCNQ1 has also provided similar mechanistic insight; for more details we refer the interested reader to another review to appear in this issue (Wrobel et al., submitted).

THE LOCATION OF KCNE1 IN THE KCNQ1 + KCNE1 CHANNEL

Biochemical and cysteine cross-linking assays have established proximity between various locations of the KCNE1 TM segment and KCNQ1 (Xu et al., 2008; Chung et al., 2009; Lvov et al., 2010; Chan et al., 2012; **Figure 1A**). On the extracellular side of the membrane, proximity between the KCNE1 NH_2 terminus (positions 36–43) and the tops of S1, S4, and S6 has been shown through disulfide cross-linking (Wang et al., 2011; Chan et al., 2012). An interaction between the distal KCNE1 COOH terminus and helix C of the KCNQ1 COOH terminus (**Figure 1A**) has been detected by co-immunoprecipitation (Haitin et al., 2009). However, truncation experiments indicate that removing either the extracellular NH_2 terminal domain (Takumi et al., 1991) or the cytosolic distal COOH terminus (Tapper and George, 2000; Chen et al., 2009) of KCNE1 does not prevent the right shift in voltage-dependence and slowing of activation kinetics upon coexpression with KCNQ1, indicating that these structures are not absolutely required for modulation of voltage-dependent activation in exogenous expression systems. Nevertheless, the distal COOH terminus of KCNE1 is required for imparting sensitivity to PKA phosphorylation (Kurokawa et al., 2009) downstream of β adrenergic stimulation, which is vital for the ability of I_{Ks} to regulate heart rhythm *in vivo* (Marx et al., 2002; Kurokawa et al., 2003; Volders et al., 2003). In addition, PKA-dependent phosphorylation can modify voltage-dependent activation by shifting the *G–V* curve toward less depolarized potentials and slowing deactivation kinetics (Kurokawa et al., 2003, 2009; Li et al., 2011).

In contrast, truncation and chimera studies show that the KCNE1 TM segment and proximal COOH terminus are both absolutely required for right shifting the KCNQ1 *G–V* and slowing of activation kinetics in heterologous expression systems (Tapper and George, 2000). Metal bridging of G55C in KCNE1 to C331 in KCNQ1 (Tapper and George, 2001) and mutant cycle analyses (Strutz-Seebohm et al., 2011) have provided evidence for an interaction between the KCNE1 TM segment and the outer aspect of the PGD. Cysteine cross-linking indicates that the proximal KCNE1 COOH terminus is in interaction with the KCNQ1 S4/S5 linker and S6 gate, key structures of the gating machinery (Lvov et al., 2010). An early study showed that mutation of the KCNE1 proximal COOH terminus strongly affects the activity of channels consisting of exogenously expressed KCNE1 and the KCNQ1 homolog that is endogenously expressed in the *Xenopus* oocyte (Takumi et al., 1991). Of note, the proximal COOH terminus is among the most highly conserved regions across the KCNE family, although this region may be of lower importance for the regulation of KCNQ1 activation by other KCNE family members (Melman et al., 2001, 2002; Gage and Kobertz, 2004).

These experimental results have been used to build various models of the KCNQ1 + KCNE1 channel complex using the atomic coordinates of $K_V1.2$ as a template for KCNQ1 (Kang et al., 2008; Xu et al., 2008; Chung et al., 2009; Strutz-Seebohm et al., 2011; Van Horn et al., 2011; Chan et al., 2012). These models consistently locate the KCNE1 TM segment in a cleft that is formed between two VSDs and adjacent to the outer face of the PGD (**Figure 1A**). From this position, KCNE1 participates in a broad set of interactions with KCNQ1 that span the entire length of the KCNE1 peptide. This interface includes interactions with both the VSD and the PGD, and contacts are made with as many as three KCNQ1 subunits of the tetramer. These structural models do not identify the likely mechanism for how KCNE1 modulates the voltage-dependent activation of KCNQ1 as the interactions with the VSD, PGD, and S4/S5 linker suggest that regulation of VSD movement, PGD opening, and electromechanical coupling are all plausible. These results are consistent with the biophysical experiments as reviewed below.

KCNE1 REGULATION OF VSD ACTIVATION

The biophysical effects of KCNE1 on the KCNQ1 VSD have been explored in several studies. First the state-dependent accessibility of a cysteine engineered into the NH_2 terminal part of S4 (positions 226–230) has been probed with MTS reagents to track S4 movement in response to membrane depolarization (Nakajo and Kubo, 2007; Rocheleau and Kobertz, 2008). In these studies, coexpression of KCNE1 with KCNQ1 slowed the rate of S4 cysteine modification. However, this result alone does not conclusively indicate that KCNE1 slows the movement of the KCNQ1 VSD since the kinetics of chemical modification are dependent on the solvent accessibility and chemical environment of the engineered cysteine (Rocheleau and Kobertz, 2008). In our hands, coexpression of KCNE1 with KCNQ1 exposes a cysteine engineered into the KCNQ1 VSD (E160C in S2) to extracellular MTS reagents (Wu et al., 2010a) indicating that KCNE1 can change either the solvent penetration into the VSD or the electrostatic environment within the VSD. Tryptophan and alanine scanning of the S4 segment with and without KCNE1 shows that KCNE1 changes the tolerance to mutation at positions within the VSD (Shamgar et al., 2008; Wu et al., 2010b) suggesting an alteration in the protein packing between S4 and the rest of the VSD or the PGD. These effects on protein packing were most dramatic for mutations of the intracellular half of S4 (Wu et al., 2010b). Changes in the solvent penetration or protein packing within the voltage sensor will change the profile of the electric field surrounding the S4 gating charges and thereby directly alter voltage sensation within the VSD. Recently, the voltage-clamp fluorometry (VCF) technique has been used to directly track VSD movement revealing that the voltage-dependence of VSD activation extends to far more hyperpolarized potentials in the presence of KCNE1 relative to KCNQ1 alone (Osteen et al., 2010). Together these results indicate that KCNE1 changes the structure and movements of the VSD. However, these changes do not offer a clear mechanism for the slow current kinetics and right shifted *G–V* relationship observed upon coexpression of KCNE1 with KCNQ1. As shown by MTS modification and VCF experiments, the kinetics of VSD activation are much faster than the current activation in the presence of KCNE1 (Rocheleau and Kobertz, 2008; Osteen et al., 2010), and the voltage-dependence of VSD movements is shifted by KCNE1 in the opposite direction (i.e., left) relative to the shift in the *G–V* relationship (Osteen et al., 2010).

KCNE1 REGULATION OF PGD OPENING

Study of either wild-type or mutant KCNE1 showed that KCNE1 alters single channel conductance (Sesti and Goldstein, 1998; Yang and Sigworth, 1998), ion selectivity (Goldstein and Miller, 1991), and channel block (Goldstein and Miller, 1991; Wang et al.,

1996a; Tai and Goldstein, 1998) suggesting that KCNE1 affects the structure of the KCNQ1 channel pore. Transplantation of the KCNQ1 PGD and cytosolic COOH terminus into K_V1.4 yielded a chimeric channel that coassembles with and is regulated by KCNE1 (Melman et al., 2004). Similarly, a recent study shows that KCNE1 shifts the *G–V* and activation kinetics of human and invertebrate KCNQ1 homologs differently, and chimeric channels between the two show that parts of the human KCNQ1 PGD (especially the S5–S6 pore loop) are required to endow the chimeric channel with the human phenotype of KCNE1 regulation (Nakajo et al., 2011). An interaction between KCNE1 and the PGD could modulate steady-state voltage-dependence by changing the energetic gap between the closed and open state of the PGD; also, this interaction could change activation kinetics by changing the energy of the transition between the open and closed state.

KCNE1 MODULATION OF COUPLING

As mentioned previously, disulfide cross-linking establishes an interaction between the KCNE1 proximal COOH terminus (residues 70–81) and the KCNQ1 S4/S5 linker (residues 251–257) as well as the S6 gate (residues 342–370; Lvov et al., 2010). The protein contacts between the S4/S5 linker and S6 gate are probably the major structural pathway for coupling VSD activation to PGD opening in KCNQ1, similar to electromechanical coupling in other K_V channels (see Introduction). Central to the coupling interface in the K_V1.2 crystal structure is a phenylalanine residue in the S6 gate that is highly conserved among K_V family channels (Haddad and Blunck, 2011; F481 in shaker, F351 in KCNQ1). Interestingly, an artificial mutation at this position in the KCNQ1 S6 (i.e., F351A; Boulet et al., 2007) as well as two naturally occurring LQTS mutations (R243C and W248R; Franqueza et al., 1999) and several artificial mutations (Labro et al., 2011) in the KCNQ1 S4/S5 linker all result in a right shifted *G–V* relationship and slow gating kinetics when the mutant α subunits were expressed alone. Thus, perturbing the internal coupling interface in KCNQ1 can mimic the phenotype of KCNE1 modulation of KCNQ1. Decoupling of PGD opening from VSD movements by KCNE1 is shown by the recent KCNQ1 VCF data as KCNE1 coexpression shifts the *F–V* (VSD activation) toward more hyperpolarized potentials while the *G–V* (PGD opening) is shifted to more depolarized potentials (Osteen et al., 2010).

A second interaction interface for coupling between the K_V VSD and the PGD has been identified between S1 and the pore loop (see Introduction). Interestingly, a cluster of gain of function KCNQ1 mutation that are associated with AF (S140G, V141M, Q147R) are located in this part of S1. Furthermore, these mutations have little impact on the function of homomeric KCNQ1 channels, but cause defective deactivation in the presence of KCNE1 (Chen et al., 2003; Hong et al., 2005; Lundby et al., 2007; Chan et al., 2012). These results indicate that KCNE1 may affect the coupling of the VSD and the PGD at both the intracellular and extracellular face of the membrane.

BK CHANNEL β SUBUNITS

BK channels have a unitary conductance of ∼100–300 pS (Marty, 1981). The opening of BK channels repolarizes the membrane and shuts down the voltage-dependent Ca^{2+} channels, thereby reducing Ca^{2+} influx. Through this negative feedback mechanism, BK channels regulate membrane excitability and intracellular Ca^{2+} signaling (Lancaster and Nicoll, 1987; Storm, 1987; Brayden and Nelson, 1992). BK channels are composed of pore-forming α subunits (Slo1) and accessory β subunits. The Slo1 subunit contains three structural domains, which are the VSD, the cytosolic domain (CTD) and PGD. In BK channels the opening of the PGD is controlled by voltage-sensing in the VSD, as in other K_V channels, and by Ca^{2+} binding in the CTD. In addition to the canonical VSD (S1–S4) of K_V channels, Slo1 contains a unique TM segment (S0; Wallner et al., 1996) which affects VSD activation (Koval et al., 2007; **Figure 1B**). A prominent feature of BK channel activation is the allosteric coupling between the VSD and the activation gate, i.e., the PGD can open when the VSDs are either in the resting or activated state but the activation of the VSDs promotes channel opening (Horrigan et al., 1999).

Four types of 2TM β subunit (β1–β4, encoded by the genes *KCNMB1–4*; Knaus et al., 1994; Wallner et al., 1999; Xia et al., 1999, 2000; Behrens et al., 2000; Brenner et al., 2000; Meera, 2000) and one 1TM β subunit (leucine-rich-repeat-containing protein 26, LRRC26; Yan and Aldrich, 2010) have been identified to date. Since the BK channel α subunit is encoded by a single gene (*slo1*), the tissue specific expression and differential modulation among these β subunits provide a major mechanism for generating a diversity of BK channel phenotypes in different tissues. The effects of β subunits on BK channel function are multifaceted, including altering voltage-dependent activation (Cox and Aldrich, 2000; Wang et al., 2006), changing Ca^{2+} sensitivity (McManus et al., 1995; Nimigean and Magleby, 1999; Wallner et al., 1999; Xia et al., 1999; Brenner et al., 2000), conferring inactivation (Wallner et al., 1999; Xia et al., 1999, 2000; Brenner et al., 2000), and endowing sensitivity to extracellular ligands (Valverde et al., 1999). Here we focus on the structural and functional interactions between different β subunits and Slo1 to elucidate how BK channel β subunits regulate voltage-dependent activation. Readers may refer to excellent reviews elsewhere for other perspectives of BK β subunits (Orio et al., 2002; Torres et al., 2007; Pongs and Schwarz, 2010; Wu and Marx, 2010).

LOCALIZATION OF 2TM β SUBUNITS IN BK CHANNELS

Among the four 2TM β subunits, β1, β2, and β3 share higher sequence homology (53% similarity between β2 and β1; 37% similarity between β3 and β1), whereas β4 is less conserved (less than 20% similarity with β1; Wallner et al., 1999; Brenner et al., 2000; Xia et al., 2000). However, all four β subunits adopt a similar membrane topology that includes two TM segments (TM1 and TM2), a large extracellular loop (116–128 amino acid residues) and short cytosolic NH_2 and COOH termini (Knaus et al., 1994; Xia et al., 1999; Brenner et al., 2000; Orio et al., 2002; **Figure 1B**).

Different Slo1 orthologs respond to β subunits modulation differently. For instance, the β1 and β2 subunits alter the voltage- and Ca^{2+}-dependent activation of mammalian Slo1 (human hSlo1 and mouse mSlo1) channels more prominently than drosophila Slo1 (dSlo1; Wallner et al., 1996; Lee et al., 2010). Studies of chimerical channels of mammalian Slo1 and dSlo1 revealed that the S0 TM segment is important for the functional effects of β subunits (Wallner et al., 1996; Morrow et al., 2006; Lee et al., 2010).

By engineering disulfide linkages, Marx and colleagues model S0 outside of the VSD adjacent to the S3 and S4 helices, while the two TM segments of the β subunits (TM1 and TM2) are packed close to each other at the mouth of the cleft between VSDs of two adjacent Slo1 subunits (Liu et al., 2008a, 2010; **Figure 1B**). Within this cleft, TM1 is close to S1 of one VSD and TM2 close to S0 of the adjacent VSD (Liu et al., 2008b, 2010; Wu et al., 2009; Zakharov et al., 2009). This model gives rise to the possibility of direct interactions between β subunits and the Slo1 VSD within the membrane. Interestingly, although experimental data suggest that the TM segments of β1, β2, and β4 subunits similarly localize with the Slo1 VSD, the functional effects of these β subunits on the voltage-dependent activation of BK channels differ (see below).

The extracellular loop of β subunits has been shown to alter BK channel block by charybdotoxin (CTX) and iberiotoxin (IbTX; Hanner et al., 1998; Meera, 2000; Chen et al., 2008). These peptide toxins block the channel pore by binding to the extracellular vestibule. The extracellular loop of β subunits interacts with these toxins to either enhance or reduce channel block, suggesting that the extracellular loop may extend from the TM domain at the channel periphery into the external vestibule and alter the entrance of the channel pore (**Figure 1B**). This picture was supported by another study regarding the rectification mechanism of BK channels in the presence of β3, in which the authors suggested that the extracellular loop of the β3 subunit associates with the Slo1 subunit near the axis of the permeation pathway to form gates blocking ion permeation (Zeng et al., 2003). The extracellular loop of the β1 subunit affects voltage-dependent activation. A recently published work (Gruslova et al., 2012) identified a functional domain in the extracellular loop of β1, consisting of residues Y74, S104, Y105, and I106, that alters voltage-dependent activation, possibly by promoting VSD activation and reducing the intrinsic open probability of the PGD. The extracellular loop connects the channel periphery to the pore so that it may modulate voltage-dependent activation by providing an additional linkage between the VSD and PGD or through direct interactions with these Slo1 structural domains.

The location of the cytosolic termini of β subunits relative to the Slo1 subunit is not clear except that the NH_2 terminus of β2 subunits is known to contain an inactivating domain that blocks the entrance to the intracellular pore with a "ball-and-chain" mechanism indicating that the NH_2 can reach the internal vestibule (Wallner et al., 1999; Xia et al., 1999, 2003; Bentrop et al., 2001; Zhang et al., 2006, 2009; Li et al., 2007). Nevertheless, deletion mutations of the cytosolic NH_2 and COOH termini eliminate the major effects of the β1 subunit on voltage-dependent activation (Wang and Brenner, 2006), indicating that the termini play an important role in Slo1-β subunits interactions. Consistently, a study of the chimeras between the β1 and β2 subunits showed that switching the cytosolic termini between the two β subunits switched the phenotypes of modulation of voltage-dependence and kinetics of activation (Orio et al., 2006).

2TM β SUBUNITS REGULATION OF VSD ACTIVATION, PGD OPENING, AND COUPLING

The β1 subunit

Among four types of 2TM β subunits, the β1 subunit has the largest effect on voltage-dependent activation. Recordings of macroscopic and single channel currents in the absence of Ca^{2+} show that the β1 subunit shifts the G–V or P_o–V relationship to more positive voltages (∼+20 mV) and decreases the steepness of these curves, indicating that the β1 subunit reduces voltage-sensitivity of the channel (McManus et al., 1995; Cox and Aldrich, 2000; Nimigean, 2000; Orio and Latorre, 2005). The β1 subunit may alter all three general steps of voltage-dependent activation based on the following evidence. First, gating current recordings show that the β1 subunit shifts the voltage-dependence of gating charge movements (Q–V curve) to more negative voltages in the absence of Ca^{2+} (Bao and Cox, 2005), indicating an impact of the β1 subunit on VSD activation. Second, at negative voltages, where the VSDs are at the resting state, the open probability of the channel is reduced in the presence of the β1 subunit, indicating that the intrinsic opening of the PGD is affected (Orio and Latorre, 2005; Wang and Brenner, 2006). Finally, evidence for the β1 subunit modulating the coupling between the VSD and the activation gate comes from fitting the above data to the HCA model (Horrigan et al., 1999) that describes the allosteric mechanism of voltage-dependent activation of BK channels. In the HCA model the VSDs activate when the channel is either open or closed, but at the open state VSD activation is more likely at any given voltage (the resting-activation equilibrium increases D fold, D is called the allosteric factor describing coupling between VSD activation and PGD opening). Studies from various laboratories show that the β1 subunit alters the allosteric factor D (Cox and Aldrich, 2000; Bao and Cox, 2005; Orio and Latorre, 2005; Wang and Brenner, 2006), indicating changes in the coupling between VSD activation and PGD opening.

The modulation of voltage-dependant activation may be a major mechanism underlying another predominant effect of the β1 subunit: increasing Ca^{2+} sensitivity, i.e., a Ca^{2+} concentration change from 0 to 100 μM elicits a larger shift of the G–V relation toward negative voltages in the presence of the β1 subunit (McManus et al., 1995). In studies by a number of laboratories, the effects of the β1 subunit were fitted to the HA model that describes allosteric voltage- and Ca^{2+}-dependent activation of BK channels (Horrigan and Aldrich, 2002). These model fittings show that changes of VSD activation and the intrinsic probability of PGD opening account for a large portion of increased Ca^{2+} sensitivity observed in experiments, while the changes in Ca^{2+} binding and its coupling to the activation gate are relatively minor (Orio and Latorre, 2005; Wang and Brenner, 2006). Such a correlation between altered VSD activation and increased Ca^{2+} sensitivity may not be a coincidence. Mutations in the Slo1 VSD that alter VSD activation (Ma et al., 2006) have been shown to reduce the effect of the β1 subunit on Ca^{2+} sensitivity; interestingly, the degree to which a mutation alters voltage-sensor activation is inversely correlated with the magnitude of the β1 subunit's effects on Ca^{2+} sensitivity of the mutant channel (Yang et al., 2008). These results suggest that the β1 subunit increases Ca^{2+} sensitivity of BK channels by altering VSD activation. However, the molecular mechanism of how changes in VSD activation alter Ca^{2+} sensitivity is not clear.

Other β subunits

Unlike the β1 subunit, the β2 subunit effects on voltage-dependent activation of BK channels are minimal (Orio and Latorre, 2005).

While both β subunits enhance Ca^{2+} sensitivity, β2 does not shift the *G–V* curve of BK channels in the absence of Ca^{2+} (Orio and Latorre, 2005; Lee et al., 2010). Mutations in the Slo1 VSD that alter VSD activation and reduce the β1 subunit modulation of Ca^{2+} sensitivity have little impact on the β2 subunit modulation of Ca^{2+} sensitivity (Yang et al., 2008). On the other hand, the NH_2 terminus of the CTD (the AC region) and the peptide linker between S6 and the CTD (the C-linker) are important for the modulation of Ca^{2+} sensitivity by β2 but not β1 (Lee et al., 2010). These results suggest that the β2 subunit targets the CTD, not the VSD, to modulate BK channel Ca^{2+} sensitivity. Nevertheless, using VCF, Savalli et al. (2007) showed that the β2 subunit shifts the *F–V* relationship toward hyperpolarized potentials when the S3–S4 linker of the Slo1 was labeled with thiol-reactive fluorescent dyes to track VSD activation. This result suggests that association with β2 subunits alters voltage-sensor activation. A further study comparing the gating current generated in the absence and in the presence of the β2 subunit may shed additional light on whether the β2 subunit alters voltage-dependent activation.

The β4 subunit reduces the intrinsic open probability of the PGD in the absence of Ca^{2+} binding as well as voltage-sensor activation (Wang et al., 2006), which reduces channel opening and shifts the *G–V* relation to more positive voltages at $[Ca^{2+}]$ of $< \sim 6\,\mu M$ (Brenner et al., 2000; Wang et al., 2006; Lee and Cui, 2009). However, at $[Ca^{2+}] > \sim 10\,\mu M$, the β4 subunit shifts the *G–V* relation to less positive voltages due to a shift of voltage-sensor activation that compensates for the reduced intrinsic opening of the PGD (Wang et al., 2006). Thus, the β4 subunit seems to modify voltage-dependent activation similarly as the β1 subunit.

1TM LRRCs MODULATION OF VOLTAGE-DEPENDENT ACTIVATION

Leucine-rich-repeat-containing protein 26 (Yan and Aldrich, 2010) is a newly identified BK channel β subunit; the protein sequence and structure of which are unrelated to the 2TM BK β subunits. LRRC proteins constitute a large protein family. LRRC26 belongs to an extracellular leucine-rich-repeat-only (Elron) cluster (Dolan et al., 2007) that consists of members a single TM segment, an extracellular LRR motif, and a short cytosolic COOH tail containing a stretch of acidic residues (**Figure 1B**). LRRC proteins have recently begun to gain appreciation as β subunits of K_V channels. LRRC52, another member of Elron, is enriched in testis and a β subunit of Slo3 (Yang et al., 2011). Slo3 is activated by voltage and H^+ and is the α subunit of Ksper, the voltage and acid activated K^+ channel in sperm (Schreiber et al., 1998; Navarro et al., 2007). LRRC52 association shifts the Slo3 *G–V* to negative voltages that match with the *G–V* relation of native Ksper *in vivo* (Yang et al., 2011). Amphoterin-induced gene and ORF (AMIGO) is a LRRC protein belonging to a large LRRC-IG/FN3 protein cluster (Kuja-Panula, 2003). AMIGO has a single TM domain, an extracellular LRR motif and an extracellular immunoglobulin motif. AMIGO associates with and also left shifts the *G–V* relation of the $K_V2.1$ channel (Peltola et al., 2011).

The leftward shift of the *G–V* relationship caused by LRRC26 is dramatic, around −140 mV, which makes BK channels activate at negative voltages without rises in Ca^{2+} concentration. The effect of LRRC26 on channel activation is independent of Ca^{2+} since mutations of both Ca^{2+} binding sites of BK channels (Ca^{2+} bowl deleted and D362A/D367A) have no effect on LRRC26 modulation. Fitting the HCA model showed that LRRC26 modulates BK channel activation mainly through a large enhancement (∼20-fold) of the allosteric factor *D*, suggesting that LRRC26 affects coupling between the VSD and PGD. The location of LRRC26 relative to Slo1 is not known. However, coexpression of Slo1 with both LRRC26 and the 2TM β1 subunit results in channels with the phenotype of Slo1 + β1, suggesting that the β1 subunit may compete with LRRC26 for a similar association site and prevent LRRC26 from binding. Functional analyses of LRRC26 deletion mutants indicate that except for the fifth leucine-rich-repeat (LRR5) motif and the cytosolic polyPD motif that contains multiple proline and aspartate repeats (residues 304–316), deletion of any region abolishes the function of LRRC26, while only the putative TM segment is necessary for association with Slo1 (Yan and Aldrich, 2010). These results further suggest that the TM segment of LRRC26 may be localized in the cleft between VSDs of the adjacent Slo1 subunits, similar to the 2TM BK channel β subunits and KCNE peptides.

CONCLUDING REMARKS

The studies of TM β subunits' regulation of K_V channels reveal common properties. First, the inter VSD cleft provides a docking site for the TM segment(s) offering the starting point for regulation of voltage-dependent activation. This conserved structural feature may be the basis for the promiscuity of some of the TM β subunits. Second, all three domains of the β subunits (extracellular, TM, intracellular) participate in the interactions with the K_V α subunit that modulate voltage-dependent activation; although, the specific interactions governing phenotypical changes are not entirely clear. Third, consistent with the structural understanding, β subunit interaction may affect all three general events of voltage-dependent activation; i.e., VSD activation, coupling, and PGD opening. All these results suggest that there is no single deciding interaction, or even a simple additive sum of individual interactions, that is responsible for the phenotype changes that are observed experimentally. Rather, the cooperation among multiple individual interactions may synergistically bring about the unique structure and function of the K_V α+β complex.

AUTHOR CONTRIBUTION

Mark A. Zaydman wrote the part on KCNEs; Xiaohui Sun wrote the part on BK channel β subunits; Jianmin Cui, Xiaohui Sun, and Mark A. Zaydman integrated the whole paper.

ACKNOWLEDGMENTS

We thank Dr. Yoram Rudy for reading and commenting on the KCNEs part of the manuscript. This work was supported by National Institutes of Health Grants R01-HL70393 and R01-NS060706 (Jianmin Cui). Jianmin Cui is the Professor of Biomedical Engineering on the Spencer T. Olin Endowment.

REFERENCES

Abbott, G. W., Sesti, F., Splawski, I., Buck, M. E., Lehmann, M. H., Timothy, K. W., Keating, M. T., and Goldstein, S. A. (1999). MiRP1 forms IKr potassium channels with HERG and is associated with cardiac arrhythmia. *Cell* 97, 175–187.

Angelo, K., Jespersen, T., Grunnet, M., Nielsen, M. S., Klaerke, D. A., and Olesen, S.-P. (2002). KCNE5 induces time- and voltage-dependent modulation of the KCNQ1 current. *Biophys. J.* 83, 1997–2006.

Bao, L., and Cox, D. H. (2005). Gating and ionic currents reveal how the BKCa channel's Ca^{2+} sensitivity is enhanced by its beta1 subunit. *J. Gen. Physiol.* 126, 393–412.

Barhanin, J., Lesage, F., Guillemare, E., Fink, M., Lazdunski, M., and Romey, G. (1996). K(V)LQT1 and lsK (minK) proteins associate to form the I(Ks) cardiac potassium current. *Nature* 384, 78–80.

Behrens, R., Nolting, A., Reimann, F., Schwarz, M., Waldschutz, R., and Pongs, O. (2000). hKCNMB3 and hKCNMB4, cloning and characterization of two members of the large-conductance calcium-activated potassium channel beta subunit family. *FEBS Lett.* 474, 99–106.

Bellocq, C., Van Ginneken, A. C. G., Bezzina, C. R., Alders, M., Escande, D., Mannens, M. M. A. M., Baro, I., and Wilde, A. A. M. (2004). Mutation in the KCNQ1 gene leading to the short QT-interval syndrome. *Circulation* 109, 2394–2397.

Bentrop, D., Beyermann, M., Wissmann, R., and Fakler, B. (2001). NMR structure of the "ball-and-chain" domain of KCNMB2, the beta 2-subunit of large conductance Ca^{2+}- and voltage-activated potassium channels. *J. Biol. Chem.* 276, 42116–42121.

Bezanilla, F. (2008). How membrane proteins sense voltage. *Nat. Rev. Mol. Cell Biol.* 9, 323–332.

Boulet, I. R., Labro, A. J., Raes, A. L., and Snyders, D. J. (2007). Role of the S6 C-terminus in KCNQ1 channel gating. *J. Physiol.* 585, 325–337.

Brayden, J. E., and Nelson, M. T. (1992). Regulation of arterial tone by activation of calcium-dependent potassium channels. *Science* 256, 532–535.

Brenner, R., Jegla, T. J., Wickenden, A., Liu, Y., and Aldrich, R. W. (2000). Cloning and functional characterization of novel large conductance calcium-activated potassium channel beta subunits, hKCNMB3 and hKCNMB4. *J. Biol. Chem.* 275, 6453–6461.

Busch, A. E., Busch, G. L., Ford, E., Suessbrich, H., Lang, H. J., Greger, R., Kunzelmann, K., Attali, B., and Stühmer, W. (1997). The role of the IsK protein in the specific pharmacological properties of the IKs channel complex. *Br. J. Pharmacol.* 122, 187–189.

Chan, P. J., Osteen, J. D., Xiong, D., Bohnen, M. S., Doshi, D., Sampson, K. J., Marx, S. O., Karlin, A., and Kass, R. S. (2012). Characterization of KCNQ1 atrial fibrillation mutations reveals distinct dependence on KCNE1. *J. Gen. Physiol.* 139, 135–144.

Chen, J., Zheng, R., Melman, Y. F., and McDonald, T. V. (2009). Functional interactions between KCNE1 C-terminus and the KCNQ1 channel. *PLoS ONE* 4, e5143. doi:10.1371/journal.pone.0005143

Chen, M., Gan, G., Wu, Y., Wang, L., and Ding, J. (2008). Lysine-rich extracellular rings formed by hβ2 subunits confer the outward rectification of BK channels. *PLoS ONE* 3, e2114. doi:10.1371/journal.pone.0002114

Chen, Y.-H., Xu, S.-J., Bendahhou, S., Wang, X.-L., Wang, Y., Xu, W.-Y., Jin, H.-W., Sun, H., Su, X.-Y., Zhuang, Q.-N., Yang, Y.-Q., Li, Y.-B., Liu, Y., Xu, H.-J., Li, X.-F., Ma, N., Mou, C.-P., Chen, Z., Barhanin, J., and Huang, W. (2003). KCNQ1 gain-of-function mutation in familial atrial fibrillation. *Science* 299, 251–254.

Chung, D. Y., Chan, P. J., Bankston, J. R., Yang, L., Liu, G., Marx, S. O., Karlin, A., and Kass, R. S. (2009). Location of KCNE1 relative to KCNQ1 in the I(KS) potassium channel by disulfide cross-linking of substituted cysteines. *Proc. Natl. Acad. Sci. U.S.A.* 106, 743–748.

Cox, D. H., and Aldrich, R. W. (2000). Role of the beta1 subunit in large-conductance Ca(2+)-activated K (+) channel gating energetics. Mechanisms of enhanced Ca(2+) sensitivity. *J. Gen. Physiol.* 116, 411–432.

Das, S., Makino, S., Melman, Y. F., Shea, M. A., Goyal, S. B., Rosenzweig, A., Macrae, C. A., and Ellinor, P. T. (2009). Mutation in the S3 segment of KCNQ1 results in familial lone atrial fibrillation. *Heart rhythm* 6, 1146–1153.

Dolan, J., Walshe, K., Alsbury, S., Hokamp, K., O'Keeffe, S., Okafuji, T., Miller, S. F. C., Tear, G., and Mitchell, K. J. (2007). The extracellular leucine-rich repeat superfamily; a comparative survey and analysis of evolutionary relationships and expression patterns. *BMC Genomics* 8, 320. doi:10.1186/1471-2164-10-230

Franqueza, L., Lin, M., Shen, J., Splawski, I., Keating, M. T., and Sanguinetti, M. C. (1999). Long QT syndrome-associated mutations in the S4–S5 linker of KvLQT1 potassium channels modify gating and interaction with minK subunits. *J. Biol. Chem.* 274, 21063–21070.

Gage, S. D., and Kobertz, W. R. (2004). KCNE3 truncation mutants reveal a bipartite modulation of KCNQ1 K+ channels. *J. Gen. Physiol.* 124, 759–771.

Goldstein, S. A., and Miller, C. (1991). Site-specific mutations in a minimal voltage-dependent K+ channel alter ion selectivity and open-channel block. *Neuron* 7, 403–408.

Grabe, M., Lai, H. C., Jain, M., Jan, Y. N., and Jan, L. Y. (2007). Structure prediction for the down state of a potassium channel voltage sensor. *Nature* 445, 550–553.

Grunnet, M., Jespersen, T., Rasmussen, H. B., Ljungstrøm, T., Jorgensen, N. K., Olesen, S.-P., and Klaerke, D. A. (2002). KCNE4 is an inhibitory subunit to the KCNQ1 channel. *J. Physiol.* 542, 119–130.

Gruslova, A., Semenov, I., and Wang, B. (2012). An extracellular domain of the accessory beta1 subunit is required for modulating BK channel voltage sensor and gate. *J. Gen. Physiol.* 139, 57–67.

Haddad, G. A., and Blunck, R. (2011). Mode shift of the voltage sensors in Shaker K+ channels is caused by energetic coupling to the pore domain. *J. Gen. Physiol.* 137, 455–472.

Haitin, Y., Wiener, R., Shaham, D., Peretz, A., Cohen, E. B.-T., Shamgar, L., Pongs, O., Hirsch, J. A., and Attali, B. (2009). Intracellular domains interactions and gated motions of I(KS) potassium channel subunits. *EMBO J.* 28, 1994–2005.

Hanner, M., Vianna-Jorge, R., Kamassah, A., Schmalhofer, W. A., Knaus, H. G., Kaczorowski, G. J., and Garcia, M. L. (1998). The beta subunit of the high conductance calcium-activated potassium channel. Identification of residues involved in charybdotoxin binding. *J. Biol. Chem.* 273, 16289–16296.

Hedley, P. L., Jørgensen, P., Schlamowitz, S., Wangari, R., Moolman-Smook, J., Brink, P. A., Kanters, J. K., Corfield, V. A., and Christiansen, M. (2009). The genetic basis of long QT and short QT syndromes: a mutation update. *Hum. Mutat.* 30, 1486–1511.

Hong, K., Piper, D. R., Diaz-Valdecantos, A., Brugada, J., Oliva, A., Burashnikov, E., Santos-De-Soto, J., Grueso-Montero, J., Diaz-Enfante, E., Brugada, P., Sachse, F., Sanguinetti, M. C., and Brugada, R. (2005). De novo KCNQ1 mutation responsible for atrial fibrillation and short QT syndrome in utero. *Cardiovasc. Res.* 68, 433–440.

Horrigan, F. T., and Aldrich, R. W. (2002). Coupling between voltage sensor activation, Ca^{2+} binding and channel opening in large conductance (BK) potassium channels. *J. Gen. Physiol.* 120, 267–305.

Horrigan, F. T., Cui, J., and Aldrich, R. W. (1999). Allosteric voltage gating of potassium channels I. Mslo ionic currents in the absence of Ca(2+). *J. Gen. Physiol.* 114, 277–304.

Jost, N., Papp, J. G., and Varró, A. (2007). Slow delayed rectifier potassium current (IKs) and the repolarization reserve. *Ann. Noninvasive Electrocardiol.* 12, 64–78.

Kang, C., Tian, C., Sönnichsen, F. D., Smith, J. A., Meiler, J., George, A. L., Vanoye, C. G., Kim, H. J., and Sanders, C. R. (2008). Structure of KCNE1 and implications for how it modulates the KCNQ1 potassium channel. *Biochemistry* 47, 7999–8006.

Knaus, H. G., Folander, K., Garcia-Calvo, M., Garcia, M. L., Kaczorowski, G. J., Smith, M., and Swanson, R. (1994). Primary sequence and immunological characterization of beta-subunit of high conductance Ca(2+)-activated K^+ channel from smooth muscle. *J. Biol. Chem.* 269, 17274–17278.

Koval, O. M., Fan, Y., and Rothberg, B. S. (2007). A role for the S0 transmembrane segment in voltage-dependent gating of BK channels. *J. Gen. Physiol.* 129, 209–220.

Kuja-Panula, J. (2003). AMIGO, a transmembrane protein implicated in axon tract development, defines a novel protein family with leucine-rich repeats. *J. Cell Biol.* 160, 963–973.

Kurokawa, J., Bankston, J. R., Kaihara, A., Chen, L., Furukawa, T., and Kass, R. S. (2009). KCNE variants reveal a critical role of the beta subunit carboxyl terminus in PKA-dependent regulation of the IKs potassium channel. *Channels (Austin)* 3, 16–24.

Kurokawa, J., Chen, L., and Kass, R. S. (2003). Requirement of subunit

expression for cAMP-mediated regulation of a heart potassium channel. *Proc. Natl. Acad. Sci. U.S.A.* 100, 2122–2127.

Labro, A. J., Boulet, I. R., Choveau, F. S., Mayeur, E., Bruyns, T., Loussouarn, G., Raes, A. L., and Snyders, D. J. (2011). The S4–S5 linker of KCNQ1 channels forms a structural scaffold with the S6 segment controlling gate closure. *J. Biol. Chem.* 286, 717–725.

Lancaster, B., and Nicoll, R. A. (1987). Properties of two calcium-activated hyperpolarizations in rat hippocampal neurones. *J. Physiol.* 389, 187–203.

Ledwell, J. L., and Aldrich, R. W. (1999). Mutations in the S4 region isolate the final voltage-dependent cooperative step in potassium channel activation. *J. Gen. Physiol.* 113, 389–414.

Lee, S.-Y., Banerjee, A., and Mackinnon, R. (2009). Two separate interfaces between the voltage sensor and pore are required for the function of voltage-dependent K^+ channels. *PLoS Biol.* 7, e47. doi:10.1371/journal.pbio.1000047

Lee, U. S., and Cui, J. (2009). {beta} subunit-specific modulations of BK channel function by a mutation associated with epilepsy and dyskinesia. *J. Physiol.* 587, 1481–1498.

Lee, U. S., Shi, J., and Cui, J. (2010). Modulation of BK channel gating by the ss2 subunit involves both membrane-spanning and cytoplasmic domains of Slo1. *J. Neurosci.* 30, 16170–16179.

Lerche, C., Seebohm, G., Wagner, C. I., Scherer, C. R., Dehmelt, L., Abitbol, I., Gerlach, U., Brendel, J., Attali, B., and Busch, A. E. (2000). Molecular impact of MinK on the enantiospecific block of I(Ks) by chromanols. *Br. J. Pharmacol.* 131, 1503–1506.

Li, H., Yao, J., Tong, X., Guo, Z., Wu, Y., Sun, L., Pan, N., Wu, H., Xu, T., and Ding, J. (2007). Interaction sites between the Slo1 pore and the NH2 terminus of the beta2 subunit, probed with a three-residue sensor. *J. Biol. Chem.* 282, 17720–17728.

Li, Y., Zaydman, M. A., Wu, D., Shi, J., Guan, M., Virgin-Downey, B., and Cui, J. (2011). KCNE1 enhances phosphatidylinositol 4,5-bisphosphate (PIP2) sensitivity of IKs to modulate channel activity. *Proc. Natl. Acad. Sci. U.S.A.* 108, 9095–9100.

Liu, G., Niu, X., Wu, R. S., Chudasama, N., Yao, Y., Jin, X., Weinberg, R., Zakharov, S. I., Motoike, H., Marx, S. O., and Karlin, A. (2010). Location of modulatory beta subunits in BK potassium channels. *J. Gen. Physiol.* 135, 449–459.

Liu, G., Zakharov, S. I., Yang, L., Deng, S. X., Landry, D. W., Karlin, A., and Marx, S. O. (2008a). Position and role of the BK channel alpha subunit S0 helix inferred from disulfide crosslinking. *J. Gen. Physiol.* 131, 537–548.

Liu, G., Zakharov, S. I., Yang, L., Wu, R. S., Deng, S. X., Landry, D. W., Karlin, A., and Marx, S. O. (2008b). Locations of the 1 transmembrane helices in the BK potassium channel. *Proc. Natl. Acad. Sci. U.S.A.* 105, 10727–10732.

Long, S. B., Campbell, E. B., and Mackinnon, R. (2005). Voltage sensor of Kv1.2: structural basis of electromechanical coupling. *Science* 309, 903–908.

Lu, Z., Klem, A. M., and Ramu, Y. (2001). Ion conduction pore is conserved among potassium channels. *Nature* 413, 809–813.

Lundby, A., Ravn, L. S., Svendsen, J. H., Olesen, S.-P., and Schmitt, N. (2007). KCNQ1 mutation Q147R is associated with atrial fibrillation and prolonged QT interval. *Heart rhythm* 4, 1532–1541.

Lvov, A., Gage, S. D., Berrios, V. M., and Kobertz, W. R. (2010). Identification of a protein–protein interaction between KCNE1 and the activation gate machinery of KCNQ1. *J. Gen. Physiol.* 135, 607–618.

Ma, Z., Lou, X. J., and Horrigan, F. T. (2006). Role of charged residues in the S1–S4 voltage sensor of BK channels. *J. Gen. Physiol.* 127, 309–328.

Marty, A. (1981). Ca-dependent K channels with large unitary conductance in chromaffin cell membranes. *Nature* 291, 497–500.

Marx, S. O., Kurokawa, J., Reiken, S., Motoike, H., D'Armiento, J., Marks, A. R., and Kass, R. S. (2002). Requirement of a macromolecular signaling complex for beta adrenergic receptor modulation of the KCNQ1-KCNE1 potassium channel. *Science* 295, 496–499.

McManus, O. B., Helms, L. M., Pallanck, L., Ganetzky, B., Swanson, R., and Leonard, R. J. (1995). Functional role of the beta subunit of high conductance calcium-activated potassium channels. *Neuron* 14, 645–650.

Meera, P. (2000). A neuronal beta subunit (KCNMB4) makes the large conductance, voltage- and Ca^{2+}-activated K^+ channel resistant to charybdotoxin and iberiotoxin. *Proc. Natl. Acad. Sci. U.S.A.* 97, 5562–5567.

Melman, Y. F., Domènech, A., De La Luna, S., and McDonald, T. V. (2001). Structural determinants of KvLQT1 control by the KCNE family of proteins. *J. Biol. Chem.* 276, 6439–6444.

Melman, Y. F., Krumerman, A., and McDonald, T. V. (2002). A single transmembrane site in the KCNE-encoded proteins controls the specificity of KvLQT1 channel gating. *J. Biol. Chem.* 277, 25187–25194.

Melman, Y. F., Um, S. Y., Krumerman, A., Kagan, A., and McDonald, T. V. (2004). KCNE1 binds to the KCNQ1 pore to regulate potassium channel activity. *Neuron* 42, 927–937.

Morrow, J. P., Zakharov, S. I., Liu, G., Yang, L., Sok, A. J., and Marx, S. O. (2006). Defining the BK channel domains required for beta1-subunit modulation. *Proc. Natl. Acad. Sci. U.S.A.* 103, 5096–5101.

Nakajo, K., and Kubo, Y. (2007). KCNE1 and KCNE3 stabilize and/or slow voltage sensing S4 segment of KCNQ1 channel. *J. Gen. Physiol.* 130, 269–281.

Nakajo, K., Nishino, A., Okamura, Y., and Kubo, Y. (2011). KCNQ1 subdomains involved in KCNE modulation revealed by an invertebrate KCNQ1 orthologue. *J. Gen. Physiol.* 138, 521–535.

Navarro, B., Kirichok, Y., and Clapham, D. E. (2007). KSper, a pH-sensitive K^+ current that controls sperm membrane potential. *Proc. Natl. Acad. Sci. U.S.A.* 104, 7688–7692.

Nimigean, C. M. (2000). Functional coupling of the beta1 subunit to the large conductance Ca^{2+}-activated K^+ channel in the absence of $Ca2^+$: increased Ca^{2+} sensitivity from a Ca^{2+}-independent mechanism. *J. Gen. Physiol.* 115, 719–736.

Nimigean, C. M., and Magleby, K. L. (1999). The beta subunit increases the Ca^{2+} sensitivity of large conductance $Ca2^+$-activated potassium channels by retaining the gating in the bursting states. *J. Gen. Physiol.* 113, 425–440.

Orio, P., and Latorre, R. (2005). Differential effects of beta 1 and beta 2 subunits on BK channel activity. *J. Gen. Physiol.* 125, 395–411.

Orio, P., Rojas, P., Ferreira, G., and Latorre, R. (2002). New disguises for an old channel: MaxiK channel beta-subunits. *News Physiol. Sci.* 17, 156–161.

Orio, P., Torres, Y., Rojas, P., Carvacho, I., Garcia, M. L., Toro, L., Valverde, M. A., and Latorre, R. (2006). Structural determinants for functional coupling between the beta and alpha subunits in the Ca^{2+}-activated K^+ (BK) channel. *J. Gen. Physiol.* 127, 191–204.

Osteen, J. D., Gonzalez, C., Sampson, K. J., Iyer, V., Rebolledo, S., Larsson, H. P., and Kass, R. S. (2010). KCNE1 alters the voltage sensor movements necessary to open the KCNQ1 channel gate. *Proc. Natl. Acad. Sci. U.S.A.* 107, 22710–22715.

Peltola, M. A., Kuja-Panula, J., Lauri, S. E., Taira, T., and Rauvala, H. (2011). AMIGO is an auxiliary subunit of the Kv2.1 potassium channel. *EMBO Rep.* 12, 1293–1299.

Piccini, M., Vitelli, F., Seri, M., Galietta, L. J., Moran, O., Bulfone, A., Banfi, S., Pober, B., and Renieri, A. (1999). KCNE1-like gene is deleted in AMME contiguous gene syndrome: identification and characterization of the human and mouse homologs. *Genomics* 60, 251–257.

Pongs, O., and Schwarz, J. R. (2010). Ancillary subunits associated with voltage-dependent K^+ channels. *Physiol. Rev.* 90, 755–796.

Pusch, M., Magrassi, R., Wollnik, B., and Conti, F. (1998). Activation and inactivation of homomeric KvLQT1 potassium channels. *Biophys. J.* 75, 785–792.

Rocheleau, J. M., and Kobertz, W. R. (2008). KCNE peptides differently affect voltage sensor equilibrium and equilibration rates in KCNQ1 K^+ channels. *J. Gen. Physiol.* 131, 59–68.

Sanguinetti, M. C., Curran, M. E., Zou, A., Shen, J., Spector, P. S., Atkinson, D. L., and Keating, M. T. (1996). Coassembly of K(V)LQT1 and minK (IsK) proteins to form cardiac I(Ks) potassium channel. *Nature* 384, 80–83.

Sanguinetti, M. C., and Jurkiewicz, N. K. (1990). Two components of cardiac delayed rectifier K^+ current. Differential sensitivity to block by class III antiarrhythmic agents. *J. Gen. Physiol.* 96, 195–215.

Savalli, N., Kondratiev, A., De Quintana, S. B., Toro, L., and Olcese, R. (2007). Modes of operation of the BKCa channel beta2 subunit. *J. Gen. Physiol.* 130, 117–131.

Schreiber, M., Wei, A., Yuan, A., Gaut, J., Saito, M., and Salkoff, L. (1998). Slo3, a novel pH-sensitive K^+ channel from mammalian spermatocytes. *J. Biol. Chem.* 273, 3509–3516.

Schroeder, B. C., Waldegger, S., Fehr, S., Bleich, M., Warth, R., Greger, R., and Jentsch, T. J. (2000). A constitutively open potassium channel formed by

KCNQ1 and KCNE3. *Nature* 403, 196–199.

Sesti, F., and Goldstein, S. A. (1998). Single-channel characteristics of wild-type IKs channels and channels formed with two minK mutants that cause long QT syndrome. *J. Gen. Physiol.* 112, 651–663.

Shamgar, L., Haitin, Y., Yisharel, I., Malka, E., Schottelndreier, H., Peretz, A., Paas, Y., and Attali, B. (2008). KCNE1 constrains the voltage sensor of Kv7.1 K^+ channels. *PLoS ONE* 3, e1943. doi:10.1371/journal.pone.0001943

Silva, J., and Rudy, Y. (2005). Subunit interaction determines IKs participation in cardiac repolarization and repolarization reserve. *Circulation* 112, 1384–1391.

Soler-Llavina, G. J., Chang, T. H., and Swartz, K. J. (2006). Functional interactions at the interface between voltage-sensing and pore domains in the Shaker K(v) channel. *Neuron* 52, 623–634.

Splawski, I., Tristani-Firouzi, M., Lehmann, M. H., Sanguinetti, M. C., and Keating, M. T. (1997). Mutations in the hminK gene cause long QT syndrome and suppress IKs function. *Nat. Genet.* 17, 338–340.

Storm, J. F. (1987). Action potential repolarization and a fast after-hyperpolarization in rat hippocampal pyramidal cells. *J. Physiol.* 385, 733–759.

Strutz-Seebohm, N., Pusch, M., Wolf, S., Stoll, R., Tapken, D., Gerwert, K., Attali, B., and Seebohm, G. (2011). Structural basis of slow activation gating in the cardiac I Ks channel complex. *Cell. Physiol. Biochem.* 27, 443–452.

Tai, K. K., and Goldstein, S. A. (1998). The conduction pore of a cardiac potassium channel. *Nature* 391, 605–608.

Takumi, T., Moriyoshi, K., Aramori, I., Ishii, T., Oiki, S., Okada, Y., Ohkubo, H., and Nakanishi, S. (1991). Alteration of channel activities and gating by mutations of slow ISK potassium channel. *J. Biol. Chem.* 266, 22192–22198.

Takumi, T., Ohkubo, H., and Nakanishi, S. (1988). Cloning of a membrane protein that induces a slow voltage-gated potassium current. *Science* 242, 1042–1045.

Tapper, A. R., and George, A. L. (2000). MinK subdomains that mediate modulation of and association with KvLQT1. *J. Gen. Physiol.* 116, 379–390.

Tapper, A. R., and George, A. L. (2001). Location and orientation of minK within the I(Ks) potassium channel complex. *J. Biol. Chem.* 276, 38249–38254.

Tinel, N., Diochot, S., Borsotto, M., Lazdunski, M., and Barhanin, J. (2000). KCNE2 confers background current characteristics to the cardiac KCNQ1 potassium channel. *EMBO J.* 19, 6326–6330.

Tombola, F., Pathak, M. M., and Isacoff, E. Y. (2005). How far will you go to sense voltage? *Neuron* 48, 719–725.

Torres, Y. P., Morera, F. J., Carvacho, I., and Latorre, R. (2007). A marriage of convenience: beta-subunits and voltage-dependent K+ channels. *J. Biol. Chem.* 282, 24485–24489.

Tristani-Firouzi, M., Chen, J., and Sanguinetti, M. C. (2002). Interactions between S4–S5 linker and S6 transmembrane domain modulate gating of HERG K^+ channels. *J. Biol. Chem.* 277, 18994–19000.

Tristani-Firouzi, M., and Sanguinetti, M. C. (1998). Voltage-dependent inactivation of the human K^+ channel KvLQT1 is eliminated by association with minimal K^+ channel (minK) subunits. *J. Physiol.* 510(Pt 1), 37–45.

Valverde, M. A., Rojas, P., Amigo, J., Cosmelli, D., Orio, P., Bahamonde, M. I., Mann, G. E., Vergara, C., and Latorre, R. (1999). Acute activation of Maxi-K channels (hSlo) by estradiol binding to the beta subunit. *Science* 285, 1929–1931.

Van Horn, W. D., Vanoye, C. G., and Sanders, C. R. (2011). Working model for the structural basis for KCNE1 modulation of the KCNQ1 potassium channel. *Curr. Opin. Struct. Biol.* 21, 283–291.

Vetter, D. E., Mann, J. R., Wangemann, P., Liu, J., Mclaughlin, K. J., Lesage, F., Marcus, D. C., Lazdunski, M., Heinemann, S. F., and Barhanin, J. (1996). Inner ear defects induced by null mutation of the isk gene. *Neuron* 17, 1251–1264.

Volders, P. G. A., Stengl, M., Van Opstal, J. M., Gerlach, U., Spätjens, R. L. H. M. G., Beekman, J. D. M., Sipido, K. R., and Vos, M. A. (2003). Probing the contribution of IKs to canine ventricular repolarization: key role for beta-adrenergic receptor stimulation. *Circulation* 107, 2753–2760.

Wallner, M., Meera, P., and Toro, L. (1996). Determinant for beta-subunit regulation in high-conductance voltage-activated and Ca(2+)-sensitive K^+ channels: an additional transmembrane region at the N terminus. *Proc. Natl. Acad. Sci. U.S.A.* 93, 14922–14927.

Wallner, M., Meera, P., and Toro, L. (1999). Molecular basis of fast inactivation in voltage and Ca^{2+}-activated K^+ channels: a transmembrane beta-subunit homolog. *Proc. Natl. Acad. Sci. U.S.A.* 96, 4137–4142.

Wang, B., and Brenner, R. (2006). An S6 mutation in BK channels reveals beta1 subunit effects on intrinsic and voltage-dependent gating. *J. Gen. Physiol.* 128, 731–744.

Wang, B., Rothberg, B. S., and Brenner, R. (2006). Mechanism of beta4 subunit modulation of BK channels. *J. Gen. Physiol.* 127, 449–465.

Wang, K. W., Tai, K. K., and Goldstein, S. A. (1996a). MinK residues line a potassium channel pore. *Neuron* 16, 571–577.

Wang, Q., Curran, M. E., Splawski, I., Burn, T. C., Millholland, J. M., Vanraay, T. J., Shen, J., Timothy, K. W., Vincent, G. M., De Jager, T., Schwartz, P. J., Toubin, J. A., Moss, A. J., Atkinson, D. L., Landes, G. M., Connors, T. D., and Keating, M. T. (1996b). Positional cloning of a novel potassium channel gene: KVLQT1 mutations cause cardiac arrhythmias. *Nat. Genet.* 12, 17–23.

Wang, Y. H., Jiang, M., Xu, X. L., Hsu, K.-L., Zhang, M., and Tseng, G.-N. (2011). Gating-related molecular motions in the extracellular domain of the IKs channel: implications for IKs channelopathy. *J. Membr. Biol.* 239, 137–156.

Wu, D., Delaloye, K., Zaydman, M. A., Nekouzadeh, A., Rudy, Y., and Cui, J. (2010a). State-dependent electrostatic interactions of S4 arginines with E1 in S2 during Kv7.1 activation. *J. Gen. Physiol.* 135, 595–606.

Wu, D., Pan, H., Delaloye, K., and Cui, J. (2010b). KCNE1 remodels the voltage sensor of Kv7.1 to modulate channel function. *Biophys. J.* 99, 3599–3608.

Wu, R. S., Chudasama, N., Zakharov, S. I., Doshi, D., Motoike, H., Liu, G., Yao, Y., Niu, X., Deng, S. X., Landry, D. W., Karlin, A., and Marx, S. O. (2009). Location of the beta 4 transmembrane helices in the BK potassium channel. *J. Neurosci.* 29, 8321–8328.

Wu, R. S., and Marx, S. O. (2010). The BK potassium channel in the vascular smooth muscle and kidney: alpha- and beta-subunits. *Kidney Int.* 78, 963–974.

Xia, X. M., Ding, J. P., and Lingle, C. J. (1999). Molecular basis for the inactivation of Ca^{2+}- and voltage-dependent BK channels in adrenal chromaffin cells and rat insulinoma tumor cells. *J. Neurosci.* 19, 5255–5264.

Xia, X. M., Ding, J. P., and Lingle, C. J. (2003). Inactivation of BK channels by the NH2 terminus of the beta2 auxiliary subunit: an essential role of a terminal peptide segment of three hydrophobic residues. *J. Gen. Physiol.* 121, 125–148.

Xia, X. M., Ding, J. P., Zeng, X. H., Duan, K. L., and Lingle, C. J. (2000). Rectification and rapid activation at low Ca^{2+} of Ca^{2+}-activated, voltage-dependent BK currents: consequences of rapid inactivation by a novel beta subunit. *J. Neurosci.* 20, 4890–4903.

Xu, X., Jiang, M., Hsu, K.-L., Zhang, M., and Tseng, G.-N. (2008). KCNQ1 and KCNE1 in the IKs channel complex make state-dependent contacts in their extracellular domains. *J. Gen. Physiol.* 131, 589–603.

Yan, J., and Aldrich, R. W. (2010). LRRC26 auxiliary protein allows BK channel activation at resting voltage without calcium. *Nature* 466, 513–516.

Yang, C., Zeng, X.-H., Zhou, Y., Xia, X.-M., and Lingle, C. J. (2011). LRRC52 (leucine-rich-repeat-containing protein 52), a testis-specific auxiliary subunit of the alkalization-activated Slo3 channel. *Proc. Natl. Acad. Sci. U.S.A.* 108, 19419–19424.

Yang, H., Zhang, G., Shi, J., Lee, U. S., Delaloye, K., and Cui, J. (2008). Subunit-specific effect of the voltage sensor domain on Ca^{2+} sensitivity of BK channels. *Biophys. J.* 94, 4678–4687.

Yang, Y., and Sigworth, F. J. (1998). Single-channel properties of IKs potassium channels. *J. Gen. Physiol.* 112, 665–678.

Yellen, G. (1998). The moving parts of voltage-gated ion channels. *Q. Rev. Biophys.* 31, 239–295.

Zagotta, W. N., Hoshi, T., and Aldrich, R. W. (1994). Shaker potassium channel gating. III: Evaluation of kinetic models for activation. *J. Gen. Physiol.* 103, 321–362.

Zakharov, S. I., Wu, R. S., Liu, G., Motoike, H., Karlin, A., and Marx, S. O. (2009). "Locations of the Beta2 transmembrane helices in the BK potassium channel," in *53rd Annual Biophysical Society Meeting*, Boston, MA.

Zeng, X. H., Xia, X. M., and Lingle, C. J. (2003). Redox-sensitive extracellular gates formed by auxiliary beta subunits of calcium-activated potassium channels. *Nat. Struct. Biol.* 10, 448–454.

Zhang, Z., Zeng, X. H., Xia, X. M., and Lingle, C. J. (2009). N-terminal inactivation domains of beta subunits are protected from trypsin digestion by binding within the antechamber of BK channels. *J. Gen. Physiol.* 133, 263–282.

Zhang, Z., Zhou, Y., Ding, J. P., Xia, X. M., and Lingle, C. J. (2006). A limited access compartment between the pore domain and cytosolic domain of the BK channel. *J. Neurosci.* 26, 11833–11843.

Conflict of Interest Statement: The authors declare that the research was conducted in the absence of any commercial or financial relationships that could be construed as a potential conflict of interest.

Received: 09 February 2012; accepted: 29 March 2012; published online: 17 April 2012.

*Citation: Sun X, Zaydman MA and Cui J (2012) Regulation of voltage-activated K^+ channel gating by transmembrane β subunits. Front. Pharmacol. **3**:63. doi: 10.3389/fphar.2012.00063*

This article was submitted to Frontiers in Pharmacology of Ion Channels and Channelopathies, a specialty of Frontiers in Pharmacology.

frontiers in
PHARMACOLOGY

REVIEW ARTICLE
published: 02 August 2012
doi: 10.3389/fphar.2012.00142

The KCNE tango – how KCNE1 interacts with Kv7.1

Eva Wrobel [1,2]***, Daniel Tapken*** [3] ***and Guiscard Seebohm*** [2]******

[1] *Cation Channel Group, Department of Biochemistry I, Faculty of Chemistry and Biochemistry, Ruhr University Bochum, Bochum, Germany*
[2] *Myozelluläre Elektrophysiologie und Molekularbiologie, Westfälische Wilhelms-Universität Münster, Münster, Germany*
[3] *Department of Drug Design and Pharmacology, University of Copenhagen, Copenhagen, Denmark*

Edited by:
Gildas Loussouarn, University of Nantes, France

Reviewed by:
Robert Kass, Colombia University in the city of New York, USA
Tom V. McDonald, Albert Einstein College of Medicine, USA

****Correspondence:***
Guiscard Seebohm, Myozelluläre Elektrophysiologie und Molekularbiologie, Westfälische Wilhelms-Universität Münster, Domagkstraße 3, 48149 Münster, Germany.
e-mail: guiscard.seebohm@gmx.de

The classical tango is a dance characterized by a 2/4 or 4/4 rhythm in which the partners dance in a coordinated way, allowing dynamic contact. There is a surprising similarity between the tango and how KCNE β-subunits "dance" to the fast rhythm of the cell with their partners from the Kv channel family. The five KCNE β-subunits interact with several members of the Kv channels, thereby modifying channel gating via the interaction of their single transmembrane-spanning segment, the extracellular amino terminus, and/or the intracellular carboxy terminus with the Kv α-subunit. Best studied is the molecular basis of interactions between KCNE1 and Kv7.1, which, together, supposedly form the native cardiac I_{Ks} channel. Here we review the current knowledge about functional and molecular interactions of KCNE1 with Kv7.1 and try to summarize and interpret the tango of the KCNEs.

Keywords: Kv channel, Kv7.1, β-subunit, KCNE1

INTRODUCTION

Voltage-gated potassium channels (Kv) are ubiquitously expressed in human tissues. They enable the rapid, selective movement of potassium ions through cellular membranes, thereby regulating physiological processes such as transmembrane ion passage and hormone secretion, vesicle cycling, and cell excitability. Kv channels display a huge diversity due to the large number of different α-subunits, alternative splicing, post-transcriptional modifications, and their ability to form heteromeric channels with other pore-forming α-subunits. To complicate the situation even more, the number of functionally different Kv channels in native tissues is further increased by interaction with regulatory β-subunits. These accessory subunits modify subcellular localization as well as biophysical properties of Kv channels such as gating kinetics, ion selectivity, and pharmacology. Among the best studied modulations of Kv channels by regulatory β-subunits is the effect of KCNE1 on Kv7.1.

Kv7.1-EXPRESSION AND PHYSIOLOGICAL FUNCTION

The *KCNQ1* gene was first identified by Wang et al. (1996b) in a linkage study of patients with long QT syndrome (LQTS1). Its gene product, Kv7.1 (also termed KvLQT1 or KCNQ1), is a voltage-gated potassium channel α-subunit, and its expression was detected in several mammalian tissues, including heart, epithelia, and smooth muscle (**Figure 1**; **Table A1** in Appendix). Kv7.1 can assemble with different members of the KCNE family of regulatory β-subunits to fulfill a variety of physiological functions.

In the heart, Kv7.1 is involved in the termination of the cardiac action potential. The repolarizing potassium current, I_K, consists of two major components, the rapid delayed rectifier potassium current I_{Kr} and the slow delayed rectifier potassium current I_{Ks} (Sanguinetti and Jurkiewicz, 1990). Kv7.1 coassembles with the KCNE1 β-subunit to form the channel complex that mediates I_{Ks} (Barhanin et al., 1996; Sanguinetti et al., 1996). Although KCNE1 is the major accessory subunit assembling with Kv7.1 in the heart, other subunits of the KCNE family might be present (Bendahhou et al., 2005), serving as additional regulators of I_{Ks} (Wu et al., 2006). The significance of Kv7.1 and its accessory β-subunits for maintaining normal rhythmicity is further emphasized by the numerous *KCNQ1* and *KCNE* mutations associated with cardiac arrhythmias (http://www.fsm.it/cardmoc/). Most of these mutations lead to loss of channel function causing LQTS, a disorder predisposing affected individuals to *torsade de pointes* arrhythmia and cardiac sudden death.

Besides its cardiac function, several lines of evidence suggest an important role of Kv7.1 and its accessory β-subunit KCNE1 in the hearing process. In patients suffering from Jervell and Lange-Nielsen syndrome – the recessive form of inherited LQTS – cardiac arrhythmia is accompanied by profound bilateral deafness. Mutations in both *KCNQ1* and *KCNE1* genes have been reported to cause this disorder (Jervell and Lange-Nielsen, 1957; Neyroud et al., 1997; Schulze-Bahr et al., 1997). In addition, targeted disruption of the *KCNQ1* gene in mice leads to deafness caused by morphological abnormalities of the inner ear (Lee et al., 2000; Casimiro et al., 2001). Expression of Kv7.1 and KCNE1 has been detected in the marginal cells of the *stria vascularis* of the cochlea and the vestibular dark cells (Neyroud et al., 1997; Nicolas et al., 2001; Knipper et al., 2006; Hur et al., 2007). Both cell types are involved in the generation of the potassium-rich endolymph, and Kv7.1/KCNE1 channels have been suggested to be key mediators of this K^+ secretion (Marcus and Shen, 1994; Shen et al., 1995; Wangemann, 1995; Wangemann et al., 1995; Sunose et al., 1997).

In addition to the inner ear epithelium, Kv7.1 has been detected in a variety of other epithelial cell types, where it participates in secretory transduction. In the kidney, Kv7.1/KCNE1 channels seem to be located in the proximal tubule of the nephron

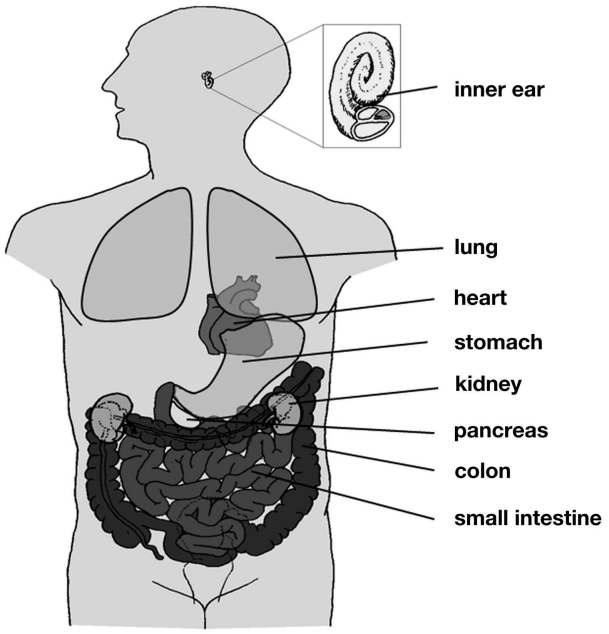

FIGURE 1 | Distribution of Kv7.1. Kv7.1 is expressed in several tissues throughout the human body, including heart, lung, inner ear, kidney, and the gastrointestinal tract.

(Sugimoto et al., 1990; Vallon et al., 2001), conducting a K^+ current to counterbalance membrane depolarization induced by electrogenic Na^+-coupled transport of glucose or amino acids (Vallon et al., 2001, 2005). The relevance of Kv7.1/KCNE1 channels for renal function is further underlined by the observation that KCNE1 knockout mice suffer from hypokalemia, urinary and fecal salt wasting, and volume depletion (Arrighi et al., 2001; Warth and Barhanin, 2002). Kv7.1 expression has also been detected in the small intestine and the colon (Schroeder et al., 2000; Dedek and Waldegger, 2001; Demolombe et al., 2001; Kunzelmann et al., 2001; Horikawa et al., 2005). In colonic crypt cells Kv7.1 is believed to assemble with another accessory β-subunit, KCNE3, and to mediate a K^+ conductance that provides the driving force for chloride secretion (Schroeder et al., 2000; Kunzelmann et al., 2001). Two further examples of Kv7.1 expression and function in chloride-secreting tissues are pancreatic acinar cells and airway epithelium (Kim and Greger, 1999; Kottgen et al., 1999; Mall et al., 2000; Demolombe et al., 2001; Grahammer et al., 2001b; Lee et al., 2004). In parietal cells of the stomach Kv7.1 coassembles with KCNE2 and participates in gastric acid secretion (Dedek and Waldegger, 2001; Demolombe et al., 2001; Grahammer et al., 2001a; Heitzmann et al., 2004). In KCNQ1 knockout mice gastric hyperplasia and profound hypochlorhydria have been observed, indicating the importance of Kv7.1 in normal stomach development and function (Lee et al., 2000). Kv7.1 expression has also been detected in the human thyroid gland, and it has been shown that mice lacking functional Kv7.1 develop hypothyroidism (Frohlich et al., 2011). Recently, Kv7.1 channels have been shown to relax systemic and pulmonary arteries upon pharmacological activation (Chadha et al., 2012).

REGULATION OF Kv7.1 BY ACCESSORY β-SUBUNITS OF THE KCNE GENE FAMILY

All five members of the KCNE family of regulatory β-subunits can functionally coassemble with Kv7.1 to subunit-specifically change its current characteristics (for an excellent review about KCNEs, see McCrossan and Abbott, 2004). The founding member KCNE1 (previously termed MinK or I_{sK}) was identified in 1988 (Takumi et al., 1988). As its expression in *Xenopus* oocytes produced slowly activating potassium currents resembling the cardiac I_{Ks}, KCNE1 was originally believed to be the ion channel α-subunit forming the I_{Ks} channel. However, it is now well established that KCNE1 cannot form functional K^+ channels alone, but can serve as a regulatory β-subunit for several voltage-gated cation channels, including Kv7.1 (Barhanin et al., 1996; Sanguinetti et al., 1996). The I_{Ks}-like potassium currents observed in oocytes upon heterologous expression of KCNE1 were actually caused by coassembly with endogenous Kv7.1. So far, four other members of the KCNE family, KCNE2-KCNE5 (also termed MiRP1-4) have been identified (Abbott et al., 1999; Piccini et al., 1999), and their influence on Kv7.1 channels has been studied extensively in heterologous expression systems. Kv7.1 expressed alone forms a classical delayed rectifier potassium-selective channel with fast activation, delayed partial inactivation, and relatively slow deactivation (Pusch et al., 1998; Tristani-Firouzi and Sanguinetti, 1998). The presence of KCNE1 drastically modifies Kv7.1 activity by increasing unitary conductance as well as macroscopic currents, slowing activation, right-shifting voltage dependence of activation, suppressing currents at low activating voltages, suppressing partial inactivation, increasing Q_{10}-value, and modulating pharmacology (**Figures 2A–C**; Barhanin et al., 1996; Sanguinetti et al., 1996; Pusch, 1998; Pusch et al., 1998; Sesti and Goldstein, 1998; Tristani-Firouzi and Sanguinetti, 1998; Lerche et al., 2000; Seebohm et al., 2001a,b,c, 2003a,b,c, 2005; Morokuma et al., 2008). Coassembly of Kv7.1 and KCNE2 gives rise to currents with decreased amplitude, instantaneous activation, rapid partial deactivation, and a linear current-voltage relationship (Tinel et al., 2000). KCNE3 also converts Kv7.1 to a channel with nearly instantaneous activation and a linear current-voltage relationship (Schroeder et al., 2000; Seebohm et al., 2003c), but in contrast to Kv7.1/KCNE2, complexes containing KCNE3 show some time dependency of gating at positive potentials and increased current densities (Schroeder et al., 2000; Melman et al., 2001; Mazhari et al., 2002). KCNE4 completely suppresses Kv7.1 currents at physiologically relevant membrane potentials (Grunnet et al., 2002) and KCNE5 shifts the voltage dependence of Kv7.1 activation to more positive potentials toward an activation threshold of about +40 mV (**Figure 2D**; Angelo et al., 2002; Seebohm et al., 2003c).

GATING OF Kv7.1 AND ITS MODULATION BY KCNE1

The biophysical properties of voltage-gated Kv7.1 channels change dramatically when they coassemble with KCNEs. Homotetrameric Kv7.1 channels activate with relatively fast kinetics with $\tau_{activation}$ by about 80−100 ms at 60 mV (**Figure 2**; Pusch et al., 1998; Tristani-Firouzi and Sanguinetti, 1998). The channels undergo partial inactivation, with about 60% of the channels being inactivated at 60 mV in steady-state (**Figure 2**). The kinetic behavior of

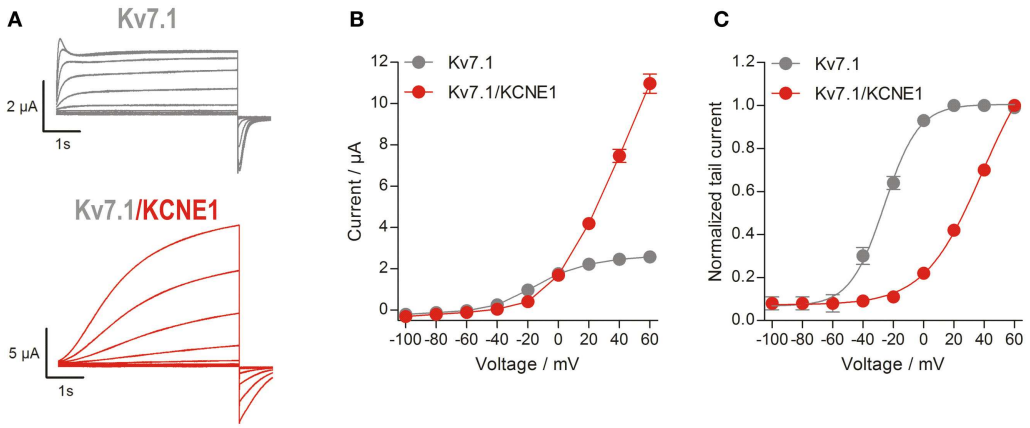

D

	Current amplitude	Voltage-independent open component	Right shift of the activation curve	Rb^+/K^+ conductance
KCNE1	+	-	+	+/-
KCNE2	-	+	+	?
KCNE3	+	++	+	+/-
KCNE4	- -	-	++ *	?
KCNE5	-	-	+	++

FIGURE 2 | Characteristics of Kv7.1/KCNE-mediated currents. (A) Representative current traces of Kv7.1 homomers and Kv7.1/KCNE1 heteromers. Channels were expressed in *Xenopus* oocytes, and currents were elicited with 7 s pulses to potentials of −100 to +60 mV, applied in 20 mV increments from a holding potential of −80 mV. Tail currents were recorded at −120 mV. **(B)** Current-voltage relationships. At voltages between −60 and −40 mV KCNE1 suppresses currents, whereas it stimulates them at voltages above 0 mV. **(C)** Voltage dependence of channel activation determined by tail current analysis. Activation curves were fitted to a Boltzmann function. Note: Kv7.1/KCNE1 channels are not fully activated at +60 mV. **(D)** Effects of different KCNE subunits on Kv7.1 currents. "+" and "++" indicate increased and strongly increased effects, while "−" and "−−" indicate decreased and strongly decreased effects, respectively. *Effect shown in the calmodulin binding-deficient $KCNE4^{L69–L72}$ mutant (Ciampa et al., 2011). The Rb^+/K^+ conductance tightly correlates with the partial inactivation, and KCNE5 slightly increases it, whereas KCNE1/3 decreases it compared to Kv7.1 (Seebohm et al., 2003c).

Kv7.1 can be approximated by a linear gating scheme of the form (Pusch et al., 1998; Tristani-Firouzi and Sanguinetti, 1998):

model 1:

$$C_1 \Leftrightarrow C_2 \Leftrightarrow C_3 \Leftrightarrow O_1 \Leftrightarrow O_2 \Leftrightarrow I$$

In this model $C_1 \Leftrightarrow C_2$, $C_2 \Leftrightarrow C_3$, and $O_1 \Leftrightarrow O_2$ are the voltage-dependent gating steps. Recently, an alternative circular gating scheme was proposed by Ma et al. (2011).

model 2:

$$C_1 \Leftrightarrow C_2 \Leftrightarrow O_1 \Leftrightarrow O_2$$

This novel gating scheme accounts for an open fraction that is determined by allosteric coupling of residues in the S4–S5 linker/pore domain (PD). $C_1 \Leftrightarrow C_2$ and $O_1 \Leftrightarrow O_2$ are the voltage-dependent gating steps.

Kv7.1/KCNE1 heteromeric channels activate far more slowly and at more positive potentials than homomeric Kv7.1 channels, do not partially inactivate, and have an increased single-channel conductance compared to homomeric Kv7.1 recorded in standard extracellular solutions (Barhanin et al., 1996; Sanguinetti et al., 1996; Pusch, 1998; Pusch et al., 1998; Tristani-Firouzi and Sanguinetti, 1998). It is believed that Kv7.1/KCNE1 channel currents resemble the cardiac repolarizing, slowly activating potassium current I_{Ks} and that LQTS1/5 mutations might directly or allosterically modify interactions of Kv7.1 and the β-subunit KCNE1 (e.g., Schmitt et al., 2000; Seebohm et al., 2001c; Osteen et al., 2010; Wang et al., 2011b). Cui et al. (1994) proposed two linear-branched gating schemes for Kv7.1/KCNE1 heteromers, which depend on varying KCNE1 amounts coexpressed with Kv7.1 and imply interactions among individual channel proteins during activation. Yet Tzounopoulos et al. reported on a crossover gating phenomenon after prepulsing to different voltages that cannot be explained by a classical *Cole–Moore* shift in a linear gating model of Kv7.1/KCNE1 channels and presented results that argue for a circular gating model similar to model 2 (Cole and Moore, 1960; Tzounopoulos et al., 1998). However, a branched model can account for this crossover gating phenomenon after prepulsing to different voltages as well (Strutz-Seebohm et al., 2011):

model 3:

$$\begin{array}{l} C_1 \Leftrightarrow C_2 \Leftrightarrow O_1 \Leftrightarrow O_2 \\ \quad\quad \Updownarrow \\ \quad\quad C_2{}^* \end{array}$$

Further gating schemes have been proposed to describe Kv7.1/KCNE1 gating (Silva and Rudy, 2005, 2010; Osteen et al., 2010; Ghosh et al., 2011). In summary, the gating behaviors of Kv7.1 and Kv7.1/KCNE1 are relatively complex, and simple, linear gating models reach too short to approximate a realistic mathematical description.

STOICHIOMETRY OF THE Kv7.1/KCNE1 COMPLEX

After the discovery that the channel complex mediating the cardiac I_{Ks} is composed of Kv7.1 α-subunits and KCNE1 β-subunits (Barhanin et al., 1996; Sanguinetti et al., 1996), detailed investigations on the nature of this association started. Like all members of the Kv channel family, Kv7.1 α-subunits assemble into tetramers to form functional channels. Each α-subunit consists of six transmembrane segments, S1–S6, flanked by intracellular amino- and carboxy-terminal domains. The central pore domain (PD) of the channel, which contains the ion conduction pathway and the activation gate, is formed by segments S5 and S6 and the pore loop between them. The pore loop carries the K^+ channel signature sequence TTIGYGD allowing rapid ion conduction and potassium selectivity. The PD is surrounded and controlled by four voltage-sensing domains (VSDs) formed by segments S1–S4 from each subunit (**Figures 3A,B**). S4 contains several positively charged amino acids and is a key element of voltage sensing. Further charged residues in S1–S3 may contribute additional charge to allow for voltage sensing. Tetrameric assembly of Kv7.1 α-subunits is mediated via their C-terminal domains (Schmitt et al., 2000; Schwake et al., 2003). Although Kv7.1 homotetramers are functional, the presence of the accessory β-subunit KCNE1 is needed to produce currents with characteristics of native I_{Ks} (**Figure 2A**). KCNE1 is a small, integral membrane protein with a single transmembrane-spanning segment flanked by an extracellular N-terminal and an intracellular C-terminal domain (**Figure 3A**). The number of KCNE1 β-subunits recruited by tetrameric Kv7.1 channels has been a matter of extensive debate (**Figure 3B**). Previous studies have either suggested a fixed stoichiometry of four Kv7.1 subunits and two KCNE1 subunits (Wang and Goldstein, 1995; Chen et al., 2003a; Kang et al., 2008; Morin and Kobertz, 2008) or a variable stoichiometry with up to four KCNE1 subunits assembling with a Kv7.1 tetramer (Cui et al., 1994; Wang et al., 1998, 2011a; Morokuma et al., 2008; Nakajo et al., 2010; Zheng et al., 2010; Strutz-Seebohm et al., 2011). A summary of the data obtained during the last two decades is provided in **Table 1**. The results reported leave the possibility open that KCNE1 subunits coassemble with Kv7.1 in different modes allowing up to four KCNE1 subunits to approach the Kv7.1 tetramer but permitting only formation of 4 Kv7.1 : 2 KCNE1 assemblies in specific regions of the heteromeric channels. Prerequisites for such an interaction would be variable and dynamic interactions. Indeed, several studies suggest interactions of Kv7.1 with KCNE1 at different protein regions in the various channel states (summarized in **Table 2**). However, further studies are required to support such a hypothesis.

STRUCTURAL BASIS OF Kv7.1/KCNE1 INTERACTION

The structural basis of the Kv7.1/KCNE1 interaction has been studied extensively over the last 20 years. Experimental data obtained from deletion analysis, chimeric approaches, and site-directed mutagenesis identified regions in both Kv7.1 and KCNE1 that might be crucial for association and modulation (summarized in **Table 2**). Based on these data it has been suggested that the transmembrane segment and the C-terminal domain of KCNE1 mediate its ability to modulate Kv7.1 (Takumi et al., 1991; Tapper and George, 2000). Molecular key elements of KCNE1 function seem to be three glycines, several bulky, aromatic phenylalanines, and the threonine 58 located at the center of the KCNE1 transmembrane segment (Melman et al., 2001, 2002; Strutz-Seebohm et al., 2011). A comparison with other KCNE subunits underscores the importance of the transmembrane segment for KCNE function: interactions of Kv7.1 with KCNE1 and Kv7.1 with KCNE3 show similar chemical modification rates within the transmembrane region (Rocheleau and Kobertz, 2008), and the KCNE4 transmembrane segment modulates voltage dependence of Kv7.1 activation (Ciampa et al., 2011). A recent study indicates that different KCNE proteins contact different regions in Kv7.1 all located within the transmembrane segments (Nakajo et al., 2011). In segment S6 of Kv7.1, a three amino acid motif (S338, F339,

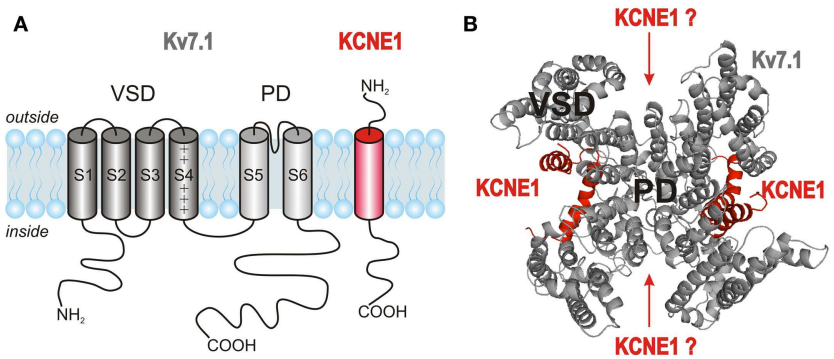

FIGURE 3 | Topology and stoichiometry of Kv7.1/KCNE1 channels. **(A)** Kv7.1 α-subunits are made of six membrane-spanning segments S1–S6 and intracellular N- and C-terminal domains. The segments S1–S4 form the voltage-sensing domain (VSD), while the pore domain (PD) consists of segments S5 and S6. KCNE1 β-subunits contain a single transmembrane segment flanked by an extracellular N-terminus and a cytosolic C-terminus. **(B)** Four Kv7.1 α-subunits assemble to form a functional channel. The number of KCNE1 β-subunits associating with Kv7.1 tetramers is still a matter of extensive debate (Strutz-Seebohm et al., 2011).

Table 1 | Stoichiometry of Kv7.1/KCNE1 channels.

Experimental evidence leading to conclusion of fixed stoichiometry (4:2)	Reference
Suppression of current induced by coexpression of wildtype and mutant KCNE1 indicates 4:2 stoichiometry	Wang and Goldstein (1995)
Kv7.1/Kv7.1/KCNE1 fusion proteins and naturally assembled Kv7.1/KCNE1 channels show similar characteristics of CTX inhibition; quantification of Kv7.1 and KCNE1 subunits using ^{3}H-CTX and an antibody indicates a 4:2 stoichiometry	Chen et al. (2003a)
Chemical subunit counting experiments indicate that association of two KCNE1 subunits with the Kv7.1 tetramer is sufficient to induce KCNE1-typical modulation of channel properties	Morin and Kobertz (2008)
Computational model of Kv7.1/KCNE1 channels indicates that binding of more than two KCNE1 subunits to the Kv7.1 tetramer might be sterically hindered	Kang et al. (2008)
Experimental evidence leading to conclusion of variable stoichiometry	**Reference**
Current amplitude, activation kinetics, and voltage dependence of Kv7.1/KCNE1 channels vary with the amount of KCNE1	Cui et al. (1994)
Both Kv7.1/KCNE1 fusion proteins and Kv7.1–Kv7.1 with additional KCNE1 produce currents with activation kinetics and voltage dependence similar to naturally assembled Kv7.1/KCNE1 channels	Wang et al. (1998)
Voltage dependence of activation of Kv7.1/KCNE1 channels varies with the amount of KCNE1	Morokuma et al. (2008)
Single-molecule fluorescent bleaching studies indicate that up to four KCNE1 subunits associate with the Kv7.1 tetramer depending on the relative densities of the two subunits	Nakajo et al. (2010)
Effects of free KCNE1 C-terminals on voltage dependence of activation of Kv7.1 and Kv7.1/KCNE1 channels are complex, indicating multiple stoichiometries or saturation of possible binding sites	Zheng et al. (2010)
Overexpression of KCNE1 markedly changed activation kinetics and voltage dependence of native I_{Ks}, indicating assembly of additional KCNE1 subunits with endogenous channels	Wang et al. (2011a)
Modeling of transmembrane domain suggests that variable stoichiometry seems possible in this region	Strutz-Seebohm et al. (2011)

F340) has been identified that might constitute a site of specific interaction with KCNE1, especially with its residue T58 (Melman et al., 2004; Panaghie et al., 2006; Strutz-Seebohm et al., 2011). Further residues in the pore region of Kv7.1 (F270, G272, and L273 in S5, V307, V310, and T311 in the lower pore helix, and V324 and V334 in the upper S6) are crucial for an accurate modulation by KCNE1 (Seebohm et al., 2001c, 2003c; Nakajo et al., 2011).

Based on experimental evidence, localizations of KCNE1 in the channel complex have been suggested. A series of observations obtained from cysteine scanning mutagenesis combined with chemical modifications (Cd^{2+} coordination, MTS reagent binding, and spontaneous disulfide formation) indicate that KCNE1 lies in close proximity to both the PD and the VSD of the Kv7.1 tetramer (summarized in **Table 2**). First interpretations suggested that KCNE1 lines the conduction pathway (Wang et al., 1996a; Tai and Goldstein, 1998). However, subsequent studies indicate that the KCNE1 transmembrane segment is located outside the PD and interacts with the outer S5 and S6 segments of Kv7.1 (Lerche et al., 2000; Kurokawa et al., 2001; Tapper and George, 2001; Chung et al., 2009; Strutz-Seebohm et al., 2011). Its extracellular flank seems to face the extracellular ends of segments S1 and S6 of Kv7.1, with the residues interacting with segment S1 varying dependent on the specific channel state (Xu et al., 2008; Chung et al., 2009). In addition to segment S1 of the VSD and S5/S6 of the PD, the transmembrane domain of KCNE1 gets in close contact with the primary cationic voltage sensor S4 (Nakajo and Kubo, 2007; Shamgar et al., 2008; Silva et al., 2009; Strutz-Seebohm et al., 2011). A possible interaction of KCNE1 with the VSD of Kv7.1 is further underscored by the fact that the abnormal phenotypes of several disease-causing mutations in S1, S4, or the S4–S5 linker of Kv7.1 *in vitro* only manifest in the presence of KCNE1 (summarized in **Table 2**; Franqueza et al., 1999; Chouabe et al., 2000; Chen et al., 2003c; Chan et al., 2012). The cytoplasmic portion directly following the transmembrane segment of KCNE1 seems to interact with the gating machinery of Kv7.1 (Lvov et al., 2010). A hallmark of all Kv7 channels is their sensitivity to muscarinic signaling, which gave them the name M-channels. The Kv7.1 membrane-proximal region may link membrane lipid metabolism of phosphoinositide $PI(4,5)P_2$ to the gating machinery to allow for integration of muscarinic signaling into gating alterations in Kv7.1 (Ikeda and Kammermeier, 2002; Loussouarn et al., 2003). The lower S6 is expected to be in close proximity to allow for electrostatic interaction with the $PI(4,5)P_2$ head groups, and $PI(4,5)P_2$ binding sites have been reported to be positioned close to the lower S6-helices bundle in the PD of Kv7.1 (Loussouarn et al., 2003; Thomas et al., 2011). However, it may be mentioned that further $PI(4,5)P_2$ binding sites may exist in the TM domain. KCNE1 residues $R^{67}SKKLEH^{73}$ in the vicinity of the inner membrane leaflet increase the $PI(4,5)P_2$ sensitivity of Kv7.1 by a factor of 100, possibly by electrostatic interaction with $PI(4,5)P_2$ head groups and/or Kv7.1 residues interacting with $PI(4,5)P_2$ (Li et al., 2011). Thus, $PI(4,5)P_2$ may function as a molecular coupler of Kv7.1 and KCNE1 to modulate gating in complex ways.

Recent structural modeling approaches generated 3D models of the transmembrane region of Kv7.1/KCNE1 that are in large agreement with the various experimental data. Specifically, homology modeling of the Kv7.1 S1–S6 region and *Rosetta*-based docking of the KCNE1 transmembrane domain produced an open and a closed state model of the heteromeric channel complex (Smith et al., 2007; Kang et al., 2008). Very recently, homology modeling of Kv7.1 with manual docking of the KCNE1 transmembrane domain was used to generate a pre-open closed state model of

Table 2 | Structural basis of Kv7.1/KCNE1 interaction.

Approach	Conclusion	Reference
Deletion analysis, chimeric approach, and/or site-directed mutagenesis	TM segment and cytoplasmic portion immediately following TM segment of KCNE1 mediate KCNE1 function	Takumi et al. (1991)
	TM segment and C-terminal domain of KCNE1 mediate KCNE1 function	Tapper and George (2000)
	Residues 57–59 of KCNE1 are important for KCNE1 function ("activation triplet")	Melman et al. (2001)
	Residue L273 of Kv7.1 is important for normal modulation by KCNE1	Seebohm et al. (2001c)
	Residue T58 is a key element of KCNE1 function	Melman et al. (2002)
	Requirements to interact with KCNE1 are located in regions C-terminal to S5; Residues S338, F339, and F340 in S6 are important for normal modulation by KCNE1	Melman et al. (2004)
	Residues S338, F339, and F340 in S6 are possible interaction sites of KCNE1	Panaghie et al. (2006)
	KCNE1 C-terminus is crucial for channel assembly, open state destabilization, kinetics of deactivation	Chen et al. (2009)
	Amino acids important for normal modulation by KCNE1 are located in S5 and S6 (G272, V324, V334) of Kv7.1	Nakajo et al. (2011)
Cysteine scanning mutagenesis combined with chemical modifications (Cd^{2+} coordination, MTS reagent binding, and spontaneous disulfide formation)	TM segment of KCNE1 lines the conduction pathway	Wang et al. (1996a)
	TM segment of KCNE1 lines the conduction pathway	Tai and Goldstein (1998)
	KCNE1 is located outside the conduction pathway	Kurokawa et al. (2001)
	KCNE1 is located outside the conduction pathway but in very close proximity to S6 of Kv7.1	Tapper and George (2001)
	E44 in KCNE1 is close to A226 in S4 of Kv7.1 in the open state; KCNE1 is close to or possibly interacts with the VSD	Nakajo and Kubo (2007)
	KCNE1 makes state-dependent contact with S1 of Kv7.1; KCNE1 is in close proximity to the VSD	Xu et al. (2008)
	KCNE1 is located close to S1 and S4 of two adjacent VSDs	Shamgar et al. (2008)
	C-terminal region directly following the KCNE1 TM segment interacts with activation gate of Kv7.1	Lvov et al. (2010)
Proof of direct physical interaction or close proximity (e.g., co-immunoprecipitation, FRET)	C-terminus of KCNE1 directly interacts with the pore region of Kv7.1	Romey et al. (1997)
	C-termini of Kv7.1 and KCNE1 move close to each other during channel activation; distal C-terminus of KCNE1 interacts with dimeric coiled coil helix C of Kv7.1	Haitin et al. (2009)
	Physical interaction between C-termini of Kv7.1 and KCNE1; portion of A-helix and its linker to S6 bind KCNE1	Zheng et al. (2010)
Analysis of disease-causing mutations	Functional interaction of KCNE1 with S4/S4–S5 linker of Kv7.1	Franqueza et al. (1999)
	Functional interaction of KCNE1 with S4/S4–S5 linker of Kv7.1	Chouabe et al. (2000)
	Functional interaction of KCNE1 with S1 of Kv7.1	Chan et al. (2012)
Computational model	KCNE1 is located in a cleft between the pore domain and the VSD of Kv7.1	Kang et al. (2008)
	KCNE1 binds to the outer face of the Kv7.1 channel pore, KCNE1 is located in a cleft between pore domain and VSD of Kv7.1	Strutz-Seebohm et al. (2011)

the Kv7.1/KCNE1 channel (Strutz-Seebohm et al., 2011). All three models are relatively stable in molecular dynamics simulations, which suggests that they are close to native states.

The C-termini of Kv7.1 and KCNE1 are in close proximity and physically interact, as indicated by FRET measurements and co-immunoprecipitation, yet the structural basis of this interaction is unknown (Haitin et al., 2009; Zheng et al., 2010). The cytosolic domain of Kv7.1/KCNE1 channels represents a multimodular structure serving multiple functions. It contains several amphipathic α-helices. Structural prediction algorithms place two α-helices, A and B, to the proximal C-terminus of Kv7.1 (Haitin and Attali, 2008). These α-helices may contain functionally relevant calmodulin interaction motifs. The residues $Kv7.1^{586–618}$ form α-helix D that contain a leucine-zipper and a coiled coil fold (Kanki et al., 2004). This parallel, four-stranded coiled coil allows for specific tetrameric assembly of Kv7.1 channel subunits (Schmitt et al., 2000; Schwake et al., 2003; Nakajo and Kubo, 2008). Recently, Xu and Minor (2009) presented a high-resolution X-ray crystal structure (1.7 Å resolution) of $Kv7.1^{583–611}$ confirming the predictions of the coiled coil assembly specificity domain. Interestingly, helix D is supposedly two helical turns longer in this crystal structure than helices D of the closely related Kv7.2–5 channels, which allows for specific homomeric assembly with other Kv7.1 subunits but not for heteromeric assemblies with other family members (Haitin and Attali, 2008; Xu and Minor, 2009). The S6 transmembrane segment and the

A-domain are linked by the region Kv7.1$^{350–582}$, which according to *in silico* prediction assumes an apo-chloroperoxidase fold and can thus be modeled using the structural coordinates of apo-chloroperoxidase (pdb: 1VNS; Macedo-Ribeiro et al., 1999). However, these predictions appear somewhat preliminary, and several assumptions have to be made to incorporate the modeled region into the rest of the Kv7.1–3D model. Further, how exactly the proposed helices A/B and linker region containing the calmodulin binding site can be integrated into this fold is speculative. The structural folds of the N-terminal region Kv7.1$^{1–115}$ and the most distal residues Kv7.1$^{612–676}$ remain completely unknown.

PI(4,5)P_2 modulates function of Kv7.1/KCNE1 channels, and functional PI(4,5)P_2 interaction sites were reported not only for the lower S6 segment but also for the C-terminus, where a cluster of basic amino acids may form a PI(4,5)P_2 interaction site allowing for electrostatic interactions with the PI(4,5)P_2 head groups (Loussouarn et al., 2003; Zhang et al., 2003; Delmas and Brown, 2005). This PI(4,5)P_2 interaction site may functionally and physically overlap with the calmodulin binding sites in the inter helix A/B linker region (Hernandez et al., 2008). The Kv7.1–calmodulin interaction can be modulated by coassembly with KCNE4. This modulation is dependent on a juxtamembrane tetraleucine motif (L69–L72) in KCNE4. However, deletion of this motif leaves the kinetic effects on Kv7.1 mediated by the KCNE4 transmembrane domain intact (Ciampa et al., 2011). Possibly, PI(4,5)P_2 and calmodulin "glue" these C-terminal regions to the transmembrane proximal regions mentioned above and allow for modulation of gating at the activation gate and the VSD. Clearly, further evidence is needed to prove this hypothesis (Li et al., 2011).

The C-termini of Kv7.1/KCNE1 channels physically interact with several proteins like the AKAP yotiao, epidermal growth factor receptor kinase, and NEDD4.2 (Marx et al., 2002; Kanki et al., 2004; Kurokawa et al., 2004; Jespersen et al., 2007; Dong et al., 2010). The protein kinase A phosphorylates Ser27 in the N-terminus of Kv7.1 and modulates Kv7.1/KCNE1 function (Marx et al., 2002). This modulation critically depends on the presence of KCNE1 (Marx et al., 2002; Kurokawa et al., 2004). This observation suggests that the Kv7.1 N-terminus contributes to Kv7.1/KCNE1 subunit interaction. The binding sites for these proteins have to be located at the surface of the C-terminal structure to be accessible for interaction. This information will be of help for further structural modeling. A 3D model of the Kv7.1/KCNE1 channel satisfying most of the aforementioned hypotheses is shown in **Figure 4**.

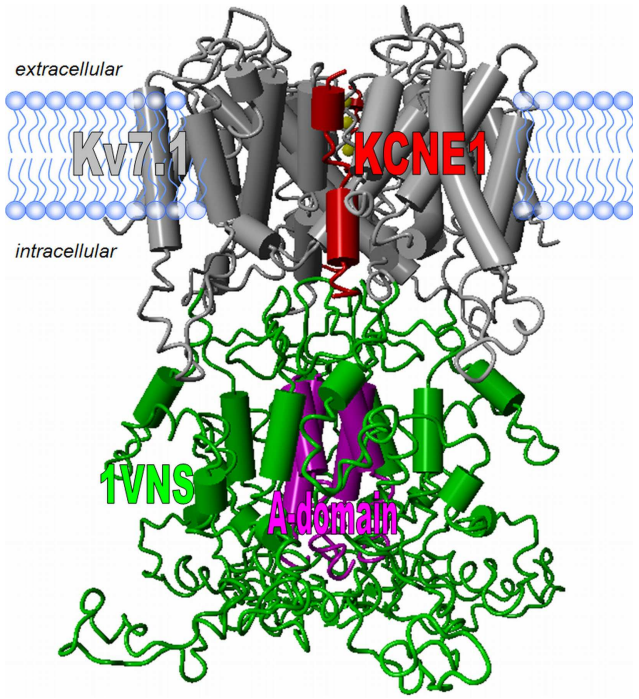

FIGURE 4 | Structural model of the Kv7.1 channel. The transmembrane domain of the Kv7.1 channel bears the common Kv channel structure. Homology models using the solved crystal structural constraints allow for good model predictions (gray). For docking experiments the solved NMR-structural data of the full-length KCNE1 in lipid environments can be used (here only the transmembrane segment is shown in red; Tian et al., 2007; Kang et al., 2008). The structure of the Kv7.1 tetrameric assembly domain (A-domain) was solved and can be incorporated into a model (Xu and Minor, 2009). The region linking the S6 and the A-domain shows amino acid similarity to the structure 1VNS.pdb. No structures or even template coordinates for the Kv7.1 N-terminus and the distal C-terminus are available and thus homology modeling is currently problematic.

TOWARD A DYNAMIC VIEW ON STRUCTURAL REARRANGEMENTS DURING Kv7.1/KCNE1 GATING

In the last 14 years a wealth of potassium channel crystal structures have been reported. Although central structural elements in Kv7.1 clearly differ from classical Shaker-type Kv channels, the available crystal structures are well-suited templates to model the Kv7.1 S1–S6 region in different states (Seebohm et al., 2006; Silva et al., 2009). Direct interactions of the transmembrane segments of Kv7.1 with KCNE1 have been proposed, but the specific amino acid interactions remain controversial (summarized in **Table 2**). CD spectra in a membrane-like environment and the NMR solution structure of KCNE1 transmembrane peptides show that this peptide adopts an α-helical structure (Aggeli et al., 1998; Strutz-Seebohm et al., 2011). Recently, two NMR structures of full-length KCNE1 confirmed that the transmembrane segment of KCNE1 folds an α-helix (Tian et al., 2007; Kang et al., 2008). An open and a closed state model of Kv7.1/KCNE1 channels were proposed based on the NMR-structural coordinates and *Rosetta*-dockings of KCNE1 to Kv7.1 that suggest binding of KCNE1 to the so-called "gain-of-function cleft", a space formed between two adjacent voltage sensor domains and the outer PD (Smith et al., 2007; Kang et al., 2008).

Localized to the center of the α-helical KCNE1 transmembrane segment are the residues G^{52}FFGFFTLG^{60}. As predicted, this α-helical transmembrane domain allows for flexibility at glycine residues G52, G55, and G60 (Tian et al., 2007; Kang et al., 2008; Strutz-Seebohm et al., 2011). Key to functional modulation of Kv7.1 by KCNE1 is the residue T58 (Melman et al., 2002). The surrounding phenylalanine residues generate a bulky aromatic cuff. The combination of these structural elements may enable formation of a stable hydrogen bond with residue S338 in Kv7.1 and

diverse van der Waals interactions with residues in S4 and the S4–S5 linker region as well as S5/S6 amino acids F270, F339, and F340 to stabilize a pre-open closed state. The combination of the Kv7.1/KCNE1 models, the closed state, the pre-open closed state and the open state model are in good agreement with published results of several experimental studies (Smith et al., 2007; Kang et al., 2008; Strutz-Seebohm et al., 2011). The modeled transmembrane domain structures can be used to assess a molecular view on the slow activation of I_{Ks} (**Figure 5**). The three states closed, pre-open, and open can be used for morphing calculations (Echols et al., 2003). The basic idea is that the channel undergoes conformational transitions from closed (C) to pre-open (C*), from pre-open (C*) to open (O), and from open (O) to closed (C) states. These seem to represent the major steps in the Kv7.1 and Kv7.1/KCNE1 gating (Silva et al., 2009). The position of the voltage sensor is "down" for the closed state and "up" for the pre-open and open states (Tian et al., 2007; Kang et al., 2008; Silva et al., 2009; Strutz-Seebohm et al., 2011). The interaction of KCNE1^{T58} with Kv7.1^{S338} and Kv7.1^{F339} may uncouple the gate at the lower S6 from the S4–S5 linker, which leads to S6 bundle crossing and closure of the gate (Strutz-Seebohm et al., 2011). The formation of the S6 bundle upon S4–S5 linker uncoupling may be supported by the lack of a central S6 gating hinge (Seebohm et al., 2006). The uncoupling of S4–S5 by KCNE1 during closed state inactivation shows similarities to an uncoupling event of the PD from the voltage sensor domain during closed state inactivation of some Kv channels as described by the group of Bähring et al. (2012). In the light of the ongoing discussion about fixed stoichiometry of two KCNE1 subunits per Kv7.1 tetramer vs. variable stoichiometry it is fair to study a channel complex with two KCNE1 subunits docked to four Kv7.1 subunits (Strutz-Seebohm et al., 2011). This stoichiometry is consistent with both hypotheses. Morphing experiments have been performed (**Figure 5**). As expected the gating is associated with large structural rearrangements in the voltage sensor domain. On the other hand the PD is rather rigid in the region around the selectivity filter. The KCNE1 transmembrane segment undergoes relatively small rearrangements during the gating steps C ⇔ C* and O ⇔ C but dramatic structural alterations during the C* ⇔ O transition (**Figure 5**; the extent of structural rearrangement around key residue KCNE1 T^{58} is indicated by a yellow arrow). This dramatic rearrangement of KCNE1 associated with the C* ⇔ O transition may generate an energetic barrier that can only slowly be overcome, resulting in dramatically slowed activation, the pivotal characteristic of Kv7.1/KCNE1 gating. Clearly, these models present a preliminary view on the dynamics of Kv7.1/KCNE1 channels. Silva et al. (2009) modeled further structural closed states of the Kv7.1 voltage sensor module. Incorporation of these data in future Kv7.1/KCNE1 morphing experiments may prove valuable. Increase in knowledge combined with the already available data, upcoming improvements in computational methodology, and decreasing computational costs will allow for much more facilitated dynamic modeling of Kv7.1/KCNE1 channel gating in the future.

The novel structural "snapshots" allow for a better understanding of Kv7.1/KCNE1 molecular pharmacology. Several Kv7.1/KCNE1 inhibitors and activators bind to distinct sites in state-dependent manner (Lerche et al., 2000, 2007; Seebohm et al., 2001b, 2003a; Chen et al., 2003b). Docking of various compounds to the different models and experimental verifications are now possible. An interesting observation is that the KCNE1 transmembrane segment induces large fenestrations in the Kv7.1 channel pre-open state that may allow for a novel access pathway not present in Kv7.1 homomeric channels (Strutz-Seebohm et al., 2011). Affected by these structural effects is the central cavity, the binding and blocking site of several Kv7.1/KCNE1 inhibitors (Lerche et al., 2000, 2007; Seebohm et al., 2003a). This altered structure could be used as a scaffold for the computer-aided design of specific Kv7.1/KCNE1 modulators not targeting homomeric Kv7.1 channels, which would be a prerequisite for tissue specific pharmacology (Seebohm et al., 2003b; Strutz-Seebohm et al., 2011). Insights into KCNE1-specific molecular pharmacology will be highly valuable for both drug development and safety pharmacology alike (Towart et al., 2009; Pugsley et al., 2011).

Upcoming physiological, pathophysiological, pharmacological, and structural analyses will fill the gaps in our current knowledge, and therefore the old Kv7.1/KCNE1 channel faces an exciting future. Let's dance the KCNQ1 tango!

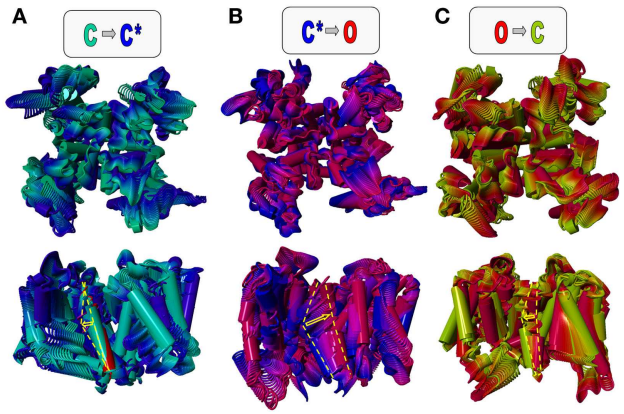

FIGURE 5 | Dynamic model of gating transitions in Kv7.1/KCNE1 channels. The closed (C), pre-open (C*), and open (O) state models described by Smith et al. (2007) and Strutz-Seebohm et al. (2011) were used to generate dynamic models using simple morphing approaches. The gating of Kv7.1/KCNE1 channels can be approximated by a simplified circular gating model. Major gating steps are C ⇒ C* **(A)**, C* ⇒ O **(B)**, and O ⇒ C **(C)** (colors as indicated in the letters above the models). For clarity the central axes of the KCNE1 start and end models are marked by the yellow dashed lines, and the direction and extent of the proposed motion is indicated by the yellow arrow. In **(A)** the KCNE1 start model is shown in red and the end model in magenta. The morphs indicate larger motions of KCNE1 during channel gating in the gating cleft of Kv7.1 channels. A particularly large gating motion around Thr58 is seen from C* ⇒ O **(B)**, suggesting a major energetic barrier. This may be the molecular basis of the dramatically slowed activation of Kv7.1 by association with KCNE1. However, calculation of energies on the models is highly speculative because specific interactions with surrounding membrane molecules [e.g., $PI(4,5)P_2$] would be highly influential, and the current knowledge on lipid-channel interactions is not sufficient to allow for precise calculations.

REFERENCES

Abbott, G. W., Sesti, F., Splawski, I., Buck, M. E., Lehmann, M. H., Timothy, K. W., Keating, M. T., and Goldstein, S. A. (1999). MiRP1 forms IKr potassium channels with HERG and is associated with cardiac arrhythmia. *Cell* 97, 175–187.

Aggeli, A., Bannister, M. L., Bell, M., Boden, N., Findlay, J. B., Hunter, M., Knowles, P. F., and Yang, J. C. (1998). Conformation and ion-channeling activity of a 27-residue peptide modeled on the single-transmembrane segment of the IsK (minK) protein. *Biochemistry* 37, 8121–8131.

Angelo, K., Jespersen, T., Grunnet, M., Nielsen, M. S., Klaerke, D. A., and Olesen, S. P. (2002). KCNE5 induces time- and voltage-dependent modulation of the KCNQ1 current. *Biophys. J.* 83, 1997–2006.

Arrighi, I., Bloch-Faure, M., Grahammer, F., Bleich, M., Warth, R., Mengual, R., Drici, M. D., Barhanin, J., and Meneton, P. (2001). Altered potassium balance and aldosterone secretion in a mouse model of human congenital long QT syndrome. *Proc. Natl. Acad. Sci. U.S.A.* 98, 8792–8797.

Bähring, R., Barghaan, J., Westermeier, R., and Wollberg, J. (2012). Voltage sensor inactivation in potassium channels. *Front. Pharmacol.* 3:100. doi:10.3389/fphar.2012.00100

Barhanin, J., Lesage, F., Guillemare, E., Fink, M., Lazdunski, M., and Romey, G. (1996). K(V)LQT1 and lsK (minK) proteins associate to form the I(Ks) cardiac potassium current. *Nature* 384, 78–80.

Bendahhou, S., Marionneau, C., Haurogne, K., Larroque, M. M., Derand, R., Szuts, V., Escande, D., Demolombe, S., and Barhanin, J. (2005). In vitro molecular interactions and distribution of KCNE family with KCNQ1 in the human heart. *Cardiovasc. Res.* 67, 529–538.

Brahmajothi, M. V., Morales, M. J., Rasmusson, R. L., Campbell, D. L., and Strauss, H. C. (1997). Heterogeneity in K+ channel transcript expression detected in isolated ferret cardiac myocytes. *Pacing Clin. Electrophysiol.* 20, 388–396.

Brueggemann, L. I., Moran, C. J., Barakat, J. A., Yeh, J. Z., Cribbs, L. L., and Byron, K. L. (2007). Vasopressin stimulates action potential firing by protein kinase C-dependent inhibition of KCNQ5 in A7r5 rat aortic smooth muscle cells. *Am. J. Physiol. Heart Circ. Physiol.* 292, H1352–H1363.

Casimiro, M. C., Knollmann, B. C., Ebert, S. N., Vary, J. C. Jr., Greene, A. E., Franz, M. R., Grinberg, A., Huang, S. P., and Pfeifer, K. (2001). Targeted disruption of the Kcnq1 gene produces a mouse model of Jervell and Lange-Nielsen Syndrome. *Proc. Natl. Acad. Sci. U.S.A.* 98, 2526–2531.

Chadha, P. S., Zunke, F., Davis, A. J., Jepps, T. A., Linders, J. T., Schwake, M., Towart, R., and Greenwood, I. A. (2012). Pharmacological dissection of K(v) 7.1 channels in systemic and pulmonary arteries. *Br. J. Pharmacol.* 166, 1377–1387.

Chan, P. J., Osteen, J. D., Xiong, D., Bohnen, M. S., Doshi, D., Sampson, K. J., Marx, S. O., Karlin, A., and Kass, R. S. (2012). Characterization of KCNQ1 atrial fibrillation mutations reveals distinct dependence on KCNE1. *J. Gen. Physiol.* 139, 135–144.

Chen, H., Kim, L. A., Rajan, S., Xu, S., and Goldstein, S. A. (2003a). Charybdotoxin binding in the I(Ks) pore demonstrates two MinK subunits in each channel complex. *Neuron* 40, 15–23.

Chen, H., Sesti, F., and Goldstein, S. A. (2003b). Pore- and state-dependent cadmium block of I(Ks) channels formed with MinK-55C and wild-type KCNQ1 subunits. *Biophys. J.* 84, 3679–3689.

Chen, Y. H., Xu, S. J., Bendahhou, S., Wang, X. L., Wang, Y., Xu, W. Y., Jin, H. W., Sun, H., Su, X. Y., Zhuang, Q. N., Yang, Y. Q., Li, Y. B., Liu, Y., Xu, H. J., Li, X. F., Ma, N., Mou, C. P., Chen, Z., Barhanin, J., and Huang, W. (2003c). KCNQ1 gain-of-function mutation in familial atrial fibrillation. *Science* 299, 251–254.

Chen, J., Zheng, R., Melman, Y. F., and McDonald, T. V. (2009). Functional interactions between KCNE1 C-terminus and the KCNQ1 channel. *PLoS ONE* 4, e5143. doi:10.1371/journal.pone.0005143

Chouabe, C., Neyroud, N., Guicheney, P., Lazdunski, M., Romey, G., and Barhanin, J. (1997). Properties of KvLQT1 K+ channel mutations in Romano-Ward and Jervell and Lange-Nielsen inherited cardiac arrhythmias. *EMBO J.* 16, 5472–5479.

Chouabe, C., Neyroud, N., Richard, P., Denjoy, I., Hainque, B., Romey, G., Drici, M. D., Guicheney, P., and Barhanin, J. (2000). Novel mutations in KvLQT1 that affect Iks activation through interactions with Isk. *Cardiovasc. Res.* 45, 971–980.

Chung, D. Y., Chan, P. J., Bankston, J. R., Yang, L., Liu, G., Marx, S. O., Karlin, A., and Kass, R. S. (2009). Location of KCNE1 relative to KCNQ1 in the I(KS) potassium channel by disulfide cross-linking of substituted cysteines. *Proc. Natl. Acad. Sci. U.S.A.* 106, 743–748.

Ciampa, E. J., Welch, R. C., Vanoye, C. G., and George, A. L. Jr. (2011). KCNE4 juxtamembrane region is required for interaction with calmodulin and for functional suppression of KCNQ1. *J. Biol. Chem.* 286, 4141–4149.

Cole, K. S., and Moore, J. W. (1960). Potassium ion current in the squid giant axon: dynamic characteristic. *Biophys. J.* 1, 1–14.

Cui, J., Kline, R. P., Pennefather, P., and Cohen, I. S. (1994). Gating of IsK expressed in *Xenopus oocytes* depends on the amount of mRNA injected. *J. Gen. Physiol.* 104, 87–105.

Dedek, K., and Waldegger, S. (2001). Colocalization of KCNQ1/KCNE channel subunits in the mouse gastrointestinal tract. *Pflugers Arch.* 442, 896–902.

Delmas, P., and Brown, D. A. (2005). Pathways modulating neural KCNQ/M (Kv7) potassium channels. *Nat. Rev. Neurosci.* 6, 850–862.

Demolombe, S., Franco, D., de Boer, P., Kuperschmidt, S., Roden, D., Pereon, Y., Jarry, A., Moorman, A. F., and Escande, D. (2001). Differential expression of KvLQT1 and its regulator IsK in mouse epithelia. *Am. J. Physiol., Cell Physiol.* 280, C359–C372.

Dong, M. Q., Sun, H. Y., Tang, Q., Tse, H. F., Lau, C. P., and Li, G. R. (2010). Regulation of human cardiac KCNQ1/KCNE1 channel by epidermal growth factor receptor kinase. *Biochim. Biophys. Acta* 1798, 995–1001.

Echols, N., Milburn, D., and Gerstein, M. (2003). MolMovDB: analysis and visualization of conformational change and structural flexibility. *Nucleic Acids Res.* 31, 478–482.

Finley, M. R., Li, Y., Hua, F., Lillich, J., Mitchell, K. E., Ganta, S., Gilmour, R. F. Jr., and Freeman, L. C. (2002). Expression and coassociation of ERG1, KCNQ1, and KCNE1 potassium channel proteins in horse heart. *Am. J. Physiol. Heart Circ. Physiol.* 283, H126–H138.

Franqueza, L., Lin, M., Shen, J., Splawski, I., Keating, M. T., and Sanguinetti, M. C. (1999). Long QT syndrome-associated mutations in the S4–S5 linker of KvLQT1 potassium channels modify gating and interaction with minK subunits. *J. Biol. Chem.* 274, 21063–21070.

Frohlich, H., Boini, K. M., Seebohm, G., Strutz-Seebohm, N., Ureche, O. N., Foller, M., Eichenmuller, M., Shumilina, E., Pathare, G., Singh, A. K., Seidler, U., Pfeifer, K. E., and Lang, F. (2011). Hypothyroidism of gene-targeted mice lacking Kcnq1. *Pflugers Arch.* 461, 45–52.

Gaborit, N., Le Bouter, S., Szuts, V., Varro, A., Escande, D., Nattel, S., and Demolombe, S. (2007). Regional and tissue specific transcript signatures of ion channel genes in the non-diseased human heart. *J. Physiol. (Lond.)* 582, 675–693.

Ghosh, S., Silva, J. N., Canham, R. M., Bowman, T. M., Zhang, J., Rhee, E. K., Woodard, P. K., and Rudy, Y. (2011). Electrophysiologic substrate and intraventricular left ventricular dyssynchrony in nonischemic heart failure patients undergoing cardiac resynchronization therapy. *Heart Rhythm* 8, 692–699.

Grahammer, F., Herling, A. W., Lang, H. J., Schmitt-Graff, A., Wittekindt, O. H., Nitschke, R., Bleich, M., Barhanin, J., and Warth, R. (2001a). The cardiac K+ channel KCNQ1 is essential for gastric acid secretion. *Gastroenterology* 120, 1363–1371.

Grahammer, F., Warth, R., Barhanin, J., Bleich, M., and Hug, M. J. (2001b). The small conductance K+ channel, KCNQ1: expression, function, and subunit composition in murine trachea. *J. Biol. Chem.* 276, 42268–42275.

Grunnet, M., Jespersen, T., Rasmussen, H. B., Ljungstrom, T., Jorgensen, N. K., Olesen, S. P., and Klaerke, D. A. (2002). KCNE4 is an inhibitory subunit to the KCNQ1 channel. *J. Physiol. (Lond.)* 542, 119–130.

Haitin, Y., and Attali, B. (2008). The C-terminus of Kv7 channels: a multifunctional module. *J. Physiol. (Lond.)* 586, 1803–1810.

Haitin, Y., Wiener, R., Shaham, D., Peretz, A., Cohen, E. B., Shamgar, L., Pongs, O., Hirsch, J. A., and Attali, B. (2009). Intracellular domains interactions and gated motions of I(KS) potassium channel subunits. *EMBO J.* 28, 1994–2005.

Han, W., Bao, W., Wang, Z., and Nattel, S. (2002). Comparison of ion-channel subunit expression in canine cardiac Purkinje fibers and ventricular muscle. *Circ. Res.* 91, 790–797.

Heitzmann, D., Grahammer, F., von Hahn, T., Schmitt-Graff, A., Romeo, E., Nitschke, R., Gerlach, U., Lang, H. J., Verrey, F., Barhanin, J., and Warth, R. (2004). Heteromeric KCNE2/KCNQ1 potassium channels in the luminal membrane of

gastric parietal cells. *J. Physiol. (Lond.)* 561, 547–557.

Heitzmann, D., and Warth, R. (2007). No potassium, no acid: K+ channels and gastric acid secretion. *Physiology (Bethesda)* 22, 335–341.

Hernandez, C. C., Zaika, O., and Shapiro, M. S. (2008). A carboxy-terminal inter-helix linker as the site of phosphatidylinositol 4,5-bisphosphate action on Kv7 (M-type) K+ channels. *J. Gen. Physiol.* 132, 361–381.

Horikawa, N., Suzuki, T., Uchiumi, T., Minamimura, T., Tsukada, K., Takeguchi, N., and Sakai, H. (2005). Cyclic AMP-dependent Cl- secretion induced by thromboxane A2 in isolated human colon. *J. Physiol. (Lond.)* 562, 885–897.

Hur, D. G., Lee, J. H., Oh, S. H., Kim, Y. H., Lee, J. H., Shin, D. H., Chang, S. O., and Kim, C. S. (2007). KCNQ1/KCNE1 K+ channel and P2Y4 receptor are co-expressed from the time of birth in the apical membrane of rat strial marginal cells. *Acta Otolaryngol. Suppl.* 558, 30–35.

Iannotti, F. A., Panza, E., Barrese, V., Viggiano, D., Soldovieri, M. V., and Taglialatela, M. (2010). Expression, localization, and pharmacological role of Kv7 potassium channels in skeletal muscle proliferation, differentiation, and survival after myotoxic insults. *J. Pharmacol. Exp. Ther.* 332, 811–820.

Ikeda, S. R., and Kammermeier, P. J. (2002). M current mystery messenger revealed? *Neuron* 35, 411–412.

Jervell, A., and Lange-Nielsen, F. (1957). Congenital deaf-mutism, functional heart disease with prolongation of the Q-T interval and sudden death. *Am. Heart J.* 54, 59–68.

Jespersen, T., Membrez, M., Nicolas, C. S., Pitard, B., Staub, O., Olesen, S. P., Baro, I., and Abriel, H. (2007). The KCNQ1 potassium channel is down-regulated by ubiquitylating enzymes of the Nedd4/Nedd4-like family. *Cardiovasc. Res.* 74, 64–74.

Joshi, S., Sedivy, V., Hodyc, D., Herget, J., and Gurney, A. M. (2009). KCNQ modulators reveal a key role for KCNQ potassium channels in regulating the tone of rat pulmonary artery smooth muscle. *J. Pharmacol. Exp. Ther.* 329, 368–376.

Kang, C., Tian, C., Sonnichsen, F. D., Smith, J. A., Meiler, J., George, A. L. Jr., Vanoye, C. G., Kim, H. J., and Sanders, C. R. (2008). Structure of KCNE1 and implications for how it modulates the KCNQ1 potassium channel. *Biochemistry* 47, 7999–8006.

Kanki, H., Kupershmidt, S., Yang, T., Wells, S., and Roden, D. M. (2004). A structural requirement for processing the cardiac K+ channel KCNQ1. *J. Biol. Chem.* 279, 33976–33983.

Kim, S. J., and Greger, R. (1999). Voltage-dependent, slowly activating K+ current (I(Ks)) and its augmentation by carbachol in rat pancreatic acini. *Pflugers Arch.* 438, 604–611.

Knipper, M., Claussen, C., Ruttiger, L., Zimmermann, U., Lullmann-Rauch, R., Eskelinen, E. L., Schroder, J., Schwake, M., and Saftig, P. (2006). Deafness in LIMP2-deficient mice due to early loss of the potassium channel KCNQ1/KCNE1 in marginal cells of the stria vascularis. *J. Physiol. (Lond.)* 576, 73–86.

Knollmann, B. C., Sirenko, S., Rong, Q., Katchman, A. N., Casimiro, M., Pfeifer, K., and Ebert, S. N. (2007). Kcnq1 contributes to an adrenergic-sensitive steady-state K+ current in mouse heart. *Biochem. Biophys. Res. Commun.* 360, 212–218.

Kottgen, M., Hoefer, A., Kim, S. J., Beschorner, U., Schreiber, R., Hug, M. J., and Greger, R. (1999). Carbachol activates a K+ channel of very small conductance in the basolateral membrane of rat pancreatic acinar cells. *Pflugers Arch.* 438, 597–603.

Kunzelmann, K., Hubner, M., Schreiber, R., Levy-Holzman, R., Garty, H., Bleich, M., Warth, R., Slavik, M., von Hahn, T., and Greger, R. (2001). Cloning and function of the rat colonic epithelial K+ channel KVLQT1. *J. Membr. Biol.* 179, 155–164.

Kurokawa, J., Motoike, H. K., and Kass, R. S. (2001). TEA(+)-sensitive KCNQ1 constructs reveal pore-independent access to KCNE1 in assembled I(Ks) channels. *J. Gen. Physiol.* 117, 43–52.

Kurokawa, J., Motoike, H. K., Rao, J., and Kass, R. S. (2004). Regulatory actions of the A-kinase anchoring protein Yotiao on a heart potassium channel downstream of PKA phosphorylation. *Proc. Natl. Acad. Sci. U.S.A.* 101, 16374–16378.

Lambrecht, N. W., Yakubov, I., Scott, D., and Sachs, G. (2005). Identification of the K efflux channel coupled to the gastric H-K-ATPase during acid secretion. *Physiol. Genomics* 21, 81–91.

Lee, J. E., Park, H. S., Uhm, D. Y., and Kim, S. J. (2004). Effects of KCNQ1 channel blocker, 293B, on the acetylcholine-induced Cl- secretion of rat pancreatic acini. *Pancreas* 28, 435–442.

Lee, M. P., Ravenel, J. D., Hu, R. J., Lustig, L. R., Tomaselli, G., Berger, R. D., Brandenburg, S. A., Litzi, T. J., Bunton, T. E., Limb, C., Francis, H., Gorelikow, M., Gu, H., Washington, K., Argani, P., Goldenring, J. R., Coffey, R. J., and Feinberg, A. P. (2000). Targeted disruption of the Kvlqt1 gene causes deafness and gastric hyperplasia in mice. *J. Clin. Invest.* 106, 1447–1455.

Lee, W. K., Torchalski, B., Roussa, E., and Thevenod, F. (2008). Evidence for KCNQ1 K+ channel expression in rat zymogen granule membranes and involvement in cholecystokinin-induced pancreatic acinar secretion. *Am. J. Physiol. Cell Physiol.* 294, C879–C892.

Lerche, C., Bruhova, I., Lerche, H., Steinmeyer, K., Wei, A. D., Strutz-Seebohm, N., Lang, F., Busch, A. E., Zhorov, B. S., and Seebohm, G. (2007). Chromanol 293B binding in KCNQ1 (Kv7.1) channels involves electrostatic interactions with a potassium ion in the selectivity filter. *Mol. Pharmacol.* 71, 1503–1511.

Lerche, C., Seebohm, G., Wagner, C. I., Scherer, C. R., Dehmelt, L., Abitbol, I., Gerlach, U., Brendel, J., Attali, B., and Busch, A. E. (2000). Molecular impact of MinK on the enantiospecific block of I(Ks) by chromanols. *Br. J. Pharmacol.* 131, 1503–1506.

Li, Y., Zaydman, M. A., Wu, D., Shi, J., Guan, M., Virgin-Downey, B., and Cui, J. (2011). KCNE1 enhances phosphatidylinositol 4,5-bisphosphate (PIP2) sensitivity of IKs to modulate channel activity. *Proc. Natl. Acad. Sci. U.S.A.* 108, 9095–9100.

Liang, G. H., Jin, Z., Ulfendahl, M., and Jarlebark, L. (2006). Molecular analyses of KCNQ1-5 potassium channel mRNAs in rat and guinea pig inner ears: expression, cloning, and alternative splicing. *Acta Otolaryngol.* 126, 346–352.

Loussouarn, G., Park, K. H., Bellocq, C., Baro, I., Charpentier, F., and Escande, D. (2003). Phosphatidylinositol-4,5-bisphosphate, PIP2, controls KCNQ1/KCNE1 voltage-gated potassium channels: a functional homology between voltage-gated and inward rectifier K+ channels. *EMBO J.* 22, 5412–5421.

Lvov, A., Gage, S. D., Berrios, V. M., and Kobertz, W. R. (2010). Identification of a protein-protein interaction between KCNE1 and the activation gate machinery of KCNQ1. *J. Gen. Physiol.* 135, 607–618.

Ma, L. J., Ohmert, I., and Vardanyan, V. (2011). Allosteric features of KCNQ1 gating revealed by alanine scanning mutagenesis. *Biophys. J.* 100, 885–894.

Macedo-Ribeiro, S., Hemrika, W., Renirie, R., Wever, R., and Messerschmidt, A. (1999). X-ray crystal structures of active site mutants of the vanadium-containing chloroperoxidase from the fungus *Curvularia inaequalis*. *J. Biol. Inorg. Chem.* 4, 209–219.

Mackie, A. R., Brueggemann, L. I., Henderson, K. K., Shiels, A. J., Cribbs, L. L., Scrogin, K. E., and Byron, K. L. (2008). Vascular KCNQ potassium channels as novel targets for the control of mesenteric artery constriction by vasopressin, based on studies in single cells, pressurized arteries, and in vivo measurements of mesenteric vascular resistance. *J. Pharmacol. Exp. Ther.* 325, 475–483.

Mall, M., Wissner, A., Schreiber, R., Kuehr, J., Seydewitz, H. H., Brandis, M., Greger, R., and Kunzelmann, K. (2000). Role of K(V)LQT1 in cyclic adenosine monophosphate-mediated Cl(-) secretion in human airway epithelia. *Am. J. Respir. Cell Mol. Biol.* 23, 283–289.

Marcus, D. C., and Shen, Z. (1994). Slowly activating voltage-dependent K+ conductance is apical pathway for K+ secretion in vestibular dark cells. *Am. J. Physiol.* 267, C857–C864.

Marx, S. O., Kurokawa, J., Reiken, S., Motoike, H., D'Armiento, J., Marks, A. R., and Kass, R. S. (2002). Requirement of a macromolecular signaling complex for beta adrenergic receptor modulation of the KCNQ1-KCNE1 potassium channel. *Science* 295, 496–499.

Mazhari, R., Nuss, H. B., Armoundas, A. A., Winslow, R. L., and Marban, E. (2002). Ectopic expression of KCNE3 accelerates cardiac repolarization and abbreviates the QT interval. *J. Clin. Invest.* 109, 1083–1090.

McCallum, L. A., Greenwood, I. A., and Tribe, R. M. (2009). Expression and function of K(v)7 channels in murine myometrium throughout oestrous cycle. *Pflugers Arch.* 457, 1111–1120.

McCrossan, Z. A., and Abbott, G. W. (2004). The MinK-related peptides. *Neuropharmacology* 47, 787–821.

Melman, Y. F., Domenech, A., de la Luna, S., and McDonald, T. V. (2001). Structural determinants of KvLQT1 control by the KCNE family of proteins. *J. Biol. Chem.* 276, 6439–6444.

Melman, Y. F., Krumerman, A., and McDonald, T. V. (2002). A single transmembrane site in the KCNE-encoded proteins controls the specificity of KvLQT1 channel gating. *J. Biol. Chem.* 277, 25187–25194.

Melman, Y. F., Um, S. Y., Krumerman, A., Kagan, A., and McDonald, T. V. (2004). KCNE1 binds to the KCNQ1 pore to regulate potassium channel activity. *Neuron* 42, 927–937.

Morin, T. J., and Kobertz, W. R. (2008). Counting membrane-embedded KCNE beta-subunits in functioning K+ channel complexes. *Proc. Natl. Acad. Sci. U.S.A.* 105, 1478–1482.

Morokuma, J., Blackiston, D., Adams, D. S., Seebohm, G., Trimmer, B., and Levin, M. (2008). Modulation of potassium channel function confers a hyperproliferative invasive phenotype on embryonic stem cells. *Proc. Natl. Acad. Sci. U.S.A.* 105, 16608–16613.

Nakajo, K., and Kubo, Y. (2007). KCNE1 and KCNE3 stabilize and/or slow voltage sensing S4 segment of KCNQ1 channel. *J. Gen. Physiol.* 130, 269–281.

Nakajo, K., and Kubo, Y. (2008). Second coiled-coil domain of KCNQ channel controls current expression and subfamily specific heteromultimerization by salt bridge networks. *J. Physiol. (Lond.)* 586, 2827–2840.

Nakajo, K., Nishino, A., Okamura, Y., and Kubo, Y. (2011). KCNQ1 subdomains involved in KCNE modulation revealed by an invertebrate KCNQ1 orthologue. *J. Gen. Physiol.* 138, 521–535.

Nakajo, K., Ulbrich, M. H., Kubo, Y., and Isacoff, E. Y. (2010). Stoichiometry of the KCNQ1 – KCNE1 ion channel complex. *Proc. Natl. Acad. Sci. U.S.A.* 107, 18862–18867.

Neyroud, N., Tesson, F., Denjoy, I., Leibovici, M., Donger, C., Barhanin, J., Faure, S., Gary, F., Coumel, P., Petit, C., Schwartz, K., and Guicheney, P. (1997). A novel mutation in the potassium channel gene KVLQT1 causes the Jervell and Lange-Nielsen cardioauditory syndrome. *Nat. Genet.* 15, 186–189.

Ng, F. L., Davis, A. J., Jepps, T. A., Harhun, M. I., Yeung, S. Y., Wan, A., Reddy, M., Melville, D., Nardi, A., Khong, T. K., and Greenwood, I. A. (2011). Expression and function of the K+ channel KCNQ genes in human arteries. *Br. J. Pharmacol.* 162, 42–53.

Nicolas, C. S., Park, K. H., El Harchi, A., Camonis, J., Kass, R. S., Escande, D., Merot, J., Loussouarn, G., Le Bouffant, F., and Baro, I. (2008). IKs response to protein kinase A-dependent KCNQ1 phosphorylation requires direct interaction with microtubules. *Cardiovasc. Res.* 79, 427–435.

Nicolas, M., Dememes, D., Martin, A., Kupershmidt, S., and Barhanin, J. (2001). KCNQ1/KCNE1 potassium channels in mammalian vestibular dark cells. *Hear. Res.* 153, 132–145.

Ohya, S., Sergeant, G. P., Greenwood, I. A., and Horowitz, B. (2003). Molecular variants of KCNQ channels expressed in murine portal vein myocytes: a role in delayed rectifier current. *Circ. Res.* 92, 1016–1023.

Osteen, J. D., Gonzalez, C., Sampson, K. J., Iyer, V., Rebolledo, S., Larsson, H. P., and Kass, R. S. (2010). KCNE1 alters the voltage sensor movements necessary to open the KCNQ1 channel gate. *Proc. Natl. Acad. Sci. U.S.A.* 107, 22710–22715.

Panaghie, G., Tai, K. K., and Abbott, G. W. (2006). Interaction of KCNE subunits with the KCNQ1 K+ channel pore. *J. Physiol. (Lond.)* 570, 455–467.

Park, K. S., Pang, B., Park, S. J., Lee, Y. G., Bae, J. Y., Park, S., Kim, I., and Kim, S. J. (2011). Identification and functional characterization of ion channels in CD34(+) hematopoietic stem cells from human peripheral blood. *Mol. Cells* 32, 181–188.

Piccini, M., Vitelli, F., Seri, M., Galietta, L. J., Moran, O., Bulfone, A., Banfi, S., Pober, B., and Renieri, A. (1999). KCNE1-like gene is deleted in AMME contiguous gene syndrome: identification and characterization of the human and mouse homologs. *Genomics* 60, 251–257.

Pugsley, M. K., Towart, R., Authier, S., Gallacher, D. J., and Curtis, M. J. (2011). Innovation in safety pharmacology testing. *J. Pharmacol. Toxicol. Methods* 64, 1–6.

Pusch, M. (1998). Increase of the single-channel conductance of KvLQT1 potassium channels induced by the association with minK. *Pflugers Arch.* 437, 172–174.

Pusch, M., Magrassi, R., Wollnik, B., and Conti, F. (1998). Activation and inactivation of homomeric KvLQT1 potassium channels. *Biophys. J.* 75, 785–792.

Rasmussen, H. B., Moller, M., Knaus, H. G., Jensen, B. S., Olesen, S. P., and Jorgensen, N. K. (2004). Subcellular localization of the delayed rectifier K(+) channels KCNQ1 and ERG1 in the rat heart. *Am. J. Physiol. Heart Circ. Physiol.* 286, H1300–H1309.

Rocheleau, J. M., and Kobertz, W. R. (2008). KCNE peptides differently affect voltage sensor equilibrium and equilibration rates in KCNQ1 K+ channels. *J. Gen. Physiol.* 131, 59–68.

Romey, G., Attali, B., Chouabe, C., Abitbol, I., Guillemare, E., Barhanin, J., and Lazdunski, M. (1997). Molecular mechanism and functional significance of the MinK control of the KvLQT1 channel activity. *J. Biol. Chem.* 272, 16713–16716.

Roura-Ferrer, M., Sole, L., Martinez-Marmol, R., Villalonga, N., and Felipe, A. (2008). Skeletal muscle Kv7 (KCNQ) channels in myoblast differentiation and proliferation. *Biochem. Biophys. Res. Commun.* 369, 1094–1097.

Sanguinetti, M. C., Curran, M. E., Zou, A., Shen, J., Spector, P. S., Atkinson, D. L., and Keating, M. T. (1996). Coassembly of K(V)LQT1 and minK (IsK) proteins to form cardiac I(Ks) potassium channel. *Nature* 384, 80–83.

Sanguinetti, M. C., and Jurkiewicz, N. K. (1990). Two components of cardiac delayed rectifier K+ current. Differential sensitivity to block by class III antiarrhythmic agents. *J. Gen. Physiol.* 96, 195–215.

Schmitt, N., Schwarz, M., Peretz, A., Abitbol, I., Attali, B., and Pongs, O. (2000). A recessive C-terminal Jervell and Lange-Nielsen mutation of the KCNQ1 channel impairs subunit assembly. *EMBO J.* 19, 332–340.

Schroeder, B. C., Waldegger, S., Fehr, S., Bleich, M., Warth, R., Greger, R., and Jentsch, T. J. (2000). A constitutively open potassium channel formed by KCNQ1 and KCNE3. *Nature* 403, 196–199.

Schulze-Bahr, E., Wang, Q., Wedekind, H., Haverkamp, W., Chen, Q., Sun, Y., Rubie, C., Hordt, M., Towbin, J. A., Borggrefe, M., Assmann, G., Qu, X., Somberg, J. C., Breithardt, G., Oberti, C., and Funke, H. (1997). KCNE1 mutations cause Jervell and Lange-Nielsen syndrome. *Nat. Genet.* 17, 267–268.

Schwake, M., Jentsch, T. J., and Friedrich, T. (2003). A carboxy-terminal domain determines the subunit specificity of KCNQ K+ channel assembly. *EMBO Rep.* 4, 76–81.

Seebohm, G., Chen, J., Strutz, N., Culberson, C., Lerche, C., and Sanguinetti, M. C. (2003a). Molecular determinants of KCNQ1 channel block by a benzodiazepine. *Mol. Pharmacol.* 64, 70–77.

Seebohm, G., Pusch, M., Chen, J., and Sanguinetti, M. C. (2003b). Pharmacological activation of normal and arrhythmia-associated mutant KCNQ1 potassium channels. *Circ. Res.* 93, 941–947.

Seebohm, G., Sanguinetti, M. C., and Pusch, M. (2003c). Tight coupling of rubidium conductance and inactivation in human KCNQ1 potassium channels. *J. Physiol. (Lond.)* 552, 369–378.

Seebohm, G., Lerche, C., Busch, A. E., and Bachmann, A. (2001a). Dependence of I(Ks) biophysical properties on the expression system. *Pflugers Arch.* 442, 891–895.

Seebohm, G., Lerche, C., Pusch, M., Steinmeyer, K., Bruggemann, A., and Busch, A. E. (2001b). A kinetic study on the stereospecific inhibition of KCNQ1 and I(Ks) by the chromanol 293B. *Br. J. Pharmacol.* 134, 1647–1654.

Seebohm, G., Scherer, C. R., Busch, A. E., and Lerche, C. (2001c). Identification of specific pore residues mediating KCNQ1 inactivation. A novel mechanism for long QT syndrome. *J. Biol. Chem.* 276, 13600–13605.

Seebohm, G., Strutz-Seebohm, N., Ureche, O. N., Baltaev, R., Lampert, A., Kornichuk, G., Kamiya, K., Wuttke, T. V., Lerche, H., Sanguinetti, M. C., and Lang, F. (2006). Differential roles of S6 domain hinges in the gating of KCNQ potassium channels. *Biophys. J.* 90, 2235–2244.

Seebohm, G., Westenskow, P., Lang, F., and Sanguinetti, M. C. (2005). Mutation of colocalized residues of the pore helix and transmembrane segments S5 and S6 disrupt deactivation and modify inactivation of KCNQ1 K+ channels. *J. Physiol. (Lond.)* 563, 359–368.

Sesti, F., and Goldstein, S. A. (1998). Single-channel characteristics of wild-type IKs channels and channels formed with two minK mutants that cause long QT syndrome. *J. Gen. Physiol.* 112, 651–663.

Shamgar, L., Haitin, Y., Yisharel, I., Malka, E., Schottelndreier, H., Peretz, A., Paas, Y., and Attali, B. (2008). KCNE1 constrains the voltage sensor of Kv7.1 K+ channels. *PLoS ONE* 3, e1943. doi:10.1371/journal.pone.0001943

Shen, Z., Liu, J., Marcus, D. C., Shiga, N., and Wangemann, P. (1995). DIDS increases K+ secretion through an IsK channel in apical membrane of vestibular dark cell epithelium of gerbil. *J. Membr. Biol.* 146, 283–291.

Silva, J., and Rudy, Y. (2005). Subunit interaction determines IKs participation in cardiac repolarization and repolarization reserve. *Circulation* 112, 1384–1391.

Silva, J. R., Pan, H., Wu, D., Nekouzadeh, A., Decker, K. F., Cui, J., Baker, N. A., Sept, D., and Rudy, Y. (2009). A multiscale model linking ion-channel molecular dynamics and electrostatics to the cardiac action potential. *Proc. Natl. Acad. Sci. U.S.A.* 106, 11102–11106.

Silva, J. R., and Rudy, Y. (2010). Multiscale electrophysiology modeling: from atom to organ. *J. Gen. Physiol.* 135, 575–581.

Smith, J. A., Vanoye, C. G., George, A. L. Jr., Meiler, J., and Sanders, C. R. (2007). Structural models for the KCNQ1 voltage-gated potassium channel. *Biochemistry* 46, 14141–14152.

Strutz-Seebohm, N., Pusch, M., Wolf, S., Stoll, R., Tapken, D., Gerwert, K., Attali, B., and Seebohm, G. (2011). Structural basis of slow activation gating in the cardiac I Ks channel complex. *Cell. Physiol. Biochem.* 27, 443–452.

Strutz-Seebohm, N., Seebohm, G., Fedorenko, O., Baltaev, R., Engel, J., Knirsch, M., and Lang, F. (2006). Functional coassembly of KCNQ4 with KCNE-beta- subunits in Xenopus oocytes. *Cell. Physiol. Biochem.* 18, 57–66.

Sugimoto, T., Tanabe, Y., Shigemoto, R., Iwai, M., Takumi, T., Ohkubo, H., and Nakanishi, S. (1990). Immunohistochemical study of a rat membrane protein which induces a selective potassium permeation: its localization in the apical membrane portion of epithelial cells. *J. Membr. Biol.* 113, 39–47.

Sunose, H., Liu, J., Shen, Z., and Marcus, D. C. (1997). cAMP increases apical IsK channel current and K+ secretion in vestibular dark cells. *J. Membr. Biol.* 156, 25–35.

Tai, K. K., and Goldstein, S. A. (1998). The conduction pore of a cardiac potassium channel. *Nature* 391, 605–608.

Takumi, T., Moriyoshi, K., Aramori, I., Ishii, T., Oiki, S., Okada, Y., Ohkubo, H., and Nakanishi, S. (1991). Alteration of channel activities and gating by mutations of slow ISK potassium channel. *J. Biol. Chem.* 266, 22192–22198.

Takumi, T., Ohkubo, H., and Nakanishi, S. (1988). Cloning of a membrane protein that induces a slow voltage-gated potassium current. *Science* 242, 1042–1045.

Tapper, A. R., and George, A. L. Jr. (2000). MinK subdomains that mediate modulation of and association with KvLQT1. *J. Gen. Physiol.* 116, 379–390.

Tapper, A. R., and George, A. L. Jr. (2001). Location and orientation of minK within the I(Ks) potassium channel complex. *J. Biol. Chem.* 276, 38249–38254.

Thomas, A. M., Harmer, S. C., Khambra, T., and Tinker, A. (2011). Characterization of a binding site for anionic phospholipids on KCNQ1. *J. Biol. Chem.* 286, 2088–2100.

Tian, C., Vanoye, C. G., Kang, C., Welch, R. C., Kim, H. J., George, A. L. Jr., and Sanders, C. R. (2007). Preparation, functional characterization, and NMR studies of human KCNE1, a voltage-gated potassium channel accessory subunit associated with deafness and long QT syndrome. *Biochemistry* 46, 11459–11472.

Tinel, N., Diochot, S., Borsotto, M., Lazdunski, M., and Barhanin, J. (2000). KCNE2 confers background current characteristics to the cardiac KCNQ1 potassium channel. *EMBO J.* 19, 6326–6330.

Towart, R., Linders, J. T., Hermans, A. N., Rohrbacher, J., van der Linde, H. J., Ercken, M., Cik, M., Roevens, P., Teisman, A., and Gallacher, D. J. (2009). Blockade of the I(Ks) potassium channel: an overlooked cardiovascular liability in drug safety screening? *J. Pharmacol. Toxicol. Methods* 60, 1–10.

Tristani-Firouzi, M., and Sanguinetti, M. C. (1998). Voltage-dependent inactivation of the human K+ channel KvLQT1 is eliminated by association with minimal K+ channel (minK) subunits. *J. Physiol. (Lond.)* 510(Pt 1), 37–45.

Tzounopoulos, T., Maylie, J., and Adelman, J. P. (1998). Gating of I(sK) channels expressed in Xenopus oocytes. *Biophys. J.* 74, 2299–2305.

Vallon, V., Grahammer, F., Richter, K., Bleich, M., Lang, F., Barhanin, J., Volkl, H., and Warth, R. (2001). Role of KCNE1-dependent K+ fluxes in mouse proximal tubule. *J. Am. Soc. Nephrol.* 12, 2003–2011.

Vallon, V., Grahammer, F., Volkl, H., Sandu, C. D., Richter, K., Rexhepaj, R., Gerlach, U., Rong, Q., Pfeifer, K., and Lang, F. (2005). KCNQ1-dependent transport in renal and gastrointestinal epithelia. *Proc. Natl. Acad. Sci. U.S.A.* 102, 17864–17869.

Wang, K., Terrenoire, C., Sampson, K. J., Iyer, V., Osteen, J. D., Lu, J., Keller, G., Kotton, D. N., and Kass, R. S. (2011a). Biophysical properties of slow potassium channels in human embryonic stem cell derived cardiomyocytes implicate subunit stoichiometry. *J. Physiol. (Lond.)* 589, 6093–6104.

Wang, Y. H., Jiang, M., Xu, X. L., Hsu, K. L., Zhang, M., and Tseng, G. N. (2011b). Gating-related molecular motions in the extracellular domain of the IKs channel: implications for IKs channelopathy. *J. Membr. Biol.* 239, 137–156.

Wang, K. W., and Goldstein, S. A. (1995). Subunit composition of minK potassium channels. *Neuron* 14, 1303–1309.

Wang, K. W., Tai, K. K., and Goldstein, S. A. (1996a). MinK residues line a potassium channel pore. *Neuron* 16, 571–577.

Wang, Q., Curran, M. E., Splawski, I., Burn, T. C., Millholland, J. M., VanRaay, T. J., Shen, J., Timothy, K. W., Vincent, G. M., de Jager, T., Schwartz, P. J., Toubin, J. A., Moss, A. J., Atkinson, D. L., Landes, G. M., Connors, T. D., and Keating, M. T. (1996b). Positional cloning of a novel potassium channel gene: KVLQT1 mutations cause cardiac arrhythmias. *Nat. Genet.* 12, 17–23.

Wang, W., Xia, J., and Kass, R. S. (1998). MinK-KvLQT1 fusion proteins, evidence for multiple stoichiometries of the assembled IsK channel. *J. Biol. Chem.* 273, 34069–34074.

Wangemann, P. (1995). Comparison of ion transport mechanisms between vestibular dark cells and strial marginal cells. *Hear. Res.* 90, 149–157.

Wangemann, P., Liu, J., and Marcus, D. C. (1995). Ion transport mechanisms responsible for K+ secretion and the transepithelial voltage across marginal cells of stria vascularis in vitro. *Hear. Res.* 84, 19–29.

Warth, R., and Barhanin, J. (2002). The multifaceted phenotype of the knockout mouse for the KCNE1 potassium channel gene. *Am. J. Physiol. Regul. Integr. Comp. Physiol.* 282, R639–R648.

Wu, D. M., Jiang, M., Zhang, M., Liu, X. S., Korolkova, Y. V., and Tseng, G. N. (2006). KCNE2 is colocalized with KCNQ1 and KCNE1 in cardiac myocytes and may function as a negative modulator of I(Ks) current amplitude in the heart. *Heart Rhythm* 3, 1469–1480.

Xu, Q., and Minor, D. L. Jr. (2009). Crystal structure of a trimeric form of the K(V)7.1 (KCNQ1) A-domain tail coiled-coil reveals structural plasticity and context dependent changes in a putative coiled-coil trimerization motif. *Protein Sci.* 18, 2100–2114.

Xu, X., Jiang, M., Hsu, K. L., Zhang, M., and Tseng, G. N. (2008). KCNQ1 and KCNE1 in the IKs channel complex make state-dependent contacts in their extracellular domains. *J. Gen. Physiol.* 131, 589–603.

Yang, W. P., Levesque, P. C., Little, W. A., Conder, M. L., Shalaby, F. Y., and Blanar, M. A. (1997). KvLQT1, a voltage-gated potassium channel responsible for human cardiac arrhythmias. *Proc. Natl. Acad. Sci. U.S.A.* 94, 4017–4021.

Yeung, S. Y., Pucovsky, V., Moffatt, J. D., Saldanha, L., Schwake, M., Ohya, S., and Greenwood, I. A. (2007). Molecular expression and pharmacological identification of a role for K(v)7 channels in murine vascular reactivity. *Br. J. Pharmacol.* 151, 758–770.

Zhang, H., Craciun, L. C., Mirshahi, T., Rohacs, T., Lopes, C. M., Jin, T., and Logothetis, D. E. (2003). PIP(2) activates KCNQ channels, and its hydrolysis underlies receptor-mediated inhibition of M currents. *Neuron* 37, 963–975.

Zheng, R., Thompson, K., Obeng-Gyimah, E., Alessi, D., Chen, J., Cheng, H., and McDonald, T. V. (2010). Analysis of the interactions between the C-terminal cytoplasmic domains of KCNQ1 and KCNE1 channel subunits. *Biochem. J.* 428, 75–84.

Zhong, X. Z., Harhun, M. I., Olesen, S. P., Ohya, S., Moffatt, J. D., Cole, W. C., and Greenwood, I. A. (2010). Participation of KCNQ (Kv7) potassium channels in myogenic control of cerebral arterial diameter. *J. Physiol. (Lond.)* 588, 3277–3293.

Zicha, S., Moss, I., Allen, B., Varro, A., Papp, J., Dumaine, R., Antzelevich, C., and Nattel, S. (2003). Molecular basis of species-specific expression of repolarizing K+ currents in the heart. *Am. J. Physiol. Heart Circ. Physiol.* 285, H1641–H1649.

Conflict of Interest Statement: The authors declare that the research was conducted in the absence of any commercial or financial relationships that could be construed as a potential conflict of interest.

Received: 29 March 2012; accepted: 29 June 2012; published online: 02 August 2012.

*Citation: Wrobel E, Tapken D and Seebohm G (2012) The KCNE tango – how KCNE1 interacts with Kv7.1. Front. Pharmacol. **3**:142. doi: 10.3389/fphar.2012.00142*

This article was submitted to Frontiers in Pharmacology of Ion Channels and Channelopathies, a specialty of Frontiers in Pharmacology.

APPENDIX

Table A1 | Kv7.1 expression in mammalian tissues.

Specified tissue	Species	mRNA/protein	Reference
Brain	Mouse	mRNA	Lee et al. (2000)
	Mouse	mRNA	Ohya et al. (2003)
	Mouse	mRNA	Yeung et al. (2007)
	Mouse	mRNA	Iannotti et al. (2010)
Inner ear	Mouse	mRNA	Neyroud et al. (1997)
	Mouse	mRNA/protein	Nicolas et al. (2001)
	Mouse	Protein	Knipper et al. (2006)
	Rat	mRNA	Liang et al. (2006)
	Rat	Protein	Hur et al. (2007)
	Guinea pig	mRNA	Liang et al. (2006)
Trachea	Mouse	mRNA/protein	Grahammer et al. (2001b)
Thyroid gland	Mouse	mRNA/protein	Frohlich et al. (2011)
	Human	mRNA	Yang et al. (1997)
	Human	mRNA	Frohlich et al. (2011)
Thymus	Mouse	mRNA	Demolombe et al. (2001)
	Human	mRNA	Chouabe et al. (1997)
Lung	Mouse	mRNA	Demolombe et al. (2001)
	Human	mRNA	Wang et al. (1996b)
	Human	mRNA	Sanguinetti et al. (1996)
	Human	mRNA	Chouabe et al. (1997)
	Human	mRNA	Yang et al. (1997)
Heart	Mouse	mRNA	Barhanin et al. (1996)
	Mouse	mRNA	Lee et al. (2000)
	Mouse	mRNA	Casimiro et al. (2001)
	Mouse	mRNA	Demolombe et al. (2001)
	Mouse	mRNA	Ohya et al. (2003)
	Mouse	mRNA	Yeung et al. (2007)
	Mouse	mRNA	Iannotti et al. (2010)
	Mouse	mRNA	Strutz-Seebohm et al. (2006)
	Mouse	Protein	Knollmann et al. (2007)
	Rat	Protein	Rasmussen et al. (2004)
	Guinea pig	mRNA/protein	Zicha et al. (2003)
	Guinea pig	Protein	Nicolas et al. (2008)
	Ferret	mRNA	Brahmajothi et al. (1997)
	Rabbit	mRNA/protein	Zicha et al. (2003)
	Horse	Protein	Finley et al. (2002)
	Canine	mRNA/protein	Han et al. (2002)
	Human	mRNA	Wang et al. (1996b)
	Human	mRNA	Sanguinetti et al. (1996)
	Human	mRNA	Chouabe et al. (1997)
	Human	mRNA	Yang et al. (1997)
	Human	mRNA	Bendahhou et al. (2005)
	Human	mRNA	Gaborit et al. (2007)
	Human	mRNA	Frohlich et al. (2011)
	Human	mRNA/protein	Zicha et al. (2003)
Liver	Mouse	mRNA	Lee et al. (2000)
	Mouse	mRNA	Demolombe et al. (2001)
Spleen	Mouse	mRNA	Demolombe et al. (2001)
	Human	mRNA	Chouabe et al. (1997)

(Continued)

Table A1 | Continued

Specified tissue	Species	mRNA/protein	Reference
Pancreas	Mouse	mRNA	Demolombe et al. (2001)
	Rat	Protein	Lee et al. (2008)
	Human	mRNA	Sanguinetti et al. (1996)
	Human	mRNA	Chouabe et al. (1997)
	Human	mRNA	Yang et al. (1997)
Stomach	Mouse	mRNA	Lee et al. (2000)
	Mouse	mRNA	Demolombe et al. (2001)
	Mouse	mRNA/protein	Dedek and Waldegger (2001)
	Mouse	Protein	Grahammer et al. (2001a)
	Mouse	Protein	Heitzmann et al. (2004)
	Mouse	Protein	Heitzmann and Warth (2007)
	Rat	mRNA/protein	Lambrecht et al. (2005)
	Human	mRNA	Yang et al. (1997)
	Human	mRNA	Frohlich et al. (2011)
	Human	Protein	Grahammer et al. (2001a)
Colon	Mouse	mRNA/protein	Dedek and Waldegger (2001)
	Rat	mRNA	Kunzelmann et al. (2001)
	Human	mRNA	Chouabe et al. (1997)
	Human	mRNA	Yang et al. (1997)
	Human	mRNA	Frohlich et al. (2011)
	Human	mRNA/protein	Horikawa et al. (2005)
Small intestine	Mouse	mRNA	Demolombe et al. (2001)
	Mouse	mRNA/protein	Dedek and Waldegger (2001)
	Human	mRNA	Chouabe et al. (1997)
	Human	mRNA	Yang et al. (1997)
Kidney	Mouse	mRNA	Barhanin et al. (1996)
	Mouse	mRNA	Lee et al. (2000)
	Mouse	mRNA	Demolombe et al. (2001)
	Mouse	Protein	Vallon et al. (2001)
	Human	mRNA	Wang et al. (1996b)
	Human	mRNA	Sanguinetti et al. (1996)
	Human	mRNA	Chouabe et al. (1997)
	Human	mRNA	Yang et al. (1997)
Uterus	Mouse	mRNA/protein	McCallum et al. (2009)
Placenta	Human	mRNA	Wang et al. (1996b)
	Human	mRNA	Sanguinetti et al. (1996)
	Human	mRNA	Chouabe et al. (1997)
	Human	mRNA	Yang et al. (1997)
Ovary	Human	mRNA	Chouabe et al. (1997)
Prostate	Human	mRNA	Chouabe et al. (1997)
	Human	mRNA	Yang et al. (1997)
Testis	Human	mRNA	Chouabe et al. (1997)
Blood vessels	Mouse	mRNA/protein	Ohya et al. (2003)
	Mouse	mRNA/protein	Yeung et al. (2007)
	Rat	mRNA	Brueggemann et al. (2007)
	Rat	mRNA	Mackie et al. (2008)
	Rat	mRNA	Joshi et al. (2009)
	Rat	mRNA/protein	Zhong et al. (2010)
	Human	mRNA/protein	Ng et al. (2011)
Skeletal muscle	Mouse	mRNA	Demolombe et al. (2001)
	Mouse	mRNA	Iannotti et al. (2010)
	Rat	mRNA	Roura-Ferrer et al. (2008)
Peripheral blood leukocytes	Human	mRNA	Chouabe et al. (1997)
Hematopoietic stem cells	Human	mRNA	Park et al. (2011)

frontiers in
PHARMACOLOGY

ORIGINAL RESEARCH ARTICLE
published: 11 June 2012
doi: 10.3389/fphar.2012.00109

Acidosis differentially modulates inactivation in $Na_V1.2$, $Na_V1.4$, and $Na_V1.5$ channels

Yury Y. Vilin, Colin H. Peters and Peter C. Ruben*

Molecular Cardiac Physiology Group, Department of Biomedical Physiology and Kinesiology, Simon Fraser University, Burnaby, BC, Canada

Edited by:
Gildas Loussouarn, University of Nantes, France

Reviewed by:
Jean-Pierre Benitah, INSERM U637, France
Jean-Sebastien Rougier, University of Bern, Switzerland

***Correspondence:**
Peter C. Ruben, Department of Biomedical Physiology and Kinesiology, Simon Fraser University, 8888 University Drive, Burnaby, BC, Canada V5A 1S6.
e-mail: pruben@sfu.ca

Na_V channels play a crucial role in neuronal and muscle excitability. Using whole-cell recordings we studied effects of low extracellular pH on the biophysical properties of $Na_V1.2$, $Na_V1.4$, and $Na_V1.5$, expressed in cultured mammalian cells. Low pH produced different effects on different channel subtypes. Whereas $Na_V1.4$ exhibited very low sensitivity to acidosis, primarily limited to partial block of macroscopic currents, the effects of low pH on gating in $Na_V1.2$ and $Na_V1.5$ were profound. In $Na_V1.2$ low pH reduced apparent valence of steady-state fast inactivation, shifted the $\tau(V)$ to depolarizing potentials and decreased channels availability during onset to slow and use-dependent inactivation (UDI). In contrast, low pH delayed open-state inactivation in $Na_V1.5$, right-shifted the voltage-dependence of window current, and increased channel availability during onset to slow and UDI. These results suggest that protons affect channel availability in an isoform-specific manner. A computer model incorporating these results demonstrates their effects on membrane excitability.

Keywords: gating, activation, fast inactivation, slow inactivation, patch-clamp, sodium channels

INTRODUCTION

Extracellular pH is a major factor that controls activity of many physiological processes. Under normal physiological conditions, pH is maintained at approximately 7.4. Previous studies *in vivo* and *in situ* demonstrated that pathological conditions, such as hypoxia and/or ischemia considerably decrease extracellular pH. During focal ischemia in rabbit brain, extracellular pH drops to as low as 6.0 (Meyer, 1990). Physical exercise of medium-to-maximum intensity may decrease pH in human skeletal muscle to 6.4 (Hermansen and Osnes, 1972). Myocardial ischemia, including regional and global ischemia, can lower pH from 7.4 to 6.13 (Maruki et al., 1993). Acidification decreases peak conductance of voltage-gated sodium channels (Na_V) by two mechanisms; protonation of outer vestibule carboxylates (Mozhayeva et al., 1984; Khan et al., 2002, 2006) and depolarizing the voltage-dependence of gating by surface charge screening (Hille, 1968; Benitah et al., 1997). Unlike neuronal ($Na_V1.2$) and skeletal muscle ($Na_V1.4$) subtypes, the cardiac sodium channel subtype ($Na_V1.5$) may exhibit persistent Na currents (I_{NaP}) in response to low extracellular pH, which is considered to be a predisposing factor for cardiac arrhythmias (Amin et al., 2010). The I_{NaP} induced by low pH in only $Na_V1.5$ raises a question regarding the possible specificity of pH effects on different Na_V subtypes.

In this study we report differential effects of low pH on kinetic properties of fast, slow, and UDI in $Na_V1.2$, $Na_V1.4$, and $Na_V1.5$ channels. Using whole-cell patch-clamp recordings, we found that low pH modified properties of $Na_V1.2$ inactivation resulting in decreased maximum availability during prolonged depolarization trains. Under similar conditions, $Na_V1.5$ demonstrated enhanced maximum availability. $Na_V1.4$ was relatively unaffected by low pH. Using computer modeling, we found that low pH produces opposing effects on action potential (AP) generation: inhibitory for neuronal APs and excitatory for cardiac APs.

Some of these data have been presented previously in abstract form (Vilin and Ruben, 2010).

MATERIALS AND METHODS

Chinese hamster ovary (CHO) cells stably expressing the rat $Na_V1.2$ channel (a gift from W. A. Catterall) were grown in filtered sterile DMEM (Gibco) with glutamine, supplemented with 2 g/L $NaCHO_3$, 100 units/ml penicillin, 0.01 mg/ml streptomycin, 50 mg/ml G418 at pH 7.4, 5% FBS and maintained in a humidified environment at 37°C with 5% CO_2. Human Embryonic Kidney (HEK293; Cedarlanes) were transiently transfected with DNA encoding $Na_V1.4$ and $Na_V1.5$ α-subunits using the PolyFect kit (Qiagen). Channel expression was confirmed with EGFP. HEK293 cells were maintained under the same conditions with the exclusion of G418 from media. Twenty-four hours prior to electrophysiology experiments, cells were dissociated with 0.25% trypsin-EDTA (Gibco) and then plated on sterile cover slips at a density conducive to patch-clamp experiments. Whole-cell recordings were performed in a chamber containing (in mM): 140 NaCl, 4 KCl, 2 $CaCl_2$, 1 $MgCl_2$, 10 HEPES, pH 7.4, using pipettes fabricated with a P-1000 puller using borosilicate glass (Sutter Instruments, CA, USA), dipped in dental wax to reduce capacitance, then thermally polished to a resistance of 1.1–1.2 MΩ. Pipettes were filled with intracellular solution, containing (in mM): 120 CsF, 20 CsCl, 10 NaCl, 10 HEPES, pH 7.4.

All recordings were made using an EPC-9 patch-clamp amplifier (HEKA, Lambrecht, Germany) digitized at 20 kHz via an ITC-16 interface (Instrutech, Great Neck, NY, USA). Voltage clamping and data acquisition was controlled and low-pass-filtered (5 kHz) using PatchMaster/FitMaster software (HEKA Elektronik, Lambrecht, Germany) running on Apple iMac. Leak subtraction was performed automatically by software using a P/4 procedure following the test pulse. Leak subtraction was performed off-line in

slow inactivation experiments. Bath solution was maintained at 22.0 + 0.2°C using a Peltier device controlled by an HCC-100A temperature controller (Dagan, Minneapolis, MN, USA). Gigaseals were allowed to stabilize in the on-cell configuration for 1 min prior to establishing the whole-cell configuration. All data were acquired >5 min after attaining the whole-cell configuration. Holding potential between protocols was −60 mV.

Fitting and graphing were done using FitMaster software (HEKA Elektronik, Lambrecht, Germany) and Igor Pro (Wavemetrics, Lake Oswego, OR, USA) with statistical information derived using InStat (Graphpad Software Inc., San Diego, CA, USA). All data acquisition programs were run on an Apple iMac computer (Apple Computer, Cupertino, CA, USA).

Conductance [$G(V)$] curves were calculated from the equation:

$$G = \frac{I_{\max}}{V_{\mathrm{m}} - E_{\mathrm{Na}}} \tag{1}$$

where G is conductance, $I_{\max}$ represents peak test pulse current, V_{m} is the test pulse voltage, and E_{Na} is the measured equilibrium potential. The midpoint and apparent valence of activation were derived by fitting the $G(V)$ curves with a Boltzmann equation:

$$\frac{G}{G_{\max}} = \frac{1}{1 + \left(\exp\left(-ze_0\left(V_{\mathrm{M}} - V_{1/2}\right)\right)/kT\right)} \tag{2}$$

where the normalized conductance $G/G_{\max}$ is derived from Eq. 1, V_{M} is the test potential, z is the apparent valence, e_0 is the elementary charge, $V_{1/2}$ is the midpoint voltage, k is the Boltzmann constant, and T is temperature in °K.

Descriptions of test pulse inactivation rates given as time constants (t) were derived using monoexponential or double exponential fits with following the equations:

$$I(t) = \mathrm{Offset} + a_1 \exp\left(\frac{-t}{t}\right) \tag{3}$$

$$I(t) = \mathrm{Offset} + a_1 \exp\left(\frac{-t}{t_1}\right) + a_2 \exp\left(\frac{-t}{t_2}\right) \tag{4}$$

where $I(t)$ is current amplitude as function of time, Offset is the amplitude plateau (asymptote), a_1 and a_2 are the components for the corresponding time constants (τ) τ_1 and τ_2 is the time constant (in s or ms). Steady-state FI (SS-FI) probability between activated and non-inactivated states were fit using the Boltzmann equation:

$$\frac{I}{I_{\max}} = \frac{1}{1 + \exp\left(-ze_0\left(V_{\mathrm{M}} - V_{1/2}\right)kT\right)} \tag{5}$$

where $I_{\max}$ is the maximum normalized current amplitude, z is apparent valence, e_0 is the elementary charge, V_{m} is the prepulse potential, $V_{1/2}$ is the midpoint voltage of the SS-FI curve, k is the Boltzmann constant, and T is absolute temperature. Steady-state slow inactivation (SS-SI) curves were fit with the following modified Boltzmann equation that takes into account changes in the steady-state probability of slow inactivation:

$$\frac{I}{I_{\max}} = \frac{I_1 - I_2}{\left[1 + \exp\left(-ze_0\left(V_m - V_{1/2}\right)/kT\right)\right] + I_2} \tag{6}$$

where $I/I_{\max}$ is the maximum probability, I_1 and I_2 are maximum and minimum values in the fit, respectively, z is apparent valence, e_0 is the elementary charge, V_{m} is the prepulse potential, $V_{1/2}$ is the midpoint voltage of the SS-SI curve, k is the Boltzmann constant, and T is degrees Kelvin.

Window current areas were analyzed by converting activation and inactivation curves to percents (Wang et al., 1996) and calculating the area under both curves by integration using MS Excel; the position of area peak was estimated in Igor Pro.

The descriptions of first-order, two-state reaction kinetics were derived by fitting τ vs. voltage curves according to the following equation:

$$\tau(V_m) = \frac{1}{k_{\mathrm{f}} + k_{\mathrm{b}}}, \tag{7}$$

where $\tau(V_{\mathrm{m}})$ represents the time constant of progression to equilibrium as a function of membrane potential; k_{f} is the rate of the forward reaction (not inactivated:inactivated), and k_{b} is the rate of the backward reaction (inactivated:not inactivated).

$$k_{\mathrm{f}} = A_{\exp} + \frac{e(1-d)\left(V_m - V_{1/2}\right)}{kT} \tag{8}$$

$$k_{\mathrm{b}} = A_{\exp} - \frac{ed\left(V_m - V_{1/2}\right)}{kT} \tag{9}$$

where $A = 1/2$ rate at V_0, e = total reaction valence (in electronic charge); d = fractional barrier distance; V_{m} = membrane potential (in mV); $V_{1/2}$ = midpoint potential (in mV); k = Boltzmann constant, and T = temperature in degrees Kelvin.

NEURONAL ACTION POTENTIAL MODEL

The neuronal AP model was programmed using Python operating language and the module NumPy (Enthought). The sodium current was modeled following the formulas of Hodgkin and Huxley (1952; Eq. 10), with 0 mV defined as an absolute value, instead of the resting membrane potential.

$$I_{\mathrm{Na}} = G_{\mathrm{Na}} \cdot m^3 \cdot h \cdot j \cdot (V - E_{\mathrm{Na}}) \tag{10}$$

where I_{Na} is the fast sodium current, G_{Na} is the maximal sodium conductance value, m is the conductance gate, h is the FI gate, j is the slow inactivation gate, V is the membrane potential, and E_{Na} is the Nernst potential for sodium.

The conductance (m) gate and FI (h) gate steady-states (see Eqs A4 and A5 in Appendix) were fit to the experimental data using Eqs 2 and 5, respectively. The steady-state of the slow inactivation (j) gate (see Eq. A7 in Appendix) was fit to Eq. 6. Activation time constants were chosen to be constant following previously published reports (Spampanato et al., 2001, 2003). The time constant vs. voltage curve of FI (see Eq. A6 in Appendix) was fit to an asymmetric inverse hyperbolic cosine function (Eq. 11).

$$\tau = \frac{2\left(T_{\max}\right)}{\exp\left[\left(V - V_{1/2}\right)/k_1\right] + \exp\left[\left(V - V_{1/2}\right)/k_2\right]} \tag{11}$$

where τ is the time constant, $T_{\max}$ is the maximum time constant, $V_{1/2}$ is the membrane potential at which the maximal time

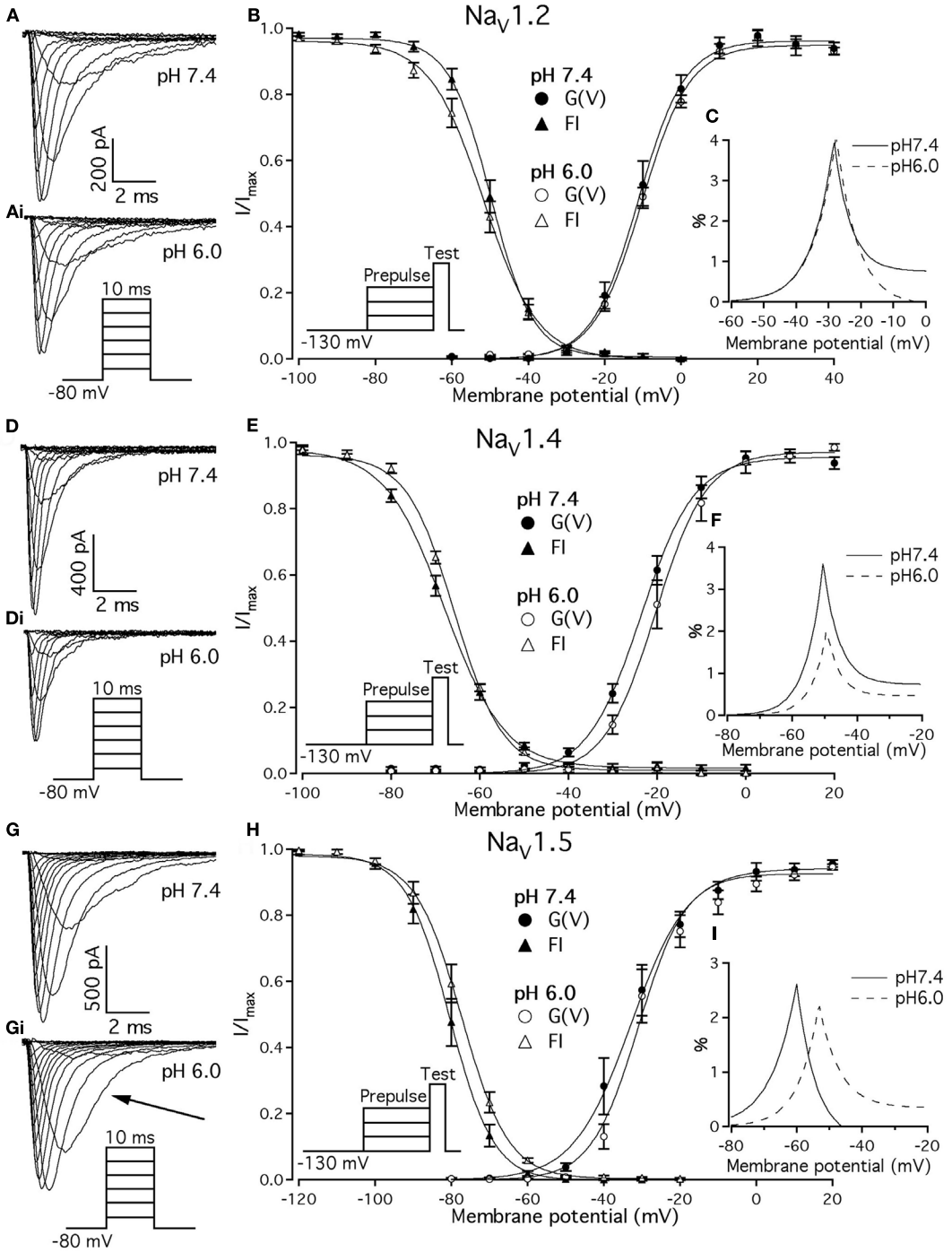

FIGURE 1 | Effects of pH on macroscopic ionic currents and window currents in $Na_V1.2$, $Na_V1.4$, and $Na_V1.5$. (A,Ai) Families of $Na_V1.2$ currents in response to the pulse protocol (**Ai**, inset) at pH 7.4 **(A)** and pH 6.0 **(Ai)**. **(B)** $Na_V1.2$ $G(V)$ curves (triangles) and steady-state FI curves (circles) are plotted as a function of membrane potential at pH 7.4 (filled symbols) and at pH 6.0 (open symbols). **(C)** Shows magnified window current area at pH 7.4 (solid lines) and at pH 6.0 (dotted lines). Values in **(C)** were converted to percents. **(D,Di)** Show families of $Na_V1.4$ currents in response to the pulse protocol (**Di**, inset) at pH 7.4 **(D)** and pH 6.0 **(Di)**. **(E)** $Na_V1.4$ $G(V)$ curves (triangles) and steady-state FI curves (circles) are plotted vs. membrane potential at pH 7.4 (filled symbols) and at pH 6.0 (open symbols). **(F)** Shows magnified window current area at pH = 7.4 (solid lines) and at pH 6.0 (dotted lines). Values in **(F)** are in percents. **(G)** Gi show families of $Na_V1.5$ currents in response to the pulse protocol (**Gi**, inset) at pH 7.4 **(G)** and pH 6.0 **(Gi)**. **(H)** $Na_V1.5$ $G(V)$ curves (triangles) and steady-state FI curves (circles) are plotted vs. membrane potential at pH 7.4 (filled symbols) and at pH 6.0 (open symbols). **(I)** Shows magnified window current area at pH 7.4 (solid lines) and at pH 6.0 (dotted lines). Values in **(I)** are in percents. Solid lines in **(B,E,H)** are Boltzmann fits to corresponding datapoints in **(B,E,H)** (Eq. 2 in Materials and Methods). Data represent mean ± SEM (n = 9–12).

constant occurs, and k_1 and k_2 are the slopes of the left and right halves of the curve.

Slow inactivation time constants (see Eq. A8 in Appendix) were fit in the same method as (Spampanato et al., 2001, 2003) with a Gaussian distribution (Eq. 12).

$$\tau = T_{\max} \exp\left[\frac{(V - V_{1/2})}{k_1}\right]^2 \quad (12)$$

where τ is the time constant, $T_{\max}$ is the maximum time constant, $V_{1/2}$ is the membrane potential at which the maximal time constant occurs, and k_1 is the slope factor of the curve.

A non-inactivating potassium current (Eqs A9–A13 in Appendix) and maximal conductance, Nernst potential, and cell capacitance parameters were used based on previously published formulas (Yuen and Durand, 1991; Spampanato et al., 2001, 2003). Stimulation protocols were done with a continuous stimulation over 105 ms at amplitudes ranging from −1 to −20 pA/pF.

CARDIAC ACTION POTENTIAL MODEL

The original ten Tusscher model (Ten Tusscher et al., 2004) was programmed into Python code making use of the module NumPy (Enthought). The code was then updated to include calcium current and slow delayed potassium current equations (Ten Tusscher and Panfilov, 2006). A late persistent sodium current was added (Eqs A24–A29 in Appendix ; Hund and Rudy, 2004). The maximal sodium conductance value was replaced with the Luo–Rudy passive model value to better reflect our experimental data (Luo and Rudy, 1991). The slow delayed rectifier potassium conductance (G_{Ks}; Eq. A30 in Appendix) was changed to incorporate the role of internal calcium concentrations on gKs (Terrenoire et al., 2005). The late sodium maximal conductance value was changed to reflect the data collected by (Zygmunt et al., 2001). The sodium current was modeled using Eq. 10. Our sodium channel conductance steady-states at both pH 7.4 and pH 6.0 (Eq. A14 in Appendix) were fit with Eq. 2 with the conductance value multiplied by the proton block in the pH 6.0 model. FI steady-state curves at both pH values (Eq. A18 in Appendix) were fit with Eq. 5. Slow inactivation steady-states curves at both pH values (Eq. A20 in Appendix) were fit with Eq. 6. Time constants of FI at both pH values (Eq. A19 in Appendix) were fit to an asymmetric inverse hyperbolic cosine function, Eq. 11. Activation and slow inactivation time constants (Eqs A15–A17 and A21–A23 in Appendix) were as described by the ten Tusscher model. The sodium channel parameters were then Q10 adjusted following the methods used in the model (Ten Tusscher and Panfilov, 2003) which used the work of Nagatomo et al. (1998). The simulation was run as an endocardial ventricular myocyte with a 1-ms stimulus pulse of amplitude −60 pA/pF. The stimulus protocol had a cycle length of 400 ms for the first 15 APs, 350 ms for the next 15, 325 ms for the next 10, and 300 ms for all subsequent APs. This was done to step the stimulus rate up to 3.33 Hz gradually and allow AP shortening. AP parameters were measured at both 2.5 Hz (150 beats per minute) and 3.33 Hz (200 beats per minute) to study the AP properties that acidosis of the cardiac voltage-gated sodium channel modulates at high heart rates. Measurements of APD were obtained from the time of stimulus to the time at which the membrane potential reaches a value of −70 mV. Maximal depolarization rise rates were measured as the maximum slope between two sequential membrane potentials after the stimulus current was ended. Equations modified from the original Tusscher model are listed in the Appendix.

All statistical values, both in the text and in the figures, are given as means ± standard error of the mean (SEM). Statistical differences were derived from Student's t-test using the Instat software package (GraphPad Software, Inc., San Diego, CA, USA).

RESULTS

EFFECTS OF LOW pH ON ACTIVATION AND STEADY-STATE FI IN $Na_V1.2$, $Na_V1.4$, $Na_V1.5$

Previous studies demonstrated that acidic pH decreases the amplitude of macroscopic sodium currents. **Figures 1A,D,G** show typical families of $Na_V1.2$, $Na_V1.4$, and $Na_V1.5$ recorded at control pH 7.4 in response to a depolarizing pulse protocol shown in insets of **Figure 1**. The current amplitude decreased in all three channel isoforms when pH was lowered to 6.0 (**Figure 1**, compare **Figures 1A,Ai,D,Di,G,Gi**). Amplitudes decreased by 32 ± 5, 35 ± 4.3, and 53 ± 7% for $Na_V1.2$, $Na_V1.4$, and $Na_V1.5$, respectively. In contrast to $Na_V1.2$ and $Na_V1.4$, the decay of macroscopic currents in $Na_V1.5$ at pH 6.0 was slower (denoted with the arrow in **Figure 1Gi**) compared to the control family of currents at pH 7.4 (**Figure 1G**). These results suggest that low pH alters properties of open-state inactivation.

We examined the effects of low pH on activation in $Na_V1.2$, $Na_V1.4$, and $Na_V1.5$. Data in **Figures 1B,E,H** represent normalized control maximum conductance derived from $I(V)$ relationships at pH 7.4 (filled circles) and pH 6.0 (open circles). Normalized conductance was plotted as a function of membrane potential and fit with the Boltzmann function (Eq. 1, Materials and Methods) to obtain values for $V_{1/2}$ and apparent valence (z). The $G(V)$ parameters we measured are shown in **Table 1**. At pH 6.0 the apparent valence of activation in $Na_V1.5$ was significantly

Table 1 | Parameters of $G(V)$ in $Na_V1.2$, $Na_V1.4$, and $Na_V1.5$ at pH 7.4 and 6.0.

Channel	z (pH 7.4)	z (pH 6.0)	$V_{1/2}$, mV (pH 7.4)	$V_{1/2}$, mV (pH 6.0)
$Na_V1.2$	4.4 ± 0.2	3.9 ± 0.1	−11.7 ± 1.56	−10.4 ± 1.4
$Na_V1.4$	3.8 ± 0.3	4.2 ± 0.5	−24.0 ± 1.1	−18.4 ± 2.8
$Na_V1.5$	3.8 ± 0.2	4.6 ± 0.6	−32.6 ± 2.8	−30.4 ± 2.2

n = 9–12.

Table 2 | Parameters of steady-state fast inactivation in $Na_V1.2$, $Na_V1.4$, and $Na_V1.5$ at pH 7.4 and 6.0.

Channel	z (pH 7.4)	z (pH 6.0)	$V_{1/2}$, mV (pH 7.4)	$V_{1/2}$, mV (pH 6.0)
$Na_V1.2$	−4.6 ± 0.2	−3.6 ± 0.1[(1)]	−50.1 ± 1.3	−52.0 ± 1.6
$Na_V1.4$	−3.5 ± 0.2	−4.2 ± 0.3	−67.5 ± 0.7	−66.0 ± 0.4
$Na_V1.5$	−4.4 ± 0.1	−4.1 ± 0.1	−80.6 ± 1.3	−77.5 ± 1.4

[(1)] $p < 0.05$ vs. apparent valence; (z) at pH 7.4 in $Na_V1.2$. n = 7–12.

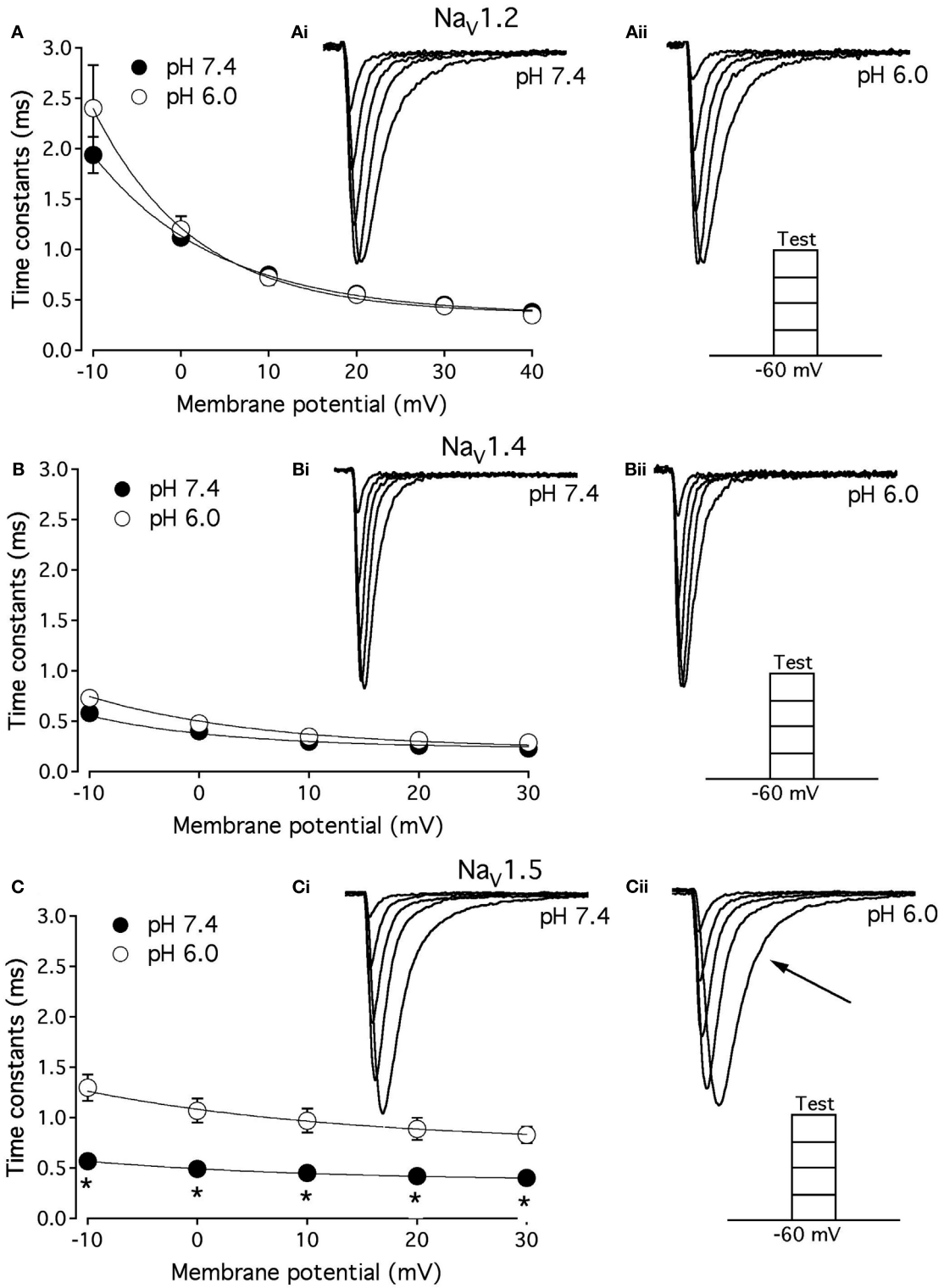

FIGURE 2 | Low pH decelerates kinetics of open-state inactivation in $hNa_v1.5$. (A) Open-state inactivation time constants in $Na_v1.2$ at pH 7.4 (filled circles) and pH 6.0 (open circles) are derived from single exponential fits (not shown) to the decay of currents in **(Ai,Aii)**. **(B)** Open-state inactivation time constants in $Na_v1.4$ at pH 7.4 (filled circles) and pH 6.0 (open circles) are derived from single exponential fits (not shown) to the decay of currents in **(Bi,Bii)**. **(C)** Open-state inactivation time constants in $Na_v1.5$ at pH 7.4 (filled circles) and pH 6.0 (open circles) are derived from single exponential fits (not shown) to the decay of currents in **(Ci,Cii)**. Arrow in **Cii** denotes deceleration of current decay in $Na_v1.5$ at pH 6.0. Asterisks denote $p < 0.05$ between open states FI at pH 7.4 (filled circles) and pH 6.0 (open circles). Data in **(A–C)** are fitted with single exponential for visual guidance. Data represent mean ± SEM ($n = 15$).

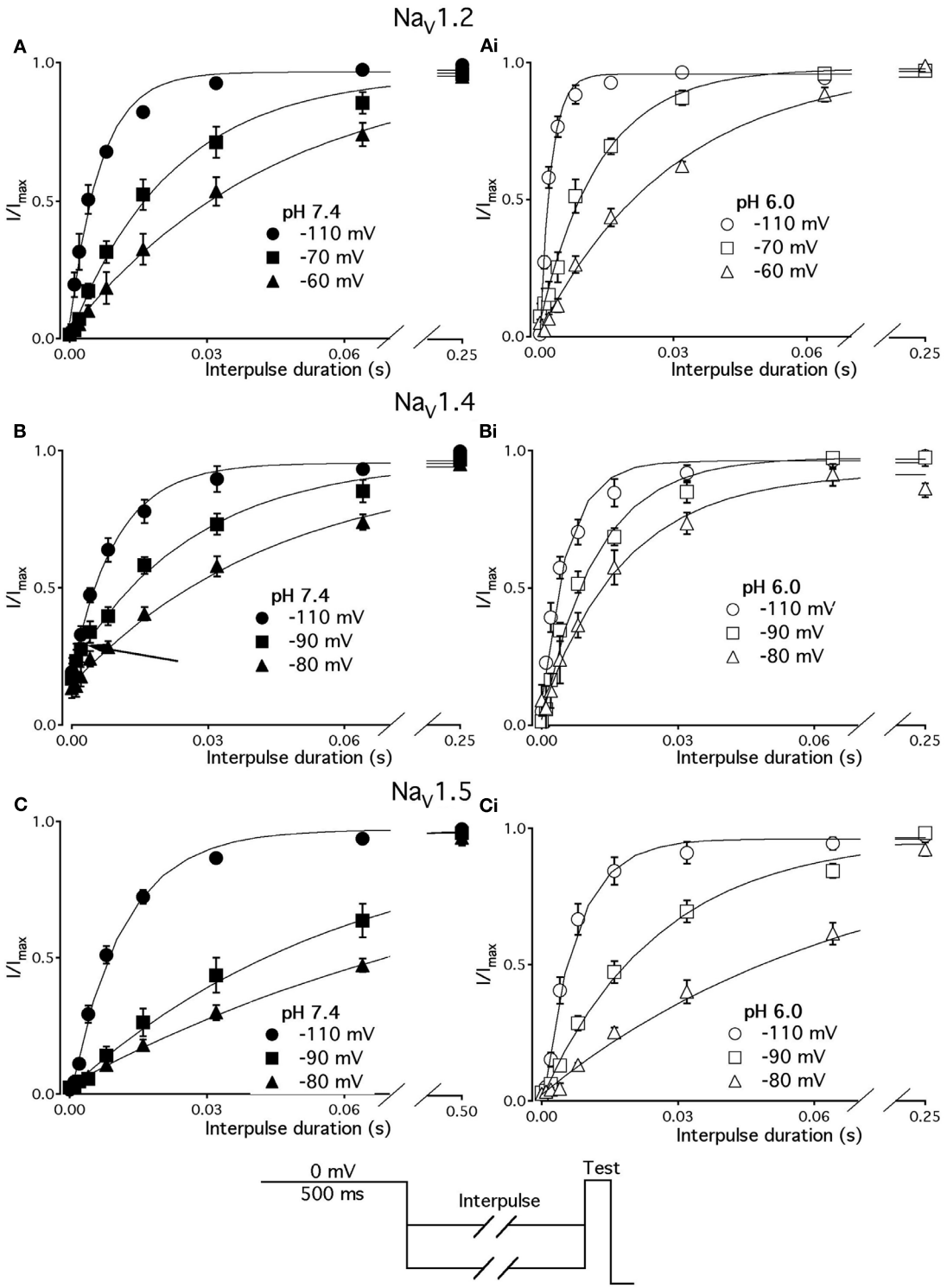

FIGURE 3 | Low pH accelerates recovery from FI. (A–C) The time course of recovery from FI at pH 7.4 (filled circles) and at pH 6.0 (open circles) for $Na_V1.2$, $Na_V1.4$, and $Na_V1.5$, respectively. The averaged, normalized currents obtained during 0 mV test pulse, following an interpulse of increasing duration over a range of potentials (−130 to −80 mV, pulse protocol is shown at the bottom) are plotted vs. interpulse duration and fit with single exponential. Solid lines are single exponential fits to datapoints (Equation, Materials and Methods). Data for only −80 mV prepulse are shown. Data represent mean ± SEM ($n = 10$–12).

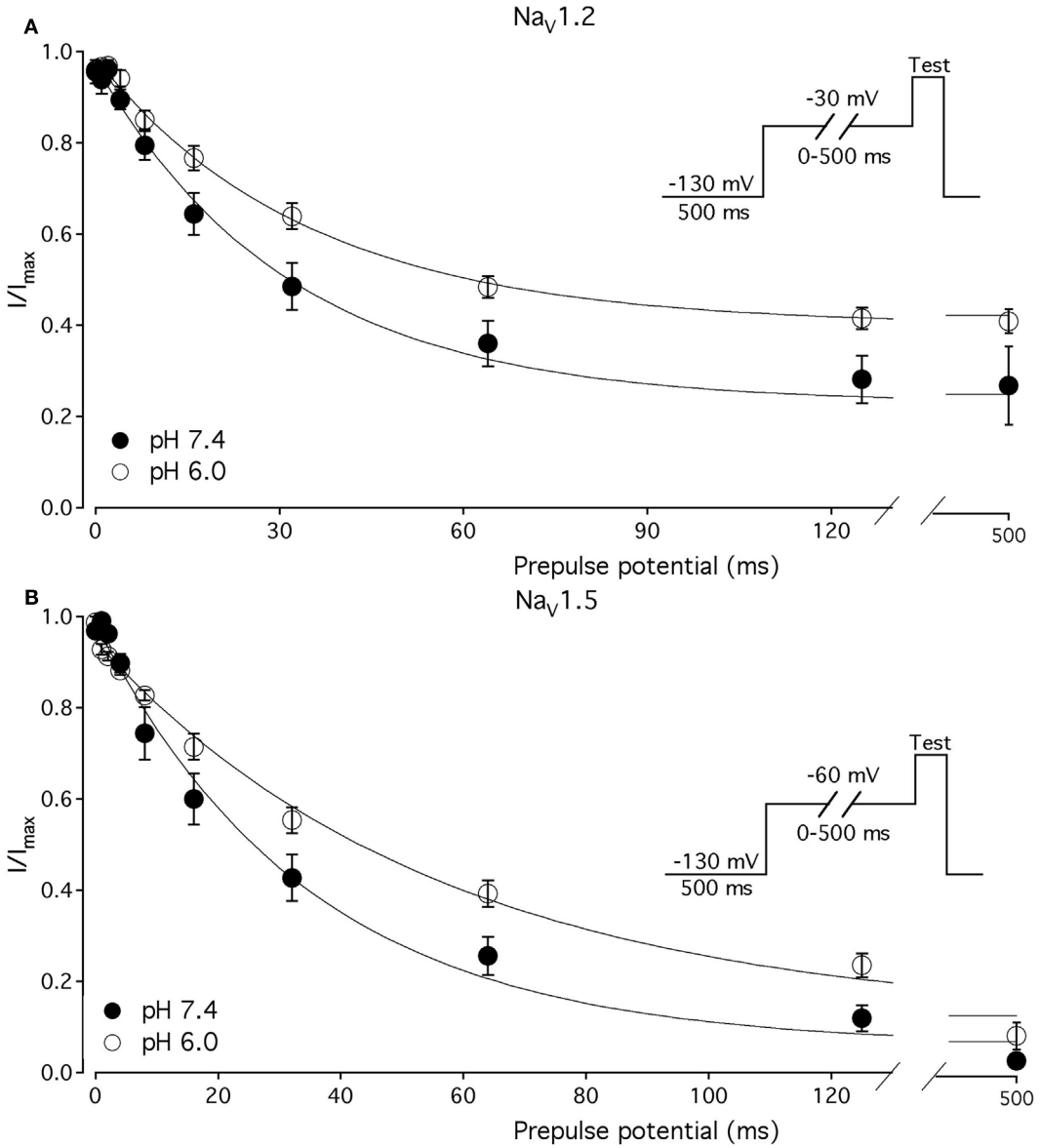

FIGURE 4 | Low pH slows the rate of onset to FI in Na$_v$1.2 and Na$_v$1.5. (A) The time course of onset to FI in Na$_V$1.2 at pH 7.4 (filled circles) and at pH 6.0 (open circles). Data represent averaged and normalized current peaks recorded during test potential following the −30 mV prepulse of variable duration (0–500 ms) plotted vs. prepulse potential. Diagram of used pulse protocols shown in **(A)**, *inset*. **(B)** The time course of onset to FI in Na$_V$1.5 at pH 7.4 (filled circles) and at pH 6.0 (open circles). Data represent averaged and normalized current peaks recorded during test potential following the −60-mV prepulse of variable duration (0–500 ms) plotted vs. prepulse potential. Diagram of used pulse protocols shown in **(B)**, *inset*. Solid lines are single exponential fits (Eq. 3, Materials and Methods). Data represent mean ± SEM ($n = 10$–12)

increased ($p < 0.05$). The $V_{1/2}$ of activation in Na$_V$1.5 was unaffected by low pH. In contrast, neither apparent valence nor the $V_{1/2}$ in Na$_V$1.2 and Na$_V$1.4 were altered by low pH ($p > 0.05$, **Figures 1B,E**, respectively).

To quantify the effects of low pH on voltage-dependent steady-state channel availability in fast-inactivated state, we compared the apparent valence (z) and $V_{1/2}$ from Boltzmann fits (Eq. 5, Materials and Methods) to steady-state FI data for Na$_V$1.2 (**Figure 1B**), Na$_V$1.4 (**Figure 1E**), and Na$_V$1.5 (**Figure 1H**) at pH 7.4 (filled triangles) and at pH 6.0 (open triangles). These data represent averaged, normalized current amplitudes obtained with a test pulse to 0 mV following a 500-ms prepulse (pulse protocol is shown in insets). Normalized current amplitudes were plotted as a function of prepulse potential. At pH 6.0 the apparent valence of steady-state FI in NaV1.2 was reduced from that at pH 7.4 to the value measured at pH 6.0 ($n = 11$). The $V_{1/2}$ of inactivation was not affected by low pH (**Table 2**). Low pH had no effect on steady-state FI in Na$_V$1.4 (**Table 2**). In Na$_V$1.5 the apparent valence was not altered at pH 6.0, but the $V_{1/2}$ was depolarized compared to the $V_{1/2}$ at pH 7.4.

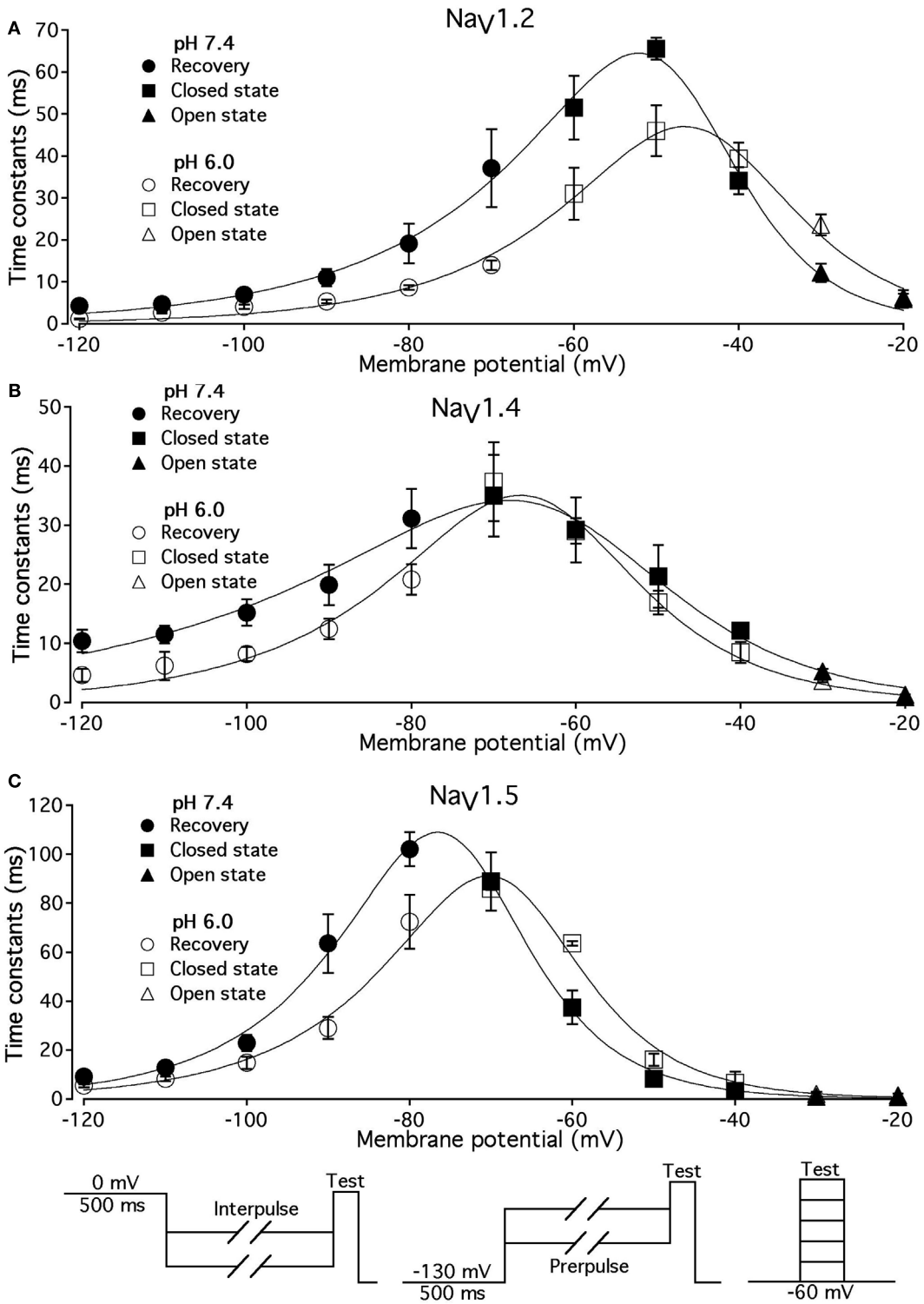

FIGURE 5 | Low pH alters the voltage dependency of FI time constants in $Na_v1.2$, $Na_v1.4$, and $Na_v1.5$. Time constants of FI in $Na_v1.2$ **(A)**, $Na_v1.4$ **(B)**, and $Na_v1.5$ **(C)** were derived from single exponential fits to recovery, onset, and decay of macroscopic currents in response to pulse protocols shown at the bottom (also see Materials and Methods) and plotted vs. membrane voltage. Circles represent recovery time constants, squires represent time constants of closed-state inactivation and triangles denote time constants for the open-state inactivation. Filled symbols represent time constants obtained at pH = 7.4 and open symbols represent time constants at pH 6.0. The solid lines are predictions of a first-order reaction model (inactivated ↔ not inactivated, Materials and Methods). Diagrams at the bottom of Figure depict pulse protocols used in this series of experiments. Data represent mean ± SEM ($n = 10$–12).

Table 3 | Parameters of $\tau(V)$ in $Na_V1.2$, $Na_V1.4$, and $Na_V1.5$ at pH 7.4 and 6.0.

	$Na_V1.2$	$Na_V1.4$	$Na_V1.5$
τ_{max}, ms (pH 7.4)	65	35	109
τ_{max}, ms (pH 6.0)	47	38	90
e, Total reaction value (pH 7.4)	4.1	2.5	4.5
e, Total reaction value (pH 6.0)	3.6	3.6	4.2
Barrier distance (pH 7.4)	0.3	0.3	0.4
Barrier distance (pH 6.0)	0.4	0.4	0.4
$V_{1/2}$, mV (pH 7.4)	−47.2	−63.4	−74.5
$V_{1/2}$, mV (pH 6.0)	−44	−66	−68

Table 4 | Parameters of steady-state slow inactivation in $Na_V1.2$ and $Na_V1.5$ at pH 7.4 and 6.0.

	$Na_V1.2$	$Na_V1.5$
SS_SI_{max},% (pH 7.4)	91.0 ± 1.1	64.0 ± 4.6
SS_SI_{max},% (pH 6.0)	98.0 ± 2.5	58.0 ± 3.5
z, Apparent valence (pH 7.4)	3.1 ± 0.6	1.9 ± 0.12
z, Apparent valence (pH 6.0)	3.7 ± 0.5	1.4 ± 0.1[(2)]
$V_{1/2}$, mV (pH 7.4)	−52.5 ± 2.8	−71.4 ± 3.2
$V_{1/2}$, mV (pH 6.0)	61.1 ± 3.7[(1)]	−57.4 ± 3.1[(3)]

[(1)] $p < 0.05$ vs. $V_{1/2}$ at pH = 7.4 in $Na_V1.2$.

[(2)] $p < 0.05$ vs. apparent valence (z) at pH = 7.4 in $Na_V1.5$.

[(3)] $p < 0.05$ vs. $V_{1/2}$ at pH = 7.4 in $Na_V1.5$; $n = 6$.

Changes in activation and steady-state inactivation slope and $V_{1/2}$ may alter the area of overlap between activation and steady-state FI curves, known as "window current." We studied this possibility by comparing this area at both pH 7.4 and 6.0 for $Na_V1.2$, $Na_V1.4$, and $Na_V1.5$. **Figures 1C,F,I** shows window current at pH 7.4 (solid line) and at pH 6.0 (dotted line) of $Na_V1.2$, $Na_V1.4$, and $Na_V1.5$, respectively. Data in these graphs were converted to percents (Wang et al., 1996) and plotted as a function of membrane potential. To compare the effects of pH on window currents, window currents were analyzed as described in Materials and Methods to find the area and peak position relative to membrane potential on the horizontal axis. Low pH had no significant effect on window currents in $Na_V1.2$ (**Figure 1C**, $p > 0.05$). Window current area in $Na_V1.4$ (**Figure 1E**) was reduced at pH 6.0 by 47 ± 4.5% ($p < 0.05$), however peak position was not changed: −51 ± 1.3 mV at pH 7.4 vs. −49 ± 1.0 mV at pH 6.0. Window current area in $Na_V1.5$ was not significantly altered by low pH, but the peak was shifted from −60.4 ± 0.7 mV (pH 7.4) to −53 ± 0.8 mV (1I, $p < 0.05$). The latter finding indicates a possible destabilization of FI gating in $Na_V1.5$ at low pH.

OPEN-STATE FAST INACTIVATION IN $Na_V1.5$ IS DECELERATED AT pH 6.0

As shown above, the decay of $Na_V1.5$ macroscopic currents was decelerated at pH 6.0. We asked whether this effect is specific to NaV1.5. **Figure 2** compares the effects of pH on open-state FI (FI) in $Na_V1.2$, $Na_V1.4$, and $Na_V1.5$. Data in **Figures 2A–C** represent time constants of open-state FI derived from exponential fits to decay of macroscopic current recorded from $Na_V1.2$ (**Figures 2Ai,Aii**), $Na_V1.4$ (**Figures 2Bi,ii**), $Na_V1.5$ (**Figure 2Ci,ii**) at pH 7.4 and pH 6.0. Pulse protocols are shown in **Figures 2Aii,Bii,Cii** *insets*. Time constants were plotted as a function of membrane potential and fitted with single exponential for visual guidance. **Figure 2A** shows that time course of open-state inactivation in $Na_V1.2$ at pH 7.4 (filled circles) is statistically identical ($p > 0.05$) to that at pH 6.0 (open circles). Similarly to $Na_V1.2$, the open-state inactivation in $Na_V1.4$ (**Figure 2B**) at pH 7.4 (filled circles) was not affected ($p > 0.05$) by low pH (open circles). However, the time course of open-state inactivation in $Na_V1.5$ at pH 6.0 (**Figure 2C**, open circles) was significantly slower than that recorded at pH 7.4 (**Figure 2C**, filled circles, asterisks denote $p < 0.05$), also see **Figures 2Ci,ii** *arrow*. Thus, data in **Figure 2** suggest that deceleration of rate of open-state FI due to low pH is specific to $Na_V1.5$, and is not seen in $Na_V1.2$ or $Na_V1.4$.

LOW pH ALTERS VOLTAGE-DEPENDENCE OF FAST INACTIVATION TIME CONSTANTS IN $Na_V1.2$, $Na_V1.4$, AND $Na_V1.5$

We studied effects of pH on the time course of recovery from fast-inactivated state (**Figure 3**), onset to FI (**Figure 4**), and consequently, the $\tau(V)$ dependence of FI (**Figure 5**). The rate of recovery from FI was studied using a double-pulse protocol (shown in **Figure 3**, inset). The fraction of recovered channels was measured from the peak current during a 0-mV test pulse. The current amplitude following recovery was normalized to the current amplitude during a pulse to 0 mV from −130 mV, a voltage at which all channels should be available (not inactivated). Recovery from FI in $Na_V1.2$, $Na_V1.4$, and $Na_V1.5$ was recorded with interpulse voltages from −120 to −80 mV. The rate of recovery from fast inactivation was greater in all three channel isoforms at low pH. **Figure 3** shows the time course of recovery from fast inactivation at pH 7.4 (filled circles) and at pH 6.0 (open circles) in $Na_V1.2$ (**Figure 3A**), $Na_V1.4$ (**Figure 3B**), and $Na_V1.5$ (**Figure 3C**). Data represent averaged and normalized current amplitudes recorded in response to test pulse following a −80-mV interpulse (see pulse protocol diagram in **Figure 3** *inset*), plotted as a function of interpulse duration (ms). For clarity, recovery data for other interpulse voltages are not shown. Solid lines are single exponential fits (Eq. 3), used to extract time constants to compare recovery at pH 7.4 and pH 6.0. We also found that more $Na_V1.4$ channels are available for recovery at the beginning ($t = 0$) of interpulse (**Figure 3B**, filled circles, arrow) at pH = 7.4 compared to pH = 6.0 (open circles, **Figure 3B**).

The effects of low pH on the rate of FI onset (**Figure 4**) were studied by measuring the test pulse current amplitude after a 0- to 500-ms prepulse of defined voltage (see protocol diagrams in **Figures 4A,B**). In response to increasing duration of prepulse, the fraction of inactivated channels, assayed with 0 mV test pulse is increased, as shown in **Figures 4A,B**. Data in **Figure 4** are normalized and averaged test pulse currents plotted as a function of prepulse duration. The rate of onset (given as a time constant) and steady-state fraction of inactivated channels (given as an asymptote) was quantified by fitting data with single exponential (Eq. 3). Onset of FI in $Na_V1.4$ at pH 7.4 was not different ($p < 0.05$) from that at pH 6.0 at prepulse potentials of −70, −60, −50, and −40 mV (data not shown). However, the onset to FI in $Na_V1.2$ (**Figure 4A**) and in $Na_V1.5$ (**Figure 4B**) was differentially

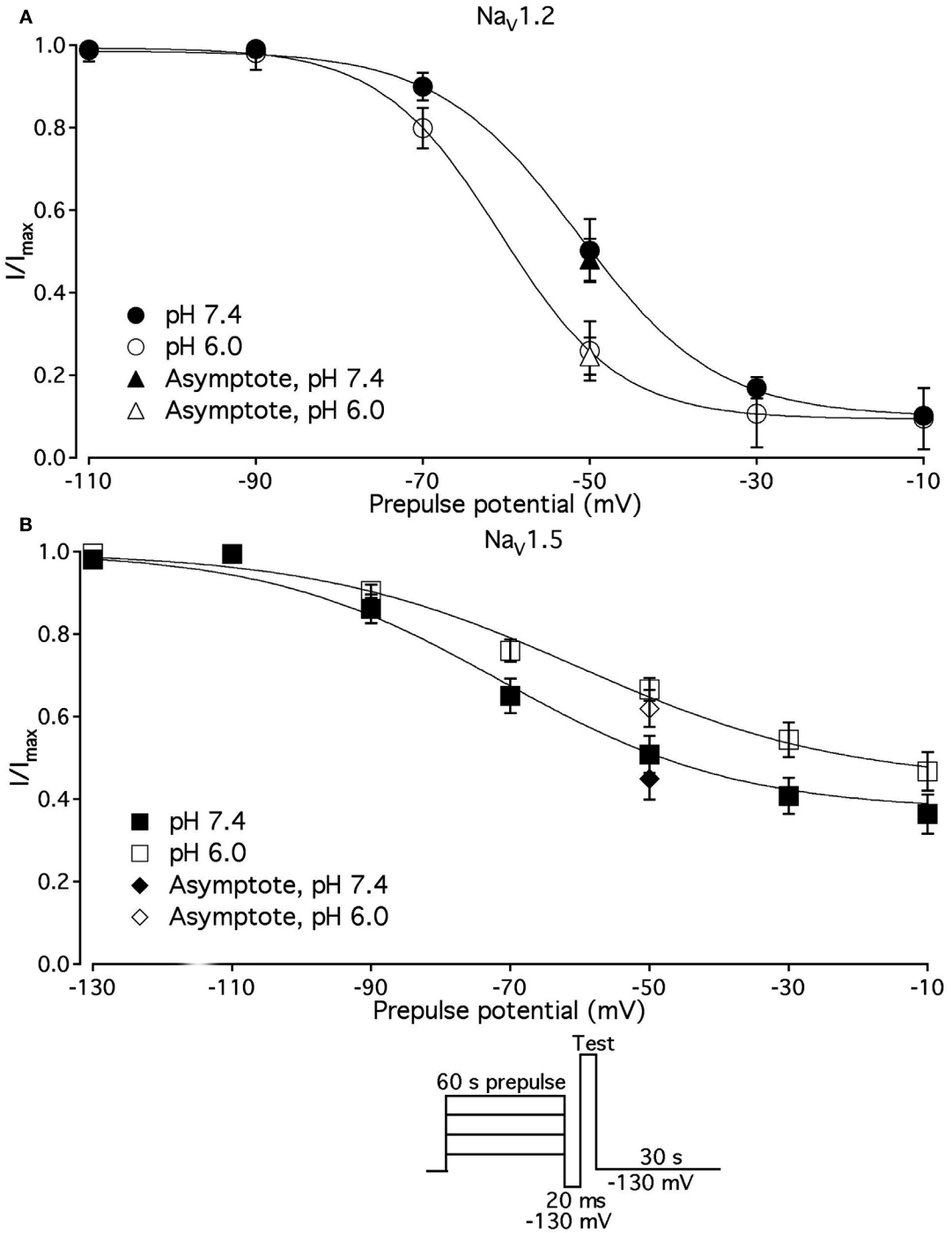

FIGURE 6 | Low pH alters properties of slow inactivation in $Na_V1.2$ and in $Na_V1.5$. (A) Steady-state slow inactivation in $Na_V1.2$ at pH 7.4 (filled circles) and at pH 6.0 (open circles) is plotted as averaged normalized current amplitude vs. 60-s prepulse voltage. Asymptotic values for $Na_V1.2$ derived from double exponential fit to slow inactivation onset **(B)** at pH 7.4 (filled triangles) and at pH 6.0 (open triangles) are superimposed with steady-state slow inactivation data at corresponding prepulse voltage (−50 mV). **(B)** Steady-state slow inactivation in $Na_V1.5$ at pH 7.4 (filled squares) and at pH 6.0 (open squares) is plotted as averaged normalized current amplitudes vs. 60-s prepulse voltage. Asymptotic values for $Na_V1.5$ derived from double exponential fits to slow inactivation onset **(B)** at pH 7.4 (filled triangles) and at pH 6.0 (open triangles) are superimposed with steady-state slow inactivation data at corresponding prepulse voltage (−50 mV). Data were obtained with pulse protocol shown in **(B)** *inset* and fit with a modified Boltzmann function (Eq. 6, Material and Methods). Data represent mean ± SEM ($n = 7$–10).

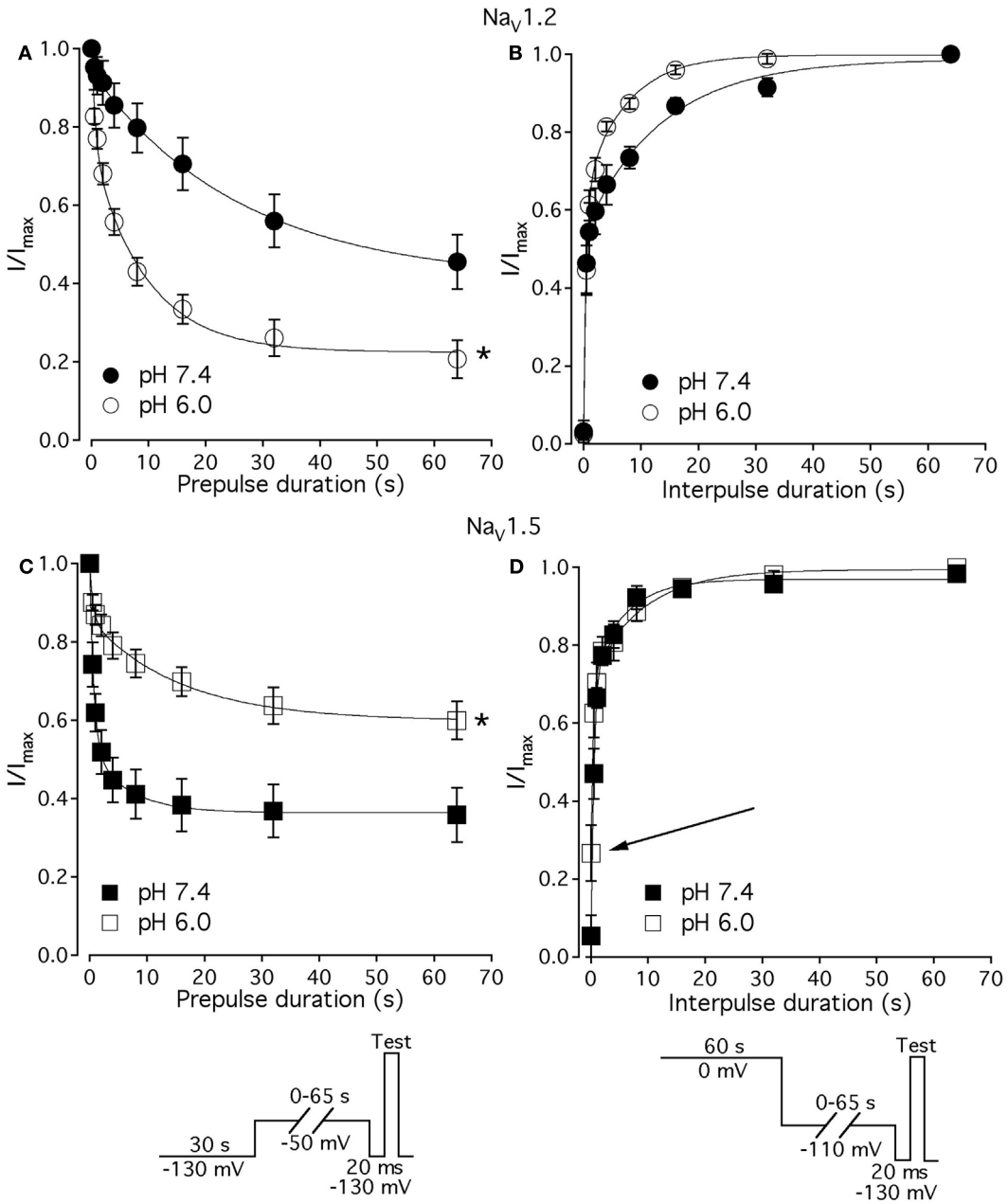

FIGURE 7 | Low pH alters kinetics of slow inactivation in Na$_V$1.2 and in Na$_V$1.5. (A) The time course of slow inactivation onset in Na$_V$1.2 at pH 7.4 (filled circles) and at pH 6.0 (open circles) is plotted vs. prepulse voltage as averaged and normalized currents, obtained with pulse protocol shown in **(C)** *inset*. **(B)** The time course of recovery from slow inactivation in Na$_V$1.2 at pH 7.4 (filled circles) and at pH 6.0 (open circles) is plotted vs. interpulse voltage as averaged and normalized currents, obtained with pulse protocol in **(D)** *inset*. **(C)** The time course of slow inactivation onset in Na$_V$1.5 at pH 7.4 (filled squares) and at pH 6.0 (open squares). **(D)** The time course of recovery from slow inactivation in Na$_V$1.5 at pH 7.4 (filled squares) and at pH 6.0 (open squares). Data represent mean ± SEM ($n = 7$–10). Asterisks denote statistical difference ($p < 0.05$).

affected by low pH. A direct comparison of pH effects on FI onset between Na$_V$1.2 and in Na$_V$1.5 at pH = 7.4 (filled circles) and at pH = 6.0 (open circles) was confounded by an isoform- and pH-dependent difference in the peak of the $\tau(V)$ curve (shown in **Figure 5**). The steady-state fraction of inactivated channels in Na$_V$1.2, Na$_V$1.4, and Na$_V$1.5 was not altered by low pH ($p > 0.05$, data not shown).

Different voltage protocols were used in Na$_V$1.2 and Na$_V$1.5 to assess the effects of pH on the onset of fast inactivation, as shown in **Figure 4**, because of a difference in $\tau(V)$ relationships between these two isoforms. As shown in **Figure 5**, the $\tau(V)$ for Na$_V$1.2 is depolarized relative to Na$_V$1.5. Had we compared −60 mV for both isoforms, we would have measured recovery from fast inactivation in Na$_V$1.2 and onset of fast inactivation in Na$_V$1.5. We chose

Table 5 | Parameters of time course of slow inactivation in $Na_V1.2$ and $Na_V1.5$ at pH 7.4 and 6.0.

	$Na_V1.2$	$Na_V1.5$
SI onset τ_1, (pH 7.4)	1.8 ± 0.5	0.8 ± 0.2
SI onset τ_1, (pH 6.0)	1.0 ± 0.5	0.7 ± 0.1
SI onset τ_2, (pH 7.4)	29.0 ± 5.1	6.0 ± 1.1
SI onset τ_2, (pH 6.0)	$12.0 \pm 1.7^{(1)}$	$16.3 \pm 1.8^{(4)}$
SI onset asymptote, % (pH 7.4)	48.0 ± 6	45.0 ± 5.4
SI onset asymptote, % (pH 6.0)	$25.0 \pm 5^{(2)}$	$64.2 \pm 4.1^{(5)}$
SI recovery τ_1, (pH 7.4)	0.3 ± 0.1	0.5 ± 0.1
SI recovery τ_1, (pH 6.0)	0.5 ± 0.1	0.3 ± 0.1
SI recovery τ_2, (pH 7.4)	18 ± 2	7.9 ± 2.9
SI recovery τ_2, (pH 6.0)	$8.2 \pm 1.2^{(3)}$	9.5 ± 3.0
SI recovery asymptote, % (pH 7.4)	99.0 ± 0.2	98.0 ± 1.9
SI recovery asymptote, % (pH 6.0)	99.0 ± 0.9	99.0 ± 0.7

(1) $p < 0.05$ vs. SI onset τ_2 at pH 7.4 in $Na_V1.2$.
(2) $p < 0.05$ vs. SI onset asymptote at pH 7.4 in $Na_V1.2$.
(3) $p < 0.05$ vs. SI recovery τ_2 at pH 7.4 in $Na_V1.2$.
(4) $p < 0.05$ vs. SI onset τ_2 at pH 7.4 in $Na_V1.5$.
(5) $p < 0.05$ vs. SI onset asymptote at pH 7.4 in $Na_V1.5$; $n = 6–7$.

Table 6 | Parameters of UDI in $Na_V1.2$, $Na_V1.2$, and $Na_V1.5$ at pH 7.4 and 6.0.

	$Na_V1.2$	$Na_V1.4$	$Na_V1.5$
UDI τ_1, s (pH 7.4)	2.0 ± 0.3	0.3 ± 0.1	2.4 ± 0.3
UDI τ_1, s (pH 6.0)	1.8 ± 0.2	0.4 ± 0.1	$5.8 \pm 0.3^{(3)}$
UDI τ_2, s (pH 7.4)	13.3 ± 1.3	4.5 ± 0.9	18.0 ± 1.1
UDI τ_2, s (pH 6.0)	$7.7 \pm 1.0^{(1)}$	4.9 ± 0.9	$36.2 \pm 4.6^{(4)}$
UDI asymptote, % (pH 7.4)	71.8 ± 1.9	63.0 ± 2.1	55.4 ± 3.0
UDI asymptote, % (pH 6.0)	$87.8 \pm 2.3^{(2)}$	60.0 ± 1.3	$69.0 \pm 0.7^{(5)}$

(1) $p < 0.05$ vs. UDI τ_2 at pH 7.4 in $Na_V1.2$.
(2) $p < 0.05$ vs. UDI asymptote at pH 7.4 in $Na_V1.2$.
(3) $p < 0.05$ vs. UDI τ_1 at pH 7.4 in $Na_V1.5$.
(4) $p < 0.05$ vs. UDI τ_2 at pH 7.4 in $Na_V1.5$.
(5) $p < 0.05$ vs. UDI asymptote at pH 7.4 in $Na_V1.5$; $n = 5–11$.

to compare −30 mV in $Na_V1.2$ with −60 mV in $Na_V1.5$ because of their similar positions relative to the peak of their respective $\tau(V)$ curves, as seen in **Figure 5**.

In **Figure 5**, the averaged time constants of FI recovery (circles), closed-state FI onset (squares), and open-state FI onset (triangles) are plotted as a function membrane (interpulse and prepulse) potential at pH 7.4 (solid symbols) and pH 6.0 (open symbols). The averaged time constants were fit using a two-state (not inactivated ↔ inactivated) Eyring first-order reaction model (solid lines, Eqs 7–9, Materials and Methods). The coefficients of fits to FI time constants are summarized in **Table 3**. Low pH strongly affects the $\tau(V)$ in $Na_V1.2$ and $Na_V1.5$ by accelerating rate of recovery from FI, slowing rate entry to FI and producing depolarizing shift in maximum of $\tau(V)$ curve. In contrast, effects of low pH on $\tau(V)$ in $Na_V1.4$ are limited to an increase in the rate of recovery from FI (**Figure 5B**).

pH DIFFERENTIALLY ALTERS SLOW INACTIVATION IN $Na_V1.2$ AND $Na_V1.5$

We compared the effects of low pH on steady-state slow inactivation (SS-SI) in $Na_V1.2$, $Na_V1.4$, and $Na_V1.5$ (**Figure 6**). SS-SI was measured using a 60-s prepulse followed by a 20-ms, −150 mV FI recovery pulse immediately before the 0-mV test. After the test pulse, channels were hyperpolarized to −130 mV for 30 s before every prepulse to completely recover channels from both fast and slow inactivation (Featherstone et al., 1996). Data points represent averaged and normalized amplitudes of currents recorded during test pulse (see pulse protocol diagram in **Figure 6** *inset*). **Figure 6A** shows SS-SI in $Na_V1.2$ at pH 7.4 (filled circles) and pH 6.0 (open circles). **Figure 6B** shows SS-SI in $Na_V1.5$ at pH 7.4 (filled squares) and at pH 6.0 (open squares). Data are plotted as a function of prepulse potential. Data sets were fitted with modified Boltzmann function (**Figure 6**, solid lines, Eq. 6, Materials and Methods) to obtain values for maximum probability, apparent valence (z), and $V_{1/2}$, summarized in **Table 4**. Data in **Figure 6** were closely matched by asymptotic values of exponential fits to the data in **Figures 7A,C** at corresponding voltages (−50 mV).

Our results revealed no significant differences in properties of SS-SI in $Na_V1.4$ recorded at pH 7.4 and at pH 6.4 (data not shown). However, low pH produced shifts in $V_{1/2}$: hyperpolarizing for $Na_V1.2$ and depolarizing for $Na_V1.5$ (see **Table 4**).

Figures 7A,C show time course of onset of SI in $Na_V1.2$ at pH 7.4 (filled circles) and at pH 6.0 (open circles) and in $Na_V1.5$ at pH 7.4 (filled squares) and at pH 6.0 (open squires), respectively. The onset of SI was assessed by recording peak currents during the test pulse preceded by −50 mV prepulse of varied duration (0–64 s). As with the pulse protocol for steady-state SI (**Figure 6**), a 20-ms, −130 mV pulse immediately prior to a test pulse was used to recover channels from accumulated FI. After the test pulse, channels were hyperpolarized to −130 mV for 30 s before every prepulse to completely recover channels from both fast and SI. The pulse protocol is shown below **Figure 7C**. Data points in **Figures 7A,C** are averaged and normalized amplitudes of peak currents recorded in response to a test pulse (as described above). The time course of SI onset was fit with double exponential (solid lines, Eq. 4, Materials and Methods) and time constants were extracted. Parameters, derived from the double exponential fits are summarized in **Table 5**. Asymptotic values of onset to SI at both pH values were added **Figure 6** to verify SS-SI data. In $Na_V1.2$, at pH 6.0 the asymptotic value of onset of SI was significantly decreased. Also, at low pH the slow time constant (τ_2) was significantly smaller at pH 6.0 compared to pH 7.4. In contrast, the asymptotic value of onset of SI in $Na_V1.5$ was significantly increased at pH 6.0 compared with pH 7.4 ($p < 0.05$, $n = 7$), and the slow component (τ_2) of SI onset was significantly smaller at pH 6.0 compared to pH 7.4 at pH 7.4 ($p < 0.05$, $n = 7$).

Figures 7B,D show time course of recovery from SI in $Na_V1.2$ at pH 7.4 (filled circles) and at pH 6.0 (open circles) and in $Na_V1.5$ at pH 7.4 (filled squares) and at pH 6.0 (open squares), respectively. The recovery from SI was measured as follows: channels were inactivated with 60 s prepulse at 0 mV, and then recovered from inactivation with a −110-mV interpulse of variable duration (0–64 s, see Materials and Methods for details about the interpulse duration protocol). A short pulse of 20 ms, at −130 mV immediately prior

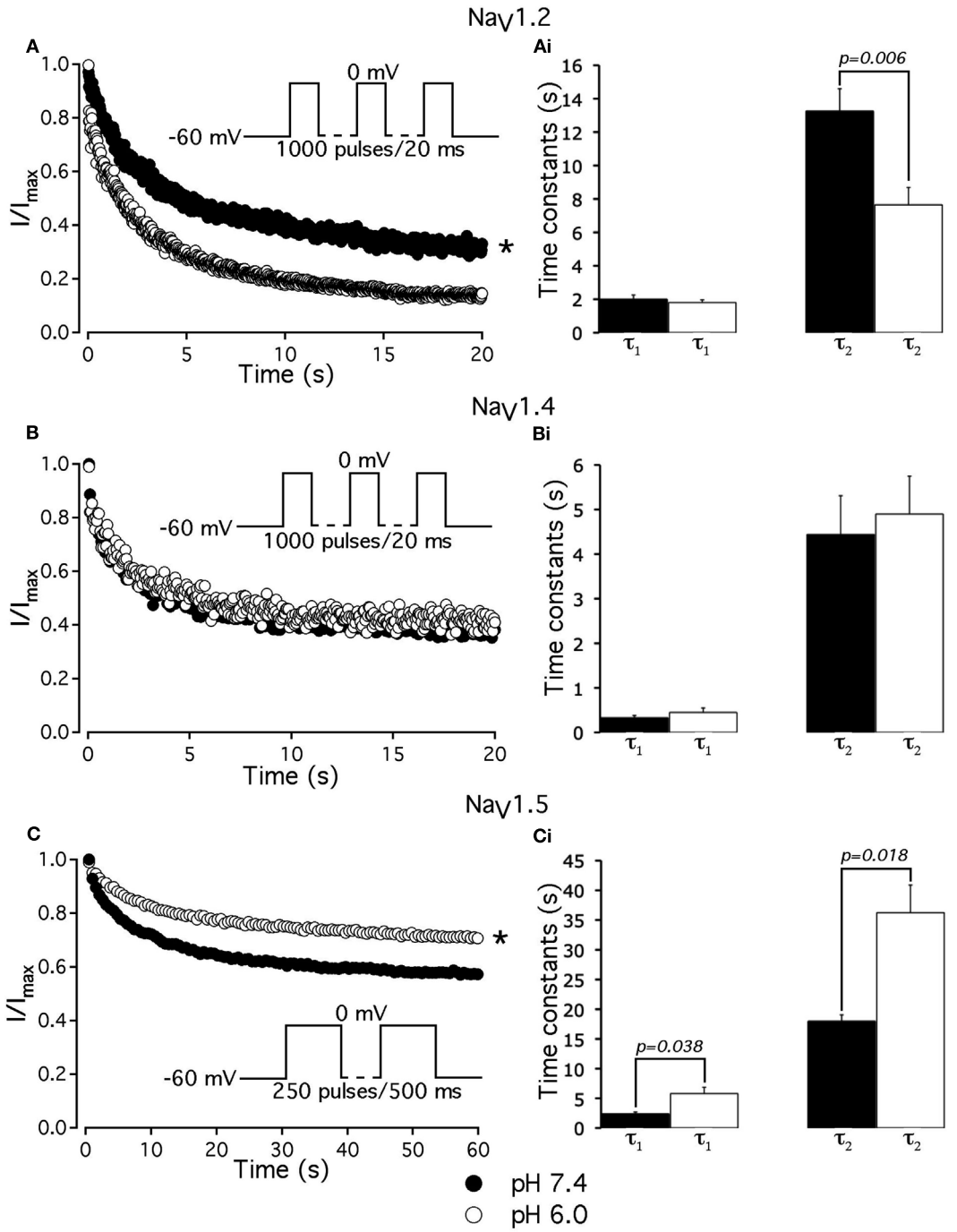

FIGURE 8 | Low pH differentially affects use-dependent inactivation. **(A,B,C)** Use-dependent inactivation at pH 7.4 (filled symbols) and at pH 6.0 (open symbols) in $Na_V1.2$, $Na_V1.4$ and $Na_V1.5$, respectively. Cells were held at −60 mV and repetitively stimulated either with one thousand 20 ms test pulses to 0 mV (for $Na_V1.2$ and $Na_V1.4$) or with 120 500 ms test pulses to 0 mV (for $Na_V1.5$). Corresponding pulse protocol diagrams are shown in **(A,B,C)** insets. Peak currents from test pulses were normalized to the amplitude of the first current in the series and values were plotted vs. number of pulses. **(A)** Use-dependent inactivation in $Na_V1.2$ at pH 7.4 (filled symbols) and at pH 6.0 (open symbols). **Ai** time constants of double exponential use-dependent inactivation in $Na_V1.2$ at pH 7.4 (filled histograms) and at pH 6.0 (open histograms). **(B)** Use-dependent inactivation in $Na_V1.4$ at pH 7.4 (filled symbols) and at pH 6.0 (open symbols). **Bi** time constants of double exponential use-dependent inactivation in $Na_V1.4$ at pH 7.4 (filled histograms) and at pH 6.0 (open histograms). **(C)** Use-dependent inactivation in $Na_V1.5$ at pH 7.4 (filled symbols) and at pH 6.0 (open symbols). **Ci** time constants of double exponential use-dependent inactivation in $Na_V1.5$ at pH 7.4 (filled histograms) and at pH 6.0 (open histograms). Data represent mean ± SEM ($n = 9$–12). Asterisks denote statistical difference ($p < .05$).

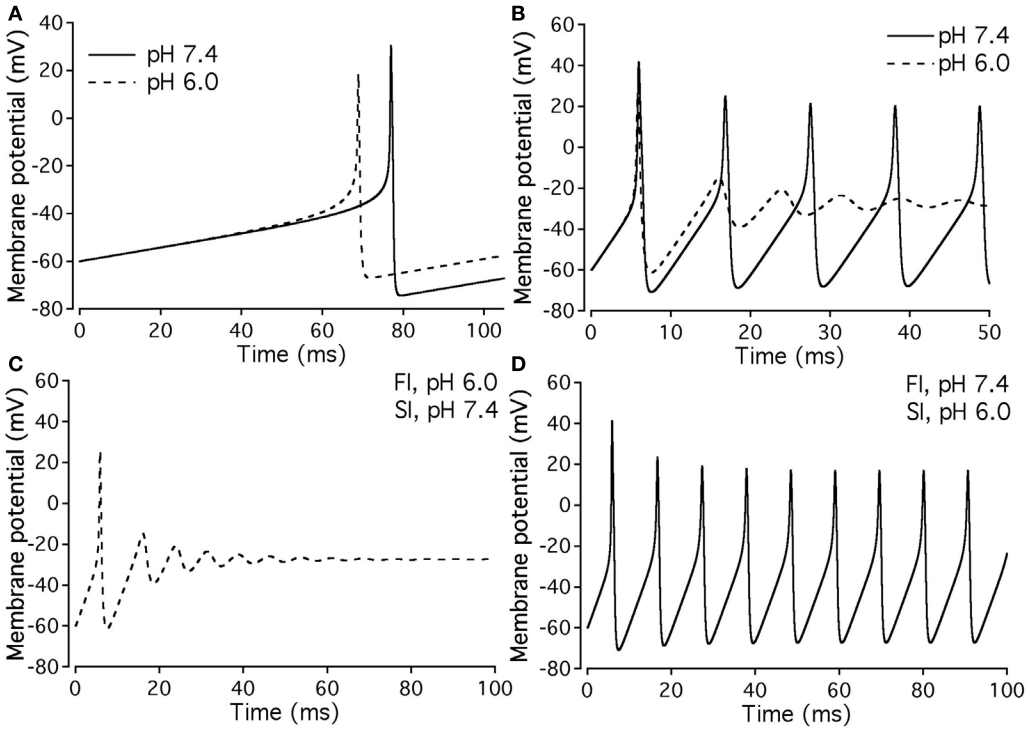

FIGURE 9 | Effects of pH on neuronal action potential. (A) An overlap of a two neuronal APs with sodium currents at pH 7.4 (solid line) and pH 6.0 (dashed line). The APs were elicited by a continuous stimulus current of 1 pA/pF. **(B)** Continuous APs with sodium currents at pH 7.4 (solid line) and pH 6.0 (dashed line). The continuous firing was induced with a continuous current of 20 pA/pF. **(C)** Continuous APs of a neuron expressing a sodium channel "pH chimera" whose parameters of conductance and FI correspond to those at pH 6.0 and the parameters of slow inactivation correspond to those at pH 7.4. The APs were stimulated with a continuous current of 20 pA/pF. **(D)** Continuous APs of a neuron expressing a sodium channel "pH chimera" whose parameters of conductance and FI correspond to those at pH 7.4 and the parameters of slow inactivation correspond to those at pH 6.0. The APs were stimulated with a continuous current of 20 pA/pF.

to the test pulse was used to recover channels from FI. The fraction of channels recovered from SI was assessed with a 0-mV test pulse. The pulse protocol is shown below **Figure 7D**. Currents, recorded during the test pulse were normalized, averaged, and plotted vs. interpulse duration. The time course of recovery from SI in $Na_V1.2$ was fitted with a double exponential (Eq. 4, Materials and Methods) to obtain time constants and asymptotic values, summarized in **Table 5**. Low pH did not significantly affect the faster component (τ_1) of recovery from SI in $Na_V1.2$. However, the slower time constant (τ_2) of recovery from SI was significantly decreased at pH 6.0 ($p < 0.05$, $n = 6$, **Figure 7B**). The asymptotic value of time course from recovery from SI in NaV1.2 at pH 6.0 was not different ($p > 0.05$) from that at pH 7.4.

Figure 7D shows time course of recovery from SI in NaV1.5 at pH 7.4 (filled squares) and at pH 6.0 (open squares). Comparing the time constants extracted from double exponential fits revealed no significant ($p > 0.05$) effect of low pH on either on τ_1 or τ_2. However, we found that, at pH 6.0, more NaV1.5 channels are available for recovery at the beginning ($t = 0$) of interpulse (**Figure 7D**, open squares, arrow) as compared to pH 7.4 (**Figure 7C**, filled squares). The asymptotic values for recovery from SI in $Na_V1.5$ at pH 6.0 were not different ($p > 0.05$) from those at pH 7.4 (**Table 5**).

Our experiments revealed no significant effects of low pH kinetics of SI in $Na_V1.4$ channels (data not shown).

pH DIFFERENTIALLY ALTERS USE-DEPENDENT INACTIVATION IN $Na_V1.2$ AND $Na_V1.5$

To further investigate the effects of low pH on inactivation in $Na_V1.2$ and $Na_V1.5$, we compared use-dependent current reduction at pH 7.4 and pH 6.0. The frequency of pulse stimulation for each channel isoform was chosen to emulate its tissue-specific activity prior to/during an ischemic event, such as epileptic episode or stroke (Kjekshus, 1986; Adeli et al., 2003). **Figure 8A** shows use-dependent inactivation (UDI) in $Na_V1.2$ at pH 7.4 (filled circles) and at pH 6.0 (open circles). Peak current amplitudes, recorded during a series of 1000, 20 ms test pulses to 0 mV are plotted as a function of pulse number. The interval between adjacent pulses was 1 ms, holding potential was −60 mV to emulate neuronal resting potential *in vivo*. The resulting frequency was approximately 45 ± 5 Hz, which roughly corresponds to frequency of AP firing during epileptic episode (Adeli et al., 2003). Peak currents were normalized to the peak amplitude of the first current record of the series and fit with a double exponential function to determine time constants, τ_1 and τ_2, and steady-state fraction of inactivated channels (asymptote). UDI parameters are summarized in **Table 6**.

At pH 7.4 (**Figure 8A**, filled circles) the asymptote of UDI in $Na_V1.2$ was significantly ($p < 0.05$) decreased compared to that at pH 6.0 (**Figure 8A**, open circles). Also, acidification accelerated the τ_2 of UDI in $Na_V1.2$ (**Figure 8Ai**, open histogram), **Table 6**. Data shown in **Figures 8B,Bi** indicate that both time course and

Table 7 | Parameters of repetitively firing neurons at a stimulus of −20 pA/pF for pH 7.4 model neurons, pH 6.0 model neurons, and pH 6.0 model neurons with either pH 7.4 slow inactivation or fast inactivation parameters.

	pH 7.4	pH 6.0	pH 6.0 with pH 7.4 FI	pH 6.0 with pH 7.4 SI
First AP depolarization	41.5 mV	25.8 mV	41.1 mV	25.8 mV
Subsequent AP depolarization	19.8 mV	n/a	17.2 mV	n/a
First AP hyperpolarization	−70.9 mV	−61.4 mV	−70.9 mV	−61.4 mV
Subsequent AP hyperpolarization	−68.9 mV	n/a	−67.9 mV	n/a
Firing frequency	94.3 Hz	0 Hz	94.7 Hz	0 Hz

Measured parameters are the maximal membrane potential reached on the initial depolarization and subsequent depolarization, the minimum membrane potential on the first hyperpolarization and subsequent hyperpolarizations as well as the action potential firing rate.

maximum probability of UDI in $Na_V1.4$ at pH 7.4 (filled circles and histograms) were statistically similar ($p > 0.05$) to those at pH 6.0 (open circles and histograms), **Table 6**. In $Na_V1.5$ the effects of low pH on UDI were essentially reversed as compared to $Na_V1.2$. At pH 7.4 the asymptote of UDI (**Figure 8C**, filled circles) was increased as compared to that at pH 6.0 (**Figure 8Ci**, open circles), **Table 6**. Also, low pH decelerated both τ_1 (**Figure 8Ci**, filled histograms) and τ_2 (**Figure 8Ci**, filled histograms) of the UDI, **Table 6**. Note that different depolarization durations for UDI pulse protocols were used (see pulse protocols in **Figure 8** and description in the figure legend) to account for differences in AP durations between neurons and skeletal muscles ($Na_V1.2$ and 1.4) vs. myocytes ($Na_V1.5$).

Our results suggest acidification produces differential effects on inactivation properties of $Na_V1.2$ and $Na_V1.5$, but not in $Na_V1.4$, suggesting that changes in pH would affect AP generation and propagation in neuronal and cardiac tissue but not in skeletal muscle.

MODELING: EFFECTS OF LOW pH ON NEURONAL ACTION POTENTIAL

Our experimental data were used as the basis for computer modeling (see Materials and Methods) to measure characteristics of neuronal APs at either normal or acidic pH. **Figure 9** shows the results of neuronal modeling. Simulations to elicit APs were done at a continuous stimulus of −1 pA/pF in both pH 6.0 (dashed line) and pH 7.4 (solid line) over a period of 105 ms (**Figure 9A**). The membrane potentials of the model neurons at each pH value were plotted as a function of time (**Figure 9A**). Three main differences were observed between the two pH values: (1) the pH 6.0 neuron reached its maximal depolarization at 68.90 ms, faster than the pH 7.4 neuron at 76.98 ms; (2) the membrane potential at peak depolarization was 18.7 mV in the pH 6.0, a more positive depolarization than the 30.40-mV observed in the pH 7.4 neuron; and (3) the maximum hyperpolarization voltage was less negative in the pH 6.0 neuron, with a value of −67 mV compared to −74.4 mV found in the pH 7.4 neuron.

Figure 9B compares repetitive AP firing in a model neuron at pH 7.4 (solid line) and at pH 6.0 (dashed line). Data shown are for neurons injected with a constant stimulus of −20 pA/pF although simulations were also performed at stimulus amplitudes of −3, −5, −10, and −15 pA/pF with the same data trends obtained (data not shown). In the first AP, the maximum depolarization and hyperpolarization trends seen in the single AP studies, are reproduced (**Table 7**). The pH 7.4 neuron continues to fire APs at a rate of 94.3 Hz, but with a decreased maximum depolarization and less negative undershoot (**Table 7**). In contrast, the pH 6.0 model neuron failed to repetitively fire.

Since our model takes into account both fast and slow gating, we have modeled "AP chimeras" to study the specific effects of both inactivation types on the neuronal AP. Chimera 1 (**Figure 9C**) consists of pH 6.0 data programmed in for the activation and FI and pH 7.4 data programmed in for the slow inactivation gate. Chimera 2 (**Figure 9D**) has pH 6.0 data programmed in for the activation and slow inactivation gates and pH 7.4 data programmed in for the FI gate. Chimera 2 (**Figure 9D**) was found to have similar characteristics to the pH 7.4 neuronal model, in which the repetitive firing was preserved (**Figure 9B**, solid line). In contrast, Chimera 1 (**Figure 9C**) results were similar to the pH 6.0 model (**Table 7**). These modeling results suggest FI defects induced by decreased pH are responsible for the failure of the neuronal model to display repetitive AP firing.

MODELING: EFFECTS OF LOW pH ON CARDIAC ACTION POTENTIAL

Figures 10A,B, show the modeled sodium current during the 15th and 200th APs (firing frequency of 2.5 and 3.33 Hz, respectively) at pH 7.4 (solid line) and at pH (6.0). Plotted are the sodium current densities in pA/pF over the initial 5 ms of the cardiac AP. The sodium current is reduced and delayed in the pH 6.0 model during both 15th and 200th APs. At pH 6.0 there is a decreased level of activation and a decreased level of FI as described in **Table 7**; **Figure 10C** is the full 15th AP at both pH values; **Figures 10Ci,ii** show expanded views of the rising phase and repolarization phase respectively. The membrane potential of the model cardiac myocytes is plotted on the vertical axis, with −85.9 mV as the resting membrane potential, vs. a single cycle length. The maximum rise rate in the pH 6.0 model is reduced from 62.1 mV/ms, at pH 7.4, to 18.6 mV/ms, and was also delayed by 0.6 ms at pH 6.0. There also was a delay in the peak plateau potential at pH 6.0, but there was no significant difference in the AP duration (APD) between the models (**Table 7**). **Figures 10D,Di,ii** show the 200th AP as well as expanded views of the rise phase and repolarization phase. As in **Figure 10C**, the membrane potential of the model cardiac AP is plotted as a function of the time of a single cycle length, with the resting membrane potential at −85.9 mV. There was a decreased maximal rise rate in the pH 6.0 AP (41.1 mV/ms at pH 7.4 compared to 11.0 mV/ms at pH 6.0) and a delay in the peak plateau depolarization (**Table 7**). There also was a 3.7-mV difference in the peak plateau membrane potential at pH 6.0 as well as a 1.4-ms delay in the repolarization of the pH 6.0 AP.

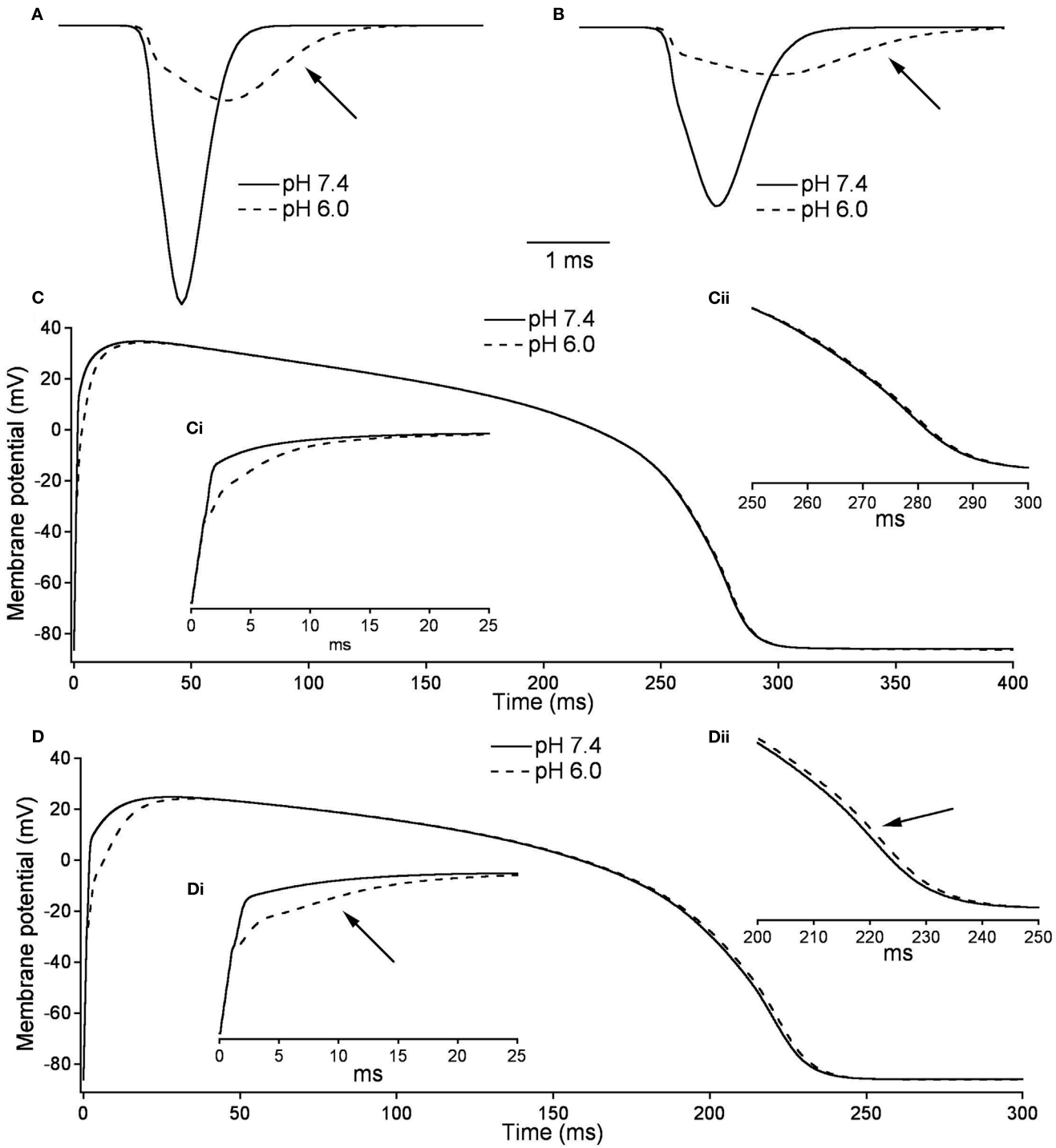

FIGURE 10 | Effects of pH on cardiac action potential. (A) The fast sodium current of a cardiac AP at pH 7.4 (solid line) and pH 6.0 (dashed line). The sodium current is recorded on the 15th AP in an endocardial myocyte stimulated at a frequency of 2.5 Hz. **(B)** The fast sodium current of a cardiac AP at pH 7.4 (solid line) and pH 6.0 (dashed line). The sodium current is recorded on the 200th AP in a endocardial myocyte stimulated at a frequency of 3.33 Hz. **(C)** The membrane potential over the time of one endocardial myocyte AP with sodium currents at pH 7.4 (solid line) and pH 6.0 (dashed line). The AP is the 15th produced in a model ventricular endocardial myocyte stimulated at 2.5 Hz. **(Ci)** The first 25 ms of the 15th endocardial AP stimulated at 2.5 Hz with sodium currents at pH 7.4 (solid line) and pH 6.0 (dashed line). **(Cii)** The last 50 ms of the 15th endocardial AP stimulated at 2.5 Hz with sodium currents at pH 7.4 (solid line) and pH 6.0 (dashed line). **(D)** The membrane potential over the time of one endocardial myocyte AP with sodium currents at pH 7.4 (solid line) and pH 6.0 (dashed line). The AP is the 200th produced in a model ventricular endocardial myocyte stimulated at 3.33 Hz. **(Di)** The first 25ms of the 200th endocardial AP stimulated at 3.33 Hz with sodium currents at pH 7.4 (solid line) and pH 6.0 (dashed line). **(Dii)** The last 50 ms of the 200th endocardial AP stimulated at 3.33 Hz with sodium currents at pH 7.4 (solid line) and pH 6.0 (dashed line).

DISCUSSION

The goal of this study was to compare the effects of extracellular acidosis on biophysical properties of $Na_V1.2$, $Na_V1.4$, and $Na_V1.5$ channels. We observed both similarities and differences between the responses of the different subtypes to changing pH from 7.4 to 6.0. On one hand, peak current amplitudes in all three channel isoforms were approximately equally suppressed due to proton block (**Figures 1A,Ai,D,Di,G,Gi**), consistent with previously published data (Hille, 1968; Benitah et al., 1997; Khan et al., 2006). However, more detailed study revealed that effects of low pH significantly differ between these channel subtypes, suggesting a specificity of effects that acidosis might have on voltage-gated sodium channels and, consequently, the tissues in which the different subtypes are found. In contrast to NaV1.2 and NaV1.5, $Na_V1.4$ channels are practically insensitive to changes in pH; activation, and both fast and slow inactivation were largely unaffected by acidosis (**Figures 1D,Di,E,F**, **2B**, and **5B**) and the UDI at pH 7.4 was statistically identical to that at pH 6.0 (**Figure 8B**). These data suggest that steady-state and kinetic properties of activation and inactivation in $Na_V1.4$ are pH-insensitive and the decrease in macroscopic current amplitudes at low pH (**Figures 1D,Di**) can be entirely attributed to proton block (Hille, 1968; Mozhayeva et al., 1984; Yatani et al., 1984; Benitah et al., 1997; Khan et al., 2006; Zhang et al., 2007). This apparent resistance to changes in extracellular pH may reflect the role of $Na_V1.4$ in skeletal muscle function and its requirement to maintain normal functionality during exercise-induced acidosis.

On the other hand, inactivation in $Na_V1.2$ and $Na_V1.5$ was modified at low pH in opposite ways. First, the time course of open-state inactivation was delayed in $Na_V1.5$ (**Figure 2C**), but not in $Na_V1.2$ (**Figure 2A**). Longer time constants of $Na_V1.5$ open-state inactivation indicate destabilization of the fast inactivation state, which in turn may result in elevated electrical excitability of cardiac tissue (Nerbonne and Kass, 2005; Wang et al., 2009). Second, the peak of window current area was shifted toward depolarized potentials in $Na_V1.5$ (**Figure 1I**), but not in $Na_V1.2$ (**Figure 1C**). This also may lead to overexcitability of cardiac tissue via elongation of the plateau phase of the cardiac AP (Abriel et al., 2001). Third, at pH 6.0, there was increased maximum channel availability in $Na_V1.5$ (**Figure 7B**). In contrast, maximum availability in $Na_V1.2$ is decreased in acidic conditions (**Figure 6B**). These data agree well with the maximum probability of UDI in $Na_V1.2$ and $Na_V1.5$ (**Figures 8A,C**, respectively), which is another indication that acidic conditions have opposite effects on $Na_V1.2$ (decreased availability) and $Na_V1.5$ (increased availability).

These hypotheses were tested with computer modeling. The results of modeling these data support *in vivo* experiments on acidosis and suggest mechanisms as to how the changes that occur in electrical signals at low pH are brought about. Neuronal modeling has shown the presence of both acidosis-inhibited and acidosis-stimulated neurons (Wang and Richerson, 2000; Wang et al., 2001). Our models showed complete inhibition of firing when only sodium channel parameters were changed (**Figure 9B**), which agrees with previous reports (Zhang et al., 2007). This suggests that acidosis inhibition of neurons is in part due to inhibited sodium currents, more specifically the altered FI kinetics (**Figures 9C,D**). Experiments on ventricular myocyte have shown reduced rise rates in APs at low pH (Kagiyama et al., 1982), which may be attributed in our modeling data to a decrease in sodium current amplitude (**Figure 10**). Decreases in initial rise rate are a potential cause of slow conduction velocity at low pH (Fry and Poole-Wilson, 1981; Kagiyama et al., 1982), a condition associated with ventricular arrhythmias (Cranefield et al., 1972). Decreased sodium current amplitude would normally suggest an early repolarization. Our data, however, suggests this is not the case (**Figures 10C,D**), and *in vivo* experiments have shown that acidosis leads to delays in repolarization. Our data further suggests that elongated macroscopic sodium currents are part of this effect. Sodium currents were present for almost twice as long at low pH (**Figures 10A,B**), probably due to delays in open-state inactivation at pH 6.0 (**Figure 4**).

The interpretation of our modeling is necessarily limited by the fact that only sodium channel properties were modified. The contribution of other channel types, and the effect of low pH on them, will inevitably alter the results we report. Nevertheless, our data, and the models we derive, provide the first direct comparison of the effects of low pH on sodium channel gating. Future studies using potassium and calcium channels, as well as other sodium channel subtypes, will provide the data necessary for a more complete picture of the effects of low pH on electrical excitability of nerve and muscle.

Our present results with $Na_V1.5$ and the effects of low pH are consistent with our previous observations (Jones et al., 2011b). In our previous work, we observed similar effects of low pH on SS-FI, window current, $\tau(V)$, and UDI in $Na_V1.5$ channels recorded using the cut-open oocyte voltage clamp. The effects of low pH on this sodium channel subtype thus are independent of the expression system and recording technique. The similarity of the $Na_V1.5$ data we report here to that in Jones et al. (2011b), addresses what we therefore consider to be an unlikely possibility that the differences between Na_V isoforms might be due to differences between expression systems.

Our results do not distinguish definitively between charge screening and pore block by protons. Since the peak I_{Na} amplitude is diminished in all the isoforms we tested, we conclude the same mechanism described by Khan et al. (2002) is responsible for this effect. Our previous results (Jones et al., 2011a), however, suggest the proton-dependent decrease in current amplitude is mediated by mechanism and molecular underpinnings different from than that by which kinetic properties are affected.

We can, at this point, only speculate as to the molecular basis for isoform-dependent differences in responses to low pH. The most likely place to explore the structural underpinnings of differential pH_0 sensitivity is in residues that face the external milieu. Our previously published results (Jones et al., 2011b) suggest that histidine residues, with a pK_a of 6.5, close to the pK_a of 6.1 measured for pH-dependent decrease in peak I_{Na} in NaV1.5, could be Na_V pH sensors. In addition, histidine residues in potassium channels have been reported to function as pH sensors (Kehl et al., 2002). Finally, our preliminary experiments also suggest histidine residues may be pH sensors (Jones et al., 2011a), although other

reports suggest C373 in NaV1.5 might fulfill this role (Khan et al., 2006). Future studies will explore the possibility that there may be several residues that may be protonated under low external pH conditions.

ACKNOWLEDGMENTS

This project was funded by a Discovery Grant from NSERC to Peter C. Ruben. We thank David K. Jones for his insight and fruitful discussions.

REFERENCES

Abriel, H., Cabo, C., Wehrens, X. H. T., Rivolta, I., Motoike, H. K., Memmi, M., Napolitano, C., Priori, S. G., and Kass, R. S. (2001). Novel arrhythmogenic mechanism revealed by a long-QT syndrome mutation in the cardiac Na channel. *Circ. Res.* 88, 740.

Adeli, H., Zhou, Z., and Dadmehr, N. (2003). Analysis of EEG records in an epileptic patient using wavelet transform. *J. Neurosci. Methods* 123, 69–87.

Amin, A. S., Asghari-Roodsari, A., and Tan, H. L. (2010). Cardiac sodium channelopathies. *Pflugers Arch.* 460, 223–237.

Benitah, J. P., Balser, J. R., Marban, E., and Tomaselli, G. F. (1997). Proton inhibition of sodium channels: mechanism of gating shifts and reduced conductance. *J. Membr. Biol.* 155, 121–131.

Cranefield, P. F., Wit, A. L., and Hoffman, B. F. (1972). Conduction of the cardiac impulse. *J. Gen. Physiol.* 59, 227.

Featherstone, D., Richmond, J., and Ruben, P. (1996). Interaction between fast and slow inactivation in Skm1 sodium channels. *Biophys. J.* 71, 3098–3109.

Fry, C. H., and Poole-Wilson, P. A. (1981). Effects of acid-base changes on excitation–contraction coupling in guinea-pig and rabbit cardiac ventricular muscle. *J. Physiol. (Lond.)* 313, 141.

Hermansen, L., and Osnes, J. B. (1972). Blood and muscle pH after maximal exercise in man. *J. Appl. Physiol.* 32, 304.

Hille, B. (1968). Charges and potentials at the nerve surface. *J. Gen. Physiol.* 51, 221.

Hodgkin, A. L., and Huxley, A. F. (1952). A quantitative description of membrane current and its application to conduction and excitation in nerve. *J. Physiol. (Lond.)* 117, 500.

Hund, T. J., and Rudy, Y. (2004). Rate dependence and regulation of action potential and calcium transient in a canine cardiac ventricular cell model. *Circulation* 110, 3168–3174.

Jones, D. K., Claydon, T. W., and Ruben, P. C. (2011a). Turret histidines in pH modulation of the cardiac voltage-gated sodium channel. *Biophys. J.* 100, 422a.

Jones, D. K., Peters, C. H., Tolhurst, S. A., Claydon, T. W., and Ruben, P. C. (2011b). Extracellular proton modulation of the cardiac voltage-gated sodium channel, NaV.15. *Biophys. J.* 101, 2147–2156.

Kagiyama, Y., Hill, J. L., and Gettes, L. S. (1982). Interaction of acidosis and increased extracellular potassium on action potential characteristics and conduction in guinea pig ventricular muscle. *Circ. Res.* 51, 614.

Kehl, S. J., Eduljee, C., Kwan, D. C., Zhang, S., and Fedida, D. (2002). Molecular determinants of the inhibition of human Kv1.5 potassium currents by external protons and Zn^{2+}. *J. Physiol. (lond.)* 541, 9–24.

Khan, A., Kyle, J. W., Hanck, D. A., Lipkind, G. M., and Fozzard, H. A. (2006). Isoform-dependent interaction of voltage-gated sodium channels with protons. *J. Physiol. (Lond.)* 576, 493.

Khan, A., Romantseva, L., Lam, A., Lipkind, G., and Fozzard, H. A. (2002). Role of outer ring carboxylates of the rat skeletal muscle sodium channel pore in proton block. *J. Physiol. (Lond.)* 543, 71.

Kjekshus, J. K. (1986). Importance of heart rate in determining beta-blocker efficacy in acute and long-term acute myocardial infarction intervention trials. *Am. J. Cardiol.* 57, 43F–49F.

Luo, C., and Rudy, Y. (1991). A model of the ventricular cardiac action potential. Depolarization, repolarization, and their interaction. *Circ. Res.* 68, 1501.

Maruki, Y., Koehler, R. C., Eleff, S. M., and Traystman, R. J. (1993). Intracellular pH during reperfusion influences evoked potential recovery after complete cerebral ischemia. *Stroke* 24, 697.

Meyer, F. B. (1990). Intracellular brain pH and ischemic vasoconstriction in the white New Zealand rabbit. *Stroke* 21, IV117–IV119.

Mozhayeva, G. N., Naumov, A. P., and Nosyreva, E. D. (1984). A study on the potential-dependence of proton block of sodium channels. *Biochim. Biophys. Acta* 775, 435–440.

Nagatomo, T., Fan, Z., Ye, B., Tonkovich, G. S., January, C. T., Kyle, J. W., and Makielski, J. C. (1998). Temperature dependence of early and late currents in human cardiac wild-type and long QT DeltaKPQ Na channels. *Am. J. Physiol.* 275, H2016.

Nerbonne, J. M., and Kass, R. S. (2005). Molecular physiology of cardiac repolarization. *Physiol. Rev.* 85, 1205.

Spampanato, J., Escayg, A., Meisler, M. H., and Goldin, A. L. (2001). Functional effects of two voltage-gated sodium channel mutations that cause generalized epilepsy with febrile seizures plus type 2. *J. Neurosci.* 21, 7481.

Spampanato, J., Escayg, A., Meisler, M. H., and Goldin, A. L. (2003). Generalized epilepsy with febrile seizures plus type 2 mutation W1204R alters voltage-dependent gating of Na(v)1.1 sodium channels. *Neuroscience* 116, 37–48.

Ten Tusscher, K., Noble, D., Noble, P. J., and Panfilov, A. V. (2004). A model for human ventricular tissue. *Am. J. Physiol. Heart Circ. Physiol.* 286, H1573.

Ten Tusscher, K., and Panfilov, A. V. (2003). Reentry in heterogeneous cardiac tissue described by the Luo-Rudy ventricular action potential model. *Am. J. Physiol. Heart Circ. Physiol.* 284, H542.

Ten Tusscher, K., and Panfilov, A. V. (2006). Cell model for efficient simulation of wave propagation in human ventricular tissue under normal and pathological conditions. *Phys. Med. Biol.* 51, 6141.

Terrenoire, C., Clancy, C. E., Cormier, J. W., Sampson, K. J., and Kass, R. S. (2005). Autonomic control of cardiac action potentials: role of potassium channel kinetics in response to sympathetic stimulation. *Circ. Res.* 96, e25.

Vilin, Y., and Ruben, P. C. (2010). Differential pH-dependent regulation of NaV channels. *Biophys. J.* 98, 111a.

Wang, L., Sun, L., Zhang, Y., Wu, H., Li, C., Pan, Z., Lu, Y., and Yang, B. (2009). Ionic mechanisms underlying action potential prolongation by focal cerebral ischemia in rat ventricular myocytes. *Cell. Physiol. Biochem.* 23, 305–316.

Wang, W., and Richerson, G. B. (2000). Chemosensitivity of non-respiratory rat CNS neurons in tissue culture. *Brain Res.* 860, 119–129.

Wang, W., Tiwari, J. K., Bradley, S. R., Zaykin, R. V., and Richerson, G. B. (2001). Acidosis-stimulated neurons of the medullary raphe are serotonergic. *J. Neurophysiol.* 85, 2224.

Wang, W., Yazawa, K., George, A. Jr., and Bennett, P. (1996). Characterization of human cardiac Na^+ channel mutations in the congenital long QT syndrome. *Proc. Natl. Acad. Sci. U.S.A.* 93, 13200–13205.

Yatani, A., Brown, A. M., and Akaike, N. (1984). Effect of extracellular pH on sodium current in isolated, single rat ventricular cells. *J. Membr. Biol.* 78, 163–168.

Yuen, G. L. F., and Durand, D. (1991). Reconstruction of hippocampal granule cell electrophysiology by computer simulation. *Neuroscience* 41, 411–423.

Zhang, R. Z., Nadler, J. V., and Schwartz-Bloom, R. D. (2007). Impaired firing and sodium channel function in CA1 hippocampal interneurons after transient cerebral ischemia. *J. Cereb. Blood Flow Metab.* 27, 1444–1452.

Zygmunt, A. C., Eddlestone, G. T., Thomas, G. P., Nesterenko, V. V., and Antzelevitch, C. (2001). Larger late sodium conductance in M cells contributes to electrical heterogeneity in canine ventricle. *Am. J. Physiol. Heart Circ. Physiol.* 281, H689.

Conflict of Interest Statement: The authors declare that the research was conducted in the absence of any commercial or financial relationships that could be construed as a potential conflict of interest.

Received: 27 April 2012; accepted: 22 May 2012; published online: 11 June 2012.
*Citation: Vilin YY, Peters CH and Ruben PC (2012) Acidosis differentially modulates inactivation in $Na_V1.2$, $Na_V1.4$, and $Na_V1.5$ channels. Front. Pharmacol. **3**:109. doi: 10.3389/fphar.2012.00109*
This article was submitted to Frontiers in Pharmacology of Ion Channels and Channelopathies, a specialty of Frontiers in Pharmacology.

APPENDIX

GENERAL EQUATIONS

$$\frac{dV}{dt} = \frac{I}{C} \tag{A1}$$

where V is membrane potential, I is total current, C is capacitance, and t is time.

$$\frac{dy}{dt} = \frac{(y^{\infty} - y)}{\tau y} \tag{A2}$$

where y is the value of any gate, $y\infty$ is its steady-state value and τy is its time constant value.

Neuron

$$I = I_{\text{na}} + I_k + I_{\text{stimulus}} \tag{A3}$$

$C = -3.5\,\mu\text{F/cm}^2$
$G_{\text{na}} = 200\,\text{mS/cm}^2$
$E_{\text{na}} = 50\,\text{mV}$
$\tau_{\text{m}} = 0.15\,\text{ms}$
$G_{\text{k}} = 40\,\text{mS/cm}^2$
$E_{\text{k}} = -80\,\text{mV}$

Fast sodium current.

$$\begin{aligned} m^{\infty} &= \frac{1}{1 + \exp\left[-1\left[(V + 11.7)/9.074\right]\right]} \text{ if pH} = 7.4 \\ m^{\infty} &= \frac{1}{1 + \exp\left[-1\left[(V + 10.35)/10.04\right]\right]} \text{ if pH} = 6.0 \end{aligned} \tag{A4}$$

$$\begin{aligned} h^{\infty} &= \frac{1}{1 + \exp\left[-1\left((V + 50.1)/-8.599\right)\right]} \text{ if pH} = 7.4 \\ h^{\infty} &= \frac{1}{1 + \exp\left[-1\left((V + 52.0)/-11.056\right)\right]} \text{ if pH} = 6.0 \end{aligned} \tag{A5}$$

$$\begin{aligned} \tau_h &= \frac{46}{0.5\{\exp[(V + 50.0)/14.0] + \exp[(V + 50.0)/-13.0]\}} \text{ if pH} = 7.4 \\ \tau_h &= \frac{65.58}{0.5\{\exp[(V + 50)/9.20 + \exp[(V + 50)/-16.0]\}} \text{ if pH} = 6.0 \end{aligned} \tag{A6}$$

$$\begin{aligned} j^{\infty} &= \frac{0.92}{1 + \exp[-1((V + 52.5)/-12.73)]} + 0.08 \text{ if pH} = 7.4 \\ j^{\infty} &= \frac{0.95}{1 + \exp[-1((V + 61.0)/-10.73)]} + 0.05 \text{ if pH} = 6.0 \end{aligned} \tag{A7}$$

$$\begin{aligned} \tau j &= 29000 \exp\left\{-0.5\left\{\left[\frac{(V + 52.5)}{60}\right]^2\right\}\right\} \text{ if pH} = 7.4 \\ \tau j &= 12300 \exp\left\{-0.5\left\{\left[\frac{(V + 61.0)}{54.5}\right]^2\right\}\right\} \text{ if pH} = 6.0 \end{aligned} \tag{A8}$$

Potassium current.

$$I_{\mathrm{k}} = G_{\mathrm{k}} \cdot n^4 \cdot (V - E_{\mathrm{k}}) \tag{A9}$$

$$n^{\infty} = \frac{\alpha_n}{(\alpha_n + \beta_n)} \tag{A10}$$

$$\tau_n = \frac{1}{(\alpha_n + \beta_n)} \tag{A11}$$

$$\alpha_n = \frac{-0.07\,[(V + 60) - 47]}{\exp\left[((V + 60) - 47)/-6\right] - 1} \tag{A12}$$

$$\beta_n = (0.264)\exp\frac{(V + 60) - 22}{40} \tag{A13}$$

Cardiac

$G_{\mathrm{na}} = 23\ \mathrm{mS/cm^2}$
$G_{\mathrm{nal}} = 0.065\ \mathrm{mS/cm^2}$
$\tau_{\mathrm{hl}} = 600\ \mathrm{ms}$

Fast sodium current.

$$\begin{aligned} m^{\infty} &= \frac{0.846}{1 + \exp\left[-1[(V + 32.58)/7.04]\right]}\ \text{if pH} = 7.4 \\ m^{\infty} &= \frac{0.482}{1 + \exp\left[-1[(V + 32.58)/7.86]\right]}\ \text{if pH} = 6.0 \end{aligned} \tag{A14}$$

$$\tau_m = \alpha_m * \beta_m \tag{A15}$$

$$\alpha_m = \frac{1}{1 + \exp[(-60 - V)/5]} \tag{A16}$$

$$\beta_m = \frac{0.1}{1 + \exp\left[(V + 35)/5\right] + 0.1/1 + \exp[(V - 50)/200]} \tag{A17}$$

$$\begin{aligned} h^{\infty} &= \frac{1}{1 + \exp[-1((V + 80.6)/-6.108)]}\ \text{if pH} = 7.4 \\ h^{\infty} &= \frac{1}{1 + \exp\left[-1((V + 77.54)/-6.509)\right]}\ \text{if pH} = 6.0 \end{aligned} \tag{A18}$$

$$\begin{aligned} \tau_h &= \frac{378.5}{0.5\{\exp[(V + 80.6)/11.5] + \exp[(V + 80.6)/-10.5]\}}\ \text{if pH} = 7.4 \\ \tau_h &= \frac{319.15}{0.5\{\exp[(V + 70)/9.5] + \exp[(V + 70)/-12.5]\}}\ \text{if pH} = 6.0 \end{aligned} \tag{A19}$$

$$\begin{aligned} j^{\infty} &= \frac{0.588}{1 + \exp[-1((V + 71.4)/-14.08)]} + 0.3305\ \text{if pH} = 7.4 \\ j^{\infty} &= \frac{0.5324}{1 + \exp[-1((V + 57.4)/-19.12)]} + 0.3856\ \text{if pH} = 6.0 \end{aligned} \tag{A20}$$

$$\tau_j = \frac{1000}{(\alpha_j + \beta_j)} \tag{A21}$$

$$\begin{aligned} \alpha_j &= 0\ \text{if}\ V \geq -40\ \mathrm{mV} \\ \alpha_j &= \frac{\{(V + 37.78)\{-0.000006948\exp[-0.04391 * V] - 25428\exp[0.2444 * V]\}\}}{\{1 + \exp[0.311(V + 79.23)]\}}\ \text{else} \end{aligned} \tag{A22}$$

$$\begin{aligned} \beta_j &= \frac{0.6\exp[0.057(V)]}{1 + \exp[-0.1(V + 32)]}\ \text{if}\ V \geq -40\mathrm{mV} \\ \beta_j &= \frac{0.02424\exp[-0.01052(V)]}{1 + \exp[-0.1378(V + 40.14)]}\ \text{else} \end{aligned} \tag{A23}$$

Late sodium current.

$$I_{\mathrm{nal}} = G_{\mathrm{nal}} \cdot \mathrm{ml3} \cdot \mathrm{hl} \cdot (V - E_{\mathrm{na}}) \tag{A24}$$

$$\mathrm{ml}^{\infty} = \frac{\alpha\mathrm{ml}}{(\alpha\mathrm{ml} + \beta\mathrm{ml})} \tag{A25}$$

$$\tau\mathrm{ml} = \frac{1}{(\alpha\mathrm{ml} + \beta\mathrm{ml})} \tag{A26}$$

$$\alpha\mathrm{ml} = \frac{0.482(V + 47.13)}{1 - \exp\left[-0.1(V + 47.13)\right]} \tag{A27}$$

$$\beta\mathrm{ml} = 0.192 \exp\left(\frac{V}{-11}\right) \tag{A28}$$

$$\mathrm{hl}^{\infty} = \frac{1}{1 + \exp[(91 + V)/6.1]} \tag{A29}$$

Slow delayed rectifier current conductance.

$$G_{\mathrm{Ks}} = 0.433 \left\{1 + \left[\frac{0.68}{\left(1 + (0.000038/\mathrm{Cai})^{1.4}\right)}\right]\right\} \tag{A30}$$